



**Andreia de Freitas  
Silva**

**Oligomerização de olefinas leves na presença de  
catalisadores ácidos inorgânicos porosos**

**Oligomerization of light olefins in the presence of  
porous inorganic acid catalysts**





**Andreia de Freitas  
Silva**

**Oligomerização de olefinas leves na presença de  
catalisadores ácidos inorgânicos porosos**

**Oligomerization of light olefins in the presence of  
porous inorganic acid catalysts**

Tese apresentada à Universidade de Aveiro para cumprimento dos requisitos necessários à obtenção do grau de Doutor em Engenharia Química, realizada sob a orientação científica da Doutora Anabela Tavares Aguiar Valente, Equiparada a Investigadora Principal do CICECO-Instituto de Materiais de Aveiro, Departamento de Química da Universidade de Aveiro, e coorientação científica do Doutor Carlos Manuel Santos da Silva, Professor Associado do Departamento de Química da Universidade de Aveiro.

Apoio financeiro do POCTI no âmbito  
do III Quadro Comunitário de Apoio.

Apoio financeiro da FCT  
(PD/BD/101018/2014), e do POPH/FSE  
no âmbito do III Quadro Comunitário de  
Apoio.



Dedico este trabalho aos meus pais e irmão, pelo incansável apoio e carinho.



## **o júri**

presidente

**Prof. Doutor António Manuel Rosa Pereira Caetano**  
Professor Catedrático do Departamento de Matemática da Universidade de Aveiro

**Prof. Doutor João Carlos Matias Celestino Gomes da Rocha**  
Professor Catedrático do Departamento de Química da Universidade de Aveiro

**Prof. Doutora Maria Filipa Gomes Ribeiro**  
Professora Associada com Agregação do Departamento de Engenharia Química e Biológica do Instituto Superior Técnico, Universidade de Lisboa

**Prof. Doutor Joaquim Silvério Marques Vital**  
Professor Auxiliar do Departamento de Química da Faculdade de Ciências e Tecnologia da Universidade Nova de Lisboa

**Prof. Doutor José Eduardo dos Santos Félix Castanheiro**  
Professor Auxiliar do Departamento de Química da Universidade de Évora

**Doutora Anabela Tavares Aguiar Valente**  
Equiparada a Investigadora Principal do Departamento de Química da Universidade de Aveiro



## agradecimentos

Um especial muito obrigado aos meus orientadores científicos. À Doutora Anabela Valente gostaria de expressar o meu sincero agradecimento por me ter aceitado como aluna de doutoramento e pelo enorme apoio, disponibilidade e dedicação incondicional durante todas as etapas do meu trabalho, sem exceção; agradeço, também, a partilha de conhecimento, sempre com muita simpatia e paciência, a motivação, amizade e compreensão nos momentos mais difíceis. Ao Professor Doutor Carlos Manuel Silva agradeço por me ter aconselhado a fazer o doutoramento e, também, pela sua disponibilidade, apoio, ensinamentos e palavras de reconhecimento, motivação e amizade, que foram muito importantes para mim nesta jornada.

Gostaria de agradecer as valiosas ajudas da Professora Filipa Ribeiro e do Doutor Auguste Fernandes (Instituto Superior Técnico, Universidade de Lisboa) pelas medidas das propriedades ácidas, e da Doutora Sílvia Rocha (QOPNA & LAQV-REQUIMTE) e Doutora Patrícia Neves (CICECO-Instituto de Materiais de Aveiro) pelas análises GC×GC-ToFMS.

Agradeço imensamente às seguintes pessoas pelos seus apoios técnicos, competências e disponibilidades (Universidade de Aveiro): Doutora Rosário Soares (DRX de pós) e Mestre Celeste Azevedo (análises térmicas) do CICECO-Instituto de Materiais de Aveiro; Doutora Paula Santos (RMN de estado sólido), Lic. Hilário Tavares (RMN de estado líquido) e Lic. Manuela Marques (análise elementar) do Departamento de Química; Lic. Maria João Bastos e Lic. Célia Miranda (isotérmicas de adsorção de N<sub>2</sub>) e mestres Marta Ferro e Tiago Silva (microscopia eletrónica) do Departamento de Engenharia de Materiais e Cerâmica.

À Doutora Inês Portugal (Universidade de Aveiro) agradeço a generosidade de emprestar equipamentos. Ao Engenheiro Jorge Correia Ribeiro (Galp) agradeço a partilha de conhecimentos e o generoso fornecimento de uma amostra de diesel. Agradeço também a generosidade da Saint-Gobain Ceramic Materials AS (amostras de SiC (SIKA)), da Clarian Produkte GmbH, Germany (amostra de catalisador COD-900) e da Sibelco Portuguesa, Lda (amostras de caulinite).

Um agradecimento especial à Doutora Margarida Antunes e Doutora Patrícia Neves pela ajuda e disponibilidade constante, e também pela simpatia e amizade. Agradecimentos carinhosos a todos os meus colegas do grupo EgiChem pela ajuda, partilha de conhecimentos, amizade e boa disposição, facilitando um bom ambiente de trabalho ao longo desta jornada.

À Universidade de Aveiro, em particular ao CICECO e ao Departamento de Química por me terem aceite como aluna de doutoramento e me terem facultado as condições necessárias para desenvolver o meu trabalho de investigação. À Fundação para a Ciência e Tecnologia (FCT) e ao Fundo Social Europeu (FSE) pela minha bolsa de doutoramento (SFRH/BD/101018/2014) e por todos os subsídios concedidos. Este trabalho foi, em parte, desenvolvido no âmbito do projeto CICECO-Instituto de Materiais de Aveiro, Ref<sup>a</sup>. FCT UID/CTM/50011/2019, financiado por fundos nacionais através da FCT/MCTES.

Um muito obrigado aos meus amigos mais próximos por serem bons ouvintes e pelo conforto nos momentos de maior dificuldade. E o maior obrigado é para os meus pais, Rita e José Manuel, e irmão Sérgio pelo amor e amizade. Apesar da distância, nunca faltaram palavras de carinho, apoio e encorajamento, que foram tão preciosas nos momentos mais difíceis desta jornada. Acima de tudo, agradeço por acreditarem sempre em mim, encorajando-me a não desistir e a ultrapassar todos os obstáculos com que me deparava. Obrigada por acreditarem em mim nos momentos em que eu própria não acreditei.



## palavras-chave

Alcenos leves, aluminossilicatos mesoporosos, 1-buteno, catálise heterogénea, combustíveis líquidos, desenho fatorial de experiências, diesel, oligomerização, otimização, reator contínuo, zeólitos

## resumo

Com o aumento global do consumo de combustíveis para o setor dos transportes e as crescentes preocupações ambientais, a oligomerização de alcenos leves provenientes de fontes fósseis ou renováveis, ou de efluentes de refinarias, representa uma *via* de valorização promissora para produzir combustíveis limpos com reduzidos teores de compostos aromáticos e enxofre, e outros produtos químicos de valor acrescentado. Esta tese incide na oligomerização do 1-buteno em produtos do tipo *diesel* sintético, em reator contínuo, a alta pressão, usando catalisadores heterogéneos ácidos.

A oligomerização de alcenos leves envolve mecanismos reacionais complexos. Os rendimentos e as características dos produtos dependem das propriedades dos materiais catalíticos e das condições de operação. Estes aspetos foram investigados com o objetivo prático de produzir diesel limpo, usando catalisadores ácidos inorgânicos porosos à base de óxidos de silício e alumínio. Os materiais foram preparados por diversas metodologias e caracterizados por técnicas complementares, com especial atenção dada às propriedades morfológicas, texturais e ácidas. Os desempenhos catalíticos foram avaliados em termos de atividade, seletividade para produtos do tipo diesel e estabilidade, com base em estudos experimentais e o recurso a ferramentas estatísticas de análise multivariada. As misturas de produtos reacionais foram caracterizadas com base em cromatografia de gás bidimensional abrangente acoplada a espectrometria de massa com analisador por tempo de voo (GC×GC-ToFMS) e espectroscopia por ressonância magnética nuclear (RMN).

À descoberta de catalisadores promissores, o trabalho de investigação evoluiu de aluminossilicatos mesoporosos do tipo TUD-1 sintetizados por metodologias relativamente limpas (sem agentes tensoativos) e um composto de nanocristais de zeólito Beta dispersos numa matriz do tipo TUD-1, até zeótipos micro- e mesoporosos possuindo diferentes topologias (BEA, MFI) e preparados por estratégias *bottom-up* (não destrutivas) ou *top-down*. Os desempenhos dos catalisadores preparados foram comparados com zeólitos comerciais e um catalisador que foi desenvolvido para processos comerciais de oligomerização, nomeadamente o COD-9 (baseado na topologia MFI).

Os zeótipos micro/mesoporosos apresentaram melhores desempenhos do que os zeólitos comerciais (Beta, ZSM-5, COD-9), obtendo-se conversões de butenos até 86 % e seletividades para produtos do tipo *diesel* até 71 % (m/m), a 200 °C, 30 bar e 2.2 g g<sub>cat</sub><sup>-1</sup> h<sup>-1</sup>. Com base em análise estatística de componentes principais (PCA) foram estabelecidas relações de atividade-estrutura que apontaram para a necessidade de haver compromissos entre as propriedades texturais e ácidas para maximizar os rendimentos em *diesel* limpo – concentrações intermédias de centros ácidos e elevada mesoporosidade resultaram em melhores desempenhos catalíticos.

Um dos catalisadores mais promissores foi o MZS-0.4-CI preparado pela abordagem *top-down* a partir do zeólito comercial ZSM-5. Foram realizados estudos de otimização para a oligomerização do 1-buteno usando este tipo de catalisador. A otimização baseou-se no desenho fatorial de experiências (DoE, com uma matriz Box-Behnken) e a metodologia da superfície de resposta (RSM), contemplando os rendimentos em produtos do tipo *diesel*, assim como aspetos da qualidade dos produtos (teor de compostos aromáticos). Estes estudos indicaram as seguintes gamas de condições de operação mais favoráveis: 220-250 °C de temperatura de reação, 30-40 bar de pressão e 2.5-3.5 g<sub>1C4</sub> g<sub>cat</sub><sup>-1</sup> h<sup>-1</sup> de velocidade espacial por unidade de massa de catalisador. Por fim, estudos de PCA com todos os materiais estudados nesta tese mostraram que a influência das propriedades dos materiais nos desempenhos não é trivial.



**keywords**

1-butene, continuous flow reactor, design of experiments, diesel, fuels, heterogeneous catalysis, light olefins, mesoporous aluminosilicates, oligomerization, optimization, zeolites, zeotypes

**abstract**

With the global growth in fuel demand for transportation and increasing environmental concerns, the oligomerization of light olefins obtainable from fossil or renewable sources and refinery streams, represents a promising route for producing clean synthetic fuels with low aromatics and sulphur contents, and other added-value chemicals. This thesis deals with the oligomerization of 1-butene to produce diesel range products, under high pressure and continuous operation, in the presence of heterogeneous acid catalysts.

The oligomerization of light olefins is a complex reaction system. The yields and characteristics of the products are governed by the properties of the catalytic materials and the operating conditions. These aspects were investigated with the practical goal of producing clean diesel range products, using porous inorganic acid catalysts based on silicon and aluminium oxides. The materials were prepared *via* different methodologies and characterized by complementary techniques, with special attention given to morphological, textural and acid properties. The catalytic performances were evaluated in terms of activity, selectivity to clean diesel type products and stability, based on experimental studies and multivariate statistical tools. The characteristics of the catalytic reaction products were studied based on comprehensive two-dimensional gas chromatography coupled to time-of-flight mass spectrometry (GCxGC-ToFMS) and nuclear magnetic resonance (NMR) spectroscopy.

In the search for promising catalysts, the research work evolved from eco-friendly mesoporous aluminosilicate of the type TUD-1 prepared *via* one-pot or stepwise approaches, and a composite material comprising BEA nanocrystallites embedded in a TUD-1 siliceous matrix, to micro/mesoporous zeotypes possessing different topologies (BEA, MFI) prepared *via* bottom-up or top-down approaches. The catalysts were benchmarked with commercially available zeolites and a catalyst based on the MFI topology which was developed for commercial oligomerization processes, namely COD-9.

The micro/mesoporous zeotypes outperformed the commercial zeolites (Beta, ZSM-5, COD-9), leading to conversions of butenes of up to 86 % and selectivity to diesel ranged products of up to 71 wt.%, at 200 °C, 30 bar and 2.2 g g<sub>cat</sub><sup>-1</sup> h<sup>-1</sup>. Based on principal component analysis (PCA), structure-activity relationships were established that pointed to the importance of good compromises between textural and acid properties for maximizing the yields of clean diesel range products - intermediate concentrations of acid sites and enhanced mesoporosity resulted in superior catalytic performances.

One of the best-performing catalysts was MZS-0.4-CI prepared *via* top-down approach from commercial ZSM-5. Optimization studies were carried out for 1-butene oligomerization over this type of catalyst. The optimization was based on a Box-Behnken design of experiments (DoE) and response surface methodology (RSM), contemplating the yields of the diesel range products, as well as the product quality (reduced aromatics content). These studies indicated that the favourable operating conditions were in the ranges 220-250 °C of reaction temperature, 30-40 bar and 2.5-3.5 g<sub>1C4</sub> g<sub>cat</sub><sup>-1</sup> h<sup>-1</sup> weight hourly space velocity. Finally, PCA studies were conducted for all materials studied in this thesis, to show the complex interplay of material properties influencing the catalytic performances.



# Thesis outline

Thesis outline.....	i
List of abbreviations.....	v
List of tables.....	viii
List of figures.....	xii

## Chapter 1: Motivation, objectives and thesis plan

1.1. Motivation.....	2
1.2. Objectives .....	3
1.3. Thesis plan .....	4
1.4. References.....	7

## Chapter 2: Literature review

2.1. Transportation fuels .....	11
2.1.1. Global and European demands.....	11
2.1.2. Production processes.....	13
2.1.3. Gasoline and diesel quality properties.....	20
2.2. Catalytic olefin oligomerization of light olefins.....	24
2.2.1. Industrial technologies.....	24
2.2.2. Emerging bio-based processes.....	32
2.2.3. Mechanistic considerations.....	33
2.2.4. Catalyst scope for olefin oligomerization.....	37
2.3. Zeolites and zeotype acid catalysts for olefin oligomerization.....	45
2.3.1. Zeolites - microporous systems.....	45
2.3.2. Zeolites - acidity and shape-selectivity.....	47
2.3.3. Improved versions of zeolites.....	52
2.3.4. Catalytic performances of zeolites/zeotypes for propene and butenes oligomerization.....	68
2.4. References.....	95

## Chapter 3: Experimental section

3.1. Chemicals.....	113
---------------------	-----

3.2.	Methods.....	115
3.2.1.	Characterization of the catalysts.....	115
3.2.2.	Quantification of the reaction products by GC-FID.....	118
3.2.3.	Identification of the liquid reaction products by GC×GC-ToFMS.....	123
3.2.4.	Determination of the cetane number, isoparaffinic index and aromatic content....	124
3.3.	Laboratory Setup 1 of the catalytic test unit.....	125
3.4.	Laboratory Setup 2 of the catalytic test unit.....	128
3.4.1.	Experimental procedure.....	134
3.5.	References.....	138

## **Chapter 4: General considerations**

4.1.	Reproducibility tests .....	140
4.2.	Studies of mass transfer limitations.....	140
4.3.	Thermodynamics of 1-butene isomerization.....	144
4.4.	References.....	145

## **Chapter 5: TUD-1 type aluminosilicate acid catalysts for 1-butene oligomerization**

5.1.	Introduction.....	149
5.2.	Synthesis of the catalytic materials.....	150
5.3.	Characterization studies of the catalytic materials.....	152
5.4.	Catalytic studies: general considerations.....	159
5.5.	Cetane number and GC×GC-ToFMS analysis of reaction products.....	162
5.6.	Influence of the reaction conditions.....	163
5.7.	Catalyst stability and benchmarking.....	165
5.8.	Conclusions.....	169
5.9.	References.....	171

## **Chapter 6: Mesostructured oligomerization catalysts based on the BEA topology for 1-butene oligomerization**

6.1.	Introduction.....	177
6.2.	Synthesis of the catalytic materials.....	179
6.3.	Characterization studies of the catalytic materials.....	180
6.3.	Catalytic studies: general considerations.....	187
6.4.	Influence of material properties on the catalytic performance.....	191

6.5.	Influence of the reaction conditions.....	194
6.6.	Catalyst stability and benchmarking.....	196
6.7.	Influence of catalyst activation temperature.....	202
6.8.	Conclusions.....	205
6.9.	References.....	206

**Chapter 7: 1-Butene oligomerization over nanocrystalline MFI-based micro/mesoporous zeotypes synthesized *via* bottom-up approaches**

7.1.	Introduction.....	213
7.2.	Synthesis of the catalytic materials.....	215
7.3.	Characterization studies of the catalytic materials.....	218
7.4.	Catalytic studies: general considerations.....	224
7.5.	Influence of material properties on the catalytic performance.....	230
7.6.	Influence of the reaction conditions.....	232
7.7.	Catalyst stability.....	233
7.8.	Conclusions.....	238
7.9.	References.....	239

**Chapter 8: Modified versions of zeolite ZSM-5 synthesized *via* top-down approaches for oligomerization of 1-butene**

8.1.	Introduction.....	245
8.2.	Synthesis of the catalytic materials.....	246
8.3.	Characterization studies of the catalytic materials.....	250
8.4.	Methods of statistical analysis of data.....	260
8.5.	Principal component analysis (PCA) of the material properties.....	262
8.6.	Catalytic studies: general considerations.....	264
8.7.	Influence of material properties on the catalytic performance.....	267
8.8.	Conclusions.....	273
8.9.	References.....	273

**Chapter 9: Optimization of heterogeneous catalytic oligomerization of 1-butene by design of experiments and response surface methodology**

9.1.	Introduction.....	281
9.2.	Synthesis of the catalytic materials.....	283
9.3.	Design of experiments (DoE) and response surface methodology (RSM).....	284

9.3.	Characterization studies of the catalytic materials.....	287
9.4.	Catalytic studies: general considerations.....	289
9.5.	Optimization studies of 1-butene oligomerization.....	294
9.6.	Conclusions.....	299
9.7.	References.....	300

## **Chapter 10: Conclusions and future work**

10.1.	General conclusions.....	308
10.2.	Future work.....	315
10.3.	References.....	317

## **Appendix A**

Supplementary Material - Chapter 3.....	320
Supplementary Material - Chapter 4.....	329
Supplementary Material - Chapter 6.....	332
Supplementary Material - Chapter 7.....	336
Supplementary Material - Chapter 8.....	338
Supplementary Material - Chapter 9.....	343
Supplementary Material - Chapter 10.....	348
References of Appendix A.....	350

## List of abbreviations

1C4	1-Butene
AARD	Average absolute relative deviation
ACH	Aluminum chlorohydrate
AIP	Aluminum(III) isopropoxide
ASTM	Standard test method (formerly, American Society for Testing and Materials)
ATR	Attenuated total reflection
B	Brønsted acid sites
BET	Brunauer, Emmett and Teller
BJH	Barrett-Joyner-Halenda
BPR	Back-pressure regulator
BTL	Biomass to liquids
C <sub>12</sub> TMABr	Dodecyltrimethylammonium bromide
C3	Propene
C4	Butenes
Catpoly	Catalytic polymerization
COD	Conversion of olefins to distillates
CN	Cetane number
CTABr	Hexadecyltrimethylammonium bromide
CTL	Coal to liquids
D <sub>cut</sub>	Cut of diesel type products
DFT	Density functional theory
DoE	Design of experiments
D <sub>p</sub>	Pore size (width)
DSC	Differential scanning calorimetry
EA	Elemental analysis
EDS	Energy dispersive X-ray spectroscopy
EFAL	Extra-framework aluminum
FCC	Fluid catalytic cracking
FID	Flame ionization detector
FT	Fischer-Tropsch
FT-IR	Fourier-transform infrared spectroscopy
HF	Hierarchy factor
GC	Gas chromatography
GCxGC-ToFMS	Two-dimensional gas chromatography with a time-of-flight mass spectrometry
GHG	Greenhouse gas
GTL	Gas to liquids
ICP-AES	Inductively coupled plasma atomic emission spectroscopy
IHF	Indexed hierarchy factor
L	Lewis acid sites
L+B	Total (Brønsted plus Lewis) acid sites
LCN	Light-cracked naphtha

LPG	Liquefied petroleum gas
MAS NMR	Magic angle spinning nuclear magnetic resonance (solid state)
MCM-41	Mobil Composition of Matter No. 41
MFC	Mass flow controller
MOGD	Mobil olefins to gasoline and distillate
MON	Motor octane number
MR	Membered ring
$N_{cut}$	Cut of naphtha type products
NMR	Nuclear magnetic resonance (liquid state)
ON	Octane number
Ox	Oxalic acid
P	Pressure
PCA	Principal componente analysis
PDADMAC	Polydiallyldimethylammonium chloride
PDD-AM	Poly(acrylamide-co-diallyldimethylammonium chloride)
PHAPTMS	[3-(Phenylamino)propyl]trimethoxysilane
PLD	Product lump distribution
PSD	Pore size distribution
PTFE	Polytetrafluoroethylene
PXRD	X-ray powder diffraction
RF	Response factor
RGO	Reference gas oil
RON	Research octane number
RSM	Response surface methodology
SAC	Steam-assisted crystallization
$S_{BET}$	BET specific surface area
$S_{ext}$	External specific surface area
$S_{meso}$	Mesoporous specific surface area
SC	Steam cracking
SDA	Structure directing agent
SEM	Scanning electron microscopy
SiC	Silicon carbide
SPA	Solid phosphoric acid
STEM	Scanning transmission electron microscopy
STY	Space time yield (based on total liquid products)
$STY_{Dcut}$	Space time yield (based on diesel type products)
$STY_{Ncut}$	Space time yield (based on naphtha type products)
T	Temperature
$T_{act}$	Catalyst activation temperature
TEA	Triethanolamine
TEAOH	Tetraethylammonium hydroxide
TEOS	Tetraethylorthosilicate
TEM	Transmission electron microscopy
TGA	Thermogravimetric analysis
TOS	Time on stream
TPAOH	Tetrapropylammonium hydroxide
TPD	Temperature-programmed desorption
TUD-1	Technische Universital Delft, number one

$V_{\text{meso}}$	Mesoporous volume
$V_{\text{micro}}$	Microporous volume
$V_p$	Total pore volume
VGO	Vacuum gas oil
$X_{C4}$	Conversion of butenes
$X_{1C4}$	Conversion of 1-butene
WHSV	Weight hourly space velocity
ZSM-5	Zeolite Socony Mobil-5

# List of tables

## **Chapter 2**

Table 2.1. Specifications of the products of petroleum distillation and refining. <sup>[9,12]</sup> .....	15
Table 2.2. Main advantages and disadvantages of conventional and alternative fuels and respective production technologies. <sup>[9,10,13,21-25]</sup> .....	18
Table 2.3. Some quality properties of most fuels used in the EU, and their normative values (EN 228:2012 for gasoline and EN 590:2013 for diesel). <sup>[26-28]</sup> .....	20
Table 2.4. Influence of the fuel composition on fuel properties. <sup>[35,39]</sup> .....	24
Table 2.5. Olefins oligomerization technologies mainly for middle distillates production. <sup>[47]</sup> .....	25
Table 2.6. Types of catalysts reported in the literature for olefin oligomerization .....	40
Table 2.7. Selected published review articles on olefin oligomerization. ....	42
Table 2.8. Selected published review articles on ethene oligomerization .....	43
Table 2.9. Zeolite classification according to micropore sizes, and examples with indication of the respective channel dimensionality. <sup>[139,145]</sup> .....	46
Table 2.10. Pore systems of selected zeolites reported in the literature for olefin oligomerization. <sup>[139,146]</sup> .....	47
Table 2.11. Types of shape-selectivity of zeolites. Adapted from ref. [52].....	51
Table 2.12. Effect of several processes parameters on the final zeolite properties. <sup>[179,183]</sup> .....	54
Table 2.13. Strategies for introducing mesoporosity in zeolites. <sup>[140,185,199,217,224,237]</sup> .....	65
Table 2.14. Selected studies of oligomerization processes involving different types of feed, zeolites and operating conditions. <sup>[a]</sup> .....	80
Table 2.15. Propene oligomerization studies, performed in fixed-bed reactors, over zeolites or other aluminosilicates and metal oxides.....	85
Table 2.16. Butene oligomerization studies, performed in fixed-bed reactors, over zeolites or other aluminosilicates and metal oxides.....	89

## **Chapter 3**

Table 3.1. Chemicals used in the synthesis of the catalysts. <sup>[a]</sup> .....	113
Table 3.2. Chemical compounds and commercial zeolites used for the catalytic tests. <sup>[a]</sup> .....	114
Table 3.3. Column specifications and GC method for ASTM D2887-04 and the liquid phase products method used in this work. ....	120
Table 3.4. Results for ASTM D2887 Reference Gas Oil n.º 1, according to the test method ASTM D2887 and the liquid phase method developed in this work. ....	121
Table 3.5. GC×GC-ToFMS analytical conditions. ....	123

## **Chapter 5**

Table 5.1. Elemental analyses and textural properties of the mesoporous silicas/silicates prepared, and the benchmark catalyst ZSM-5.....155

Table 5.2. Acid properties of the prepared mesoporous silicas/silicates.<sup>[a]</sup>.....158

## **Chapter 6**

Table 6.1. Elemental analyses and textural properties of the zeolite Beta based materials.....183

Table 6.2. Acid properties of the zeolite Beta based materials.<sup>[a]</sup>.....186

Table 6.3. Acid properties measured at 200 °C or 450 °C on X<sub>C4</sub>, STY, and catalytic activity for the bulk Beta based catalysts (BEA-hier, BEA-nano, BEA-micro) activated at 200 °C prior to catalytic reaction. ....192

Table 6.4. Textural properties of the catalysts before and after use (activated at 200 °C or 450 °C).<sup>[a]</sup>.....197

Table 6.5. Catalytic results for BEA-hier and the benchmark catalysts.<sup>[a]</sup>.....200

Table 6.6. Comparison of the catalytic results for BEA-hier and ZSM-5 (this work) to literature data, for catalysts based on the BEA or MFI zeolites, tested for the reaction of 1-butene using a fixed-bed reactor (it is included studies where feed mixtures containing 1-butene were used).<sup>[a]</sup>.....201

## **Chapter 7**

Table 7.1. Bottom-up protocols and synthesis conditions of the zeotypes based on the MFI topology.....215

Table 7.2. Elemental analyses and textural properties of the MFI-based materials.<sup>[a]</sup>.....219

Table 7.3. Al-species and acid properties of the MFI-based materials.....224

Table 7.4. Comparison of the catalytic results for hZSM-5(20)-PZSi (this work) to literature data, for catalysts based on the MFI topology, tested for the reaction of butene (the isomer is not always specified) using a fixed-bed reactor (includes studies where the feed was multicomponent and contained 1-butene).<sup>[a]</sup>.....228

Table 7.5. Influence of the catalyst activation temperature (T<sub>act</sub>) and reaction conditions (T, P) on the catalytic reaction.....232

Table 7.6. Elemental analyses and textural properties of the original and used MFI-based materials.<sup>[a]</sup>.....235

Table 7.7. Al-species and acid properties of the original and used MFI-based materials.....236

## **Chapter 8**

Table 8.1. Top-down protocols and synthesis conditions of the MFI based catalysts.....249

Table 8.2. Composition and textural properties of HZSM-5 and its modified versions.....251

Table 8.3. Types of aluminum species and acid properties of selected catalysts.....259

Table 8.4. Data matrix used in the construction of the PCA biplot (Figure 8.10).....262

## **Chapter 9**

Table 9.1. Gasoline and distillate mode operating conditions used in light olefins oligomerization technologies.....	281
Table 9.2. Levels and codification of the factors (independent variables) used in the optimization of the catalytic oligomerization process.....	285
Table 9.3. Performance parameters (responses) for the evaluation of 1-butene oligomerization....	86
Table 9.4. Aliphatic products formed in the catalytic reactions of 1-butene, at 225 °C, 32.5 bar, 3.5 g <sub>1C4</sub> g <sub>cat</sub> <sup>-1</sup> h <sup>-1</sup> (sample 1), or 300 °C, 45 bar, 3.5 g <sub>1C4</sub> g <sub>cat</sub> <sup>-1</sup> h <sup>-1</sup> (sample 2). <sup>[a]</sup> .....	291
Table 9.5. Experimental design matrix using a three-level Box-Behnken design with three factors (in terms of uncoded units) and the experimental responses.....	295
Table 9.6. Reduced models for the responses of the DoE.....	296
Table 9.7. Experimental and calculated responses (by the RSM reduced models) for the catalytic assay performed at 45 bar, 255 °C, 2.0 g <sub>1C4</sub> g <sub>cat</sub> <sup>-1</sup> h <sup>-1</sup> , and the AARDs for this catalytic assay and for the RSM reduced models.....	296

## **Appendix A**

Table S3.1. Critical properties and acentric factor of 1-butene and nitrogen.....	326
Table S3.2. Yields of different products considered in the material balances, for the different materials (Chapter 5-8) tested in the 1-butene oligomerization at 200 °C, 30 bar and WHSV of 2.2 g <sub>1C4</sub> g <sub>cat</sub> <sup>-1</sup> h <sup>-1</sup> . <sup>[a]</sup> .....	327
Table S3.3. Yields of different products considered in the material balances, for the hierZ-MFI (Chapter 9) tested in the 1-butene oligomerization at different reaction conditions. <sup>[a]</sup> .....	328
Table S4.1. Butene isomers distributions for the different materials tested in the 1-butene oligomerization at 200 °C, 30 bar and WHSV of 2.2 g <sub>1C4</sub> g <sub>cat</sub> <sup>-1</sup> h <sup>-1</sup> .....	330
Table S4.2. Butene isomers distributions for the different materials tested in different operating conditions.....	331
Table S6.1. Acid properties measured at 200 °C or 450 °C on X <sub>C4</sub> , STY, and catalytic activity for the bulk Beta based catalysts (BEA-hier, BEA-nano, BEA-micro) activated at 200 °C prior to catalytic reaction.....	335
Table S8.1. Data matrix used in the construction of the PCA biplot of Figure S8.4.....	339
Table S8.2. Data matrix used in the construction of the PCA biplot of Figure 8.15.....	340
Table S8.3. Cetane number, paraffin index and content of aromatic compounds for the best catalysts.....	340
Table S9.1. Aromatic and diaromatic contents determined by GC×GC-ToFMS, and aromatic content, isoparaffinic index and cetane number determined by <sup>1</sup> H NMR, for the different assays.....	343
Table S9.2. Aromatic products formed in the catalytic reactions of 1-butene, at 225 °C, 32.5 bar, and 3.5 g <sub>1C4</sub> g <sub>cat</sub> <sup>-1</sup> h <sup>-1</sup> (sample 1), or 300 °C, 45 bar, and 3.5 g <sub>1C4</sub> g <sub>cat</sub> <sup>-1</sup> h <sup>-1</sup> (sample 2). <sup>[a]</sup> .....	343
Table S9.3. Reduced experimental models, with codified variables, for the responses of the DoE..	347

Table S9.4. Aromatics distribution in the Dcut and Ncut products.....	347
Table S10.1. Data matrix used in the construction of the PCA biplots of Figure 10.2 and Figure 10.3.....	348

# List of figures

## Chapter 2

Figure 2.1. Projections for 2040 of the global energy consumption by sector and global greenhouse gas emission by sector in 2014. Adapted from refs. [1,2].	12
Figure 2.2. Projections for 2040 of the global energy consumption by transportation fuel and EU energy demand by transportation fuel (2010-2050) (others include biodiesel and hydrogen). Adapted from refs. [1,5]	13
Figure 2.3. Scheme of a petroleum refinery process to obtain liquid hydrocarbons. Adapted from refs. [9,11].	14
Figure 2.4. Simplified flow diagram of a Fischer-Tropsch (FT) based facility. Adapted from ref. [15].	16
Figure 2.5. Simplified representation of high temperature (HT) FT syncrude refining coupled with an oligomerization unit. Adapted from ref. [20].	16
Figure 2.6. Pure component CN as function of the number of carbon atoms for different classes of hydrocarbons. Adapted from ref. [36].	22
Figure 2.7. MOGD process flow for operation in Distillate mode. Adapted from ref. [60].	28
Figure 2.8. COD process with indication of the feed and products compositions. Adapted from refs. [86,87]	29
Figure 2.9. Polyfuel process using the IP 811 (amorphous silica-alumina) catalyst. Adapted from ref. [92].	31
Figure 2.10. Polynaphtha in a FlexEne configuration for gasoline (red arrows) and distillates (purple arrows) production. Adapted from ref. [95].	32
Figure 2.11. Production of synthetic liquid fuels from lignocellulose (LA=levulinic acid, FA=formic acid, SBP=2-sec-butylphenol, GVL= $\gamma$ -valerolactone). Adapted from ref. [55].	33
Figure 2.12. Carbenium ion mechanism of acid-catalyzed oligomerization reactions, exemplified for 1-butene as initial monomer (R and R' stands for alkyl groups with different number of carbons atoms or configurations). Adapted from ref. [17].	35
Figure 2.13. Possible mechanism of olefin aromatization, exemplified for 1-heptene. Adapted from ref. [105].	36
Figure 2.14. Simplified representation of the steps involved in a heterogeneous catalytic reaction process (A stands for reactant, P for product, and * for active site). Adapted from ref. [126].	39
Figure 2.15. (A) Silicon and aluminum atoms in tetrahedral coordination, and sodium cations compensating the negatively charged framework. (B) Example of a zeolite structure (LTA type) possessing a sodalite cage (the white lines represent T-O-T bridges). Adapted from ref. [139].	46
Figure 2.16. Simplified representation of Brønsted acid sites (“bridging hydroxyl groups”) and formation of Lewis acid sites in zeolites. Adapted from ref. [99].	48
Figure 2.17. Effect of pore size on the diffusion of large (purple) and small (black) molecules within macropores (red), mesopores (yellow) and micropores (blue), with indication of the approximate ranges of diffusivities. Adapted from ref. [178].	52
Figure 2.18. Typical operations involved in zeolite synthesis.	53
Figure 2.19. Bottom-up and top-down strategies for synthesizing hierarchical zeolites.	56

Figure 2.20. Influence of the Al content of precursor MFI zeolites on the desilication treatment, and possible treatments to overcome drawbacks associated with a high or low Al content. Adapted from ref. [200].....	58
Figure 2.21. Hard templating method to prepare hierarchical zeolites. Adapted from ref. [220].....	60
Figure 2.22. Soft templating strategies using organosilanes or silylated polymers. Adapted from refs. [221,227,228].....	62
Figure 2.23. Solid-state and steam-assisted crystallizations methods. Adapted from refs. [238,239].....	64
Figure 2.24. Ultrasounds-assisted method. Adapted from ref. [232].....	64

### **Chapter 3**

Figure 3.1. GC calibration curve for 1-butene, used for quantification of the gas phase reaction products, for loop 4, where $[1C4]_{loop}$ stands for the molar concentration of 1-butene at the PT condition of the loop (1 bar, 200 °C), and A stands for the peak area of 1-butene.....	119
Figure 3.2. GC calibration curve for C6-C24 <i>n</i> -paraffins, used for the quantification of liquid reaction products ( $C_0$ and $A_0$ stand for the concentration and area of the internal standard ( <i>n</i> -pentane), respectively), accompanied by the response factors (RS, slope of the calibration curves), for each <i>n</i> -paraffin.....	119
Figure 3.3. Calibration curve for the <i>n</i> -alkanes series (ASTM D2887 calibration mix) (BP and RT stand for boiling point and retention time, respectively).....	121
Figure 3.4. Process flow diagram of Setup 1 for the catalytic test unit. The red lines represent heating hoses and the red areas represent closed heated boxes. ....	126
Figure 3.5. Photograph of the laboratory Setup 1.....	127
Figure 3.6. Process flow diagram of Setup 2 for the catalytic test unit. The red lines represent heating hoses and the red areas represent closed heated boxes.....	129
Figure 3.7. Photograph of the laboratory Setup 2.....	130
Figure 3.8. Feed section (A) of the laboratory Setup 2.....	131
Figure 3.9. Reaction section (B) of the laboratory Setup 2.....	132
Figure 3.10. Detailed design of the fixed-bed tubular reactor (Paralab) of Setup 2.....	133
Figure 3.11. Products section (C) of the laboratory Setup 2. ....	134

### **Chapter 4**

Figure 4.1. Conversion of butenes ( $X_{C4}$ ) as a function of TOS for: (A) the commercial zeolites BEA-nano ( $\diamond, \diamond$ ), BEA-micro ( $\blacktriangle, \blacktriangle$ ) and ZSM-5 ( $\bullet, \bullet$ ); or (B) the synthesized aluminosilicate Al-TUD-1(25)-HT ( $\blacksquare, \blacksquare$ ).....	140
Figure 4.2. Conversion ( $X_{C4}$ ) as function of TOS (A,C,E) and PLD curves (B, D, F) using BEA-nano (A,B) and ZSM-5 (C,D), and Al-TUD-1(25)-HT (E,F).....	143
Figure 4.3. Butene isomers distribution for different reaction temperatures (150-250 °C), and different catalysts (Al-TUD-1(25)-HT ( $\bullet$ ), BEA-hier ( $\bullet$ ) and hZSM-5(20)-PZSi ( $\bullet$ )); and thermodynamic equilibrium compositions ( $\bullet$ ).....	145

## Chapter 5

- Figure 5.1. (A) Low angles PXRD patterns of Al-TUD-1(25)-HT (fresh (a); used (b)), Al-TUD-1(50)-HT (fresh (c); used (d)), Al-TUD-1(PG) (fresh (e); used (f)), TUD-1 (fresh (g)), Al-LP(PG) (fresh (h); used (i)), and LP (fresh (j)); (B) wide angles PXRD patterns of fresh catalysts: Al-TUD-1(25)-HT (a), Al-TUD-1(50)-HT (b), Al-TUD-1(PG) (c), TUD-1 (d), Al-LP(PG) (e), and LP (f)...153
- Figure 5.2. SEM images and Si, Al mappings of Al-TUD-1(25)-HT (a), Al-TUD-1(50)-HT (b), Al-TUD-1(PG) (c), TUD-1 (d), Al-LP(PG) (e), and LP (f).....154
- Figure 5.3. Nitrogen adsorption-desorption isotherms (at  $-196\text{ }^{\circ}\text{C}$ ) for (A) Al-TUD-1(25)-HT (fresh ( $\square$ ); used ( $\times$ )), (B) Al-TUD-1(50)-HT (fresh ( $\square$ ); used ( $\times$ )), (C) Al-TUD-1(PG) (fresh ( $\square$ ); used ( $\times$ )) and TUD-1 (fresh ( $-$ )), and (D) Al-LP(PG) (fresh ( $\square$ ); used ( $\times$ )) and LP (fresh ( $-$ )). Insets are the mesopore size distributions for the corresponding materials (using the same symbols).....155
- Figure 5.4. (A) FT-IR spectra in the OH stretching region of the materials Al-TUD-1(25)-HT (dashed black line), Al-TUD-1(50)-HT (dashed grey line), Al-TUD-1(PG) (solid black line), and Al-LP(PG) (solid grey line), after evacuation at  $450\text{ }^{\circ}\text{C}$ ; the inset is a zoom into a narrower spectral region. (B) FT-IR spectra of pyridine (base probe) adsorbed, at  $200\text{ }^{\circ}\text{C}$ , on Al-TUD-1(25)-HT (a), Al-TUD-1(50)-HT (b), Al-TUD-1(PG) (c), and Al-LP(PG) (d).....157
- Figure 5.5.  $^{27}\text{Al}$  MAS NMR spectra of Al-TUD-1(25)-HT (a), Al-TUD-1(50)-HT (b), Al-TUD-1(PG) (c), and Al-LP(PG) (d).....157
- Figure 5.6. Conversion ( $X_{C4}$ ) and STY of Dcut and Ncut products for the different OMPS catalysts. ....160
- Figure 5.7. (A) Molar proportions of Dcut (black bars) and Ncut (grey bars) products, and (B) PLD profiles for the reaction of 1-butene in the presence of the OMPS catalysts.....160
- Figure 5.8. Influence of Lewis acid site density on (A) conversion ( $\bullet$ ) and intrinsic activity ( $\circ$ ), and (B) molar ratio of Dcut/Ncut products.....161
- Figure 5.9. Influence of reaction conditions on the catalytic reaction of 1C4 in the presence of Al-TUD-1(25)-HT. Conversion ( $X_{C4}$  ( $\times$ )) and STY of Dcut ( $\bullet$ ) and Ncut products ( $\circ$ ) (A, C), and PLD profiles (B, D) for different reaction pressures (A, B) and temperature (C, D).....164
- Figure 5.10. Influence of reaction conditions on the catalytic reaction of 1C4 in the presence of Al-TUD-1(25)-HT. Conversion ( $X_{C4}$  ( $\times$ )) and STY of Dcut ( $\bullet$ ) and Ncut products ( $\circ$ ) (E), and PLD profiles (F) for different WHSV.....165
- Figure 5.11. SEM images and Si, Al mappings of the catalysts after the reaction in the presence of Al-TUD-1(25)-HT (A), Al-TUD-1(50)-HT (B), Al-TUD-1(PG) (C), and Al-LP(PG) (D).....166
- Figure 5.12. Conversion ( $X_{C4}$ ) as a function of TOS, using Al-TUD-1(25)-HT as catalyst. The inset shows the PLD profiles for the products collected after 8 h and 32 h on-stream.....167
- Figure 5.13. Catalyst benchmarking with ZSM-5. (A) Conversion and mass ratio of Dcut/Ncut products, and (B) PDL profiles for Al-TUD-1(25)-HT and ZSM-5. ....168
- Figure 5.14. Conversion ( $X_{C4}$ ) versus Lewis acid site strength (based on the molar ratio  $L_{450}/L_{200}$ ) for the OMPS catalysts prepared and the benchmark catalyst, ZSM-5.....168
- Figure 5.15. Dependence of conversion ( $X_{C4}$ ) on TOS for Al-TUD-1(25)-HT ( $\circ$ ), Al-TUD-1(50)-HT ( $\square$ ), Al-TUD-1(PG) ( $\Delta$ ), Al-LP(PG) ( $+$ ), and ZSM-5 ( $\square$ ).....169

## Chapter 6

- Figure 6.1. (A) PXRD patterns of BEA-micro (fresh (a); used (b)), BEA-hier (fresh (c); used (d)), BEA-nano (fresh (e); used (f)), BEA/TUD (fresh (g); used (h)). (B) Low angles PXRD patterns of BEA-hier (fresh (a); used (b)), BEA/TUD (fresh (c); used (d)), TUD-1 (e).....180
- Figure 6.2. SEM images of BEA-nano (a), BEA-micro (b), and BEA-hier (c), and SEM images with corresponding Si and Al mappings of BEA/TUD (d), BEA+TUD-1 (e), and BEA-hier (f).....181
- Figure 6.3. TEM image of BEA-nano (a), TUD-1 (b), BEA/TUD (c), and BEA-hier (d and e).....182
- Figure 6.4. Nitrogen adsorption-desorption isotherms (at -196 °C) for (A) composite BEA/TUD ( $\square$ ) and its counterparts BEA-nano ( $\times$ ) and TUD-1 (-), and (B) BEA-hier ( $\diamond$ ), BEA-micro ( $\Delta$ ). Inset of (A) are the mesopore size distributions for BEA/TUD ( $\square$ ) and TUD-1 (-). Inset of (B) is the bimodal pore size distributon for BEA-hier ( $\diamond$ ).....184
- Figure 6.5.  $^{27}\text{Al}$  MAS NMR spectra of BEA-micro (a), BEA-hier (b), BEA-nano (c), and BEA/TUD (d). The asterisk indicate a sideband.....185
- Figure 6.6. FT-IR spectra in the OH stretching region after evacuation at 450 °C (A), and FT-IR spectra of pyridine (base probe) adsorbed at 200 °C (B) for BEA-micro (a), BEA-hier (b), BEA-nano (c), and BEA/TUD (d).....186
- Figure 6.7. SEM image (a) and Si (b), Al (c) mappings of the commercial benchmark catalyst ZSM-5 (obtained *via* calcination of CBV3024E, Zeolyst).....187
- Figure 6.8. Conversion ( $\diamond$ ) and STY (bars) of Ncut (light colour) and Dcut (dark colour) products for the zeolite Beta based materials, and the benchmark catalysts activated at 200 °C or 450 °C prior to the catalytic reaction.....189
- Figure 6.9. Dependence of conversion ( $X_{C4}$ ) on TOS for BEA-hier ( $\square$ ), BEA/TUD ( $\diamond$ ), BEA-nano (o), and BEA-micro ( $\Delta$ ).....189
- Figure 6.10. PLD profiles for the reaction of 1-butene in the presence of BEA/TUD (a), BEA-nano (b), BEA-hier (c), BEA-micro (d), ZSM-5 (e) or COD-900 (f), activated at 200 °C (solid lines) or 450 °C (dashed lines).....190
- Figure 6.11. Influence of the acid properties measured at 200 °C on ((a), (c), (e), (g)) conversion ( $\times$ ),  $\text{STY}_{\text{Dcut}}$  ( $\bullet$ ) and  $\text{STY}_{\text{Ncut}}$  (o), and on ((b), (d), (f), (h)) catalytic activity expressed as  $\text{mmol g}^{-1} \text{h}^{-1}$  ( $\diamond$ ) or  $\text{mol mol}_{\text{L+B}}^{-1} \text{h}^{-1}$  ( $\square$ ), for the bulk Beta based catalysts (BEA-hier, BEA-nano, BEA-micro) activated at 200 °C prior to catalytic reaction.....193
- Figure 6.12. Influence of the acid properties measured at 450 °C on ((a), (c), (e)) conversion ( $\square$ ),  $\text{STY}_{\text{Dcut}}$  ( $\bullet$ ) and  $\text{STY}_{\text{Ncut}}$  (o),, and on ((b), (d), (f)) catalytic activity expressed as  $\text{mmol g}^{-1} \text{h}^{-1}$  ( $\diamond$ ) or  $\text{mol mol}_{\text{L+B}}^{-1} \text{h}^{-1}$  (\*), for the bulk Beta type catalysts (BEA-hier, BEA-nano, BEA-micro) activated at 200 °C prior to catalytic reaction.....194
- Figure 6.13. Dependence of conversion ( $\square$ ) and STY (bars) of Ncut (light color) and Dcut (dark color) products ((a) and (b)), and of the PLD curves ((c) and (d)) on the reaction temperature ((a) and (c)) or pressure ((b) and (d)), in the presence of BEA-hier.....195
- Figure 6.14. Ratio of aromatic ( $A_{\text{arom}}$ ) to aliphatic ( $A_{\text{aliph}}$ ) products ( $A_{\text{arom}}/A_{\text{aliph}}$ ; determined by GC $\times$ GC-ToFMS) of the condensed reaction products (a) for the catalysts based on the BEA or MFI topologies, or (b) for different reaction conditions using BEA-hier as catalyst.....196
- Figure 6.15. DSC curves for the used Beta based materials.....197
- Figure 6.16. Dependence of conversion ( $X_{C4}$ ) on TOS in the first (-), and second use after regeneration ( $\times$ ), for BEA-hier (A) and ZSM-5 (B). The inset shows the PLD curves for the two runs (with matching symbols).....198

Figure 6.17.  $^{27}\text{Al}$  MAS NMR spectrum of (A) BEA-hier (fresh (a) and used ( $T_{\text{act}}=200\text{ }^{\circ}\text{C}$  (b) or  $450\text{ }^{\circ}\text{C}$  (c))) and (B) the benchmark catalyst ZSM-5 (fresh (d) and used ( $T_{\text{act}}=200\text{ }^{\circ}\text{C}$  (e) or  $450\text{ }^{\circ}\text{C}$  (f))).199

Figure 6.18. Amount of coke (based on TGA) of the Beta based materials and ZSM-5 used after activation ( $T_{\text{act}}$ ) at  $200\text{ }^{\circ}\text{C}$  (black bars) or  $450\text{ }^{\circ}\text{C}$  (grey bars).....202

Figure 6.19. DSC curves for the BEA/TUD (A), BEA-nano (B), BEA-hier (C) and ZSM-5 (D); the results are given for the unused catalyst (dashed line), and the used catalyst activated ( $T_{\text{act}}$ ) at  $200\text{ }^{\circ}\text{C}$  (grey line) or  $450\text{ }^{\circ}\text{C}$  (black line).....203

Figure 6.20. (A) PXRD patterns of ZSM-5 (fresh (a); used b)), BEA-hier (fresh (c); used (d)), BEA-nano (fresh (e); used (f)), and BEA/TUD (fresh (g); used (h)). (B) Low angles PXRD patterns of BEA-hier (fresh (a); used (b)), BEA/TUD (fresh (c); used (d)).....204

## **Chapter 7**

Figure 7.1. (A) Wide angles and (B) Low angles PXRD patterns for hZSM-5(31)-noT (a), hZSM-5(20)-PZSi (b), hZSM-5(51)-PZSi (c), hZSM-5(47)-PZSiS (d), hZSM-5(31)-CoT (e), and ZSM-5(29) (f).....218

Figure 7.2. SEM (left column, a,d,g,j,m,p) and STEM (middle and right columns) images of hZSM-5(31)-noT (a, b, c), hZSM-5(20)-PZSi (d, e, f), hZSM-5(51)-PZSi (g, h, i), hZSM-5(47)-PZSiS (j, k, l), hZSM-5(31)-CoT (m, n, o), and ZSM-5(29) (p, q, r).....220

Figure 7.3. Chemical (Al, Si) mappings of ZSM-5(31)-noT (a, b, c), hZSM-5(20)-PZSi (d, e, f), hZSM-5(51)-PZSi (g, h, i), hZSM-5(47)-PZSiS (j, k, l), hZSM-5(31)-CoT (m, n, o), and ZSM-5(29) (p, q, r).....221

Figure 7.4.  $^{27}\text{Al}$  MAS NMR spectra for hZSM-5(31)-noT (a), hZSM-5(20)-PZSi (b), hZSM-5(51)-PZSi (c), hZSM-5(47)-PZSiS (d), hZSM-5(31)-CoT (e), and ZSM-5(29) (f).....222

Figure 7.5. FT-IR spectra in the OH stretching region after evacuation at  $450\text{ }^{\circ}\text{C}$  (A), and FT-IR spectra of pyridine (base probe) adsorbed at  $200\text{ }^{\circ}\text{C}$  (B) for hZSM-5(31)-noT (a), hZSM-5(20)-PZSi (b), hZSM-5(51)-PZSi (c), hZSM-5(47)-PZSiS (d), hZSM-5(31)-CoT (e), and ZSM-5(29) (f).....223

Figure 7.6. Conversion ( $\square$ ) and STY (bars) of Ncut (dark colour) and Dcut (light colour) products for the MFI-based materials prepared and the benchmark catalyst ZSM-5(29) .....225

Figure 7.7. PLD profiles for the liquid products of the reaction of 1-butene in the presence of the MFI-based materials: (A) hZSM-5(20)-PZSi (solid line), hZSM-5(51)-PZSi (dashed line), hZSM-5(47)-PZSiS (dotted line), and (B) hZSM-5(31)-noT (solid line), hZSM-5(31)-CoT (dashed line), and ZSM-5(29) (dotted line).....225

Figure 7.8. Dependence of conversion on TOS for hZSM-5(31)-noT ( $\Delta$ ), hZSM-5(20)-PZSi ( $\times$ ), hZSM-5(51)-PZSi (+), hZSM-5(47)-PZSiS ( $\square$ ), hZSM-5(31)-CoT ( $\diamond$ ), and ZSM-5(29) (o).....226

Figure 7.9. STY as a function of  $X_{\text{C}_4}$  for the MFI-based materials prepared (STY total ( $\bullet$ ),  $\text{STY}_{\text{Dcut}}$  ( $\times$ ), and  $\text{STY}_{\text{Ncut}}$  (+)).....226

Figure 7.10. Influence of the acid properties measured at  $200\text{ }^{\circ}\text{C}$  on  $X_{\text{C}_4}$  ( $\times$ ), (a, b),  $\text{STY}_{\text{Dcut}}$  ( $\blacksquare$ ) and  $\text{STY}_{\text{Ncut}}$  ( $\square$ ) (c, d), for the catalysts prepared according to the PZSi(S) protocols, namely hZSM-5(20)-PZSi, hZSM-5(51)-PZSi, and hZSM-5(47)-PZSiS.....231

Figure 7.11. DSC curves for hZSM-5(20)-PZSi (solid line), and the respective used solid after washing and drying (dashed line) or after calcination at  $550\text{ }^{\circ}\text{C}$  to remove the organic matter from the solid catalyst (dotted line).....234

Figure 7.12. PXRD patterns (A) and  $^{27}\text{Al}$  MAS NMR spectra (B) for hZSM-5(20)-PZSi (fresh (a); used (b)), hZSM-5(51)-PZSi (fresh (c); used (d)), and ZSM-5(29) (fresh (e); used (f)).....234

Figure 7.13. Dependence of conversion ( $X_{C4}$ ) on TOS for hZSM-5(20)-PZSi (A), hZSM-5(51)-PZSi (C) and ZSM-5(29) (E) in the first ( $\times$ ) and second cycle using the regenerated catalyst (-). PLD curves for the two cycles (with matching symbols) for hZSM-5(20)-PZSi (B), hZSM-5(51)-PZSi (D), and ZSM-5(29) (F)..... 237

## **Chapter 8**

Figure 8.1. Top-down synthetic approaches employed for the synthesis of the MFI based micro/mesoporous zeotypes.....247

Figure 8.2. Si/Al molar ratio as function of the NaOH concentration for the materials prepared by the SIB procedure without acid treatment ( $\times$ ), with acid treatment using HCl ( $\bullet$ ) or oxalic acid ( $\blacktriangle$ )... 250

Figure 8.3. Powder XRD patterns for (A) the materials prepared *via* the SIB procedure: HZSM-5 (a), MZS-0.2 (b), MZS-0.2-Cl (c), MZS-0.2-Ox (d), MZS-0.4 (e), MZS-0.4-Cl (f), MZS-0.4-Ox (g), MZS-0.6 (h), MZS-0.6-Cl (i), MZS-0.6-Ox (j), MZS-0.8 (k), and MZS-0.8-Cl (l); and for (B) materials prepared *via* QAH and mixB procedures: HZSM-5 (a), MZS-TPA-65 (b), MZS-TPA-65-Cl (c), MZS-TPA-85 (d), MZS-TPA-85-Cl (e), MZS-TPA/Na (f), and MZS-TPA/Na-Cl (g)..... 252

Figure 8.4. SEM images of the materials prepared *via* the SIB procedure: MZS-0.2 (a), MZS-0.2-Cl (b), MZS-0.2-Ox (c), MZS-0.4 (d), MZS-0.4-Cl (e), MZS-0.4-Ox (f), MZS-0.6 (g), MZS-0.6-Cl (h), MZS-0.6-Ox (i), MZS-0.8 (j), MZS-0.8-Cl (k), and HZSM-5 (l); and the materials prepared *via* the QAH and mixB procedures: MZS-TPA-65 (m), MZS-TPA-85 (n), MZS-TPA/Na (o), MZS-TPA-65-Cl (p), MZS-TPA-85-Cl (q), and MZS-TPA/Na-Cl (r)..... 254

Figure 8.5. Nitrogen adsorption-desorption isotherms (at -196 °C) for materials prepared by SIB procedure using NaOH concentration of 0.2 M (A), 0.4 M (B), 0.6 M (C) or 0.8 M (D); and materials prepared by QAH (E) and mixB (F) procedures. Materials without acid (Ox, Cl) treatment - thick black lines; materials treated with oxalic acid - wide dashed lines in (A), (B), (C); materials treated with HCl - grey lines; HZSM-5 - dotted black line in (A). The inset in (E) shows, separately, the pairs (a) MZS-TPA-65 and MZS-TPA-65-Cl, and (b) MZS-TPA-85 and MZS-TPA-85-Cl for better visualization..... 255

Figure 8.6. Proportion of mesoporous specific surface area (black), mesoporous volume (white) and microporous volume (grey) of each material ( $\%S_{\text{meso}}=S_{\text{meso}}/S_{\text{BET}}\times 100$ ;  $\%V_i=V_i/V_p\times 100$  where  $i$  is micro or meso and  $V_p$  is the total pore volume)..... 256

Figure 8.7.  $^{27}\text{Al}$  MAS NMR spectra for (A) HZSM-5 (a), MZS-0.2 (b), MZS-0.2-Cl (c), MZS-0.2-Ox (d), MZS-0.4 (e), MZS-0.4-Cl (f), MZS-0.4-Ox (g), and (B) MZS-0.6 (h), MZS-0.6-Cl (i), MZS-0.6-Ox (j), MZS-0.8 (k), MZS-0.8-Cl (l), MZS-TPA/Na (m), and MZS-TPA/Na-Cl (n). The asterisk denotes side bands..... 257

Figure 8.8. FT-IR spectra of pyridine (base probe) adsorbed at 200 °C (A), and FT-IR spectra in the OH stretching region after evacuation at 450 °C (B) for HZSM-5 (a), MZS-0.2 (b), MZS-0.2-Cl (c), MZS-0.2-Ox (d), MZS-0.4 (e), MZS-0.4-Cl (f), MZS-0.4-Ox (g), MZS-0.6 (h), MZS-0.6-Cl (i), MZS-0.6-Ox (j), MZS-TPA/Na (k), and MZS-TPA/Na-Cl (l)..... 258

Figure 8.9. Changes in textural and acid properties of the materials prepared by the SIB and mixB procedures: black arrows – after desilication; red arrows – after the acid treatment; ( $\uparrow$ ) represents an increase and ( $\downarrow$ ) a decrease..... 260

Figure 8.10. Two-dimensional principal component analysis biplot; the variables are represented in red color and the observations in black color; the colored circles signalize three different groups of materials (Group 1 (blue), Group 2 (green), Group 3 (purple)). PCA biplot (PC1: 45.53 % and PC2: 29.39 %) categorizing the materials according to their properties..... 263

Figure 8.11. Conversion (●) and STY (bars) of Ncut (black bars) and Dcut (grey bars) products for the MFI-based materials prepared and the benchmark catalyst HZSM-5.....	264
Figure 8.12. Dependence of conversion of butenes on TOS for materials prepared by the SIB procedure using NaOH concentration of 0.2 M (A), 0.4 M (B), 0.6 M (C) or 0.8 M (D); and materials prepared by the QAH (E; orange (65 °C), purple (85 °C)) and mixB (F) procedures: (◇) - materials without acid treatment; (Δ) - materials treated with oxalic acid; (o) - materials treated with HCl; (□) - commercial HZSM-5.....	265
Figure 8.13. STY as a function of X <sub>C4</sub> , under approximately steady state conditions, for the different catalysts prepared (STY total (●), STY <sub>Dcut</sub> (+), and STY <sub>Ncut</sub> (◆)).....	266
Figure 8.14. Product lump distributions (PLD) curves for the liquid products of the reaction of 1-butene, in the presence of the catalysts prepared <i>via</i> the SIB procedure with acid treatment using (A) oxalic acid or (B) HCl. The NaOH concentration was 0.2 M (blue), 0.4 M (red), 0.6 M (black) or 0.8 M (yellow).....	266
Figure 8.15. Two-dimensional principal component analysis biplot; the variables are represented in red color and the observations in black color; the colored highlights signalize three different groups of materials (Group 1 (blue), Group 2 (green), Group 3 (purple)). PCA biplot (PC1: 77.08 % and PC2: 21.94 %) categorizing the materials according to their catalytic performance.....	269
Figure 8.16. Influence of amount of Brønsted acid sites (A) and total amount of acid sites (B) on X <sub>C4</sub> (▲), STY <sub>Dcut</sub> (×) and STY <sub>Ncut</sub> (+), for the catalysts MZS-x-Ox and MZS-x-Cl.....	269
Figure 8.17. DSC analysis of the original, used and thermally regenerated catalyst MZS-0.4-Cl....	271
Figure 8.18. Catalytic stability of MZS-0.4-Cl for consecutive 7 h on-stream runs (original catalyst (×); regenerated catalyst MZS-0.4-Cl-r (-)); the inset is the product lump distributions (PLD) curves for the liquid products of the reaction of 1-butene in the presence of the original (×) or the regenerated (-) catalysts.....	271
Figure 8.19. (A) Powder XRD patterns for the original (black line) and recovered (grey line) solids. (B) N <sub>2</sub> adsorption-desorption isotherms (at -196 °C) for the original (black line) and recovered (grey line) solids.....	272

## **Chapter 9**

Figure 9.1. Light olefin oligomerization reaction and possible pathways involved in the complex reaction system (x and y is the carbon number and N is a number different from x and y).....	282
Figure 9.2. PXRD patterns for H-ZSM-5 (a) and hierZ-MFI (b), and respective SEM images (and Si (red), Al (blue) mapping for hierZ-MFI).....	287
Figure 9.3. (A) Nitrogen adsorption-desorption isotherms at -196 K for H-ZSM-5 (-) and hierZ-MFI (□). The inset shows the respective pore size distribution curves (with matching lines). (B) <sup>27</sup> Al MAS NMR spectra for HZSM-5 (a) and hierZ-MFI (b).....	288
Figure 9.4. GC×GC-ToFMS total ion chromatogram contour plot of the reaction product mixture for (A) sample 1 (225 °C, 32.5 bar, 3.5 g g <sub>cat</sub> <sup>-1</sup> h <sup>-1</sup> ) and (B) sample 2 (300 °C, 45 bar, 3.5 g g <sub>cat</sub> <sup>-1</sup> h <sup>-1</sup> ): <sup>1</sup> t <sub>R</sub> (horizontal axis) and <sup>2</sup> t <sub>R</sub> (vertical axis) stand for retention time (s) for the primary and secondary GC columns, respectively; as a guide, the compounds of the standard mixture (linear hydrocarbons, C <sub>i</sub> where i is the number of carbon atoms) eluted from the first column are signalized in the <sup>1</sup> t <sub>R</sub> axis. The symbols denote types of chemical compounds, namely: Bz-C <sub>i</sub> =alkyl benzenes (monocyclic), N-C <sub>i</sub> =alkyl naphthalenes, and N-th-C <sub>i</sub> =alkyl tetrahydronaphthalenes, where C <sub>i</sub> is the total number of carbon atoms in substituent groups per molecule.....	290

Figure 9.5. Pareto charts of (a)  $X_{C_4}$ , (b)  $\eta_{Dcut}$  and (c)  $\eta_{Ncut}$  considering the Box-Behnken design of Table 9.5 with confidence interval of 90 % and p-value=0.10; black and white bars refer to positive and negative impacts, respectively. Response surface plots of (d,g)  $X_{C_4}$ , (e,h)  $\eta_{Dcut}$ , (f,i)  $\eta_{Ncut}$  as function of temperature, pressure or WHSV (imposing the other variable at their zero level, i.e. (d,h,i) have  $P=32.5$  bar, and (e,f,g) have  $W=3.5$   $g_{1C_4} g_{cat}^{-1} h^{-1}$ ). Dots represent the experimental results.....298

Figure 9.6. Pareto charts of (a)  $\eta_{Arom}$ , (b)  $\eta_{Dcut,free}$  and (c)  $\eta_{Ncut,free}$  considering the Box-Behnken design of Table 9.5 with confidence interval of 90 % and p-value=0.10; black and white bars refer to positive and negative impacts, respectively. Response surface plots of (d)  $\eta_{Arom}$ , (e,g)  $\eta_{Dcut,free}$ , (f)  $\eta_{Ncut,free}$  as function of temperature, pressure or WHSV (imposing the other variable at their zero level, i.e. (e) have  $W=3.5$   $g_{1C_4} g_{cat}^{-1} h^{-1}$  and (g) have  $P=32.5$  bar). Dots represent the experimental results.....299

## **Chapter 10**

Figure 10.1. Summary of the porous solid acid catalysts explored in this work..... 309

Figure 10.2. PCA biplot (PC1: 73.85 % and PC2: 24.93 %) categorizing the materials according to their catalytic performances. The variables are represented in red text and the observations in blue text. The blue and pink colored regions signalize, respectively, the superior and poorer performing materials, in comparison to the commercial zeolites (yellow). In green is highlighted the best performing catalyst of all the studied materials. The samples names are abbreviated for better visualization: M represents MZS, Zx represents hZSM-5 (where x is the value of the molar ratio Si/Al), n represents nano and m represents micro, Al-TUD-25=Al-TUD-1(25)-HT, Al-TUD-50=Al-TUD-1(50)-HT..... 313

Figure 10.3. PCA biplot (PC1: 61.58 % and PC2: 18.75 %) categorizing the materials according to their properties. The variables are represented in red text and the observations in blue text. The blue and pink highlights (of sample names) signalize, respectively, the superior and poorer performing materials in comparison to the commercial zeolites (yellow), according to Figure 10.2. In green is highlighted the best performing catalyst of all the studied materials. The samples names are abbreviated for better visualization: M represents MZS, Zx represents hZSM-5 (where x is the value of the molar ratio Si/Al), n represents nano and m represents micro, Al-TUD-25=Al-TUD-1(25)-HT, Al-TUD-50=Al-TUD-1(50)-HT.....314

## **Appendix A**

Figure S3.1. Fluid circuit (represented by the green lines) in Setup 1 for atmospheric-pressure operation. ....323

Figure S3.2. Fluid circuit (represented by the green lines) in Setup 1 for the high-pressure operation.....324

Figure S3.3. Mass flow controller (MFC) calibration curve.....326

Figure S4.1. Chromatogram of the gas phase reaction products of the 1-butene oligomerization over BEA-hier (Chapter 6) at 200 °C, 30 bar and 2.2  $g_{1C_4} g_{cat}^{-1} h^{-1}$ , obtain using Master Fast GC-FID with the analysis method described in Chapter 3..... 329

Figure S6.1. SEM images for the spent catalysts BEA-nano (a, e), BEA-micro (b, f), BEA-hier (c, g), BEA/TUD (d, h), and ZSM-5 (i, j)..... 332

Figure S6.2. Dependence of conversion ( $X_{C_4}$ ) on TOS for (A) BEA-hier and (B) ZSM-5, at different catalyst activation temperatures: 200 °C (o), 325 °C (+) and 450 °C (□).....332

Figure S6.3. Influence of the acid properties measured at 200 °C on ((a), (c), (e), (g)) conversion (×), STY <sub>Dcut</sub> (●) and STY <sub>Ncut</sub> (o), and on ((b), (d), (f), (h)) catalytic activity expressed as mmol g <sup>-1</sup> h <sup>-1</sup> (◇) or mol mol <sub>L+B</sub> <sup>-1</sup> h <sup>-1</sup> (□), for the bulk Beta based catalysts (BEA-hier, BEA-nano, BEA-micro) activated at 450 °C prior to catalytic reaction.....	333
Figure S6.4. Influence of the acid properties measured at 450 °C on ((a), (c), (e)) conversion (□), STY <sub>Dcut</sub> (●) and STY <sub>Ncut</sub> (o), and on ((b), (d), (f)) catalytic activity expressed as mmol g <sup>-1</sup> h <sup>-1</sup> (◇) or mol mol <sub>L+B</sub> <sup>-1</sup> h <sup>-1</sup> (*), for the bulk Beta type catalysts (BEA-hier, BEA-nano, BEA-micro) activated at 450 °C prior to catalytic reaction.....	334
Figure S7.1. Pore size distribution curves (DFT method) for hZSM-5(31)-noT (a, b), hZSM-5(20)-PZSi (c, d), hZSM-5(51)-PZSi (e, f), hZSM-5(47)-PZSiS (g, h), and hZSM-5(31)-CoT (i, j).....	336
Figure S7.2. SEM and TEM images for the unused (a, b, c, g, h, i, m) and used (d, e, f, j, k, l, n) catalysts hZSM-5(20)-PZSi (a to f), hZSM-5(51)-PZSi (g to l), and ZSM-5(29) (m, n).....	337
Figure S8.1. Pore size distribution curves (DFT method) for MZS-0.2 (a), MZS-0.4 (b), MZS-0.6 (c), MZS-0.8 (d), MZS-0.2-Cl (e), MZS-0.4-Cl (f), MZS-0.6-Cl (g), MZS-0.8-Cl (h), MZS-0.2-Ox (i), MZS-0.4-Ox (j), MZS-0.6-Ox (k), HZSM-5 (l), MZS-TPA-65 (m), MZS-TPA-65-Cl (n), MZS-TPA-85 (o), MZS-TPA-85-Cl (p), MZS-TPA/Na (q) and MZS-TPA/Na-Cl (r).....	338
Figure S8.2. (A) Amount and (B) density of total (Brønsted plus Lewis) acid sites (black), and amounts of Brønsted (white) or Lewis (grey) acid sites for each catalyst.....	339
Figure S8.3. Scheme of the PCA analysis of the data matrix of Table 8.4.....	341
Figure S8.4. Two-dimensional principal component analysis biplot (PC1: 40.27 % and PC2: 33.02 %) categorizing the materials according to their properties. The set of material properties was enlarged (in relation to Figure 8.10 (Chapter 8)), and includes % Al <sub>tetra+penta</sub> , ratio Al <sub>penta</sub> /Al <sub>tetra</sub> and IHF (Table S8.1). The variables are represented in red color and the observations are signalized in black color. The colored highlights of the sample names indicate the groups of materials according to the PCA biplot presented in Figure 8.10: Group 1 (blue), Group 2 (green), Group 3 (purple).....	342
Figure S9.1. Aromatics contents (% Ar) determined by <sup>1</sup> H NMR spectroscopy versus that determined by GC×GC-ToFMS.....	346
Figure S10.1. Preparation of ZSM-5 from kaolin C30 (Sibelco) according to the procedure described in refs. [24,25], using different acid treatments of metakaolin, with or without addition of external source of Si and Al ('X' stands for materials without ZSM-5 crystalline phase and 'V' stands for material with ZSM-5 crystalline phase).....	349
Figure S10.2. (A) PXRD patterns of ZMS-5 zeolite (CBV3024E, Zeolyst) (a), ZSM5-K2 (b) and metakaolin (c). (B) PXRD patterns of ZMS-5 zeolite (CBV3024E, Zeolyst) (a), ZSM5-K4 (b), ZSM5-K3 (c), ZSM5-K1 (d), metakaolin (e), and kaolin C30 (f).....	349

# CHAPTER 1

---

## Motivation, objectives and thesis plan

### Chapter 1

#### Motivation, objectives and thesis plan

1.1. Motivation .....	2
1.2. Objectives .....	3
1.3. Thesis plan.....	4
1.4. References .....	7

## 1.1. Motivation

In face of the high demand for middle distillates in comparison to gasoline fractions, particularly in Europe, it is important to develop and implement efficient and clean processes for middle distillates production. The catalytic oligomerization of light olefins (*e.g.*, propene and butenes) is growing interest in chemical and oil refining industries for the production of ecofriendly synthetic fuels, or other important chemicals like detergents, resins, plasticizers, drugs, flavours, dyes, etc..<sup>[1]</sup>

Light olefins have long been key industrial building blocks partly due to their availability and relative cheapness, and may be obtained as by-products from petrochemical processes or from renewable sources of organic carbon.<sup>[2–5]</sup> Over the years, commercialized olefin oligomerization technologies have been strategically developed for the transportation fuels sector, and some refineries worldwide have implemented olefin oligomerization processes, using conventional porous solid acids catalysts, such as the solid phosphoric acid and medium-pore MFI zeolite.<sup>[2,6,7]</sup> Despite the important improvements which have been accomplished in oligomerization technologies, there are continued research efforts to develop catalysts with superior performances, *e.g.*, in terms of stability and selectivity to diesel type products. Different types of inorganic solid acid catalysts have been investigated for the oligomerization of light alkenes,<sup>[8,9]</sup> such as solid phosphoric acid,<sup>[2,10,11]</sup> zeolites,<sup>[12–17]</sup> amorphous silica-alumina,<sup>[18,19]</sup> and other metal oxide catalysts.<sup>[20,21]</sup>

In order to obtain high quality diesel (*e.g.*, high cetane number) with high yields, the formation of long chains hydrocarbons with reduced branching degree should be maximized and the aromatics should be avoided, albeit this is challenging. An important factor influencing the average branching degree of the products is the catalysts' pore sizes.<sup>[22]</sup> Zeolites and zeotypes show great potential as solid acids for olefin oligomerization, since they are microporous materials, relatively robust, versatile (tunable properties), with strong acidity, which may withstand the catalytic reaction conditions and catalyst regeneration treatments, and some are readily available and reached industrial application (*e.g.*, MFI, FAU, BEA topologies). Their ordered microporous systems can function as molecular sieves inducing shape selectivity towards products with lower branching degree.<sup>[23–25]</sup> However, internal mass transfer limitations may be considerable in the micropores, defaulting the

active sites accessibility and leading to pore blockage and fast catalyst deactivation, especially in reactions with relatively bulky molecules such as intermediates leading to oligomers.<sup>[17,26]</sup> Hence, compromises between structure, morphology, texture and acid properties of materials are important in order to meet superior catalytic performances. The materials' versatility is also important because the olefinic feedstocks may possess different compositions and chemical features, and thus tuning of the material properties may be important to meet superior performances.

During the last decade, important advancements have been made in materials science to minimize steric hindrance and diffusion limitations inside the microporous structures of zeolite/zeotype materials, and enhance the active site accessibility and stability for catalytic applications.<sup>[27-29]</sup> The introduction of mesoporosity *via* synthesis with templates or *via* post-synthesis (*e.g.*, desilication, dealumination), may facilitate the diffusion of reactants/products inside the pores. On the other hand, mesoporous aluminosilicates possessing high mesoporous specific surface area, defined pore size distributions and moderate acid strength, may be promising in terms of enhanced catalyst stability with time-on-stream. Last, but not least, in selecting the catalysts it is important to consider aspects of up-scalability and eco-friendliness of the synthesis methodologies and conditions.

## 1.2. Objectives

The present work focuses on the oligomerization of 1-butene to produce diesel range products, in the presence of heterogeneous acid catalysts, based on crystalline porous inorganic (Al, Si) oxides, under high pressure and continuous flow operation. A practical goal is to repurpose light olefins-containing industrial streams and/or valorize bio-based light olefins, to achieve economical and environmentally sustainable production of clean fuels and useful chemicals. The choice of the (i) catalysts and (ii) oligomerization reaction conditions are fundamental to reach high yields of the desired products. In this thesis, the two approaches were addressed in targeting clean diesel range products.

Regarding (i) the choice of the catalysts, the thermal stability is fundamental not only for the catalytic reaction, but also for the catalyst regeneration, since coking is an expected

catalyst deactivation phenomenon. Crystalline porous inorganic (Al, Si) oxides may possess relatively high thermal stability (>200 °C) in relation to organic or hybrid inorganic-organic materials. On the other hand, they are versatile with respect to crystalline and porous structures, and acid properties, making them interesting for flexible technologies.

The catalytic potentialities of mesoporous aluminosilicates of the type TUD-1 and modified versions of zeolites/zeotypes of BEA and MFI types were explored for 1-butene oligomerization. The catalytic performances were investigated in terms of activity, selectivity to diesel range products, and stability. Due to the complex nature of the reaction product mixtures, comprehensive two-dimensional gas chromatography coupled to time-of-flight mass spectrometry (GC×GC-ToFMS) and nuclear magnetic resonance (NMR) spectroscopy were used for characterizing the product mixtures. The catalyst characterization and catalytic studies were essentially to evaluate the catalytic performances and establish structure-activity relationships. Principal component analysis helped categorize the differently prepared catalysts, and gain insights into complex interplay of material properties influencing the catalytic reaction.

Regarding (ii) the operating conditions, the influence of the reaction pressure, temperature and weight hourly space velocity (WHSV) was investigated for the different catalytic materials, in order to meet superior performances and identify best-performing catalysts. For one of the best-performing catalysts, catalytic experiments were planned according to a Box-Behnken design of experiments (DoE), which together with response surface methodology (RSM) allowed the optimization of 1-butene oligomerization to clean diesel range products.

### 1.3. Thesis plan

The thesis is divided into ten chapters, of which chapters 2 to 10 are briefly described in this section.

**Chapter 2** contemplates a contextualization of the global energetic consumption, particularly focused on transportation fuels; a literature review of light olefin

oligomerization over acid catalysts, comprising an overview of the industrial oligomerization technologies, and the state of art of the research made in this field in the recent years. A more directed literature review concerning zeolites and zeotypes is presented, highlighting the promising characteristics of these types of materials for catalysis and, in particular, olefin oligomerization.

**Chapter 3** describes the experimental work, which involved the design and implementation of a new laboratory setup to carry out the catalytic oligomerization reactions at high pressure, temperature and continuous flow operation; the experimental procedure of the setup; the analytic methods for identification and quantification of the reaction products; and description of the catalysts characterization techniques.

**Chapter 4** presents some general considerations of the work, regarding reproducibility of the catalytic tests, assessment of internal and external mass transfer limitations and thermodynamics aspects of butene isomerization.

**Chapter 5 to Chapter 8** cover the study of 1-butene oligomerization at high pressure and continuous flow operation, over different inorganic porous solid acid catalysts which were synthesized and characterized *via* complementary techniques. Each chapter starts with a lead-in to the specific topic, followed by the synthesis of the materials, discussion of the characterization results, and discussion of the catalytic performance of the materials.

**Chapter 5** deals with the oligomerization of 1-butene over TUD-1 type mesoporous aluminosilicates, synthesized *via* one-pot synthesis or a stepwise approach, without using surfactants as templates (eco-friendly). The products were analyzed by GC×GC-ToFMS. The influence of the properties and process parameters on the catalytic reaction, and catalyst stability were investigated. The catalytic performances were benchmarked with ZSM-5 (zeolite used in commercial oligomerization processes) and were compared to an ordered mesoporous aluminosilicate synthesized *via* the stepwise approach using surfactants as templates. This chapter regards the article entitled “TUD-1 type aluminosilicate acid catalysts for 1-butene oligomerisation”.<sup>[30]</sup>

**Chapter 6** focuses on several mesostructured solid acid catalysts based on the BEA topology, namely hierarchical BEA zeolite prepared *via* one-pot approach using a dual function template, a composite (BEA/TUD) possessing BEA zeolite nanocrystallites

embedded in a mesoporous matrix synthesized under hydrothermal conditions. The influence of the material properties, catalyst activation temperature, reaction parameters and catalyst stability were investigated combining characterization, GC×GC-ToFMS and catalytic experiments. The catalytic performances were compared to commercial nano/microcrystalline zeolites of different topologies (BEA, MFI), and COD-900 (type of catalyst for the Conversion of Olefins to Distillates industrial process). This chapter corresponds to the article entitled “Mesostructured Catalysts Based on the BEA Topology for Olefin Oligomerisation”.<sup>[31]</sup>

**Chapter 7** comprises the oligomerization study over micro/mesoporous zeotypes based on the MFI topology, prepared *via* different non-destructive bottom-up strategies, such as crystallization of silanized protozeolitic units, co-templating with a dual function template, or using a sole structure directing agent (non-surfactant and non-polymeric) to generate mesoporosity. The influence of the material properties, reaction parameters on the catalytic reaction were investigated, along with the catalyst stability. This chapter corresponds to an article entitled “Olefin oligomerisation over nanocrystalline MFI-based micro/mesoporous zeotypes synthesised *via* bottom-up approaches”.<sup>[32]</sup>

**Chapter 8** discusses the potentialities of modified versions of zeolite ZSM-5, prepared by top-down strategies involving base-acid treatments of commercial available ZSM-5 with low Si/Al ratio. Characterization studies and multivariate/principal component analysis (PCA) were employed to help categorize the differently prepared catalysts and to gain insights into the complex interplay of material properties influencing the catalytic reaction. This chapter corresponds to the article entitled “Catalytic conversion of 1-butene over modified versions of commercial ZSM-5 to produce clean fuels and chemicals”.<sup>[33]</sup>

**Chapter 9** presents an optimization of the reaction conditions of 1-butene oligomerization, by applying the Box-Behnken design of experiments (DoE) and response surface methodology (RSM), with the aim of targeting diesel range products with low aromatics content. GC×GC-ToFMS was valuably used for characterizing the complex reaction product mixtures. This chapter corresponds to a manuscript entitled “Optimization of continuous-flow heterogeneous catalytic oligomerization of 1-butene by design of experiments and response surface methodology”.<sup>[34]</sup>

In **Chapter 10** is presented the main conclusions and suggestion for future work.

## 1.4. References

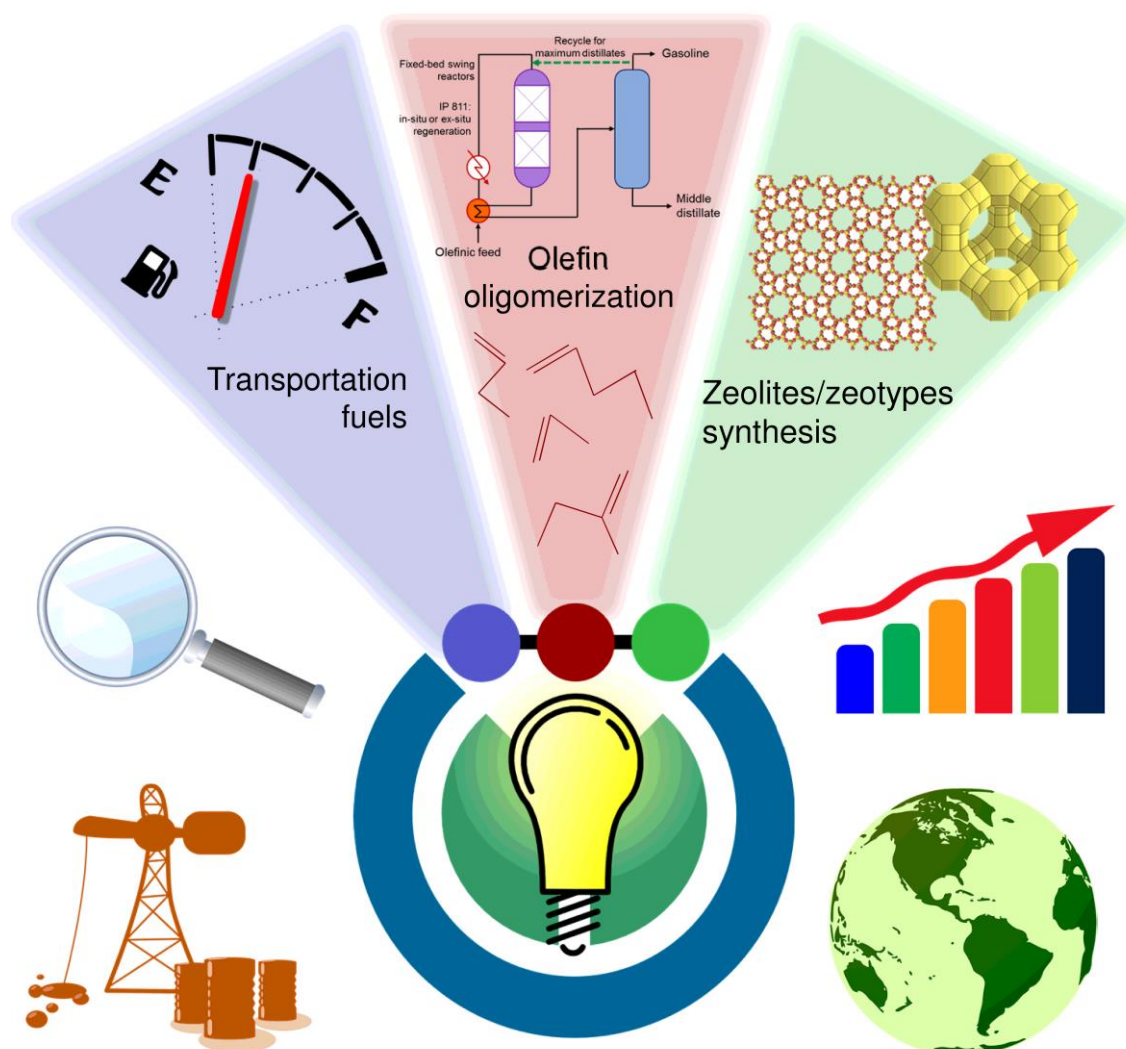
- [1] A. Corma, S. Iborra, Oligomerization of alkenes, in: *E.G., Derouane (Ed.), Catalysts for fine chemical synthesis, Volume 4, Microporous and mesoporous solid catalysts*, John Wiley & Sons, 2006: pp. 125–140.
- [2] A. De Klerk, Distillate production by oligomerization of Fischer-Tropsch olefins over solid phosphoric acid, *Energy & Fuels* 20 (2006) 439–445.
- [3] G. Bellussi, F. Mizia, V. Calemma, P. Pollesel, R. Millini, Oligomerization of olefins from light cracking naphtha over zeolite-based catalyst for the production of high quality diesel fuel, *Microporous Mesoporous Mater.* 164 (2012) 127–134.
- [4] J.Q. Bond, D.M. Alonso, D. Wang, R.M. West, J.A. Dumesic, Integrated catalytic conversion of  $\gamma$ -valerolactone to liquid alkenes for transportation fuels, *Science* 327 (2010) 1110–1114.
- [5] D.M. Alonso, J.Q. Bond, J.C. Serrano-Ruiz, J.A. Dumesic, Production of liquid hydrocarbon transportation fuels by oligomerization of biomass-derived C<sub>9</sub> alkenes, *Green Chem.* 12 (2010) 992–999.
- [6] F.J. Krambeck, S.A. Tabak, A.A. Avidan, Production of synthetic gasoline and diesel fuel from non-petroleum resources, *Am. Chem. Soc., Div. Fuel Chem.* 31 (1986) 293–299.
- [7] M.N. Harandi, H. Owen, Integrated staged conversion of methanol to gasoline and distillate, US 4899002 A, 1988.
- [8] M. Sanati, C. Hornell, S.G. Jaras, The Oligomerization of alkenes by heterogeneous catalysts, in: J.J. Spivey (Ed.), *Catalysis: volume 14 (Specialist periodical reports)*, 1999: pp. 236–287.
- [9] A. Corma, Inorganic solid acids and their use in acid-catalyzed hydrocarbon reactions, *Chem. Re.* 95 (1995) 559–614.
- [10] J.H. Coetzee, T.N. Mashapa, N.M. Prinsloo, J.D. Rademan, An improved solid phosphoric acid catalyst for alkene oligomerization in a Fischer – Tropsch refinery, *Appl. Catal. A Gen.* 308 (2006) 204–209.
- [11] J. Zhang, Y. Yan, Q. Chu, J. Feng, Solid phosphoric acid catalyst for propene oligomerization: Effect of silicon phosphate composition, *Fuel Process. Technol.* 135 (2015) 2–5.
- [12] C. Martínez, E.J. Daskocil, A. Corma, Improved THETA-1 for light olefins oligomerization to diesel: influence of textural and acidic properties, *Top. Catal.* 57 (2014) 668–682.
- [13] Y.T. Kim, J.P. Chada, Z. Xu, Y.J. Pagan-Torres, D.C. Rosenfeld, W.L. Winniford, E. Schmidt, G.W. Huber, Low-temperature oligomerization of 1-butene with H-ferrierite, *J. Catal.* 323 (2015) 33–44.
- [14] A. Coelho, G. Caeiro, M.A.N.D.A. Lemos, F. Lemos, F.R. Ribeiro, 1-Butene oligomerization over ZSM-5 zeolite: Part 1 - Effect of reaction conditions, *Fuel* 111 (2013) 449–460.
- [15] J.W. Yoon, J.-S. Chang, H.-D. Lee, T.-J. Kim, S.H. Jung, Trimerization of isobutene over a zeolite beta catalyst, *J. Catal.* 245 (2007) 253–256.
- [16] N. Kumar, P. Mäki-Arvela, T. Yläsalmi, J. Villegas, T. Heikkilä, A.-R. Leino, K. Kordás, T. Salmi, D. Yu Murzin, Dimerization of 1-butene in liquid phase reaction: Influence of structure, pore size and acidity of Beta zeolite and MCM-41 mesoporous material, *Microporous Mesoporous Mater.* 147 (2012) 127–134.
- [17] M.J. Wulfers, R.F. Lobo, Assessment of mass transfer limitations in oligomerization of butene at high pressure on H-beta, *Appl. Catal. A Gen.* 505 (2015) 394–401.
- [18] E. Rossetto, B.P. Nicola, R.F. De Souza, K. Bernardo-Gusmão, S.B.C. Pergher, Heterogeneous complexes of nickel MCM-41 with beta-diimine ligands: Applications in olefin oligomerization, *J. Catal.* 323 (2015) 45–54.

- [19] R. Catani, M. Mandreoli, S. Rossini, A. Vaccari, Mesoporous catalysts for the synthesis of clean diesel fuels by oligomerisation of olefins, *Catal. Today* 75 (2002) 125–131.
- [20] J.S. Lee, J.W. Yoon, S.B. Halligudi, J.S. Chang, S.H. Jung, Trimerization of isobutene over  $\text{WO}_x/\text{ZrO}_2$  catalysts, *Appl. Catal. A Gen.* 366 (2009) 299–303.
- [21] F. Tzompantzi, A. Mantilla, G. Del Angel, J.M. Padilla, J.L. Fernández, J.A.I. Díaz-Góngora, R. Gómez,  $\text{NiO-W}_2\text{O}_3/\text{Al}_2\text{O}_3$  catalysts for the production of ecological gasoline: Effect of both NiO and the preparation method on the isobutene oligomerization selectivity, *Catal. Today* 143 (2009) 132–136.
- [22] O. Muraza, Maximizing diesel production through oligomerization: a landmark opportunity for zeolite research, *Ind. Eng. Chem. Res.* 54 (2015) 781–789.
- [23] A.N. Mlinar, O.C. Ho, G.G. Bong, A.T. Bell, The effect of noncatalytic cations on the activity and selectivity of nickel-exchanged X zeolites for propene oligomerization, *ChemCatChem* 5 (2013) 3139–3147.
- [24] M.L. Occelli, J.T. Hsu, L.G. Galya, Propylene oligomerization with pillared clays, *J. Mol. Catal.* 33 (1985) 371–389.
- [25] S.A. Tabak, F.J. Krambeck, W.E. Garwood, Conversion of propylene and butylene over ZSM-5 catalyst, *AIChE J.* 32 (1986) 1526–1531.
- [26] J. Weitkamp, S. Ernst, L. Puppe, Shape-selective catalysis in zeolites, in: *Catalysis and Zeolites: Fundamentals and Applications*, 1999: pp. 327–376.
- [27] D.P. Serrano, J.M. Escola, P. Pizarro, Synthesis strategies in the search for hierarchical zeolites, *Chem. Soc. Rev.* 42 (2013) 4004–35.
- [28] J.C. Groen, J. a. Moulijn, J. Pérez-Ramírez, Desilication: on the controlled generation of mesoporosity in MFI zeolites, *J. Mater. Chem.* 16 (2006) 2121–2131.
- [29] T. Prasomsri, W. Jiao, S.Z. Weng, J. Garcia Martinez, Mesostructured zeolites: bridging the gap between zeolites and MCM-41, *Chem. Commun.* 51 (2015) 8900–8911.
- [30] A.F. Silva, A. Fernandes, M.M. Antunes, P. Neves, S.M. Rocha, M.F. Ribeiro, M. Pillinger, J. Ribeiro, C.M. Silva, A.A. Valente, TUD-1 type aluminosilicate acid catalysts for 1-butene oligomerisation, *Fuel* 209 (2017) 371–382.
- [31] A.F. Silva, A. Fernandes, P. Neves, M.M. Antunes, S.M. Rocha, M.F. Ribeiro, C.M. Silva, A.A. Valente, Mesostructured Catalysts Based on the BEA Topology for Olefin Oligomerisation, *ChemCatChem* 10 (2018) 2741–2754.
- [32] A.F. Silva, A. Fernandes, M.M. Antunes, M.F. Ribeiro, M. Silva, A.A. Valente, Olefin oligomerisation over nanocrystalline MFI-based micro/mesoporous zeotypes synthesised via bottom-up approaches, *Renew. Energy* (2019).
- [33] A. Silva, A. Fernandes, M.M. Antunes, M.F. Ribeiro, C.M. Silva, A.A. Valente, Catalytic conversion of 1-butene over modified versions of commercial ZSM-5 to produce clean fuels and chemicals, (Submitted to *ChemCatChem* (2019)).
- [34] A.F. Silva, P. Neves, S.M. Rocha, C.M. Silva, A.A. Valente, Optimization of continuous-flow heterogeneous catalytic oligomerization of 1-butene by design of experiments and response surface methodology, (Submitted to *Applied Catalysis A: General* (2019)).

# CHAPTER 2

---

## Literature review



## CHAPTER 2

### Literature review

2.1. Transportation fuels.....	11
2.1.1. Global and European demands .....	11
2.1.2. Production processes.....	13
2.1.3. Gasoline and diesel quality properties .....	20
2.2. Catalytic olefin oligomerization of light olefins .....	24
2.2.1. Industrial technologies .....	24
2.2.2. Emerging bio-based processes .....	32
2.2.3. Mechanistic considerations .....	33
2.2.4. Catalyst scope for olefin oligomerization .....	37
2.3. Zeolites and zeotype acid catalysts for olefin oligomerization .....	45
2.3.1. Zeolites - microporous systems .....	45
2.3.2. Zeolites - acidity and shape-selectivity.....	47
2.3.3. Improved versions of zeolites .....	52
2.3.4. Catalytic performances of zeolites/zeotypes for propene and butenes oligomerization.....	68
2.4. References .....	95

## 2.1. Transportation fuels

### 2.1.1. Global and European demand

The world is in constant change and modern society is greatly dependent on sources of energy. The social and economic progresses call for the need to meet the growing demand for energy in sustainable and secure fashions. According to the International Energy Outlook 2017 (IEO2017), the worldwide energy consumption increased from 575 quadrillion Btu in 2015 to 736 quadrillion Btu in 2040, corresponding to 28 % increase in energy consumption, partly due to the strong economic and population growths of the non-OECD (Organization for Economic Co-operation and Development) countries, mostly India and China.<sup>[1]</sup> In 2015, the global largest share of energy consumption of *ca.* 54 % regarded the industrial sector (including mining, agriculture and construction), followed by *ca.* 26 % due to the transportation sector and *ca.* 20 % due to buildings.<sup>[1]</sup> Until 2040, it is expected higher energy consumption rise for transportation and buildings (1.0 %/year and 1.1 %/year, respectively) than for the industrial sector (0.7 %/year).<sup>[1]</sup>

The increasing energy demand cause great environmental concerns with global warming. The main contributors to global greenhouse gas (GHG) emissions by economic sector were power generation (42 %), transportation (22 %), industry (20 %), followed by buildings (10 %) and others (agriculture, non-energy use, oil and gas extraction and energy transformation) (6 %) (year 2014, Figure 2.1).<sup>[2]</sup> According to the OECD Environmental Outlook Baseline, transport emissions may double between 2010 and 2050, partly due to a considerable increase of vehicles ownership and growth in aviation transportation.<sup>[3]</sup>

The transportation sector accounts for the main share of the total end-use of liquid fuels consumed; *ca.* 54 % in 2015 and expectedly 56 % by 2040. Gasoline and diesel fuels are the most consumed transportation fuels (*ca.* 36 % and *ca.* 30 %, respectively, based on projections for 2040) followed by jet fuel, natural gas, liquefied petroleum gas (LPG) and electricity (Figure 2.2).<sup>[1]</sup> The consumption of gasoline and diesel may not suffer major changes between 2015 and 2040, due to improvements in vehicles efficiency and increased preference for electric and shared vehicles, counterbalancing the growing travel demand.

Despite the improvements in energy efficiency, jet fuel consumption may double due to growth of air travel demand. Natural gas and electricity consumption showed faster growth associated with the increasing sales of electric cars.<sup>[1,4]</sup>

According to the European Union (EU) Reference Scenario 2016, the transport sector will account for 33 % of the EU energy consumption by 2050, which is roughly comparable to 31 % in 2005.<sup>[5]</sup> Diesel fuel may remain the largest transportation fuel consumed in 2050 (51 %), as the predominant fuel for passenger cars and continuing to be the primary fuel for heavy-duty vehicles (Figure 2.2). Gasoline demand may suffer the most pronounced drop, from 26 % in 2015 to 15 % by 2050, mainly based on expected higher taxes and prices compared to diesel fuel (Figure 2.2).<sup>[5,6]</sup> Jet fuel, gas, biofuels and electricity demand are expected to increase. The use of hydrogen continues limited partly due to the lack of favorable policies.<sup>[5]</sup>

The prospects of fuel demand in the transport sector depend on many factors, such as economic growth, especially of non-OCDE countries, population growth, urbanization, geopolitics, global oil reserves and supply, environmental and health concerns, government policy, technological improvements, vehicles efficiencies and social preferences.<sup>[7]</sup> Hence, it is important for refineries worldwide to be flexible, able to make the adjustments to shift their fuels production in line with market demand.

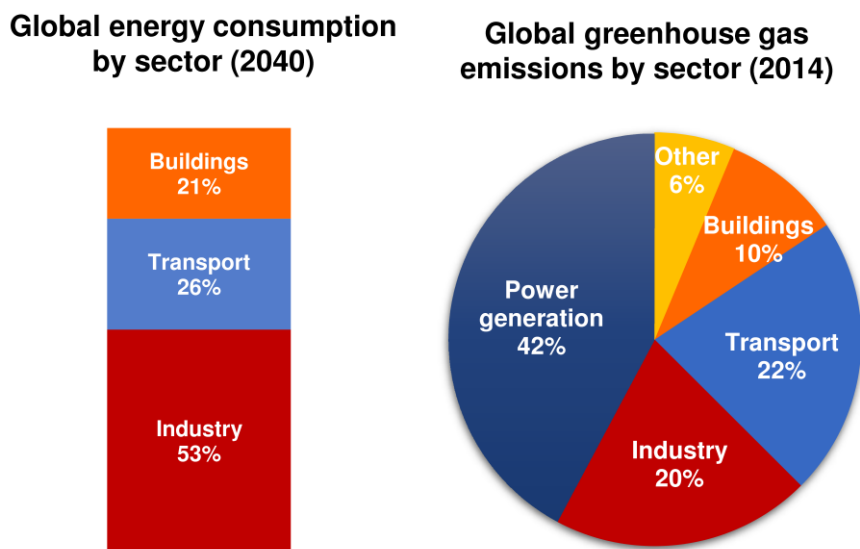


Figure 2.1. Projections for 2040 of the global energy consumption by sector and global greenhouse gas emission by sector in 2014. Adapted from refs. [1,2].

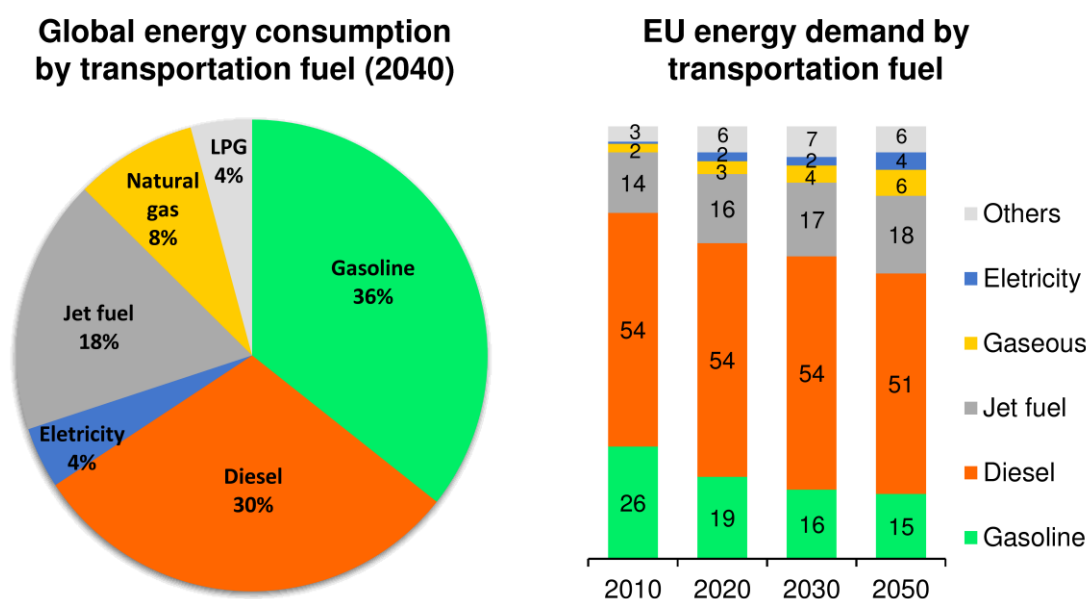


Figure 2.2. Projections for 2040 of the global energy consumption by transportation fuel and EU energy demand by transportation fuel (2010-2050) (others include biodiesel and hydrogen). Adapted from refs. [1,5].

### 2.1.2. Production processes

Currently, conventional transportation fuels such as gasoline, jet fuel (kerosene) and diesel are mainly produced *via* distillation of crude oil and subsequent refining, along with other important products in petroleum refineries, as schematically represented in Figure 2.3 (Table 2.1). Some of the world's largest refineries are Jamnagar Refinery (Reliance Industries, India, 1240 kilo-barrels per day (kbbbl/d)) and Paraguana Refinery Complex (Petróleos de Venezuela SA, Venezuela, 940 kbbbl/d).<sup>[8]</sup>

The gasoline pool produced from petroleum derives from different refining units, such as isomerate of light naphtha, reformate of heavy naphtha, hydrocracked gasoline, Fluid Catalytic Cracking (FCC) gasoline, alkylate of butenes/pentenes, and coker naphtha. (Figure 2.3). Jet fuel and diesel fuel are obtained by atmospheric distillation of crude oil, followed by merox treatment and hydrotreatment, respectively, with the aim of reducing the sulphur content (*e.g.*, mercaptans) in jet fuel and reducing the contents of sulphur, nitrogen, oxygen, aromatics and metals in diesel in order to meet fuel specifications. Diesel may be obtained by catalytic hydrocracking of vacuum gas oil (VGO), and by oligomerization of light-

cracked naphtha (LCN) or coker naphtha coming from FCC unit or delayed coker, respectively (Figure 2.3).<sup>[9,10]</sup> However, oligomerization units are not implemented in petroleum refineries for diesel production.

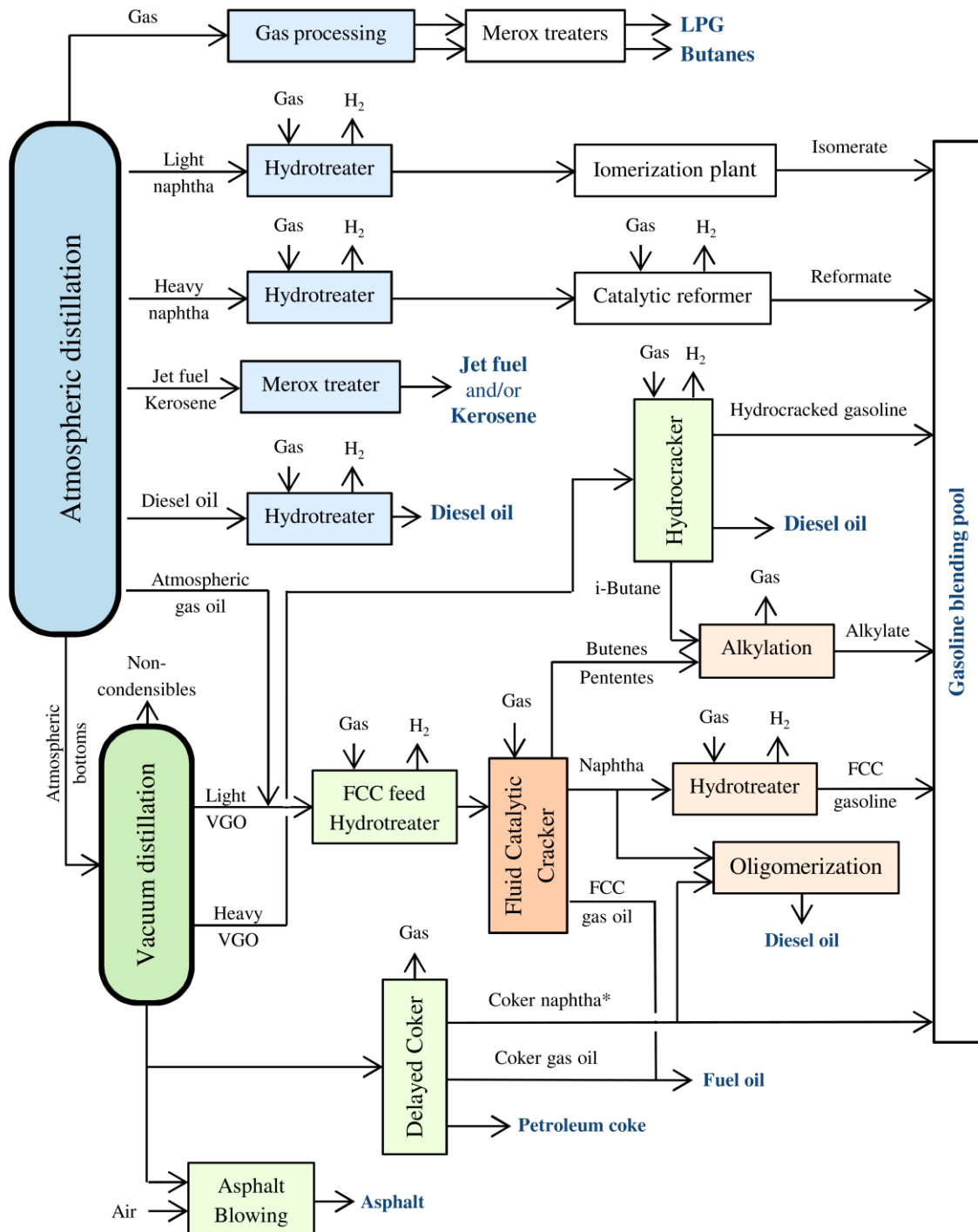


Figure 2.3. Scheme of a petroleum refinery process to obtain liquid hydrocarbons. Adapted from refs. [9,11].

Table 2.1. Specifications of the products of petroleum distillation and refining.<sup>[9,12]</sup>

Petroleum fraction	Product	Number of. C atoms	Boiling point (°C)	Final use
Petroleum gas	Methane	1	-161.6	Heating, electricity
	Ethane	2	-88.6	Plastics, petrochemicals
	Propane/Butane	3-4	-42 - -12	LPG, transport, domestic
Light ends	Naphtha	5-17	36-302	Petrochemicals, solvents, gasoline
	Gasoline	4-12	-1-216	Transport
Middle distillates <sup>[a]</sup>	Kerosene/diesel	8-18	126-258	Jet fuel, transport, heating
	Jet fuel	11-18	126-287	Transport
Heavy ends	Fuel oil	12-20	216-421	Transport, domestic/industrial use
	Lubricating oil	>20	>343	Motor oil, lubricants
Solid heavy ends	Wax	17 - >20	302 - >343	Lubricants
	Asphalt	>20	>343	Roads, roofing
	Coke	50	>1000	Steel production

<sup>[a]</sup> In this thesis, distillate fuel or distillate is generally used to denote products with similar properties to middle distillates (not necessarily obtained via petroleum distillation).

For countries with only a few crude oil reserves or not self-sufficient in terms of oil production and refining capacity, transport fuels are obtained in a Fischer-Tropsch (FT) refinery from organic carbon sources such as natural gas, coal or biomass (gas to liquid (GTL), coal to liquid (CTL) or biomass to liquid (BTL), respectively);<sup>[13]</sup> for example, Secunda CTL plant (Sasol, South Africa, 160 kbb/d), Pearl GTL plant (Shell, Qatar, 140 kbb/d), Mossel Bay GTL plant (PetroSA, South Africa, 54 kbb/d). Presently, there are no BTL industrial scale plants in operation.<sup>[8,14]</sup> Figure 2.4 shows a simplified flow diagram of a FT based facility. The carbon source is firstly pre-treated and gasified (or reformed in the case of gaseous carbon sources) to produce synthesis gas (or syngas, which consists of a mixture of hydrogen and carbon monoxide), followed by purification. The CO<sub>2</sub> by-product of the gasification can be removed from the syngas stream prior to feeding the FT synthesis reactor, allowing the capture of CO<sub>2</sub> for sequestration. The FT synthesis reaction occurs in the presence of a cobalt or iron catalyst, where the syngas is converted to water, CO<sub>2</sub> and

synthetic crude (syncrude), composed of a wide range of hydrocarbons (mainly paraffins, and oxygenated hydrocarbons). The syncrude is further refined to produce the desired products (chemicals, fuels). The nature of the selected carbon source affects the carbon efficiency (and CO<sub>2</sub> footprint) of the FT technology. In this respect, natural gas and waste plastic are preferred to biomass or coal sources, since hydrogen-rich and heteroatom-poor feedstocks are preferable.<sup>[15,16]</sup> The refining processes in FT plants share similar types of processes to petroleum plants such as atmospheric distillation, hydrotreating, hydrocracking and oligomerization (Figure 2.5). Currently, oligomerization units (technology emerged in the early 1930s) are only implemented in some FT refineries for the production of transportation fuels<sup>[17]</sup>, such as Mossel Bay GTL<sup>[18]</sup> and Secunda CTL<sup>[19]</sup> plants .

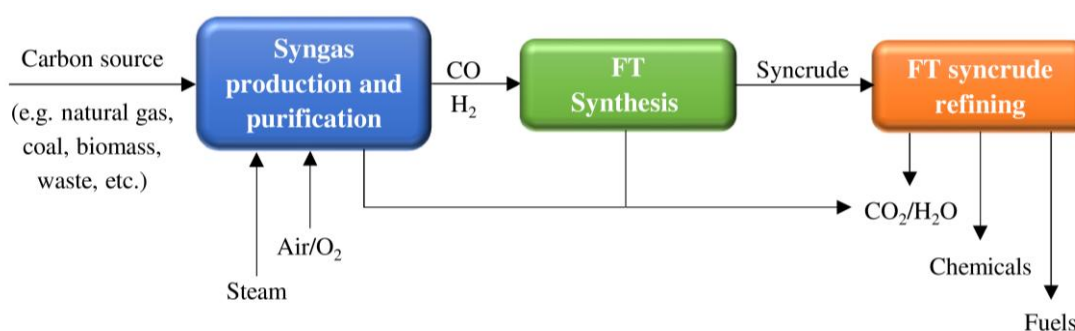


Figure 2.4. Simplified flow diagram of a Fischer-Tropsch (FT) based facility. Adapted from ref. [15].

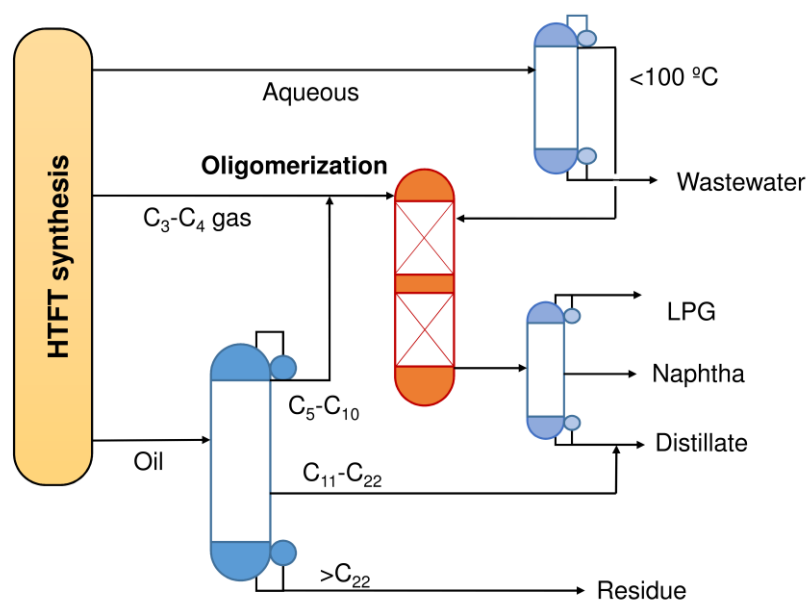


Figure 2.5. Simplified representation of high temperature (HT) FT syncrude refining coupled with an oligomerization unit. Adapted from ref. [20].

Electricity and transportation fuels alternative to diesel and gasoline, such as biodiesel, bioethanol, biogas, natural gas, and dimethyl ether, account for a small percentage of the global demand, albeit they are important, and their market is growing very fast. For instance, the biofuels (biodiesel, bioethanol, biogas) consumption is expected to grow at an average rate of 5 %/year (2004-2030), being the US the main producer, followed by Brazil.<sup>[7]</sup> These fuels may be used directly or blended with conventional gasoline or diesel. In particular biomass is a renewable source of organic carbon that may contribute to enhanced energy security, since it is independent of fluctuations of oil prices. Biomass should be complemented with other sources to meet the high fuel demand, and the sustainable intensification of biomass cultivation is important for GHG emissions mitigation and avoid negative impacts on biodiversity, soil quality, food chain and natural resources. Moreover, the production, processing and transportation of biomass should preferably not require non-renewable energy.<sup>[7]</sup> Table 2.2 summarizes the main advantages and disadvantages of the different production processes for each transportation fuel (conventional or alternative).

Table 2.2. Main advantages and disadvantages of conventional and alternative fuels and respective production technologies.<sup>[9,10,13,21–25]</sup>

Advantages	Disadvantages
<b>Petroleum refineries</b>	
<ul style="list-style-type: none"> <li>- Extraction/exploration of crude oil is a easy and economic process;</li> <li>- The refining technologies are well developed, making it easier to get valuable products;</li> <li>- Petroleum has high energy density (energy generated per volume).</li> </ul>	<ul style="list-style-type: none"> <li>- Petroleum is a non-renewable source and its extraction and burning lead to GHG emissions harmful to the environment;</li> <li>- Refining of petroleum produces toxic products (<i>e.g.</i>, CO);</li> <li>- Sustains growth of terrorism and violence;</li> <li>- Low energy ratio<sup>[a]</sup> of 0.83-0.95.</li> </ul>
<b>Fischer-Tropsch (CTL, GTL)</b>	
<ul style="list-style-type: none"> <li>- Abundant coal and natural gas reserves;</li> <li>- Flexibility in terms of variety of products produced by easily adjusting the FT reaction conditions;</li> <li>- Products with ultra-low sulphur, very few aromatics, N, Ni and V concentrations, and diesel with high cetane number (up to 75);</li> <li>- Feasible separation of CO<sub>2</sub> during syngas production;</li> <li>- Waste heat is available for electricity co-generation;</li> <li>- GTL generates reduced amounts of CO<sub>2</sub>;</li> <li>- Similar combustion properties as the petroleum derived fuels.</li> </ul>	<ul style="list-style-type: none"> <li>- Competition of coal and natural gas in electric power generation and domestic use;</li> <li>- CTL generates significant amounts of CO<sub>2</sub>;</li> <li>- Produces diesel with low density;</li> <li>- Produces gasoline and naphtha with low octane number;</li> <li>- FT diesel vehicles use 1.3–2.9 MJ of additional energy per kilometer compared to a fossil fuel derived diesel.</li> </ul>
<b>Fischer-Tropsch (BTL)</b>	
<ul style="list-style-type: none"> <li>- Biomass is a renewable and low-cost source of carbon;</li> <li>- Zero carbon footprint for some feedstocks (<i>e.g.</i>, industrial waste and residues);</li> <li>- Relatively high energy ratio<sup>[a]</sup> of 3-9.5 (depending on the biomass);</li> <li>- Produces electricity as sub-product.</li> </ul>	<ul style="list-style-type: none"> <li>- Competition of biomass for the food chain <i>versus</i> biofuels production;</li> <li>- Emission of matter that contribute to the eutrophication and acidification (when using energy crops as biomass).</li> <li>- Requires non-renewable energy for producing/handling biomass, which may have GHG emissions associated.</li> <li>- Few or none BTL commercial scale plants;</li> </ul>

Table 2.2. (continued)

Advantages	Disadvantages
<b>Transesterification of vegetable oils to biodiesel</b>	
<ul style="list-style-type: none"> <li>- Can be manufactured from a wide range of feedstocks;</li> <li>- Biodiesel is easy to use (no vehicle modification needed);</li> <li>- Biodiesel is safer to handle and to store than petroleum, because it is less toxic and flammable;</li> <li>- Biodiesel improves fuel lubricity and increases the cetane number when mixed in fossil fuel derived diesel;</li> <li>- High energy ratio<sup>[a]</sup> of 5-6 (vegetables waste) or 8.5-9.5 (palm oil);</li> <li>- Good performance and cost efficiency;</li> <li>- The presence of oxygen in biodiesel can reduce the ignition delay time, and the fuel may burn more completely, which reduces CO, particulate matter, and other exhaust emissions.</li> </ul>	<ul style="list-style-type: none"> <li>- More expensive than petroleum diesel fuel;</li> <li>- Needs fossil fuel derived methanol;</li> <li>- Produces high amounts of glycerol as co-product;</li> <li>- Less suitable for use at low temperature;</li> <li>- Low concentration blends with conventional diesel;</li> <li>- Lower energy density;</li> <li>- The high oxygen content of biodiesel increases the probability of combination with nitrogen, at high temperature, leading to an increase in NO<sub>x</sub> emissions.</li> </ul>
<b>Fermentation of biomass to bioethanol</b>	
<ul style="list-style-type: none"> <li>- Can be manufactured from a wide range of feedstocks;</li> <li>- Can be used directly as pure ethanol or blended with gasoline, enhancing the octane number and heats of vaporization;</li> <li>- Less toxic and biodegradable;</li> <li>- Cleaner emissions;</li> <li>- Reduced GHG emissions.</li> </ul>	<ul style="list-style-type: none"> <li>- Crops grow slowly in countries with low levels of sunlight and temperatures;</li> <li>- Expensive energy-consuming distillation step;</li> <li>- Bioethanol has lower energy density than gasoline;</li> <li>- Bioethanol has high miscibility with water;</li> <li>- Low concentration blends with gasoline;</li> <li>- Low flame luminosity, lower vapor pressure;</li> <li>- Toxic for the ecosystems;</li> <li>- Bioethanol can only be used in Flexible-Fuel Vehicles (FFV), which have a very small share in the market.</li> </ul>

<sup>[a]</sup> Ratio of the energy output of the end product to the fossil energy required for producing the desired fuel.

### 2.1.3. Gasoline and diesel quality properties

Gasoline and diesel are very complex mixtures composed of hydrocarbons (comprising linear, branched and cyclic paraffins, olefins, and aromatics) in the range of approximately C4–C12 and C8–C18, respectively.<sup>[9]</sup> Besides the need to increase gasoline and diesel production in relation to present and future demand, the fuel properties need to meet standard and restricted requirements (Table 2.3) to allow efficient atomization in the internal combustion engine (ICE), avoid engine damage and minimize air pollution.

Table 2.3. Some quality properties of most fuels used in the EU, and their normative values (EN 228:2012 for gasoline and EN 590:2013 for diesel).<sup>[26–28]</sup>

Quality property	Gasoline (Unleaded Petrol grade)	Diesel (values for temperate weather)
RON/MON, min	95/85	-
CN, min	-	51
Density @ 15°C (Kg m <sup>-3</sup> ), min-max	720 to 775	820 to 845
Viscosity @ 37.8°C (cSt), min-max	-	2.0 to 4.5
RVP <sup>[a]</sup> @ 37.8°C (KPa), min-max	45 to 60 (Class A) 70 to 100 (Class F <sub>1</sub> )	-
Sulfur (ppm), max	10	10
Lead (mg/L), max	5	-
Aromatics (Vol %), max	35	-
Flash point (°C), min	-	55
Cloud Point (°C), max	-	-10 to -34 <sup>[b]</sup>

<sup>[a]</sup> RVP=reid vapor pressure. <sup>[b]</sup> Only applicable to countries with arctic or severe winter conditions.

The fuel properties may be divided into 3 groups: (i) operational properties (*e.g.*, octane number, cetane number, heating value) or properties related to the durability, chemical stability and chemical composition (*e.g.*, volatility, density, viscosity); (ii)

properties related to the transportation and storage safety of fuels (*e.g.*, flash point); and (iii) properties related to environmental legislation (*e.g.*, acidity, sulphur and aromatic contents).<sup>[29]</sup>

The combustion performance of gasoline is given by the octane number (ON). Gasoline with high ON tolerates higher compression ratios before igniting and thus, may be used in high performance gasoline engines. Gasoline with low ON may cause engine knocking problems. Conventionally, the Research Octane Number (RON, measured according to ASTM D2699), and the Motor Octane Number (MON, measured according to ASTM D2700) describe the antiknock performance under different conditions. The tests are performed in Cooperative Fuel Research (CFR) engines operating at low (RON) or high speed (MON), by comparing the gasoline with standard mixtures of 2,2,4-trimethylpentane (isooctane) and *n*-heptane.<sup>[30]</sup> Thus, the octane number and isoparaffinic index (I, which is a measure of the amount of branching, determined as the ratio  $\text{CH}_3:\text{CH}_2$  in the paraffins) of gasoline vary between the values for isooctane (ON=100; I=5.0) and those for *n*-heptane (ON=0; I=0.4).<sup>[31,32]</sup> The ON (for gasoline) is greatly influenced by the isoparaffinic and aromatic contents. Isoparaffins with higher values of isoparaffinic index are more resistant to self-ignition, thus presenting higher ON. Conversely, longer chain paraffins and olefins are more susceptible to self-ignition, presenting lower ON. Aromatic compounds increase the ON of gasoline, since they, *per se*, present high RON (typically 110) and MON (typically 100).<sup>[32]</sup> Additives (*e.g.*, alcohols, organic compounds, etc.) may be added to gasoline to increase the ON.<sup>[32–34]</sup>

The CN is a measure of the ignition delay of a diesel fuel. Diesel with high CN has a small ignition delay and can burn completely, allowing the engine to run more smoothly and powerfully, while producing less emissions of black and white smoke and noise. On the other hand, diesel with low CN has a significant delay that may cause starting difficulties, engine knocking, leading to poor fuel economy, power loss and sometimes engine damage. Most diesel fuels for standard ICE vehicles possess CN between 45 and 55.<sup>[35]</sup> The CN depends essentially on the molecular composition of the diesel product. Figure 2.6 shows the CN for pure compounds as function of the number of carbon atoms for different classes of hydrocarbons. The CN increases with the number of carbon atoms, and is higher for *n*-paraffins, followed by olefins, cycloparaffins, isoparaffins and aromatics. Diaromatics have lower CN due to their high chemical stability. CN may be measured according to the ASTM

D613 standard engine test, where CN is defined as the percentage by volume of normal cetane ( $C_{16}H_{34}$ ) in a blend with isocetane (2,2,4,4,6,8,8-heptamethylnonane), which matches the ignition quality of the diesel fuel being rated under the specified test conditions. This test requires 1 L of diesel, which is a large amount for performing catalyst evaluation tests in laboratory-scale reactors for research purposes. Therefore, some models, *e.g.*, Ghosh and Jaffe (2006),<sup>[36]</sup> Kapur et al. (2001)<sup>[37]</sup> and O'Connor et al. (1992)<sup>[38]</sup> were developed to estimate the CN based on the diesel chemical composition determined by GC-MS analysis or  $^1H$  NMR spectroscopy.

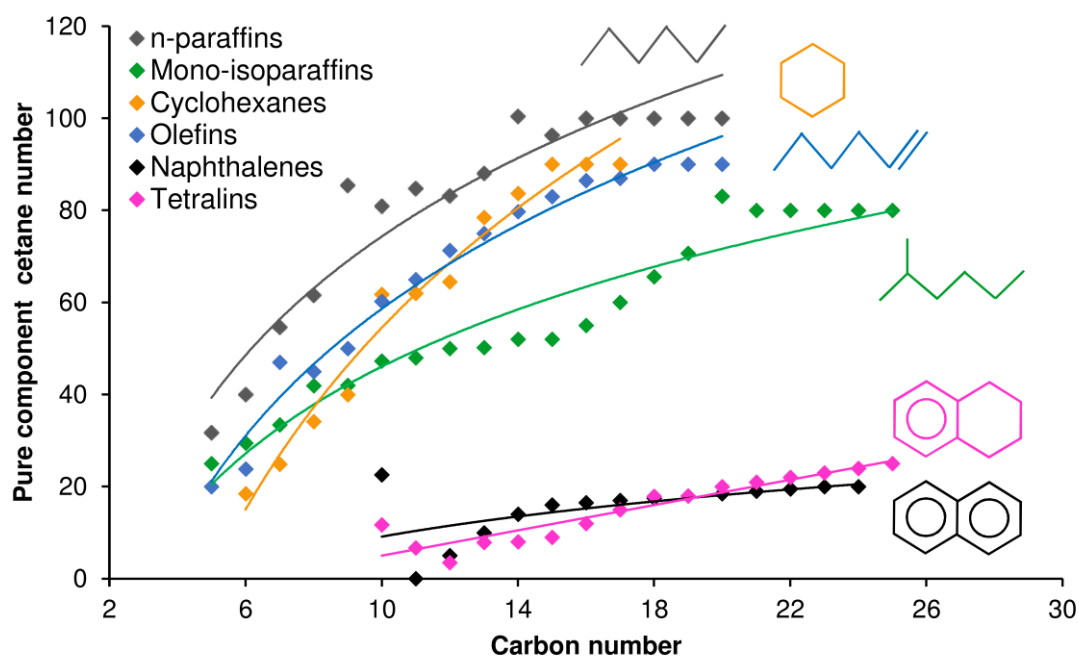


Figure 2.6. Pure component CN as function of the number of carbon atoms for different classes of hydrocarbons. Adapted from ref. [36].

The quality of fuels depends on various properties, besides ON and CN. The heating value is the amount of heat released per mass or volume of fuel *via* complete combustion, which affects the fuel economy. The higher the heating value of the fuel, the more power the engine may generate. Fuel volatility affects the vehicle performance and emissions. Fuels should preferably possess an optimum proportion of low boiling compounds for easy cold starting and fast warm-up, and high boiling point compounds for providing power and fuel economy. Too high or too low volatility may favor smoking and carbon deposits. On the

other hand, fuel viscosity affects the atomization and fuel delivery rate. Too high viscosity may deteriorate the injection system and cause engine starting difficulties, whereas too low viscosity causes poor lubricity of the plungers and injectors. The fuel density influences of the fuel-air mixture and, consequently, the engine output power, whereas high fuel density may cause smoke formation and starting difficulties.<sup>[35]</sup> Flash point is the minimum temperature at which the fuel needs to be heated before a flammable vapor is produced (which may undesirably ignite). The lower the flash point, the higher the risk of explosion during transportation or storage. Legislation is increasingly stringent with respect to sulphur and aromatics contents of fuels. High sulphur leads to corrosion and wear of the engine components and contributes to air pollution, and, on the other hand, high content of heavier aromatics may lead to combustion chamber deposits.<sup>[35]</sup>

Table 2.4 shows the relationship between the main classes of hydrocarbons and some fuel properties.<sup>[10,35,39]</sup> While *n*-paraffins contribute for low ON and good CN, aromatics have the opposite effect leading to good ON and poor CN. On the other hand, the presence of *n*-paraffins is responsible for low heating value, density, cold-flow properties and smoking tendency, whereas the aromatics provide good values for these properties. Isoparaffins and olefins have a similar effect on fuel properties, leading to moderate-good ON and low CN, heating value, density, cold-flow properties and smoking tendency. Cyclic paraffins have moderate effects on fuel properties. Aromatics and olefins may increase engine deposits (worsen engine cleanliness), and lead to carcinogenic compounds (benzene, polyaromatic compounds) in exhaust gases. Olefins in gasoline may lead to enhanced concentration of reactive olefins in exhaust gases, some of which may be carcinogenic and toxic.<sup>[10,39]</sup> The goal is to have the optimum distribution of hydrocarbons that satisfies established regulations and performance needs. In summary, all fuel properties should be considered in the evaluation of the fuel quality. Additives may be needed to meet the good requirements for gasoline and diesel.

Fuels obtained *via* olefin oligomerization can be analyzed by different techniques: simulated distillation analysis (SDA, ASTM-D2887) to determine the boiling point ranges; differential scanning calorimetry (DSC) to determine the *n*-paraffin content; gel permeation chromatography (GPC) and gas chromatography-mass spectrometry (GC-MS) to determine the molecular weight distribution and identify the chemical compounds, respectively; and proton nuclear magnetic resonance (<sup>1</sup>H NMR) spectroscopy to determine the CN.<sup>[40]</sup>

Table 2.4. Influence of the fuel composition on fuel properties.<sup>[35,39]</sup>

Type of hydrocarbon	ON	CN	Heating value	Density	Smoking tendency
<i>n</i> -Paraffins	Low	Good	Poor	Low	Low
Isoparaffins	Good	Low	Poor	Low	Low
Cyclic paraffins	Moderate	Moderate	Moderate	Moderate	Moderate
Olefins	Moderate	Low	Poor	Low	Moderate
Aromatics	Good	Poor	Good	High	High

## 2.2. Catalytic olefin oligomerization of light olefins

### 2.2.1. Industrial technologies

The oligomerization of light olefins (C3-C6) is an important topic to refineries (*e.g.*, petroleum), and several patents were published since the 80's.<sup>[39,41-46]</sup> It represents a promising and sustainable route to produce sulphur-free synthetic fuels (gasoline, diesel, jet fuel) and reduced aromatics content. The fuel products may have wide applications profile: land/sea/air transportation, domestic/commercial heating, power generation, construction/agricultural machinery; or for producing intermediates for lubricants, surfactants, heavy oils, plasticizers, pharmaceuticals, dyes, resins, detergents and additives.<sup>[17,47-49]</sup> Light olefins (C3-C6) are by-products (in considerable quantities) of petrochemical processes, such as FCC, SC, delayed coking, and FT synthesis,<sup>[19,20,42,50-53]</sup> or may be obtained from renewable sources of carbon, *e.g.*, carbohydrate biomass and biobased ethanol/butanol.<sup>[54-59]</sup>

Olefin oligomerization technologies for the production of gasoline and/or middle distillates have been improving along decades (Table 2.5). In 1935, Universal Oil Products (UOP) implemented the Catalytic Polymerization (CatPoly) technology to convert propene and butene compounds to distillate fuels, in the presence of a solid phosphoric acid catalyst.<sup>[19]</sup> However, this technology presented several drawbacks (specified ahead in subsection: Catpoly). Later, in the 1980s Mobil Oil (now ExxonMobil) developed the Mobil

Olefins to Gasoline and Distillate (MOGD) technology using zeolite H-ZSM-5 (MFI topology) as catalyst to produce high-quality distillate fuels, gasoline and lubricating oils<sup>[60]</sup> The same type of catalyst, namely COD-9 (MFI topology), was employed in the Conversion of Olefins to Distillate (COD) technology developed by Mossgas (presently, PetroSA) in 1992, to produce high-quality distillate fuels.<sup>[61]</sup> Axens developed new flexible technologies (Polynaphtha, PolyFuel and FlexEne) to be licensed by other companies; the processes used an amorphous silica-alumina catalyst and allow to easily swift production according to the market demand, without requiring significant investments and plant modifications.<sup>[62,63]</sup> Petron Corp. (Philippines) selected in 2011 Axens' technologies for processing heavier crudes into higher quality products and propene production, including C4 olefins oligomerization unit (Polynaphtha).<sup>[64]</sup> OMV Petrom (Romania) selected in 2016 Axens' PolyFuel technology in order to maximize diesel production by converting olefins present in LPGs and LCN from the FCC unit into distillates, while targeting Euro V specifications for gasoline and diesel pools.<sup>[65]</sup>

Table 2.5. Olefins oligomerization technologies mainly for middle distillates production.<sup>[47]</sup>

Technology	Development	Operation	Catalyst
CatPoly	1930-1935 Universal Oil Products	Sasol Synfuels HTFT refineries, South Africa	Solid phosphoric acid (SPA)
MOGD	1970 Exxon Mobil	Not commercialized	Zeolite Socony Mobil-5 (ZSM-5)
COD	1992 Mossgas refinery	PetroSA at Mossel Bay, South Africa	MFI type zeolite: COD-9
PolyNaphtha Polyfuel FlexEne	1986 2008 Axens	Licensed to different companies	Amorphous silica- alumina: IP 811

**Catalytic Polymerization (CatPoly).** The CatPoly technology employs solid phosphoric acid (SPA, discovered by Ipatieff<sup>[66,67]</sup>) as catalyst to convert olefins, usually propene/butene mixtures, in the gas-phase, to gasoline and diesel range iso-olefins.<sup>[68]</sup> The reaction process involves dimerization and trimerization reactions, *via* an ester mechanism,<sup>[69]</sup> whereby a

phosphoric acid ester stabilizes the polarized hydrocarbon intermediates. SPA is a cheap catalyst consisting of a mixture of orthophosphoric acid with kieselguhr (also known as diatomaceous earth, a natural form of highly pure silica), followed by extrusion and calcination at high temperature to form a composite material.<sup>[68]</sup> The final catalyst is composed of *ca.* 60 wt.% phosphorus pentoxide ( $P_4O_{10}$  or  $P_2O_5$ ) and *ca.* 40 wt.% kieselguhr.<sup>[70]</sup> The active phase is a viscous layer of phosphoric acid on the inactive kieselguhr support.<sup>[71]</sup> The CatPoly process presents several disadvantages,<sup>[15,47,68]</sup> mainly associated with the SPA catalyst, such as:

- Reduced catalyst lifetime as a result of the collapse of the catalyst particles (related to catalyst crushing strength), causing high pressure drops in the catalytic bed and, ultimately, premature shut-downs;
- Very limited possibilities to tailor the catalyst properties to product specifications/demand;
- Above certain amounts of water and oxygenates, the catalyst may suffer structural collapse and deactivation;
- The spent catalyst is not regenerable, and there exist environmental issues related to catalyst disposal (though the spent catalyst may be repurposed if neutralized with ammonia to produce ammonium phosphate, commonly used as plant fertilizer).

Moreover, the CatPoly diesel has poor self-ignition properties and is highly branched, partly due to the absence of microporosity and steric constraints on the SPA catalyst. Therefore, CatPoly diesel has a low CN of 30 (raw) or 34 (after hydrogenation), whereas current and future European standards require CN of at least 51.<sup>[16,72]</sup> Nevertheless, the CatPoly diesel has low viscosity of 1.8 cP at 40 °C and excellent cold-flow properties.<sup>[73]</sup> Therefore, CatPoly process is more suitable for high-quality gasoline production (RON=95-97 and MON=81-82), since it leads to highly branched products with good octane quality.<sup>[74]</sup> The Catpoly technology continues to be in operation in Secunda Sasol refinery nowadays, and in the recent years there has been new research on olefin oligomerization over SPA catalyst, in order to improve the catalyst and the technology.<sup>[19,75-77]</sup>

**Mobil olefins to gasoline and distillate (MOGD).** In the MOGD process, methanol is first converted to light olefins (MTO) over H-ZSM-5 as catalyst and, in a second stage, the olefins are converted to gasoline and diesel fuel over the same type of catalyst.<sup>[42,60]</sup> The catalyst possesses a molar ratio Si/Al of approximately 70, and is extruded with 35 wt.% of alumina.<sup>[78,79]</sup> The MOGD process is highly flexible in terms of feedstock and operability design. It is adequate for a variety of feed streams, ranging from ethene to 200 °C-end boiling point olefinic naphtha coming from FCC units.<sup>[80]</sup> Propene/butene and pentene/hexene feeds led to the best distillate selectivity, partly due to the relatively high reactivity of these olefins. The process may operate under Gasoline mode (230-375 °C, 4-30 bar, 0.5-2 g<sub>olefin</sub> g<sub>cat</sub><sup>-1</sup> h<sup>-1</sup>) or Distillate mode (190-310 °C, 42-70 bar, 0.5-1.5 g<sub>olefin</sub> g<sub>cat</sub><sup>-1</sup> h<sup>-1</sup>), allowing a wide range of operating conditions in order to meet the desired product yields.<sup>[42]</sup> Figure 2.7 represents the process flow for a commercial MOGD plant operating under Distillate mode, which consists of four fixed-bed reactors: three in a series configuration, with inter-reactor coolers and liquid recycle to control the reaction heat, and a fourth reactor for catalyst regeneration. The olefinic feed is mixed with the recycle and passes through the three reactors. The reactor effluent is fractionated to produce distillate-rich and gasoline-rich streams. Part of the gasoline-rich stream is used for reactor recycle to help control the reaction heat and maximize the distillate selectivity. The distillate is subjected to a deep hydrotreatment in order to saturate the olefin oligomers and reduce the amount of aromatics. The product, after hydrogenation, consists essentially of a mixture of moderately branched paraffins in the diesel range (C10-C20).<sup>[60]</sup>

ZSM-5 is an established catalyst in the petroleum industry, for hydrocarbon isomerization reactions. This material is a medium pore zeolite possessing high thermal stability, specific surface area, strong acidity and may impose shape-selectivity (discussed in section 2.3).<sup>[79,81]</sup> The degree of branching of the MOGD products is influenced by the shape-selective constraints imposed by the microporous system of zeolite ZSM-5. The structure of the longer carbon chain products consists mainly of moderately methyl-branched olefins with an average of one methyl side chain per chain of five carbon atoms.<sup>[79]</sup> After hydrogenation, these products are converted to iso-paraffins, which have very good distillate properties, low sulphur, nitrogen and aromatic contents, very low pour and cloud points, and high CN (>55). These outstanding distillate fuel properties account for the high potential of

the MOGD process in meeting future demand for cleaner, low aromatics transportation fuels.<sup>[82]</sup>

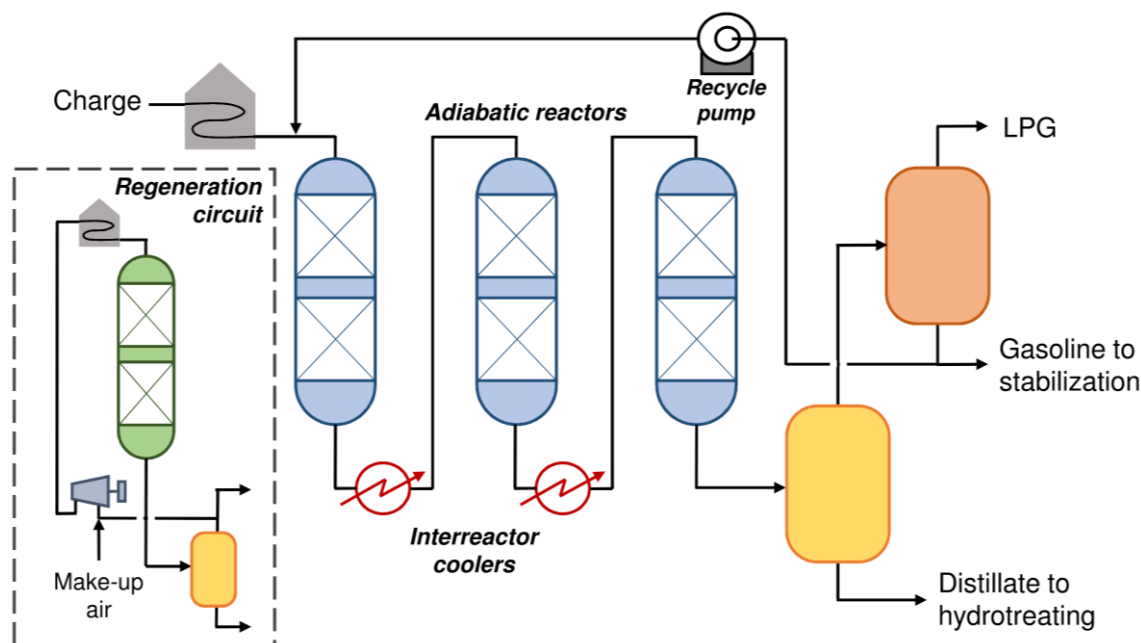


Figure 2.7. MOGD process flow for operation in Distillate mode. Adapted from ref. [60].

In summary, the MOGD process has a great potential for refinery, petrochemical and synthetic fuel applications. The first application of the MODG process occurred in 1982 in the former Mobil refinery in Paulsboro (New Jersey), in which the process was tested using a commercially produced catalyst, giving good results in terms of controllability in large scale, catalyst regeneration, product yields and selectivity, demonstrating that the MOGD process could be scaled-up for industrial production.<sup>[60]</sup> However, it is not yet commercialized. It is worth mentioning that ZSM-5 catalysts show good activity for olefin oligomerization, but they may suffer from relatively fast deactivation.<sup>[83,84]</sup>

**Conversion of Olefins to Distillate (COD).** The COD process is only operated by PetroSA at Mossel Bay, one of the world's largest GTL complexes producing high-quality fuels compared to conventional oil refiners.<sup>[61]</sup> This process is a modification of the MOGD process, which was developed specifically for the conversion (oligomerization and isomerization) of olefins ( $C_3$  to  $C_6$ ) derived from FT synthesis, over COD-9 (H-ZSM-5 type)

catalyst supplied by Süd-Chemie.<sup>[16,85]</sup> In a similar fashion to the MOGD, the COD process may operate under Gasoline mode (223-350 °C, 58 bar, 0.5 g<sub>olefin</sub> g<sub>cat</sub><sup>-1</sup> h<sup>-1</sup>) or Distillate mode (233-375 °C, 4-58 bar, 0.5 g<sub>olefin</sub> g<sub>cat</sub><sup>-1</sup> h<sup>-1</sup>).<sup>[86]</sup> The catalyst regeneration is performed *in-situ* under a flow of nitrogen mixed with small amounts of oxygen, in order to remove coke. The COD process may lead to gasoline, propane and distillates (Figure 2.8). The gasoline and propane produced may be included in the gasoline or liquefied petroleum gas blend pool, respectively; the distillates may be further processed to specialty distillate products by hydrotreating processes giving low aromatic kerosene (LAK) and low aromatic diesel (LAD).<sup>[87]</sup> If required, fractionation may be carried out after hydrotreatment in order to obtain a range of finer cut distillates for special applications.<sup>[87]</sup> These are amongst the cleanest marketed fuels.

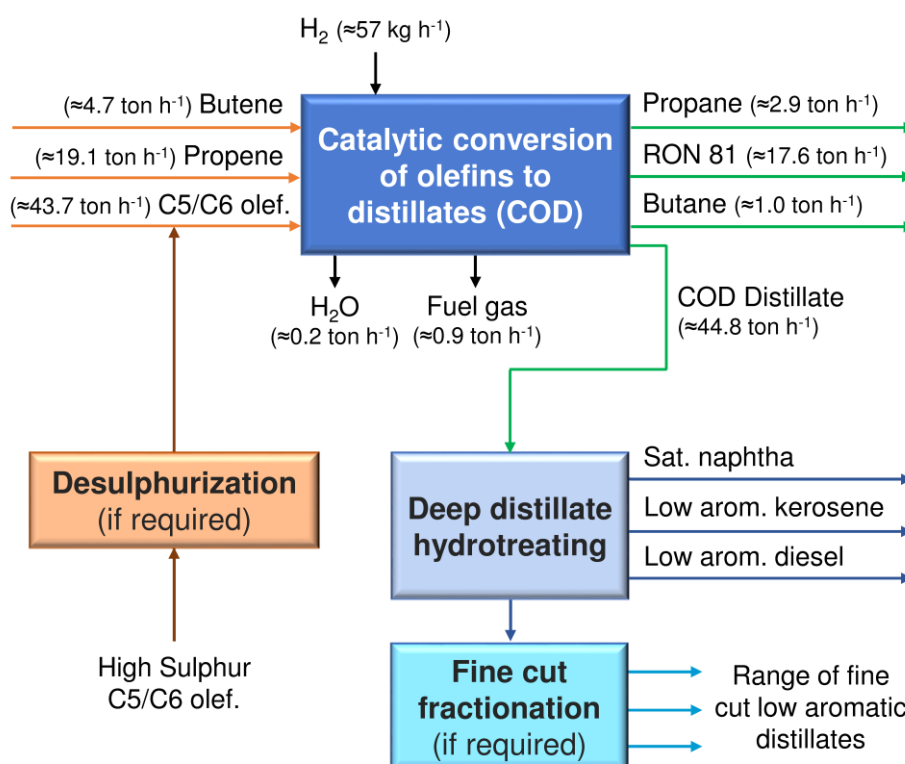


Figure 2.8. COD process with indication of the feed and products compositions. Adapted from refs. [86,87].

Overall, the COD process is very advantageous to increase diesel yield and product value, since it converts mixed olefins (generally used for gasoline products) to higher value

distillates with low sulphur and aromatics contents. These fuels have better exhaust emission and cold-flow properties than conventional fuels, making them particularly suitable as blends for fossil or bio-derived fuels, and very attractive transportation fuels for countries with colder winter seasons. After deep hydrotreatment, the LAD and LAK may be used as indoor fuels and solvents. LAD may be used for lubricants, rolling oils, eco-diesel and copper extraction fuels.<sup>[87]</sup> Due to the above advantages, the COD process is considered a very promising fuel technology.

**Polynaphtha, Polyfuel and FlexEne.** Axens developed several technologies to enhance middle distillates production.<sup>[62]</sup> The Polynaphtha technology<sup>[88]</sup> allows a wide choice of feedstocks (propene and mixed-butene fractions present in C<sub>3</sub>/C<sub>4</sub> cuts from LPG, FCC or SC, and C<sub>5</sub> olefins from the FCC unit) and a wide range of products (high octane blending components for gasoline; high smoke point blending components for kerosene, jet fuel and diesel). Moreover, the Polynaphtha technology is well suited for revamping existing phosphoric acid polymerization units. When gasoline demand falls, the co-produced C<sub>4</sub> olefins (normally used for alkylate production) and light gasoline olefins may be converted to distillate fuel *via* oligomerization.<sup>[89]</sup>

The PolyFuel technology<sup>[90]</sup> appeared later as an improved technology to maximize the middle distillates production *via* the conversion of light olefins from gasoline, at minimum cost while fulfilling more stringent product requirements. The feedstock for this process may be pre-treated olefin-rich components derived from cracking processes (*e.g.*, FCC, SC) or other olefin sources (*e.g.*, effluent from paraffin dehydrogenation processes). Nevertheless, the preferred feed is the C<sub>5</sub>-C<sub>6</sub> olefinic cut from the Prime-G<sup>+</sup> process; Prime G<sup>+</sup> is an ideal feed pre-treatment process to lower the contents of dienes and sulphur in light C<sub>5</sub>-C<sub>6</sub> fractions.<sup>[91]</sup> In the Polyfuel process (Figure 2.9), light olefins are oligomerized using two fixed-bed reactors (one swing reactor), with on-stream catalyst regeneration. The operation of the reactors is optimized to maximize catalyst on-stream lifetime. Conversion and selectivity are controlled by reactor temperature adjustment, while the heat of reaction is simply removed by heat exchange between the feed and effluent. The reactor effluent is fractionated, producing gasoline depleted in olefins, and middle distillates. The gasoline fraction is partly recycled to the reactor aiming at enhanced distillate production; on the other

hand, the middle distillate stream is typically sent to existing kerosene and diesel hydrotreatment units.<sup>[91]</sup>

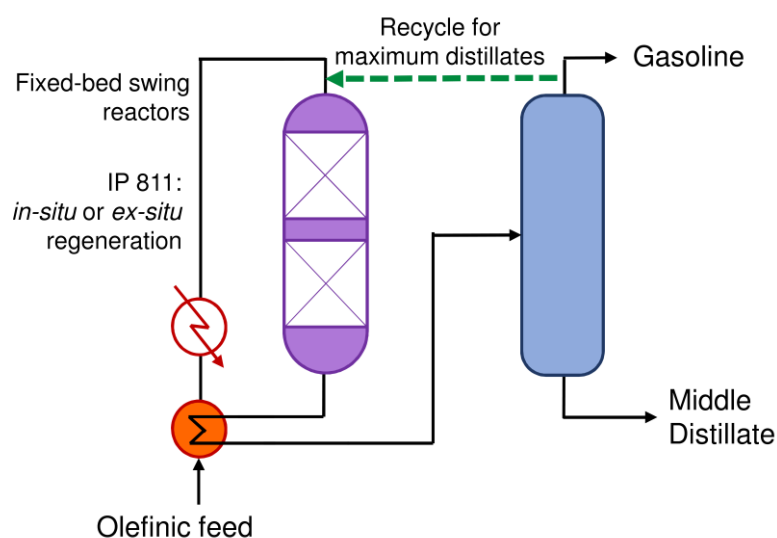


Figure 2.9. Polyfuel process using the IP 811 (amorphous silica-alumina) catalyst. Adapted from ref. [92].

The type of catalyst used in the Polynaphtha and PolyFuel technologies consists of amorphous silica-alumina (IP 811) with a trilobe extrudate shape. This material is considered an environmentally friendly catalyst that does not lead to acidic waste effluents and presents long on-stream lifetime, besides high activity. The catalytic material possesses high mechanical strength, may be regenerated multiple times (*in-situ* or *ex-situ*) and is stable in the presence of water and other impurities.<sup>[93]</sup> These characteristics of the catalyst avoid pressure drop problems and allow operation under severe reaction conditions to maximize the middle distillate production.

The FlexEne technology<sup>[94]</sup> was developed in 2008 to provide refineries the flexibility in face of fluctuating demand. It is an innovative combination of two well-proven technologies: FCC and oligomerization (Polynaphtha/PolyFuel), designed to process light FCC olefins and recycle valuable feed coming from the oligomerization unit, back to the FCC unit (without any reactor modification) to maximize gasoline or distillate yields. Figure 2.10 shows the Polynaphtha oligomerization process in a FlexEne configuration. Depending on the operating conditions, types of light olefins feed, catalyst formulation, and product cut to recycle, the FCC process operates in different modes, providing product based flexibility

according to the market trends: “Maxi Distillate”, “Maxi Gasoline” and “High Propylene”. In the Maxi Distillate mode, selected olefins in the C<sub>3</sub>-C<sub>9</sub> range are converted to distillate range products in the oligomerization unit. The gasoline olefin oligomers are highly reactive and may be selectively cracked to propene and butenes in the FCC unit under normal cracking conditions, thereby producing higher amounts of feed for the oligomerization unit, leading to enhanced distillate production. In this fashion, the refinery is recovering the desired product, and recycling the undesired product. Overall, FlexEne may be easily implemented in an existing refinery, while providing product based flexibility to help the refiner respond to the market needs and maximize returns.<sup>[94]</sup>

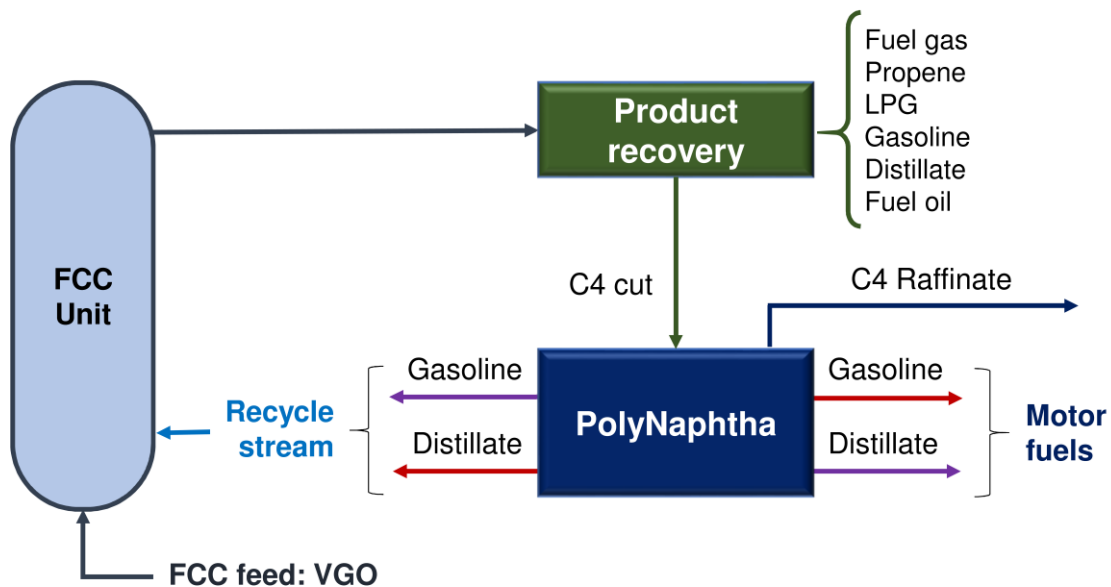


Figure 2.10. Polynaphtha in a FlexEne configuration for gasoline (red arrows) and distillates (purple arrows) production. Adapted from ref. [95].

### 2.2.2. Emerging bio-based processes

Besides the “traditional” technologies, new processes involving olefin oligomerization to produce synthetic fuels from cellulosic biomass were proposed in the literature. Figure 2.11 exemplifies a case, specifically a technology proposed by Bond et al.<sup>[55]</sup> where lignocellulose is firstly pre-treated using hot water extraction to obtain (i) an aqueous solution of xylo-oligomers for producing furfural, and (ii) cellulose and lignin that

are subsequently treated with diluted sulfuric acid in a CSTR reactor or steam-gun for producing levulinic acid (LA) and formic acid (FA) in aqueous solution. Lignin and humins are recovered by filtration and sent to a boiler generator to produce heat and power. LA is recovered from the hydrolysate *via* extraction using 2-*sec*-butylphenol (SBP), and subsequently converted (without separation) to  $\gamma$ -valerolactone (GVL) via hydrogenation over a RuSn/C catalyst. Then, GVL undergoes decarboxylation over SiO<sub>2</sub>/Al<sub>2</sub>O<sub>3</sub> catalyst to form butene isomers and CO<sub>2</sub>. The butene products can be directly used as feedstock for an oligomerization conversion unit to produce liquid fuels which will be subsequently refined (hydrotreatment, distillation) to increase the desired product quality.<sup>[55]</sup>

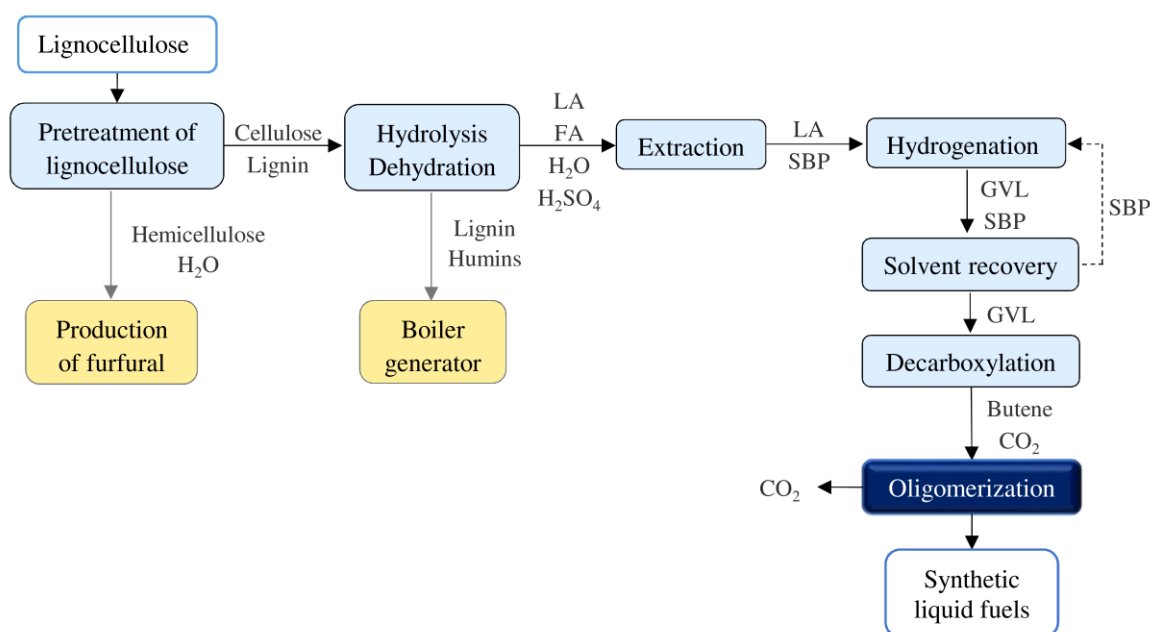


Figure 2.11. Production of synthetic liquid fuels from lignocellulose (LA=levulinic acid, FA=formic acid, SBP=2-*sec*-butylphenol, GVL= $\gamma$ -valerolactone). Adapted from ref. [55].

### 2.2.3. Mechanistic considerations

Olefin oligomerization involves consecutive reactions between light olefins to produce higher molecular weight products composed of 2-100 repeating units (monomers), *i.e.* oligomers. If the number of repeating units ( $n$ ) is equal to 2, the reaction is designated dimerization, whereas for  $n > 100$  it is a polymerization reaction.<sup>[47]</sup> The reaction mechanism

of olefins over solid acid catalysts may follow a classic carbenium route (exemplified in Figure 2.12 for 1-butene). Three main steps may be considered. Step 1 involving the protonation of an olefin over an acid site (initiation step – (1a)) leading to the formation of a secondary alkyl-carbenium ion. Step 2 where the alkyl-carbenium ion may undergo double bond isomerization ((2a) and (2b)) giving *cis*- and *trans*-2-butene, or skeletal isomerization (2c) giving isobutene (*via* rearrangement of the secondary carbenium ion into a protonated cyclopropane intermediate and subsequently an unstable primary carbenium ion). The alkyl-carbenium may react with an olefin molecule (propagation step – (1b) and (1c)) to give longer carbon chain olefins. Alternatively, step 3 involved the termination of the chain growth *via*, for example, deprotonation (termination step – (1d)) to give an olefin and the initial acid site.<sup>[17,47,70]</sup> Olefin reactivity tends to increase with chain length, and the molecular weight of the products formed depends on the rate constants of propagation and termination,  $k_p$  and  $k_t$ , respectively.<sup>[96]</sup> If  $k_p \gg k_t$ , polymers will be formed; if  $k_p \ll k_t$ , dimers are formed, and if  $k_p \cong k_t$ , oligomers are formed.<sup>[97]</sup> These rate constants are strongly dependent on the reaction conditions.

The carbenium ions formed may undergo isomerization *via* hydride shifts (3a and 3b in Figure 2.12) or alkyl shifts (3c, Figure 2.12), or cracking (4, Figure 2.12) (*via*  $\beta$ -scission, the classical cracking mechanism<sup>[98]</sup>) giving mixtures of oligomeric olefins in which the number of carbon atoms per molecule may be a multiple of the total number of carbon atoms of the olefin molecule in the feed, or possess odd number of C atoms (not a multiple number).<sup>[17]</sup> Cracking mechanisms may involve the classical bimolecular cracking *via* carbenium ions, or the non-classical monomolecular cracking *via* carbonium ions state. At low reaction temperature, high reactant partial pressure and high conversion, the classical cracking mechanism is gradually replaced by oligomerization cracking, where substantial oligomerization precedes the cracking process; nevertheless, the fundamental chemistry related to this cracking mechanism is basically the same as that for classical cracking.

The non-classical monomolecular cracking is known as the Haag-Dessau mechanism of protolytic cracking, where unstable carbonium ion transition state is formed and “collapses” to give alkanes (or dihydrogen, depending on whether a C-C or C-H bond is protonated), olefins and the free Brønsted acid sites.<sup>[99,100]</sup> The changes in the relative contributions of the different mechanisms to the overall reaction may be evaluated based on

the product selectivities; propane and propene were taken as indicator of monomolecular cracking contribution, and isobutane and isobutene were taken as indicator of the bimolecular and oligomeric cracking contribution.<sup>[101]</sup>

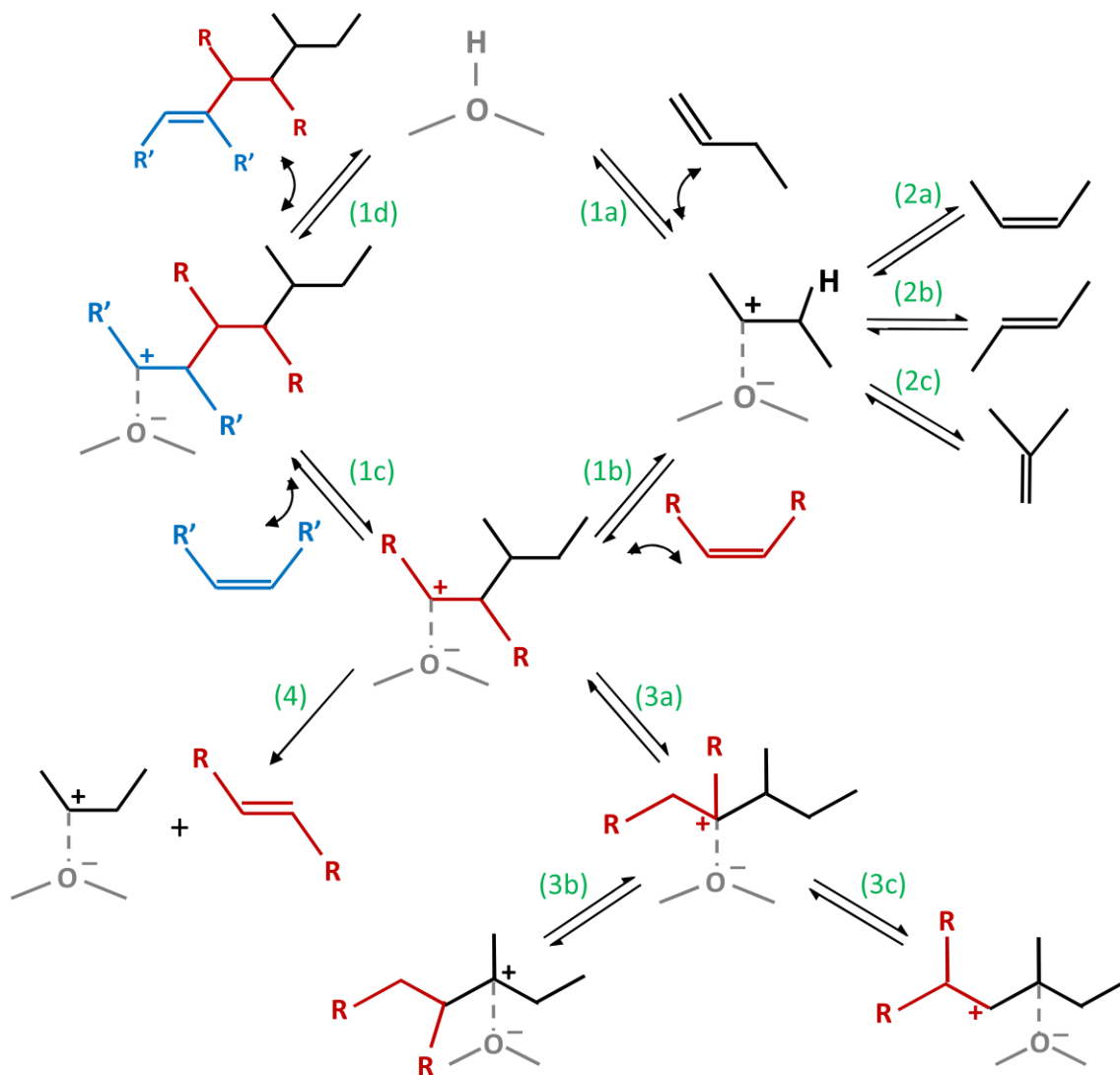


Figure 2.12. Carbenium ion mechanism of acid-catalyzed oligomerization reactions, exemplified for 1-butene as initial monomer (R and R' stands for alkyl groups with different number of carbon atoms or configurations). Adapted from ref. [17].

The Haag-Dessau mechanism<sup>[102]</sup> was reported as the predominating one for reactions carried out at high reaction temperature, low reactant concentrations and low conversions, and using small or medium (*e.g.*, ZSM-5) pore zeolites capable of imposing

steric hindrance on bimolecular (hydride transfer) reactions of classical cracking.<sup>[99,102]</sup> Large pore zeolites (*e.g.*, Y) may favor hydrocarbons cracking *via* bimolecular reactions (classical cracking).<sup>[101,102]</sup> The acid properties may lead to differences in mechanisms; *e.g.*, low acid site density may favor protolytic cracking.<sup>[99,100]</sup> Overall, the reaction mechanism may be complex; in addition to hydrocarbon products, H<sub>2</sub> may be formed and activated on Brønsted acid sites leading to Haag–Dessau hydrocracking.<sup>[103]</sup>

The olefin products may undergo hydride transfer (H-transfer) and cyclization reactions, through carbenium ion intermediates, leading to aromatic compounds (Figure 2.13). The aromatic compounds may become entrapped inside the catalyst pore system, blocking the access to the acid sites, resulting in decreased catalytic activity.<sup>[70,97,104]</sup>

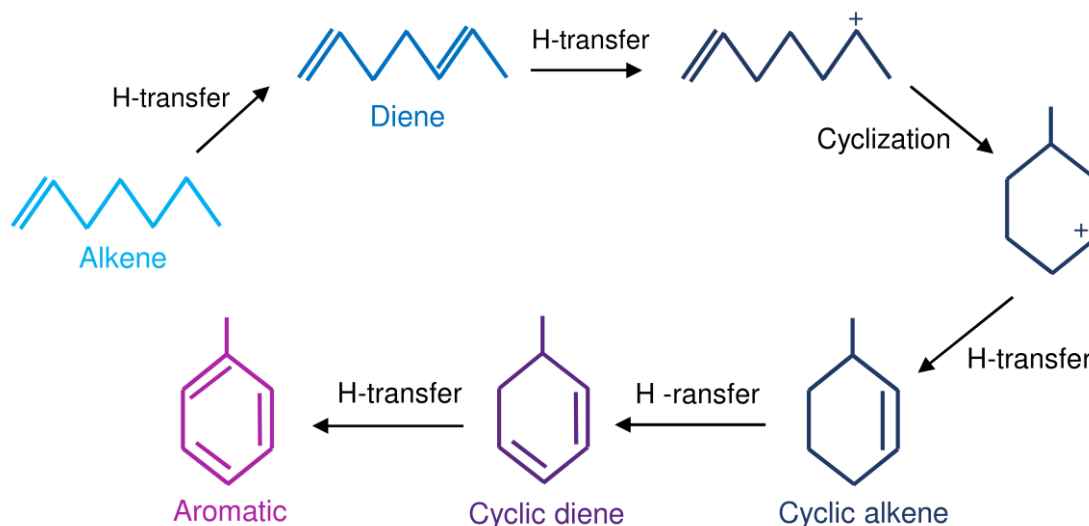


Figure 2.13. Possible mechanism of olefin aromatization, exemplified for 1-heptene. Adapted from ref. [105].

The reaction rates of olefins may decrease as the carbon chain length increases; *e.g.*, propene may react faster than 1-decene, due to the lower mobility of the longer chain olefins inside the catalyst pores. On the other hand, based on the same number carbon atoms,  $\alpha$ -olefins (abbreviated as terminal olefins) tend to react more easily over solid acid catalysts than olefins with internal C=C bonds (or internal olefins), since the coupling of internal olefins over solid acids is more difficult.<sup>[56,81]</sup>

The oligomerization process may be described by thermodynamic and kinetic phenomena.<sup>[97]</sup> The operating conditions will influence the relative rates of the various pathways, and will lead to product mixtures with different properties (such as branching degree, molecular weight, boiling point, etc.).<sup>[9,35]</sup> For obtaining high-quality fuel, olefin oligomerization must be favored over other reactions and preferably lead to hydrocarbons with the desired chain lengths and branching degree. Depending on the degree of branching and oligomer chain length, the fuel products can be of gasoline or diesel type. An ideal gasoline, with high ON, is partly composed of highly branched paraffins with 8–10 carbon atoms, whereas an ideal diesel fuel, with high CN, is partly composed of linear or slightly branched paraffins with 12-22 carbon atoms.<sup>[106]</sup>

The development of rigorous kinetic models of olefins oligomerization systems is important to reach optimal performances and desired product yields; however, this is not trivial due to the complex reaction mechanisms involved. Olefin oligomerization may be very exothermic, with heat of reaction of *ca.*  $-1.05$  to  $-1.38$  kJ g<sup>-1</sup> of reacted olefin.<sup>[107]</sup> The reaction involves reduction in the total number of moles of the system, and therefore low temperature (< 200 °C) and high pressure are thermodynamically favorable. However, at relatively low temperature the chain growth is kinetically limited, whereas too high temperature (> 300 °C) promotes undesirable reactions, such as cracking, hydride transfer (and aromatization) and disproportionation.<sup>[17,70,108,109]</sup> Low weight hourly space velocity (WHSV; mass flow rate of olefin feed per unit mass of catalyst) may favor olefin oligomerization.<sup>[51,70]</sup> Overall, the feedstock, reaction conditions and catalytic properties need to be carefully chosen.

#### **2.2.4. Catalyst scope for olefin oligomerization**

Table 2.6 summarizes the most common types of catalysts and their advantages and disadvantages for olefin oligomerization. Homogeneous and heterogeneous acid catalysts were studied, albeit the latter are preferable since they may possess higher thermal stability, relatively good selectivity, may be easily separated from the reaction mixture and regenerated, and are more adequate for continuous flow processes (in line with industrial oligomerization processes).<sup>[110]</sup> Since the late 50's several organic and inorganic catalysts

were reported in the literature for carrying out olefin oligomerization (Table 2.6). The most studied organocatalysts were acid ion-exchange resins.<sup>[111–113]</sup> On the other hand, inorganic catalysts included solid phosphoric acid<sup>[19,68,75]</sup>, zeolites<sup>[53,114,115]</sup>, amorphous silica-alumina (ASA)<sup>[116,117]</sup> and other metal oxide catalysts<sup>[118,119]</sup>, and ionic liquids<sup>[120–123]</sup>. Other materials include variety of immobilized metal complexes (combining properties of homogeneous and heterogeneous catalysts), albeit these materials may decompose under the reaction conditions.

The most investigated heterogeneous catalysts for olefin oligomerization can be divided into two types: transition metal-free (TM-free) acid catalysts (which include zeolites and other types of aluminosilicates) and TM-containing catalysts (mostly based on nickel).<sup>[47,97]</sup> While nickel-containing catalysts were mainly used for dimerization reactions, TM-free acid catalysts seem preferred for the conversion of light olefins to distillate fuels.<sup>[79]</sup>

Solid acid catalysts (*e.g.*, SPA, zeolites, sulfonic resins) are widely studied for ethene oligomerization. However, the rate of the acid-catalyzed ethene oligomerization is much lower than that of other olefins, especially under mild thermal conditions. Much research on ethene oligomerization was focused mainly on catalysts based on nickel oxide supported on inorganic porous materials, or nickel complexes immobilized on oxide and polymeric supports.<sup>[110,124,125]</sup> On the other hand, many types of heterogeneous acid catalysts (in particular zeolites) were studied for the oligomerization of propene and butenes. The use of zeolites as catalysts may require higher temperature and pressure than SPA and sulfonic acid resins; the harsher reaction conditions may favor side reactions.<sup>[110]</sup> Nevertheless, zeolites may present superior stability to other catalysts, leading to enhanced productivity.

The catalytic reaction over porous catalysts involves different steps, in a dynamic fashion; molecules diffusing from site to site until the reaction occurs, products desorb, etc. (Figure 2.14). Preferably, the overall process should operate under kinetic regime (negligible diffusion limitations). The steps involved for a heterogeneous catalyst are:

- 1) Transport of reactants from the fluid bulk to the catalyst particle surface (external diffusion and adsorption);
- 2) Transport of reactants (and solvents or carrier gas molecules) inside the catalyst's pores (internal diffusion);
- 3) Adsorption of reactants on the active sites;

- 4) Chemical reaction involving adsorbed species (molecules, atoms);
- 5) Desorption of products from the active sites;
- 6) Diffusion of the products to the external surface of the particle (internal diffusion);
- 7) Desorption of products from the catalyst surface and diffusion to the fluid bulk (external diffusion).

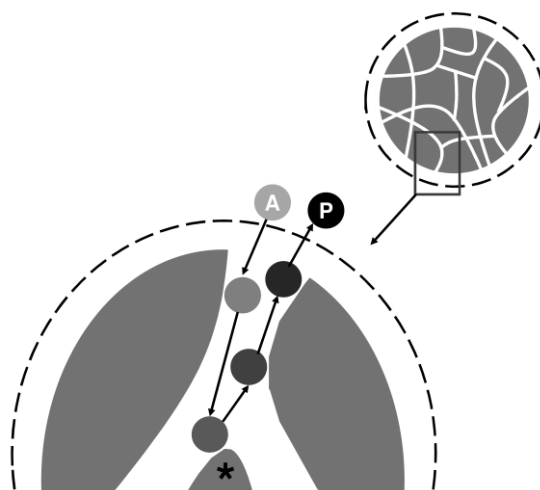


Figure 2.14. Simplified representation of the steps involved in a heterogeneous catalytic reaction process (A stands for reactant, P for product, and \* for active site). Adapted from ref. [126].

The design of efficient catalysts capable of leading to high selectivity to the desired products at high conversion, and possess good stability over long time on-stream, is challenging. Much research was done over the years covering dimerization and oligomerization reactions of light olefins over different types of porous acid catalysts, targeting  $\alpha$ -olefins, gasoline, diesel or jet fuel type products. The studies were mostly based on pure olefins diluted either in inert solvents ( $N_2$  and He) or in an alkane (*e.g.*, butane, pentane, hexane). Few studies used mixtures of small olefins and paraffins to mimic industrial olefinic streams. Review articles on olefin oligomerization addressed various aspects (Table 2.7). Most reviews in recent years were mainly focused on the oligomerization of ethene which is of academic and industrial interest for the production of linear  $\alpha$ -olefins in the C4-C10 range, the demand of which has grown very fast (Table 2.8).

Table 2.6. Types of catalysts reported in the literature for olefin oligomerization.

Types of Catalysts	Characteristics	Advantages	Disadvantages	Examples
Acid ion-exchange resins	Macroporous; Strong acidity associated with sulfonic acid groups (active sites).	Long lifetime if regenerated; Good selectivity towards high molecular weight oligomers.	High cost; Low thermal stability ( <i>e.g.</i> , 150 °C), limiting temperature range and hinders regeneration <i>via</i> calcination; Recovery <i>via</i> washing with hydrocarbons, but the recovered resins presents lower activity and higher deactivation rates.	Amberlyst-15, -35 and -36, Purolite-CT275, Indion-125 and -130
Solid phosphoric acid (SPA)	Mixture of kieselguhr (support) and concentrated phosphoric acid (active component).	Low cost.	SPA is not regenerated and deactivates rapidly; Difficulty to remove the catalyst from the reaction mixture; May cause equipment corrosion; Environmental issues related to catalyst disposal; Low selectivity towards distillates due to the formation of highly branched products.	SPA
Amorphous alumina-silica (ASA)	Exhibit cation-exchange capacity; Possess Brønsted and Lewis acid sites.	Relatively high mechanical strength; More robust and less expensive compared to zeolites; More cost effective compared to SPA.	Relatively fast deactivation; Intrinsic activity (conversion rate per aluminum site) tends to be lower than for zeolites; Lower acidity than zeolites; No shape-selectivity; Higher activity for hydride transfer reactions; Low selectivity to distillates, with the formation of highly branched products.	ASA
Ionic liquids	Can possess acid groups.	Considered eco-friendly; Can be reused (with some deactivation); Good thermal stability.	Difficulties in product purification or ionic liquid recycling; Issues for application in continuous flow reactors.	1-(4-sulfonic acid)-butyl-3-alkylimidazolium triflate

Table 2.6. (continued)

<b>Types of Catalysts</b>	<b>Characteristics</b>	<b>Advantages</b>	<b>Disadvantages</b>	<b>Examples</b>
Zeolites	Microporous structure and uniform pores; Aluminosilicates with significant specific surface area; Cation-exchange capacity; Possess Brønsted and Lewis acid sites.	Relatively high activity; Shape-selectivity; Facile regeneration by calcination to burn the coke; Facile disposal; Fairly high thermal stability.	Relatively fast deactivation.	ZSM-5, Faujasites Y and X, Mordenite, Beta, ZSM-12, TON

Table 2.7. Selected published review articles on olefin oligomerization.

<b>Ref.</b>	<b>Title (year)</b>	<b>Content/Approach</b>
[17]	Applications of light olefin oligomerization to the production of fuels and chemicals (2017)	Discussion of reaction mechanisms and showcase of catalysts and processes of olefin oligomerization commercially practiced. Discussion of multifunctional materials possessing both acid and metal active sites. Discussion of processes where oligomerization is a key step in a multi-step or multi-reaction process.
[110]	Heterogeneous oligomerization of light alkenes: 80 years in oil refining (2016)	Overview of the existing industrial technologies for the production of motor fuel compounds by the heterogeneous oligomerization of light C <sub>2</sub> –C <sub>4</sub> alkenes. Special attention is given to the dimerization of iso-butylene to iso-octene and its subsequent hydrogenation to iso-octane.
[11]	Maximizing diesel production through oligomerization: a landmark opportunity for zeolite research (2015)	Challenges in the acid-catalyzed oligomerization of olefins with the aim of diesel production, essentially regarding mass transport and accessibility to the acid sites for one-dimensional pore zeolites. Possible solutions to improve the mass transfer properties of one-dimensional pore zeolites, either by introducing mesoporosity or using nanosized zeolites, are discussed.
[111]	Alkenes oligomerization with resin catalysts (2015)	Catalytic oligomerization of propene, butene, isobutene and isoamylene over cation-exchange resins, discussing the influence of the resin (resin-type and their physical and structural properties), the operating conditions and additives used (polar compounds like alcohols), upon oligomerization conversion and selectivity.
[124]	Oligomerization of $\alpha$ -olefins to higher oligomers (1991)	Comprehensive study of the catalysts and the process for ethylene, propylene, and higher olefins oligomerization, discussing the industrial processes and the olefin oligomerization mechanism (based on the literature up to December 1989).
[79]	Alkene oligomerization (1990)	The oligomerization of alkenes, the thermodynamics and kinetics of the reaction and the use of both homogeneous and heterogeneous catalysts are discussed. Particular attention is given to the use of acid catalysts, especially zeolites, and homogeneous and heterogeneous nickel catalysts.

Table 2.8. Selected published review articles on ethene oligomerization.

Ref.	Title (year)	Content/Approach
[127]	Carbocyclic-fused N,N,N-pincer ligands as ring-strain adjustable supports for iron and cobalt catalysts in ethylene oligo-/polymerization (2018)	Recent progress in the application of homogeneous iron and cobalt catalysts in ethylene oligo-/polymerization, with emphasis on the tuning of catalyst performance through the introduction of controlled amounts of ring strain to the ligand frame.
[128]	Chromium catalysts for selective ethylene oligomerization to 1-hexene and 1-octene: recent results (2017)	Analysis of recent publication results (July 2010 to February 2017) obtained for selective ethylene oligomerization toward 1-hexene and 1-octene catalyzed by chromium-based catalytic systems, considering scientific and patent literature. The results of the studies concerning oligomerization mechanisms are also included in this review.
[125]	Nickel-based solid catalysts for ethylene oligomerization – a review (2014)	The main properties of Ni-based inorganic porous materials and their catalytic performances in ethylene oligomerization reactions performed under mild conditions. The influence of the catalyst pore size and reaction conditions (temperature, pressure) on the productivity and product distribution in oligomerization are discussed.
[129]	Recent progresses of late-transition metal complexes with nonsymmetric diimine ligands in ethylene polymerization and oligomerization (2014)	Recent developments in the research of ethylene polymerization and oligomerization catalyzed by late-transition metal complexes with unsymmetric diimine ligands, with discussion of the influence of complex structure of the catalyst on the catalytic performance.
[130]	Tetramerization of ethylene to octene-1 (A review) (2012)	Summary and analysis of data on the activity, selectivity, and reaction conditions for the selective oligomerization of ethylene to octene-1 mediated by chromium-containing organic compounds in combination with organoaluminum compounds. Discussion of possible mechanisms of the formation of octene-1, byproduct cyclic hydrocarbons and higher (>C8) linear olefins.

Table 2.8. (continued).

Ref.	Title (year)	Content/Approach
[131]	Selective ethylene oligomerization: recent advances in chromium catalysis and mechanistic investigations (2011)	Discussion of the most recent advances in chromium chemistry related to selective olefin oligomerization. Aspects regarding ligand design, catalyst generation, selectivity for different products, and reaction mechanism are presented. Isotopic labeling protocols designed to distinguish between various mechanisms of catalysis are reviewed.
[132]	Early-transition-metal catalysts with phenoxy–imine-type ligands for the oligomerization of ethylene (2011)	Highlight of recent advances in (selective) ethylene oligomerization with early-transition-metal complexes bearing phenoxy–imine-type ligands for the formation of linear $\alpha$ -olefins and high-molecular-weight linear $\alpha$ -olefins, which have had an important impact on ethylene oligomerization chemistry and on the synthesis of ethylene-based functionalized materials.
[133]	Olefin oligomerization <i>via</i> metallacycles: dimerization, trimerization, tetramerization, and beyond (2011)	Studies of ethylene trimerization to 1-hexene (from 2004) and of alkene (especially ethylene) dimerization to short-chain linear $\alpha$ -olefins (comonomers). The possibility of large ring metallacycles leading to polyethylene formation was covered as well.
[134]	Catalytic ethylene dimerization and oligomerization: recent developments with nickel complexes containing P,N-chelating ligands (2006)	Overview of comparative studies aiming at modulating the coordinating properties of functional ligands for a metal, such as nickel (which is used in oligomerization industrial processes targeting $\alpha$ -olefins), that lead to beneficial effects in catalytic ethylene oligomerization.
[135]	Advances in selective ethylene trimerisation – a critical overview (2004)	Historical overview of all developments in the field of selective olefin trimerization, giving attention to the catalyst system (mainly homogeneous catalysts), catalyst activity, reaction selectivity and relative catalyst cost. Various mechanistic aspects are discussed in detail.

## 2.3. Zeolites and zeotype acid catalysts for olefin oligomerization

Zeolites are widely used as heterogeneous catalysts in oil refineries and petrochemical industry.<sup>[136,137]</sup> Zeolites are crystalline microporous aluminosilicates, which may be of natural origin (*e.g.*, Faujasite (FAU), Mordenite (MOR), Offretite (OFF), and Ferrierite (FER)) or synthetic (*e.g.*, ZSM-5 (MFI), Beta (BEA), and Y (FAU)).<sup>[138,139]</sup> These materials have a unique combination of properties which includes high specific surface area, well-defined microporosity, fairly high hydrothermal and thermal stabilities, adsorption and ion-exchange capacities, and the ability to confine different types of active species. Zeolites may possess much higher internal specific surface area than external surface area and high microporous volume, allowing chemical reactions to occur mainly at active sites in confined environments, enhancing product selectivity. Zeolites may possess the stability for thermally demanding reactions, and they may be regenerated at high temperature and reused, enhancing the productivity; moreover, they are not environmentally harmful.<sup>[140,141]</sup>

Zeolites are highly recognized as heterogeneous acid catalysts.<sup>[137,142]</sup> Some zeolites were reported as thermally stable acid catalysts for the oligomerization of light olefins.<sup>[53,83,112,115,143]</sup> The type of products formed during oligomerization over zeolites is influenced by the pore structure and sizes (shape-selectivity) and acid properties. In this section, the structural features of zeolites and their influence on olefin oligomerization are described, based on a literature survey.

### 2.3.1. Zeolites - microporous systems

According to IUPAC classification, zeolites are crystalline microporous materials ( $d_p \leq 2.0$  nm), and are chemically composed of elementary tetrahedral units of silicon tetraoxide ( $\text{SiO}_4$ ) and aluminum tetraoxide ( $\text{AlO}_4^-$ ), Figure 2.15.<sup>[144]</sup> The empirical formula for zeolites is  $\text{M}_{x/n}^{n+} \text{Al}_x \text{Si}_{1-x} \text{O}_2 \cdot y\text{X}$ , where  $\text{M}^{n+}$  represents an inorganic or organic cation with oxidation state  $n+$ ,  $y\text{X}$  represents  $y$  moles of a physically adsorbed compound  $\text{X}$  (*e.g.*, water), and the subscripts are the number of moles of each atom or ion (sometimes the silicon

or aluminum are generically denoted T atoms). Adjacent tetrahedra ( $\text{TO}_4$ ) share oxygen atoms, forming T-O-T bridges. The trivalent aluminum atoms in tetrahedral coordination give rise to a negatively charged framework, which is charge-balanced by exchangeable cations (*e.g.*,  $\text{Na}^+$ ,  $\text{K}^+$ ,  $\text{NH}_4^+$ ). The tetrahedral units may assemble into composite building units (*e.g.*, sodalite cage,  $\alpha$ -cavity), and the latter, in turn, assemble to give different topologies of porous systems (*i.e.*, framework types), Table 2.9 and Table 2.10.<sup>[142]</sup>

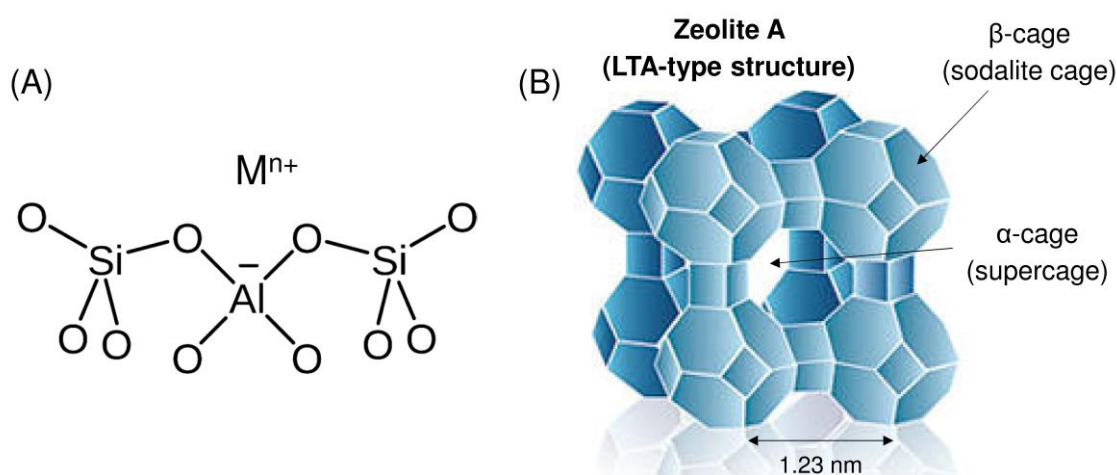


Figure 2.15. (A) Silicon and aluminum atoms in tetrahedral coordination, and sodium cations compensating the negatively charged framework. (B) Example of a zeolite structure (LTA type) possessing a sodalite cage (the white lines represent T-O-T bridges). Adapted from ref. [139].

Table 2.9. Zeolite classification according to micropore sizes, and examples with indication of the respective channel dimensionality.<sup>[139,145]</sup>

Classification	MR <sup>[a]</sup>	Pore diameter, d (nm)	Zeolites (Channel dimensionality)
Small pore	8	$0.3 < d < 0.5$	Erionite (3D), A (3D), ITQ-3 (2D)
Medium pore	10	$0.5 < d < 0.6$	ZSM-5 (3D), ZSM-11 (3D), ITQ-1 (2D), ferrierite (2D), Theta-1 (1D), ZSM-22 (1D)
Large pore	12	$0.6 < d < 0.9$	X (3D), Y (3D), Beta (3D), $\Omega$ (3D), Mordenite (1D), ITQ-7 (3D)
Extra-large pore	18	$0.9 < d$	MCM-9 (1D), VIP-5 (1D)

<sup>[a]</sup> MR stands for membered-ring channels, *i.e.* number of T-O-T bridges in pore openings.

Zeolites may be classified according to the micropore sizes (Table 2.9) or channel dimensionality, as exemplified in Table 2.10 for common zeolites studied in olefin oligomerization.<sup>[139]</sup> For porous structures of the same dimensionality, the pore sizes may differ significantly.<sup>[139]</sup> The channel/pore size is related to the number of T-O-T bridges forming the pore apertures.

Table 2.10. Pore systems of selected zeolites reported in the literature for olefin oligomerization.<sup>[139,146]</sup>

Framework type code (channel dimensionality) <sup>[a]</sup>	Ring sizes <sup>[b]</sup>		Pore sizes (Å) <sup>[c]</sup>	Maximum diameter of a sphere (Å) <sup>[d]</sup>	
				Included	Diffused
MFI (3D)	Channel	system	5.1 × 5.5 5.3 × 5.6	6.36	4.46
BEA (3D)	Channel	system	6.6 × 6.7 5.6 × 5.6	6.68	5.95
MOR (2D)	Channel	system	7.0 × 6.5 5.7 × 2.6	6.7	6.45
FER (2D)	Channel	system	5.4 × 4.2 4.8 × 3.5	6.31	4.89
FAU (3D)	Channel	system	7.4	11.24	7.35
		with 12 MR, and supercages			

<sup>[a]</sup> Channel dimensionality is indicated based on channels with at least 8 MR (Membered-ring). <sup>[b]</sup> Channels with at least 10 MR are indicated whenever the topology contemplates them. <sup>[c]</sup> Two pore dimensions referent to channels in different orientations. <sup>[d]</sup> Maximum diameter of a sphere that can be included or than can diffuse along the channels of the zeolite.

### 2.3.2. Zeolites - acidity and shape-selectivity

The catalytic performances of zeolites for olefin oligomerization may be influenced by the type of crystalline structure, and the textural and acid properties.

The acid properties refer to the type of acid sites (Brønsted or Lewis), and the amount, density, strength and location of the acid sites (on the external or internal surface of the



Transform Infrared (FT-IR) spectroscopy of an adsorbed base probe, or TPD of chemisorbed ammonia are mostly used. In particular, FT-IR spectroscopy of adsorbed pyridine (Py, as base probe) allows to determine the amount and strength of acid sites, distinguishing between Brønsted and Lewis acidity.<sup>[149,150]</sup> On the other hand, TPD of ammonia<sup>[151]</sup> allows to determine the amount of weak, medium and strong acid sites, without distinguishing the type of acid sites.<sup>[152,153]</sup> The chemical environments of the Si and Al sites may be evaluated by <sup>29</sup>Si and <sup>27</sup>Al Magic Angle Spinning Nuclear Magnetic Resonance (MAS NMR) spectroscopy, respectively, which may give insights into the types of acid sites.<sup>[154,155]</sup>

Brønsted and Lewis acid sites of zeolites may initiate catalytic reactions *via* proton transfer or hydride abstraction,<sup>[147,156,157]</sup> and negatively charged framework oxygen may stabilize intermediates such as carbenium ions.<sup>[158,159]</sup> In olefin oligomerization systems, the Lewis acidity may enhance conversion and promote the formation of branched oligomers. Intracrystalline Brønsted acid site density tends to favor the catalytic activity leading to higher diesel production.<sup>[160,161]</sup> The formation of long chain linear oligomers (contributing to high cetane number (CN) and viscosity) may be favored by Brønsted acid sites located on the internal surface of the crystals. On the other hand, high density of Brønsted acid sites on the external surface of the crystals may lead to the formation of short chain highly branched oligomers, due to the lack of shape-selectivity effects. The elimination of the outer surface acidity is possible *via* treatment with bulky amines or acids.<sup>[47]</sup> For instance, propene oligomerization over ZSM-5 treated with 4-methylquinoline led to the formation of linear oligomers.<sup>[162]</sup> The same reaction over ZSM-23, ZSM-22 and ZSM-35 treated with oxalic acid,<sup>[163]</sup> and ZSM-23 treated with bulky 2,4,6-collidine<sup>[164]</sup> also led essentially to the formation of linear oligomers.

An important feature of zeolites is that their pore openings, channel intersections and/or cages are of molecular dimensions (0.2-1.5 nm), and thus these materials may act as molecular sieves (Figure 2.15).<sup>[142,165]</sup> The geometric features of the microporous systems may impose shape-selectivity effects on the reactions. Shape-selectivity is an important concept in olefin oligomerization. The catalytic performance of zeolites in olefin oligomerization may depend on a favorable distribution of Brønsted acid sites inside regular pores of molecular dimensions, where the initiation step of the oligomerization reaction occurs.<sup>[11,81]</sup> As the kinetic diameters of the olefins increase with respect to the pores sizes of the molecular sieve, the access to the internal pore system may be more difficult or not

possible.<sup>[166–168]</sup> The catalytic properties may be modified by changing the Si/Al ratio of the synthesized zeolites, and/or by post-synthesis treatments.<sup>[114,161]</sup>

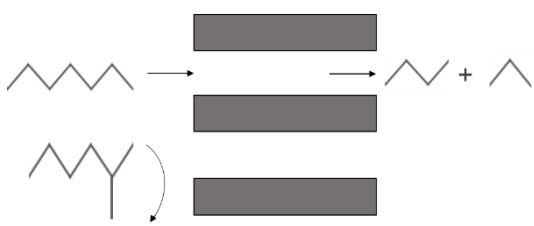
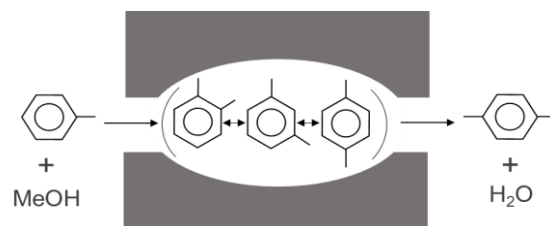
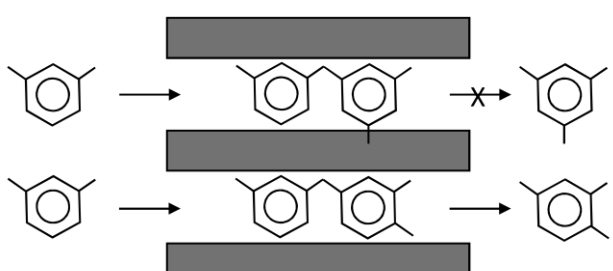
There are essentially three main types of shape-selectivity in zeolites: reactant, product and transition state shape-selectivity (Table 2.11).<sup>[52,142,165]</sup> Zeolites, with their well-defined pore dimensions, may discriminate reactants and products by size and shape (channel differentiation<sup>[169]</sup>). The reactant and product shape-selectivity have their origin in mass transfer effects and steric hindrance, which may be enhanced (or avoided) by using larger (or smaller) crystals of the same zeolite, *i.e.* by lengthening (or shortening) the intracrystallite diffusional paths; alternatively, different types of zeolites with slightly narrower (or wider) pores may be used. Product selectivity may be verified when the products present significant differences in diffusivity through a given microporous system.<sup>[52,142,165,169,170]</sup> The transition state shape-selectivity is not trivial to assess experimentally, and may depend on the surface chemistry and structural constraints associated with the zeolite cavities.<sup>[169,170]</sup> Shape-selectivity in zeolites can be a more complex phenomenon, with several concepts being reported in the literature, such as: molecular traffic control, inverse shape-selectivity, nest effect, cage or window effect and pore mouth and key–lock catalysis.<sup>[99,165,167,171,172]</sup> For instance, the molecular traffic control is common in zeolites with different types of channels like ZSM-5 (sinusoidal and linear pore channels), because different molecules have preferential diffusion paths depending on their size/geometry of the channels. For example, while *n*-paraffins may diffuse preferentially through sinusoidal channels, isoparaffins and aromatics may diffuse preferentially through linear channels.<sup>[173]</sup>

An important drawback of zeolites is that the microporous systems may lead to mass transfer limitations. In this sense, various strategies were developed in recent years to enhance the accessibility to the active sites and avoid internal mass transfer limitations in zeolites (discussed ahead in section 2.3.3). Diffusion in zeolites may control the overall reaction process. Three diffusion mechanisms may occur, depending on the characteristics of the diffusing molecules and the porous structure, namely: restricted or configurational diffusion, Knudsen diffusion, and bulk or molecular diffusion (Figure 2.17).<sup>[174–176]</sup>

Restricted, configurational or intracrystalline diffusion (typical of microporous zeolites) occurs when the sizes of the molecules are similar to the cross section of the

channels in which they are diffusing, and thus the diffusion may be relatively slow. This mechanism depends on the reactant molecules' size and polarity, the zeolite's composition, crystallite size and morphology, channel geometry, connectivity and dimensions, presence of carbonaceous deposits on the internal surface, and reaction temperature. Configurational diffusion may lead to mass transfer limitations and catalyst deactivation due to pore blockage (organic matter that builds-up inside the microporous system).<sup>[177]</sup> Knudsen diffusion (typical in mesopores) occurs when the mean free path of the diffusing molecules is significantly greater than the cross section of the pores, and the molecular motion occurs by free flight interrupted by momentary adsorption on the wall and desorption; the Knudsen diffusivities are several orders of magnitude higher than the configurational ones. In the bulk or molecular diffusion mechanism (typical in macropores), the molecules diffuse freely through the catalyst pores.<sup>[174,175]</sup>

Table 2.11. Types of shape-selectivity of zeolites. Adapted from ref. [52].

<p><b>Reactant shape-selectivity</b><sup>[142,165]</sup></p> <p>The pore openings of some zeolites only allow some reactants to diffuse through the channels and reach the active site.</p> 	<p><b>Product shape-selectivity</b><sup>[52,142,165]</sup></p> <p>Refers to different diffusivities of the reaction products formed inside the pores or entrapment of some products inside cavities and channels.</p> 
<p><b>Restricted transition state/intermediate shape-selectivity</b><sup>[165]</sup></p> <p>The formation of certain intermediates is more or less sterically hindered depending on the pore size and shape, thus only certain intermediate configurations are possible.</p> 	

While the reactions at active sites on the internal surface may be subjected to shape-selectivity, the active sites located on the external surface present no size or shape restrictions.<sup>[47]</sup> Thus, the product selectivity may be changed when reducing the external/internal surface area ratio.<sup>[11,174]</sup> In oligomerization processes, the coking of the catalyst is an important deactivation phenomenon. Coke formation may be favored when no steric hindrance exists, or when the pore system is too small that the products cannot diffuse out of the pores and react further.<sup>[166]</sup>

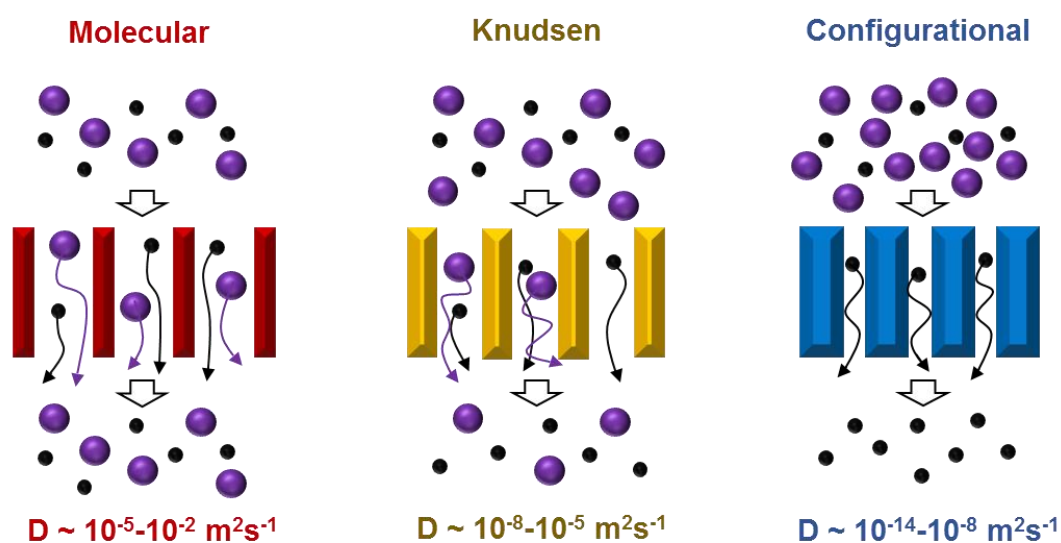


Figure 2.17. Effect of pore size on the diffusion of large (purple) and small (black) molecules within macropores (red), mesopores (yellow) and micropores (blue), with indication of the approximate ranges of diffusivities. Adapted from ref. [178].

### 2.3.3. Improved versions of zeolites

Conventional zeolites are typically prepared in the laboratory (small scale) *via* the sol-gel synthesis method, comprising a series of sequential steps, as illustrated in Figure 2.18. The sol-gel method involves the transformation of the synthesis aqueous solution containing sources of silicon and aluminum (pure chemicals or minerals), alkaline agent, and structure directing agents (SDAs, typically organic amine or alkyl ammonium compounds), into a hydrogel (crosslinked polymeric network structure, capable of retaining considerable amounts of water), comprising silicate species. The synthesis procedure can be divided into

the following main steps: formation of the hydrogel (*via* hydrolysis, polycondensation and gelation), ageing, separation of the solid-phase (decantation, filtration or centrifugation depending on the solid particle sizes), washing of the solid with water, thermal treatment (drying and calcination) to remove the solvent and synthesis compounds, formulation and catalyst activation.<sup>[179–182]</sup>

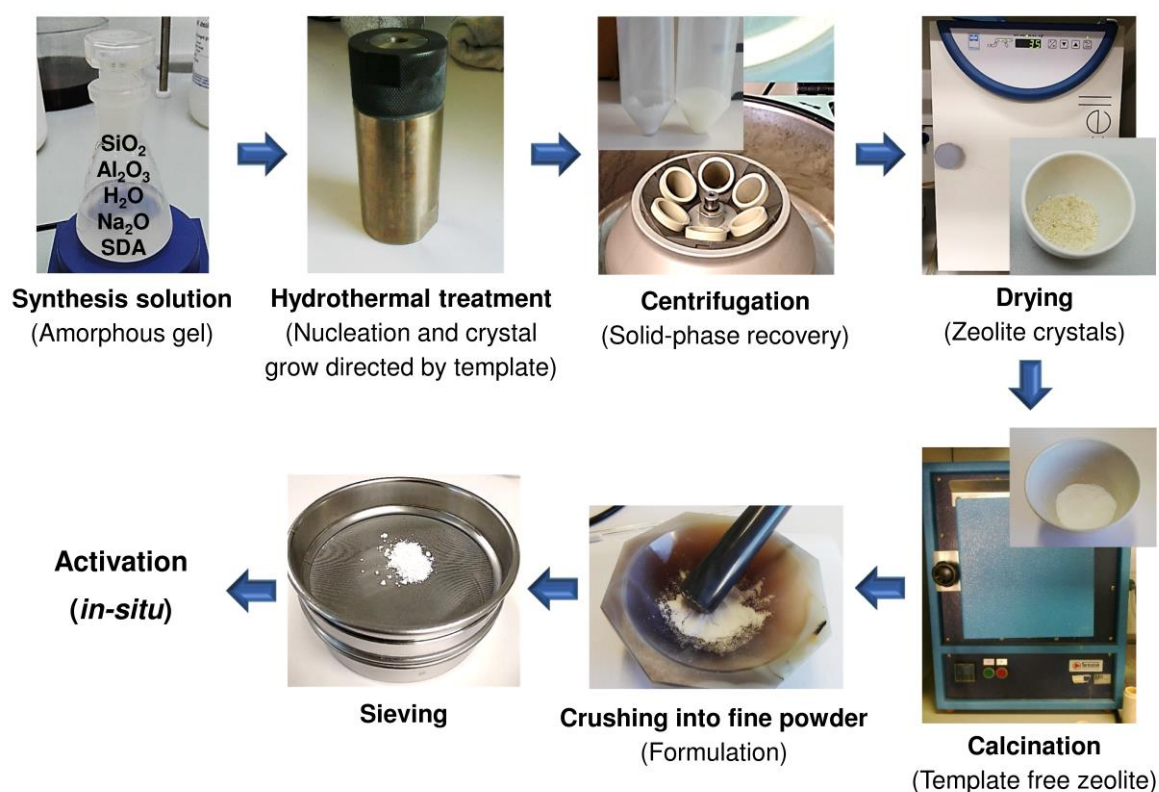


Figure 2.18. Typical operations involved in zeolite synthesis.

The ageing at high temperature is a critical step for the formation of the desired zeolite. In this step, it occurs the dissolution of the gel to form clusters of  $\{\text{SiO}_4\}$  and  $\{\text{AlO}_4\}$  (building blocks of zeolites), polymerization of the clusters and crystallization of the zeolite seeds around the SDA producing the porous network, stiffening and shrinkage (expulsion of the liquid from the pores).<sup>[182]</sup> Ageing is usually performed under hydrothermal conditions in an autoclave (100–300 °C and autogenous pressure), being important variables the time, temperature and stirring rate. At the end of the hydrothermal treatment, the zeolite containing

the occluded organic template is calcined to remove the SDA and desorb water and volatile compounds from the pores. After synthesis, the obtained solid may be a powder or formulated into pellets or granulates with desirable shape and size, depending on the type of reactor, hydrodynamics, and heat and mass transport aspects. Increasing the particle resistance towards crushing and abrasion, with binders (*e.g.*, *via* impregnation) may be useful to minimize bed pressure drops and temperature gradients. Prior to the catalytic reaction, the catalyst may be activated inside the reactor (*in-situ*), in an inert atmosphere (*e.g.*, He, N<sub>2</sub>); activation is not considered strictly to be a preparation procedure.<sup>[179]</sup>

The sol-gel method is versatile and allows a good control over composition, homogeneity, and textural and structural properties of the final product. The versatility of this preparation method lies on the number of parameters that can be varied in different steps, such as: type and amounts of raw materials (SiO<sub>2</sub> and Al<sub>2</sub>O<sub>3</sub> contents), concentration of water and SDAs, pH, temperature, pressure and time, which influence the type of framework and zeolite properties (Table 2.12).<sup>[179,180]</sup>

Table 2.12. Effect of several processes parameters on the final zeolite properties.<sup>[179,183]</sup>

<b>Parameters</b>	<b>Affected properties</b>
Solution composition	Phase, purity, composition
SDA	Phase, homogeneity
Template and additives	Morphology, textural properties
pH	Phase
Temperature	Phase, textural properties
Solvent	Crystallinity, textural properties
Mixing sequence	Composition, homogeneity
Aging	Purity, crystallinity, textural properties

Zeolite catalysts benefit from structure crystallinity, and well-defined pore sizes (which confer them shape-selectivity properties), large internal specific surface area, surface chemistry (furnished with active sites), hydrothermal stability, mechanical strength, recovery/regeneration via relatively easy procedures.<sup>[183]</sup> However, the ordered microporous systems of zeolites may account for mass transfer limitations in reaction systems involving

relatively bulky molecules, hinder the access of reactants to the active sites and suffer pore blockage by organic products causing fast catalyst deactivation.<sup>[142,168,184]</sup>

During the last decade, various strategies were used to prepare zeotypes (*i.e.* modified zeolites) possessing reduced steric hindrance inside the micropores, enhanced accessibility to the active sites and high specific surface area,<sup>[140,185,186]</sup> such as:

- Synthesis of zeolites with crystallite sizes in the nanometer range (<100 nm);<sup>[187–189]</sup>
- Synthesis of zeolitic composites consisting of nanocrystalline zeolites embedded in a mesoporous matrix (*e.g.*, of the type MCM-41, SBA-15, TUD-1), where the mesoporous phase is interconnected with the microporous phase;<sup>[190,191]</sup>
- Delamination of layered zeolite precursors to form accessible zeolitic nanosheets (few nanometers thick) with enhanced external surface area;<sup>[192–194]</sup>
- Introduction of mesoporosity (2-50 nm width, according to the IUPAC classification<sup>[144]</sup>) in zeolites *via* post-synthesis modifications or hydrothermal synthesis, giving the so-called hierarchical zeotypes (possessing micro- and mesoporosity).<sup>[185,195]</sup>

Interest in hierarchical materials is growing rapidly due to their great potential in different areas.<sup>[196,197]</sup> There are different approaches for introducing mesoporosity in zeolites, which may be categorized in two types: destructive or top-down approaches, and constructive or bottom-up approaches (Figure 2.19).<sup>[185]</sup> Regardless of the preparation method, catalytic reactions over hierarchical zeotypes benefit from facilitated mass transfer (diffusion) and enhanced accessibility to the active sites, which account for higher catalytic activities and longer catalyst lifetimes than conventional microporous zeolites, impacting positively on productivity.<sup>[198]</sup> There exist several review articles concerning hierarchical materials.<sup>[140,185,186,195,199]</sup> Table 2.13 summarizes the main advantages and disadvantages of different approaches.

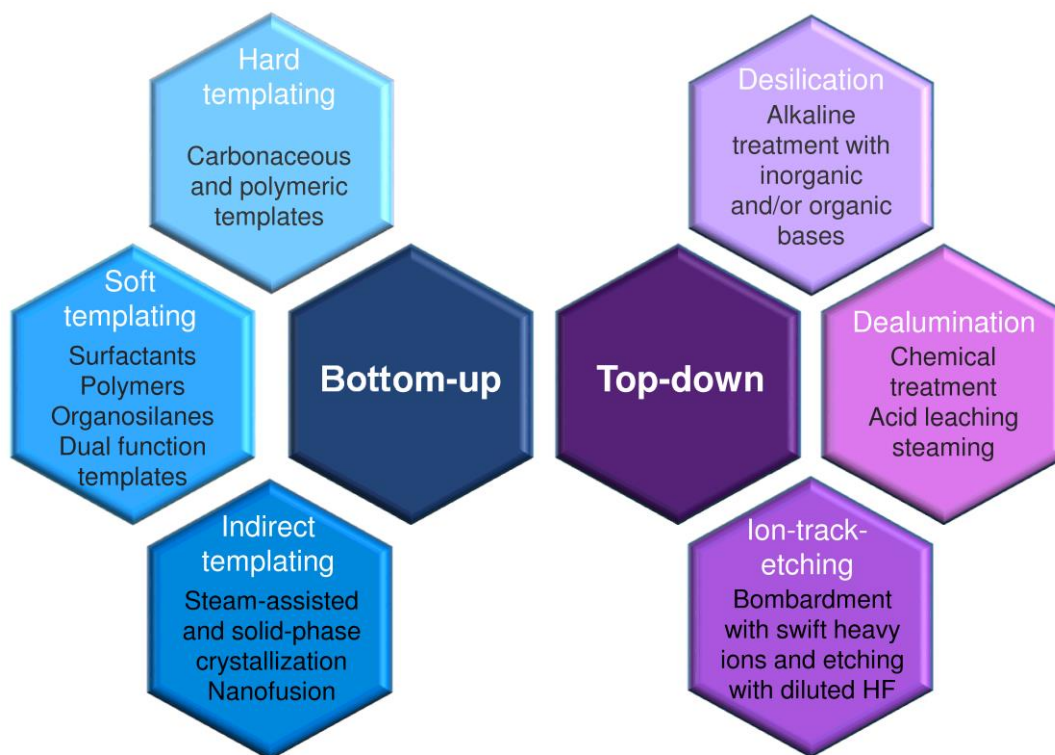


Figure 2.19. Bottom-up and top-down strategies for synthesizing hierarchical zeolites.

***Top-down approach to hierarchical zeotypes - desilication.*** Desilication consists of extraction of silicon from the zeolite framework *via* alkaline treatment under controlled conditions. This process may be preferentially initiated at boundaries or defect sites of the zeolite crystals, resulting in lower Si/Al ratio and formation of mesopores.<sup>[140,185]</sup> The role of framework aluminum is important in this process (Figure 2.20). Si/Al ratios in the range 25-50 of the MFI precursor zeolite seem adequate for desilication in a controlled manner with significant generation of mesoporosity, while preserving microporosity and acid properties. For zeolites with lower Si/Al ratio (<25), the high aluminum content stabilizes the surrounding silicon atoms, suppressing the extraction of silicon from the framework and preferential dissolution of the crystal boundaries may occur; this results in low degree of mesoporosity. In order to enhance the mesoporosity in these materials, severe treatment conditions may be required, affecting considerably the crystallinity and acid properties. On the other hand, for zeolites with high Si/Al ratio (>50), the dissolution of silica may be excessive, leading to lower mesoporous specific surface area.<sup>[185,200]</sup> Besides the framework Si/Al ratio, the alkaline treatment conditions such as treatment temperature, time, type and concentration of base are important parameters influencing the desilication process.

Increasing the temperature (55-65 °C), time (15-30 min) and base concentration, contributes to a higher degree of mesoporosity. However, if the conditions are too severe, loss of mechanical resistance and acidity may occur.<sup>[201,202]</sup>

The degree of mesoporosity produced by the desilication treatment may be determined as the hierarchy factor (HF),<sup>[203]</sup> Eq. (1), or the indexed hierarchy factor (IHF),<sup>[204]</sup> Eq. (2). These factors give a measure of the changes in textural properties of the zeolite, enabling comparisons between different materials. The higher the values of HF and IHF, the higher the degree of mesoporosity.

$$HF = \frac{V_{\text{micro}}}{V_{\text{p}}} \times \frac{S_{\text{meso}}}{S_{\text{BET}}} \quad (1)$$

$$IHF = \frac{V_{\text{micro}}}{V_{\text{micro,max}}} \times \frac{S_{\text{meso}}}{S_{\text{meso,max}}} \quad (2)$$

where  $V_{\text{micro}}$  and  $V_{\text{p}}$  are the micropore and total pore volumes of the desilicated zeolite, respectively;  $S_{\text{meso}}$  and  $S_{\text{BET}}$  are the mesoporous and BET specific surface areas of the desilicated zeolite, respectively;  $V_{\text{micro,max}}$  and  $S_{\text{meso,max}}$  are, respectively, the maximum micropore volume (corresponding to that of the parent zeolite) and the maximum mesoporous surface area (corresponding to that of the desilicated sample possessing the highest mesoporous surface area).

Organic bases (*e.g.*, tetrapropylammonium hydroxide (TPAOH) and tetrabutylammonium hydroxide (TBAOH)) may be used as desilication agents, but require treatment at higher temperature and/or longer time than inorganic bases (*e.g.*, NaOH), since the former bases are less effective for silicon dissolution. The relatively bulky tetraalkylammonium cations ( $\text{TPA}^+$  or  $\text{TBA}^+$ ) may interact with the zeolite external surface, leading to steric effects that may protect the zeolite crystals against the  $\text{OH}^-$  attack. The dissolution rates are lower than those for inorganic bases, allowing a more controlled desilication process, leading to the lower degree of mesoporosity (and smaller pores), while significantly preserving the microporosity. Moreover, treatments with organic bases do not require a final ion-exchange step to obtain the protonic form of the zeolite, since the ammonium ions are decomposed to protons during the calcination step.<sup>[205–208]</sup>

Several strategies may be used to overcome the constraints discussed above, associated with the Si/Al ratio of the starting zeolite (Figure 2.20). A two-step procedure involving the addition of high concentrations of an alkali aluminate solution (*e.g.*, sodium aluminate) as desilication agent, with subsequent acid washing (to remove silicate debris and alkali ions), may favor the desilication of zeolites with Si/Al ratio in the range 2-1000.<sup>[209]</sup> The degree of Si leaching in sodium aluminate solution is much lower than in NaOH solution, since the  $\text{Al}(\text{OH})_3$  species formed form a protective barrier/layer on the external surface hindering silicon extraction by  $\text{OH}^-$ . Thus desilication occurs in a more controlled manner.<sup>[209]</sup> On the other hand, a two-step procedure involving desilication with high concentration of base and subsequent washing with HCl may be effective for zeolites with low Si/Al ratio; the high base concentration will increase mesoporosity, and the acid washing will remove the aluminum-rich debris from the pores. However, the synthesis yields may be less than 50%.<sup>[204]</sup>

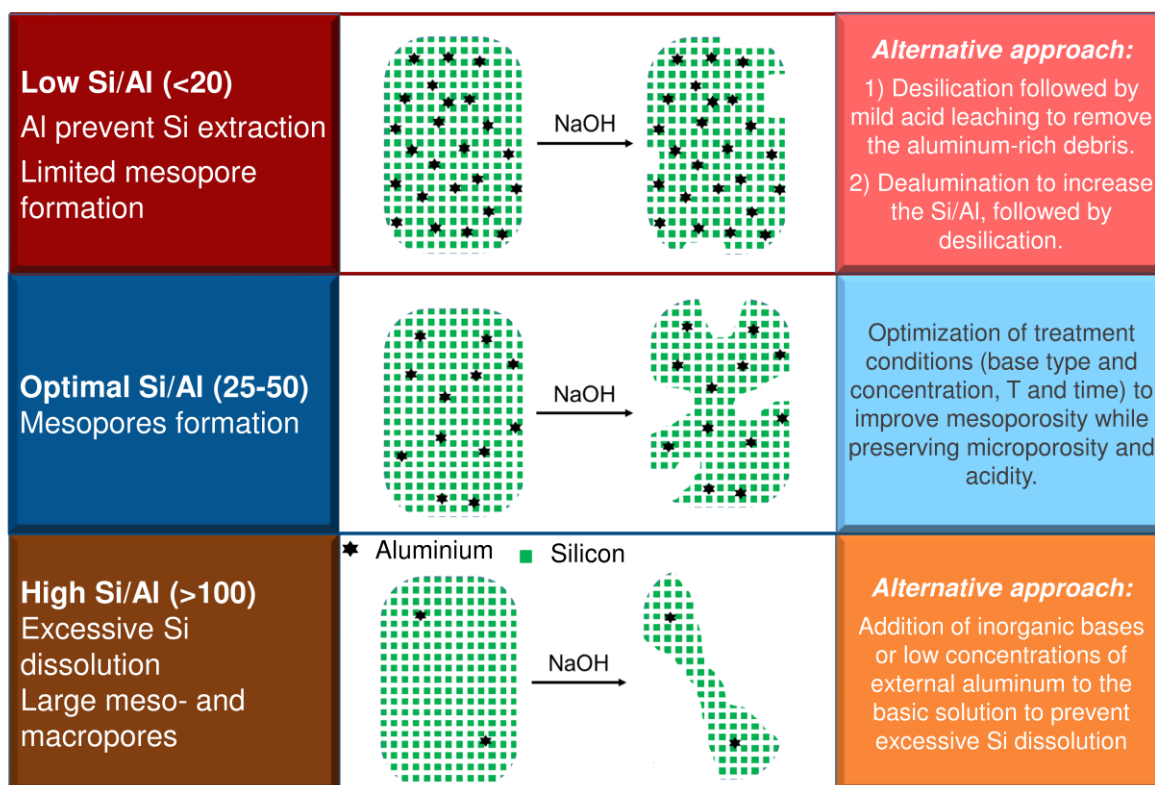


Figure 2.20. Influence of the Al content of precursor MFI zeolites on the desilication treatment, and possible treatments to overcome drawbacks associated with a high or low Al content. Adapted from ref. [200].

Alternatively, the starting zeolite may be dealuminated to increase the Si/Al ratio, prior to the desilication step (dealumination procedures are described ahead).<sup>[210]</sup> In a different approach, mixtures of inorganic and organic bases with optimal ratio of organic/inorganic cations may be effective for desilication of zeolites with high Si/Al ratio, leading to the formation of mesoporosity, while preserving microporosity.<sup>[205]</sup> The addition of low concentrations of an aluminum source to the alkaline solution (*e.g.*, aluminum nitrate that forms  $\text{Al}(\text{OH})_4^-$  complexes under alkaline conditions) is another way of promoting desilication of high Si/Al zeolites, since it will act as pore-directing agent (*i.e.* has the ability to regulate the process of silicon extraction towards mesopore formation), in a similar fashion to that for organic bases, allowing the generation of intracrystalline mesoporosity without excessive Si dissolution (this shows that framework Al is not a mandatory prerequisite for desilication<sup>[205]</sup>).

***Top-down approach - dealumination.*** Dealumination may be accomplished by chemical treatment, acid leaching or steaming. The extraction of aluminum is resultant from the hydrolysis of the Al-O-Si bonds of the zeolite framework, resulting in an increase of the Si/Al ratio and formation of vacancies in the mesopore size range, and partial collapse of the zeolite structure. The type of dealumination treatment and conditions will influence the acid properties of the modified material.<sup>[185,199,211,212]</sup> The chemical treatment may be performed using strong chelating agents (*e.g.*, ethylenediaminetetraacetic acid (EDTA)) or chemicals capable of isomorphic substitution of aluminum for silicon (*e.g.*, ammonium hexafluorosilicate (AFS), silicon tetrachloride).<sup>[213]</sup> The acid treatment involves the use of high concentration of inorganic ( $\text{HCl}$ ,  $\text{H}_2\text{SO}_4$ ,  $\text{HNO}_3$ ) or organic (oxalic, acetic, tartaric) acids.<sup>[214]</sup> The type of acid and the pH influence the effectiveness of the treatment. The steaming treatment (>500-600 °C) of zeolites in the ammonium or protonic form, leads to the hydrolysis of the Al-O-Si bonds and the removal of Al atoms from the framework, creating vacancies that may be repaired by mobile silicon species or may grow to form mesopores; a subsequent mild acid-leaching treatment is performed to remove extra-framework species.<sup>[215]</sup>

**Top-down approach to hierarchical zeotypes - Ion-track-etching process.** This method, developed by Valtchev et al.<sup>[216]</sup>, involves the bombardment of the zeolite crystal with swift heavy ions (SHI: high energy heavy ions that have energy ranging from few tens of MeV to few GeV). As SHI pass through the target zeolite, it is produced latent tracks inside the crystal (induced by linear energy transfer). These tracks are damaged regions with cylindrical shape and diameters ranging from a few nanometers to a few tens of nanometers. This process is followed by etching with diluted HF and subsequently washing with water.<sup>[216]</sup>

**Bottom-up approach to hierarchical zeotypes - hard templating.** The hard templating technique consists of hydrothermal synthesis carried out in the presence of inert porous/hollow carbonaceous or polymeric matrices, with relatively rigid structures. Different materials may be used as hard templates, such as metal-oxide nanoparticles, plant-based materials, resin beads or aerogels, but carbon-based compounds (*e.g.*, carbon nanoparticles, nanotubes and aerogels) are most frequently used.<sup>[195,217–219]</sup> The zeolite crystallization takes place in confined space of cavities/pores, preventing the growth of the zeolite crystals to sizes larger than the sizes of the matrix's pores. In the first step, the solution, containing the reagents and zeolite precursor, fills the pores/cavities of the solid template; then, the crystallization occurs in the hard template by thermal treatment in single or multiple steps. Finally, the template is removed by combustion (for organic templates) or dissolution processes (for inorganic templates) (Figure 2.21). Depending on the interconnectivity degree of the zeolite nanocrystals after the template removal, secondary porosity is formed coming from intra and/or interparticle cavities.<sup>[185,186]</sup>

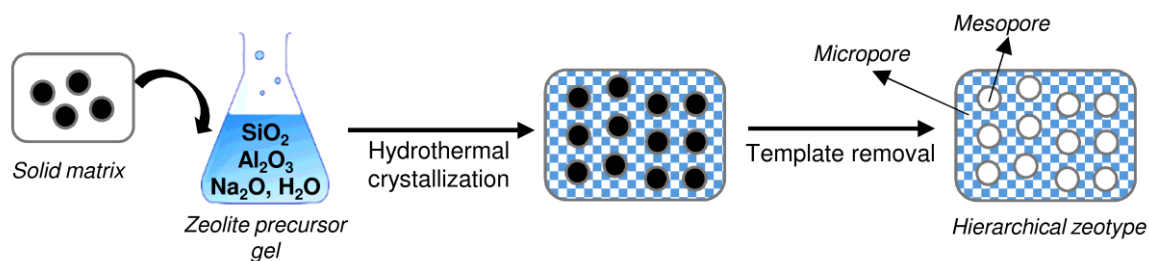


Figure 2.21. Hard templating method to prepare hierarchical zeolites. Adapted from ref. [220].

***Bottom-up approach to hierarchical zeotypes - soft templating.*** The soft templating approach consists of a hydrothermal synthesis using aluminum and silicon precursors, plus micropore and mesopore SDAs. The micropore SDAs are usually those employed in the preparation of conventional zeolites, whereas the mesopore SDAs are (macro)molecular templates with inherent flexibility, such as: surfactants, soluble polymers, organosilanes, silylated polymers and cationic polymers.

Surfactants may self-organize to give micelles, which prevent the aggregation of the zeolites nanocrystals, leading to mesoporosity. On the other hand, polymers may lead to the formation of mesoporosity in zeolites *via* inclusion in the zeolite crystals or by assisting in the aggregation of zeolite particles, leading to interparticle mesoporosity.<sup>[217,220]</sup>

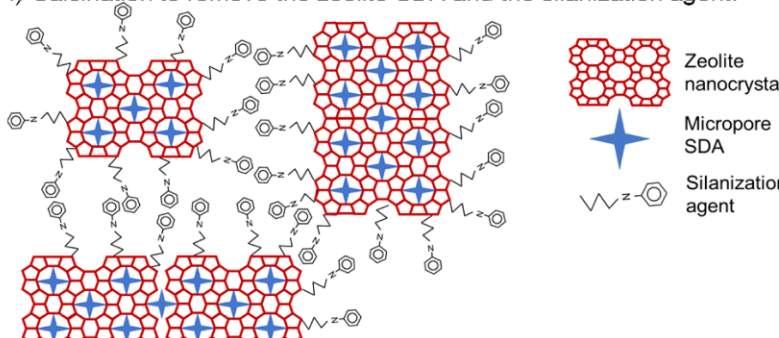
Novel soft templates possessing dual functionality, *i.e.* able to simultaneously generate micro and mesoporosity, were reported recently, such as dual function polyquaternary ammonium surfactants (*e.g.*, [3-(trimethoxysilyl)propyl]hexadecyldimethylammonium chloride (TPHAC)<sup>[221]</sup> and dual function polymers (*e.g.*, polydiallyldimethylammonium chloride (PDADMAC),<sup>[222]</sup> dimethyldiallyl ammonium chloride acrylamide (PDD-AM)<sup>[223]</sup>). These templates are furnished with micropore directing multi-ammonium centers, responsible for nucleating the zeolite domains, and on the other hand, “mesopore directing alkyl tails” responsible for the formation of mesoporous channels.

Organosilanes may be used as soft templates, which are anchored to zeolitic nanoparticles/seeds *via* reaction with external surface silanol groups, leading to the formation of organofunctionalized zeolitic structures. Subsequent crystallization gives organic-inorganic composites. This process avoids the zeolite growth into larger crystals. The organic groups are removed *via* calcination resulting in secondary porosity (porosity not associated with the zeolite structure). The size, configuration and chemical nature of the organosilane, and the temperature of the crystallization step, influence the properties of the hierarchical zeotype (*e.g.*, morphology, texture).<sup>[185,224]</sup> Depending on the type of silanization agent employed, the crystallization process may differ: crystallization of silanized protozeolitic nanounits,<sup>[198,225]</sup> crystallization using amphiphilic organosilanes

(acting as dual function templates),<sup>[221,226]</sup> and crystallization using silylated polymers (

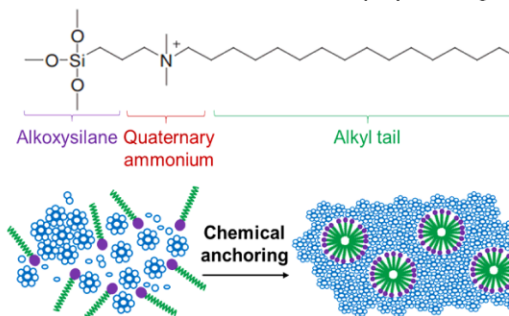
### Crystallization of silanized protozeolitic units

- 1) Pre-crystallization of the synthesis gel to promote the formation of small zeolitic seeds or protozeolitic units.
- 2) Functionalization of the external surface of the zeolitic seeds with the organosilane, forming a protective layer.
- 3) Crystallization of the functionalized zeolite gel under hydrothermal conditions.
- 4) Calcination to remove the zeolite SDA and the silanization agent.



### Crystallization with amphiphilic

- 1) Attachment of the Si-OH groups of the hydroxylated zeolite (-Si-(OH)<sub>3</sub>) to Si species in the synthesis gel, forming aluminosilicate species or external hydroxyl groups.
- 2) Formation of mesoscale micellar structures between the chain alkyl tails, while the inorganic part grows from the crystal seeds, with the contribution of the quaternary ammonium group, acting as micropore SDA.
- 3) Calcination to remove the amphiphile organosilane.



### Crystallization with silylated polymers

- 1) Nucleation of the zeolite phase and grafting of the silane-functionalized polymer (silylated polymer) over the external outer surface of the protozeolitic units through covalent Si-O-Si linkages.
- 2) Aggregation of the protozeolitic units into bigger entities and phase-segregation of the incorporated polymer from the zeolite matrix, forming an intracrystal polymer network covalently linked to the zeolite framework.
- 3) Calcination to remove the SDA and the polymer.

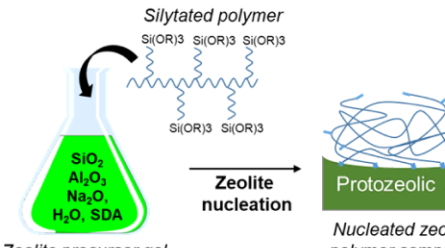


Figure 2.22).

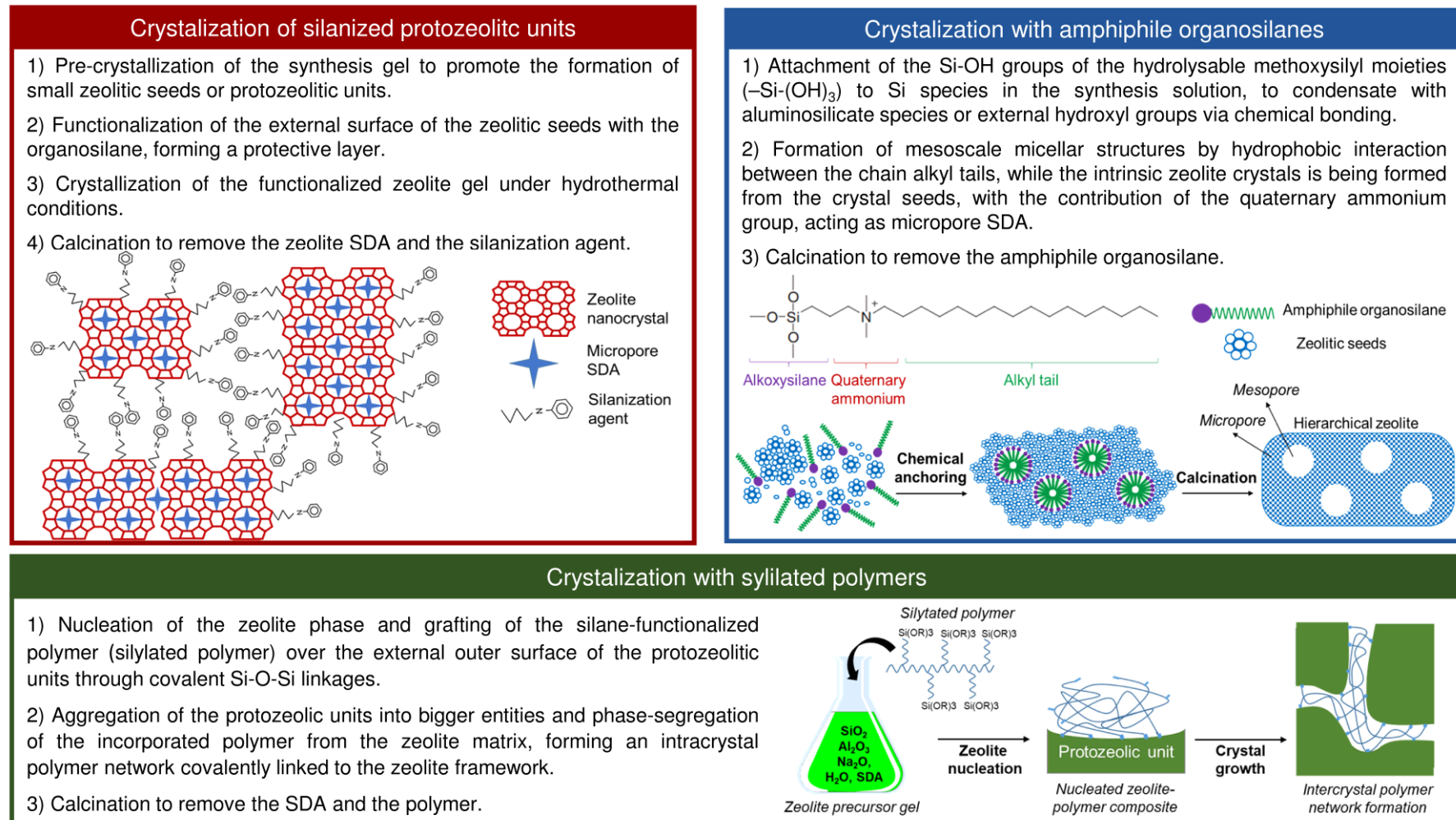


Figure 2.22. Soft templating strategies using organosilanes or silylated polymers. Adapted from refs. [221,227,228].

**Bottom-up approach to hierarchical zeotypes - indirect templating.** The indirect templating methods involve the assemble of zeolite nanoparticles into larger mechanically resistant aggregates possessing mesoporosity, without additional templates for the mesophase. There are several protocols reported in the literature, such as: steam-assisted crystallization/conversion (SAC),<sup>[229]</sup> solid-state crystallization,<sup>[230]</sup> nanofusion,<sup>[231]</sup> ultrasounds-assisted method,<sup>[232]</sup> synthesis using natural clays as raw materials (*e.g.*, kaolin<sup>[233]</sup> and rectorite<sup>[234]</sup>), crystallization of the amorphous walls of mesoporous materials<sup>[235,236]</sup> and other methods discussed in review articles<sup>[237]</sup>.

The solid-state crystallization and SAC methods involve crystallization of an aluminosilicate dry gel (containing the micropore SDA) in the solid state, and treatment with water vapor, respectively, in an autoclave, as illustrated in Figure 2.23.<sup>[185]</sup> In the SAC method, firstly the dense dry gel is prepared by solvent evaporation (at high temperature) of the precursor gel, followed by steam treatment. The steam leads to very high nucleation rate and formation of a large amount of individual nucleation centers; then crystallization of the nucleation centers during the initial stages of the SAC treatment gives nanocrystallites. The small crystallites form aggregates with mesoporosity corresponding to interparticle voids. For both methods, the water content is a critical parameter for crystallization (to provide fast nucleation and recrystallization into ordered, crystalline networks).<sup>[229]</sup>

In the solid-state crystallization method, the aluminosilicate nanogels are formed by sol-gel process at relatively low temperature, with subsequent solvent evaporation (at low temperature, with control over the dehydration level of the solid), resulting in amorphous aluminosilicates. These are then converted to nanocrystals upon thermal treatment (involving hydrolysis with water present in the solid, and condensation of silicon and aluminum species). Then, adjacent nanogels are brought together as large ensembles, by weak solid-solid interactions, forming nanocrystals. The stacking or aggregation of the nanocrystals gives rise to mesoporosity corresponding to intercrystal voids.<sup>[230]</sup>

The nanofusion method involves the preparation of a highly concentrated precursor solution (containing the micropore SDA) that is subjected to hydrothermal treatment, resulting in the formation of a viscous translucent gel containing individual nanoparticles. Then, the viscous gel is immediately dried giving a powder of compacted particles corresponding to the hierarchical zeotype.<sup>[231]</sup>

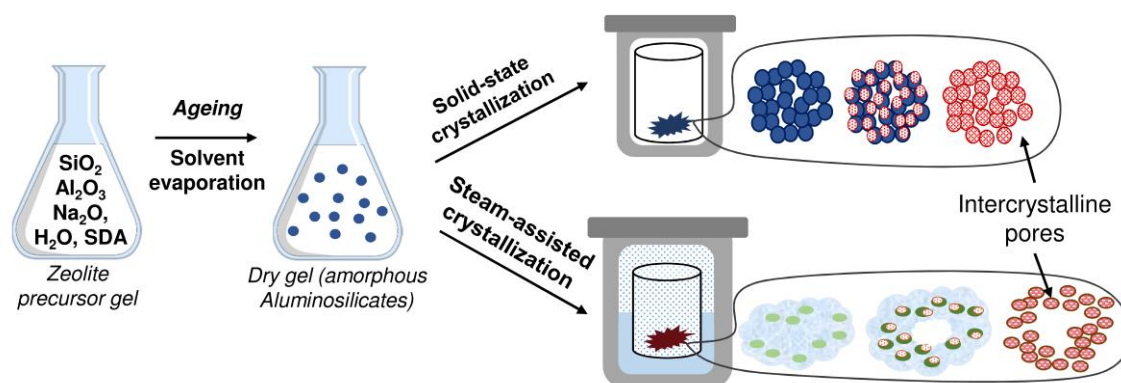


Figure 2.23. Solid-state and steam-assisted crystallizations methods. Adapted from refs. [238,239].

In the ultrasounds-assisted method, the zeolite precursor mixture is subjected to a short ultrasonic treatment involving hot spot heating (from collapse of steam bubbles) and sufficient energy is released to overcome the interparticle forces, without affecting the chemical bonding. Subsequently, the mixture is vigorously stirred for some time to promote the aggregation of nanoparticles to give larger zeolite particles, which will allow the formation of intracrystal mesopores during crystallization under hydrothermal conditions (Figure 2.24).<sup>[232]</sup> The ultrasonic treatment and the stirring have a critical role in the success of this synthesis process.<sup>[232]</sup>

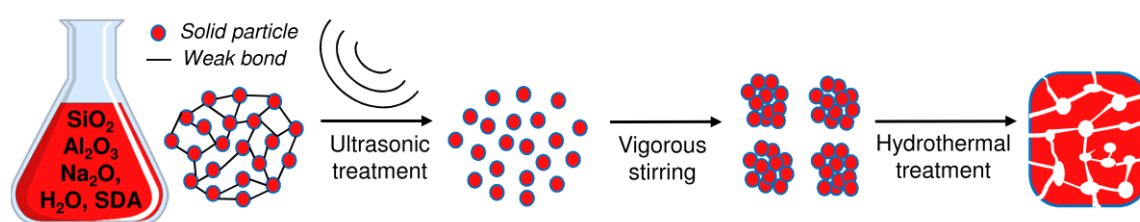


Figure 2.24. Ultrasounds-assisted method. Adapted from ref. [232].

Table 2.13. Strategies for introducing mesoporosity in zeolites.<sup>[140,185,199,217,224,237]</sup>

<b>Advantages</b>	<b>Disadvantages</b>
<b><i>Desilication/dealumination</i></b>	
<p>Simple, versatile, low-cost.</p> <p>Reproducibility of desilication may be remarkably good.</p> <p>Desilication in a continuous manner was accomplish with good quality of the final product, being suitable for high-scale production.</p>	<p>Destructive technique (mass loss of zeolite).</p> <p>Changes in acidity and possible reduction of crystallinity.</p> <p>Desilication is efficient for a specific Si/Al range (<i>e.g.</i>, 25-50 for MFI zeolites).</p> <p>Dealumination induces partial amorphization of the zeolite and passivation of the surface by deposition of amorphous matter. The mesopores may be random and not interconnected to form a mesoporous network.</p>
<b><i>Ion-track</i></b>	
<p>Allows to create parallel distribution of meso/macropores.</p>	<p>Use of uranium and the scale-up of this procedure are not straightforward.</p>
<b><i>Hard templating</i></b>	
<p>Hard templates are chemically inert, structurally diverse and easy to remove by combustion or dissolution.</p> <p>Common and versatile method, applicable to a wide range of zeolites, being economic considering that it involves few steps to synthesize the final product.</p> <p>Compared with demetallation, this approach allows simultaneously high crystallinity and uniform mesoporosity, and to tailor the pore architecture by using templates with different shapes and textures.</p>	<p>The preparation of ordered mesoporous matrices may be expensive and time-consuming.</p> <p>Loss of somewhat expensive template (removed <i>via</i> calcination). The severity of the calcination conditions may damage the microporous structure of the zeolite, resulting in lower mechanical resistance.</p> <p>Polymeric matrices are thermally sensitive, thus the crystallization temperature needs to be adjust by the glass transition temperature of the polymeric material.</p>

Table 2.13. (continued).

Advantages	Disadvantages
<b><i>Soft templating with surfactants</i></b>	
<p>Allows a more precise control of the mesopore size distribution compared to hard templating method, and the zeolite structure is well preserved.</p>	<p>Time-consuming methods and very dependent on the synthesis conditions. The operational window concerning chemical composition is relatively narrow.</p> <p>Surfactants are expensive and involve complex preparation processes, which restrict their industrial application.</p> <p>Phase separation may occur, since the surfactants may separate from the zeolite domains during crystallization.</p>
<b><i>Soft templating with dual function templates</i></b>	
<p>The cost-factor can be reduced by employing small amounts of template or using cheap dual function templates, which are commercially available.</p> <p>Avoids phase separation.</p>	<p>The zeolitic microporous structure may be favored over the formation of mesopores, or <i>vice-versa</i>.</p>
<b><i>Soft templating with organosilanes</i></b>	
<p>Organosilanes exhibit high affinity for aluminosilicate species and a large number is commercially available.</p> <p>The mesopore diameter could be easily tuned by changing the chain length of the organosilanes.</p> <p>Applicable to several zeolite topologies.</p> <p>Prevents phase separation and gives materials with very high BET and mesopore specific surface area and high synthesis yields (when using organosilanes).</p> <p>Relatively uniform mesopore size distribution (when using silylated polymers and amphiphile organosilanes).</p>	<p>High cost of organosilanes.</p> <p>Few silylated polymers and amphiphile organosilanes are commercially available.</p> <p>Broad mesopore size distribution (when using organosilanes).</p> <p>Reproducibility and crystallinity issues (when using amphiphile organosilanes).</p>

Table 2.13. (continued).

Advantages	Disadvantages
<b><i>Soft templating with organosilanes</i></b>	
<p>Avoids phase separation (when using amphiphile organosilanes).</p> <p>The synthesis using amphiphilic organosilanes gives zeotypes possessing mesopore walls with large amounts of silanol groups, thus being feasible for organic functionalization by post-synthesis treatment.</p>	
<b><i>Indirect templating</i></b>	
<p>Simple and less expensive, since it does not require a secondary template.</p> <p>Gives hierarchical zeotypes with short intraparticle diffusion pathways and not very large external surface area.</p> <p>Solid-state crystallization leads to materials with high crystallinity, good hydrothermal stability, and similar acid properties to zeolites prepared <i>via</i> conventional methods. Does not require expensive templates, nor high quantity of solvents, reducing the toxic liquid waste.</p> <p>Nanofusion is a simple route to tune the size of the interstitial mesopores and gives high synthesis yields.</p> <p>The ultrasounds-assisted method is a facile and economic route to materials with high stability and enhanced acidity.</p> <p>In the SAC method, the crystallization proceeds faster, and the consumption of SDA is minimized. No need for wastewater treatment or secondary processing. The hierarchical zeotype may be obtained with the same Si/Al ratio of the precursor gel. Allows to obtain materials with Si/Al ratios that are otherwise difficult to obtain. Prevents phase separation.</p>	<p>Compared with hard and soft templating routes, indirect templating is still a less general method to extend to different zeolite topologies synthesis.</p> <p>Successful synthesis always depends on the rigorous conditions. For instance, inadequate stirring in the ultrasounds-assisted method will lead to the formation of nanosized zeolites instead of hierarchical zeolites.</p> <p>The methods have relatively low control on the mesopore size.</p> <p>For some methods, the mechanism of the formation of mesopores is still unclear.</p> <p>The SAC method is very sensitive to the amount of water, thus the water content needs to be adjusted for the amount of sample loading, temperature and reactor volume, which may create upscaling issues. In this method, the potential reactor volume is reduced, since it is necessary to separate the dry gel (inside the reactor) from the water used for steam production (surrounding the reactor which is inside an autoclave).</p>

### 2.3.4. Catalytic performances of zeolites/zeotypes for propene and butenes oligomerization

This section presents the state of the art of the catalytic oligomerization of propene and butenes over zeolites and other silicates, carried out in fixed-bed reactors, in resemblance to the industrial technologies (Table 2.15 and Table 2.16). The following aspects are discussed with the objective of producing high molecular weight products (C<sub>10</sub><sup>+</sup>): the influence of the zeolite framework, porous system and Al content on the catalytic performance, as well as the incorporation of different metals in the catalysts; improved shape-selectivity due to poisoning of the external surface acid sites, and facilitated mass transport associated with reduced crystal sizes of the catalysts or the existence of mesoporosity; olefins scope and the influence of the operating conditions.

The oligomerization of ethene was not included in this overview, since (i) ethene possesses relatively low reactivity and the reported catalysts are predominantly homogeneous and contain transition metals, distinct from that for larger olefins; moreover, scientific research of ethene oligomerization is mostly focused on the production linear  $\alpha$ -olefin products as building blocks for producing materials and chemicals such as plastics, lubricants, surfactants (rather than synthetic fuels).<sup>[133]</sup> There are not many research studies using zeolites as catalysts for the oligomerization of heavy olefins, possibly due to important steric constraints.<sup>[240–243]</sup>

***Small, medium and large pore zeolites with different Si/Al ratios.*** Medium pore ZSM-5 zeolite was developed and used by Mobil for the methanol to gasoline (MTG), methanol to olefins (MTO) and Mobil olefins to gasoline and distillate (MOGD) processes.<sup>[60,244,245]</sup> The MOGD process (feedstock consisting of C<sub>3</sub>-C<sub>4</sub> hydrocarbons, with 53 wt.% olefins and 47 wt.% paraffins) using this zeolite allowed good selectivity to high-quality diesel range (C<sub>10</sub>-C<sub>20</sub>) iso-olefinic compounds (which were subsequently hydrogenated to the corresponding iso-paraffins).<sup>[245]</sup> Aiming at improved catalytic results for producing clean synthetic fuels *via* olefin oligomerization, scientists working in the fields of catalysis and materials science have put efforts into developing improved versions of ZSM-5 or exploring different zeolites or related materials. The fact that the pore sizes of ZSM-5 (0.5-0.6 nm) are smaller than the

dimensions of multi-branched molecules (*e.g.*, kinetic diameter in the range 0.5-0.62 nm for 2-methylhexane and 2,2,3-trimethylbutane<sup>[246]</sup>), the branching degree during oligomerization may be restricted *via* shape-selective effects, resulting in improved CN and viscosity properties of the distillates. On the other hand, geometrical constraints imposed by the 10 MR pores of MFI catalysts, together with high Si/Al ratios may avoid extensive coking.<sup>[247]</sup> Small pore zeolites may suffer very rapid deactivation due to coking, whereas large and extra-large pore zeolites may lead to high branching degree in olefin oligomerization.<sup>[83]</sup> On the other hand, the pore dimensions and networks may influence the diffusion of reactants and products, and the overall rate of olefin oligomerization.

Ocelli et al.<sup>[83,248]</sup> reported the oligomerization of propene at high pressure (30-50 bar) and temperature (38-399 °C), over zeolites of different topologies (H-ZSM-5 (MFI), HY (FAU), H-Mordenite (MOR),  $\Omega$  (MAZ), Boralite (MFI)), and possessing different Si/Al ratios. The average molecular size of the oligomers formed was considered to depend mainly on the pore sizes. The branching degree decreased with decreasing pore sizes (nm):  $\Omega$  (1) > HY (0.8) > MOR (0.6-0.65) > ZSM-5 (0.55-0.6) > Boralite (0.55-0.6).<sup>[83,248]</sup> Zeolite  $\Omega$  possessing large pores led to high molecular weight oligomers and high amounts of aromatic products than the remaining zeolites. Fast catalyst deactivation due coking and pore blockage was reported for the large pore zeolites Mordenite and HY, being less pronounced for the MFI catalysts. It is important to evaluate the acid properties. Stronger acidity and acid site density led to rapid coking, formation of aromatics and deactivation (particularly for zeolites HY and Mordenite).<sup>[83]</sup>

Kim et al.<sup>[143]</sup> reported the oligomerization of butenes (15 bar, 350 °C, WHSV=10 h<sup>-1</sup>) over medium pore ZSM-5 (Si/Al=11.5-140) and large pore zeolites Y (Si/Al=2.6-30) and Beta (Si/Al=12.5-150) for production jet fuel type products (C8–C16). The Si/Al ratio may influence the acid properties. It was verified that for all catalysts, excluding zeolite Y, the conversion of butenes and selectivity to jet fuel type products (C8<sup>+</sup>) increased with decreasing Si/Al up to Si/Al=12.5 for Beta (reaching *ca.* 36 % conversion and *ca.* 21 % selectivity), and up to Si/Al=25 for ZSM-5 (reaching *ca.* 80 % conversion and *ca.* 55 % selectivity). Among the studied materials, ZSM-5 with Si/Al=25 led to higher butene conversion and selectivity to jet fuel type products, and was more stable over 6 h on-stream. Zeolites Y and Beta possessed higher amounts of acid sites than ZSM-5, which could not solely explain the poorer performances of the former. A comparative study of the porous

structure of the zeolites indicated that large pore zeolites led to the formation of bulky aromatics responsible for rapid catalyst deactivation, whereas medium pore zeolites were more resistance to coking and led to high-quality middle distillates.<sup>[143]</sup>

Schwarz et al.<sup>[249]</sup> studied the effect of synthesis parameters of ZSM-5 on the catalytic performance for propene oligomerization (50 bar, 220-300 °C, WHSV=12 h<sup>-1</sup>). Increasing the Si/Al ratio of the synthesis gel (20-500) led to an increase of crystallinity (59-99 %) and amount of strong acid sites (0.05-0.46 mmol g<sup>-1</sup>). On the other hand, an increase of synthesis time (1-10 days) led to the growth of the crystal size (0.8-1.2 μm (1-6 days) for Si/Al=40, and 1.8-3.0 μm (1-6 days) for Si/Al=20) and enhanced crystallinity (69-83 % (1-3 days) for Si/Al=40, and 59-71 % (1-6 days) for Si/Al=20). The acidity remained rather similar for the same Si/Al ratio used. Decreasing the Si/Al ratio (20-500) enhanced the catalytic activity (27-99 % conversion at 300 °C). The effect of synthesis time was not straightforward; for Si/Al of 40, increasing the synthesis time up to 6 days enhanced catalytic activity, whereas for Si/Al of 18, the effect was opposite (activity decreased possibly due to changes in morphology for longer synthesis times, which may influence the diffusion and coking phenomena). The best performance was reported for materials possessing average crystal sizes of 1.1-1.2 μm, and 77-83 % crystallinity (Si/Al ratio of synthesis gel=40; synthesis time=3 or 6 days). These catalysts possessed longer lifetime and led to 94-98 % propene conversion (at 270 °C). The material synthesized during 3 days led to approximately 65 % of diesel range products (b.p. 165-343 °C) (determined using the standard ASTM distillation boiling curve), compared to 79 % for the MOGD process<sup>[245]</sup>.<sup>[249]</sup>

Mlinar et al.<sup>[250]</sup> investigated how the proximity of the Brønsted acid sites in ZSM-5 catalysts (Si/Al in the range 12-140) influenced the activity and selectivity for propene oligomerization at atmospheric pressure and 200-270 °C. High Al content (Si/Al<40) led to decreased catalytic activity and enhanced selectivity to dimers, which could not be explained by differences in acidity, presence of EFAL species or mass transfer phenomena. The limited growth of propene oligomers was attributed to molecular crowding near the acid sites (oligomers adsorbed on proximal acid sites, which was studied by quantum chemical analysis of the energetics of the reaction). The proximity of Brønsted acid sites may favor the formation of aromatics.<sup>[250]</sup>

Kojima et al.<sup>[251]</sup> studied the oligomerization of a C3/C4 mixture (82 wt.% of butenes) from Sasol, at 51 bar, 200 °C, WHSV=3.5-11 h<sup>-1</sup>) over (large pore) Na-Mordenite ion-exchanged with ammonium chloride, using different Na<sup>+</sup>-NH<sub>4</sub><sup>+</sup> exchange levels, followed by calcination at different temperatures (300-600 °C). For the same calcination temperature, the increased degree of ion-exchange (11-97 % NH<sub>4</sub><sup>+</sup>) led to increased catalytic activity and selectivity to trimers and tetramers. However, above 50 % ammonium ion content, the conversion to liquid products did not increase prominently, and the selectivity did not depend on NH<sub>4</sub><sup>+</sup>-exchange levels. Calcination temperatures of 400-500 °C were found to be optimal for butene oligomerization.<sup>[251]</sup> Oligomerization of a butene/butane feed (50 bar, 300 °C, WHSV=1 h<sup>-1</sup>) over calcined Na-exchanged Y zeolite was accompanied by fast deactivation due to coke formation, regardless of the amount of Na<sup>+</sup> in the zeolite and the calcination temperature. Butene conversion and coke formation increased with increasing Na-exchange degrees, and the reaction products were highly branched, suggesting that Na-Y zeolite was not suitable for synthesizing long linear hydrocarbons.<sup>[252]</sup>

Wilshier et al.<sup>[162]</sup> explored different approaches based on chemical treatment of the zeolite surface, in order to enhance shape-selectivity (formation of less branched oligomers) of propene oligomerization over ZSM-5 (24 bar, 0.7 h<sup>-1</sup>). Specifically, the external surface acid sites were poisoned with 4-methylquinoline or hexamethyldisilazane (silylated ZSM-5), or using an alcohol-containing feed (iso-propanol). The untreated ZSM-5 (1.22 wt.% Al content) led to the highest propene conversion to liquids (90 % at 284 °C) and selectivity to C<sub>10</sub><sup>+</sup> hydrocarbons (62 % at 90 % conversion), although the products were highly branched compared to the modified zeolites, ascertained by gas-chromatography coupled with mass spectrometry analyses of the hydrogenated liquid reaction products. The reaction mechanism possibly involved cationic oligomerization on the external surface without shape-selectivity effects, since the ZSM-5 channels may become occluded by oligomeric product. Of the different poisoning methods, the silylated ZSM-5 led to the most pronounced decrease in conversion (37 % at 350 °C) and selectivity to C<sub>10</sub><sup>+</sup> (31 % at 37 % conversion); this catalyst seemed superior in terms of shape-selectivity than ZSM-5 treated with 4-methylquinoline (42 % selectivity at 68 % conversion, 300 °C). The treatment with iso-propanol led to 80 % conversion to liquid products (at 310 °C), and *ca.* 34 % C<sub>10</sub><sup>+</sup> selectivity.<sup>[162]</sup> Chen et al.<sup>[253]</sup> successfully obtained near linear C<sub>20</sub><sup>+</sup> hydrocarbons by shape-selective oligomerization of propene, 1-decene and isobutene (batch operation) over ZSM-5 in which the external surface

was deactivated with 2,6-di-tert-butylpyridine. Branching was more pronounced at higher temperature and the type of products structure seemed more dependent on temperature than on the type of olefin substrate; the products were analyzed *via*  $^{13}\text{C}$  NMR spectroscopy and related to the viscosity index (measure of the variation in kinematic viscosity due to changes in temperature).<sup>[253]</sup>

***Porous aluminosilicates with different metals.*** Metals (Me; *e.g.*, Ga, Fe, B, V, Zn, Ti, Zr, and Ni) were introduced in the zeolite frameworks to enhance the catalytic performance for olefin (*e.g.*, propene, butenes) oligomerization.<sup>[254]</sup> The Me incorporation was accomplished *via* hydrothermal synthesis (isomorphic substitution of Al for Me) or post-synthesis treatments (*e.g.*, ion-exchange or wet impregnation).

Miller et al.<sup>[255]</sup> evaluated the performance of ZSM-5 with Si/Al=39, for the propene oligomerization at high pressure and low temperature (111 bar, 54 °C). This catalyst presented low hydrogen transfer activity, based on the hydrogen transfer index (HTI) test. It was suggested that the reaction occurred mainly on the external surface of the zeolite, with lack of shape-selectivity, since the formation of linear olefins was poor. However, selectivity to linear olefins was improved for Ni-ZSM-5 as catalyst (54 °C).<sup>[255]</sup>

High pressure propene oligomerization was studied over Zr-ZSM-5 (Si/Al=15, Si/Zr=50-300),<sup>[256]</sup> and Ni-ZSM-5 (Si/Al=25, 0.76-5.05 wt.% Ni)<sup>[257]</sup>, targeting diesel type products. The incorporation of increasing amounts of Zr in ZSM-5, by isomorphic substitution of aluminum, led to decreasing amounts of strong Brønsted acid sites.<sup>[256]</sup> It was verified a maximum conversion of propene (*ca.* 88 % at 40 bar, 260 °C, 1 h<sup>-1</sup>) and selectivity to diesel type products (*ca.* 80 %) for zeolites with intermediate Zr content (acidity).<sup>[256]</sup> On the other hand, the incorporation of Ni by wet impregnation, led to an increase of the strong Brønsted and Lewis acid sites.<sup>[257]</sup> The incorporation of Ni (3.58 wt.%) promoted a slight decrease in conversion, but enhanced significantly the selectivity to diesel (up to 81 % selectivity at 76 % conversion, at 40 bar, 270 °C, 4 h<sup>-1</sup>).<sup>[257]</sup> The Ni-catalyst was stable for 72 h on-stream. Increasing the Ni content above 3.58 wt.% did not affect considerably the catalytic results.<sup>[257]</sup> The incorporation of chromium (Cr-exchange) and tungsten (W) in ZSM-5 for propene oligomerization (25 bar, 270 °C), indicated that Cr-ZSM-5 led to slightly better catalytic results than H-ZSM-5, whereas W-ZSM-5 performed similarly to H-ZSM-5.

Lower Cr or W content was preferable; the products were mostly C6-C10 olefins with low branching degree.<sup>[258]</sup>

The catalytic performance of Ni-ZSM-5 (Si/Al=30 or 160) was compared to Ni-Beta (Si/Al=16), both prepared *via* impregnation, for olefin trimerization using mixed butene:butane:propane as feed (10 bar, 350 °C, 4.03 h<sup>-1</sup>). The doping of Ni in ZSM-5 and Beta followed by calcination at 550 °C led to a slight decrease of the total and external surface area, increase of the amount of acid sites (especially the weak/medium Lewis acid sites) and enhanced ratio of Lewis to Brønsted acid sites (L/B); these changes improved the catalytic performance. The yield to trimers plus tetramers (C<sub>12</sub><sup>+</sup>) reached a maximum of 24 wt.%, and increased in the order: ZSM-5(30) < ZSM-5(160) < Beta < 1 %Ni-ZSM-5(160) < 1 %Ni-Beta < 1.6 %Ni-Beta, which was correlated with the amount of the external surface acid sites. The authors reported that an intermediate amount of external acid sites and high L/B ratio favored the formation of larger oligomers.<sup>[259]</sup>

Beside zeolites, mesoporous silicates such as MCM-41 (M41S family) type materials were studied for olefin oligomerization. These types of materials possess relatively high thermal stability, specific surface area, and regular arrangement of mesoporous channels, favoring mass transfer and avoiding diffusional limitations for reactions of larger molecules. The incorporation of metals in zeolites may confer the necessary activity for different types of chemical reactions. The catalyst Al-MCM-41 (Si/Al=10-70) led to promising results for oligomerization of 1-butene/butane feed (50 bar, 160 °C, WHSV=5.3-5.6 h<sup>-1</sup>). Al-MCM-41 with Si/Al of 20 led to the best catalytic results; *ca.* 74 % selectivity to diesel type products at *ca.* 99 % conversion, without significant deactivation over 3 h on-stream. The incorporation of small amounts of noble metals (Rh and Pt) had almost no effect on the catalytic performance, and the incorporation of Ni led to lower selectivity to diesel. The CN (based on O'Connor correlation of the hydrogenated samples<sup>[38]</sup>) was in the range 27-30 for noble metal-containing catalysts, compared to 25 without metal.<sup>[117]</sup> The effect of metal-containing MCM-41 (Si/Me=100 or 200) was studied for propene oligomerization at atmospheric pressure and 300 °C; catalytic activity increased with the increasing Si/Me ratio. The catalytic activity increased in the order, Ga-MCM-41 < Fe-MCM-41 < Al-MCM-4, albeit conversions were quite low (3-7 % after 2 h on-stream) and the products were mainly in the gasoline range (C<sub>10</sub>).<sup>[260]</sup>

Although it is not an aluminosilicate, it is worth mentioning very recently studies of N-doped carbon-supported cobalt oxide (CoOx/N-C) as catalyst for olefin oligomerization.<sup>[261,262]</sup> Zhao et al.<sup>[262]</sup> studied the oligomerization of 1-butene (31 bar, 80 °C, WHSV=0.4-14.1 h<sup>-1</sup>) over CoOx/N-C (prepared by treating activated carbon with nitric acid and subsequently with ammonia at different temperatures (200-800 °C), followed by impregnation with cobalt) and over 2A-CoOx/N-C (2A stands for doubly-ammoniated), prepared by treatment with ammonium hydroxide solution followed by impregnation with cobalt. The authors verified that the doubly-ammoniated procedure resulted in lower catalytic performance. The catalytic performance of CoOx/N-C increased with the ammonia treatment temperature (increase of nitrogen content), and the oligomers selectivity increased with 1-butene conversion (up to 49 % at 92 % conversion, WHSV=0.71 h<sup>-1</sup>), for the material prepared at 800 °C. The oligomers were mainly linear olefins (>70 %), albeit the selectivity to larger oligomers (C12<sup>+</sup>) was rather low (*ca.* 7.5 %).<sup>[262]</sup> Thus, despite of the good catalytic results, this material did not seem appropriate for diesel production.

***Strategies to improve shape-selectivity and accessibility to the acid sites of zeolites.***

Medium-pore zeolites (especially ZSM-5) may be preferred catalysts for light olefin oligomerization to produce diesel, whereas large pore zeolites deactivated rapidly and led to hydrocarbons with high branching degree (impacting on the quality of diesel). However, for obtaining higher yields of high-quality diesel and minimize catalyst deactivation, especially in the oligomerization of mixtures of larger olefins (*e.g.*, C3-C6 olefins present in petrochemical processes streams), it is important to design catalysts with a good compromise between textural and acid properties.<sup>[11]</sup> Olefin oligomerization over zeolites with reduced crystal sizes allows to shorten the diffusion path lengths, facilitating mass transfer and accessibility to the acid sites.<sup>[160,161]</sup> Corma et al.<sup>[161]</sup> reported propene oligomerization (40 bar, 200 °C, WHSV=5.9 h<sup>-1</sup>) over MFI catalysts possessing different crystal sizes. Smaller crystal sizes (0.16-0.17 μm) favored propene conversion and presented good stability with time on-stream; larger crystals deactivated faster due to the formation of higher amounts of (refractory) coke. Thus, the catalytic reaction seemed to benefit from shorter intracrystallite diffusion paths in smaller crystals. The acid properties need to be simultaneously evaluated, since zeolites possessing similar crystal sizes may perform differently due to differences in acid properties. Propene conversion (*ca.* 80 %), selectivity to diesel (*ca.* 74 %) and catalyst

stability were superior for a zeolite sample possessing lower Si/Al (11) and higher Brønsted acid sites density.<sup>[161]</sup>

Later, Popov et al.<sup>[160]</sup> studied the effect of the polycrystal size of MFI type catalysts possessing similar Si/Al ratios, on the continuous-flow oligomerization of a butene/butane mixture (15 bar, 300 °C). The catalysts consisted of aggregates (0.2-3 μm size) of nanocrystallites (*ca.* 40-70 nm). The conversion of butenes was influenced by the polycrystal sizes, indicating that internal diffusion limitations may be important. The authors found a linear correlation between the initial reaction rate and the amount of Brønsted acid sites located on the external surface of the crystals (determined by IR spectroscopy of adsorbed 2,6-di-tert-butylpyridine as base probe), and no correlation was found with the total amount of Brønsted acid sites (determined by IR spectroscopy of adsorbed pyridine). Hence, the external surface Brønsted acid sites were responsible for the oligomerization reaction. The initial catalytic activity was higher for smaller crystals (0.1-0.3 μm), although the latter led to extensive coking (involving hydrogen transfer reactions), favored the formation of (light) C4-C5 hydrocarbons (cracking *via* β-scission), and high branching degree. The products spectrum suggested that the effective acid sites were those located on the external surface or pore mouths of the zeolite polycrystals, where shape-selectivity was not important. In addition to the favorable effects of reducing the crystal sizes, the removal of the external acid sites should be considered for the formation of high molecular weight hydrocarbons.<sup>[160]</sup> In a different study, the same authors carried out detailed studies of the influence of selective poisoning of external surface acid sites of ZSM-5, for the same catalytic reaction.<sup>[263]</sup> The poisoning procedure involved incipient wetness impregnation of the zeolite with organosilanes (with sizes that were greater than the zeolite pore diameter) and with metal-containing (Zn, Ga and La) solutions. The poisoning with the organosilicons led to a 60-75 % reduction of the external surface Brønsted acid sites, resulting in a slight decrease of conversion, and increase in the yield of C5<sup>+</sup> products (up to 90 % at 15 bar, 300 °C); moreover, the introduction of gallium as promoter metal avoided coking, enhancing the catalyst stability with time on-stream.<sup>[263]</sup>

With the aim of improving the active sites accessibility for olefin oligomerization, modified zeolite-type materials (zeotypes) possessing micro/mesoporosity (hierarchical zeotypes) were prepared by post-synthesis desilication and dealumination treatments,

presenting advantages in terms of simplicity of catalyst preparation and costs.<sup>[114,161,264–267]</sup> Corma et al.<sup>[161]</sup> studied the effect of desilication treatments under different conditions (0.2–0.8 M NaOH, 65 or 85 °C, 30 or 90 min, with or without subsequent acid leaching) to generate mesoporosity in ZSM-5 (Si/Al=10–30), and tested the modified catalyst in propene and pentene oligomerization (40 bar, 200 °C). NaOH concentrations  $\geq 0.5$  M and longer desilication time (90 min) were required to introduce significant mesoporosity in the Al-rich ZSM-5 parent zeolite (Si/Al=11); conversely, the introduction of mesoporosity in a zeolite precursor with a higher Si/Al ratio of 20 was much easier. The washing with oxalic acid step of the desilicated zeolites was found important for micropore volume preservation, although it caused decrease of Brønsted acidity. This treatment led to decreased total Al content (including EFAL species), and also removed Al from the external zeolite surface, aiming at low branching degree of the reaction products. The best catalytic results were obtained with the parent zeolite (Si/Al=11) desilicated with 0.5 M NaOH at 85 °C during 90 min, followed by washing with oxalic acid; this catalyst led to *ca.* 92 % propene conversion and *ca.* 73 % selectivity to diesel. The same treatment employed in the ZSM-5 with Si/Al of 20 and similar crystal size, did not improve the catalytic performance, due to significant decrease in the amount of Brønsted acid sites. Therefore, ZSM-5 possessing mesoporosity led to superior catalytic results when the acidity was sufficiently preserved. The authors evaluate the performance of the best modified ZSM-5 zeolite in the oligomerization of pentene, which indicated that the presence of a secondary mesopore system was advantageous for the oligomerization of larger olefins.<sup>[161]</sup>

10-MR zeolites with 3D topology (like ZSM-5) may favor the formation of methyl-branched hydrocarbon chains. Decreasing the branching degree is of interest to produce high-quality diesel products. The use of 1D 10-MR zeolites may lead to lower branching degree, albeit the 1D pore system may impose significant diffusional limitations (relatively slow mass transport to/from the acid sites), leading to the formation of bulkier coke precursors which may block the pores, rapidly deactivating the catalyst. Thus, the introduction of mesoporosity in 1D materials was investigated to improve acid site accessibility, and this needs to be done in a controlled manner to preserve the catalyst acidity (necessary for olefin conversion) and microporosity (retaining some shape-selectivity to low-branched diesel type products).<sup>[11,114]</sup> In this sense, Martínez et al.<sup>[114]</sup> reported an optimized combination of desilication with NaOH and dealumination with oxalic acid,

applied to zeolite Theta-1 (TON) with Si/Al ratio of 25 and 50, in order to introduce mesoporosity to facilitate the internal mass transport, while preserving microporosity and Brønsted acidity. The modified materials were tested for propene oligomerization (40 bar, 200 °C), and revealed increased initial activity, catalyst stability and selectivity to diesel range products, compared to the parent Theta-1 zeolite. The best modified materials (prepared from the parent zeolite with Si/Al of 25 or 50) were obtained *via* desilication with 0.2 M NaOH at 85 °C (Si/Al=50) or 95 °C (Si/Al=25) during 30 min, followed by dealumination with oxalic acid. The materials showed increased mesoporosity without significant changes in the micropore volume and Brønsted acid site density, leading to propene conversion of *ca.* 90-93 % (Si/Al=25-50), and selectivity towards diesel of *ca.* 61-63 % (Si/Al=25-50), with relatively high stability over 8-10 h on-stream. If the desilication treatment was too severe, the diffusion paths lengths may be too short, and the products spectrum consisted mainly of dimers and trimers (that possibly left the catalyst pores without undergoing further oligomerization to larger hydrocarbons).<sup>[114]</sup>

Modified zeolites prepared by bottom-up strategies were hardly studied for olefin oligomerization. Modified MFI zeolite was prepared *via* bottom-up approach under hydrothermal conditions, and evaluated for 1-butene oligomerization (40 bar, 270 °C).<sup>[268]</sup> Specifically, small amounts of hemicellulose and initiating agents (ammonium persulfate (APS) and tetramethylethylenediamine (TMEDA)) were added to the precursor gel. Compared to the conventional ZSM-5, the modified material possessed slightly higher specific surface area and pore volume and significant higher Brønsted and Lewis acidity, associated with the abundancy of hydroxyl groups of hemicellulose. The modified material outperformed the parent zeolite ZSM-5 in terms of butene conversion (91 % compared to 21 %) and selectivity to diesel type products (87 % compared to 80 %). The catalyst showed high stability over 72 h on-stream and for two runs (conversion > 80 %), with regeneration (calcination at 700 °C) between runs.<sup>[268]</sup> This catalyst synthesis method seemed simple, involved few steps (synthesis time of 72 h), not too expensive reactants and led to good catalytic results for diesel production. However, scale-up of bottom-up preparation methodologies may not be trivial.

***Influence of feedstock and reaction conditions.*** Tabak et al.<sup>[245]</sup> reported that at constant temperature and pressure, and for a sufficiently long reaction time, the molecular weight distribution of the products reached equilibrium and was independent of the feed composition.<sup>[245]</sup> Nevertheless, there are several studies reporting the influence of the feed composition on olefin oligomerization; *e.g.*, type of olefin, feed consisting of one or more types of olefins, solvent (*e.g.*, organic compound, N<sub>2</sub>, He).

Schwarzs et al.<sup>[249]</sup> reported for olefin oligomerization over ZSM-5 at 50 bar and 270 °C, that 1-butene was more reactive than propene, which in turn was more reactive than 1-hexene. The main oligomeric products were: tetramers and hexamers for the propene; dimers, trimers and tetramers for 1-butene; and dimers for 1-hexene. In all cases, C<sub>12</sub><sup>+</sup> products were the main oligomers formed.<sup>[249]</sup> Xu et al.<sup>[262]</sup> studied the oligomerization of ethene (C<sub>2</sub>), propene (C<sub>3</sub>), 1-butene (1C<sub>4</sub>) and 1-hexene (1C<sub>6</sub>), over 2A-CoOx/N-C catalyst, at 31 bar and 80 °C. The yield of oligomers for the reaction of the different substrates increased in the order: 1C<sub>4</sub> (11 %) < C<sub>3</sub> (16 %) < 1C<sub>6</sub> (17 %) < C<sub>2</sub> (40 %), being the oligomers formed mainly dimers. Mechanisms explaining the product distribution for the oligomerization of the different olefins are proposed.<sup>[262]</sup>

Klerk et al.<sup>[269]</sup> verified that the type of feedstock had a great impact on the properties (viscosity, density, volatility, RON and CN) of the fuels produced *via* oligomerization of Fischer-Tropsch type feed (propene (91 %)/propane; or 1-hexene (53 %)/*n*-hexane mixtures) over ZSM-5, under typical industrial conditions (265-270 °C, 48 bar, LHSV=1 h<sup>-1</sup>). For the two feeds, very high conversion (>95 %) was reached. However, the distillate yield was lower for propene than for 1-hexene oligomerization. The products from propene possessed higher branching degree and consequently higher octane number and lower cetane number.<sup>[269]</sup>

Bellussi et al.<sup>[51]</sup> reported the ZSM-5 catalyzed oligomerization of light cracked naphtha (LCN, derived from a FCC unit, and pre-treated to remove heteroatoms) containing C<sub>4</sub>-C<sub>6</sub> paraffins (42 %) and olefins (52 %) to middle distillates, at 60 bar, 240 °C, 0.5-1.5 h<sup>-1</sup>. The selectivity to oligomers was approximately 100 % (formation of coke and light cracking products was negligible). The oligomers were predominantly in the middle distillate range products, suggesting that co-oligomerization and that “true” oligomerization (which gives dimers and trimers in the range of gasoline products) was less important. The

products possessed no sulfur, low density, and relatively high CN. A shift to lighter products was verified for high space velocities; a space velocity of  $1.0 \text{ h}^{-1}$  was recommended considering productivity and product quality.<sup>[51]</sup>

Yoon et al.<sup>[112,266,270,271]</sup> studied the oligomerization of a isobutene:butane (50:50 (wt)) mixture over different types of zeolites (ZSM-5, Ferrierite, Mordenite, Beta, Y, and USY) and zirconia supported tungsten oxide catalyst ( $\text{WO}_x/\text{ZrO}_2$ ), at 15 bar and  $70 \text{ }^\circ\text{C}$ . Zeolites Beta ( $\text{Si}/\text{Al}=12.5$ )<sup>[112]</sup> and Ferrierite ( $\text{Si}/\text{Al}=10$ )<sup>[270]</sup> led to the best catalytic results in terms of isobutene conversion (100 %) over long times on-stream (50-70 h) and selectivity to trimers and tetramers (89-90 %). These catalysts were easy to regenerate (*via* calcination in air at  $550 \text{ }^\circ\text{C}$ ), without loss in catalytic performance after regeneration. Aluminum chloride-loaded USY zeolite ( $\text{Al}/\text{USY}$ )<sup>[271]</sup> and dealuminated Y zeolite (by steaming)<sup>[266]</sup> performed superiorly (84 % selectivity to trimers and tetramers at 98 % conversion, for dealuminated Y zeolite,  $\text{WHSV}=1.4 \text{ h}^{-1}$ ; 79 % selectivity at 99 % conversion for  $\text{Al}/\text{USY}$ ,  $\text{WHSV}=10 \text{ h}^{-1}$ ) to the respective parent zeolites USY (40 % selectivity at 85 % conversion,  $\text{WHSV}=10 \text{ h}^{-1}$ ) and Y (67 % selectivity at 83 % conversion,  $\text{WHSV}=1.4 \text{ h}^{-1}$ ). The isobutene conversion for zeolites  $\text{Al}/\text{USY}$  and dealuminated Y was in the same range (98-99 %) as for Beta and Ferrierite (100 %), although the former two catalysts were not so stable over time, and the selectivity to trimers and tetramers was not so high (79-84 % compared to 89-90 %). The  $\text{WO}_x/\text{ZrO}_2$  oxide, prepared by impregnation and calcination at different temperatures, showed remarkable catalytic activity (100 % isobutene conversion) and stability over 100 h on-stream, as well as high selectivity for trimers plus tetramers (90 %), when the tetragonal structure of zirconia was present (required calcination temperature of at least  $700 \text{ }^\circ\text{C}$ ).<sup>[118]</sup>

Several studies were reported for different types of zeolites in order to gain insights into the influence of the oligomerization conditions, such as reaction pressure, temperature,  $\text{WHSV}$ , and feed composition, on the reaction (Table 2.14).<sup>[53,115,184,245,256,270,272,273]</sup>

A wide range of operating conditions were used. High olefin conversions seemed favored by high temperature, olefin partial pressure and total pressure, and by low  $\text{WHSV}$  (high residence time). Regarding the products molecular weight distribution, high olefin partial pressure (high olefin composition in the feed) and high total pressure may favor the formation of heavier products. High temperature enhances the oligomerization rate and the formation of high molecular weight products. In the higher temperature range ( $>200 \text{ }^\circ\text{C}$ ), an

increase of temperature may shift the product distribution to lighter hydrocarbons due to cracking reactions which become important. Decreasing WHSV may favor the formation of heavy oligomers by enhancing bimolecular oligomerization over monomolecular cracking reactions; nevertheless, in the higher temperature region, low WHSV tends to favor formation of cracking products, due to the extension of secondary reactions.<sup>[53,115,245,256,270,274]</sup>

Table 2.14. Selected studies of oligomerization processes involving different types of feed, zeolites and operating conditions.<sup>[a]</sup>

Ref.	Zeolite (Si/Al)	Feed <sup>[b]</sup> ¶	Operation conditions			
			P (bar)	T (°C)	WHSV (g <sub>olefin</sub> g <sub>cat</sub> <sup>-1</sup> h <sup>-1</sup> )	Olefin composition (%)
[53]	ZSM-5 (15)	1C4:N <sub>2</sub>	1	150-250	13.5-80	12.5-50 mol.%
[115]	FER (10)	1C4:H <sub>2</sub>	6.9-62.7	100-250	0.18-49.7	23-100 mol.%
[184]	Beta (17)	1C4:N <sub>2</sub>	14.7-28.5	205-245	85-345	90 mol.%
[270]	Ferrierite (10)	iC4:C4 <sup>0</sup>	15	40-100	2.5-20	50 wt.%
[274]	ZSM-5 (25-95)	2C4:C4 <sup>0</sup>	30-50	210-300	0.5-1 <sup>[c]</sup>	90 n.s. %.
[272]	ZSM-5 (30)	C3:N <sub>2</sub>	1	200-450	n.s.	5-30 mol.%
[256]	Zr-ZSM-5 (15)	C3:N <sub>2</sub>	20-40	210-280	1 a 4	33 vol %
[245]	ZSM-5 (n.s.)	C3/C4 mix	41	150-270	1-3	C3/C3 <sup>0</sup> /1C4/iC4 <sup>0</sup> 17/11/36/27 wt.%
[273]	ZSM-5 (n.s.)	FCC naphtha	30-60	80-300	1-2 <sup>[c]</sup>	C4-C6, b.p. 31-88 °C

<sup>[a]</sup> n.s.=not specified. <sup>[b]</sup> 1C4=1-butene, 2C4=2-butene, iC4=isobutene, C4<sup>0</sup>=butane, C3=propene. <sup>[c]</sup> Liquid hourly space velocity (LHSV).

Li et al.<sup>[256]</sup> reported that the conversion of propene over Zr-ZSM-5 increased with temperature in the range 210-280 °C (at 40 bar, 1 h<sup>-1</sup>), with pressure in the range 20-40 bar (at 260 °C, 1 h<sup>-1</sup>), and with the decreasing WHSV in the range 1-4 h<sup>-1</sup> (at 40 bar, 260 °C). On the other hand, selectivity to diesel decreased with temperature.<sup>[256]</sup> A further increase of

temperature up to 290 °C and pressure up to 50 bar led to a decrease of conversion and selectivity to diesel.

ZSM-5 with different Si/Al ratio (25-95) was tested for the oligomerization of 2-butene, under different reaction temperature (210-300 °C), pressure (30-50 bar), and LHSV (0.5-1.5 h<sup>-1</sup>). Lower Si/Al ratio (enhanced acidity, determined by NH<sub>3</sub>-TPD) enhanced the liquid products yield and C<sub>9</sub><sup>+</sup> selectivity. Increasing the temperature and pressure up to 260 °C and 40 bar, and decreasing LHSV to 0.5 h<sup>-1</sup> led to an increase in the liquid products yield and selectivity to C<sub>9</sub><sup>+</sup> products. Lower branching degree was reported for low temperature (<270 °C) and moderate pressure (40 bar). The results were compared to those for silica-supported phosphoric acid (SSPA) at lower temperature (180-220 °C); the latter (mesoporous) material possessed higher total acidity (1377 μmol g<sup>-1</sup>) compared to ZSM-5 (860 μmol g<sup>-1</sup>), but was not advantageous for targeting heavier oligomers or reduced branching degree. These results may be associated with the lack of microporosity and shape-selectivity for SSPA, and its higher total amount of acid sites (including the strong acid sites) favored cracking reactions leading to C<sub>5</sub>-C<sub>7</sub> products.<sup>[274]</sup>

Kriván et al.<sup>[273]</sup> verified that the most favorable combination of process parameters for oligomerization of light FCC naphtha (C<sub>2</sub>-C<sub>6</sub>) olefins over ZSM-5, was 240 °C, 50 bar, and LHSV=2 h<sup>-1</sup>. Under these conditions, the olefin conversions were *ca.* 40 % and the portion of C<sub>12</sub><sup>+</sup> hydrocarbons in the oligomer product was 9.0 %. The authors investigated the influence of having two layered bed in the catalytic reactor, and the largest portion of oligomers was formed at 270 °C, 40 bar, 1 h<sup>-1</sup>, which allowed to double the trimers selectivity in the middle distillate boiling point range; although the yield of liquid products was lower for the reaction at 270°C than that at 240 °C, since cracking reactions were favored at higher temperature (>250 °C).<sup>[273]</sup>

Kim et al.<sup>[115]</sup> performed a detailed study of 1-butene oligomerization over Ferrierite at different temperatures (10-250 °C), WHSV (0.03-49.7 h<sup>-1</sup>), olefin partial pressures (14.2-62.7 bar), and with or without co-feed (*n*-hexane). They performed two-dimensional gas chromatography coupled with mass spectrometry (GC×GC-MS) to identify the gas and liquid phase reaction products, which included olefins, paraffins, aromatics and cycloalkanes. Mainly gaseous products were formed (butene isomers, C<sub>2</sub>-C<sub>8</sub> olefins and C<sub>1</sub>-C<sub>5</sub> paraffins) and small amounts of liquid products (C<sub>5</sub>-C<sub>19</sub> olefins, C<sub>7</sub>-C<sub>20</sub> paraffins). The

authors verified that butene (C4 isomers) conversion increased with temperature, 1-butene partial pressure, and with decreasing WHSV. The product selectivity was strongly influenced by the reaction temperature (100-250 °C, 6.9 bar, 0.03 h<sup>-1</sup>). Below 200 °C, the products were essentially C8 olefins (indicating that dimerization was favored) and a small portion of C4 paraffins (formed *via* hydride transfer to butenes). C8<sup>+</sup> hydrocarbons were not formed at 100 or 150 °C. As the reaction temperature increased (100-250 °C), the selectivity to C8 olefins and to C4 paraffins decreased, while the selectivity to C3 and C5-C7 olefins increased, likely due to cracking. Above 200 °C, hydrogen transfer reactions were favored leading to increasing amounts of C8-C20 paraffins and small amounts of aromatics and cycloalkanes.<sup>[115]</sup> An increase of WHSV may shift the product distribution to lower molecular weight products.<sup>[115,143]</sup> The selectivity to olefin products (mainly C8, C12 and C16) increased in detriment of the decreasing paraffin (C13<sup>-</sup>) selectivity, which indicated that the oligomerization was favored in detriment of hydride transfer reactions. The selectivity to aromatic and cycloalkane compounds also increased, although these were formed in small amounts. As the WHSV decreased, the selectivity to dimers decreased, whereas the selectivity to trimers, tetramers and pentamers increased. The selectivity to C9–C11, C13–C15, and C17–C19 olefins and C5-C15 paraffins also increased, due to oligomerization–cracking–re-alkylation over H-FER.<sup>[115]</sup> These reaction products followed the Schulz–Flory chain growth model.<sup>[275,276]</sup> Moreover, the olefin branching degree increased with butene conversion (and lower WHSV), and was directed correlated with butene conversion, which is consistent with a carbocation-based oligomerization mechanism.<sup>[115]</sup>

The same authors studied the influence of co-feeding 1-butene with *n*-hexane in different proportions at 62.7 bar, 150 °C or 250 °C (1-butene in the gas phase). When the hexane/1-butene molar ratio increased from 3.1 to 18.7, the C4 conversion and selectivity to higher molecular weight products increased considerably, even at lower temperature (150 °C). A further increase of the hexane/1-butene ratio to 34.3 led to a decrease of selectivity to C12<sup>+</sup> at 150 °C; at 250 °C, the selectivity to C12<sup>+</sup> was not affected by the solvent:olefin ratio.<sup>[115]</sup> The catalyst deactivation rates (evaluated for 8-26 h on-stream) decreased with increasing 1C4 partial pressure (at 150 °C) and increasing temperature (100-250 °C, using low 1C4 partial pressure in the feed, *i.e.* 0.14 bar or 2 mol.% 1C4). The catalyst used at lower reaction temperature had more coke deposits. In turn, the catalyst deactivation rate decreased

with the decrease of the WHSV in the range of 0.03-0.18 h<sup>-1</sup> and with the decrease of the hexane/1-butene ratio in the range 18.1-34.3, at 150 °C. At 250 °C, the deactivation seems to be independent of the hexane/1-butene ratio.<sup>[115]</sup>

### Final remarks

Overall, oligomerization in the presence of inorganic heterogeneous catalysts may be attractive for synthesizing fuels without sulphur and reduced content of aromatics, fulfilling the increasing fuel needs. Control over oligomerization degree, product selectivity and catalyst deactivation may be challenging. Many studies using different olefinic feedstock and catalysts were reported in the literature, investigating the types of reaction products as a function of the type of acid sites (amount, acid strength and nature), size of the reactant molecules, feed solvent, reaction conditions (temperature, pressure, space velocity), and shape and size of the porous system of the catalyst. The shape and structure of the product molecules may be influenced by the pore geometry and size, whereas the hydrocarbons distribution may be influenced by the reaction conditions.

The acid strength, density and distribution (acid sites on the internal *versus* external surface) may be tuned by changing the framework Si/Al ratio of the zeolite. The amount of framework aluminum ratio may influence the ratio L/B and crystallite sizes (crystallite sizes may increase as the aluminum content decreases). Incorporation of other metals in the zeolitic framework may alter the acidity of zeolites, without affecting significantly the crystallite dimensions. Elements such as B, Cu, Ni, Zr, Co, Fe, Ga and Zn were introduced to change the acidity.<sup>[254,257-259]</sup> The selective poisoning of external surface acid sites may prevent the reactions to occur at the zeolite crystals surface, where shape-selectivity effects do not exist and highly branched products may be formed (impacting negatively on CN). On the other hand, micro- and mesoporous versions of zeolites, prepared by bottom-up and top-down approaches, may enhance mass transport and accessibility to the acid sites, preventing fast catalyst deactivation and good catalytic performances. Bottom-up approaches are under-investigated for light olefin oligomerization.

It is important to bear in mind the difference between the reactant grade of the feedstock employed in laboratory or pilot scale oligomerization processes, from real feed

compositions coming from refineries. The presence of impurities in the feed may cause catalyst deactivation. Thus, pre-treatments may be required to remove the impurities (in the same fashion as the industrial oligomerization technologies).<sup>[51,277,278]</sup> Several inorganic catalysts were studied without clean olefinic feed (impurities may be present, influencing the catalytic performances). The operation conditions (temperature, pressure and space velocity) influence the activity and product selectivity. The temperature impacts on the rate of oligomerization and cracking reactions. Temperature below approximately 200 °C favors oligomerization, while higher temperature favors cracking and aromatization reactions of the formed oligomer products.<sup>[53,115,245,256,270,274]</sup> However, low temperature leads to slow reaction kinetics. Increasing pressure favored heavier oligomer products. Increasing the space velocity (or decreasing the residence time) may improve the selectivity towards heavier oligomeric products or may favor cracking reactions, depending on the reaction temperature range.<sup>[53,115,245,256,270,274]</sup>

Although olefin oligomerization has been investigated for some decades, several challenges remain concerning the types of catalysts and their performances (versatile, stable and productive cheap catalysts), operating conditions (optimization is important) and process design.

Table 2.15. Propene oligomerization studies, performed in fixed-bed reactors, over zeolites or other aluminosilicates and metal oxides.

Ref	Catalyst (Si/Al, S <sub>BET</sub> ) <sup>[a]</sup>	Catalytic assays conditions						Catalytic results			
		Activation (°C, h, flow)	P (bar)	T (°C)	WHSV (h <sup>-1</sup> )	TOS (h)	Feed <sup>[b]</sup>	Conditions	Conversion	Selectivity	
										Naphtha or C10 <sup>-</sup> products	Diesel or C10 <sup>+</sup> products
[161]	<sup>[c]</sup> ZSM-5 (10-30, 364-397)	519, n.s., N <sub>2</sub>	40	200	5.9	6 h	C3:C3 <sup>0</sup> 60:40 (mol)	Si/Al, crystal size 11, 173 nm 10, 912 nm 10, 1805 nm 15, 200 nm 20, 163 nm 31, 580 nm	(TOS=4 h) 80 % 10 % 3 % (2.5 h) 45 % 70 % 31 %	(TOS=3-6 h) 21 % n.s. n.s. 37 % 26 % 39 %	(TOS=3-6 h) 74 % n.s. n.s. 62 % 715 60 %
[161]	<sup>[c,d]</sup> ZSM-5 (7-47,375-547)	520, n.s., N <sub>2</sub>	40	200	5.9-12.5	6 h	C3:C3 <sup>0</sup> 60:40 (mol)	Si/Al=11 ZSM-5-unmodified ZSM-5-modified	81 % 92 %	21 % 25 %	74 % 73 %
[249]	ZSM-5 (18-487,n.s.)	500, 8, air	50	220- 300	12	60 h	C3:C3 <sup>0</sup> 85:15 (wt)	300 °C  Si/Al=18, 1 day Si/Al=40, 3 day Si/Al=40, 6 day	27-99 % (Si/Al=197-18) 90-100 % (220-270 °C) 84-94 % (220-270 °C) 93-98 % (220-270 °C)	(wt.) 49-62 (Si/Al=18-197) 52-53 (220-270 °C) 40-47 (220-270 °C) 41-46 (220-270 °C)	(wt.) 38-51 (Si/Al=18-197) 57-58 (270-220 °C) 53-60 (270-220 °C) 54-59 (220-270 °C)
[272]	ZSM-5 (30,n.s.)	n.s.	1	200- 450	n.s.	45 min	C3:N <sub>2</sub> 5-30:95- 70 (mol)	5 % C3 15 % C3 30 % C3	40-64 % (450-300 °C) 66-81 % (450-300 °C) 72-87 % (450-300 °C)		C8 <sup>-</sup> 100 mol.%
[250]	ZSM-5 (12-140,n.s.)	500, 3,air	1	200- 275	n.s.	3 h	C3:He 25:75 (vol)	250 °C  275 °C	3-24 % (Si/Al=12-140) 10-75 % (Si/Al=12-140)	n.s.	n.s.

Table 2.15. (continued).

Ref	Catalyst (Si/Al, S <sub>BET</sub> ) <sup>[a]</sup>	Catalytic assays conditions						Catalytic results			
		Activation (°C, h, flow)	P (bar)	T (°C)	WHSV (h <sup>-1</sup> )	TOS (h)	Feed <sup>[b]</sup>	Conditions	Conversion	Selectivity	
										Naphtha or C10 <sup>-</sup> products	Diesel or C10 <sup>+</sup> products
[269]	<sup>[e]</sup> ZMS-5 (n.s.,n.s.)	480, 1, H <sub>2</sub>	48	265- 270	1	96 h	C3:C30 91:9 (n.s.) 1C6:C6 <sup>0</sup> 53:47 (n.s.) HTFT-1/2 84 %/72 % olefins	C3:C3 <sup>0</sup> 1C6 (97 %) 1C6:C6 <sup>0</sup> HTFT-1 C5-C6 HTFT-2 C5-C6 (38 bar)	99 % (RON=80, CN=40) 96 % (RON=66, CN=47) 66 % (RON=73, CN=41) 95 % (RON=80, CN=48) 91 % (RON=76, CN=45)	59 % 32 % 66 % 44 % 39 %	41 % 68 % 34 % 56 % 61 %
[162]	<sup>[e]</sup> ZSM-5 (n.s.,n.s.)	n.s.	24	189- 359	0.7	n.s.	n.s.	ZSM-5 <sup>[f]</sup> : 1.22 wt.% Al 0.1 wt.% Al 4-methyl- quinoline) HMDS iso-propanol <sup>[g]</sup>	Conversion to liquids 90 wt.% (189-284 °C) 36-73 wt.% (298-359 °C) 53 wt.% (304 °C) 37 wt.% (351 °C) 80 wt.% (309 °C)	38-42 (284-189 °C) 63-67 (359-298 °C) 57 (304 °C) 68 (351 °C) 66 (309 °C)	58-62 (189-284 °C) 33-37 (298-359 °C) 42 (304 °C) 31 (351 °C) 34 (309 °C)
[83]	<sup>[h]</sup> ZSM-5 (39,380) Y (1.8,n.s.) Mordenite (4.7,n.s.) Ω (3.9,299) Offretite (3.8,430) Boralite (-,372)	n.s.	30-50	38-399	0.75-1	16 h	C3:C3 <sup>0</sup> 3:1 (mol)	P=41-48 bar H-ZSM-5 HY H-Mordenite Ω Offretite Boraline	(wt.%) 5-98 (204-371 °C) 3-36 (38-315 °C) 0.4-22 (149-315 °C) 22-98 (149-260 °C) 3-92 (204-343 °C) 3-96 (204-315 °C)	(wt.%) 78-85 (204-371 °C) 69-70 (102-160 °C) 77-79 (315-343 °C) 59-65 (260-149 °C) 71-79 (343-399 °C) 78-82 (315-329 °C)	(wt.%) 15-20 (371-204 °C) 24-27 (160-102 °C) 19-21 (343-315 °C) 30-31 (149-260 °C) 19-24 (399-343 °C) 17-19 (329-315 °C)
[258]	<sup>[i]</sup> ZSM-5 (44,401) Cr-ZSM-5 (43-95,344-389) W-ZSM-5 (43-47,393-485)	n.s.	25	270	n.s.	6 h	C3:N <sub>2</sub> 5:95 (n.s.)	H-ZSM-5 Cr-ZSM-5 W-ZSM-5	48 % 52 % 46 %	n.s. 57 % 56 %	n.s. 23 23

Table 2.15. (continued).

Ref	Catalyst (Si/Al, S <sub>BET</sub> ) <sup>[a]</sup>	Catalytic assays conditions						Catalytic results			
		Activation (°C, h, flow)	P (bar)	T (°C)	WHSV (h <sup>-1</sup> )	TOS (h)	Feed <sup>[b]</sup>	Conditions	Conversion	Yield or Selectivity	
										Naphtha or C10 <sup>-</sup> products	Diesel or C10 <sup>+</sup> products
[256]	Zr-ZSM-5 (15,314-363)	500, 2, N <sub>2</sub>	20-40	210- 280	1 a 4	ns	C3 <sup>=</sup> /N <sub>2</sub>  1/3 (vol)	260 °C, 40 bar, 1 h <sup>-1</sup> : Zr-ZSM-5 (0.94wt.% Zr) Zr-ZSM-5 (0.57wt.% Zr) 0.94 % Zr, 40 bar, 1 h <sup>-1</sup> 0.94 % Zr, 260 °C, 1 h <sup>-1</sup> 0.94 % Zr, 260 °C, 40 bar	91 88-81 % (25-200 h) 58-90 % (220-280 °C) 67-88 % (20-40 bar) 88-73 % (1-4 h <sup>-1</sup> )	ns	58 60-58(25-200 h) 67-58 (220-280 °C) 44-60 (20-40 bar) 61-43 (1-4 h <sup>-1</sup> )
[257]	Ni-ZSM-5 (25,291-388)	400, 4, N <sub>2</sub>	40	270	4.03	6 a 72 h	ns	HZSM-5 (0.76 wt.%)Ni-HZSM-5 (2.21 wt.%)Ni-HZSM-5 (3.58 wt.%)Ni-HZSM-5 (5.05 wt.%)Ni-HZSM-5	77.7 % 65.7 % 75.4 % 75.8 % 79.6 %	32.02 % 21.1 % 21.18 % 19.41 % 18.57 %	67.97 % 78.9 % 78.88 % 80.59 % 81.51 %
[279]	<sup>[j]</sup> Ni-Na-X (1.3,n.s.)	500, 3, air	1.25-5 partial P	180- 220	ns	270 min	C3 <sup>=</sup> (99.9 %)	(9.3 wt.%)Ni-Na-X (0.6 wt.%)Ni-Na-X	0.3 % 1.2 %	n.s.	n.s.
[114]	<sup>[c]</sup> Theta-1 (15-51,139-264)	520, 2, N <sub>2</sub>	40	200	5.9	6-8 h	C3/C3 <sup>0</sup> 60/40 (mol)	<sup>[k]</sup> T1-50 T1-50-des T1-50-des+deal T1-25 T1-52-des T1-25-des+deal	TOS=6h 5 % 72 % 93 % <10 % 73 % 90 %	TOS=0-3 h 64 % 27 % 35 % 51 % 39 % 31 %	TOS=0-3 h 34 % 68 % 63 % 48 % 59 % 61 %
[280]	<sup>[l]</sup> MSA (25,778-806)	n.s.	35	155	4	20-200 h	C3 <sup>=</sup> /C3 (70/30 (wt))	MSA-1 MSA-2 MSA-3	63-35 % (20-200 h) 74-45 % (20-200 h) 95-78 % (20-200 h)	n.s.	n.s.

Table 2.15. (continued).

Ref	Catalyst (Si/Al, S <sub>BET</sub> ) <sup>[a]</sup>	Catalytic assays conditions						Catalytic results			
		Activation (°C, h, flow)	P (bar)	T (°C)	WHSV (h <sup>-1</sup> )	TOS (min)	Feed <sup>[b]</sup>	Conditions	Conversion	Selectivity	
										Naphtha or C10 <sup>-</sup> products	Diesel or C10 <sup>+</sup> products
[260]	MCM-41 (-,1300) Al-MCM-41 (100-200,1210-1300) Ga-MCM-41 (100-200,1220-1270) Fe-MCM-41 (50-200,1210-1190)	500, 0.5, N <sub>2</sub>	1	150- 400	500 (GHSV)	150 min	C3 (n.s.)	MCM-41 Al-MCM-41 (200) Ga-MCM-41 (200) Fe-MCM-41 (200)	7-1.8 % (5-120 min) 34.8-7 % (5-120 min) 19.8-5.1 % (5-120 min) 12.7-3.6 % (5-120 min)	TOS=5 min 100 % 100 % 100 %	TOS=5 min 0 % 0 % 0 %

<sup>[a]</sup> n.s.= no specified. S<sub>BET</sub>=BET specific surface area (m<sup>2</sup>g<sup>-1</sup>). Red text color represent commercial catalysts, whereas black text color represent synthesized catalysts. <sup>[b]</sup> C3=propene and C3<sup>0</sup>=propane. <sup>[c]</sup> Catalyst diluted with silicon carbide (SiC) (n.s.). <sup>[d]</sup> Modified zeolite by desilication treatment (0.5 M NaOH at 85 °C during 90 min) followed by acid leaching. <sup>[e]</sup> Catalyst diluted with acid-washed sand (80 wt.%). <sup>[f]</sup> ZSM-5 zeolite with different Al content and poisoned with 4-methyl-quinoline and HMDS. <sup>[g]</sup> Substitution of C3 feed for iso-propanol feed. <sup>[h]</sup> Catalyst diluted with spanish sepiolite (20 wt.%). <sup>[i]</sup> Catalyst diluted with pseudo-bohemite or kaolin (60 %). Results shown for bohemite. <sup>[j]</sup> SiC (33 wt.%). <sup>[k]</sup> Modified theta-1 zeolite by desilication (des) (0.2 M NaOH at 85 °C (T1-50) or 95 °C (T1-25) during 30 min) and subsequent dealumination with oxalic acid (deal). <sup>[l]</sup> Catalyst diluted with pseudo-bohemite (39 % wt).

Table 2.16. Butene oligomerization studies, performed in fixed-bed reactors, over zeolites or other aluminosilicates and metal oxides.

Ref	Catalyst (Si/Al, S <sub>BET</sub> ) <sup>[a]</sup>	Catalytic assays conditions						Catalytic results			
		Activation (°C, h, flow)	P (bar)	T (°C)	WHSV (h <sup>-1</sup> )	TOS	Feed <sup>[b]</sup>	Conditions	Conversion	Selectivity	
										Naphtha or C10 <sup>-</sup> products	Diesel or C10 <sup>+</sup> products
<i>1-butene (1C4) and 2-butene (2C4)</i>											
[249]	ZSM-5 (44,n.s.)	n.s.	50	270	12	60 h	1C4 99.5 wt.%	ZSM-5	67-99 % (28-10 h)	24 wt.%	76 wt.%
[272]	ZSM-5 (30,n.s.)	n.s.	1	200-450	n.s.	45 min	1C4:N <sub>2</sub> 5-30:95-70 (mol)	300 °C, 1C4:N <sub>2</sub> (30:70)	68 % (20 min)	n.s.	n.s.
[53]	ZSM-5 (15,50)	450, 8, N <sub>2</sub>	1	150-250	13.5-80	21 min	1C4:N <sub>2</sub> 12.5-50:87.5-50 (mol)	200 °C, 50 mol.% 1C4 80 h <sup>-1</sup> , 50 mol.% 1C4	4-10 % (80-13.5 h <sup>-1</sup> ) 4-21 % (150-250 °C)	55-77 wt.% (80-13.5 h <sup>-1</sup> ) 55-84 wt.% (150-250 °C)	23-43 wt.% (13.5-80 h <sup>-1</sup> ) 16-45 wt.% (250-150 °C)
[268]	<sup>[c]</sup> ZSM-5 (25,344-391)	450, 1, N <sub>2</sub>	40	270	4.8	72 h	Butene :N <sub>2</sub> (n.s.)	TOS=24 h ZSM-5 ZSM-5-Hc-S <sup>[d]</sup>	21 % 86-91 % (72-24h)	20 % 10-12 % (72-24h)	80 % 88-90 % (24-72h)
[274]	<sup>[e]</sup> ZSM-5 (25-95,n.s.) SSPA (38 % P <sub>2</sub> O <sub>5</sub> ,n.s.)	500, 0.5, N <sub>2</sub>	30-50	210-300	0.5-1 (LHSV)	n.s.	2C4:C4 <sup>0</sup> 90:10 (n.s.)	ZSM-5 (Si/Al=30) 45 bar, 1 h <sup>-1</sup> 45 bar, 230 °C 230 °C, 1 h <sup>-1</sup> 230 °C, 1 h <sup>-1</sup> , 45 bar SSPA (220 °C, 40 bar, 1 h <sup>-1</sup> )	Liquid yield: 54-86 % (230-260 °C) 43-70 % (1.5-0.5 h <sup>-1</sup> ) 61-67 % (30-40 bar) 39-67 % (Si/Al=95, 25) 67 %	n.s. 4.5-6.4 % (0.5-1.5 h <sup>-1</sup> ) n.s. n.s. 72 %	51-78 % (230-260 °C) 39-59 % (1.5-0.5 h <sup>-1</sup> ) n.s. 33-57 % (Si/Al=95, 25) 38 %
[184]	<sup>[f]</sup> Beta (17,600) ZSM-5 (40,429) Pillared ZSM-5 (75,602)	500, 2, N <sub>2</sub>	14.7-28.5	205-245	85-345	6 h	1C4:N <sub>2</sub> 90:10 (mol)	24 bar, 225 °C, 345 h <sup>-1</sup> H-beta H-ZSM-5 Pillared ZSM-5	<sup>[g]</sup> C4s conversion: 2 % 3 % 3.5 %	80 % 86 % 87 %	12 % 8 % 7 %

Table 2.16. (continued).

Ref	Catalyst (Si/Al, S <sub>BET</sub> ) <sup>[a]</sup>	Catalytic assays conditions						Catalytic results			
		Activation (°C, h, flow)	P (bar)	T (°C)	WHSV (h <sup>-1</sup> )	TOS (h)	Feed <sup>[b]</sup>	Conditions	Conversion	Selectivity	
										Naphtha or C10 <sup>-</sup> products	Diesel or C10 <sup>+</sup> products
<b><i>1-butene (1C4) and 2-butene (2C4)</i></b>											
[281]	BEA (26,623) MFI (25,400) ASA (6,405) MTS (27-30,782-987)	500, 4, N <sub>2</sub>	15-20	150	3-9	33 h	1C4:N <sub>2</sub> 17:83 (mol)	19 bar, 150 °C, 9 h <sup>-1</sup> : BEA, MFI, ASA MTS-3 15 bar, 250 °C, 4.7 h <sup>-1</sup> : MTS-3	TOS=400 min 0 % 8 % 12 %	TOS=400 min n.s. 85 % n.s.	TOS=400 min n.s. 15 % n.s.
[115]	H-FER (10,44)	500, 2, He	6.9- 62.7	100- 250	0.18- 49.7	160 h	2-100 mol.% 1C4 in He or C6 <sup>0</sup> /1C4 3.1-34.3 (mol)	6.79 bar, 2 mol.% 1C4, No solvent 150 °C, 62.7 bar, WHSV=0.03 h <sup>-1</sup> 250 °C, 62.7 bar, WHSV=0.03 h <sup>-1</sup> 150 °C, 62.7 bar	[g] 5-70 % (150-250 °C) 14-81 % (3.1-8.7, C6 <sup>0</sup> /1C4) 90-92 % (34.3-18.1, C6 <sup>0</sup> /1C4) 19-99 (9.51-0.18 h <sup>-1</sup> )	C9 <sup>-</sup> 90-100 % (250-150 °C) 38-84 % (18.1-3.1, C6 <sup>0</sup> /1C4) 81 % (34.3-18.1, C6 <sup>0</sup> /1C4) 31-83 (0.18-9.51 h <sup>-1</sup> )	C9 <sup>+</sup> 0-10 % (150-250 °C) 16-62 % (3.1-18.1, C6 <sup>0</sup> /1C4) 19 % (18.1-34.3, C6 <sup>0</sup> /1C4) 17-69 (9.51-0.18 h <sup>-1</sup> )
[117]	Al-MCM-41 (10-70, 700-820) Ni,Pt,Rh-Al- MCM-41 (20, 818)	550, 5, air	15-50	140- 250	2-11	180 min	1C4:C4 <sup>0</sup> 88:12 (wt)	50 bar, 5.6 h <sup>-1</sup> , Si/Al=10 50 bar, 5.3 h <sup>-1</sup> , 160 °C Me-Al-MCM-41 (1 wt.%)	[g] 4-91 % (140-160 °C) 97-99 % (Si/Al=10-70) 98, 99, 98 % (Rh, Ni, Pt)	21-32 % (160-140 °) 20-26 % (Si/Al=10-70) 21, 18, 20 % (Rh, Ni, Pt)	57 % (140-160 °C) 70-74 % (Si/Al=70-10) 74,67,73 % (Rh, Ni, Pt)
[262]	<sup>[h]</sup> CoOx/N-C (13 wt.% Co, 341-409)	230, 2, He	31	80	0.4-14.1	120 h	1C4 (99.9 %)	WHSV=0.71 h <sup>-1</sup> 400-CoOx/N-C 800-CoOx/N-C 600-CoOx/N-C 600-CoOx/N-C (0.4 h <sup>-1</sup> )	<sup>[i]</sup> TOS= 64-69 h 94 %, 28 % oligom. 92 %, 49 % oligom. 92 %, 35 % oligom. 97 %, 48 % oligom.	TOS= 64-69 h 95.4 % 92.5 % 94 % 92.8 %	TOS= 64-69 h 4.6 % 7.5 % 6 % 7.2 %

Table 2.16. (continued).

Ref	Catalyst (Si/Al, S <sub>BET</sub> ) <sup>[a]</sup>	Catalytic assays conditions						Catalytic results			
		Activation (°C, h, flow)	P (bar)	T (°C)	WHSV (h <sup>-1</sup> )	TOS	Feed <sup>[b]</sup>	Conditions	Conversion	Selectivity	
										Naphtha or C10 <sup>-</sup> products	Diesel or C10 <sup>+</sup> products
<b>Isobutene (iC4)</b>											
[118]	<sup>[j]</sup> WO <sub>x</sub> /ZrO <sub>2</sub> (-,54-119) T <sub>calc</sub> =550-800 °C	300, 10, N <sub>2</sub>	15	70	5 a 20	550 h	iC4:C4 <sup>0</sup> 50:50 (wt.%)	WO <sub>x</sub> /ZrO <sub>2</sub> (800 °C) WO <sub>x</sub> /ZrO <sub>2</sub> (700 °C) WO <sub>x</sub> /ZrO <sub>2</sub> (550 °C)	94 % (100 h) 72-100 % (550-100 h) 65 % (100 h)	7 % (100 h) 10-23 % (100-550 h) 26 % (100 h)	93 % (100 h) 90 % (100 h) 74 % (100 h)
[270]	Ferrierite (10,400) ZSM-5 (25,425) Mordenite (12.5,500)	300, 10, N <sub>2</sub>	15	40- 100	2.5-20	60 h	iC4: C4 <sup>0</sup> 50:50 (wt.%)	70 °C, 15 bar, 10 h <sup>-1</sup> : Ferrierite ZSM-5 Mordenite	100 % (12-50 h) 40 % (11 h) 20 % (12 h)	11-20 % (10-50 h) 83 % (10 h) 89 % (10 h)	80-89 % (50-10 h) 17 % (10 h) 11 % (10 h)
[266]	HY (1.4,722) <sup>[k]</sup> HY-deal (n.s.,382-660)	300, 10, N <sub>2</sub>	15	70	1.375	12 h	iC4: C4 <sup>0</sup> 50:50 (wt.%)	TOS=6 h HY HY-deal-500 HY-deal-600 HY-deal-600 (TOS=20 h)	83 % 91 % 98 % 58 %	33 % 26 % 16 % 50 %	67 % 74 % 84 % 50 %
[271]	USY (30,750) <sup>[l]</sup> Al/USY (n.s.,745)	300, 10, N <sub>2</sub>	15	70	10	120 h	iC4: C4 <sup>0</sup> 50:50 (wt.%)	USY (20 h) Al/USY (20 h) Al/USY (120 h)	85 % 99 % 71 %	60 % 21 % 55 %	40 % 79 % 45 %
[112]	Beta (9-19,680- 710) USY (30,720) Mordenite (12.5,500)	n.s.	15	40- 100	10-20	25 h	iC4:C4 <sup>0</sup> 50:50 (wt.%)	12 h, 70 °C, 10 h <sup>-1</sup> : Beta (12.5) USY Mordenite	100 % (12-70 h) 90 % 20 %	10 % 38 % 90 %	90 % 62 % 10 %
[119]	W <sub>2</sub> O <sub>3</sub> /Al <sub>2</sub> O <sub>3</sub> (-,345) NiO-W <sub>2</sub> O <sub>3</sub> /Al <sub>2</sub> O <sub>3</sub> (-,121-227)	n.s.	1	50- 150	9	5.5 h	iC4: C4 <sup>0</sup> 50:50 (wt.%)	W <sub>2</sub> O <sub>3</sub> /Al <sub>2</sub> O <sub>3</sub> NiO-W <sub>2</sub> O <sub>3</sub> /Al <sub>2</sub> O <sub>3</sub>	1.0-2.1 % (50-150 °C) 7.4-14.6 % (50-150 °C)	35-74 mol.% (50-150 °C) 42-66 mol.% (50-150 °C)	26-65 mol.% (150-50 °C) 34-58 mol.% (150-50 °C)

Table 2.16. (continued).

Ref	Catalyst (Si/Al, S <sub>BET</sub> ) <sup>[a]</sup>	Catalytic assays conditions						Catalytic results			
		Activation (°C, h, flow)	P (bar)	T (°C)	WHSV (h <sup>-1</sup> )	TOS	Feed <sup>[b]</sup>	Conditions	Conversion	Selectivity	
										Naphtha or C10 <sup>-</sup> products	Diesel or C10 <sup>+</sup> products
<b>Butene mixtures (C4s)</b>											
[245]	ZSM-5 (n.s.,n.s.)	n.s.	41	150- 270	1-3	n.s.	<sup>[m]</sup> C3-C4 mix:N <sub>2</sub> 10-60:90-40 (mol)	41 bar, 260 °C: 13 mol.% olefin 27 mol.% olefin 45 mol.% olefin 41 bar, 27 mol.%: 180 °C 230 °C	51-75 % (2-1 h <sup>-1</sup> ) 88-95 % (2-1 h <sup>-1</sup> ) 97-99 % (2-1 h <sup>-1</sup> ) 57-67 % (2-1 h <sup>-1</sup> ) 83-95 % (2-1 h <sup>-1</sup> )	n.s.	n.s.
[263]	ZSM-5 (40,n.s.) ZSM-5 (40,n.s.)	n.s.	15	300	n.s.	200 h	C4s:C4s <sup>0</sup> 20:77 (n.s.)	ZSM-5 ZSM-5+PMS ZSM-5+TEOS Ga-ZSM-5+TEOS	98 % 96 % 94 % 96 %	C5 <sup>+</sup> :85 % C5 <sup>+</sup> :90 % C5 <sup>+</sup> :90 % C5 <sup>+</sup> :95 %	
[160]	ZSM-5 (26-29,n.s.)	550, 1, N <sub>2</sub>	15	300	3-40	330 min	<sup>[n]</sup> 1C4:2C4 9:63 (wt)	MFI-1 (40–45 nm, 0.1–0.3 μm) MFI-3 (60–70 nm, 2–3 μm)	TOS=310 min 63 % (40 h <sup>-1</sup> ) 73 % (3.3 h <sup>-1</sup> )	TOS=250 min 82 mol.% 78 mol.%	TOS=250 min 18 mol.% 22 mol.%
[143]	Y (2.6-30,n.s.) Beta (12.5-150,n.s.) ZSM-5 (11.5-140,n.s.)	n.s.	15	350	7-12	6 h	1C4:2C4 44:56 (n.s.)	WHSV=10 h <sup>-1</sup> HY H-Beta HZSM-5	8-15 % (Si/Al=5.2-60) 20-36 % (Si/Al=300-25) 67-80 % (Si/Al=280-50)	C8 <sup>+</sup> : 3-9 % (Si/Al=5.2-60) C8 <sup>+</sup> : 15-21 % (Si/Al=300-25) C8 <sup>+</sup> : 46-55 % (Si/Al=280-50)	
[252]	<sup>[o]</sup> Na-HY (2.4-2.7,n.s)	400, 3, air	50	100 -400	1	35 h	Sasol C4 stream (84 wt.% C4s) <sup>[n]</sup>	Na-HY (99 % exchange)	1.40 % (300 °C)	28 wt.% (300 °C)	17 wt.% (300 °C)

Table 2.16. (continued).

Ref	Catalyst (Si/Al, S <sub>BET</sub> ) <sup>[a]</sup>	Catalytic assays conditions						Catalytic results			
		Activation (°C, h, flow)	P (bar)	T (°C)	WHSV (h <sup>-1</sup> )	TOS	Feed <sup>[b]</sup>	Conditions	Conversion	Yield or Selectivity	
										Naphtha or C10 <sup>-</sup> products	Diesel or C10 <sup>+</sup> products
<b>Butene mixtures (C4s)</b>											
[251]	H-Mordenite (5.8,n.s.) NH <sub>4</sub> Na- Mordenite (6, n.s.)	n.s.	51	200	3.5-11	36- 222	Sasol C4 stream (82 wt.% C4s) <sup>[p]</sup>	TOS=90-114 min, WHSV=3.5 h <sup>-1</sup> H-Mor NH <sub>4</sub> Na-Mor	Conversion to liquids: 60 wt.% 31-82 wt.% (33-97 % NH <sub>4</sub> )	71 wt.% 59-79 wt.% (97-33 % NH <sub>4</sub> )	29 wt.% 21-39 wt.% (33-97 % NH <sub>4</sub> )
[259]	HZSM-5 (30-160,243- 309) Ni-HZSM-5 (160,305) H-Beta (16,319) Ni-H-Beta (16,312-316)	450, 0.5, N <sub>2</sub>	10	350	2	75 h	C4 <sup>0</sup> :1C4:2C4: C3 <sup>0</sup> 54:15:25:6 (wt)	TOS=24h HZSM-5 (30) HZSM-5 (160) Ni-HZSM-5 (1 wt.% Ni) H-Beta Ni-H-Beta (1 wt.% Ni) Ni-H-Beta (1.6 wt.% Ni)	Conv. to liquids: 45 wt.%, 51 wt.% liq. 58 wt.%, 60 wt.% liq. 67 wt.%, 74 wt.% liq. 71 wt.%, 68 wt.% liq. 74 wt.%, 66 wt.% liq. 78 wt.%, 64 wt.% liq.	98 wt.% 94 wt.% 56 wt.% 69 wt.% 55 wt.% 51 wt.%	2 wt.% 6 wt.% 44 wt.% 31 wt.% 45 wt.% 49 wt.%
<b>Olefinic mixtures</b>											
[51]	<sup>[q]</sup> ZSM-5 (26,360)	150, n.s. N <sub>2</sub>	60	240	0.5-1.5	96 h	<sup>[r]</sup> LCN 52 wt.% olefins	TOS=35 h	58-80 % (1.5-0.5 h <sup>-1</sup> )	Yield (wt.%) 52-71 % (1.5-0.5 h <sup>-1</sup> )	Yield (wt.%) 29-47 % (0.5-1.5 h <sup>-1</sup> )
[273]	ZSM-5 (n.s.,189-328)	400, n.s. H <sub>2</sub>	30-60	80- 300	1-2	n.s.	Light FCC- naphtha (C4- C6, b.p. 31- 88 °C)	30bar, 2 h <sup>-1</sup> 240 °C, 2 h <sup>-1</sup>  270°C, 40 bar	14-35 % (160-260 °C) 35-40 % (30-60 bar) 19-31 % (2-1 h <sup>-1</sup> )	C12 <sup>-</sup> 97 % 91-95 % (60-30 bar) 82-83 % (2-1 h <sup>-1</sup> )	C12 <sup>+</sup> 3 % 5-9 % (30-60 bar) 17-18 % (1-2 h <sup>-1</sup> )
[19]	<sup>[s]</sup> ASA (10,n.s.)	n.s.	40-60	140- 235	0.5	432 h	C3-C6 HTFT condensate	150 °C, 60 bar	92 %	30-35 %	65-70 %

Table 2.16. (continued).

Ref	Catalyst (Si/Al, S <sub>BET</sub> ) <sup>[a]</sup>	Catalytic assays conditions						Catalytic results			
		Activation (°C, h, flow)	P (bar)	T (°C)	WHSV (h <sup>-1</sup> )	TOS	Feed <sup>[b]</sup>	Conditions	Conversion	Selectivity	
										Naphtha or C10 <sup>-</sup> products	Diesel or C10 <sup>+</sup> products
<i>Olefinic mixtures</i>											
[261]	<sup>[l]</sup> 2A-CoO <sub>x</sub> /N-C (-,321)	230, 2, He	31	80	14.1	8 h	C2:He 50:50 (n.s) C3,1C4, 1C6 - 100 %	TOS=2 h C2 C3 1C4  1C6	<sup>[i]</sup> 39 %, 100 % oligom. 16 %, 100 % oligom. 53 %, 21 % oligom. + 79 % isom 94 %, 18 % oligom. + 82 % isom	99.6 % 100 % 99.7 % 100 %	0.4 % 0 % 0.3 % 0 %
[249]	ZSM-5 (44,n.s.)	n.s.	50	220- 300	12	60 h	C3:C30 85:15 (wt.%) 1C4 (99.5 wt.%) 1C6:C6 isomers 96:4 (wt.%)	TOS=25 h C3 1C4 1C6	84 % 99 % 38 %	C12 <sup>-</sup> 30 % 27 % 0 %	C12 <sup>+</sup> 70 % 77 % 100 %

<sup>[a]</sup> n.s.=not specified. S<sub>BET</sub>=BET specific surface area (m<sup>2</sup>g<sup>-1</sup>). Red text color represent commercial catalysts, whereas black text color represent synthesized catalysts. <sup>[b]</sup> 1C4=1-butene, 2C4=2-butene, iC4=iso-butene, C4<sup>0</sup>=butane, C4<sub>s</sub>=butenes, C4<sub>s</sub><sup>0</sup>=butanes, C3=propene, C6=hexane, C2=ethene, and 1C6=1-hexene. <sup>[c]</sup> Catalyst diluted with silicon carbide (SiC) (50 vol.%). <sup>[d]</sup> ZSM-5-Hc-S stands for ZSM-5 synthesized using hemicellulose, APS and TMEDA. <sup>[e]</sup> Catalyst diluted with calcined acid-washed quartz (87.5 wt.%). SSPA=silica-supported phosphoric acid. <sup>[f]</sup> Catalyst binded with 15-20 wt.% clay. <sup>[g]</sup> Conversion of butenes (1-butene isomers were not accounted as reaction products) <sup>[h]</sup> CoO<sub>x</sub>/N-C=cobalt oxide on N-doped carbon. <sup>[i]</sup> oligom.=oligomerization products (the remaining fraction refers to isomerization (isom) products). <sup>[j]</sup> WO<sub>x</sub>/ZrO<sub>2</sub> calcined at different temperatures (T<sub>calc</sub>). Catalyst diluted with quartz beads (83 wt.%). <sup>[k]</sup> HY dealuminated (deal) by steam-treatment at 600 °C. <sup>[l]</sup> AlCl<sub>3</sub>-loaded USY zeolite. <sup>[m]</sup> C3/C4 mixture composed by C3:C3<sup>0</sup>:1C4:iC4<sup>0</sup> in the proportion 17:11:36:27 (wt). <sup>[n]</sup> The remaining feed components are iC4, C3<sup>0</sup>, C4<sup>0</sup>, iC4<sup>0</sup> (iso-butane), and C5<sup>0</sup> (pentane). <sup>[o]</sup> Catalyst prepared by sodium ion-exchange, binded with 25 wt.% kaolinite. <sup>[p]</sup> The remaining feed components are C3<sup>0</sup>, C3, iC4<sup>0</sup>, C4<sup>0</sup>. <sup>[q]</sup> Catalyst binded with 20 wt.% alumina. <sup>[r]</sup> LCN=light cracked naphtha. <sup>[s]</sup> Catalyst diluted with acid-washed sand (28 vol.%). <sup>[t]</sup> 2A-CoO<sub>x</sub>/N-C = doubly ammoniated cobalt oxide on N-doped carbon.

## 2.4. References

- [1] U.S. Administration energy information, International energy outlook 2017, 2017. [https://www.eia.gov/outlooks/ieo/pdf/0484\(2017\).pdf](https://www.eia.gov/outlooks/ieo/pdf/0484(2017).pdf) (Accessed November 10, 2018).
- [2] I.E. Agency, World energy outlook special report, 2015. <https://eneken.ieej.or.jp/data/6508.pdf> (Accessed November 10, 2018).
- [3] V. Marchal, R. Dellink, D. van Vuuren, C. Clapp, J. Chateau, E. Lanzi, B. Magne, J. van Vliet, Climate change - OECD environmental outlook to 2050, 2011. <https://www.oecd.org/env/indicators-modelling-outlooks/49846090.pdf> (Accessed November 10, 2018).
- [4] BP, BP energy outlook 2018, 2018. [https://www.bp.com/content/dam/bp-country/de\\_ch/PDF/Energy-Outlook-2018-edition-Booklet.pdf](https://www.bp.com/content/dam/bp-country/de_ch/PDF/Energy-Outlook-2018-edition-Booklet.pdf) (Accessed November 10, 2018).
- [5] E.C., EU reference scenario: energy, transport and GHG emissions trends to 2050, Eur. Comm. (2016) 27. [https://ec.europa.eu/energy/sites/ener/files/documents/20160713%20draft\\_publication\\_REF2016\\_v13.pdf](https://ec.europa.eu/energy/sites/ener/files/documents/20160713%20draft_publication_REF2016_v13.pdf) (Accessed November 10, 2018).
- [6] FuelsEurope, FuelsEurope statistical report 2017, 2017. [https://www.fuelseurope.eu/wp-content/uploads/2017/06/20170704-Graphs\\_FUELS\\_EUROPE-\\_2017\\_WEBFILE.pdf](https://www.fuelseurope.eu/wp-content/uploads/2017/06/20170704-Graphs_FUELS_EUROPE-_2017_WEBFILE.pdf) (Accessed November 10, 2018).
- [7] W.E. Council, Global transport scenarios 2050, 2011. <http://www.scopus.com/inward/record.url?eid=2-s2.0-33750120750&partnerID=40&md5=dbf2ffb8e0467d56353c0486dc0c200>. (Accessed November 10, 2018).
- [8] List of oil refineries, [https://en.wikipedia.org/wiki/List\\_of\\_oil\\_refineries#South\\_Africa](https://en.wikipedia.org/wiki/List_of_oil_refineries#South_Africa) (accessed January 3, 2019).
- [9] J. Speight, The chemistry and technology of petroleum, 4<sup>th</sup> ed., CRC press, 2014.
- [10] Robert A. Meyers, Handbook of petroleum refining processes, 4<sup>th</sup> ed., McGraw-Hill, 2004.
- [11] O. Muraza, Maximizing diesel production through oligomerization: a landmark opportunity for zeolite research, *Ind. Eng. Chem. Res.* 54 (2015) 781–789.
- [12] World energy council, World energy resources 2016, 2016. <https://www.worldenergy.org/wp-content/uploads/2016/10/World-Energy-Resources-Full-report-2016.10.03.pdf> (Accessed December 5, 2018).
- [13] A. Andrews, Fischer-Tropsch fuels from coal, natural gas, and biomass: background and policy, report, 2008, <https://digital.library.unt.edu/ark:/67531/metadc821070/> (Accessed 13/02/2019)
- [14] I. Dimitriou, H. Goldingay, A. V. Bridgwater, Techno-economic and uncertainty analysis of Biomass to Liquid (BTL) systems for transport fuel production, *Renew. Sustain. Energy Rev.* 88 (2018) 160–175.
- [15] A. De Klerk, Fischer–Tropsch refining: technology selection to match molecules, *Green Chem.* 10 (2008) 1249–1279.
- [16] D. Leckel, Diesel production from Fischer-Tropsch: the past, the present, and new concepts, *Energy & Fuels* 23 (2009) 2342–2358.
- [17] C.P. Nicholas, Applications of light olefin oligomerization to the production of fuels and chemicals, *Appl. Catal. A Gen.* 543 (2017) 82–97.

- [18] C. Knottenbelt, Moss gas “gas-to-liquid” diesel fuels - An environmentally friendly option, *Catal. Today* 71 (2002) 437–445.
- [19] A. De Klerk, Distillate production by oligomerization of Fischer - Tropsch olefins over solid phosphoric acid, *Energy & Fuels* 20 (2006) 439–445.
- [20] A. de Klerk, Can Fischer-Tropsch syncrude be refined to on-specification diesel fuel?, *Energy & Fuels* 23 (2009) 4593–4604.
- [21] V. Balan, Current challenges in commercially producing biofuels from lignocellulosic biomass, *ISRN Biotechnol.* 2014 (2014) 1–31.
- [22] S. Bhardwaj, P. Das, A review: advantages and disadvantages of biogas, *Int. Res. J. Eng. Technol.* 4 (2017) 530–535.
- [23] C.N. Ibeto, A.U. Ofoefule, K.E. Agbo, A global overview of biomass potentials for bioethanol production: a renewable alternative fuel, *Trends Appl. Sci. Res.* 6 (2011) 410–425.
- [24] S.S. Ail, S. Dasappa, Biomass to liquid transportation fuel via Fischer Tropsch synthesis – Technology review and current scenario, *Renew. Sustain. Energy Rev.* 58 (2016) 267–286.
- [25] J.C. Ge, S.K. Yoon, N.J. Choi, Using canola oil biodiesel as an alternative fuel in diesel engines : a review, *Appl. Sci.* 7 (2017) 881.
- [26] Unleaded petrol BS EN 228:2012, (2016). [https://www.mabanaft.com/fileadmin/content/global\\_content/downloads/mabanaft/Mabanaft-Ltd\\_Prod-Spec\\_Regular-Unleaded-Petrol.pdf](https://www.mabanaft.com/fileadmin/content/global_content/downloads/mabanaft/Mabanaft-Ltd_Prod-Spec_Regular-Unleaded-Petrol.pdf) (Accessed January 5, 2019).
- [27] Sulphur free diesel BS EN 590:2013, (2015). [https://www.mabanaft.com/fileadmin/content/global\\_content/downloads/mabanaft/Mabanaft-Ltd\\_Prod-Spec\\_Diesel.pdf](https://www.mabanaft.com/fileadmin/content/global_content/downloads/mabanaft/Mabanaft-Ltd_Prod-Spec_Diesel.pdf). (Accessed January 5, 2019).
- [28] H. Energy, International fuel quality standards and their implications for Australian standards, 2014. <https://www.environment.gov.au/system/files/resources/f83ff2dc-87a7-4cf9-ab24-6c25f2713f9e/files/international-fuel-quality-standards.pdf> (accessed January 10, 2019).
- [29] J. Matijošius, E. Sokolovskij, Research into the quality of biocomponents on the fuel quality, *Transport.* 24 (2009) 212–217.
- [30] G. Mendes, H.G. Aleme, P.J.S. Barbeira, Determination of octane numbers in gasoline by distillation curves and partial least squares regression, *Fuel* 97 (2012) 131–136.
- [31] W. Dabelstein, A. Reglitzky, A. Schütze, K. Reders, Automotive fuels, in: Ullmann’s encyclopedia of industrial chemistry, Wiley-VCH, 2007: pp. 425–458.
- [32] M.E. Myers, J. Stollsteimer, A.M. Wims, Determination of gasoline octane numbers from chemical composition, *Anal. Chem.* 47 (1975) 2301–2304.
- [33] N.H. Al-mashhadani, A.A. Mohamed, E.M. Ali, A.S. Mahmood, M.M. Khudhair, Z.A. Al Kareem, E.A.A.L. Mohsun, M.M. Jaseem, Improvement of gasoline octane number by using organic, *Baghdad Sci. J.* 11 (2014) 502–508.
- [34] A. Demirbas, M.A. Balubaid, A.M. Basahel, W. Ahmad, Octane Rating of Gasoline and Octane Booster Additives, *Pet. Sci. Technol.* 33 (2015) 1190–1197.
- [35] Chevron, Diesel fuels technical review, (2007). <https://www.chevron.com/-/media/chevron/operations/documents/diesel-fuel-tech-review.pdf>.
- [36] P. Ghosh, S.B. Jaffe, Detailed composition-based model for predicting the cetane number of diesel fuels, *Ind. Eng. Chem. Res.* 45 (2006) 346–351.
- [37] G.S. Kapur, A. Ecker, R. Meusinger, Establishing quantitative structure-property relationships (QSPR) of diesel samples by proton-NMR & multiple linear regression (MLR) analysis, *Energy and Fuels* 15 (2001) 943–948.

- [38] C.T. O'Connor, R.D. Forrester, M.S. Scurrrell, Cetane number determination of synthetic diesel fuels, *Fuel* 71 (1992) 1323–1327.
- [39] F.B. Du Toit, Process and apparatus for the production of diesel fuels by oligomerisation of olefinic feed streams, US 0287565 A1, 2006.
- [40] R. Rodríguez, J.J. Espada, B. Coto, Structural characterization of fuels obtained by olefin oligomerization, *Energy and Fuels* 24 (2010) 464–468.
- [41] F.T. DiGuseppi, S. Han, R.H. Heck, Process for converting olefins to higher hydrocarbons, US 5264643 A, 1993.
- [42] M.N. Harandi, H. Owen, Integrated staged conversion of methanol to gasoline and distillate, US 4899002 A, 1988.
- [43] N.A. Bhore, Q.N. Le, G.H. Yokomizo, Catalytic oligomerization process using synthetic mesoporous crystalline material, US 5134243 A, 1992.
- [44] F. Nierlich, J. Neumeister, T. Wildt, W. Droste, F. Obenaus, Oligomerization of olefins, US 5177282, 1993.
- [45] S.J. Miller, Low pressure oligomerization of gaseous olefins, US 4423268, 1983.
- [46] C. Flego, C. Perego, M. Marchionna, Process for obtaining a “diesel cut” fuel by the oligomerization of olefins or their mixtures, US 6914165 B2, 2005.
- [47] A. Corma, S. Iborra, Oligomerization of alkenes, in: E.G., Derouane (Ed.), *Catalysts for fine chemical synthesis, Volume 4, Microporous and mesoporous solid catalysts*, John Wiley & Sons, 2006: pp. 125–140.
- [48] T. Imai, Preparation of metal oxide-supported boron fluoride catalysts, US 4407731 A, 1983.
- [49] F.T.T. Ng, G.L. Rempel, B. Nkosi, Composite catalyst for the selective oligomerization of lower alkenes and the production of high octane products, WO 2005056503 A1, 2005.
- [50] E. Kriván, I. Valkai, J. Hancsók, Investigation of production of motor fuel components on heterogeneous catalyst with oligomerization, *Top Catal.* 56 (2013) 831–838.
- [51] G. Bellussi, F. Mizia, V. Calemma, P. Pollesel, R. Millini, Oligomerization of olefins from light cracking naphtha over zeolite-based catalyst for the production of high quality diesel fuel, *Microporous Mesoporous Mater.* 164 (2012) 127–134.
- [52] M.A. Maseloane, Dimerization of naphtha-range Fischer-Tropsch olefins into diesel-range products over zeolite H-ZSM-5 and amorphous silica-alumina, thesis, University of Cape Town, 2011.
- [53] A. Coelho, G. Caeiro, M.A.N.D.A. Lemos, F. Lemos, F.R. Ribeiro, 1-Butene oligomerization over ZSM-5 zeolite: Part 1 - Effect of reaction conditions, *Fuel* 111 (2013) 449–460.
- [54] J.Q. Bond, D.M. Alonso, D. Wang, R.M. West, J.A. Dumesic, Integrated catalytic conversion of  $\gamma$ -valerolactone to liquid alkenes for transportation fuels, *Science* 327 (2010) 1110–1114.
- [55] J.Q. Bond, A.A. Upadhye, H. Olcay, G.A. Tompsett, J. Jae, R. Xing, D.M. Alonso, D. Wang, T. Zhang, R. Kumar, A. Foster, S.M. Sen, C.T. Maravelias, R. Malina, S.R.H. Barrett, R. Lobo, C.E. Wyman, J. a. Dumesic, G.W. Huber, Production of renewable jet fuel range alkanes and commodity chemicals from integrated catalytic processing of biomass, *Energy Environ. Sci.* 7 (2014) 1500–1523.
- [56] D.M. Alonso, J.Q. Bond, J.C. Serrano-Ruiz, J.A. Dumesic, Production of liquid hydrocarbon transportation fuels by oligomerization of biomass-derived C<sub>9</sub> alkenes, *Green Chem.* 12 (2010) 992–999.
- [57] V.L. Dagle, C. Smith, M. Flake, K.O. Albrecht, M.J. Gray, K.K. Ramasamy, R.A. Dagle, Integrated process for the catalytic conversion of biomass-derived syngas into transportation fuels, *Green Chem.* 18 (2016) 1880–1891.

- [58] R. Palkovits, Pentenoic acid pathways for cellulosic biofuels, *Angew. Chem. Int. Ed.* 49 (2010) 4336–4338.
- [59] Isobutene process, <http://www.global-bioenergies.com/our-groupe/isobutene-process/?lang=en> (accessed March 2, 2017).
- [60] S.A. Tabak, A.A. Avidan, F.J. Krambeck, Production of synthetic gasoline and diesel fuel from non-petroleum resources, *Am. Chem. Soc., Div. Fuel Chem.* 31 (1986) 293–299.
- [61] PetroSA, COD technology, [http://www.petrosa.co.za/innovation\\_in\\_action/Pages/COD-Technology.aspx](http://www.petrosa.co.za/innovation_in_action/Pages/COD-Technology.aspx) (accessed March 24, 2016).
- [62] Axens, Oligomerization, <http://www.axens.net/our-offer/by-market/oil-refining/bottom-of-the-barrel/73/oligomerization.html> (accessed March 24, 2016).
- [63] V. Tom, V. Coupard, F. Hugues, R. Huyghe, Process for the production of middle distillates from a feedstock comprising butanol and pentanol, US 2014/0249340 A1, 2014.
- [64] Axens, Axens' technologies for Petron Corporation in the Philippines, (2011). <https://www.axens.net/news-and-events/news/160/axens-technologies-for-petron-corporation-in-the-philippines.html> (accessed February 10, 2019).
- [65] Axens, Axens awarded for a Polyfuel® contract in Romania, (2016). <https://www.axens.net/news-and-events/news/411/axens-awarded-for-a-polyfuel®-contract-in-romania.html> (accessed February 10, 2019).
- [66] V.N. Ipatieff, Catalytic polymerization of gaseous olefins by liquid phosphoric acid, *Ind. Eng. Chem.* 27 (1935) 1067–1069.
- [67] V.N. Ipatieff, V.I. Komarewsky, Isooctane production by simultaneous polymerization and hydrogenation, *Ind. Eng. Chem.* 29 (1937) 958–985.
- [68] J.H. Coetzee, T.N. Mashapa, N.M. Prinsloo, J.D. Rademan, An improved solid phosphoric acid catalyst for alkene oligomerization in a Fischer – Tropsch refinery, *Appl. Catal. A Gen.* 308 (2006) 204–209.
- [69] L. Schmerling, V.N. Ipatief, The mechanism of the polymerization of alkenes, *Adv. Catal.* 2 (1950) 21–80.
- [70] C.T. O'Connor, Oligomerization, in: G. Ertl, H. Knözinger, F. Schüth, J. Weitkamp (Eds.), *Handbook of heterogeneous catalysis*, volume 1, 2<sup>nd</sup> ed., Wiley-VCH, Weinheim, 2008: pp. 2854–2864.
- [71] T.R. Krawietz, P. Lin, K.E. Lotterhos, P.D. Torres, D.H. Barich, A. Clearfield, J.F. Haw, Solid phosphoric acid catalyst: a multinuclear NMR and theoretical study, *J. Am. Chem. Soc.* 120 (1998) 8502–8511.
- [72] ACEA, Worldwide fuel charter, 2013, [http://www.acea.be/uploads/publications/Worldwide\\_Fuel\\_Charter\\_5ed\\_2013.pdf](http://www.acea.be/uploads/publications/Worldwide_Fuel_Charter_5ed_2013.pdf) (accessed March 24, 2016).
- [73] M.E. Dry, The Sasol route to chemicals and fuels, in: D.M. Bibby, C.D. Chang, R.F. Howe, S. Yurchack (Eds.), *Studies in surface science and catalysis*, volume 36, Methane conversion, Elsevier, 1988: pp. 447–456.
- [74] B.B. Corson, V.N. Ipatief, Gasoline from ethylene by catalytic polymerization, *Ind. Eng. Chem.* 28 (1936) 860–863.
- [75] J. Zhang, Y. Yan, Q. Chu, J. Feng, Solid phosphoric acid catalyst for propene oligomerization: Effect of silicon phosphate composition, *Fuel Process. Technol.* 135 (2015) 2–5.
- [76] A. De Klerk, D.O. Leckel, N.M. Prinsloo, Butene oligomerization by phosphoric acid catalysis: Separating the effects of temperature and catalyst hydration on product selectivity, *Ind. Eng. Chem. Res.* 45 (2006) 6127–6136.

- [77] T.M. Sakuneka, A. De Klerk, R.J.J. Nel, A.D. Pienaar, Synthetic jet fuel production by combined propene oligomerization and aromatic alkylation over solid phosphoric acid, *Ind. Eng. Chem. Res.* 47 (2008) 1828–1834.
- [78] B.S. Wright, C.H. Hsia, H. Owen, Light olefin conversion to heavier hydrocarbons with sorption recovery of unreacted olefin vapor, US 4511747, 1985.
- [79] C.T.O. Connor, M. Kojima, Alkene oligomerization, *Catal. Today* 6 (1990) 329–349.
- [80] I. Romey, P.F.M. Paul, The Mobil process, in: I. Romey, P.F.M. Paul (Eds.), *Synthetic fuels from coal: status of the technology*, Graham & Trotman, 1987: pp. 70–107.
- [81] J.F. Knifton, J.R. Sanderson, Olefin oligomerization via zeolite catalysis, *Catal. Letters* 28 (1994) 223–230.
- [82] P.H. Schipper, A. V. Sapre, Q.N. Le, Chemical aspects of clean fuels production, in: H. de Lasa, G. Dogammau, A. Ravella (Eds.), *Chemical reactor technology for environmentally safe reactors and products*, 1992: pp. 147–182.
- [83] M.L. Occelli, J.T. Hsu, L.G. Galya, Propylene oligomerization over molecular sieves part I. Zeolite effects on reactivity and liquid product selectivities, *J. Mol. Catal.* 32 (1985) 377–390.
- [84] M. Henry, M. Bulut, W. Vermandel, B. Sels, P. Jacobs, D. Minoux, N. Nesterenko, S. van Donk, J.P. Dath, Low temperature conversion of linear C 4 olefins with acid ZSM-5 zeolites of homogeneous composition, *Appl. Catal. A, Gen.* 413–414 (2012) 62–77.
- [85] A. de Klerk, E. Furimsky, Oligomerization, in: *Catalysis in the refining of Fischer-Tropsch syncrude*, 2010: pp. 41–79.
- [86] R.O. Minnie, Catalytic conversion of olefins to diesel and gasoline fuel, WO 2006091986 A1, 2006.
- [87] U. of the W. Cape, PetroSA, Advancing synthetic fuels technology development and know-how through human capital development, <https://www.uwc.ac.za/Faculties/NS/SAIAMC/Pages/PSFIC.aspx> (accessed March 24, 2016).
- [88] Axens, Polynaphtha, <http://www.axens.net/product/technology-licensing/10082/polynaphtha.html> (accessed March 24, 2016).
- [89] S. Frays, S. Huchette, Gasoline and diesel imbalances in the Atlantic Basin: part II, (2011) 8. <http://www.axens.net/document/932/gasoline-and-diesel-imbalances---part-2/english.html> (accessed January 3, 2016).
- [90] Axens, PolyFuel, <http://www.axens.net/product/technology-licensing/20071/polyfuel.html> (accessed March 24, 2016).
- [91] E. Benazzi, Gasoline and diesel imbalances in the Atlantic Basin Part I: market outlook, (2011) 5. <http://www.axens.net/document/11/gasoline-and-diesel-imbalances---part-1/english.html> (accessed January 3, 2016).
- [92] M. Gagnière, A. Pucci, E. Rousseau, Tackling the gasoline/middle distillate imbalance, (2013) 31–33. <http://www.axens.net/document/1003/tackling-the-gasoline-middle-distillate-imbalance/english.html> (accessed April 1, 2016).
- [93] Axens, IP 811, <http://www.axens.net/product/catalysts-a-adsorbents/241/ip-811.html> (accessed March 24, 2016).
- [94] Axens, FlexEne, <http://www.axens.net/product/technology-licensing/11001/flexene.html> (accessed March 24, 2016).
- [95] C. Dupraz, (R)FCC product flexibility with FlexEne™, (2012). <https://www.slideshare.net/AlbaniaVillarroel/axens-flexene-artc2012cdenglish> (accessed February 10, 2019).

- [96] L.H. Sperling, Dilute solution thermodynamics, molecular weights, and sizes, in: Introduction to physical polymer, 4<sup>th</sup> ed., John Wiley & Sons, 2006: pp. 71–144.
- [97] M. Sanati, C. Hörnell, S.G. Jaras, The Oligomerization of alkenes by heterogeneous catalysts, in: J.J. Spivey (Ed.), Catalysis: volume 14 (Specialist periodical reports), Royal society of chemistry, 1999: pp. 236–287.
- [98] P.M.M. Blauwhoff, J.W. Gosselink, E.P. Kieffer, S.T. Sie, W.H.J. Stork, Zeolites as catalysts in industrial processes, in: J. Weitkamp, L. Puppe (Eds.), Catalysis and zeolites: fundamentals and applications, Springer Berlin Heidelberg, Berlin, Heidelberg, 1999: pp. 437–538.
- [99] M. Stöcker, Gas phase catalysis by zeolites, *Microporous Mesoporous Mater.* 82 (2005) 257–292.
- [100] G. Caeiro, R.H. Carvalho, X. Wang, M.A.N.D.A. Lemos, F. Lemos, M. Guisnet, F.R. Ribeiro, Activation of C2–C4 alkanes over acid and bifunctional zeolite catalysts, *J. Mol. Catal. A Chem.* 255 (2006) 131–158.
- [101] B.A. Williams, S.M. Babitz, J.T. Miller, R.Q. Snurr, H.H. Kung, The roles of acid strength and pore diffusion in the enhanced cracking activity of steamed Y zeolites, *Appl. Catal. A Gen.* 177 (1999) 161–175.
- [102] S. Kotrel, H. Knözinger, B.C. Gates, The Haag–Dessau mechanism of protolytic cracking of alkanes, *Microporous Mesoporous Mater.* 35–36 (2000) 11–20.
- [103] J. Weitkamp, Catalytic hydrocracking-mechanisms and versatility of the process, *ChemCatChem* 4 (2012) 292–306.
- [104] J.R. Shahrouzi, D. Guillaume, P. Rouchon, P. Da Costa, Stochastic simulation and single events kinetic modeling: Application to olefin oligomerization, *Ind. Eng. Chem. Res.* 47 (2008) 4308–4316.
- [105] M. Guisnet, N.S. Gnep, Aromatization of short chain alkanes on zeolite catalysts, *Appl. Catal. A, Gen.* 89 (1992) 1–30.
- [106] S. Rossini, The impact of catalytic materials on fuel reformulation, *Catal. Today* 77 (2003) 467–484.
- [107] S. Peratello, M. Molinari, G. Bellussi, C. Perego, Olefins oligomerization: thermodynamics and kinetics over a mesoporous silica-alumina, *Catal. Today* 52 (1999) 271–277.
- [108] L. Ying, J. Zhu, Y. Cheng, L. Wang, X. Li, Kinetic modeling of C2–C7 olefins interconversion over ZSM-5 catalyst, *J. Ind. Eng. Chem.* 33 (2016) 80–90.
- [109] X. Huang, D. Aihemaitijiang, W. De Xiao, Reaction pathway and kinetics of C3–C7 olefin transformation over high-silicon HZSM-5 zeolite at 400–490°C, *Chem. Eng. J.* 280 (2015) 222–232.
- [110] A. V. Lavrenov, T.R. Karpova, E.A. Buluchevskii, E.N. Bogdanets, Heterogeneous oligomerization of light alkenes: 80 years in oil refining, *Catal. Ind.* 8 (2016) 316–327.
- [111] B.M. Antunes, A.E. Rodrigues, Z. Lin, C.M. Silva, Alkenes oligomerization with resin catalysts, *Fuel Process. Technol.* 138 (2015) 86–99.
- [112] J.W. Yoon, J.-S. Chang, H.-D. Lee, T.-J. Kim, S.H. Jung, Trimerization of isobutene over a zeolite beta catalyst, *J. Catal.* 245 (2007) 253–256.
- [113] W.Y. Ji, H.J. Sung, J.S. Chang, Trimerization of isobutene over solid acid catalysts: Comparison between cation-exchange resin and zeolite catalysts, *Bull. Korean Chem. Soc.* 29 (2008) 339–341.
- [114] C. Martínez, E.J. Dorskocil, A. Corma, Improved THETA-1 for light olefins oligomerization to diesel: influence of textural and acidic properties, *Top. Catal.* 57 (2014) 668–682.

- [115] Y.T. Kim, J.P. Chada, Z. Xu, Y.J. Pagan-Torres, D.C. Rosenfeld, W.L. Winniford, E. Schmidt, G.W. Huber, Low-temperature oligomerization of 1-butene with H-ferrierite, *J. Catal.* 323 (2015) 33–44.
- [116] E. Rossetto, B.P. Nicola, R.F. De Souza, K. Bernardo-Gusmão, S.B.C. Pergher, Heterogeneous complexes of nickel MCM-41 with beta-diimine ligands: Applications in olefin oligomerization, *J. Catal.* 323 (2015) 45–54.
- [117] R. Catani, M. Mandreoli, S. Rossini, A. Vaccari, Mesoporous catalysts for the synthesis of clean diesel fuels by oligomerisation of olefins, *Catal. Today* 75 (2002) 125–131.
- [118] J.S. Lee, J.W. Yoon, S.B. Halligudi, J.S. Chang, S.H. Jung, Trimerization of isobutene over  $\text{WO}_x/\text{ZrO}_2$  catalysts, *Appl. Catal. A Gen.* 366 (2009) 299–303.
- [119] F. Tzompantzi, A. Mantilla, G. Del Angel, J.M. Padilla, J.L. Fernández, J.A. I. Díaz-Góngora, R. Gómez,  $\text{NiO-W}_2\text{O}_3/\text{Al}_2\text{O}_3$  catalysts for the production of ecological gasoline: effect of both NiO and the preparation method on the isobutene oligomerization selectivity, *Catal. Today* 143 (2009) 132–136.
- [120] S. Liu, J. Shang, S. Zhang, B. Yang, Y. Deng, Highly efficient trimerization of isobutene over silica supported chloroaluminate ionic liquid using C4 feed, *Catal. Today* 200 (2013) 41–48.
- [121] Y. Gu, F. Shi, Y. Deng,  $\text{SO}_3\text{H}$ -functionalized ionic liquid as efficient, green and reusable acidic catalyst system for oligomerization of olefins, *Catal. Commun.* 4 (2003) 597–601.
- [122] C. Fehér, E. Kriván, J. Hancsók, R. Skoda-Földes, Oligomerisation of isobutene with silica supported ionic liquid catalysts, *Green Chem.* 14 (2012) 403.
- [123] C. Fehér, E. Kriván, J. Kovács, J. Hancsók, R. Skoda-Földes, Support effect on the catalytic activity and selectivity of SILP catalysts in isobutene trimerization, *J. Mol. Catal. A Chem.* 372 (2013) 51–57.
- [124] J. Skupiński, Oligomerization of  $\alpha$ -olefins to higher oligomers, *Chem. Rev.* 91 (1991) 613–648.
- [125] A. Finiels, F. Fajula, V. Hulea, Nickel-based solid catalysts for ethylene oligomerization – a review, *Catal. Sci. Technol.* 4 (2014) 2412.
- [126] J.J.M. Órfão, Mechanisms and kinetic in heterogeneous catalysis, in: J.L. Figueiredo, M.M. Pereira, J. Faria (Eds.), *Catalysis from theory to application*, 2008: pp. 55–82.
- [127] Z. Wang, G.A. Solan, W. Zhang, W.-H. Sun, Carbocyclic-fused N,N,N-pincer ligands as ring-strain adjustable supports for iron and cobalt catalysts in ethylene oligo-/polymerization Zheng, *Coord. Chem. Rev.* 363 (2018) 92–108.
- [128] K.A. Alferov, G.P. Belov, Y. Meng, Chromium catalysts for selective ethylene oligomerization to 1-hexene and 1-octene: recent results, *Appl. Catal. A, Gen.* 542 (2017) 71–124.
- [129] G. Mao, Y. Jiang, N. Li, Q. Wang, D. Zheng, M. Li, Y. Ning, Recent progresses of late-transition metal complexes with nonsymmetric diimine ligands in ethylene polymerization and oligomerization, *Chinese Sci. Bull.* 59 (2014) 2505–2512.
- [130] G.P. Belov, Tetramerization of ethylene to octene-1 (a review), *Pet. Chem.* 52 (2012) 139–154.
- [131] T. Agapie, Selective ethylene oligomerization: recent advances in chromium catalysis and mechanistic investigations, *Coord. Chem. Rev.* 255 (2011) 861–880.
- [132] S. Kinoshita, K. Kawamura, T. Fujita, Early-transition-metal catalysts with phenoxy-imine-type ligands for the oligomerization of ethylene, *Chem. - An Asian J.* 6 (2011) 284–290.
- [133] D.S. McGuinness, Olefin oligomerization via metallacycles: dimerization, trimerization, tetramerization, and beyond, *Chem. Rev.* 111 (2011) 2321–2341.

- [134] F. Speiser, P. Braunstein, L. Saussine, Catalytic ethylene dimerization and oligomerization: recent developments with nickel complexes containing P,N-chelating ligands, *Acc. Chem. Res.* 38 (2006) 784–793.
- [135] J.T. Dixon, M.J. Green, F.M. Hess, D.H. Morgan, Advances in selective ethylene trimerisation – a critical overview, *J. Organomet. Chem.* 689 (2004) 3641–3668.
- [136] B. Yilmaz, U. Müller, Catalytic applications of zeolites in chemical industry, *Top. Catal.* 52 (2009) 888–895.
- [137] W. Vermeiren, J.P. Gilson, Impact of zeolites on the petroleum and petrochemical industry, *Top. Catal.* 52 (2009) 1131–1161.
- [138] M. Flanigen, R.W. Broach, S.T. Wilson, Introduction, in: S. Kulprathipanja (Ed.), *Zeolites in industrial separation and catalysis*, Wiley-VCH Verlag GmbH & Co. KGaA, Weinheim, 2010: pp. 1–26.
- [139] W.M. Meier, D.H. Olson, C. Baerlocher, *Atlas of zeolites*, 5<sup>th</sup> ed., Elsevier Science, 2001.
- [140] J.C. Groen, J.A. Moulijn, J. Pérez-Ramírez, Desilication: on the controlled generation of mesoporosity in MFI zeolites, *J. Mater. Chem.* 16 (2006) 2121–2131.
- [141] A. Corma, State of the art and future challenges of zeolites as catalysts, *J. Catal.* 216 (2003) 298–312.
- [142] J. Weitkamp, Zeolites and catalysis, *Solid State Ionics* 131 (2000) 175–188.
- [143] H. Kim, D. Kim, Y.P.J. Jeon, Synthesis of jet fuel through the oligomerization of butenes on zeolite catalysts, *Res. Chem. Intermed.* 44 (2018) 3823–3833.
- [144] B. Zdravkov, J. Čermák, M. Šefara, J. Janků, Pore classification in the characterization of porous materials: a perspective, *Open Chem.* 5 (2007) 385–395.
- [145] A. Chica, Zeolites: promised materials for the sustainable production of hydrogen, *ISRN Chem. Eng.* 2013 (2013) 1–19.
- [146] Atish Kulkarni, Oligomerization of pentenes by acid zeolites, Thesis, Graduate School-New Brunswick Rutgers, The State University of New Jersey, 2015.
- [147] A. Corma, Inorganic solid acids and their use in acid-catalyzed hydrocarbon reactions, *Chem. Rev.* 95 (1995) 559–614.
- [148] R.C. Deka, Acidity in zeolites and their characterization by different spectroscopic methods, *Indian J. Chem. Technol.* 5 (1998) 109–123.
- [149] J.M. Campelo, F. Lafont, J.M. Marin, Pt/SAPO-5 and Pt/SAPO-11 as catalysts for the hydroisomerization and hydrocracking of *n*-octane, *J. Chem. Soc., Faraday Trans.* 91 (1995) 1551–1555.
- [150] E.P. Parry, An infrared study of pyridine adsorbed characterization of surface, *J. Catal.* 2 (1963) 371–379.
- [151] B. Hunger, M. Heuchel, L.A. Clark, R.Q. Snurr, Characterization of acidic OH groups in zeolites of different types: An interpretation of NH<sub>3</sub>-TPD results in the light of confinement effects, *J. Phys. Chem. B* 106 (2002) 3882–3889.
- [152] G.V.A. Martins, G. Berlier, C. Bisio, S. Coluccia, H.O. Pastore, L. Marchese, Quantification of Brønsted acid sites in microporous catalysts by a combined FTIR and NH<sub>3</sub>-TPD study, *J. Phys. Chem. C* 112 (2008) 7193–7200.
- [153] B.M. Lok, B.K. Marcus, C.L. Angell, Characterization of zeolite acidity. II. Measurement of zeolite acidity by ammonia temperature programmed desorption and FTIR spectroscopy techniques, *Zeolites* 6 (1986) 185–194.

- [154] E. Lippmaa, M. Magi, A. Samoson, M. Tarmak, G. Engelhardt, S. Al, Investigation of the structure of zeolites by solid-state high-resolution  $^{29}\text{Si}$  NMR spectroscopy, *J. Am. Chem. Soc.* 103 (1981) 4992–4996.
- [155] J.B. Nagy, Z. Gabelica, G. Debras, E.G. Derouane, J.-P. Gilson,  $^{27}\text{Al}$ -n.m.r. characterization of natural and synthetic zeolites, *Zeolites* 4 (1984) 133–139.
- [156] T. Mildner, D. Freude, Proton transfer between Brønsted sites and benzene molecules in zeolites H-Y studied by in situ MAS NMR, *J. Biotechnol.* 178 (1998) 309–314.
- [157] S. Li, A. Zheng, Y. Su, H. Zhang, L. Chen, J. Yang, Brønsted/Lewis acid synergy in dealuminated HY zeolite: A combined solid-state NMR and theoretical calculation study, *J. Am. Chem. Soc.* 129 (2007) 11161–11171.
- [158] A. Bhan, E. Iglesia, A link between reactivity and local structure in acid catalysis on zeolites, *Acc. Chem. Res.* 41 (2008) 559–567.
- [159] W.E. Farneth, Methods for characterizing zeolite acidity, *Chem. Rev.* 95 (1995) 615–635.
- [160] A.G. Popov, V.S. Pavlov, I.I. Ivanova, Effect of crystal size on butenes oligomerization over MFI catalysts, *J. Catal.* 335 (2016) 155–164.
- [161] A. Corma, C. Martínez, E. Doskocil, Designing MFI-based catalysts with improved catalyst life for  $\text{C}_3=$  and  $\text{C}_5=$  oligomerization to high-quality liquid fuels, *J. Catal.* 300 (2013) 183–196.
- [162] K.G. Wilshier, P. Smart, R. Western, T. Mole, Oligomerization of propene over H-ZSM-5 zeolite, *Appl. Catal.* 31 (1987) 339–359.
- [163] M.R. Apelian, J.R. Boulton, S. Anthony Fung, Olefin oligomerization with surface modified zeolite catalyst, US 5284989 A, 1994.
- [164] N.M. Page, L.B. Young, D.A. Blain, Olefin oligomerization with surface modified zeolite catalyst, US 4870038, 1989.
- [165] M.M. Pereira, A. Fernandes, Fundamental aspects in zeolites synthesis and post-synthesis modification, in: M.M. Pereira (Ed.), *Catalysis from theory to application*, Imprensa da Universidade de Coimbra, 2008: pp. 107–144.
- [166] L. Costa, F.R. Ribeiro, Shape selective catalysis by zeolites, in: M.M. Pereira (Ed.), *Catalysis from theory to application*, Imprensa da Universidade de Coimbra, 2008: pp. 191–212.
- [167] S. Teketel, L.F. Lundegaard, W. Skistad, S.M. Chavan, U. Olsbye, K.P. Lillerud, P. Beato, S. Svelle, Morphology-induced shape selectivity in zeolite catalysis, *J. Catal.* 327 (2015) 22–32.
- [168] J. Weitkamp, S. Ernst, L. Puppe, Shape-selective catalysis in zeolites, in: *Catalysis and zeolites: fundamentals and applications*, Springer-Verlag Berlin Heidelberg, 1999: pp. 327–376.
- [169] E.G. Derouane, Shape selectivity in catalysis by zeolites: the nest effect, *J. Catal.* 100 (1986) 541–544.
- [170] G. Sastre, A. Corma, The confinement effect in zeolites, *J. Mol. Catal. A Chem.* 305 (2009) 3–7.
- [171] D.S. Santilli, T. V. Harris, S.I. Zones, Inverse shape selectivity in molecular sieves: Observations, modelling, and predictions, *Microporous Mater.* 1 (1993) 329–341.
- [172] M.C. Claude, G. Vanbutsele, J.A. Martens, Dimethyl branching of long *n*-alkanes in the range from decane to tetracosane on pt/H-ZSM-22 bifunctional catalyst, *J. Catal.* 203 (2001) 213–231.
- [173] E. Derouane, Z. Gabelica, A novel effect of shape selectivity: molecular traffic control in zeolite ZSM-5, *J. Catal.* 65 (1980) 486–489.

- [174] C.N. Satterfield, Acid and zeolite catalysts, in: *Heterogeneous catalysis in industrial practice*, 2<sup>nd</sup> ed., McGraw-Hill, New York, 1991: pp. 209–266.
- [175] J. Xiao, J. Wiewi, Diffusion mechanisms of hydrocarbons in zeolites - I. Theory, *Chem. Eng. Sci.* 47 (1992) 1123–1141.
- [176] D.M. Ruthven, Diffusion in zeolite molecular sieves, in: *Introduction to zeolite science and practice*, Elsevier Science, 2007: pp. 737–785.
- [177] N.Y. Chen, T.F.D. Jr., C.M. Smith, Molecular transport and reaction in zeolites: design and application of shape selective catalysis, John Wiley & Sons, 1994.
- [178] K. Li, J. Valla, J. Garcia-Martinez, Realizing the commercial potential of hierarchical zeolites: New opportunities in catalytic cracking, *ChemCatChem* 6 (2014) 46–66.
- [179] M. Campanati, G. Fornasari, A. Vaccari, Fundamentals in the preparation of heterogeneous catalysts, *Catal. Today* 77 (2003) 299–314.
- [180] G.J. Hutchings, C.J. Viedrine, Catalyst preparation, in: M. Baerns (Ed.), *Basic principles in applied catalysis*, Springer-Verlag Berlin Heidelberg, 2004: pp. 215–258.
- [181] J.L. Figueiredo, F.R. Ribeiro, Preparação de catalisadores, in: *Catálise heterogénea*, 2<sup>nd</sup> ed., 2007: pp. 99–172.
- [182] R.A. Sheldon, I. Arends, U. Hanefeld, Solid acids and bases as catalysts, in: *Green chemistry and catalysis*, Wiley-VCH Verlag GmbH & Co. KGaA, 2007: pp. 49–90.
- [183] E.F. Gallei, M. Hesse, E. Schwab, Preparation of solid catalysts, in: G. Ertl, H. Knözinger, F. Schüth, J. Weitkamp (Eds.), *Handbook of heterogeneous catalysis*, Volume 1, Wiley-VCH, 2008: pp. 57–720.
- [184] M.J. Wulfers, R.F. Lobo, Assessment of mass transfer limitations in oligomerization of butene at high pressure on H-beta, *Appl. Catal. A Gen.* 505 (2015) 394–401.
- [185] D.P. Serrano, J.M. Escola, P. Pizarro, Synthesis strategies in the search for hierarchical zeolites, *Chem. Soc. Rev.* 42 (2013) 4004–4035.
- [186] J. Pérez-Ramírez, C.H. Christensen, K. Egeblad, C.H. Christensen, J.C. Groen, Hierarchical zeolites: enhanced utilisation of microporous crystals in catalysis by advances in materials design, *Chem. Soc. Rev.* 37 (2008) 2530.
- [187] E. Koohsaryan, M. Anbia, Nanosized and hierarchical zeolites: a short review, *Cuihua Xuebao/Chinese J. Catal.* 37 (2016) 447–467.
- [188] L.S. Roselin, R. Selvin, M. Bououdina, Nanocrystalline ZSM-5: an efficient catalyst for regioselective acetolysis of epichlorohydrin, *Chem. Eng. Commun.* 199 (2012) 221–230.
- [189] X. Cheng, J. Mao, X. Lv, T. Hua, X. Cheng, Y. Long, Y. Tang, Fast synthesis of nanosized zeolite beta from a low-seeded, low-templated dry gel with a seeding-steam-assisted conversion method, *J. Mater. Chem. A* 2 (2014) 1247–1251.
- [190] X. Vu, U. Armbruster, A. Martin, Micro/mesoporous zeolitic composites: recent developments in synthesis and catalytic applications, *Catalysts* 6 (2016) 183–206.
- [191] J. Cejka, H. van Bekkum, *Zeolites and ordered mesoporous materials: progress and prospects*, Volume 157, 1<sup>st</sup> ed., Elsevier Science, 2005.
- [192] M.K. de Pietre, F.A. Bonk, C. Rettori, F.A. Garcia, H.O. Pastore, [V,Al]-ITQ-6: novel porous material and the effect of delamination conditions on V sites and their distribution, *Microporous Mesoporous Mater.* 145 (2011) 108–117.
- [193] U. Díaz, Layered materials with catalytic applications: pillared and delaminated zeolites from MWW precursors, *ISRN Chem. Eng.* 2012 (2012) 1–35.
- [194] U. Díaz, A. Corma, Layered zeolitic materials: an approach to designing versatile functional solids, *Dalt. Trans.* 43 (2014) 10292–10316.

- [195] K. Na, M. Choi, R. Ryoo, Recent advances in the synthesis of hierarchically nanoporous zeolites, *Microporous Mesoporous Mater.* 166 (2013) 3–19.
- [196] M.S. Holm, E. Taarning, K. Egeblad, C.H. Christensen, Catalysis with hierarchical zeolites, *Catal. Today* 168 (2011) 3–16.
- [197] K. Zhu, X. Zhou, Manipulating the architecture of zeolite catalysts for enhanced mass transfer, *Curr. Opin. Chem. Eng.* 9 (2015) 42–48.
- [198] D.P. Serrano, J.M. Escola, R. Sanz, R.A. Garcia, A. Peral, I. Moreno, M. Linares, Hierarchical ZSM-5 zeolite with uniform mesopores and improved catalytic properties, *New J. Chem.* 40 (2016) 4206–4216.
- [199] R. Chal, C. Gérardin, M. Bulut, S. van Donk, Overview and industrial assessment of synthesis strategies towards zeolites with mesopores, *ChemCatChem* 3 (2011) 67–81.
- [200] J.C. Groen, J.C. Jansen, J.A. Moulijn, J. Pe, Optimal aluminum-assisted mesoporosity development in MFI zeolites by desilication, *J. Phys. Chem. B* (2004) 13062–13065.
- [201] M. Ogura, S. Shinomiya, J. Tateno, Y. Nara, M. Nomura, E. Kikuchi, M. Matsukata, Alkali-treatment technique-new method for modification of structural and acid-catalytic properties of ZSM-5 zeolites, *Appl. Catal. A Gen.* 219 (2001) 33–43.
- [202] J.C. Groen, L.A.A. Peffer, J.A. Moulijn, Mesoporosity development in ZSM-5 zeolite upon optimized desilication conditions in alkaline medium, *Colloids Surfaces A Physicochem. Eng. Asp.* 241 (2004) 53–58.
- [203] J. Pérez-Ramírez, D. Verboekend, A. Bonilla, S. Abello, Zeolite catalysts with tunable hierarchy factor by pore-growth moderators, *Adv. Funct. Mater.* 19 (2009) 3972–3979.
- [204] D. Verboekend, S. Mitchell, M. Milina, J.C. Groen, J. Pérez-Ramírez, Full compositional flexibility in the preparation of mesoporous MFI zeolites by desilication, *J. Phys. Chem. C.* 115 (2011) 14193–14203.
- [205] D. Verboekend, J. Pérez-Ramírez, Desilication mechanism revisited: highly mesoporous all-silica zeolites enabled through pore-directing agents, *Chem. - A Eur. J.* 17 (2011) 1137–1147.
- [206] S. Abelló, A. Bonilla, J. Pérez-Ramírez, Mesoporous ZSM-5 zeolite catalysts prepared by desilication with organic hydroxides and comparison with NaOH leaching, *Appl. Catal. A Gen.* 364 (2009) 191–198.
- [207] Q. Shen, L. Zhang, M. Wu, C. He, W. Wei, N. Sun, Y. Sun, Postsynthesis of mesoporous ZSM-5 zeolites with TPAOH-assisted desilication and determination of activity performance in N<sub>2</sub>O decomposition, *J. Porous Mater.* 24 (2017) 759–767.
- [208] Y. He, M. Liu, C. Dai, S. Xu, Y. Wei, Z. Liu, X. Guo, Modification of nanocrystalline HZSM-5 zeolite with tetrapropylammonium hydroxide and its catalytic performance in methanol to gasoline reaction, *Cuihua Xuebao/Chinese J. Catal.* 34 (2013) 1148–1158.
- [209] R. Caicedo-Realpe, J. Pérez-Ramírez, Mesoporous ZSM-5 zeolites prepared by a two-step route comprising sodium aluminate and acid treatments, *Microporous Mesoporous Mater.* 128 (2010) 91–100.
- [210] S. Yang, C. Yu, L. Yu, S. Miao, M. Zou, C. Jin, D. Zhang, L. Xu, S. Huang, Bridging dealumination and desilication for the synthesis of hierarchical MFI zeolites, *Angew. Chemie.* (2017).
- [211] S. van Donk, A.H. Janssen, J.H. Bitter, K.P. De Jong, Generation, characterization, and impact of mesopores in zeolite catalysts, *Catal. Rev.* 45 (2003) 297–319.
- [212] C.S. Triantafillidis, A.G. Vlessidis, N.P. Evmiridis, Dealuminated H-Y zeolites: influence of the degree and the type of dealumination method on the structural and acidic characteristics of H-Y zeolites, *Ind. Eng. Chem. Res.* (2000) 307–319.

- [213] M.M.L.R. Carrott, P.A. Russo, C. Carvalhal, P.J.M. Carrott, Adsorption of *n*-pentane and iso-octane for the evaluation of the porosity of dealuminated BEA zeolites, *Microporous Mesoporous Mater.* 81 (2005) 259–267.
- [214] E.F.T. Lee, L.V.C. Rees, Dealumination of sodium Y zeolite with hydrochloric acid, (1987) 1531–1537.
- [215] A.W.O. Donovan, C.T.O. Connor, K.R. Koch, Effect of acid and steam treatment of Na- and H-mordenite on their structural, acidic and catalytic properties, 5 (1995) 185–202.
- [216] V. Valtchev, E. Balanzat, V. Mavrodinova, I. Diaz, E. Fallah, High energy ion irradiation-induced ordered macropores in zeolite crystals, *J. Am. Chem. Soc.* (2011) 18950–18956.
- [217] K. Möller, T. Bein, Mesoporosity – a new dimension for zeolites, *Chem Soc Rev.* 42 (2013) 3689–3707.
- [218] H.C. Bajaj, P.A. Parikh, Synthesis of hierarchical nano-crystalline zeolite beta using biomass-derived hard templates, *Int. J. Mater. Eng. Innov.* 6 (2015) 49–58.
- [219] I. Schmidt, C. Madsen, C.J.H. Jacobsen, Confined space synthesis. A novel route to nanosized zeolites, *Inorg. Chem.* 39 (2000) 2279–2283.
- [220] K. Na, M. Choi, R. Ryoo, Recent advances in the synthesis of hierarchically nanoporous zeolites, *Microporous Mesoporous Mater.* 166 (2013) 3–19.
- [221] M. Yang, B. Wang, F. Hu, X. Mi, H. Liu, H. Liu, X. Gao, Synergy between crystal seeds and amphiphilic organosilane surfactant: a facile approach for mesoporous ZSM-5 with high SiO<sub>2</sub>/Al<sub>2</sub>O<sub>3</sub> ratio, *Mater. Lett.* 222 (2018) 153–155.
- [222] Y. Yuan, P. Tian, M. Yang, D. Fan, L. Wang, S. Xu, C. Wang, D. Wang, Y. Yang, Z. Liu, Synthesis of hierarchical beta zeolite by using a bifunctional cationic polymer and the improved catalytic performance, *RSC Adv.* 5 (2015) 9852–9860.
- [223] L. Wang, Z. Zhang, C. Yin, Z. Shan, F.-S. Xiao, Hierarchical mesoporous zeolites with controllable mesoporosity templated from cationic polymers, *Microporous Mesoporous Mater.* 131 (2010) 58–67.
- [224] Y. Wei, T.E. Parmentier, K.P. de Jong, J. Zečević, Tailoring and visualizing the pore architecture of hierarchical zeolites, *Chem. Soc. Rev.* 44 (2015) 7234–7261.
- [225] Z. Xue, T. Zhang, J. Ma, H. Miao, W. Fan, Y. Zhang, R. Li, Accessibility and catalysis of acidic sites in hierarchical ZSM-5 prepared by silanization, *Microporous Mesoporous Mater.* 151 (2012) 271–276.
- [226] M. Choi, H.S. Cho, R. Srivastava, C. Venkatesan, D.-H. Choi, R. Ryoo, Amphiphilic organosilane-directed synthesis of crystalline zeolite with tunable mesoporosity, *Nat. Mater.* 5 (2006) 718–723.
- [227] D.P. Serrano, J. Aguado, G. Morales, J.M. Rodri, A. Peral, M. Thommes, Molecular and meso- and macroscopic properties of hierarchical nanocrystalline ZSM-5 zeolite prepared by seed silanization, *Chem. Mater.* 216 (2009) 641–654.
- [228] H. Wang, T.J. Pinnavaia, MFI zeolite with small and uniform untracrystal mesopores, *Angew. Chem. Int. Ed.* 45 (2006) 7603–7606.
- [229] K. Möller, B. Yilmaz, R.M. Jacubinas, U. Müller, T. Bein, One-step synthesis of hierarchical zeolite beta via network formation of uniform nanocrystals, *J. Am. Chem. Soc.* 133 (2011) 5284–5295.
- [230] Y. Wang, J. Song, N.C. Baxter, G.T. Kuo, S. Wang, Synthesis of hierarchical ZSM-5 zeolites by solid-state crystallization and their catalytic properties, *J. Catal.* 349 (2017) 53–65.
- [231] K. Möller, B. Yilmaz, U. Müller, T. Bein, Nanofusion: mesoporous zeolites made easy, *Chem. Eur. J.* 18 (2012) 7671–7674.

- [232] L. Huang, F. Qin, Z. Huang, Y. Zhuang, J. Ma, H. Xu, W. Shen, Hierarchical ZSM-5 zeolite synthesized by an ultrasound-assisted method as a long-life catalyst for dehydration of glycerol to acrolein, *Ind. Eng. Chem. Res.* 55 (2016) 7318–7327.
- [233] J. Zhu, Y. Cui, Y. Wang, F. Wei, Direct synthesis of hierarchical zeolite from a natural layered material, *Chem. Commun.* (2009) 3282–3284.
- [234] B. Wei, H. Liu, T. Li, L. Cao, Y. Fan, Natural rectorite mineral: a promising substitute of kaolin for *in-situ* synthesis of Fluid Catalytic Cracking catalysts, *AIChE J.* 56 (2010) 2913–2922.
- [235] D.T. On, S. Kaliaguine, Large-pore mesoporous materials with semi-crystalline zeolitic frameworks, *Angew. Chem. Int. Ed.* 40 (2001) 3248–3251.
- [236] D.T. On, S. Kaliaguine, Zeolite-coated mesostructured cellular silica foams, *J. Am. Chem. Soc.* 125 (2003) 618–619.
- [237] M. Moliner, Direct synthesis of functional zeolitic materials, *ISRN Mater. Sci.* 2012 (2012) 1–24.
- [238] Y. Wang, J. Song, N.C. Baxter, G.T. Kuo, S. Wang, Synthesis of hierarchical ZSM-5 zeolites by solid-state crystallization and their catalytic properties, *J. Catal.* 349 (2017) 53–65.
- [239] M. Rilyanti, R.R. Mukti, G.T.M. Kadja, M. Ogura, H. Nur, E.-P. Ng, Ismunandar, On the drastic reduction of organic structure directing agent in the steam-assisted crystallization of zeolite with hierarchical porosity, *Microporous Mesoporous Mater.* 230 (2016) 30–38.
- [240] C. Bertrand-Dira, X. wei Cheng, T. Cacciaguerra, P. Trens, G. Melinte, O. Ersen, D. Minoux, A. Finiels, F. Fajula, C. Gerardin, Mesoporous mordenites obtained by desilication: mechanistic considerations and evaluation in catalytic oligomerization of pentene, *Microporous Mesoporous Mater.* 213 (2015) 142–149.
- [241] M.R. Díaz-Rey, C. Paris, R. Martínez-Franco, M. Moliner, C. Martínez, A. Corma, Efficient oligomerization of pentene into liquid fuels on nanocrystalline Beta zeolites, *ACS Catal.* 7 (2017) 6170–6178.
- [242] N.G. Grigor, S. V. Bubennov, B.I. Kutepov, Oligomerization of  $\alpha$ -octene catalyzed by zeolites, *Catal. Chem. Petrochemical Ind.* 3 (2011) 144–150.
- [243] N.G. Grigoréva, S. V. Bubennov, A.A. Mayak, B.I. Kutepov, Oligomerization of 1-octene on micro-mesoporous zeolite catalysts, *Pet. Chem.* 53 (2013) 407–411.
- [244] R.J. Argauer, G.R. Landolt, Crystalline zeolite ZSM-5 and method of preparing the same, US 3702886, 1972.
- [245] S.A. Tabak, F.J. Krambeck, W.E. Garwood, Conversion of propylene and butylene over ZSM-5 catalyst, *AIChE J.* 32 (1986) 1526–1531.
- [246] R.W. Broach, Zeolite types and structures, in: *Zeolites in industrial separation and catalysis*, Wiley-VCH Verlag GmbH & Co, 2010: pp. 27–60.
- [247] W.O. Haag, N.Y. Chen, Catalyst design with zeolites, in: L.L. Hegedus, A.T. Bell, N.Y. Chen, W.O. Haag, J. Wei, R. Aris, M. Boudart, B.C. Gates, G.A. Somorjai (Eds.), *Catalyst design-progress and perspectives*, Wiley Interscience, New York, 1987: pp. 162–213.
- [248] L.G. Galya, M.L. Occelli, J.T. Hsu, D.C. Young, Propylene oligomerization over molecular sieves: Part II.  $^1\text{H}$  NMR and  $^{13}\text{C}$  NMR characterization of reaction products, *J. Mol. Catal.* 32 (1985) 391–403.
- [249] S. Schwarz, M. Kojima, C.T. O'Connor, Effect of silicon-to-aluminum ratio and synthesis time on high-pressure olefin oligomerization over ZSM-5, *Appl. Catal.* 56 (1989) 263–280.
- [250] A.N. Mlinar, P.M. Zimmerman, F.E. Celik, M. Head-Gordon, A.T. Bell, Effects of Brønsted-acid site proximity on the oligomerization of propene in H-MFI, *J. Catal.* 288 (2012) 65–73.

- [251] M. Kojima, M.W. Rautenbach, C.T. O'Connor, Butene oligomerization over ion-exchanged mordenite, *Ind. Eng. Chem. Res.* 27 (1988) 248–252.
- [252] C.T. O'Connor, R.E. Fasol, G.A. Foulds, The oligomerization of C4-alkenes with calcined NaHY-zeolites, *Fuel Process. Technol.* 13 (1986) 41–51.
- [253] C.S.H. Chen, R.F. Bridger, Shape-selective oligomerization of alkenes to near-linear hydrocarbons by zeolite catalysis, *J. Catal.* 161 (1996) 687–693.
- [254] X. Ding, C. Li, C. Yang, Study on the oligomerization of ethylene in fluidized catalytic cracking (FCC) dry gas over metal-loaded HZSM-5 catalysts, *Energy & Fuels* 24 (2010) 3760–3763.
- [255] S.J. Miller, Olefin oligomerization over high silica zeolites, *Stud. Surf. Sci. Catal.* 38 (1988) 187–197.
- [256] X.B. Li, X.Y. Jiang, Propylene oligomerization to produce diesel fuel on Zr-ZSM-5 catalyst, *Chem. Technol. Fuels Oils* 49 (2013) 156–164.
- [257] X. Li, D. Han, H. Wang, G. Liu, B. Wang, Z. Li, J. Wu, Propene oligomerization to high-quality liquid fuels over Ni/HZSM-5, *Fuel* 144 (2015) 9–14.
- [258] A.M.M. Arango, C.M.E. Garcés, J.L.A. Valderrama, A.G. Monsalve, L.A.P. Santos, A.E. Isaza, Oligomerization of propene over ZSM-5 modified with Cr and W | Oligomerización de propeno usando como catalizador ZSM-5 modificada con Cr y W, *Rev. Fac. Ing.* (2011) 57–65.
- [259] X. Zhang, J. Zhong, J. Wang, J. Gao, A. Liu, Trimerization of butene over Ni-doped zeolite catalyst: effect of textural and acidic properties, *Catal. Letters* 126 (2008) 388–395.
- [260] J. Kim, H. Chemistry, Synthesis of metal-incorporated mesoporous crystalline silicates for oligomerization of propene, *Catal. Letters* 36 (1996) 255–261.
- [261] Z. Xu, D. Zhao, J.P. Chada, D.C. Rosenfeld, J.L. Rogers, I. Hermans, G.W. Huber, Olefin conversion on nitrogen-doped carbon-supported cobalt catalyst: effect of feedstock, *J. Catal.* 354 (2017) 213–222.
- [262] D. Zhao, Z. Xu, J.P. Chada, C.A. Carrero, D.C. Rosenfeld, J.L. Rogers, I. Hermans, G.W. Huber, Cobalt oxide on N-doped carbon for 1-butene oligomerization to produce linear octenes, *ACS Catal.* 7 (2017) 7479–7489.
- [263] A.G. Popov, D.A. Fedosov, I.I. Ivanova, O.S. Vedernikov, A.V. Kleimenov, D.O. Kondrashev, V.D. Miroshkina, P.A. Abrashenkov, S.E. Kuznetsov, A ZSM-5 zeolite-based catalyst for oligomerization of the butane–butylene fraction, *Pet. Chem.* 56 (2016) 237–243.
- [264] N.A.S. Amin, D.D. Anggoro, Dealuminated ZSM-5 zeolite catalyst for ethylene oligomerization to liquid fuels, *J. Nat. Gas Chem.* 11 (2002) 79–86.
- [265] M.J. van Niekerk, C.T. O'Connor, J.C.Q. Fletcher, Methanol conversion and propene oligomerization productivity of dealuminated large-pore mordenites, *Ind. Eng. Chem. Res.* 35 (1996) 697–702.
- [266] J.W. Yoon, S.H. Jung, D.H. Choo, S.J. Lee, K.-Y. Lee, J.S. Chang, Oligomerization of isobutene over dealuminated Y zeolite catalysts, *Appl. Catal. A Gen.* 337 (2008) 73–77.
- [267] X. Wang, X. Hu, C. Song, K.W. Lux, M. Namazian, T. Imam, Oligomerization of biomass-derived light olefins to liquid fuel: effect of alkali treatment on the HZSM-5 catalyst, *Ind. Eng. Chem. Res.* 56 (2017) 12046–12055.
- [268] C. Li, J. Du, H. Wang, X. Li, S.S. Zhu, G. Liu, J. Wu, A hemicellulose modified HZSM-5 and their application in the light olefins oligomerization to high-quality liquid fuels reaction, *Catal. Commun.* 102 (2017) 89–92.
- [269] A. de Klerk, Properties of synthetic fuels from H-ZSM-5 oligomerization of Fischer-Tropsch type feed materials, *Energy and Fuels* 21 (2007) 3084–3089.

- [270] J.W. Yoon, J.H. Lee, J.-S. Chang, D.H. Choo, S.J. Lee, S.H. Jung, Trimerization of isobutene over zeolite catalysts: remarkable performance over a ferrierite zeolite, *Catal. Commun.* 8 (2007) 967–970.
- [271] J.W. Yoon, J.S. Lee, S.H. Jung, K.-Y. Lee, J.-S. Chang, Oligomerization of isobutene over aluminum chloride-loaded USY zeolite catalysts, *J. Porous Mater.* 16 (2009) 631–634.
- [272] P. Borges, R.R. Pinto, M.A.N.D.A. Lemos, F. Lemos, J.C. Védrine, E.G. Derouane, F.R. Ribeiro, Light olefin transformation over ZSM-5 zeolites. A kinetic model for olefin consumption, *Appl. Catal. A Gen.* 324 (2007) 20–29.
- [273] E. Kriván, S. Tomasek, J. Hancsók, Application possibilities of zeolite catalysts in oligomerization of light olefins, *Period. Polytech. Chem. Eng.* 58 (2014) 149–156.
- [274] S. Liu, G. Liu, Z. Liu, X. Sun, Butene-2 oligomerization to heavy olefins over ZSM-5 zeolite, *Pet. Sci. Technol.* 27 (2009) 1653–1660.
- [275] P.J. Flory, Molecular size distribution, *J. Am. Chem. Soc.* 62 (1940) 1561–1565.
- [276] G.J.P. Britovsek, R. Malinowski, D.S. McGuinness, J.D. Nobbs, A.K. Tomov, A.W. Wadsley, C.T. Young, Ethylene oligomerization beyond Schulz-Flory distributions, *ACS Catal.* 5 (2015) 6922–6925.
- [277] P.W. Jacobs, G.B. Brignac, T.R. Halbert, M. Acharya, T.A. Lelain, Nitrogen removal from olefinic naphtha feedstreams to improve hydrodesulfurization versus olefin saturation selectivity, US 7357856 B2, 2008.
- [278] J. Aguilhon, D. Minoux, K. Le Mapihan, C. Revault, S. van Donk, J.-P. Dath, Method for the conversion of low boiling point olefin containing hydrocarbon feedstock, WO 2013/104614 A1, 2013.
- [279] A.N. Mlinar, G.B. Baur, G.G. Bong, A.B. Getsoian, A.T. Bell, Propene oligomerization over Ni-exchanged Na-X zeolites, *J. Catal.* 296 (2012) 156–164.
- [280] C. Flego, S. Peratello, C. Perego, L.M.F. Sabatino, G. Bellussi, U. Romano, Reaction and deactivation study of mesoporous silica-alumina (MSA) in propene oligomerisation, *J. Mol. Catal. A Chem.* 204–205 (2003) 581–589.
- [281] B. Chiche, E. Sauvage, F. Di Renzo, I.I. Ivanova, F. Fajula, Butene oligomerization over mesoporous MTS-type aluminosilicates, *J. Mol. Catal. A Chem.* 134 (1998) 145–157.



# CHAPTER 3

---

## Experimental section



## Chapter 3

### Experimental section

3.1. Chemicals .....	113
3.2. Methods .....	115
3.2.1. Characterization of the catalysts .....	115
3.2.2. Quantification of the reaction products by GC-FID .....	118
3.2.3. Identification of the liquid reaction products by GC×GC-ToFMS .....	123
3.2.4. Determination of the cetane number, isoparaffinic index and aromatic content .....	124
3.3. Laboratory Setup 1 of the catalytic test unit .....	125
3.4. Laboratory Setup 2 of the catalytic test unit .....	129
3.4.1. Experimental procedure .....	135
3.5. References .....	139

## Chapter 3: Experimental section

In this chapter describes the preparation and physicochemical characterization of the porous solid acid materials used as catalysts for the oligomerization of 1-butene. For the catalytic studies, two laboratory scale installations - Setup 1 and Setup 2 – are described. Setup 1 already existed in the laboratory, but several drawbacks were verified (discussed ahead). Thus, several improvements were made to Setup1, leading to Setup 2 which was implemented in the year 2016 to carry out the olefin oligomerization experiments discussed in this thesis. The techniques used to analyze the reaction product mixtures are described.

### 3.1. Chemicals

Table 3.1 lists the chemicals used for the synthesis of the catalysts. Table 3.2 lists the chemical compounds and commercial zeolites used for the catalytic tests. The chemicals were obtained from commercial sources and used as received, if not mentioned otherwise.

Table 3.1. Chemicals used in the synthesis of the catalysts.<sup>[a]</sup>

Chemicals	Abbreviation/Formula	Supplier	Purity
Aluminum chlorohydrate	ACH	Fagron	95.4 %
Aluminum(III) isopropoxide	AIP	Aldrich	98 %
Ammonium hydroxide	-	Sigma-Aldrich	28-30 %
Ammonium nitrate	NH <sub>4</sub> NO <sub>3</sub>	Aldrich	98 %
Anhydrous isopropanol	-	Sigma-Aldrich	99.5 %
Cab-O-sil® M5	-	Sigma-Aldrich	n.a.
Colloidal silica (30 % SiO <sub>2</sub> in water)	-	Ludox	n.a.
Dodecyltrimethylammonium bromide	C <sub>12</sub> TMABr	Sigma-Aldrich	98 %
Ethanol	-	Riedel de Haen	99.9 %
Hexadecyltrimethylammonium bromide	CTABr	Aldrich	98 %

Table 3.1. (continued).

Chemicals	Abbreviation/Formula	Supplier	Purity
Mesitylene	-	Aldrich	98 %
Hydrochloric acid (37 % in water)	HCl	AnalaR NORMAPUR	n.a.
Oxalic acid dihydrate	Ox	Panreac	97 %
[3-(Phenylamino)propyl] trimethoxysilane	PHAPTMS	Aldrich	n.a.
Poly(acrylamide-co-diallyldimethylammonium chloride) (10 wt.% in water)	PDD-AM	Aldrich	n.a.
Polydiallyldimethylammonium chloride, molecular weight 400000-500000 g mol <sup>-1</sup> ; (20 % in water)	PDADMAC	Aldrich	n.a.
Sodium aluminate (50-56 % Al <sub>2</sub> O <sub>3</sub> )	NaAlO <sub>2</sub>	Riedel de Haen	n.a.
Sodium hydroxide	NaOH	Sigma-Aldrich	97 %
Sodium silicate (27 % SiO <sub>2</sub> ; 8 % Na <sub>2</sub> O)	-	Merck	n.a.
Tetraethylammonium hydroxide (35 wt.% in water)	TEAOH	Aldrich	99.9 %
Tetrapropylammonium hydroxide (40 wt.% in water)	TPAOH	Aldrich	99.9 %
Tetraethylorthosilicate	TEOS	Sigma	98 %
Triethanolamine	TEA	Fluka	97 %

<sup>[a]</sup> n.a.=information not available.

Table 3.2. Chemical compounds and commercial zeolites used for the catalytic tests.<sup>[a]</sup>

Chemicals	Abbreviation/Formula	Supplier	Purity
1-butene	1C4	Praxair	99.6 %
Nitrogen	N <sub>2</sub>	AirLiquid	99.999 %
Silicon carbide	SiC	SIKA	n.a.
Dichloromethane	DCM	Fisher Scientific	99.98 %
Ethylene glycol	-	Auchan	n.a.
<i>n</i> -pentane	C5	Fluka	95 %
ASTM D2887 calibration mixture ( <i>n</i> -paraffins C6-C44)	-	Supelco	n.a.

Table 3.2. (continued)

Chemicals	Abbreviation/Formula	Supplier	Purity
Zeolite HBEA (Si/Al=14, crystal size 0.5 $\mu\text{m}$ 931HOA)	BEA-micro	Tosoh	n.a.
Zeolite NH <sub>4</sub> BEA (Si/Al=12.5, CP814E)	BEA-nano	Zeolyst	n.a.
Zeolite NH <sub>4</sub> ZSM-5 (Si/Al=15, CBV3024E)	ZSM-5 (Chapter 4,5,6) or HZSM-5 (Chapter 9)	Zeolyst	n.a.
Zeolite NH <sub>4</sub> ZSM-5 (Si/Al=25, specific surface area=425 $\text{m}^2 \text{g}^{-1}$ )	ZSM-5(29) (Chapter 8)	Alfa-Aesar	n.a.
Zeolite COD-900 <sup>[b]</sup>	COD-900	Clariant Produkte GmbH	n.a.

<sup>[a]</sup> n.a.=information not available. <sup>[b]</sup> COD-900 sample was kindly supplied by Clariant Produkte GmbH (Munich, Germany).

## 3.2. Methods

### 3.2.1. Characterization of the catalysts

The X-ray powder diffraction (PXRD) data were collected on an Empyrean PANalytical diffractometer (Cu-K $\alpha$  X-radiation,  $\lambda=1.54060 \text{ \AA}$ ) in a Bragg-Brentano parafocusing optics configuration (45 kV, 40 mA). Samples were prepared in a spinning flat plate sample holder and step-scanned in the range from 3° to 70° (2 $\theta$ ) with steps of 0.026°. A PIXEL linear detector with an active area of 1.7462° was used with a counting time of 68 s per step. The low angle (0.5-5° 2 $\theta$ ) PXRD data were collected using the transmission mode, and with the sample deposited between Mylar foils; the samples were step-scanned in 0.01° 2 $\theta$  steps with a counting time of 80 s per linear detector active area of 2.0°.

Scanning electron microscopy (SEM) images, energy dispersive X-ray spectroscopy (EDS) analysis and elemental mappings (Al, Si) were obtained on a Hitachi SU-70 SEM microscope with a Bruker Quantax 400 detector operating at 20 kV. Transmission electron microscopy (TEM) was carried out on Hitachi H9000 or on Hitachi HD2700 instruments, whereas scanning transmission electron microscopy (STEM) was performed on Hitachi HD2700; samples were prepared by spotting carbon film-coated 400 mesh copper grids (Agar Scientific) with a suspension of the solid sample in ethanol.

Inductively coupled plasma atomic emission spectroscopy (ICP-AES) analyses (for Si, Al) were performed at the Central Analysis Laboratory (University of Aveiro); the measurements were carried out on a Horiba JobinYvon Activa W spectrometer (detection limit of *ca.* 20  $\mu\text{g dm}^{-3}$ ; experimental range of error of *ca.* 5 %). Prior to analyses, the solid samples (10 mg) were digested using 1  $\text{cm}^3$  HF and 1  $\text{cm}^3$  HNO<sub>3</sub>, and microwave heating at 180 °C.

Elemental analysis (EA; for C and H) was performed using a Truspec 630-200-200 instrument. The thermogravimetric analyses (TGA) and differential scanning calorimetry analyses (DSC) were carried out on Shimadzu TGA-50 and Shimadzu DSC-50 instruments, respectively, under air, from room temperature until 800 °C (for TGA) and 550 °C (for DSC), with a heating rate of 10 °C  $\text{min}^{-1}$ , maintain the final temperature for additional 15-30 min.

Nitrogen adsorption-desorption isotherms of the mesoporous TUD-1 type aluminosilicates (Chapter 5) and the BEA based materials (Chapter 6) were measured at -196 °C, using a Quantachrome instrument (automated gas sorption data using Autosorb iQ Station 1); the samples were pre-treated at 300 °C for 3 h, under vacuum (3 Torr). The external surface area ( $S_{\text{ext}}$ ) and micropore volume ( $V_{\text{micro}}$ ) were calculated by the t-plot method. The mesopore size distributions were determined from the BJH method (adsorption branch). The micropore size distribution was determined by the Horvath-Kawazoe method. The textural properties of the used catalysts were measured in a similar fashion using a Micromeritics Gemini V-2380 instrument (the samples were pre-treated at 300 °C for 3 h).

Nitrogen adsorption-desorption isotherms of the MFI based (Chapter 7, 8 and 9). were measured at -196 °C, using a Quantachrome instrument (automated gas sorption data using Autosorb IQ<sub>2</sub>). The samples were pre-treated at 300 °C for 3 h, under vacuum (3 Torr). The external or mesopore surface area ( $S_{\text{ext,meso}}$ ) and micropore volume ( $V_{\text{micro}}$ ), were

calculated by the t-plot method. The pore size distributions ( $D_p$ ) were determined by the density functional theory (DFT) method (adsorption branch). The textural properties of the used catalysts were measured in a similar fashion using the same instrument (the samples were pre-treated at 300 °C for 3 h).

The indexed hierarchy factor (IHF) was calculated according to that reported by the group of Pérez-Ramírez,<sup>[1]</sup> where the micropore and mesopore volumes were normalized by the maximum values.

The  $^{27}\text{Al}$  magic angle spinning (MAS) nuclear magnetic resonance (NMR) spectra were recorded at 182.432 MHz using a Bruker Avance 700 (16.4 T) spectrometer with a unique pulse, a recycle delay of 1 s, and a spinning rate of 14 kHz. Attenuated Total Reflectance Fourier Transform Infrared (ATR FT-IR) spectra were measured in absorbance mode using a Mattson 7000 FT-IR spectrometer equipped with a Specac Golden Gate Mk II ATR accessory having a diamond top-plate.

The surface acidity was measured by FT-IR spectroscopy of adsorbed pyridine as base probe, using a NexusThermo Nicolet apparatus (64 scans and resolution of 4  $\text{cm}^{-1}$ ) equipped with a home-made vacuum cell, using self-supported discs (5-10  $\text{mg cm}^{-2}$ ). After *in-situ* outgassing at 450 °C for 3 h ( $10^{-6}$  mbar), the sample was contacted with pyridine (99.99 %) at 200 °C for 10 min and subsequently evacuated at 200 °C or 450 °C for 30 min, under vacuum ( $10^{-6}$  mbar). The IR bands at *ca.* 1540 and 1455  $\text{cm}^{-1}$  related to pyridine adsorbed on Brønsted (B) and Lewis (L) acid sites, respectively, were used for quantification.<sup>[2,3]</sup> The Lewis and Brønsted molar extinction coefficients were 2.22 and 1.67  $\text{cm } \mu\text{mol}^{-1}$ , respectively.<sup>[3]</sup> The total amount of acid sites (L+B) and the molar ratios L/B were determined at the desorption temperature of 200 °C. The acid strength was evaluated by the molar ratios  $B_{450}/B_{200}$  (for B acid strength) and  $L_{450}/L_{200}$  (for L acid strength), where  $L_T$  and  $B_T$  are the amount of L and B acid sites, respectively, which remained adsorbed on the material after evacuation at  $T=450$  or 200 °C. The sites interacting with pyridine after evacuation at 450 °C ( $L_{450}$ ,  $B_{450}$ ) were considered as strong acid sites. The B acid site density (expressed as  $\text{meq nm}^{-2}$ , where meq is milliequivalents of acid sites) was calculated from the amount of B acid sites ( $\text{mol g}^{-1}$ ) and  $S_{\text{BET}}$  ( $\text{m}^2 \text{g}^{-1}$ ), using the following equation: B acid site density =  $(\mu\text{mol}_B \text{g}^{-1} \times 10^{-6} \times N_A) / (S_{\text{BET}} \times 10^{18}) \times 10^3$ , where  $N_A = 6.022 \times 10^{23} \text{ mol}^{-1}$ . The L acid site density was calculated using the same formula, but  $\mu\text{mol}_L \text{g}^{-1}$  instead of  $\mu\text{mol}_B \text{g}^{-1}$ .

### 3.2.2. Quantification of the reaction products by GC-FID

The gas and liquid phase reaction products were analyzed using a DANI Master Fast GC (C6), equipped with FID detector, split/splitless injector, and capillary column ValcoBond VB-1 (VICI, 60 m length, 0.25 mm ID, 1.50  $\mu\text{m}$  column film thickness, with poly(dimethylsiloxane) phase). The gas phase was directly injected into the GC from the 0.1 mL sample loops. The liquid phase was diluted (dilution factor of 34.3) in 0.0087 M internal standard solution of *n*-pentane in dichloromethane, and 1.0-1.6  $\mu\text{l}$  was manually injected in the GC injection port using a 10  $\mu\text{L}$  syringe (Hamilton, 700 series, cemented needle). The GC oven temperature program for the gas phase analyses was 40  $^{\circ}\text{C}$  (0 min) to 200  $^{\circ}\text{C}$  (0 min) at 10  $^{\circ}\text{C min}^{-1}$ ; and for the liquid products analyses, 40  $^{\circ}\text{C}$  (0 min) to 340  $^{\circ}\text{C}$  (15 min) at 10  $^{\circ}\text{C min}^{-1}$ . For gas and liquid products analyses, the injection port was set at split mode, with a split ratio of 20, the carrier gas was helium with a flowrate of 68  $\text{mL min}^{-1}$ , the split flowrate was 60  $\text{mL min}^{-1}$ , the septum purge flowrate was 5.0  $\text{mL/min}$ , and the flowrate in the column was 3  $\text{mL min}^{-1}$ . The injector was at 290  $^{\circ}\text{C}$  and 340  $^{\circ}\text{C}$  for the gas and liquid analysis, respectively. In both cases, the FID detector was at 350  $^{\circ}\text{C}$ , with 27  $\text{mL min}^{-1}$  nitrogen, 50  $\text{mL min}^{-1}$  hydrogen and 300  $\text{mL min}^{-1}$  air.

The quantification of the reaction products was based on calibration curves (compound concentration as function of compound peak area) for the gas and liquid products, as exemplified in Figure 3.1 and Figure 3.2, respectively. For the calibration of the gas phase, different experiments were carried out without catalyst, at 200  $^{\circ}\text{C}$  and 30 bar, using mixtures of 1-butene with molar compositions in the range 3-10 % (corresponding to [1C4] in the loop of 0.8-2.6 mM), and the effluent was analyzed by GC as described above for the gas phase. The calibration was made only for loops number 4 and 5, since these loops were leak-free (checked by several leak tests). It was obtained a response factor (RF) of 0.034 for 1-butene. For the calibration of the liquid phase it was analyzed, by GC as described above for the liquid products, different amounts of ASTM D2887 calibration mixture diluted (dilution factor of 84, 126 and 501) in 0.0087 M internal standard solution

of *n*-pentane in dichloromethane, and it was obtained the RF for the different *n*-paraffins between 0.212-0.996 ( $R^2 > 0.89$ ).

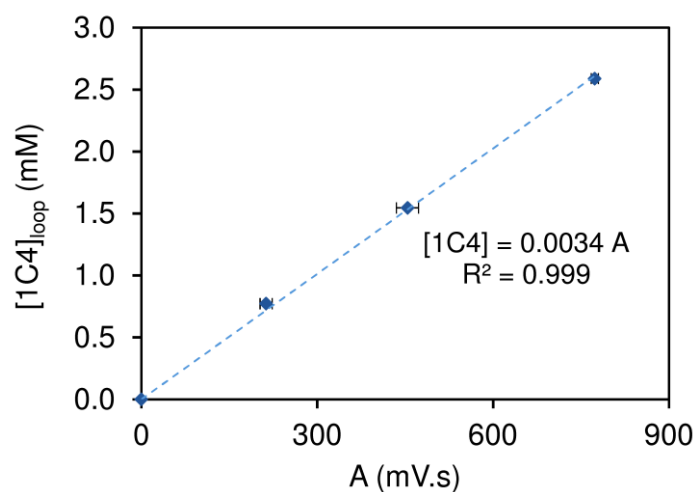


Figure 3.1. GC calibration curve for 1-butene, used for quantification of the gas phase reaction products, for loop 4, where  $[1C4]_{loop}$  stands for the molar concentration of 1-butene at the PT condition of the loop (1 bar, 200 °C), and A stands for the peak area of 1-butene.

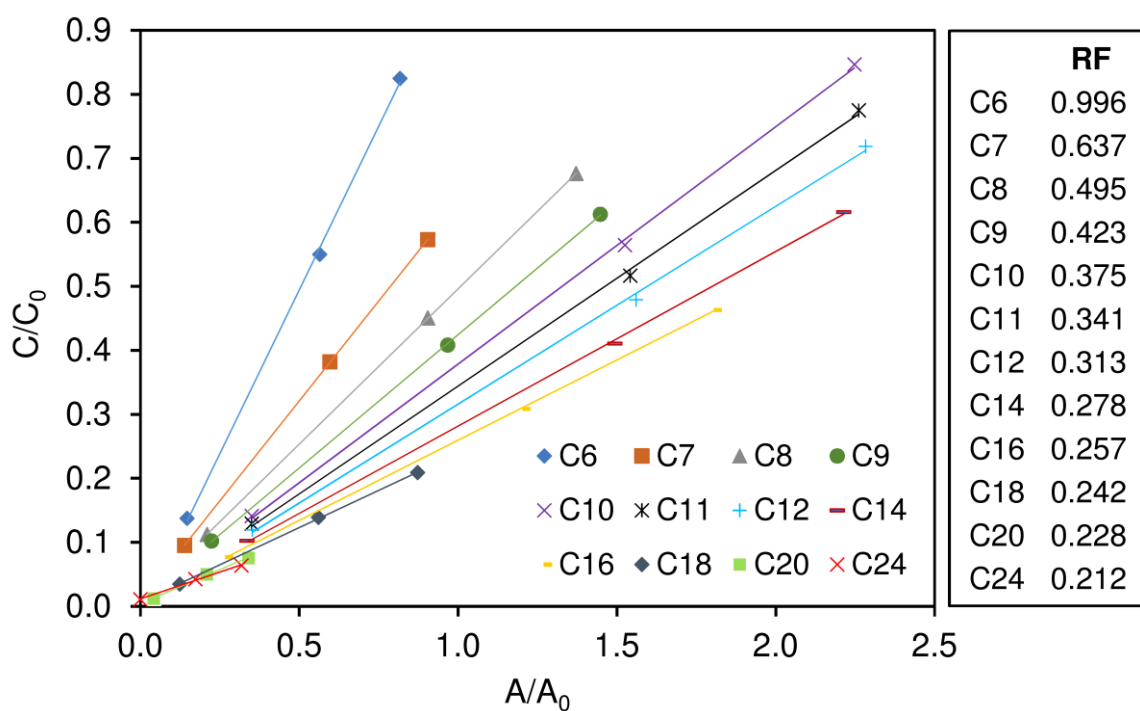


Figure 3.2. GC calibration curve for C6-C24 *n*-paraffins, used for the quantification of liquid reaction products ( $C_0$  and  $A_0$  stand for the concentration and area of the internal standard (*n*-

pentane), respectively), accompanied by the response factors (RS, slope of the calibration curves), for each *n*-paraffin.

The GC method for the liquid products analyses was adapted from methods presented in ASTM D2887 (Standard Test Method for Boiling Range Distribution of Petroleum Fractions by Gas Chromatography) (Table 3.3).<sup>[4]</sup>

Table 3.3. Column specifications and GC method for ASTM D2887-04 and the liquid phase products method used in this work.

	<b>ASTM D2887-04</b>	<b>This work (Liquid phase method)</b>
Column specifications	DB-1 (100 % poly(dimethylsiloxane)) 7.5 m x 0.53 mm x 1.5 μm T <sub>max</sub> : 325/350 °C	VB-1 (100 % poly(dimethylsiloxane)) 60 m x 0.25 mm x 1.5 μm T <sub>max</sub> : 340/360 °C
GC method	T injector: 340 °C T detector: 350 °C T oven: 40 to 340 °C (10 °C/min)	T injector: 340 °C T detector: 350 °C T oven: 40 to 340 °C (10 °C/min)

In order to validate the GC method selected in this work and the calculation algorithms, it was followed the procedure described by ASTM D2887,<sup>[4]</sup> which involved performing a blank analysis, a calibration curve, and the analysis of ASTM D 2887 Reference Gas Oil (RGO) n.º 1 (Supelco, sample 1, Batch 2).

The blank analysis consisted of running the GC method for the liquid phase, without injecting sample or solvent. The calibration (Figure 3.3) consisted of relating the boiling point (BP) with the retention time (RT) of each compound of the standard *n*-alkanes solution (ASTM D2887 calibration mix) that was analyzed using the same GC method. The analysis of RGO was made by directly injecting 0.5 μL of RGO, and then it was determined the boiling point for a given percentage of area of the RGO chromatogram (Table 3.4), using the calibration curve. Since the differences between the observed boiling point and the boiling point given by the ASTM D2887 method were within the allowable differences

range, the GC method and calculations algorithms for the liquid products analyses of this work, were validated.

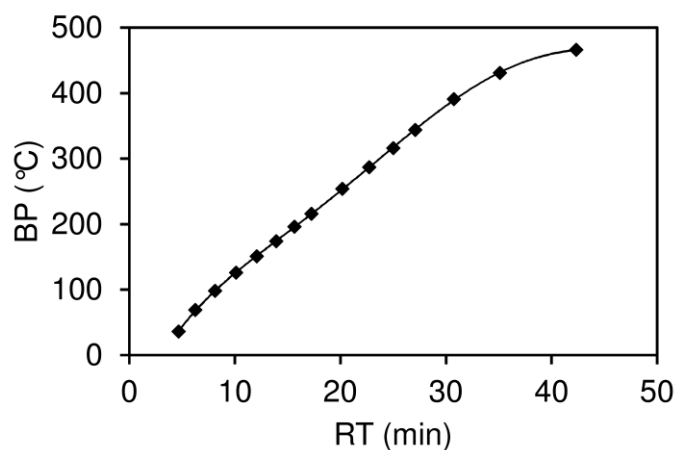


Figure 3.3. Calibration curve for the *n*-alkanes series (ASTM D2887 calibration mix) (BP and RT stand for boiling point and retention time, respectively).

Table 3.4. Results for ASTM D2887 Reference Gas Oil n.º 1, according to the test method ASTM D2887 and the liquid phase method developed in this work.

OFF(%)	ASTM D2887 method		Liquid phase method	
	BP	Allowable difference	BP	Difference
IBP <sup>[a]</sup>	115	7.6	117	1.5
5	151	3.8	151	0.2
10	176	4.1	174	1.7
15	201	4.5	198	3.1
20	224	4.9	221	3.0
30	259	4.7	258	0.5
40	289	4.3	289	0.0
50	312	4.3	314	2.4
60	332	4.3	334	1.7
70	354	4.3	356	1.9
80	378	4.3	378	0.4
90	407	4.3	407	0.5
95	428	5	431	3.2
FBP <sup>[b]</sup>	475	11.8	466	9.1

<sup>[a]</sup> IBP=initial boiling point. <sup>[b]</sup> FBP=final boiling point.

The catalytic results were expressed as conversion of butenes ( $X_{C_4}$ ) which reacted to give higher molar mass products, using Eq. (1).

$$X_{C_4}(\text{mol } \%) = \frac{[1C_4]_{\text{in}} - [C_4]_{\text{out}}}{[1C_4]_{\text{in}}} \times 100 \quad (1)$$

where  $[1C_4]_{\text{in}}$  is the molar concentration of 1C4 in the feed (in), and  $[C_4]_{\text{out}}$  is the molar concentration of butenes in the effluent stream (out), at the PT conditions of the loop (200 °C, atmospheric pressure). The feed concentration of 1-butene was determined as the ratio of the molar flowrate of 1-butene and the total volumetric flowrate at the PT conditions of the loop; this was determined using densities at different PT conditions obtained by the Peng-Robinson equation of state (PREOS).<sup>[5]</sup> In turn, the effluent concentration of butenes was determined based on the calibration curve for 1-butene (Figure 3.1).

Selectivity to a lump of compounds possessing  $y$  to  $z$  number of carbon atoms per molecule (denoted  $S_{C_{[y-z]}}$  for lump  $C_{[y-z]}$ , where  $z > y$ ) was calculated according to Eq. (2).

$$S_{C_{[y-z]}}(\text{mol } \%) = \frac{[C_{[y-z]}]}{\sum[C_{[y-z]}]} \times 100 \quad (2)$$

$$\frac{[C_{[y-z]}]}{C_0} = \overline{RF}_{C_{[y-z]}} \frac{A_{[y-z]}}{A_0} \quad (3)$$

where  $[C_{[y-z]}]$  is the concentration of product lump  $C_{[y-z]}$ , given by Eq. (3) and based on the calibration curves of Figure 3.2,  $\sum[C_{[y-z]}]$  is the total concentration of products in the range C<sub>6</sub>-C<sub>24</sub>,  $\overline{RF}_{C_{[y-z]}}$  is the average of the response factors of compound  $C_y$  and  $C_z$ ,  $A_{[y-z]}$  is the area of the sample chromatogram, subtracted by the area of the blank chromatogram, in the region between the retention times of compounds  $C_y$  and  $C_z$ ,  $C_0$  and  $A_0$  are the concentration and area of the internal standard ( $n$ -pentane), respectively.

The set of values of  $S_{C_{[y-z]}}$  give rise to the products lump distributions (PLD), that were divided in two main fractions: fractions with boiling point <170 °C, characteristic of naphtha products (Ncut, corresponding approximately to the C<sub>6</sub>-C<sub>10</sub>  $n$ -paraffinic range), and fractions with boiling points in the range 170-390 °C, characteristic of diesel products (Dcut, corresponding approximately to the C<sub>10</sub>-C<sub>24</sub>  $n$ -paraffinic range).

The space time yield (STY) was expressed as the ratio of mass of reaction products per mass of catalyst and TOS. The space time yield of naphtha ( $STY_{Ncut}$ ) or diesel ( $STY_{Dcut}$ ) cuts were determined by the multiplying the total STY and the respective selectivity (in wt.%) of naphtha or diesel cuts.

### 3.2.3. Identification of the liquid reaction products by GC×GC-ToFMS

Comprehensive two-dimensional gas chromatography (GC×GC) combined with time-of-flight mass spectrometry (ToFMS) was used to identify the liquid phase reaction products. The analyses were performed in the LECO Pegasus 4D (LECO, St. Joseph, MI, USA) GC×GC-ToFMS system, comprised by an Agilent GC 7890A gas chromatograph (Agilent Technologies, Inc., Wilmington, DE), with a dual stage jet cryogenic modulator (licensed from Zoex) and a secondary oven, as well as mass spectrometer equipped with a ToF analyzer. The analytical conditions used are indicated in Table 3.5 for the analysis of the samples related to Chapters 5 and 6 (method A) and Chapter 9 (method B).

Table 3.5. GC×GC-ToFMS analytical conditions.

	Method A	Method B
1D column, non-polar	Equity-5 column (30 m × 0.32 mm I.D., 0.25 μm) <sup>[a]</sup>	PONA column (10 m × 0.2 mm I.D., 0.5 μm) <sup>[c]</sup>
2D column, polar	DB-FFAP column (0.79 m × 0.25 mm I.D., 0.25 μm) <sup>[b]</sup>	BPX50 column (0.8 m × 0.1 mm I.D., 0.1 μm) <sup>[d]</sup>
Column oven program	1D: 35 °C (1 min) to 220 °C (1 min); 2 °C min <sup>-1</sup> 2D: 50 °C (1 min) to 235 °C (1 min); 2 °C min <sup>-1</sup>	1D: 40 °C (0.5 min) to 325 °C (1 min); 3 °C min <sup>-1</sup> 2D: 45 °C (0.5 min) to 330 °C (1 min); 3 °C min <sup>-1</sup>
Carrier gas injection system	He, 2.5 mL min <sup>-1</sup> 250 °C, 0.75 mm I.D. splitless glass liner, splitless injections (30 s), 0.5 μL	He, 1.0 mL min <sup>-1</sup> 270 °C, 4 mm I.D. splitless glass liner, split=1/80, 0.3 μL
	MS and MS transfer line at 250 °C	MS and MS transfer line at 330 °C

	10 s, 15 °C offset above primary oven, hot pulses=0.8 s, cold pulses=4.2 s	7 s, 15 °C offset above primary oven, hot pulses=0.8 s, cold pulses=2.7 s
Detector		
Modulation		

<sup>[a]</sup> Poly(5 % diphenyl/95 % dimethylsiloxane), Supelco, Inc., Bellefonte, PA, USA; <sup>[b]</sup> Nitroterephthalic-acid-modified polyethylene glycol (PEG), J&W Scientific Inc., Folsom, CA, USA; <sup>[c]</sup> Poly(dimethylsiloxane), Agilent technologies, Massy, France; <sup>[d]</sup> (50 % Phenyl)polysilphenylene-siloxane, SGE, Courtaboeuf, France.

The ToF analyser was operated at a spectrum storage rate of 100 spectra s<sup>-1</sup> with mass spectrometer running in the EI mode at 70 eV and detector voltage of -1439 (method A) or -1682 (method B), using a range of *m/z* 30-400 (method A) or 35-500 (method B). Total Ion Chromatograms (TIC) were processed using the automated data processing software ChromaTOF<sup>®</sup> (LECO) at signal-to-noise threshold of 100.

Two commercial databases (Wiley 275 and US National Institute of Science and Technology (NIST) V. 2.0 - Mainlib and Replib) were used, combined with the use of the retention index (RI) value, which was determined according to the Van den Dool and Kratz RI equation.<sup>[6]</sup> For the determination of the RI, a C8-C20 *n*-alkane series was used, and as some volatile compounds were eluted before C8, *n*-hexane was used as the solvent.

### 3.2.4. Determination of the cetane number, isoparaffinic index and aromatic content

The quality parameters of the liquid (condensed) reaction products were evaluated in terms of cetane number (CN), isoparaffinic index and aromatic content determined by proton nuclear magnetic resonance (<sup>1</sup>H NMR) spectroscopy. The <sup>1</sup>H NMR spectra were recorded using a Bruker Avance III - 300 MHz spectrometer (Bruker QNP 300MHz SB 5 mm with Z-gradient), collecting 104 scans, with a recycle delay time of 1 s, and a 30° pulse sequence. The samples were prepared by dissolving 8-10 µL of liquid sample in *ca.* 6 mL of deuterated dichloromethane, and using 5 mm NMR sample tubes. The products mixtures were not hydrogenated, and thus the CN values may be underestimated (the values were considered for rough comparisons).

The CN was determined using the correlations proposed by O'Connor et al.<sup>[7]</sup> (Eq. (4)) and by Kapur et al.<sup>[8]</sup> (Eq. (5)), based on <sup>1</sup>H NMR spectra of the samples. O'Connor et al. predicted the CN of hydrogenated synthetic diesel fuel derived from catalytic oligomerization of low-chain-length alkenes over acid catalysts, whereas Kapur et al. correlated <sup>1</sup>H NMR data of 60 commercial diesel samples with the diesel properties, using multiple linear regression modelling and statistical software to predict the CN.

$$CN = 1.8 + 43.8 \left( \frac{CH_2}{CH_3} \right) - 8.1 \left( \frac{CH_2}{CH_3} \right)^2 + 0.69 \left( \frac{CH_2}{CH_3} \right)^3 \quad (4)$$

$$CN = -0.272(A + B) + 0.570(F + G) + 0.653(H) - 0.712(J) + 3.001(K) - 0.408(L) + 0.0886(N) + 0.152(Q) \quad (5)$$

where CH<sub>2</sub>/CH<sub>3</sub> is the ratio of areas of total peaks attributed to methylene hydrogen atoms (CH<sub>2</sub>; 1.8–1.03 ppm) and methyl hydrogen atoms (CH<sub>3</sub>; 1.03–0.4 ppm); and the letters A to Q stand for the <sup>1</sup>H NMR integral intensity of various spectral regions, as defined in ref. [8].<sup>[8–10]</sup> The peak areas were obtained by integration of the spectra using software MestReNova (V. 6.0.2, 2009, Mestrelab Research S.L.).

The content of aromatic hydrocarbons was determined considering the aromatic proton content (H<sub>ar</sub>) in the <sup>1</sup>H NMR spectra region of *ca.* 6.5–9.2 ppm.<sup>[8–10]</sup> The isoparaffinic index (I), *i.e.* the ratio between the number of methyl groups and the number of methylene groups was determined using Eq. (6).

$$I = \frac{2CH_3}{3CH_2} \quad (6)$$

### 3.3. Laboratory Setup 1 of the catalytic test unit

The design of the laboratory Setup 1 is represented in Figure 3.4 and Figure 3.5, which may be divided into three sections: feed section (A), reaction section (B), and products section (C). The detailed description of Setup 1 and the experimental procedure are given in Supplementary Material-Chapter 3.

## Chapter 3

Briefly, the feed section (A) comprised a bottle of nitrogen gas, bottle of 1-butene, mass flow controller (to control the N<sub>2</sub> flowrate), syringe pump (to control the 1C<sub>4</sub> flowrate), and auxiliary equipment (needle valves, check valves, manometer, pressure transducer, and pressure indicator). The reaction section (B) comprised a tubular reactor (internal diameter of 16 mm), tubular oven, filter, back-pressure regulator, BPR manual regulator, and auxiliary equipment (thermocouples, temperature PID controllers, pressure transducer, manometer, needle valves). The products section (C) comprised a jacketed trap, bath, needle valves, and a Master Fast gas chromatograph equipped with an eleven loop system (loops of 0.5 mL).

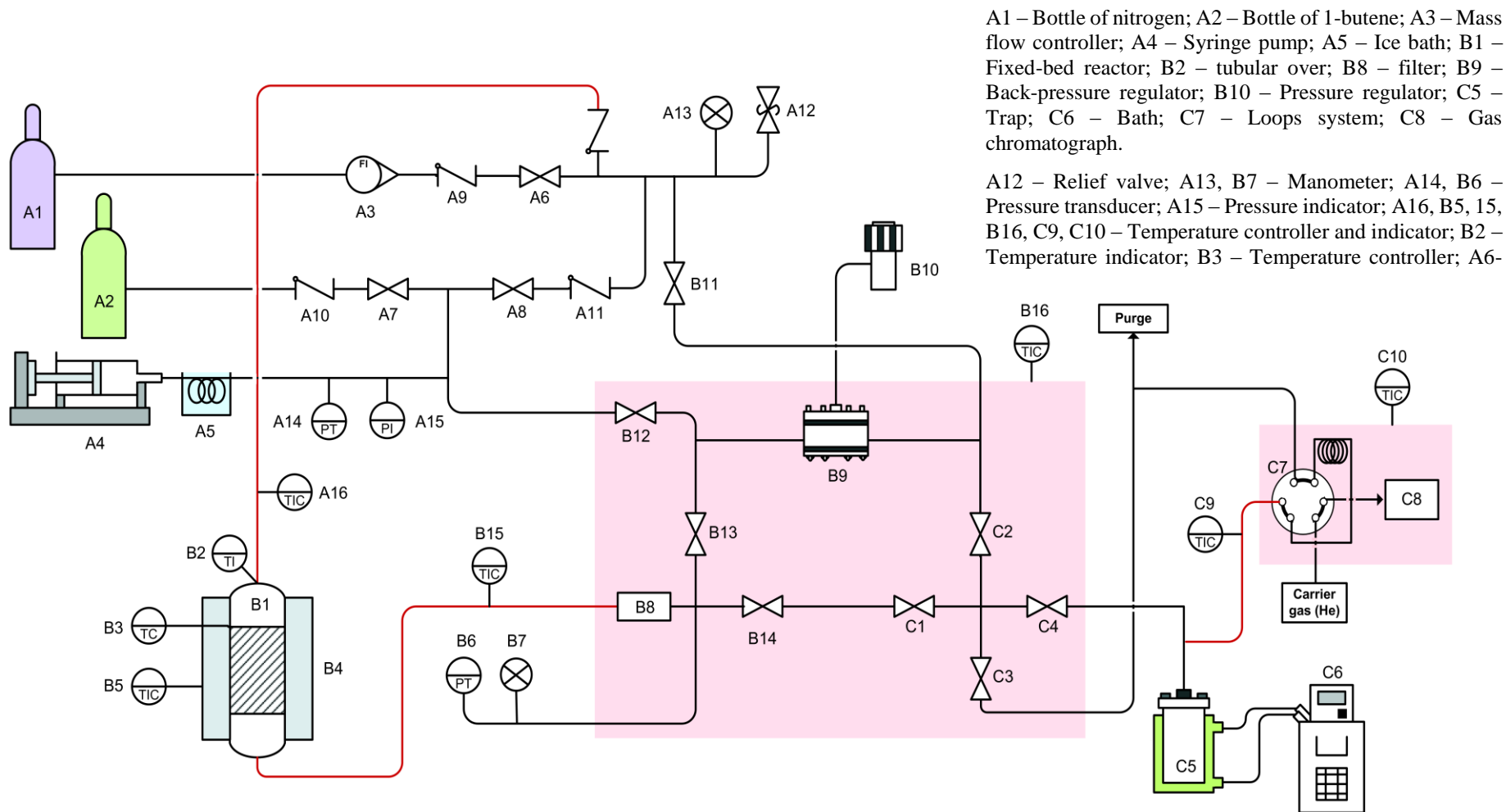


Figure 3.4. Process flow diagram of Setup 1 for the catalytic test unit. The red lines represent heating hoses and the red areas represent closed heated boxes.



Figure 3.5. Photograph of the laboratory Setup 1.

During operation of Setup 1, it was found major drawbacks in all the main sections of the installation, which compromised the quality and reproducibility of the experimental results. The first limitation was located in the feed section and related to the impossibility of filling the syringe pump with 1-butene in the liquid state. This constituted a limitation for continuous flow operation during long time on stream (TOS), without interruptions; it was necessary to feed a considerable amount of reactant (1-butene) to the reactor, without interruptions. During operation of Setup 1, this was found to be difficult, even with the help of an auxiliary 1-butene condensation system (i.e. elliptical pipeline circuit submerged in ice) and low filling rate. The installation of a dosage pump and a stainless-steel vessel between the syringe pump and the bottle of 1-butene seemed to be the best solution with minimal equipment requirements. The dosage pump allowed compressing 1-butene from the bottle into the vessel, where it was stored in the liquid state, and then used for filling the syringe pump. Moreover, the pipeline (in length and diameter) between the syringe pump and valves A8 and B12 was reduced which was advantageous in dispensing smaller amount of 1-butene in the pressurization of the 1-butene feed line.

Another important drawback of Setup 1 was the high dead volume of the installation caused by long pipelines, high amount of valves and connections and a reactor with high internal volume. This increased the time for the system to reach a steady state operation, especially when low flow rates were used (operation at high residence time). Moreover, the

many valves and long pipelines with upwards and downwards curves (necessary for the versatile operation of this setup 1, i.e. atmospheric and high-pressure operations), constituted problematic pathways for the liquid reaction products, leading to retention of liquid products and considerable wetted area, reducing significantly the total amount of liquid products. The cylinders with helical cracks placed inside the reactor to support the catalytic bed, reduced the dead volume of the reactor, but constituted a difficult path to the liquid products. Thus, to solve the problem of dead volume and difficult collection of the liquid reaction products, it was necessary to: (i) eliminate the complexity of the pipeline system, by reducing the length and diameter of the tubes and the amount of valves; (ii) design a new reactor with reduced internal volume and a catalytic bed without additional parts; and (iii) create a vertical design in sections B and C with minimal dead volume allowing the liquid reaction products to flow in one direction and to be collected with the aid of gravity.

Regarding the analytical part of the gas chromatographic analysis of the non-condensed reaction products, it was verified that high split ratios (SR=200-280) were required in order to avoid saturation of the FID detector (0.5 mL samples of non-condensed reaction products). The SR is the ratio of the volumetric flow rate at the split purge vent to the volumetric flow rate in the GC column, and by varying the SR it is possible to adjust the sample concentration that enters the GC column. Very high SR requires high split flow rates, which may cause poor sensitivity, resistance to gas flow in the split line, pressure drop issues, and excessive consumption of carrier gas.<sup>[11,12]</sup> Thus, it was necessary to implement new sample loops with smaller internal volume (0.1 mL instead of 0.5 mL) in order to reduce the SR of the GC analyses.

### **3.4. Laboratory Setup 2 of the catalytic test unit**

Several modifications were made to Setup 1, considering the drawbacks and possible solutions mentioned above, which resulted in the laboratory Setup 2, represented in Figure 3.6 and Figure 3.7, used for carrying out all the catalytic tests discussed in this thesis. The laboratory Setup 2, implemented in 2016, may be divided into three sections: feed section (A), reaction section (B), and products section (C).

### Chapter 3

A1 – Bottle of nitrogen; A2 – Bottle of 1-butene; A3 – Mass flow controller; A4 – Syringe pump; A5 – Piston screw pump; A6 – Ice bath; A7 – Vessel; B1 – Fixed-bed reactor; B4 – tubular over; B9 – Back-pressure regulator; B10 – Pressure regulator; C3 – Trap; C4 – Bath; C5 – Loops system; C6 – Gas chromatograph.

A16, A17, B7 – Manometer; B6 – Relief valve; A18, B8 – Pressure transducer; A19 – Pressure indicator; A20, B5, B11, C7, C8 – Temperature controller and indicator; B2 – Temperature indicator; B3 – Temperature controller; A8-A15, C1, C2 – Valves and check valves.

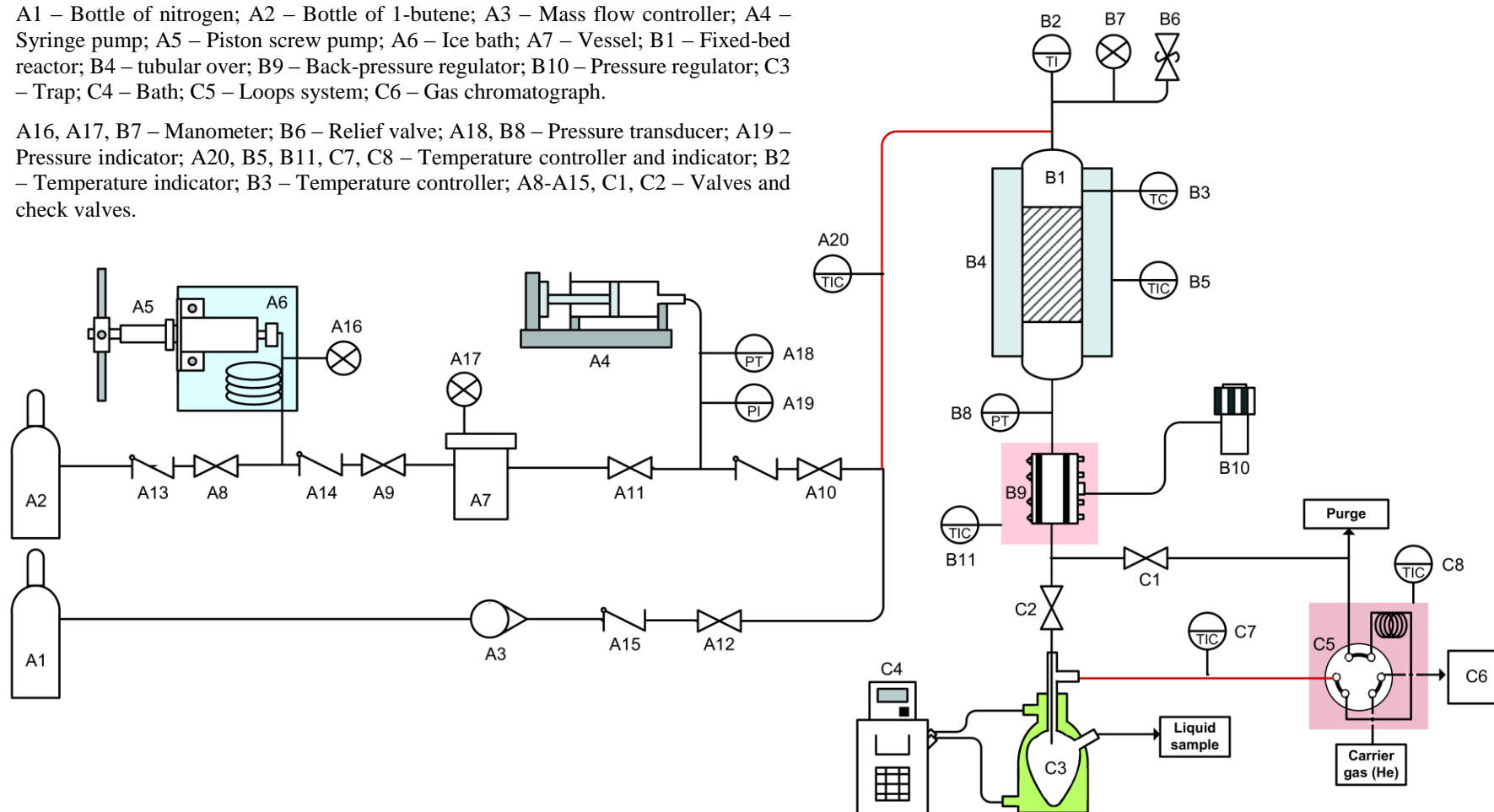


Figure 3.6. Process flow diagram of Setup 2 for the catalytic test unit. The red lines represent heating hoses and the red areas represent closed heated boxes.



Figure 3.7. Photograph of the laboratory Setup 2.

The feed section (A) is represented in Figure 3.8 and comprised the following equipment: (A1) bottle of nitrogen gas (A2) bottle of 1-butene; (A3) mass flow controller (MFC, Bronkhorst, EL-FLOW F-201CV, 3-500 mL min<sup>-1</sup>, pressure up to 64 bar, -10 to 70 °C); (A4) syringe pump (CHEMYX, Nexus 6000, with capacity of 20 mL, minimal volumetric flow of 0.1 nL min<sup>-1</sup>, accuracy < ±0.04 % error, pressure up to 78 bar, 10 to 50 °C); (A5) piston screw pump (HiP, Standard Laboratory Model 50-6-15, manually operated with a capacity per stroke of 20 mL, pressure up to 1034 bar); (A6) ice bath; (A7) stainless-steel 316 vessel with capacity of 200 mL; (A8-A9) needle valves (HiP, 15-11AF1, pressure up to 1034 bar); (A10) needle valve (HiP, 15-11AF2, pressure up to 1034 bar); (A11-A12) needle valves (Hy-lok, NV1-H-2TPK-S316, pressure up to 340 bar, temperature up to 315 °C); (A13-A15) check valves (Hy-lok, 700 series model CV1-H-2T-S316, pressure up to 206 bar, temperature up to 191 °C); (A16-A17) manometers (Wika); (A18) pressure transducer (Sensor Techniques, KTE630GL0, output of 0-10V); and (A19) pressure indicator (Paralab).

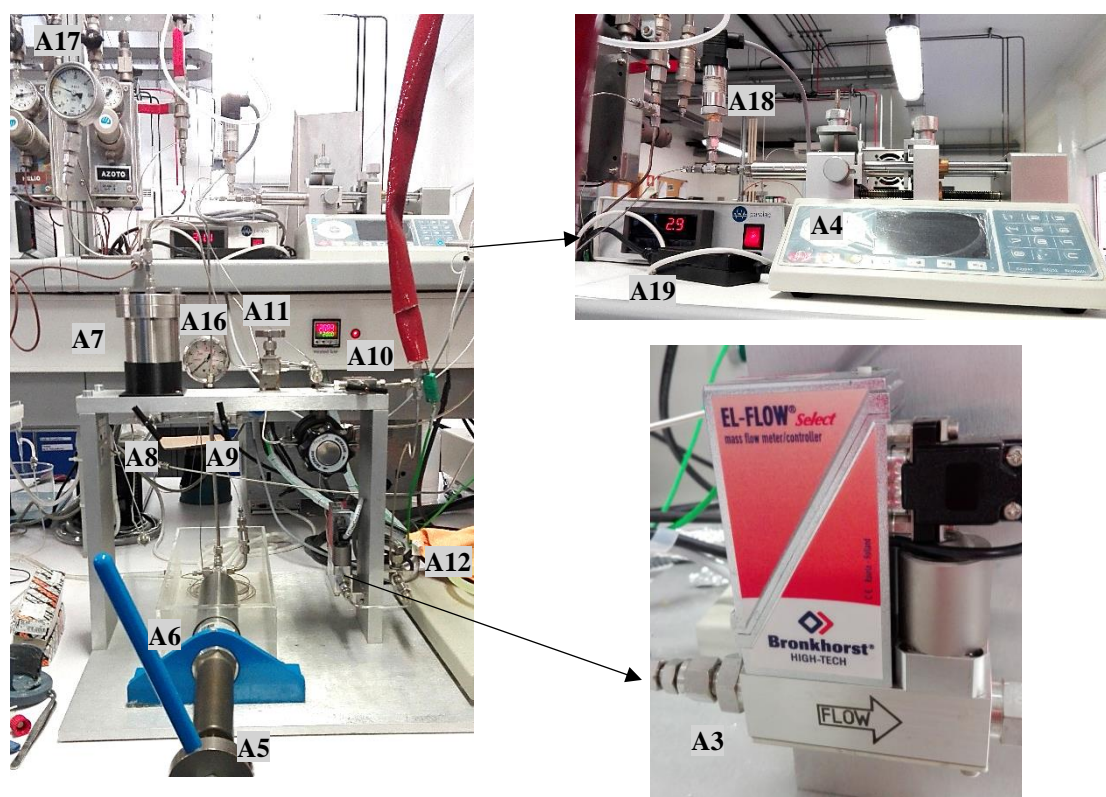


Figure 3.8. Feed section (A) of the laboratory Setup 2.

The reaction section (B) is represented in Figure 3.9 and comprised the following equipment: (B1) tubular reactor (Paralab, custom made of stainless-steel 316, length of 370 mm, I.D. of 10 mm, the I.D. is reduced to 4.35 mm at 210 mm length (Figure 3.10), where is placed a graphite sintered (6 mm diameter and 1 mm thick), temperature up to 500 °C); (B2) thermocouple (Omega, type K, CAIN-IM15U-450, temperature up to 650 °C); (B3) temperature PID controller (Shinko, model ACS); (B4) tubular oven equipped with a thermocouple (Termolab); (B5) oven temperature PID controller and indicator (Eurotherm, model 2116); (B6) relief valve (Parker, 4M4F-RH4A-VT-SS, -26 °C to 204 °C); (B7) manometer (Wika); (B8) pressure transducer (Omega, PX319-1KGI, pressure up to 69 bar, accuracy of  $\pm 0.25$  %, output of 4-20 mA); (B9) back-pressure regulator (BPR, Equilibar, Primary Research series, model LF1, diaphragm of polyamide, pressure up to 55 bar, temperature up to 150 °C); and (B10) BPR manual regulator (TESCOM, 44-1700 Series, maximum inlet pressure of 55.2 bar, -26 to 60 °C).



Figure 3.9. Reaction section (B) of the laboratory Setup 2.

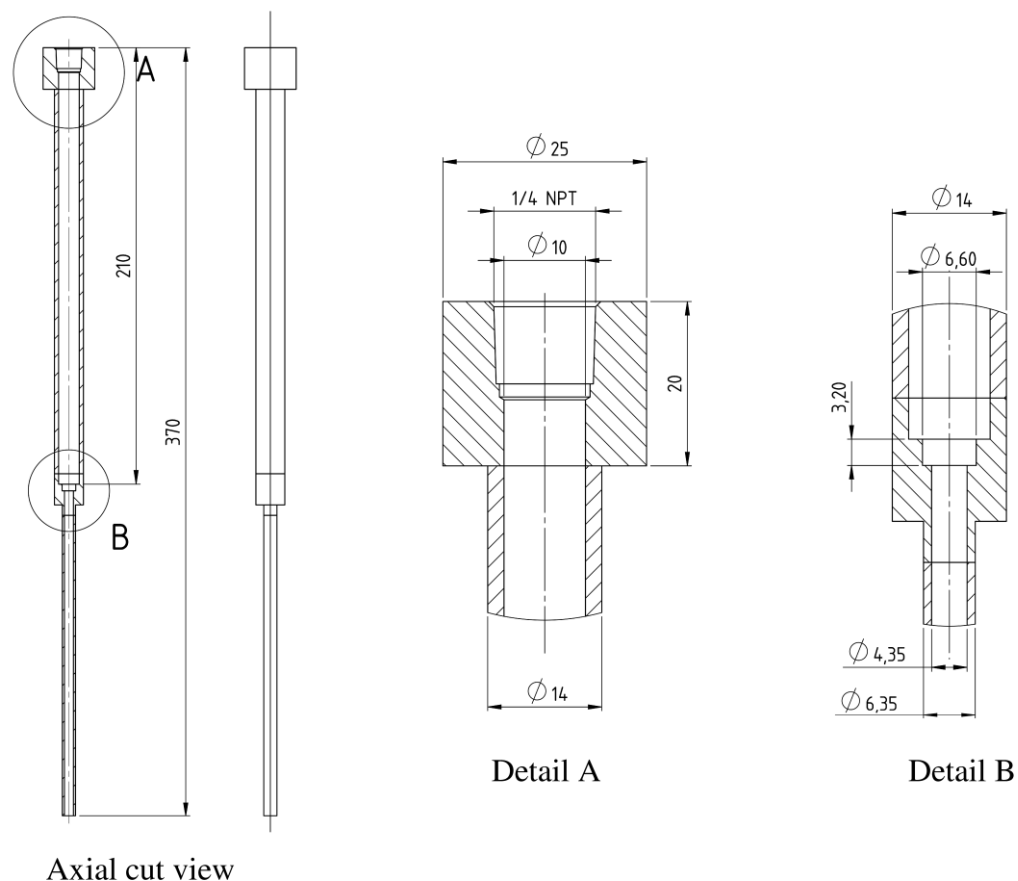


Figure 3.10. Detailed design of the fixed-bed tubular reactor (Paralab) of Setup 2.

The products section (C) is represented in Figure 3.11 and comprised the following equipment: (C1-C2) needle valves (HiP, 15-11AF2, pressure up to 1034 bar); (C3) jacketed glass trap (glass shop of University of Aveiro, custom made, with capacity of 5 mL); (C4) bath (Thermo/HAAKE, model DC10-K10 with immersion circulator, operates from 20 to 100 °C (with tap water) or -30 to 100 °C (with an appropriate liquid refrigerant)); (C5) loops system, composed by a 6 port 2-position manual valve (VICI, 4C6WE, pressure up to 27 bar, temperature up to 225 °C), and a 12 multi-position trapping path ST selector (VICI, EMT4CST12MWT), equipped with 0.1 mL loops (Paralab, pressure up to 13 bar, temperature up to 300 °C); and (C6) gas chromatograph (GC, DANI, Master Fast) equipped with FID detector, split/splitless injector, and capillary column ValcoBond VB-1 (VICI, 60 m length, 0.25 mm ID, 1.50  $\mu$ m column film thickness, with poly(dimethylsiloxane) phase, maximum temperature of 340/360 °C).

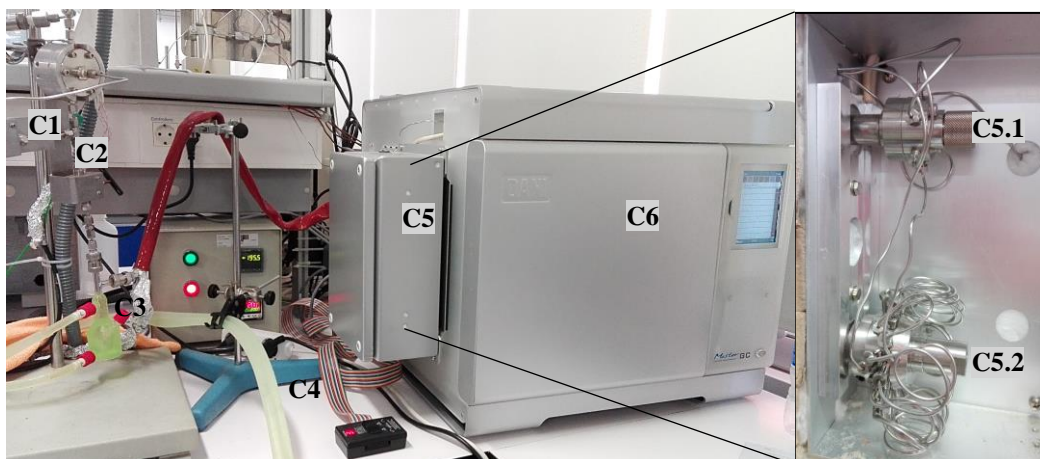


Figure 3.11. Products section (C) of the laboratory Setup 2.

The laboratory Setup 2 was composed of stainless-steel 316 tubes with O.D. of 1/8 and 1/16 inches. Two sections of 1/16 inch tube were heated by heating hoses, to avoid condensation of products. The setpoint and the measured point of several instruments was monitored *via* a LabVIEW software, created by Paralab, for this catalytic oligomerization setup.

### 3.4.1. Experimental procedure

After Setup 2 was implemented in the laboratory, preliminary tests indicated lack of pressure stability due to leakage, which required additional modifications/replacements of equipment. Subsequently, preliminary catalytic tests were carried out using a commercial catalyst in order to develop an experimental protocol, which allowed reproducibility of the catalytic results. The protocol was divided into four steps, in a total of three operating days for one catalytic assay:

- 1) **Preparation for the catalytic reaction** (1<sup>st</sup> day) – consisted of loading the reactor with a previously sieved and weighted mixture of catalyst and inert solid; assembling the reactor in the installation; leak testing; and *in-situ* activation of the catalyst, overnight, at the desired temperature, under nitrogen flow.

2) **Catalytic reaction** (2<sup>nd</sup> day) – consisted of filling the syringe pump with 1-butene in the liquid state; heating and pressurizing the installation parts; and carry out the oligomerization reaction for a given TOS. The evolution of the reaction was monitored *via* on-line GC analyses of the gaseous products in order to determine the conversion of butenes.

3) **Recovery of catalyst and products** (3<sup>rd</sup> day) – consisted of feeding the installation with solvent in order to recover liquid products that remained inside the reactor unit, separating the solvent from the reaction products by evaporation using a rotavapor, and washing and drying the used catalyst for subsequent characterization and/or catalyst stability studies.

### **Preparation for the catalytic reaction**

In order to prepare the oligomerization installation for the catalytic assays, first the reactor, in vertical position, was loaded with a sieved mixture of powdered catalyst and silicon carbide (SiC) in a mass proportion of 1:20 (0.120-0.200 g catalyst, particle size below 0.16 mm, and 2.4-4.0 g SiC, particle size of 0.31 mm), supported in one quartz wool disc (Elemental Miroanalysis, 16 mm diameter and 5 mm thick). Tracing paper was used to load the mixture into the reactor, avoiding catalyst deposition on the internal walls of the reactor. The SiC is an inert solid used to favor uniform distribution of temperature along the catalytic bed. The bed height was *ca.* 22-32 mm and a total bed volume was *ca.* 1.7-2.5 cm<sup>3</sup>. The dimensions of the catalyst particles and catalytic bed fulfil the conditions of plug flow pattern: reactor diameter at least 10 times greater than the catalyst particle size, and catalytic bed length at least 50 times greater than the catalyst particle size.<sup>[13]</sup>

The reactor was assembled in the installation and the installation was pressurized for leak tests, at room temperature, up to 20-30 bar with nitrogen (50 mL/min), while keeping valve A12 open and the remaining valves closed. The pressure stability was monitored over time (leaks were detected using a leak detector spray). If no leaks were detected, the installation was emptied by opening slowly valve C1. The next step was the *in-situ* activation of the catalyst, overnight, typically at 450 °C for 3 h (heating rate of 0.7-0.9 °C min<sup>-1</sup>), under nitrogen flow of 10 mL/min, while keeping valves A12 and C1 open and the remaining valves closed. After the activation period, the reactor was cooled to the reaction temperature (cooling rate of 2 °C min<sup>-1</sup>).

## Catalytic reaction

In day 2, 1-butene was compressed using the piston pump in order to be stored in the liquid state. In this process the pump handle is rotated counter-clockwise to withdraw fluid from the 1-butene bottle into the pump cylindrical body, while keeping valve A8 open and valve A9 close; when the pump body was full, valve A8 was closed, valve A9 was opened, and the pump handle was rotated clockwise, so that the piston compressed the fluid into the storage vessel. If enough pressure was not reached in one stroke, the vessel can be filled again: valve A9 was closed to maintain the pressure in the vessel, whereas valve A8 was opened, and the fluid was again withdrawn from the 1-butene bottle into the pump body. When the pressure of the storage vessel reached 40-50 bar, the syringe pump was filled at a flow rate in the range 0.05-0.15 mL/min. Then, the BPR was heated to 150 °C, and the trap-to-GC line and the loops were heated to 200 °C. The temperature of the feed line was set at the desired reaction temperature, and the jacketed trap was cooled to 5 °C using a bath filled with a mixture of ethylene glycol and distilled water. The installation was pressurized with nitrogen (flow rate of 50 mL/min), by rotating clockwise the manual regulator of the BPR, until the desired reaction pressure was reached.

Before initializing the catalytic reaction, the room temperature was measured with a thermometer and the atmospheric pressure was recorded from the webpage ("<http://climetua.fis.ua.pt/>"). Some calculations were made in order to determine the set-point of the MFC and the syringe pump, based on the ambient conditions and desired reaction conditions (Supplementary Material-Chapter 3). The catalytic reaction started (starting time) when the pressure of the syringe pump line equaled the pressure of the installation and valve A10 was opened. During the catalytic reaction valves A10, A12 and C2 were opened, whereas the remaining valves were closed. The 6 port 2-position manual valve was placed in the "Load" position in order to sample the effluent gas phase (non-condensed reaction products) using the loops of the trapping selector, in regular intervals of *ca.* 1 h and with a loading time of 1 or 2 min per loop (pre-programmed in the lab view software). After loading the loops, the 6 port 2-position manual valve was placed in the "Inject" position in order to inject the gas sample from the loops to the GC column for analysis.

At the end of the reaction, *i.e.* typically after the 7-8 h TOS, the 1-butene feed was stopped and valve A10 was closed; the reactor and other heated zones were cooled to

ambient temperature, and the installation was slowly depressurized by rotating the manual BPR regular counter-clockwise. The nitrogen flow was set to 30-40 mL/min for at least 30 min in order to carry residual products to the trap. Afterwards, the nitrogen flow was turned off and all valves were closed. The liquid product inside the trap was collected, labelled, weighted and stored in the freezer (*ca.* -4 °C).

### **Recovery of catalyst and liquid products**

In day 3, the reactor was disassembled from the installation, the quartz wool disc of the catalytic bed was separated and disposed, and the mixture of catalyst and SiC was transferred to a centrifuge tube. The solid mixture was washed with *ca.* 5 mL of dichloromethane and centrifuged (repeated 3-4 times) until the supernatant appeared colorless. The supernatant was separated from the solid and subjected to rotary evaporation, under vacuum at 40 °C, until dichloromethane was completely evaporated (monitored by GC analysis). The resultant residue was weighted (accounted for the material balance, Supplementary Material-Chapter 3) and stored in the freezer (*ca.* -4 °C). On the other hand, the catalyst and SiC were dried at 60 °C, overnight; the two solids were separated using a sieve with 0.16 mm aperture diameter. The used catalysts were characterized by different techniques such as TGA, DSC, ATR FT-IR spectroscopy, elemental (C and H) analysis, PXRD, <sup>27</sup>Al MAS NMR, SEM and N<sub>2</sub> adsorption-desorption at -196 °C.

Afterwards, the cleaned reactor was assembled and the inlet was connected to a HPLC pump (KNAUER, Smartline Pump 100), which, in turn, was connected to a flask containing dichloromethane. A flow rate of 2.8 mL/min of dichloromethane was used to clean the reactor and the installation sections B and C, while carrying products that remained inside the installation, to the trap. The cleaning process was repeated six times and the obtained liquid was subjected to rotary evaporation under vacuum at 40 °C, until the dichloromethane was completely evaporated (monitored by GC analysis). The residue of the evaporation consisted of heavy reaction products, which were weighted and then mixed with the liquid products that had been collected in the trap during the catalytic reaction. The total of liquid products was subsequently analyzed by GC-FID or GC×GC-ToFMS.

For the mass balance, it was accounted: as reactant the mass of 1-butene fed to the system during the total TOS; as products the unreacted 1-butene and butene isomers, the C5<sup>+</sup> gas phase products, the liquid products collected in the trap plus the products recovered from the cleaning of the installation, the products recovered from the catalyst washing; and the coke present in the catalysts (determined based on TGA and elemental analysis for C). In general, the mass balances closed in 80-95 % (Table S3.2 and Table S3.3).

### 3.5. References

- [1] D. Verboekend, S. Mitchell, M. Milina, J.C. Groen, J. Pérez-Ramírez, Full compositional flexibility in the preparation of mesoporous MFI zeolites by desilication, *J. Phys. Chem. C* 115 (2011) 14193–14203.
- [2] J.M. Campelo, F. Lafont, J.M. Marinas, Pt/SAPO-5 and Pt/SAPO-11 as catalysts for the hydroisomerization and hydrocracking of *n*-octane, *J. Chem. Soc., Faraday Trans.* 91 (1995) 1551–1555.
- [3] C.A. Emeis, Determination of integrated molar extinction coefficients for infrared absorption bands of pyridine adsorbed on solid acid catalysts, *J. Catal.* 141 (1993) 347–354.
- [4] A. D2887-04, Standard test method for boiling range distribution of petroleum fractions by gas chromatography, *Annu. B. Stand.* 05 (2002) 13.
- [5] J.S. Lopez-Echeverry, S. Reif-Acherman, E. Araujo-Lopez, Peng-Robinson equation of state: 40 years through cubics, *Fluid Phase Equilib.* 447 (2017) 39–71.
- [6] H. van den Dool, P.D. Kratz, A generalization of the retention index system including linear temperature programmed gas-liquid partition chromatography, *J. Chromatogr. A* 11 (1963) 463–471.
- [7] C.T. O'Connor, R.D. Forrester, M.S. Scurrall, Cetane number determination of synthetic diesel fuels, *Fuel* 71 (1992) 1323–1327.
- [8] G.S. Kapur, A. Ecker, R. Meusinger, Establishing quantitative structure-property relationships (QSPR) of diesel samples by proton-NMR & multiple linear regression (MLR) analysis, *Energy and Fuels* 15 (2001) 943–948.
- [9] C. Martos, B. Coto, J.J. Espada, M.D. Robustillo, S. Gómez, J.L. Peña, Experimental determination and characterization of wax fractions precipitated as a function of temperature, *Energy and Fuels* 22 (2008) 708–714.
- [10] R.M. Silverstein, F.X. Webster, D.J. Kiemle, Spectrometric identification of organic compounds, 7<sup>th</sup> ed., John Wiley & Sons, 2005.
- [11] K. Grob, Split and splitless injection for quantitative gas chromatography (concepts, processes, practical guidelines, sources of error), 4<sup>th</sup> ed., Wiley-VCH Verlag GmbH, 2001.
- [12] R.L. Grob, E.F. Barry, Modern practice of gas chromatography, 4<sup>th</sup> ed., John Wiley & Sons, 2004.
- [13] C. Perego, S. Peratello, Experimental methods in catalytic kinetics, *Catal. Today* 52 (1999) 133–145.

# CHAPTER 4

---

## General considerations

### Chapter 4

#### General considerations

4.1. Reproducibility tests .....	140
4.2. Studies of mass transfer limitations .....	140
4.3. Thermodynamics of 1-butene isomerization .....	144
4.4. References .....	145

## 4.1. Reproducibility tests

To study the reproducibility of the catalytic results and determine the experimental range of error, replicates were performed under typical 1-butene oligomerization reaction conditions: 200 °C, 30 bar, 1-butene (1C4) composition of 15 % (mol), and weight hourly space velocity (WHSV) of  $2.2 \text{ g}_{1\text{C}_4} \text{ g}_{\text{cat}}^{-1} \text{ h}^{-1}$ , using the commercial zeolites ZSM-5 (CBV3024E, Zeolyst), BEA-nano (CP814E, Zeolyst) and BEA-micro (931HOA, Tosoh) in the protonic form (prepared *via* calcination), and Al-TUD-1(25)-HT synthesized as described in Chapter 5. Figure 4.1 shows the experimental results of conversion of butenes ( $X_{\text{C}_4}$ ) *versus* time on-stream (TOS) for the four catalyts. It was verified good reproducibility of the catalytic results, and the experimental error was less than 5 %.

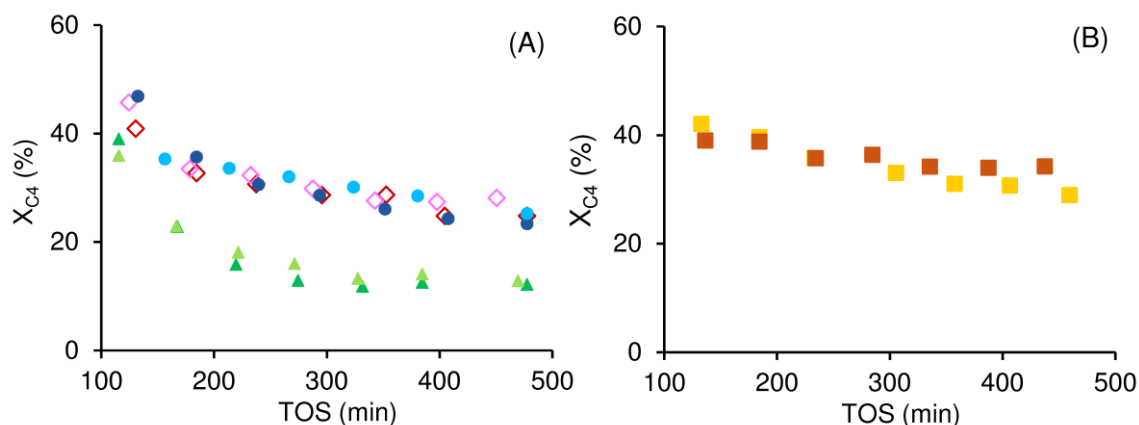


Figure 4.1. Conversion of butenes ( $X_{\text{C}_4}$ ) as a function of TOS for: (A) the commercial zeolites BEA-nano ( $\diamond, \diamond$ ), BEA-micro ( $\blacktriangle, \blacktriangle$ ) and ZSM-5 ( $\bullet, \bullet$ ); or (B) the synthesized aluminosilicate Al-TUD-1(25)-HT ( $\blacksquare, \blacksquare$ ). Reaction conditions: 200 °C, 30 bar, WHSV= $2.2 \text{ g}_{1\text{C}_4} \text{ g}_{\text{cat}}^{-1} \text{ h}^{-1}$ , catalyst activation temperature=450 °C (BEA-nano, BEA-micro and Al-TUD-1(25)-HT) or 200 °C (ZSM-5).

## 4.2. Studies of mass transfer limitations

The Weisz-Prater criterion<sup>[1,2]</sup>, valid under isothermal conditions, is commonly used for studying internal diffusion limitations in 1-butene oligomerization over porous

catalysts.<sup>[3-6]</sup> The product of the generalized effectiveness factor ( $\eta$ ) and the square of the Thiele modulus ( $\varnothing$ ) was calculated for the (packed bed of) spherical catalyst particles, according to Eq. (8).

$$\eta \cdot \varnothing^2 = \left(\frac{D_p}{6}\right)^2 \frac{n+1}{2} \frac{r_{obs} \cdot \rho_c}{C_{As} \cdot D_{eff}} \quad (8)$$

$$r_{obs} = \frac{F_{1C4,in} - F_{1C4,out}}{m_{cat}} \quad (9)$$

$$D_{eff,T2,P2} = D_{eff,T1,P1} \left(\frac{P1}{P2}\right) \left(\frac{T2}{T1}\right)^{3/2} \quad (10)$$

where  $\eta$  is the effectiveness factor,  $\varnothing$  is the Thiele modulus,  $D_p$  is the diameter of the catalyst particle (m),  $n$  is the reaction order,  $r_{obs}$  is the observed reaction rate ( $\text{mol kg}^{-1} \text{s}^{-1}$ ),  $\rho_c$  is the density of the catalyst particle ( $\text{kg m}^{-3}$ ),  $C_{As}$  is the concentration of 1-butene at the surface of the catalyst ( $\text{mol m}^{-3}$ ),  $D_{eff}$  is the effective diffusivity of the reactant 1-butene ( $\text{m}^2 \text{s}^{-1}$ ),  $F_{1C4,in}$  and  $F_{1C4,out}$  are, respectively, the molar flowrates of 1-butene in the feed and in the effluent stream ( $\text{mol s}^{-1}$ ),  $m_{cat}$  is the mass of catalyst,  $D_{AB,T1,P1}$  and  $D_{AB,T2,P2}$  are the diffusion coefficients at the conditions of pressure and temperature P1, T1 and P2, T2, respectively. Internal diffusion limitations may be neglected for  $\eta \cdot \varnothing^2 \ll 1$ .<sup>[1]</sup>

In this thesis, the above criterion was used for the catalytic oligomerization considering irreversible reaction in the early stages of the reaction; catalyst particle sizes ( $D_p$ ) less than 160  $\mu\text{m}$ ; for zeolites catalysts, the density ( $\rho_c$ ) may be considered in the range 1200-1800  $\text{kg m}^{-3}$ <sup>[7-9]</sup>; first order reaction ( $n=1$ , for early stages of the reaction); the 1-butene concentration at the surface ( $C_{As}$ ) was approximately equal to the bulk concentration, which is reasonable since it was not verified external mass transfer limitations (discussed ahead). The observed reaction rate ( $r_{obs}$ ) was determined according to Eq. (9), considering (the worst case scenario) 100 % of 1C4 conversion.

The effective diffusion coefficients were determined for the reference/benchmark zeolite ZSM-5 (CBV3024E). Jousse et al.<sup>[10]</sup> reported that the diffusion coefficient of 1-butene in the MFI channels was equal to  $9.7 \times 10^{-9} \text{ m}^2 \text{ s}^{-1}$ , based on molecular dynamics simulations at 623 K. For determining the coefficients for different operating conditions, temperature and pressure corrections were introduced according to Eq. (10).<sup>[5]</sup> The values of

$D_{eff}$  were in the range  $1.46 \times 10^{-7}$ - $2.29 \times 10^{-8}$   $\text{m}^2 \text{s}^{-1}$  for 20-45 bar and 150-300 °C (under these conditions, 1C4 in the feed mixture was in the gas phase). The internal diffusion limitations seemed negligible, since  $\eta \cdot \phi^2$  was below 0.01, which is significantly smaller than 1.

The external mass transfer limitations were studied using the Carberry (Ca) number for a spherical catalyst particle, Eq. (11).<sup>[11]</sup>

$$Ca = \frac{r_{obs} \rho_c}{C_{Ab} k_c} \left( \frac{D_p}{6} \right) \quad (11)$$

where  $r_{obs}$  is the observed reaction rate ( $\text{mol kg}^{-1} \text{s}^{-1}$ ),  $\rho_c$  is the density of the catalyst particle ( $\text{kg m}^{-3}$ ),  $D_p$  is the diameter of the catalyst particle (m),  $C_{Ab}$  is the bulk concentration of 1-butene ( $\text{mol m}^{-3}$ ), and  $k_c$  is the convective mass transfer coefficient ( $\text{m s}^{-1}$ ) determined using the j-factor analogy for very low Reynolds numbers, as proposed by Wilson and Geankoplis<sup>[12]</sup> (Eq. (12)).

$$j_M = \frac{k_c}{u} Sc^{2/3} = \frac{1.09 Re^{-2/3}}{\epsilon}, \quad 0.0016 < Re < 55 \quad 0.35 < \epsilon < 0.75 \quad (12)$$

where  $Re$  and  $Sc$  are respectively the Reynolds and Schmidt numbers,  $u$  is the superficial velocity through the bed, and  $\epsilon$  is the void fraction (porosity) of the catalytic bed. In the range of operating conditions 20-45 bar, 150-300 °C and 1.3-3.1  $\text{g}_{1C4} \text{g}_{cat}^{-1} \text{h}^{-1}$ , the Reynolds number was in the range 0.06-0.85, and consequently the mass transfer coefficient  $k_c$  was in the range  $2.6 \times 10^{-4}$ - $9.2 \times 10^{-4}$   $\text{m s}^{-1}$  (considering  $\epsilon=0.4$ ). The Carberry number was always less than 0.02, and therefore external diffusional limitations may be neglected.

In a different approach, catalytic tests were carried out to study the external diffusion limitations of 1C4,<sup>[13]</sup> using the protonic form (obtained *via* calcination) of the commercial materials  $\text{NH}_4\text{ZSM-5}$  (Si/Al=15, CBV3024E) and  $\text{NH}_4\text{BEA}$  (Si/Al=12.5, CP814E), and Al-TUD-1(25)-HT. The WHSV was kept constant, and the mass of catalyst was varied in the range 120–280 mg and the 1C4 flowrate varied in the range 0.26-0.61  $\text{g h}^{-1}$ . The tests were performed under the typical reaction conditions: 200 °C, 30 bar, 1C4 composition of 15 % (mol), and  $\text{WHSV}=2.2 \text{ g}_{1C4} \text{g}_{cat}^{-1} \text{h}^{-1}$ . For all materials tested, the conversion of butenes ( $X_{C4}$ ) was similar: 33–34 % for BEA-nano, 23-25 % for ZSM-5 and 23-25 % for Al-TUD-

1(25)-HT, and the product lump distribution (PLD) curves were comparable (Figure 4.2). Thus, external mass transfer limitations did not seem important.

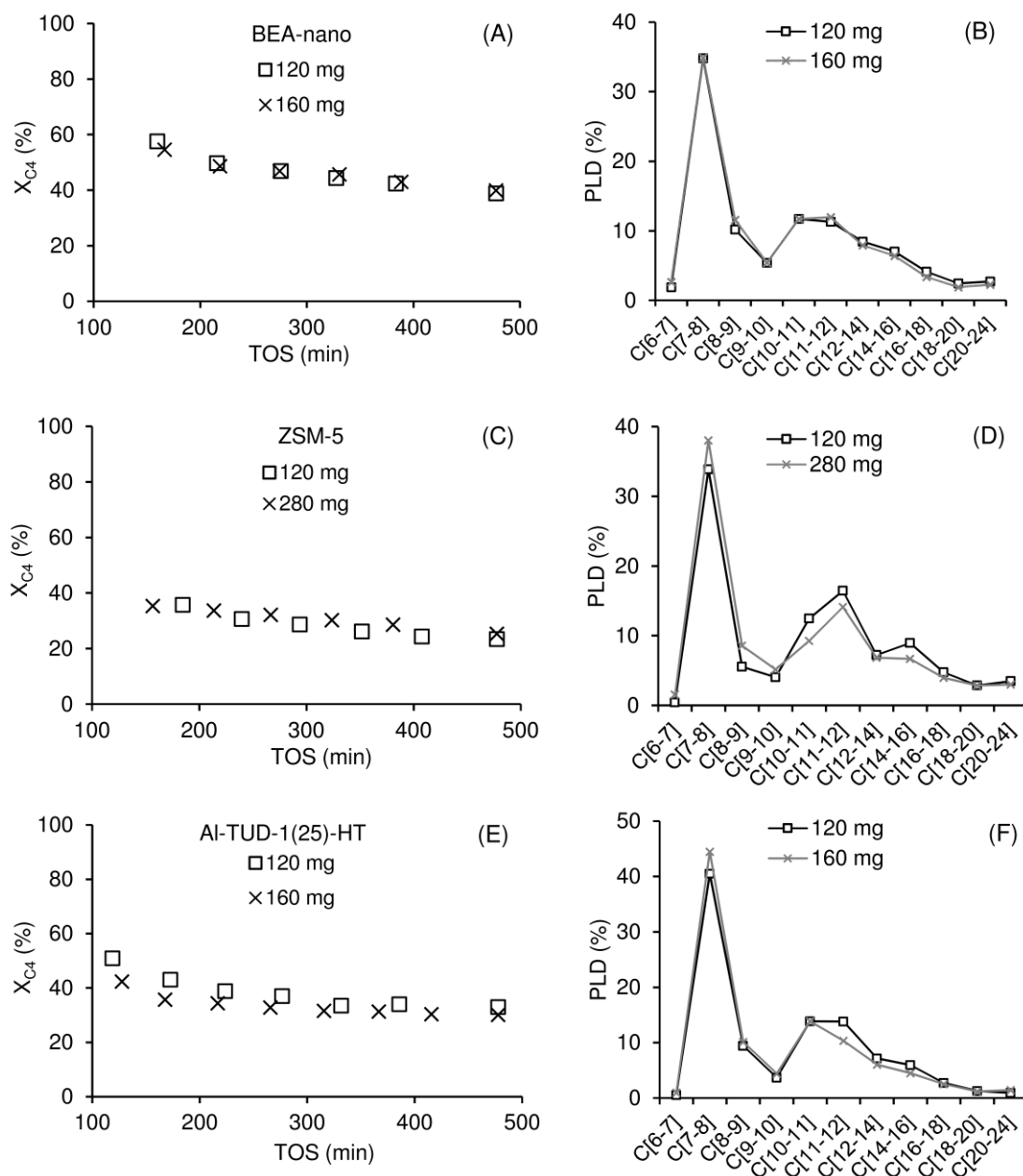


Figure 4.2. Conversion ( $X_{C_4}$ ) as function of TOS (A,C,E) and PLD curves (B, D, F) using BEA-nano (A,B), ZSM-5 (C,D), and Al-TUD-1(25)-HT (E,F). Reaction conditions: 200 °C, 30 bar,  $WHSV=2.2 \text{ g}_{cat}^{-1} \text{ h}^{-1}$ , catalyst activation temperature=200 °C (BEA-nano and ZSM-5) or 450 °C (Al-TUD-1(25)-HT).

### 4.3. Thermodynamics of 1-butene isomerization

The acid-catalyzed oligomerization of 1-butene was accompanied by double bond isomerization of 1C4 to *cis*-2-butene and *trans*-2-butene; *trans*-2-butene may further undergo skeletal isomerization to isobutene. The distribution of butene isomers was determined for 1-butene oligomerization over different catalysts studied in chapters 5-8, under different reaction conditions.

For the typical reaction conditions (200 °C, 30 bar, 1C4 composition of 15 % (mol), and  $WHSV=2.2 \text{ g}_{1C4} \text{ g}_{cat}^{-1} \text{ h}^{-1}$ ), the gaseous effluent stream contained essentially unreacted 1C4 and its isomers *cis*-2-butene and *trans*-2-butene (Figure S4.1). The distribution of butene isomers was roughly independent of the type of catalyst (Table S4.1), which is in agreement with that reported by Sarazen et al.<sup>[14]</sup> in a study of the relative rates of oligomerization, isomerization and  $\beta$ -scission reactions over different microporous and mesoporous acid catalysts (the distribution of isomers with chains of a given size seemed independent of the type of solid acid catalyst). For the catalysts tested under the typical reaction conditions, the average butene isomers distribution was:  $16\pm 2.6$  % 1-butene,  $52\pm 1.7$  % *trans*-2-butene and  $32\pm 1.0$  % *cis*-2-butene. The calculated butene isomers distribution agreed with the thermodynamic equilibrium compositions of *n*-butenes at 200 °C and 30 bar, obtained with Aspen Plus V10 simulation on RGibbs reactor and using the NRTL thermodynamic model; 13 % 1-butene, 52 % *trans*-2-butene and 35 % *cis*-2-butene. Hence, double bond isomerization seemed relatively fast compared to the oligomerization reaction.

The molar ratio of butene products:1C4 was always in the range 3-7, and the ratio of *trans*:*cis* isomers was in the range 1.6-1.7. The predominance of the *trans* isomer is in agreement with literature data for the isomerization of 1C4.<sup>[15-17]</sup> For all catalysts, it was verified that the isobutene concentration was not in equilibrium with *trans*-C4, in parallel to that reported in the literature.<sup>[16,18]</sup> This may be explained by the more demanding skeletal isomerization reaction than double bond isomerization.

For the catalysts tested under different reaction conditions (150-250 °C, 20-40 bar), namely Al-TUD-1(25)-HT (Chapter 5) and BEA-hier (Chapter 6), it was verified that the reaction temperature was the most important parameter influencing the butene isomers

distribution (consistent with the thermodynamic data, Table S4.2). For the two catalysts, increasing temperature led to higher ratio of 1C4:*trans*-C4 (reaching 0.48-0.55 at 250 °C), whereas the amount of *cis*-C4 remained constant (*ca.* 30-32 %). The values were somewhat similar to the thermodynamic equilibrium compositions, with some deviations especially for higher reaction temperature (Figure 4.3). The ratio *trans*-2-butene:*cis*-2-butene decreased from 1.8-2.0 (150 °C) to 1.5 (250 °C), which is in agreement with the results reported by Kim et al. for 1C4 conversion over H-ferrierite catalysts (100-250 °C, 6.9 bar).<sup>[16]</sup>

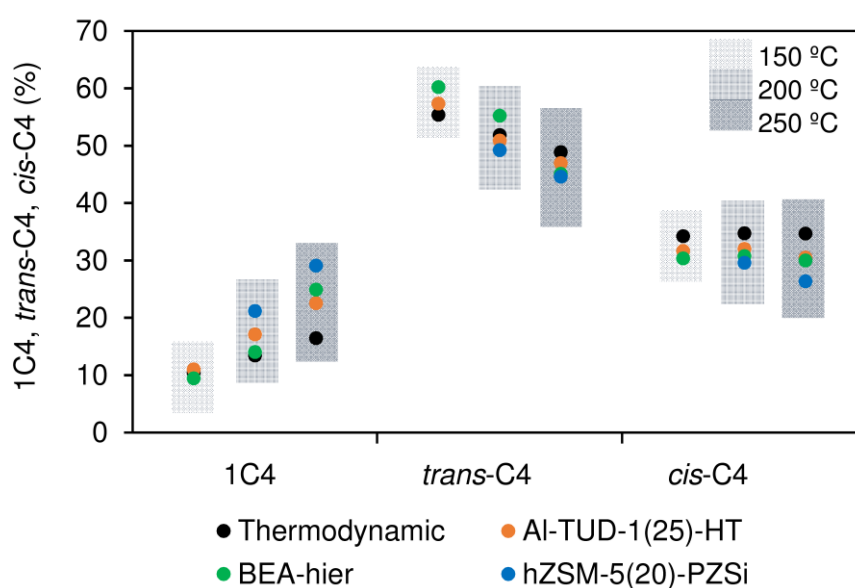


Figure 4.3. Butene isomers distribution for different reaction temperatures (150-250 °C), and different catalysts (Al-TUD-1(25)-HT (●), BEA-hier (●) and hZSM-5(20)-PZSi (●)); and thermodynamic equilibrium compositions (●). Reaction conditions: 30 bar, 1C4 composition of 15 % (mol), and  $WHSV=2.2 \text{ g}_{1C4} \text{ g}_{cat}^{-1} \text{ h}^{-1}$ , catalyst activation temperature=200 °C (BEA-hier) or 450 °C (Al-TUD-1(25)-HT and hZSM-5(20)-PZSi).

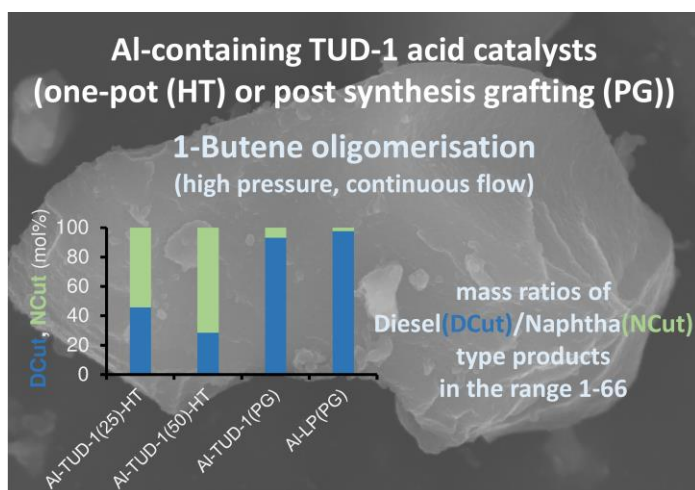
#### 4.4. References

- [1] H.S. Fogler, Diffusion and reaction in porous catalysts, in: Elements of Chemical Reaction Engineering, 4<sup>th</sup> ed., 1999: pp. 738–808.
- [2] P.B. Weisz, C.D. Prater, Interpretation of measurements in experimental catalysis, *Adv. Catal.* 6 (1954) 143–196.
- [3] A. Coelho, G. Caeiro, M.A.N.D.A. Lemos, F. Lemos, F.R. Ribeiro, 1-Butene oligomerization over ZSM-5 zeolite: Part 1 - Effect of reaction conditions, *Fuel* 111 (2013) 449–460.

- [4] M.J. Wulfers, R.F. Lobo, Assessment of mass transfer limitations in oligomerization of butene at high pressure on H-beta, *Appl. Catal. A Gen.* 505 (2015) 394–401.
- [5] G. Wittreich, Kinetic model and analysis of mass transfer limitations in oligomerization of butene at high pressure on H-beta zeolite catalyst, 2015 (Technical report, DOI: 10.13140/RG.2.1.3009.2887).
- [6] P. Borges, R.R. Pinto, M.A.N.D.A. Lemos, F. Lemos, J.C. Védrine, E.G., Derouane, F.R. Ribeiro, Light olefin transformation over ZSM-5 zeolites. A kinetic model for olefin consumption, *Appl. Catal. A Gen.* 324 (2007) 20–29.
- [7] J.B. Higgins, R.B. LaPierre, J.L. Schlenker, A.C. Rohrman, J.D. Wood, G.T. Kerr, W.J. Rohrbaugh, The framework of zeolite beta, *Zeolites* 8 (1988) 446–452.
- [8] D.H. Olson, G.T. Kokotailo, S.L. Lawton, W.M. Meier, Crystal structure and structure-related properties of ZSM-5, *J. Phys. Chem.* 85 (1981) 2238–2243.
- [9] L.D. Rollmann, E.W. Valyocsik, R. Shannon, Miscellaneous solid-state compounds, *Inorg. Synth.* 30 (1995) 1–8.
- [10] F. Jousse, L. Leherte, D.P. Vercauteren, Energetics and diffusion of butene isomers in channel zeolites from molecular dynamics simulations, *J. Mol. Catal. A Chem.* 119 (1997) 165–176.
- [11] J.A. Moulijn, P.W.N.M. van Leeuwen, R.A. van Santen, Chapter 7 catalytic reaction engineering, *Stud. Surf. Sci. Catal.* 79 (1993) 251–306.
- [12] E.J. Wilson, C.J. Geankoplis, Liquid mass transfer at very low Reynolds numbers in packed beds, *Ind. Eng. Chem. Fundam.* 5 (1966) 9–14.
- [13] C. Perego, S. Peratello, Experimental methods in catalytic kinetics, *Catal. Today* 52 (1999) 133–145.
- [14] M.L. Sarazen, E. Duskocil, E. Iglesia, Effects of void environment and acid strength on alkene oligomerization selectivity, *ACS Catal.* 6 (2016) 7059–7070.
- [15] J.G. Yates, P.N. Rowe, S.T. Whang, The isomerization of n-butenes over a fluidised silica-alumina catalyst, *Chem. Eng. Sci.* 25 (1970) 1387–1394.
- [16] Y.T. Kim, J.P. Chada, Z. Xu, Y.J. Pagan-Torres, D.C. Rosenfeld, W.L. Winniford, E. Schmidt, G.W. Huber, Low-temperature oligomerization of 1-butene with H-ferrierite, *J. Catal.* 323 (2015) 33–44.
- [17] N. Kumar, P. Mäki-Arvela, T. Yläsalmi, J. Villegas, T. Heikkilä, A.-R. Leino, K. Kordás, T. Salmi, D. Yu Murzin, Dimerization of 1-butene in liquid phase reaction: Influence of structure, pore size and acidity of Beta zeolite and MCM-41 mesoporous material, *Microporous Mesoporous Mater.* 147 (2012) 127–134.
- [18] C. Costa, J.M. Lopes, F. Lemos, F.R. Ribeiro, Activity-acidity relationship in zeolite Y. Part 1. Transformation of light olefins, *J. Mol. Catal. A Chem.* 144 (1999) 207–220.

# CHAPTER 5

## TUD-1 type aluminosilicate acid catalysts for 1-butene oligomerization



### Abstract<sup>1</sup>

TUD-1 type mesoporous aluminosilicates were explored for the acid-catalyzed oligomerization of 1-butene, under high pressure, continuous flow operation, which is an attractive route to produce sulphur-free synthetic fuels with reduced aromatics content. The solid acid catalysts were synthesized *via* one-pot synthesis (HT) or stepwise approach (PG), without using

surfactants as templates, which is an eco-friendly characteristic of the TUD-1 family. While the HT approach may be advantageous in terms of process intensification in relation to the PG one, the latter may lead to relatively low molar ratios Si/Al. The catalysts possessed Si/Al ratios in the range 3–5 and 17–35 for the PG and HT approaches, respectively, pore sizes in the range 10–14 nm, and essentially Lewis acidity. To the best of our knowledge, this is the first report of siliceous oxide TUD-1 furnished with acidity *via* post-synthesis grafting (PG) of Al-species. For comparative studies, an ordered mesoporous aluminosilicate was synthesized *via* the PG approach using surfactant mixtures. All materials prepared promoted the reaction of 1-butene to higher molar mass products. The best-performing catalyst in terms of space-time yields of the 170–390 °C cut (boiling point range) products (of the type middle distillates) was Al-TUD-1(25)-HT synthesized *via* the HT method. The products were analyzed by comprehensive two-dimensional gas chromatography (GC×GC) combined with time-of-flight mass spectrometry (ToFMS). The influence of material properties and process parameters on the catalytic reaction, and catalyst stability were studied. The catalytic performances were benchmarked with ZSM-5 (zeolite used in commercial oligomerization processes).

<sup>1</sup> Fuel 209 (2017) 371–382

## CHAPTER 5

### **TUD-1 type aluminosilicate acid catalysts for 1-butene oligomerization**

5.1.	Introduction .....	149
5.2.	Synthesis of the catalytic materials .....	150
5.3.	Characterization studies of the catalytic materials .....	152
5.4.	Catalytic studies: general considerations.....	159
5.5.	Cetane number and GC×GC–ToFMS analysis of reaction products ..	162
5.6.	Influence of the reaction conditions .....	163
5.7.	Catalyst stability and benchmarking.....	165
5.8.	Conclusions .....	169
5.9.	References .....	171

## 5.1. Introduction

Commercial oligomerization processes use heterogeneous catalysts, operating in continuous mode. In particular, zeolites (microporous crystalline aluminosilicates) with MFI topology are used as solid acid catalysts in the commercial olefin oligomerization processes, Mobil Olefins to Gasoline and Distillate (MOGD)<sup>[1,2]</sup> and Conversion of Olefins to Distillate (COD).<sup>[3,4]</sup> In processes such as these, involving relatively bulky intermediates/products, microporous catalysts may present drawbacks associated with internal diffusion limitations and/or catalyst deactivation due to pore blockage by the long chain olefins and bulky byproducts, impacting negatively on the catalyst stability and productivity. In this sense, mesostructured solid acid catalysts possessing high specific surface area and enhanced active site accessibility seem attractive.

Ordered mesoporous silicates (OMPS) of the type MCM-41 possessing aluminum sites exhibited fairly good stability (steady activity under continuous operation) for the conversion of C4 and C5 olefins,<sup>[5-7]</sup> in relation to disordered porous materials such as amorphous silica-alumina,<sup>[6]</sup> or ordered microporous materials such as BEA<sup>[6,7]</sup> and MFI<sup>[6]</sup> type zeolites. The MCM-41 family of materials are synthesized using surfactants as templates, which have negative environmental impact. Thus, OMPS were developed focusing on surfactant-free routes, such as SBA-15. It was reported that Al-containing SBA-15 promoted the oligomerization of ethene<sup>[8]</sup> and hexene<sup>[9,10]</sup>. Nevertheless, SBA-15 type materials are synthesized using copolymers as templates which are rather expensive. A nice compromise in terms of cost and eco-friendliness of OMPS synthesis methodologies was achieved with the development of TUD-1 by Maschmeyer, Hanefeld and co-workers.<sup>[11-15]</sup>

TUD-1 type materials are synthesized *via* surfactant-free and copolymer-free routes, following important sustainable chemistry principles; *e.g.*, use of less hazardous reagents, benefiting from decreased toxicity and costs.<sup>[16]</sup> TUD-1 family of materials possesses a sponge-like ordered mesoporous structure, with high specific surface area, pore volume and sizes. These textural properties may avoid severe diffusion limitations and/or fast catalyst deactivation due to pore-blockage by carbonaceous matter; particularly important for catalytic processes such as olefins oligomerization which involves intermediates and/or

products. TUD-1 may be furnished with acid properties by introducing, for example, aluminum species.<sup>[17–19]</sup>

In the present work, Al-containing TUD-1 type mesoporous solid acids were synthesized *via* different approaches, and tested as catalysts for 1-butene oligomerization, under continuous flow operation mode, in the temperature range 150–250 °C, and pressure range 20–40 bar. The catalysts were prepared *via* one-pot (HT; sol-gel process, using hydrothermal conditions)<sup>[14,17,18,20]</sup> or stepwise procedures (PG; post-synthesis grafting of Al-species on pre-made siliceous oxide TUD-1)<sup>[21]</sup>. To the best of our knowledge, this is the first report of TUD-1 type aluminosilicates prepared *via* the PG approach. The HT approach may be advantageous in terms of process intensification in relation to the PG approach; on the other hand, the latter may lead to relatively low Si/Al ratios. For comparison, a large-pore (LP) Al-containing OMPS material was synthesized *via* the PG approach, using a mixture of surfactants as structure directing agents (giving Al-LP(PG)). The type of reaction products formed were investigated by GC×GC-ToFMS. The influence of process parameters and material properties on the catalytic reaction, and benchmarking studies with zeolite ZSM-5 were carried out.

## 5.2. Synthesis of the catalytic materials

Mesoporous Al-containing TUD-1 materials with different molar ratios Si/Al were prepared *via* (surfactant-free) sol-gel technique using hydrothermal conditions (HT), or *via* post-synthesis grafting of aluminum species on the pre-made silica support TUD-1 (PG). Large pore (LP) aluminosilicates were synthesized by HT (using a mixture surfactants) and PG methods for comparative studies.

### Sol-gel technique using hydrothermal conditions (HT)

The HT synthesis was carried out following a similar procedure to that described by Lima et al.<sup>[22]</sup>, using AIP and TEOS as Al and Si sources, respectively, and TEA as templating agent. Specifically, TEOS (83.0 mmol) was added slowly to a mixture consisting

of AIP (3.33 mmol for Si/Al=25; 1.66 mmol for Si/Al=50) in isopropanol (6.5 mL) and ethanol (6.5 mL). After stirring *ca.* 20 min, a mixture of TEA (83.9 mmol) and milli-Q water (932.2 mmol) was added slowly, followed by dropwise addition of TEAOH (27.0 mmol) under vigorous stirring. The molar composition of the synthesis-gel was SiO<sub>2</sub>: (0.02 or 0.04)AIP: 0.33TEAOH: 1.01TEA: 11.23H<sub>2</sub>O. The gel obtained was stirred at room temperature for 24 h and dried at 98 °C for 22 h, followed by aging in a PTFE-lined stainless-steel autoclave at 180 °C for 8 h. The resultant solid was subjected to Soxhlet extraction with ethanol (*ca.* 3 h), dried overnight at 60 °C, and gently grinded using an Agate mortar and pestle. Finally, the solid was calcined at 600 °C in static air for 10 h (heating rate of 1 °C min<sup>-1</sup>), giving the materials denoted as Al-TUD-1(x)-HT where x is the initial molar ratio Si/Al (25 or 50) of the synthesis mixture.

### Post-synthesis grafting of aluminum (PG)

The material Al-TUD-1(PG) was synthesized *via* post-synthesis grafting (PG) of an aluminum precursor on the pre-made mesoporous silica TUD-1.<sup>[21]</sup> TUD-1 was prepared according to the procedure described by Lima et al.<sup>[23]</sup>. Specifically, TEOS (25.6 mmol) was added dropwise with stirring to a mixture of TEA (25.8 mmol) and milli-Q water (166.5 mmol). Subsequently, TEAOH (8.2 mmol) was added, and the stirring was continued for *ca.* 2 h. The molar composition of the synthesis-gel was SiO<sub>2</sub>: 0.32TEAOH: 1.01TEA: 7.09H<sub>2</sub>O. The gel was aged at room temperature for 24 h, dried at 100 °C for 22 h, followed by aging in a PTFE-lined stainless-steel autoclave at 180 °C for 8 h. The solid was subjected to Soxhlet extraction with ethanol (*ca.* 3 h), dried overnight at 60 °C, gently grinded using an Agate mortar and pestle, and finally calcined at 600 °C in static air for 10 h (heating rate of 1 °C min<sup>-1</sup>), giving TUD-1. Subsequently, wet (aqueous) impregnation of aluminum on TUD-1 was carried out by mixing TUD-1 (1.0 g) with 50 mL of an aqueous solution of ACH (0.48 mol L<sup>-1</sup> of ACH in milli-Q water, homogenized at 80 °C), and stirring for 2 h at 80 °C. The solid was separated by filtration, and thoroughly washed with milli-Q water until complete removal of chloride, which was checked by the silver nitrate test (for the filtrate). The solid was dried overnight at room temperature, and finally calcined in static air at 550 °C for 4 h (heating rate of 1 °C min<sup>-1</sup>), giving Al-TUD-1(PG).

### Large pore (LP) aluminosilicates

Material Al-LP(PG) was prepared *via* the PG method using a silica denoted as LP (possessing large pores), which, in turn, was synthesized using a mixture of surfactants (C<sub>12</sub>TMABr and C<sub>16</sub>TMACl) as structure directing agent, mesitylene as swelling agent, and sodium silicate and Cab-O-sil® M5 as silica sources, as described previously by Dias et al.<sup>[24]</sup> The molar composition of the synthesis mixture was SiO<sub>2</sub>: 0.271Na<sub>2</sub>O: 0.116C<sub>16</sub>TMACl: 0.025C<sub>12</sub>TMABr: 0.75mesitylene: 30.3H<sub>2</sub>O. The mixture was stirred for 1 h, then transferred to PTFE-lined stainless-steel autoclaves, and heated at 100 °C for 4 days, under static conditions. In 24 h intervals (in total three times), the autoclaves were cooled to room temperature and the pH of the mixture was adjusted to 10.0 with acetic acid. After 4 days, the solids were filtered, washed with water (1.5 L), ethanol (300 mL), dried at 50 °C, and finally calcined at 120 °C for 3 h and then at 560 °C for 4 h, giving LP material. Subsequently, wet impregnation of aluminum on LP was carried out in a similar fashion to that described for Al-TUD-1(PG), leading to Al-LP(PG).

### 5.3. Characterization studies of the catalytic materials

The Al-containing TUD-1 and the large-pore (LP) Al-containing OMPS materials were characterized as described in section 3.2.1.

For all materials prepared, the low angle PXRD patterns show a peak centred in the range 0.8-1.1° 2θ (Figure 5.1-A), suggesting that the materials possessed relatively narrow mesopore size distributions, in agreement with the N<sub>2</sub> adsorption studies discussed ahead. The wide angle PXRD patterns show a very broad, weak peak centred at *ca.* 24° 2θ (Figure 5.1-B), characteristic of mesoporous silicas/silicates possessing amorphous pore walls. There is no evidence of the presence of crystalline alumina or other crystalline phases in the materials. The SEM images show particles of irregular size and morphology, and the Si and Al (for the aluminosilicates) mappings suggest uniform dispersions of surface metal/metalloid species for all materials prepared (Figure 5.2).

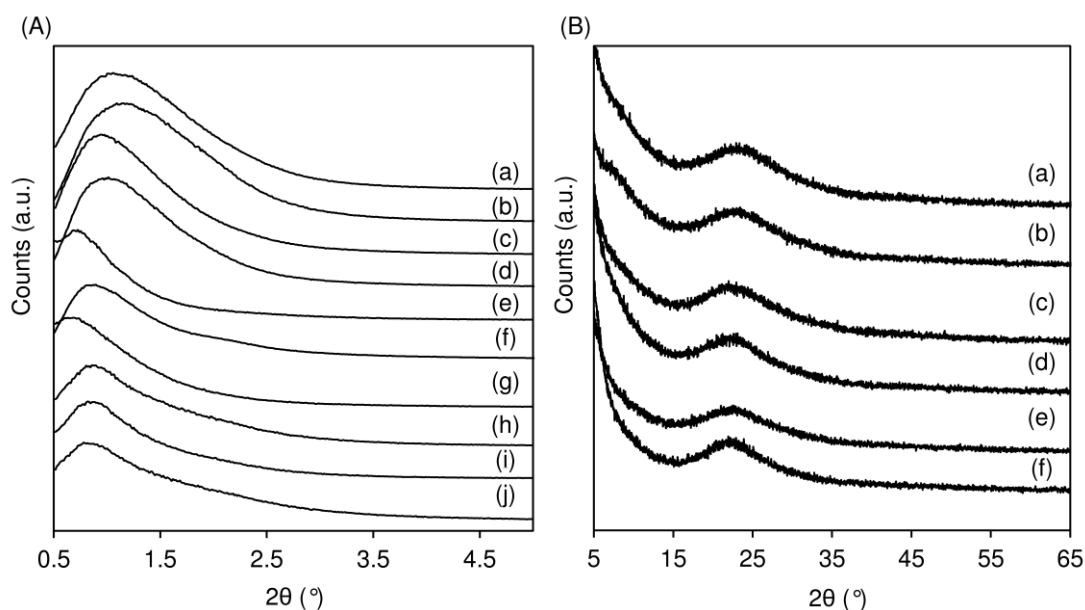


Figure 5.1. (A) Low angles PXRD patterns of Al-TUD-1(25)-HT (fresh (a); used (b)), Al-TUD-1(50)-HT (fresh (c); used (d)), Al-TUD-1(PG) (fresh (e); used (f)), TUD-1 (fresh (g)), Al-LP(PG) (fresh (h); used (i)), and LP (fresh (j)); (B) wide angles PXRD patterns of fresh catalysts: Al-TUD-1(25)-HT (a), Al-TUD-1(50)-HT (b), Al-TUD-1(PG) (c), TUD-1 (d), Al-LP(PG) (e), and LP (f).

ICP-AES indicated that the materials prepared *via* the PG method (Al-TUD-1(PG) and Al-LP(PG)) possessed much lower molar ratios Si/Al (3-5) than Al-TUD-1(25)-HT and Al-TUD-1(50)-HT (18 and 37, respectively), Table 5.1. For each material, the Si/Al ratios determined by ICP-AES (bulk analysis) and EDS (surface analysis) were roughly comparable, suggesting somewhat uniform metal/metalloid dispersions for the bulk (Al-TUD-1(x)-HT) and supported catalysts (Al-TUD-1(PG) and Al-LP(PG)).

The N<sub>2</sub> adsorption/desorption isotherms of the materials prepared are shown in Figure 5.3, and the corresponding textural parameters are given in Table 5.1. All materials exhibited type IV isotherms with a hysteresis loop, characteristic of mesoporous materials (Figure 5.3).<sup>[25]</sup> The median mesopore sizes were in the range 18-26 nm for TUD-1, and in the range 10-14 nm for the other materials (Figure 5.3). In general, the materials possessed very small microporous volume ( $V_{\text{micro}} < 0.04 \text{ cm}^3 \text{ g}^{-1}$ ). The Al-TUD-1(x)-HT materials possessed higher  $S_{\text{BET}}$  (687-741  $\text{m}^2 \text{ g}^{-1}$ ) and  $V_p$  (1.7-2.1  $\text{cm}^3 \text{ g}^{-1}$ ) than those prepared *via* the PG method (397-559  $\text{m}^2 \text{ g}^{-1}$  and 1.2-1.4  $\text{cm}^3 \text{ g}^{-1}$ ), Table 5.1. The PG approach led to 21-24 % reduction in  $S_{\text{BET}}$  of the pre-made silica supports, which was accompanied by decreased

$V_p$ . Although the metal dispersions seemed fairly uniform (discussed above), blockage of a fraction of pores by grafted Al-species cannot be completely ruled out.

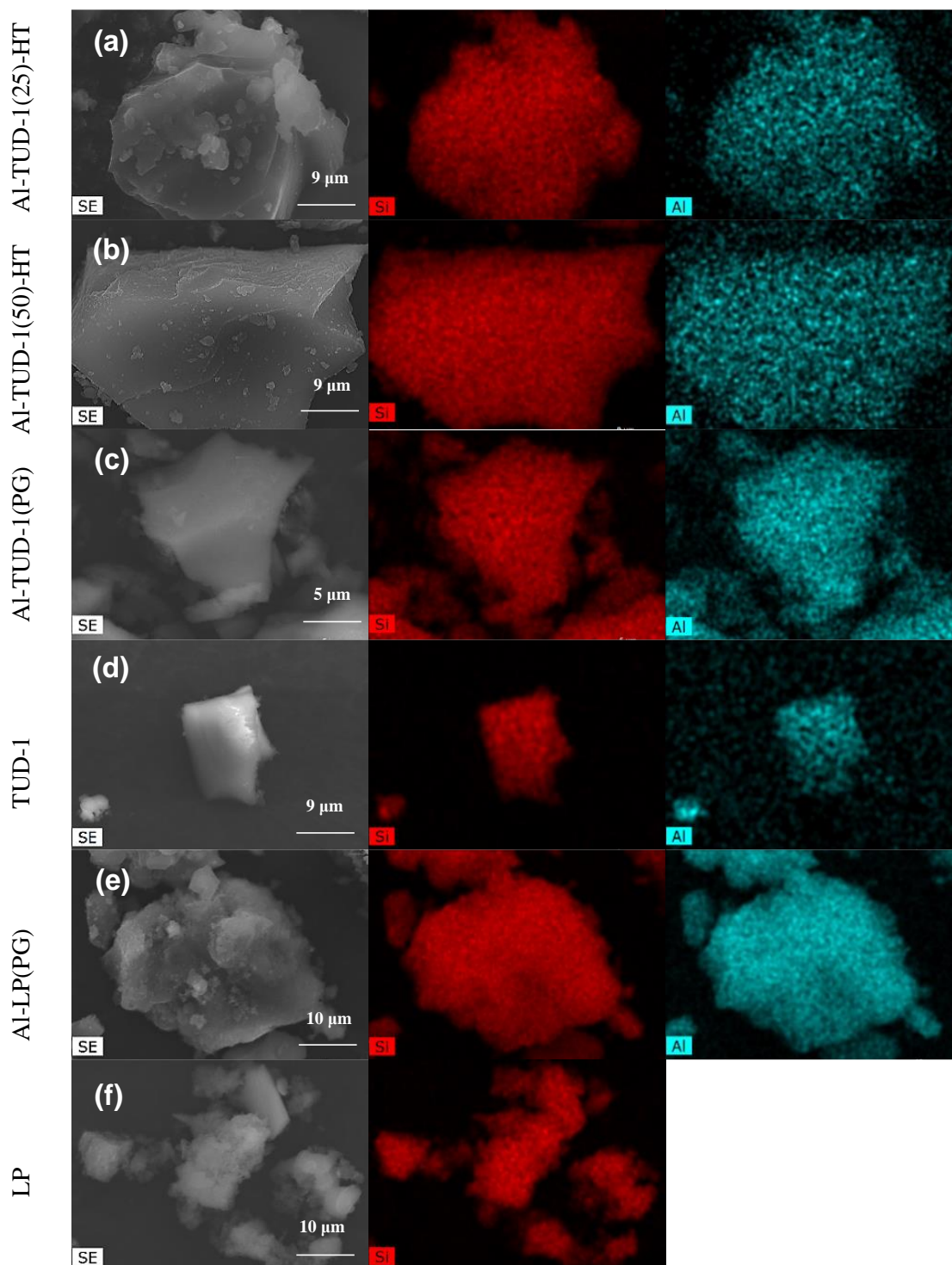


Figure 5.2. SEM images and Si, Al mappings of Al-TUD-1(25)-HT (a), Al-TUD-1(50)-HT (b), Al-TUD-1(PG) (c), TUD-1 (d), Al-LP(PG) (e), and LP (f).

Table 5.1. Elemental analyses and textural properties of the mesoporous silicas/silicates prepared, and the benchmark catalyst ZSM-5.

Sample	Si/Al <sup>[a]</sup>		Textural properties <sup>[b]</sup>		
	ICP-AES	EDS <sup>b</sup>	S <sub>BET</sub> (m <sup>2</sup> g <sup>-1</sup> )	V <sub>p</sub> (cm <sup>3</sup> g <sup>-1</sup> )	D <sub>p</sub> (nm)
Al-TUD-1(25)	18	16 (16)	741 (710)	1.7 (1.6)	10 (10)
Al-TUD-1(50)	37	29 (27)	687 (683)	2.1 (2.1)	14 (14)
Al-TUD-1(PG)	5	5 (4)	397 (344)	1.2 (1.0)	14 (14)
Al-LP(PG)	3	4	559 (511)	1.4 (1.1)	10 (10)
TUD-1	-	-	524	2.2	19
LP	-	-	713	2.0	10
ZSM-5	-	-	417	0.4	-

<sup>[a]</sup> Molar ratios determined by ICP-AES or EDS. <sup>[b]</sup> The values in parenthesis are for the spent catalysts.

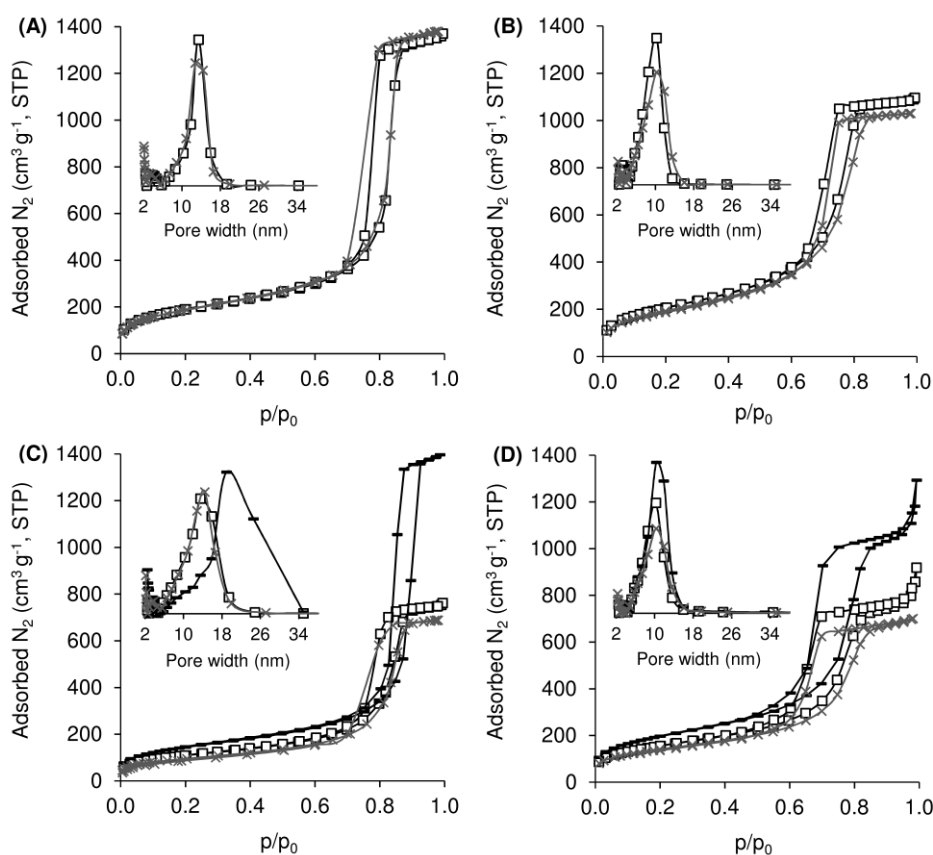


Figure 5.3. Nitrogen adsorption-desorption isotherms (at  $-196\text{ }^{\circ}\text{C}$ ) for (A) Al-TUD-1(25)-HT (fresh ( $\square$ ); used ( $\times$ )), (B) Al-TUD-1(50)-HT (fresh ( $\square$ ); used ( $\times$ )), (C) Al-TUD-1(PG) (fresh ( $\square$ ); used ( $\times$ )) and TUD-1 (fresh ( $-$ )), and (D) Al-LP(PG) (fresh ( $\square$ ); used ( $\times$ )) and LP (fresh ( $-$ )). Insets are the mesopore size distributions for the corresponding materials (using the same symbols).

The FT-IR spectra in the OH stretching region of the materials (after evacuation at 450 °C) showed a band at *ca.* 3743 cm<sup>-1</sup> assignable to OH stretching vibrations of isolated surface silanol groups (Figure 5.4-A).<sup>[26,27]</sup> The relative intensity of this band was lower for the materials prepared *via* the PG methods, which is likely due to the reaction of surface silanol groups with Al-species.

The <sup>27</sup>Al MAS NMR spectra of the materials prepared show three resonances centred at *ca.* 0 ppm, 30 ppm and 54 ppm, assigned to framework octahedral Al species (Al<sub>octa</sub>), pentahedral Al species (Al<sub>penta</sub>), and tetrahedral Al species (Al<sub>tetra</sub>), respectively (Figure 5.5). All materials exhibited a broad, asymmetric Al<sub>octa</sub> peak, suggesting wide distributions of bond angles of these types of species. The Al-TUD-1(x)-HT materials exhibited similar spectral features. The same applies for the materials prepared *via* the PG approach, albeit with differences in relation to the Al-TUD-1(x)-HT materials; the former possessed wide distributions of different types of Al-species. The spectral features of the Al-TUD-1(x)-HT materials were in agreement with literature data for similarly prepared materials.<sup>[14,22]</sup> The peaks area ratio (Al<sub>tetra</sub>+Al<sub>penta</sub>)/Al<sub>octa</sub> was higher for the Al-TUD-1(x)-HT materials (2.6 and 3.2 for x=25 and 50, respectively) than Al-TUD-1(PG) and Al-LP(PG) (1.1 and 1.3, respectively); a similar trend was verified in terms of Al<sub>tetra</sub>/Al<sub>penta</sub>, which was higher for Al-TUD-1(x)-HT (2.2 and 2.6 for x=25 and 50, respectively) than Al-TUD-1(PG) and Al-LP(PG) (1.2 and 1.0, respectively).

The acid properties of the materials were measured by FT-IR of pyridine adsorbed at 200 °C (Table 5.2, Figure 5.4-B). The materials exhibited bands characteristic of pyridinium ions due to Brønsted (B) acid Al-species (*ca.* 1545 cm<sup>-1</sup> and 1636 cm<sup>-1</sup>), pyridine coordinated with Lewis (L) acid Al-species (*ca.* 1624 cm<sup>-1</sup>, 1456 cm<sup>-1</sup> or 1443 cm<sup>-1</sup>), and a band at *ca.* 1495 cm<sup>-1</sup> associated with the two types of acid sites (Figure 5.4-B).<sup>[28,29]</sup> The B and L acid sites may be matched with species of the type Al<sub>tetra</sub> and Al<sub>penta</sub>, respectively, evidenced by <sup>27</sup>Al MAS NMR spectroscopy. The total amount of L+B acid sites followed the order Al-TUD-1(PG) ≅ Al-TUD-1(50)-HT < Al-TUD-1(25)-HT ≅ Al-LP(PG); no direct relationship with the Si/Al ratio could be established. All materials possessed mainly L type acidity. The PG approach led to higher molar ratios L/B (10-15) than the HT one (3-4), and higher L acid site density (expressed as meq<sub>L</sub> nm<sup>-2</sup>, considering S<sub>BET</sub>); 181 and 184 meq<sub>L</sub> nm<sup>-2</sup> for Al-

TUD-1(PG) and Al-LP(PG), respectively, and 108 and 89 meq<sub>L</sub> nm<sup>-2</sup> for Al-TUD-1(x)-HT with x=25 and 50, respectively.

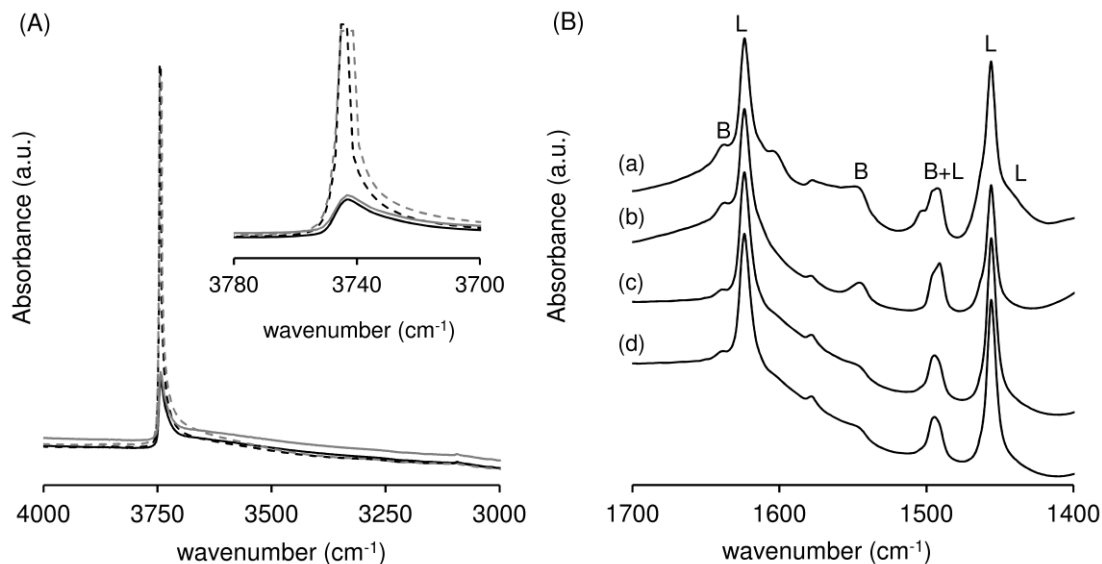


Figure 5.4. (A) FT-IR spectra in the OH stretching region of the materials Al-TUD-1(25)-HT (dashed black line), Al-TUD-1(50)-HT (dashed grey line), Al-TUD-1(PG) (solid black line), and Al-LP(PG) (solid grey line), after evacuation at 450 °C; the inset is a zoom into a narrower spectral region. (B) FT-IR spectra of pyridine (base probe) adsorbed, at 200 °C, on Al-TUD-1(25)-HT (a), Al-TUD-1(50)-HT (b), Al-TUD-1(PG) (c), and Al-LP(PG) (d).

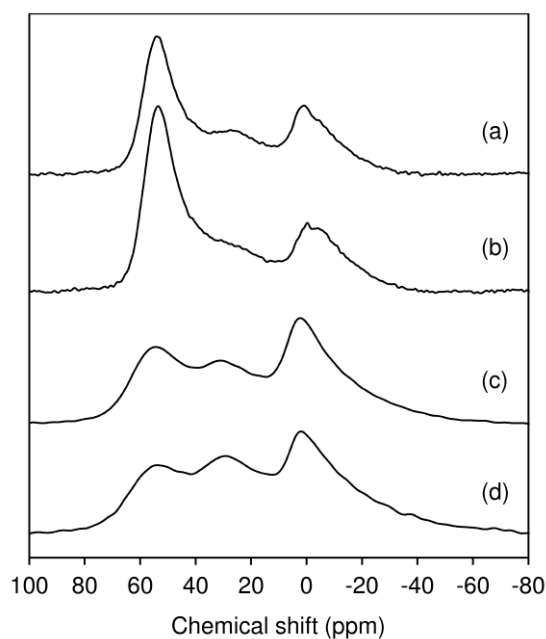


Figure 5.5. <sup>27</sup>Al MAS NMR spectra of Al-TUD-1(25)-HT (a), Al-TUD-1(50)-HT (b), Al-TUD-1(PG) (c), and Al-LP(PG) (d).

Table 5.2. Acid properties of the prepared mesoporous silicas/silicates.<sup>[a]</sup>

Material	B ( $\mu\text{mol g}^{-1}$ )	L ( $\mu\text{mol g}^{-1}$ )	L+B ( $\mu\text{mol g}^{-1}$ )	L/B	L <sub>450</sub> /L <sub>200</sub>	B <sub>450</sub> /B <sub>200</sub>
Al-TUD-1(25)	44	133	177	3.0	0.33	0
Al-TUD-1(50)	28	101	129	4	0.33	0
Al-TUD-1(PG)	8	119	127	15	0.18	0
Al-LP(PG)	17	171	188	10	0.22	0
ZSM-5	338	80	418	0.2	0.71	0.43

<sup>[a]</sup> Determined by FT-IR of adsorbed pyridine, at 200 °C; B=Brønsted acid sites, L=Lewis acid sites, B+L=total amount of acid sites.

Increasing the evacuation temperature from 200 °C to 450 °C led to a significant reduction in the amount of L acid sites (L<sub>450</sub>/L<sub>200</sub> in the range 0.18-0.33), and the disappearance of the bands associated with B acid sites. Hence, the mesoporous aluminosilicates prepared possess mainly L acidity, few strong L acid sites, and lack strong B acidity. Very recently, Yuan, Lv and coworkers reported for Al-containing SBA-15 materials prepared under hydrothermal conditions, the lack of B acidity after evacuation at 350 °C.<sup>[29]</sup> For commercial zeolite ZSM-5 possessing molar ratio Si/Al=26 and 20 % alumina binder, it was reported a molar ratio L/B of 1.15 (based on pyridine adsorbed at 200 °C), and molar ratios B<sub>400</sub>/B<sub>200</sub> and B<sub>500</sub>/B<sub>200</sub> of 0.57 and zero, respectively, indicating the lack of B acidity after evacuation at 500 °C.<sup>[30]</sup>

The benchmark catalyst, ZSM-5, obtained *via* calcination of commercial CBV3024E (Zeolyst), possessed S<sub>BET</sub> of 417 m<sup>2</sup> g<sup>-1</sup> (S<sub>ext</sub>=43 m<sup>2</sup> g<sup>-1</sup>), V<sub>p</sub> of 0.4 cm<sup>3</sup> g<sup>-1</sup> (V<sub>micro</sub>=0.1 cm<sup>3</sup> g<sup>-1</sup>), Table 5.1. These results show considerable differences in textural properties between the zeolite and the mesoporous materials, in particular the much lower S<sub>BET</sub> (which is essentially mesoporous surface for TUD-1 and LP type materials). In comparison to the mesoporous aluminosilicates prepared, ZSM-5 possesses higher total amount of acid sites (L+B), lower molar ratio L/B, and stronger acidity (Table 5.2).

#### 5.4. Catalytic studies: general considerations

The OMPS materials prepared were tested for the acid-catalyzed oligomerization of 1-butene (1C<sub>4</sub>), under high pressure, continuous flow operation, and compared under the typical reaction conditions, specifically 200 °C, 30 bar, weight hourly space velocity (WHSV) of 2.2 g<sub>1C<sub>4</sub></sub> g<sub>cat</sub><sup>-1</sup> h<sup>-1</sup> (corresponding to *ca.* 0.5 h contact time, which is somewhat reasonable from a practical point of view;<sup>[31,32]</sup> and it was verified that mass transfer limitations are avoided (Chapter 4)), and the total mass of 1C<sub>4</sub> fed to mass of catalyst was *ca.* 17.6 g g<sub>cat</sub><sup>-1</sup> (TOS≅8 h). Relatively low WHSV may improve catalytic conversion of the feedstock (for example, oligomerization technologies such as Mobil Olefins to Gasoline and Distillate (MOGD) operate at 0.5-2 h<sup>-1</sup>).<sup>[1,2]</sup>

All materials prepared led to the conversion of 1C<sub>4</sub> to higher molar mass products (Figure 5.6 and Figure 5.7). A blank experiment without catalyst led to negligible conversion, indicating that the solid acids were essential for the reaction of 1C<sub>4</sub> to occur, and that thermal reactions are not important. The materials prepared *via* the HT method (Al-TUD-1(x)-HT, x=25 or 50) led to similar conversions (33-35 % X<sub>C<sub>4</sub></sub> at *ca.* 8 h on-stream). The same applies for the materials prepared *via* the PG method (Al-TUD-1(PG) and Al-LP(PG)), albeit the conversions were lower (21-22 %) than for the Al-TUD-1(x)-HT materials (Figure 5.6). On the other hand, the materials prepared *via* the PG method favored the formation of Dcut products (with boiling point range distribution characteristic of diesel fractions), whereas the Ncut products (with boiling point range distribution characteristic of naphtha fractions) predominated in the case of the Al-TUD-1(x)-HT materials (Figure 5.7-A). Specifically, the product lump distribution (PLD) profiles show that the main portion of the liquid products was C10-C18 for Al-TUD-1(PG) and Al-LP(PG) and C7-C8 for Al-TUD-1(x)-HT materials (Figure 5.7-B). Although Al-TUD-1(PG) and Al-LP(PG) resembled somewhat comparable features in terms of catalytic performance, the choice of TUD-1 as support is particularly attractive and ecofriendly, avoiding use of surfactants.

As mentioned above, the acid properties of the materials are essential for the reaction of 1C<sub>4</sub> to occur. The OMPS prepared possessed essentially Lewis (L) acidity (Table 5.2). It was reported in the literature for different types of solid acids that Lewis (L) acidity (in

relation to Brønsted (B) acidity) may favor the selective oligomerization of butenes, and catalyst stability.<sup>[33–38]</sup>

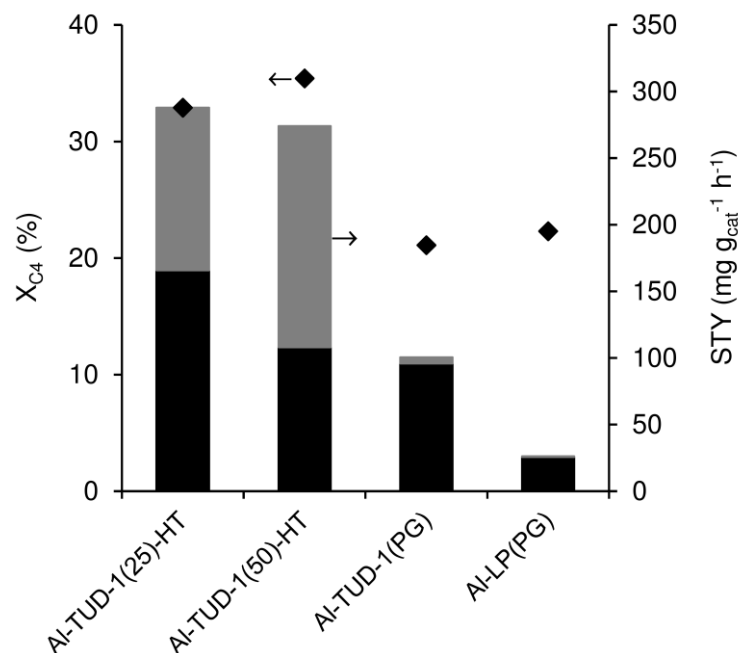


Figure 5.6. Conversion ( $X_{C4}$ ) and STY of Dcut and Ncut products for the different OMPS catalysts. Reaction conditions: 200 °C, 30 bar,  $WHSV=2.2 \text{ g}_{1C4} \text{ g}_{cat}^{-1} \text{ h}^{-1}$ , TOS=8 h,  $T_{act}=450 \text{ °C}$ .

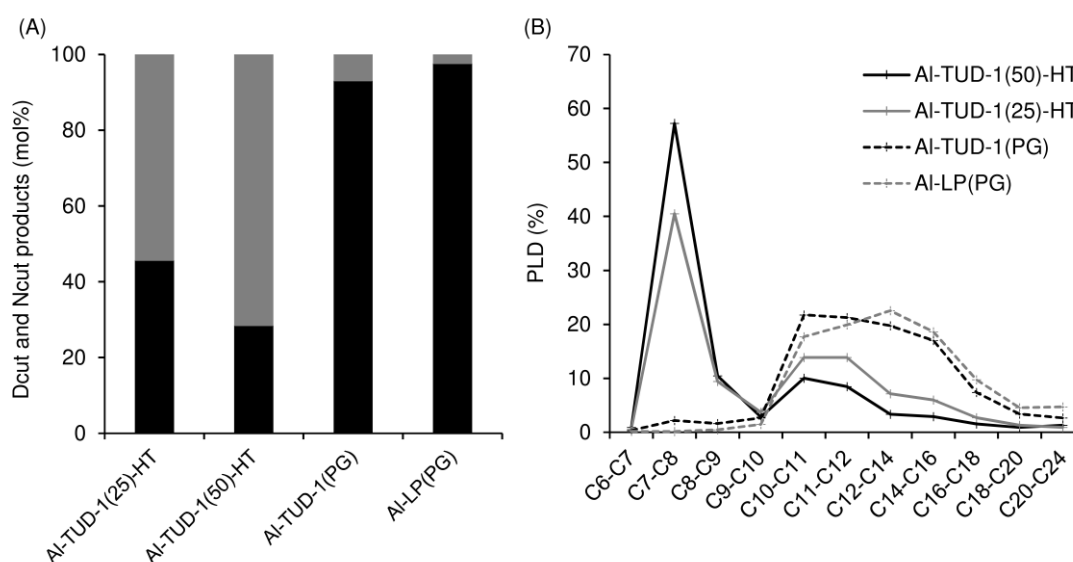


Figure 5.7. (A) Molar proportions of Dcut (black bars) and Ncut (grey bars) products, and (B) PLD profiles for the reaction of 1-butene in the presence of the OMPS catalysts. Reaction conditions: 200 °C, 30 bar,  $WHSV=2.2 \text{ g}_{1C4} \text{ g}_{cat}^{-1} \text{ h}^{-1}$ , TOS=8 h,  $T_{act}=450 \text{ °C}$ .

A relationship seems to exist between catalytic activity and L acid sites density (associated with a combination of textural and acid properties), Figure 5.8. Direct relationships between activity and (solely) textural properties could not be established. However, higher L acid sites density for Al-TUD-1(PG) and Al-LP(PG) seems to correlate with lower conversions and intrinsic catalytic activity (expressed as  $\text{mol}_{\text{C}_4} \text{mol}_{\text{L}}^{-1} \text{h}^{-1}$ ) in comparison to the Al-TUD-1(x)-HT materials (Figure 5.8-A). On the other hand, the materials with higher L acid site density led to higher ratio  $D_{\text{cut}}/N_{\text{cut}}$  (Figure 5.8-B). Possibly, the proximity of acid sites (site density) favors consecutive reactions of the formed/adsorbed intermediates, leading to higher molar mass products. Corma et al. reported for the oligomerization of propene and pentene over MFI based acid catalysts, that the formation of larger oligomers was favored by a higher B acid site density, for cases where the diffusion out of the micropores was enhanced by short intracrystalline diffusion path lengths.<sup>[39]</sup> For the OMPS prepared, no clear correlations could be established between the catalytic results and the amount or density of B acid sites. It seems that, in relation to the catalysts prepared *via* the HT method, those prepared *via* the PG method possess lower B acid sites density (lower amount of B acid sites and  $S_{\text{BET}}$ ), and led to lower  $X_{\text{C}_4}$  and higher  $D_{\text{cut}}/N_{\text{cut}}$  ratios, although there is not a straightforward trend. More detailed studies of the influence of material properties on the catalytic reactions (*e.g.*, refined studies of the influence of acid strength) may help establish clearer relationships.

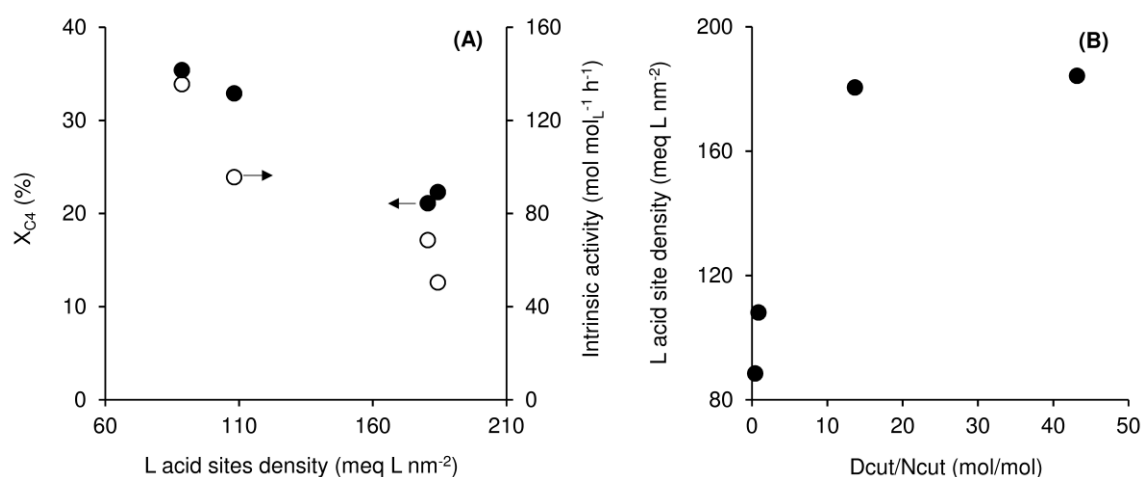


Figure 5.8. Influence of Lewis acid site density on (A) conversion (●) and intrinsic activity (○), and (B) molar ratio of  $D_{\text{cut}}/N_{\text{cut}}$  products. Reaction conditions: 200 °C, 30 bar,  $\text{WHSV}=2.2 \text{ g}_{\text{IC}_4} \text{ g}_{\text{cat}}^{-1} \text{ h}^{-1}$ ,  $\text{TOS}=8 \text{ h}$ ,  $T_{\text{act}}=450 \text{ °C}$ .

The average space-time yields (STY) is an important parameter from a practical point of view, reflecting the catalyst's productivity. The STY of Dcut products ( $STY_{Dcut}$ ) followed the order ( $mg\ g_{cat}^{-1}\ h^{-1}$ ) Al-LP(PG) (26) < Al-TUD-1(PG) (96) < Al-TUD-1(50)-HT (108) < Al-TUD-1(25)-HT (166), Figure 5.6. The materials Al-TUD-1(x)-HT led to higher  $STY_{Dcut}$ , as well as higher  $STY_{Ncut}$  (122-166  $mg\ g_{cat}^{-1}\ h^{-1}$ ). From the point of view of process economics, one could consider recycling the coproduced Ncut products into the oligomerization process or other production units in an integrated refinery.

## 5.5. Cetane number and GC×GC–ToFMS analysis of reaction products

The PLD profiles for the different catalysts prepared included products with “odd” number of carbon atoms ( $(n\pm x)$ , where  $n$  is a multiple of 4 and  $x\neq 4$ ), Figure 5.7-B. These results suggest that the overall reaction system involved side reactions such as co-oligomerization (of different olefins), and cracking, which can lead to products with  $n+x$  carbon atoms.<sup>[7,40]</sup> For the prepared catalysts, the cetane number (CN, determined by the O'Connor et al. correlation<sup>[41]</sup>) was in the range 41-46 for the TUD-1 type catalysts, and 36 for Al-LP(PG). These results are for the mixtures of Ncut plus Dcut products, without any subsequent treatment/reactions. CN values of 50-56 were reported in the literature for diesel cuts after hydrogenation (which enhances CN), produced in MODG and COD commercial processes.<sup>[3,7,42-44]</sup> Since the products mixtures were not hydrogenated for the OMPS materials, the CN values are indicated for rough comparisons. The CN was determined in a similar fashion for a crude-oil-based diesel fuel sample (denoted as GDiesel) produced by Galp Energia refinery (Portugal), with CN=50 (determined using test engines, according to ASTM D613; Standard test method for cetane number of diesel fuel oil). The O'Connor correlation gave CN=62 for GDiesel, which is higher than the values obtained using test engines, albeit not drastically different. The difference may be partly due to the fact that the O'Connor correlation gives better predictions for synthetic fuels produced *via* oligomerization of light olefins, than for crude-oil-based diesel which contains relatively high amounts of aromatics (the GDiesel produced by Galp Energia refinery contained 23 % aromatics, based on the GC×GC-ToFMS analysis).<sup>[41]</sup>

To gain insights into the types of chemical compounds formed, the mixture of reaction products for Al-TUD-1(25)-HT as catalyst, under typical conditions, was analyzed by GC×GC-ToFMS. The mixture was mainly composed of aliphatic compounds, and contained some aromatics. The ratio of total peak areas of aromatics ( $A_{\text{arom}}$ ) to aliphatics ( $A_{\text{aliph}}$ ) was *ca.* 0.04. In the ranges of the chromatogram corresponding to C10<sup>-</sup> and C10<sup>+</sup> (based on the retention times ( $^1t_{\text{R}}$ ) of the alkane series), the ratio  $A_{\text{arom}}/A_{\text{aliph}}$  was 0.009 and 0.062, respectively, indicating that the aromatics were mainly in the Dcut portion; nevertheless, the aromatics content is relatively low (*ca.* 4 %) which is an attractive feature of synthetic fuels. The low aromatics content is consistent with the fact that the <sup>1</sup>H NMR spectrum of the reaction mixture (used for determining the CN; not shown) indicated negligible contribution of aromatic rings (spectral region 9.2-6.5 ppm). The crude-oil-based diesel fuel GDiesel sample supplied by the Galp Energia refinery contained *ca.* 23 % of aromatics. The aromatic products identified for Al-TUD-1(25)-HT may be precursors of coke formation (discussed ahead).<sup>[45]</sup>

## 5.6. Influence of the reaction conditions

The influence of the process parameters on the catalytic reaction was investigated for Al-TUD-1(25)-HT (Figure 5.9 and Figure 5.10), which was the best performing catalyst in terms of  $\text{STY}_{\text{Dcut}}$ . Increasing the reaction pressure in the range 20-40 bar, at 200 °C, enhanced conversion;  $X_{\text{C}_4}$  increased by a factor of 1.4 (Figure 5.9-A). These results are consistent with the fact that oligomerization pathways are accompanied by reduction in the total number of moles, and thus increasing reaction pressure may favor conversion. The PLD profiles were roughly comparable (Figure 5.9-B), and the  $\text{STY}_{\text{Dcut}}$  was higher at 30 bar ( $166 \text{ mg g}_{\text{cat}}^{-1} \text{ h}^{-1}$ ; Figure 5.9-A).

Increasing the reaction temperature in the range 150-250 °C, at 30 bar, enhanced conversion; a temperature increment of 100 °C led to an increase in  $X_{\text{C}_4}$  by a factor of *ca.* 1.8, reaching 47 % at 250 °C;  $\text{STY}_{\text{Dcut}}$  also increased reaching  $238 \text{ mg g}_{\text{cat}}^{-1} \text{ h}^{-1}$  (Figure 5.9-C). However, the mass ratio Dcut/Ncut decreased, following the order, 150 °C (3.1) > 200 °C (1.4) > 250 °C (0.9), Figure 5.9-D. Decreasing the reaction temperature possibly favors

the formation of oligomers, since the oligomerization pathways are exothermic, albeit it impacts negatively on conversion. Increasing temperature seems to favor the formation of lighter products, possibly due to increasing importance of competitive side reactions such as cracking.<sup>[7]</sup> The influence of the WHSV on the catalytic reaction was studied in the range 1.2-3.1  $\text{g}_{1\text{C}4} \text{g}_{\text{cat}}^{-1} \text{h}^{-1}$ , at 200 °C, 30 bar, by varying the flowrate of 1-butene. Increasing WHSV had a negative effect on  $X_{\text{C}4}$  (Figure 5.10-E), without affecting considerably the PLDs (Figure 5.10-F). The mass ratio  $D_{\text{cut}}/N_{\text{cut}}$  was in the range 1-1.4, and WHSV of 2.2  $\text{g}_{1\text{C}4} \text{g}_{\text{cat}}^{-1} \text{h}^{-1}$  led to slightly higher  $\text{STY}_{D_{\text{cut}}}$  (66  $\text{mg} \text{g}_{\text{cat}}^{-1} \text{h}^{-1}$ , Figure 5.10-E).

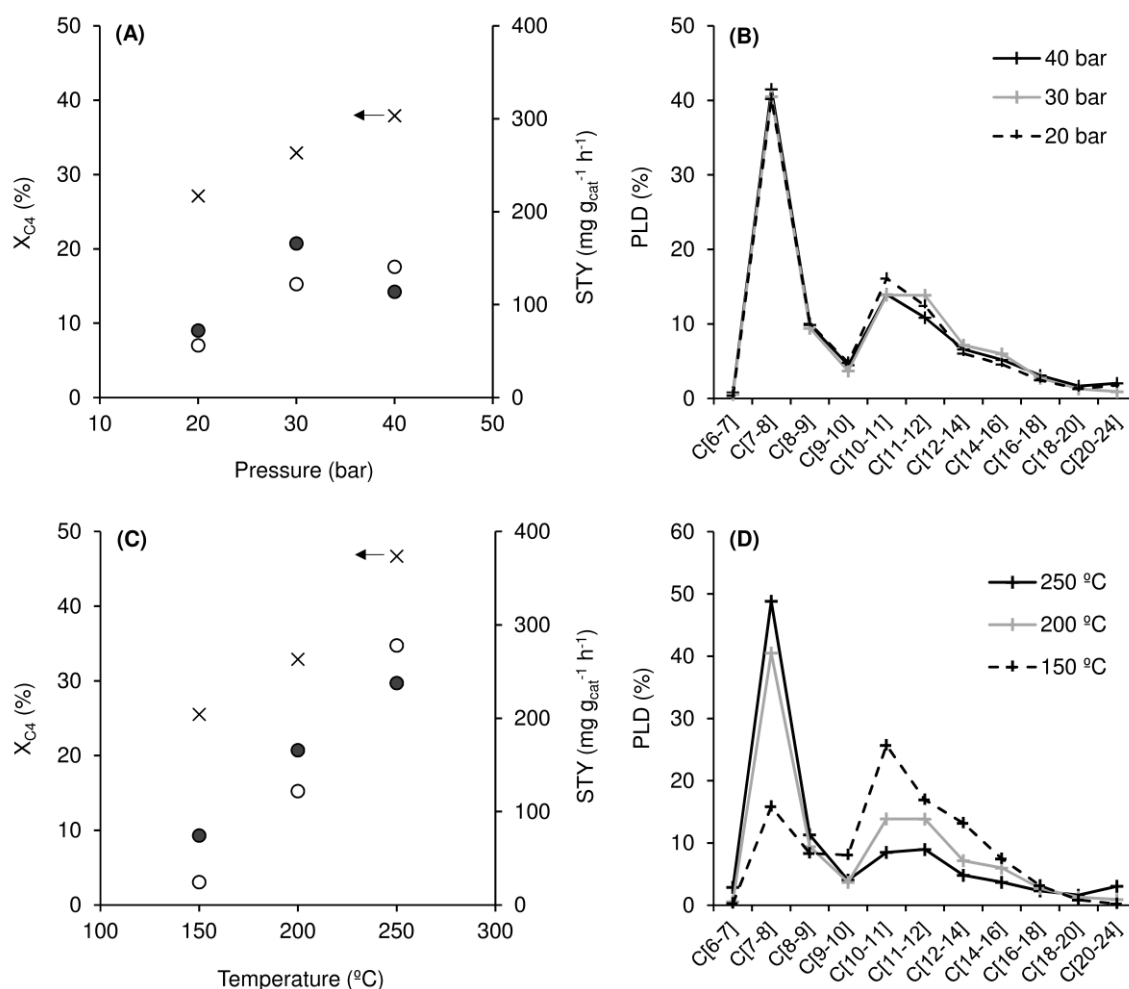


Figure 5.9. Influence of reaction conditions on the catalytic reaction of 1C4 in the presence of Al-TUD-1(25)-HT. Conversion ( $X_{\text{C}4}$ (x)) and STY of Dcut (●) and Ncut products (○) (A, C), and PLD profiles (B, D) for different reaction pressures (A, B) and temperature (C, D).

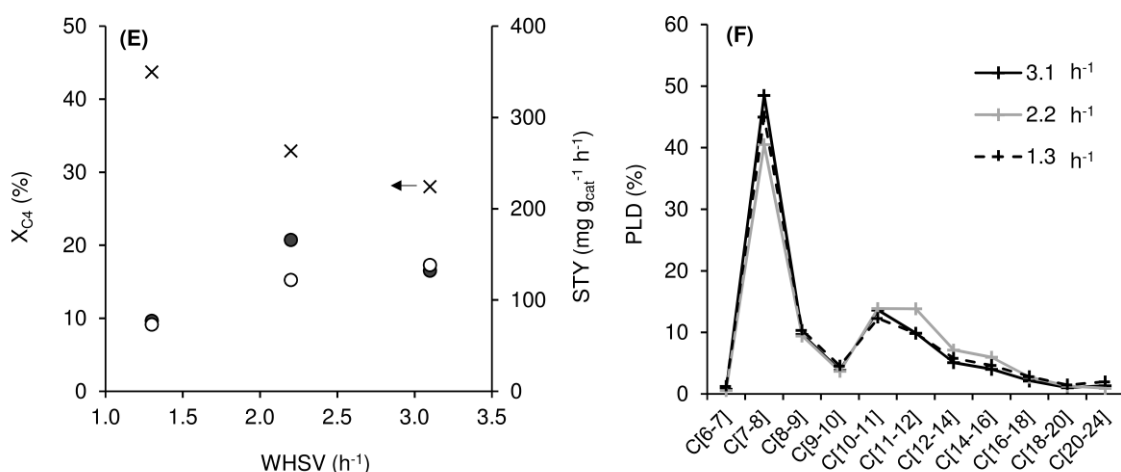


Figure 5.10. Influence of reaction conditions on the catalytic reaction of 1C4 in the presence of Al-TUD-1(25)-HT. Conversion ( $X_{C_4}$ ( $\times$ )) and STY of Dcut ( $\bullet$ ) and Ncut products ( $\circ$ ) (E), and PLD profiles (F) for different WHSV.

## 5.7. Catalyst stability and benchmarking

The recovered catalysts exhibited roughly comparable PXRD patterns (Figure 5.1), and textural properties (Table 5.1, Figure 5.3) to the corresponding original catalysts, suggesting that the structural integrity was essentially preserved. The elemental mappings (Figure 5.11) and Si/Al ratios (EDS, Table 5.1) for the used catalysts were comparable to the corresponding data for the original catalysts. Coke was formed in comparable amounts for all OMPS catalysts tested; 5.3-6.1 wt.% organic matter (TGA) and 1.6-2.5 wt.% carbon content (EA). Increasing the TOS from 8 h to 32 h, using Al-TUD-1(25)-HT as catalyst, under typical reaction conditions, led to decrease in conversion by a factor of *ca.* 1.2, suggesting that catalyst deactivation was not severe (Figure 5.12); on the other hand, the PLD profiles were comparable for the product mixtures collected after 8 h or 32 h on-stream, suggesting fairly steady products compositions with TOS. Fairly good catalyst stability with TOS was reported in the literature for OMPS of the type Al-MCM-41 in comparison to (microporous) zeolites.<sup>[6,7]</sup>

Comparison of the catalytic results for the materials prepared to literature data is not straightforward due to the considerably different process parameters used. The catalysts

prepared, excluding Al-TUD-1(50)-HT (Dcut/Ncut mass ratio=0.7), led to mass ratios of Dcut/Ncut in the range 1-67, at 200 °C, 30 bar (WHSV=2.2 g<sub>1C4</sub> g<sub>cat</sub><sup>-1</sup> h<sup>-1</sup>), and Al-TUD-1(25)-HT led to the highest STY<sub>Dcut</sub> (166 mg g<sub>cat</sub><sup>-1</sup> h<sup>-1</sup>, under these conditions; Figure 5.6). It was reported in the literature that the reaction of 1C<sub>4</sub>, in the presence of zeolite ZSM-5 (the type used in commercial oligomerization processes), at 200 °C and ambient pressure, gave mainly dimers (which are in the Ncut range).<sup>[46]</sup> At higher temperature and pressure (240 °C, 60 bar), the reaction of light olefins (C<sub>4</sub>-C<sub>6</sub>) over ZSM-5, led to a mass ratio Dcut/Ncut of *ca.* 1.1, and STY<sub>Dcut</sub> of *ca.* 410 mg g<sub>cat</sub><sup>-1</sup> h<sup>-1</sup> (with WHSV=1.5 g<sub>1C4</sub> g<sub>cat</sub><sup>-1</sup> h<sup>-1</sup>).<sup>[30]</sup> In turn, the catalyst Al-TUD-1(25)-HT, at 250 °C, 30 bar (WHSV=2.2 g<sub>1C4</sub> g<sub>cat</sub><sup>-1</sup> h<sup>-1</sup>), led to a lower ratio Dcut/Ncut (0.9) and STY<sub>Dcut</sub> (238 mg g<sub>cat</sub><sup>-1</sup> h<sup>-1</sup>).

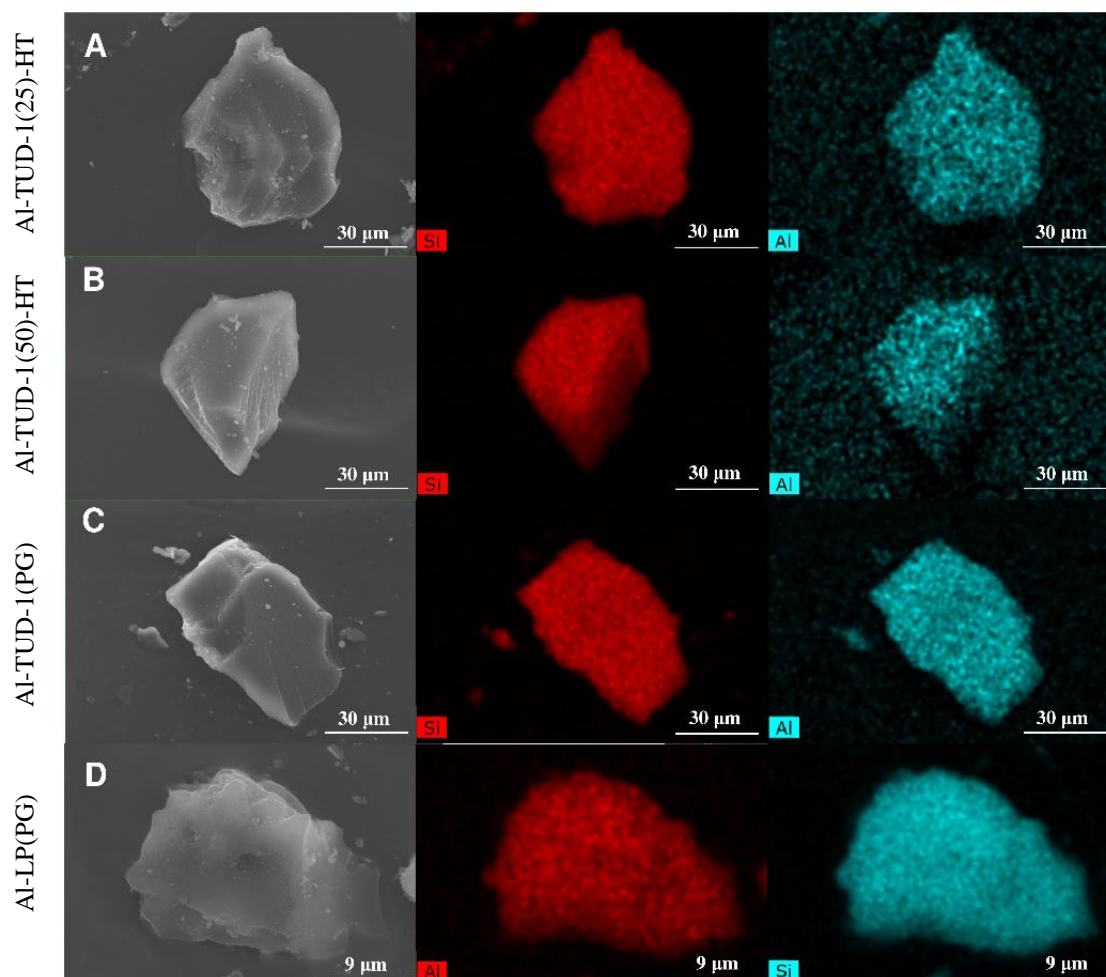


Figure 5.11. SEM images and Si, Al mappings of the catalysts after the reaction in the presence of Al-TUD-1(25)-HT (A), Al-TUD-1(50)-HT (B), Al-TUD-1(PG) (C), and Al-LP(PG) (D).

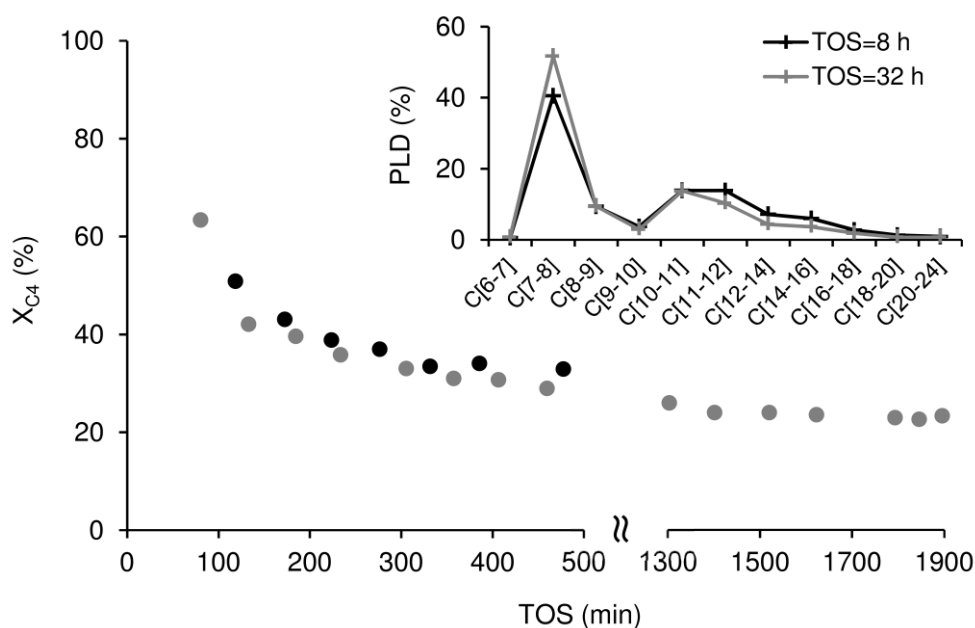


Figure 5.12. Conversion ( $X_{C4}$ ) as a function of TOS, using Al-TUD-1(25)-HT as catalyst. The inset shows the PLD profiles for the products collected after 8 h and 32 h on-stream. Reaction conditions: 200 °C, 30 bar,  $WHSV=2.2 \text{ g}_{1C4} \text{ g}_{cat}^{-1} \text{ h}^{-1}$ ,  $T_{act}=450 \text{ °C}$ .

The performance of Al-TUD-1(25)-HT was compared to that of ZSM-5 (the protonic form of commercially available CBV3024E, Zeolyst, Si/Al=15) for 1C4 conversion, under typical reaction conditions (200 °C, 30 bar,  $WHSV=2.2 \text{ g}_{1C4} \text{ g}_{cat}^{-1} \text{ h}^{-1}$ ) (Figure 5.13). The two catalysts led to comparable mass ratio  $D_{cut}/N_{cut}$  (1.3-1.4; Figure 5.13-A), PLD profiles (Figure 5.13-B), and CN (41-46). However, in relation to ZSM-5, Al-TUD-1(25)-HT led to lower conversion (39 % and 33 %, respectively) and  $STY_{Dcut}$  (293 and 166  $\text{mg g}_{cat}^{-1} \text{ h}^{-1}$ , respectively). These differences may be associated with the considerably different material properties (structure, crystallinity, acidity) for the two catalysts. Yoon et al. reported for butene oligomerization over large-pore zeolites (FAU topology) that conversion and selectivity to trimers and tetramers correlated with L acidity rather than B acidity.<sup>[35]</sup> A comparative study of the Lewis acidity for all OMPS catalysts prepared and ZSM-5, suggested that higher molar ratio  $L_{450}/L_{200}$  tended to favor  $X_{C4}$ , being highest for ZSM-5 (Table 5.2, Figure 5.14). Stronger L acid sites may possess higher intrinsic activity, enhancing conversion.

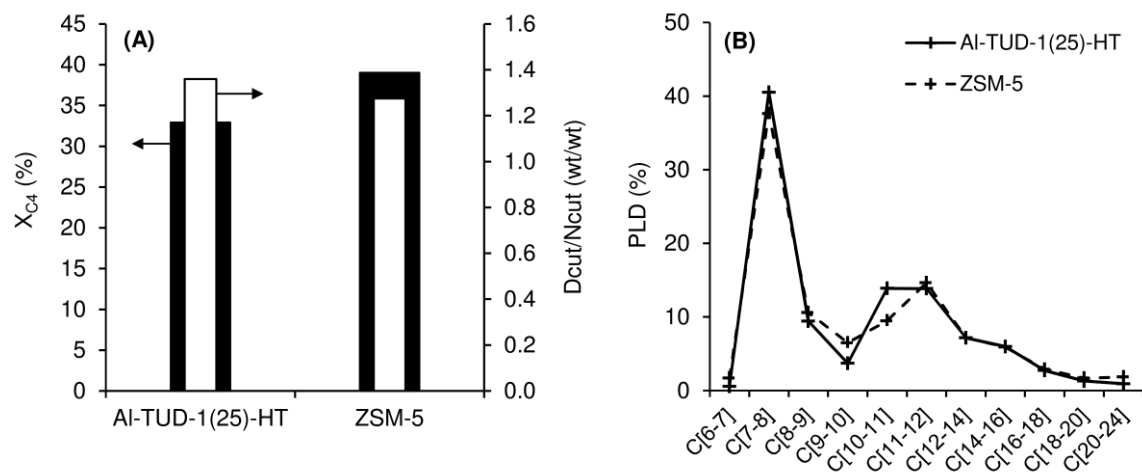


Figure 5.13. Catalyst benchmarking with ZSM-5. (A) Conversion and mass ratio of Dcut/Ncut products, and (B) PDL profiles for Al-TUD-1(25)-HT and ZSM-5.

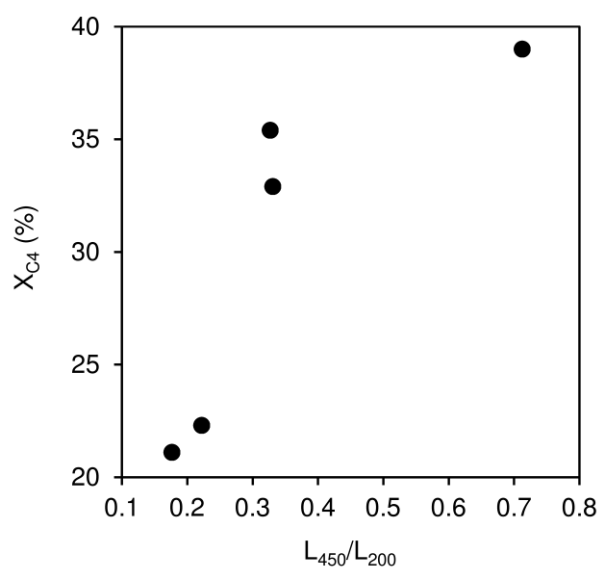


Figure 5.14. Conversion ( $X_{C_4}$ ) versus Lewis acid site strength (based on the molar ratio  $L_{450}/L_{200}$ ) for the OMPS catalysts prepared and the benchmark catalyst, ZSM-5. Reaction conditions: 200 °C, 30 bar,  $WHSV=2.2 \text{ g}_{1C_4} \text{ g}_{cat}^{-1} \text{ h}^{-1}$ ,  $T_{act}=450 \text{ °C}$ .

Virtually any porous solid acid catalyst in olefin oligomerization may suffer deactivation due to surface passivation by adsorption and building-up of organic deposits (byproducts) with TOS. The amount of coke formed in the case of ZSM-5 was approximately double that for Al-TUD-1(25)-HT (11.5 and 5.9 wt.%, respectively). From the  $X_{C_4}$  versus

TOS profiles (Figure 5.15), a slightly higher decrease in  $X_{C4}$  was observed between *ca.* 2 and 8 h on-stream for ZSM-5 than Al-TUD-1(25)-HT (factor of 1.7 and 1.5, respectively). As mentioned above, the two materials possess considerably different acid properties (and structures, crystallinity), which may impact differently on the catalytic performance with TOS. According to the literature, catalyst deactivation due to coking phenomena may be particularly important for microporous catalysts (susceptible to rapid pore blockage effects);<sup>[7,40]</sup> on the other hand, the acid properties may influence the amount and nature of the coke, and catalyst stability.<sup>[6,30,36,45,47]</sup>

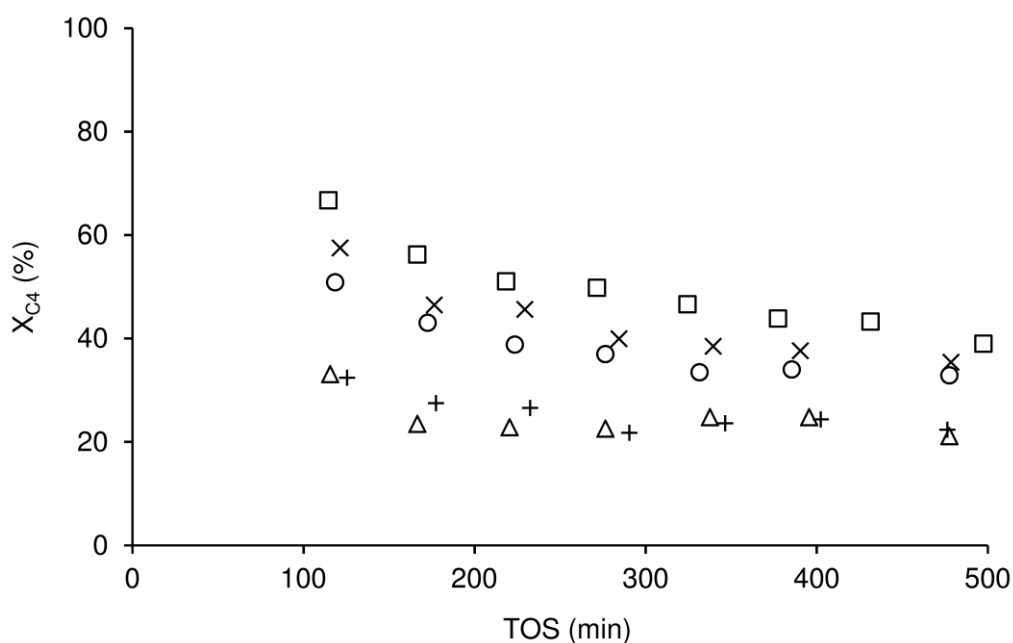


Figure 5.15. Dependence of conversion ( $X_{C4}$ ) on TOS for Al-TUD-1(25)-HT (o), Al-TUD-1(50)-HT (x), Al-TUD-1(PG) ( $\Delta$ ), Al-LP(PG) (+), and ZSM-5 ( $\square$ ). Reaction conditions: 200 °C, 30 bar,  $WHSV=2.2 \text{ g}_{1C4} \text{ g}_{cat}^{-1} \text{ h}^{-1}$ , TOS=8 h,  $T_{act}=450 \text{ }^\circ\text{C}$ .

## 5.8. Conclusions

TUD-1 was furnished with acid properties *via* one-pot synthesis (HT; giving Al-TUD-1(25)-HT and Al-TUD-1(50)-HT), an approach which is interesting in terms of process intensification, or *via* a stepwise approach (PG; post-synthesis grafting of Al-

species, giving Al-TUD-1(PG)) which allows obtaining relatively low molar ratio Si/Al. To the best of our knowledge, this is the first report of TUD-1 furnished with acidity *via* post-synthesis grafting of Al-species. For comparison, an ordered mesoporous aluminosilicate was synthesized using surfactant mixtures and the PG approach (giving Al-LP(PG)). The PG approach gave materials with Si/Al ratios in the range 3-5, and the HT one led to Si/Al ratios of 17-35. The materials possessed pore sizes in the range 10-14 nm, and essentially Lewis acidity of moderate strength. The solid acids prepared promoted 1-butene oligomerization, under high pressure, continuous flow operation. In particular, Al-LP(PG) resembled somewhat comparable features in terms of catalytic performance to the similarly prepared Al-TUD-1(PG). However, in terms of synthesis requirements, Al-TUD-1(PG) is more attractive from environmental/economic perspectives, not requiring the use of surfactants. The materials prepared *via* the PG approach led to higher molar ratios Dcut/Ncut products. However, the best-performing catalyst in terms of space-time yields of Dcut products ( $STY_{Dcut}=166 \text{ mg g}_{cat}^{-1} \text{ h}^{-1}$ , at 200 °C, 30 bar) was Al-TUD-1(25)-HT, synthesized *via* the HT approach using Si/Al ratio of 25. Studies of structure-activity relationships suggested that conversion to higher molar mass products may be influenced by the L acid sites density. Lower L acid site density of the materials prepared *via* the HT approach had a positive effect on conversion, and led to higher  $STY_{Dcut}$ . The catalytic activity was enhanced by increasing the reaction temperature (in the range 150-250 °C), pressure (20-40 bar), or decreasing the weight hourly space velocity (WHSV in the range 1.3-3.1  $\text{g}_{1C4} \text{ g}_{cat}^{-1} \text{ h}^{-1}$ ); temperature had a pronounced effect of the products distribution. Based on GC×GC-ToFMS analysis, the types of products formed (using Al-TUD-1(25)-HT as catalyst) were mainly aliphatic hydrocarbons, and relatively low amounts of aromatics.

Al-TUD-1(25)-HT was benchmarked with ZSM-5, under similar reaction conditions (200 °C, 30 bar,  $WHSV=2.2 \text{ g}_{1C4} \text{ g}_{cat}^{-1} \text{ h}^{-1}$ ). The two materials led to comparable mass ratios of Dcut/Ncut (1.3-1.4). On the other hand, the zeolite led to higher conversion (by a factor of *ca.* 0.8),  $STY_{Dcut}$  (by a factor of *ca.* 0.6), and higher amount of coke (approximately double). High relative amount of the stronger L acid sites (highest for ZSM-5) seems to favor catalytic activity. Nevertheless, for clearer relationships between the material properties and the catalytic results it may be interesting to in-depth the studies of the influence of synthesis parameters on the material properties, and of the latter on the catalytic reactions (*e.g.*, more refined studies of the influence of B acid strength).

## 5.9. References

- [1] S.A. Tabak, F.J. Krambeck, W.E. Garwood, Conversion of propylene and butylene over ZSM-5 catalyst, *AIChE J.* 32 (1986) 1526–1531.
- [2] M.N. Harandi, H. Owen, Integrated staged conversion of methanol to gasoline and distillate, US 4899002 A, 1988.
- [3] C. Knottenbelt, Mossgas “gas-to-liquid” diesel fuels - An environmentally friendly option, *Catal. Today* 71 (2002) 437–445.
- [4] R.O. Minnie, Catalytic conversion of olefins to diesel and gasoline fuel, WO 2006091986 A1, 2006.
- [5] R. Catani, M. Mandreoli, S. Rossini, A. Vaccari, Mesoporous catalysts for the synthesis of clean diesel fuels by oligomerisation of olefins, *Catal. Today* 75 (2002) 125–131.
- [6] B. Chiche, E. Sauvage, F. Di Renzo, I.I. Ivanova, F. Fajula, Butene oligomerization over mesoporous MTS-type aluminosilicates, *J. Mol. Catal. A Chem.* 134 (1998) 145–157.
- [7] N. Kumar, P. Mäki-Arvela, T. Yläsalmi, J. Villegas, T. Heikkilä, A.-R. Leino, K. Kordás, T. Salmi, D. Yu Murzin, Dimerization of 1-butene in liquid phase reaction: Influence of structure, pore size and acidity of Beta zeolite and MCM-41 mesoporous material, *Microporous Mesoporous Mater.* 147 (2012) 127–134.
- [8] R.D. Andrei, M.I. Popa, F. Fajula, V. Hulea, Heterogeneous oligomerization of ethylene over highly active and stable Ni-*AlSBA-15* mesoporous catalysts, *J. Catal.* 323 (2015) 76–84.
- [9] R. van Grieken, J.M. Escola, J. Moreno, R. Rodríguez, Direct synthesis of mesoporous M-SBA-15 (M = Al, Fe, B, Cr) and application to 1-hexene oligomerization, *Chem. Eng. J.* 155 (2009) 442–450.
- [10] R. van Grieken, J.M. Escola, J. Moreno, R. Rodríguez, Liquid phase oligomerization of 1-hexene over different mesoporous aluminosilicates (Al-MTS, Al-MCM-41 and Al-SBA-15) and micrometer/nanometer HZSM-5 zeolites, *Appl. Catal. A Gen.* 305 (2006) 176–188.
- [11] S. Telalović, A. Ramanathan, G. Mul, U. Hanefeld, TUD-1: synthesis and application of a versatile catalyst, carrier, material..., *J. Mater. Chem.* 20 (2010) 642–658.
- [12] J.S. Beck, J.C. Vartuli, W.J. Roth, M.E. Leonowicz, C.T. Kresge, K.D. Schmitt, C.T.-W. Chu, D.H. Olson, E.W. Sheppard, S.B. McCullen, J.B. Higgins, J.L. Schlenkert, A new family of mesoporous molecular sieves prepared with liquid crystal templates, *J. Am. Chem. Soc.* 114 (1992) 10834–10843.
- [13] J.C. Jansen, Z. Shan, L. Marchese, W. Zhou, N.v.d. Puil, T. Maschmeyer, A new templating method for three-dimensional mesopore networks, *Chem. Commun.* (2001) 713–714.
- [14] R. Anand, R. Maheswari, U. Hanefeld, Catalytic properties of the novel mesoporous aluminosilicate AlTUD-1, *J. Catal.* 242 (2006) 82–91.
- [15] S. Telalović, S. Kumar, A. Ramanathan, U. Hanefeld, Al-TUD-1: Introducing tetrahedral aluminum, *J. Mol. Catal. A Chem.* 368–369 (2013) 88–94.
- [16] P. Anastas, J. Warner, Principles of green chemistry, in: *Green chemistry: theory and practice*, 1<sup>st</sup> ed., Oxford University Press, New York, 1998.
- [17] C. Simons, U. Hanefeld, I.W.C.E. Arends, R.A. Sheldon, T. Maschmeyer, Noncovalent anchoring of asymmetric hydrogenation catalysts on a new mesoporous aluminosilicate: application and solvent effects, *Chem. Eur. J.* 10 (2004) 5829–5835.
- [18] Z.-X. Zhang, P. Bai, B. Xu, Z.-F. Yan, Synthesis of mesoporous alumina TUD-1 with high thermostability, *J. Porous Mater.* 13 (2006) 245–250.

- [19] S. Telalović, J.F. Ng, R. Maheswari, A. Ramanathan, G.K. Chuah, U. Hanefeld, Synergy between Brønsted acid sites and Lewis acid sites, *Chem. Commun.* 7345 (2008) 4631–4633.
- [20] Z. Shan, J.C. Jansen, W. Zhou, T. Maschmeyer, Al-TUD-1, stable mesoporous aluminas with high surface areas, *Appl. Catal. A Gen.* 254 (2003) 339–343.
- [21] R. Mokaya, Ultrastable mesoporous aluminosilicates by grafting routes, *Angew. Chem. Int. Ed.* 38 (1999) 2930–2934.
- [22] S. Lima, M.M. Antunes, A. Fernandes, M. Pillinger, M.F. Ribeiro, A.A. Valente, Acid-catalysed conversion of saccharides into furanic aldehydes in the presence of three-dimensional mesoporous Al-TUD-1, *Molecules* 15 (2010) 3863–3877.
- [23] S. Lima, M.M. Antunes, A. Fernandes, M. Pillinger, M.F. Ribeiro, A.A. Valente, Catalytic cyclodehydration of xylose to furfural in the presence of zeolite H-Beta and a micro/mesoporous Beta/TUD-1 composite material, *Appl. Catal. A Gen.* 388 (2010) 141–148.
- [24] A.S. Dias, M. Pillinger, A.A. Valente, Mesoporous silica-supported 12-tungstophosphoric acid catalysts for the liquid phase dehydration of D-xylose, *Microporous Mesoporous Mater.* 94 (2006) 214–225.
- [25] S.J. Gregg, K.S.W. Sing, Adsorption, surface area and porosity, 2<sup>nd</sup> ed., Academic Press, London, 1982.
- [26] J.M.R. Gallo, C. Bisio, G. Gatti, L. Marchese, H.O. Pastore, Physicochemical characterization and surface acid Properties of mesoporous [Al]-SBA-15 obtained by direct synthesis, *Langmuir* 26 (2010) 5791–5800.
- [27] K. Góra-Marek, M. Derewiński, P. Sarv, J. Datka, IR and NMR studies of mesoporous alumina and related aluminosilicates, *Catal. Today* 101 (2005) 131–138.
- [28] C.A. Emeis, Determination of integrated molar extinction coefficients for infrared absorption bands of pyridine adsorbed on solid acid catalysts, *J. Catal.* 141 (1993) 347–354.
- [29] S. Xing, P. Lv, J. Fu, J. Wang, P. Fan, L. Yang, Z. Yuan, Direct synthesis and characterization of pore-broadened Al-SBA-15, *Microporous Mesoporous Mater.* 239 (2017) 316–327.
- [30] G. Bellussi, F. Mizia, V. Calemma, P. Pollesel, R. Millini, Oligomerization of olefins from Light Cracking Naphtha over zeolite-based catalyst for the production of high quality diesel fuel, *Microporous Mesoporous Mater.* 164 (2012) 127–134.
- [31] C. Martínez, E.J. Doskocil, A. Corma, Improved THETA-1 for light olefins oligomerization to diesel: influence of textural and acidic properties, *Top. Catal.* 57 (2014) 668–682.
- [32] S. Peratello, M. Molinari, G. Bellussi, C. Perego, Olefins oligomerization: thermodynamics and kinetics over a mesoporous silica-alumina, *Catal. Today* 52 (1999) 271–277.
- [33] J.W. Yoon, J.-S. Chang, H.-D. Lee, T.-J. Kim, S.H. Jung, Trimerization of isobutene over a zeolite beta catalyst, *J. Catal.* 245 (2007) 253–256.
- [34] J.W. Yoon, J.S. Lee, S.H. Jung, K.-Y. Lee, J.-S. Chang, Oligomerization of isobutene over aluminum chloride-loaded USY zeolite catalysts, *J. Porous Mater.* 16 (2009) 631–634.
- [35] J.W. Yoon, S.H. Jung, D.H. Choo, S.J. Lee, K.-Y. Lee, J.S. Chang, Oligomerization of isobutene over dealuminated Y zeolite catalysts, *Appl. Catal. A Gen.* 337 (2008) 73–77.
- [36] A. Mantilla, G. Ferrat, A. López-Ortega, E. Romero, F. Tzompantzi, M. Torres, E. Ortiz-Islas, R. Gómez, Catalytic behavior of sulfated TiO<sub>2</sub> in light olefins oligomerization, *J. Mol. Catal. A Chem.* 228 (2005) 333–338.
- [37] L. Zhang, M. Ke, Z. Song, Y. Liu, W. Shan, Q. Wang, C. Xia, C. Li, C. He, Improvement of the catalytic efficiency of butene oligomerization using alkali metal, *Catalysts* 8 (2018) 298.
- [38] X. Zhang, J. Zhong, J. Wang, J. Gao, A. Liu, Trimerization of butene over Ni-doped zeolite catalyst: effect of textural and acidic properties, *Catal. Letters* 126 (2008) 388–395.

- [39] A. Corma, C. Martínez, E. Doskocil, Designing MFI-based catalysts with improved catalyst life for C<sub>3</sub>= and C<sub>5</sub>= oligomerization to high-quality liquid fuels, *J. Catal.* 300 (2013) 183–196.
- [40] Y.T. Kim, J.P. Chada, Z. Xu, Y.J. Pagan-Torres, D.C. Rosenfeld, W.L. Winniford, E. Schmidt, G.W. Huber, Low-temperature oligomerization of 1-butene with H-ferrierite, *J. Catal.* 323 (2015) 33–44.
- [41] C.T. O'Connor, R.D. Forrester, M.S. Scurrall, Cetane number determination of synthetic diesel fuels, *Fuel* 71 (1992) 1323–1327.
- [42] A. de Klerk, Fischer–Tropsch refining: technology selection to match molecules, *Green Chem.* 10 (2008) 1249–1279.
- [43] D. Leckel, Diesel production from Fischer-Tropsch: the past, the present, and new concepts, *Energy & Fuels* 23 (2009) 2342–2358.
- [44] H. de Lasa, G. Dogammau, A. Ravella, Fuels of the future and changing fuel needs, in: *Chemical reactor technology for environmentally safe reactors and products*, Springer-Science+Business Media, London, Ontario, 1992: pp. 1–182.
- [45] E. Epelde, J.I. Santos, P. Florian, A.T. Aguayo, A.G. Gayubo, J. Bilbao, P. Castaño, Controlling coke deactivation and cracking selectivity of MFI zeolite by H<sub>3</sub>PO<sub>4</sub> or KOH modification, *Appl. Catal. A Gen.* 505 (2015) 105–115.
- [46] A. Coelho, G. Caeiro, M.A.N.D.A. Lemos, F. Lemos, F.R. Ribeiro, 1-Butene oligomerization over ZSM-5 zeolite: Part 1 - Effect of reaction conditions, *Fuel* 111 (2013) 449–460.
- [47] M. Henry, M. Bulut, W. Vermandel, B. Sels, P. Jacobs, D. Minoux, N. Nesterenko, S. Van Donk, J.P. Dath, Low temperature conversion of linear C<sub>4</sub> olefins with acid ZSM-5 zeolites of homogeneous composition, *Appl. Catal. A, Gen.* 413–414 (2012) 62–77.

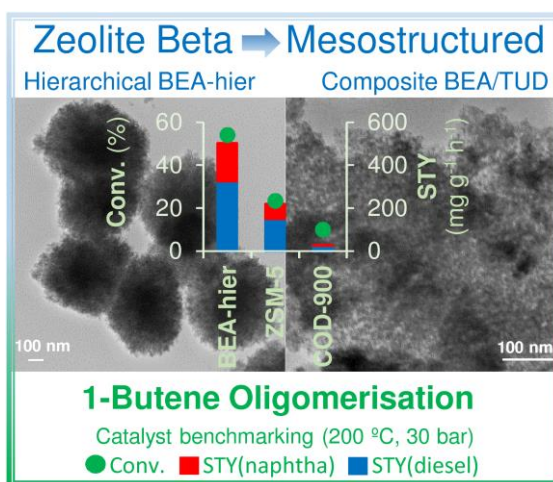


# CHAPTER 6

## Mesostructured oligomerization catalysts based on the BEA topology

### Abstract<sup>1</sup>

Mesostructured solid acid catalysts based on the BEA topology were explored for olefin oligomerization, which is an attractive synthetic route to produce clean, sulphur-free fuels or fuel additives with reduced aromatics content. Specifically, the oligomerization of 1-butene, which may derive from (non)renewable sources, was carried out under high pressure and continuous-flow operation. The mesostructured catalysts consisted of a hierarchical zeotype (BEA-hier) synthesized *via* one-pot approach using a dual function template, and, on the other hand, a composite (BEA/TUD) possessing zeolite nanocrystallites embedded in a mesoporous matrix synthesized under hydrothermal conditions. The influence of the material properties, catalyst activation temperature and reaction parameters were investigated combining characterization, GC×GC-ToFMS and catalytic studies. The catalytic performances were compared to commercial nano/microcrystalline zeolites of different topologies, and COD-900 (type of catalyst for the Conversion of Olefins to Distillates process). BEA-hier performed superiorly in terms of conversion and space-time yields to diesel cut products.



<sup>1</sup> ChemCatChem 2018, 10, 2741-2754

## CHAPTER 6

### **Mesostructured oligomerization catalysts based on the BEA topology for 1-butene oligomerization**

6.1.	Introduction .....	177
6.2.	Synthesis of the catalytic materials .....	179
6.3.	Characterization studies of the catalytic materials .....	180
6.3.	Catalytic studies: general considerations.....	187
6.4.	Influence of material properties on the catalytic performance .....	191
6.5.	Influence of the reaction conditions .....	194
6.6.	Catalyst stability and benchmarking.....	196
6.7.	Influence of catalyst activation temperature.....	202
6.8.	Conclusions .....	205
6.9.	References .....	206

## 6.1. Introduction

The oligomerization of light alkenes is an attractive industrial process for producing clean, sulphur-free synthetic fuels or fuel additives/blenders with reduced aromatics content, and products with variety of other applications, such as detergents, resins, plasticizers, drugs, flavors, perfumes, dyes, etc.<sup>[1-3]</sup> Despite the important improvements which have been accomplished in oligomerization technologies, there are continued research efforts to develop catalysts with superior performances, *e.g.*, in terms of stability and selectivity to diesel type products. The material properties and operation conditions (*e.g.*, reaction temperature, pressure and weight hourly space velocity (WHSV)) may influence product quality properties, such as cetane number (CN).<sup>[4,5]</sup> Different types of inorganic solid acid catalysts have been investigated for the oligomerization of light alkenes,<sup>[4,6]</sup> such as solid phosphoric acid,<sup>[7-9]</sup> zeolites,<sup>[10-15]</sup> amorphous silica-alumina,<sup>[16,17]</sup> and other metal oxide catalysts.<sup>[18,19]</sup> Zeolites and zeotypes are particularly promising versatile, crystalline, porous materials which may withstand the catalytic reaction conditions and catalyst regeneration treatments (*e.g.*, to burn-off coke). Zeolites with BEA topology may present high commercial potential; it was demonstrated their relatively high oligomerization activity, selectivity to C<sub>12</sub><sup>+</sup> products (in the diesel range) and somewhat enhanced stability.<sup>[13,20]</sup> However, zeolites possess microporous structures which may lead to important steric constraints and diffusion limitations of relatively bulky oligomer products from the micropores to the fluid bulk, causing pore blockage and consequently catalyst deactivation.<sup>[15,20]</sup> Comparative studies reported in the literature indicated that increasing the pore sizes of the catalysts may influence positively the catalyst stability, as demonstrated for ordered mesoporous aluminosilicates (OMAS), *e.g.*, MCM-41.<sup>[14]</sup> However, OMAS tend to be less active than zeolites, partly due to the fact that they possess amorphous pore walls and relatively weak overall acidity.<sup>[21,22]</sup>

During the last decade, there have been important advancements made in materials science to bring together the best of OMAS and zeolites; specifically, minimize steric hindrance and diffusion limitations inside the microporous structures of zeolite/zeotype materials, and enhance the active site accessibility and stability for catalytic applications.<sup>[23-25]</sup> The reduction of the crystallite size down to the nanoscale is an interesting approach to

avoid diffusion limitations, since the diffusion path lengths are shortened. However, the use of catalyst nanoparticles in catalytic processes may present several environmental and technical drawbacks, such as high pressure drops, clogging of equipment, and difficult catalyst separation/recovery.<sup>[26]</sup> These drawbacks may be avoided by dispersing and stabilizing the catalyst nanoparticles in porous matrices. The porous matrices should be preferably inorganic, possess high surface area, defined pore size distributions, and prepared *via* relatively low-cost routes. In fulfilling these requirements, TUD-1 type matrices may be advantageous in relation to other ordered mesoporous materials such as MCM-41 and SBA-15. TUD-1 is prepared *via* surfactant-free (green) protocols, and possesses a three-dimensional mesopore system which may be favorable for internal mass transfer compared to one-dimensional pore systems.<sup>[26]</sup> Other materials science strategies involve introducing mesoporosity *via* post-synthesis techniques such as desilication and dealumination (destructive techniques); or *via* direct hydrothermal synthesis using hard or soft templates (constructive techniques).<sup>[23,27–30]</sup> Regarding the soft templating methods, an interesting approach was developed more recently, and consists of using an appropriate dual function template containing simultaneously micropore-directing multi-ammonium heads and mesopore-directing alkyl tails (avoiding phases separation).<sup>[31,32]</sup>

In the present work, mesostructured materials based on the BEA topology were explored for the oligomerization of 1-butene, under high pressure and continuous-flow operation. Specifically, a composite consisting of zeolite nanocrystallites embedded in a siliceous mesoporous matrix of the type TUD-1 was synthesized under hydrothermal conditions (BEA/TUD),<sup>[26,33,34]</sup> and a hierarchical material (BEA-hier) was synthesized using a relatively cheap, commercial polymer as dual function template.<sup>[35]</sup> The catalytic performances of the mesostructured materials were compared to commercial nano- and microcrystalline zeolites possessing BEA topology (BEA-nano, BEA-micro, respectively), and benchmark catalysts possessing MFI topology, namely, ZSM-5 and COD-900 (related to the Conversion of Olefins to Distillates (COD) process; catalyst kindly supplied by Clariant Produkte GmbH, Germany). The influence of material properties and reaction parameters on the oligomerization reaction system was investigated by combining characterization, catalytic and comprehensive two-dimensional gas chromatography (GC×GC) combined with time-of-flight mass spectrometry (ToFMS) studies.

## 6.2. Synthesis of the catalytic materials

The hierarchical Beta zeolite (BEA-hier) was prepared *via* the sol-gel technique using a dual function template and hydrothermal conditions, following a similar procedure to that described by Yuan and co-workers.<sup>[35]</sup> Specifically, sodium hydroxide (17.4 mmol), NaAlO<sub>2</sub> (0.65 mmol) and milli-Q water (1.11 mol) were mixed at 30 °C, followed by the addition of colloidal silica (34.8 mmol) under vigorous stirring. The mixture was stirred for 1 h, followed by the addition of PDADMAC (5.1 mmol). The molar composition of the synthesis-gel was SiO<sub>2</sub>: 0.02Al<sub>2</sub>O<sub>3</sub>: 0.27Na<sub>2</sub>O: 45H<sub>2</sub>O: 0.15PDADMAC (0.15 stands for the molar ratio of the repeating unit in PDADMAC). The resulting mixture was stirred vigorously for 3 h in order to obtain a uniform gel, followed by crystallization at 170 °C for 9 days in a PTFE-lined stainless-steel autoclave, under static conditions. The resultant product was centrifuged, washed with milli-Q water, and dried at 100 °C overnight. The solid was gently grinded using an Agate mortar and pestle and calcined at 550 °C in static air for 5 h (heating rate of 1 °C min<sup>-1</sup>). The proton form was obtained by ion-exchange with 1 M NH<sub>4</sub>NO<sub>3</sub> aq. (1 g of calcined sample per 10 mL of solution), at 80 °C, under stirring. The solution was renewed two times, every 2 h. Finally, the solid was centrifuged, washed with milli-Q water, dried at 100 °C overnight, and calcined at 550 °C in static air for 4 h (heating rate of 1 °C min<sup>-1</sup>).

The composite BEA/TUD was synthesized following a similar procedure to that described by Maschmeyer et al.<sup>[26,33]</sup> for a composite with a BEA zeolite loading of *ca.* 40 wt.%. HBEA (protonic form) was used as zeolite precursor, which was prepared from commercial (nanocrystalline) zeolite NH<sub>4</sub>BEA (Si/Al=12.5, CP814E) *via* calcination at 550 °C for 10 h (heating rate of 1 °C min<sup>-1</sup>). Specifically, TEOS (25.6 mmol) was added dropwise with stirring to a suspension of HBEA (1.0 g) in a mixture of TEA (25.8 mmol) and milli-Q water (166.5 mmol). Subsequently, TEAOH (8.2 mmol) was added, and stirring was continued for *ca.* 2 h. The molar composition of the synthesis-gel was SiO<sub>2</sub>: 0.32TEAOH: 1.01TEA: 7.09H<sub>2</sub>O. The gel was aged at room temperature for 24 h and dried at 100 °C for 22 h, followed by aging in a PTFE-lined stainless-steel autoclave for 8 h at 180 °C. The resultant solid was subjected to Soxhlet extraction with ethanol (*ca.* 3 h), dried overnight at

60 °C, and gently grinded using an Agate mortar and pestle. Finally, the solid was calcined at 600 °C in static air for 10 h (heating rate of 1 °C min<sup>-1</sup>).

### 6.3. Characterization studies of the catalytic materials

Mesostructured versions of zeolite Beta were prepared *via* (i) the sol-gel technique using a relatively low cost dual function template as a bifunctional porogen, leading to a hierarchical material (BEA-hier), or *via* (ii) blending of nanocrystallites of zeolite Beta into the synthesis gel of a mesoporous siliceous matrix, producing a composite material (BEA/TUD). The materials were characterized according section 3.2.1. The wide angle PXRD patterns of the mesostructured materials BEA/TUD and BEA-hier, and of microcrystalline BEA-micro and nanocrystalline BEA-nano, showed the diffraction peaks at *ca.* 7.5-7.8° 2θ and *ca.* 22.5° 2θ, characteristic of the BEA topology (Figure 6.1-A).<sup>[26,34,35]</sup> There was no evidence of the presence of crystalline alumina or other phases in the materials.

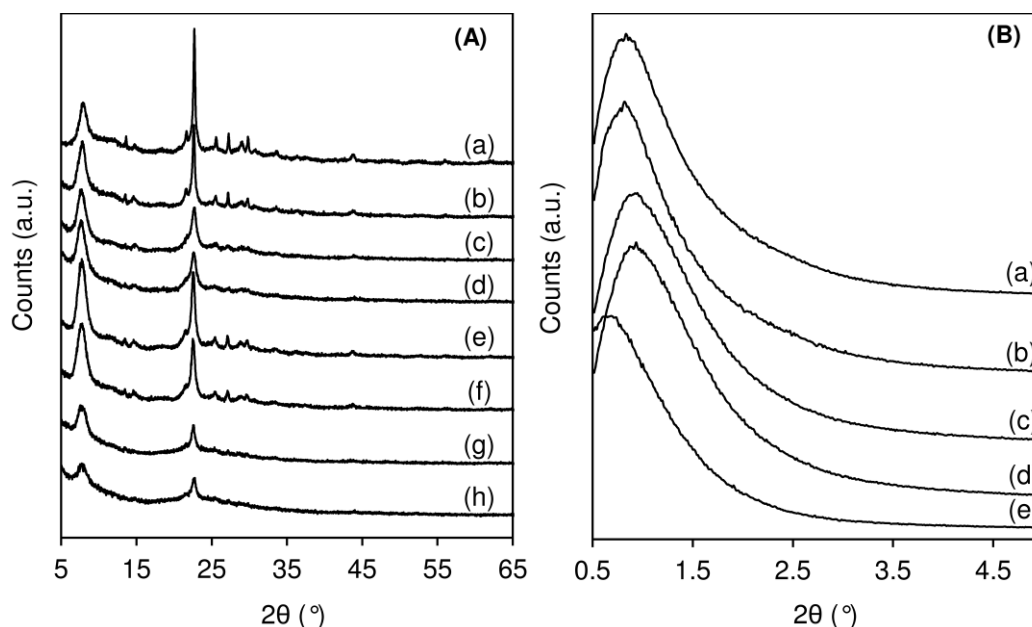


Figure 6.1. (A) PXRD patterns of BEA-micro (fresh (a); used (b)), BEA-hier (fresh (c); used (d)), BEA-nano (fresh (e); used (f)), BEA/TUD (fresh (g); used (h)). (B) Low angles PXRD patterns of BEA-hier (fresh (a); used (b)), BEA/TUD (fresh (c); used (d)), TUD-1 (e). Reaction conditions: catalyst activation=catalytic reaction temperature=200 °C, 30 bar, WHSV=2.2 g<sub>1C4</sub> g<sub>cat</sub><sup>-1</sup> h<sup>-1</sup>.

The low angle PXRD patterns of BEA/TUD and BEA-hier showed a peak centred in the range  $0.7\text{-}1.0^\circ 2\theta$  (Figure 6.1-B), suggesting that these materials possess relatively narrow mesopore size distributions (supported by the results of  $\text{N}_2$  adsorption at  $-196^\circ\text{C}$ , discussed ahead). Figure 6.2 shows the SEM images of the different materials based on the BEA topology. The composite BEA/TUD consists of particles of irregular morphology and size, which are features associated with the TUD-1 type matrix (Figure 6.2-d). The elemental mappings showed fairly uniform distributions of Si and Al (Figure 6.2-d). Conversely, the mechanical mixture of BEA plus TUD-1 consisted of distinct particles which were essentially composed of Si corresponding to pristine silica TUD-1, and, on the other hand, particles rich in Al corresponding to isolated zeolite crystals (Figure 6.2-e).

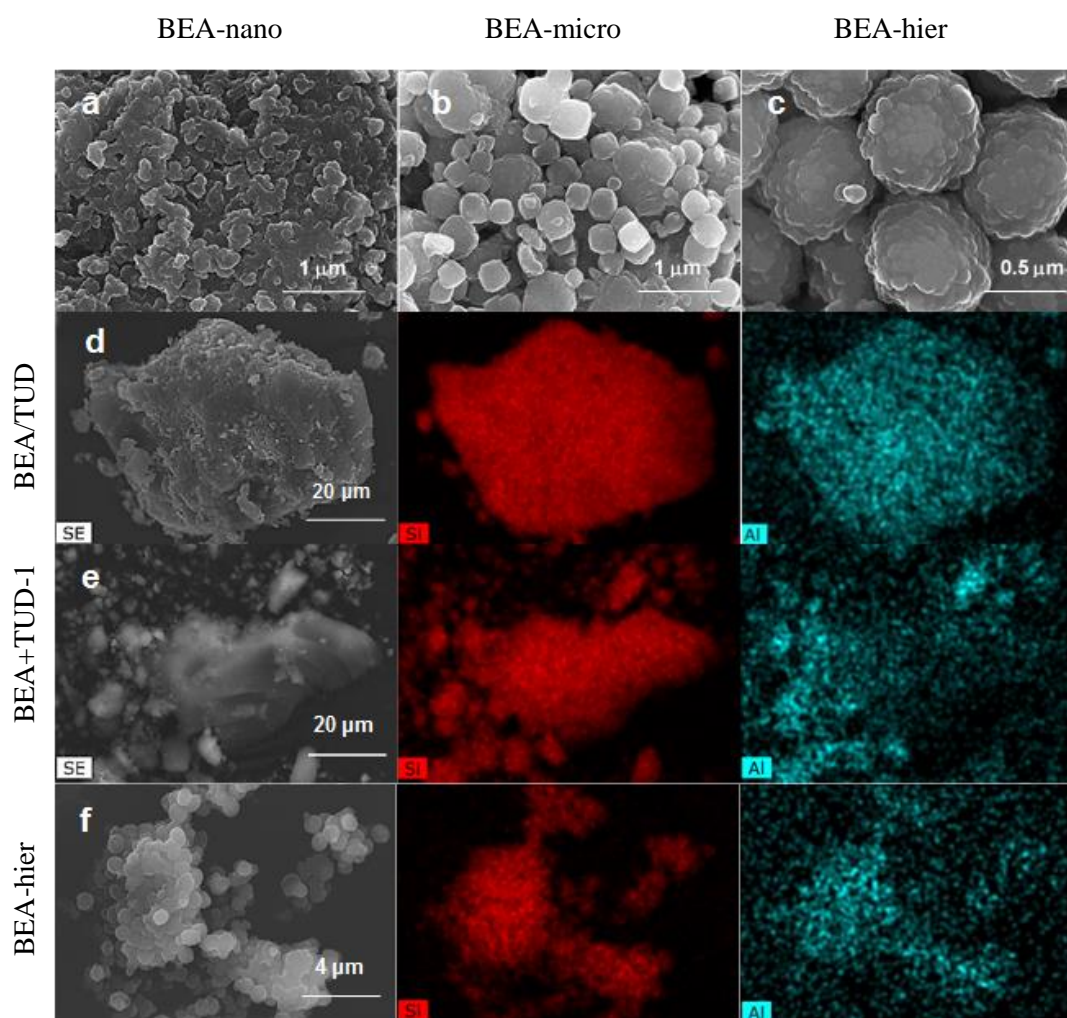


Figure 6.2. SEM images of BEA-nano (a), BEA-micro (b), and BEA-hier (c), and SEM images with corresponding Si and Al mappings of BEA/TUD (d), BEA+TUD-1 (e) and BEA-hier (f).

TEM characterization of BEA/TUD (Figure 6.3-c) and its pure components BEA-nano and TUD-1 (Figure 6.3-a,b, respectively), showed that the composite distinctly consists of a wormlike mesoporous matrix with some dark domains corresponding to embedded single zeolite Beta nanocrystals (20-30 nm) or aggregates of Beta nanocrystals (50-200 nm). In general, the zeolitic domains were fairly evenly distributed, in agreement with literature data for similarly prepared materials.<sup>[26,34]</sup> The zeolite content of BEA/TUD is *ca.* 43 wt.% (based on ICP-AES), which is similar to that introduced in the synthesis gel (*ca.* 40 wt.%), and in agreement with literature data.<sup>[26,34]</sup> The SEM (Figure 6.2-c) and TEM images (Figure 6.3-d,e) of BEA-hier showed that it consisted of relatively pseudospherical aggregates (*ca.* 500-600 nm, Figure 6.2-c and Figure 6.3-d) of nanocrystals (*ca.* 10-20 nm, Figure 6.3-e), and Si and Al were uniformly distributed in the material (Figure 6.2-f). The intercrystal voids of BEA-hier account for mesoporosity.<sup>[35]</sup>

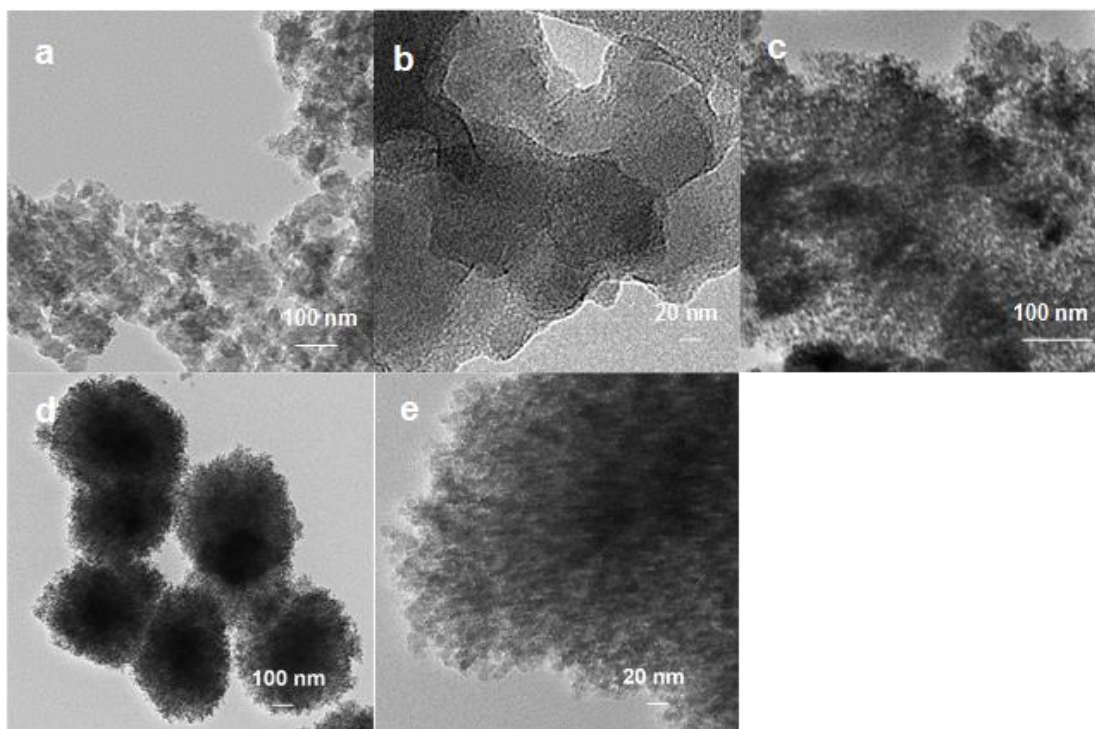


Figure 6.3. TEM image of BEA-nano (a), TUD-1 (b), BEA/TUD (c), and BEA-hier (d and e).

For all materials, excluding BEA/TUD, the molar ratios Si/Al were in the range 11-14 (ICP-AES); BEA/TUD composite possessed a bulk Si/Al ratio of 37 (Table 6.1). In

general, ICP-AES and EDS results were roughly comparable for each material, suggesting fairly uniform distributions of Si and Al, which is consistent with the elemental mappings.

The N<sub>2</sub> adsorption isotherms of BEA-micro and BEA-nano are of type I, characteristic of microporous materials (Figure 6.4). In particular, for BEA-nano it was observed an increasing N<sub>2</sub> uptake as relative pressure approaches unity, attributable to multilayer adsorption on the external surface ( $S_{\text{ext}}=260 \text{ m}^2 \text{ g}^{-1}$ , Table 6.1). On the other hand, BEA/TUD and BEA-hier exhibited type IV isotherms with a hysteresis loop associated with mesoporosity, and in agreement with literature data for similar types of materials.<sup>[26,34,35]</sup> Composite BEA/TUD possesses  $S_{\text{BET}}$  ( $589 \text{ m}^2 \text{ g}^{-1}$ ) and pore volume ( $1.4 \text{ cm}^3 \text{ g}^{-1}$ ) intermediate of its individual components BEA-nano and TUD-1, and slightly smaller mesopore sizes (*ca.* 16 nm) than TUD-1 (19 nm), which may be partly associated with the embedment of the zeolite nanocrystallites during the synthesis (Figure 6.4-A inset, Table 6.1). The material BEA-hier possesses relatively high  $S_{\text{BET}}$  ( $741 \text{ m}^2 \text{ g}^{-1}$ , Table 6.1), and bimodal pore size distribution associated with intracrystal microporosity (*ca.* 0.45-0.65 nm) and intercrystal mesoporosity (6-9 nm) (Figure 6.4-b inset, Table 6.1).<sup>[35]</sup>

Table 6.1. Elemental analyses and textural properties of the zeolite Beta based materials.

Sample	Si/Al <sup>[a]</sup>		Textural Properties <sup>[b]</sup>				
	ICP	EDS	$S_{\text{BET}}$ ( $\text{m}^2 \text{ g}^{-1}$ )	$S_{\text{ext,meso}}$ <sup>[c]</sup> ( $\text{m}^2 \text{ g}^{-1}$ )	$V_{\text{p}}$ ( $\text{cm}^3 \text{ g}^{-1}$ )	$V_{\text{micro}}$ ( $\text{cm}^3 \text{ g}^{-1}$ )	$D_{\text{p}}$ <sup>[d]</sup> (nm)
BEA/TUD	37	44	589 (598)	355 (494)	1.4 (1.5)	0.1 (<0.1)	16 (20)
BEA-nano <sup>[e]</sup>	13 <sup>[f]</sup>	-	645 (615)	260 (255)	1.1 (0.7)	0.1 (0.1)	-
TUD-1	-	-	524	-	2.2	-	19
BEA-hier	11	13	741 (765)	503 (613)	0.9 (1.0)	<0.1 (<0.1)	6-9 (6-9) <sup>[g]</sup>
BEA-micro <sup>[e]</sup>	14 <sup>[f]</sup>	14	583 (566)	20 (21)	0.4 (0.3)	0.2 (0.2)	-

<sup>[a]</sup> Molar ratios determined by ICP-AES or EDS. <sup>[b]</sup> The values in parenthesis are for the spent catalysts. <sup>[c]</sup> External or mesoporous specific surface area. <sup>[d]</sup> Mesopore size. <sup>[e]</sup> Materials obtained *via* calcination of commercial samples. <sup>[f]</sup> Values given in the technical bulletin of the commercial zeolites. <sup>[g]</sup> The material possessed a micropore size distribution centered at *ca.* 0.5 nm.

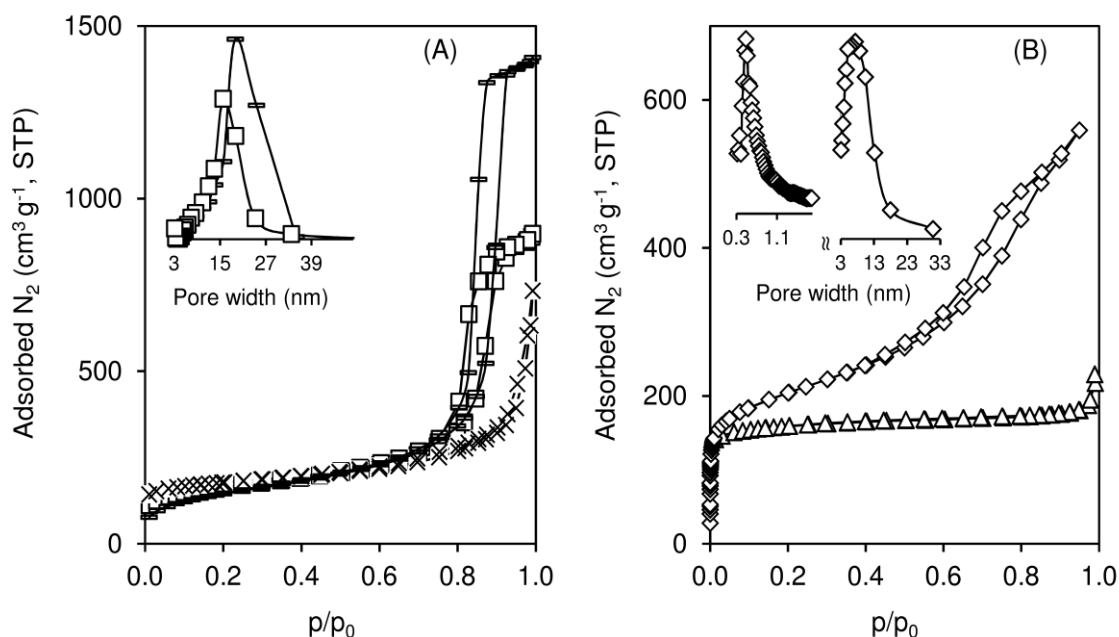


Figure 6.4. Nitrogen adsorption-desorption isotherms (at  $-196\text{ }^{\circ}\text{C}$ ) for (A) composite BEA/TUD ( $\square$ ) and its counterparts BEA-nano ( $\times$ ) and TUD-1 ( $-$ ), and (B) BEA-hier ( $\diamond$ ), BEA-micro ( $\triangle$ ). Inset of (A) are the mesopore size distributions for BEA/TUD ( $\square$ ) and TUD-1 ( $-$ ). Inset of (B) is the bimodal pore size distribution for BEA-hier ( $\diamond$ ).

The  $^{27}\text{Al}$  MAS NMR spectra of all materials based on the BEA topology showed a main resonance centred at *ca.* 54 ppm assigned to framework four-coordinate Al species ( $\text{Al}_{\text{tetra}}$ ) (Figure 6.5). In particular, BEA-hier, BEA-nano and (to smaller extent) BEA/TUD, which are based on zeolite nanocrystallites, exhibited a shoulder at *ca.* 58 ppm. According to the literature, Beta zeolite may exhibit overlapped signals in the spectral range 50-60 ppm due to wide distributions of  $\text{Al}_{\text{tetra}}$  species (*e.g.*, different Al-O-Si angles).<sup>[36,37]</sup> The crystal structure of Beta zeolite possesses crystallographically different Al sites; on the other hand, structural defects may lead to electronic effects on the Al sites.<sup>[36,37]</sup> All materials exhibited a resonance at *ca.* 0 ppm assignable to six-coordinate Al species ( $\text{Al}_{\text{octa}}$ ) partially bridged to the framework.<sup>[38-40]</sup> BEA-nano and BEA-hier exhibited a somewhat broad resonance in the range -3 to -16 ppm, which may be due to extra-framework amorphous aluminum oxide species.<sup>[34,38,41]</sup> Based on the deconvoluted spectra and peaks areas, the ratio  $\text{Al}_{\text{tetra}}/\text{Al}_{\text{octa}}$  for composite BEA/TUD and its counterpart BEA-nano were roughly comparable (2.3 and 2.7, respectively). The ratio  $\text{Al}_{\text{tetra}}/\text{Al}_{\text{octa}}$  for BEA-hier was 2.9, and that of BEA-micro was 4.0.

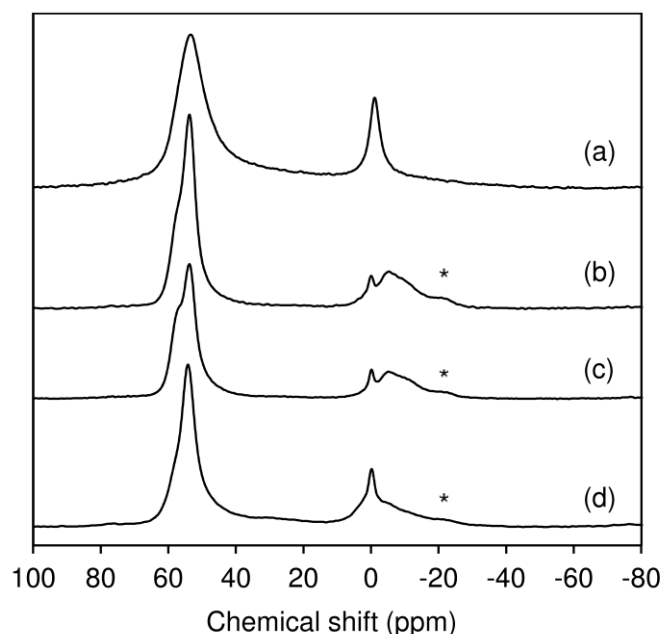


Figure 6.5.  $^{27}\text{Al}$  MAS NMR spectra of BEA-micro (a), BEA-hier (b), BEA-nano (c), and BEA/TUD (d). The asterisk indicate a sideband.

The FT-IR spectra in the OH stretching region of the materials showed a band at *ca.* 3740-3745  $\text{cm}^{-1}$  assignable to OH stretching vibrations of (non-acidic) isolated surface silanol groups (Figure 6.6-A).<sup>[42,43]</sup> This band seemed less pronounced for BEA-micro, which may be associated with the relatively large crystal sizes and possibly enhanced crystallinity (less defect sites) compared to the materials based on nanocrystallites.

The acid properties of the materials were measured by FT-IR of pyridine adsorbed at 200 °C (Table 6.2, Figure 6.6-B). The materials based on the BEA topology possessed Brønsted (B) acid sites (ascertained by the bands at *ca.* 1547  $\text{cm}^{-1}$ , 1637  $\text{cm}^{-1}$ ) and Lewis (L) acid sites (*ca.* 1622  $\text{cm}^{-1}$ , 1456  $\text{cm}^{-1}$ ); the band at *ca.* 1491  $\text{cm}^{-1}$  is associated with the two types of acid sites (Figure 6.6-B).<sup>[44,45]</sup> The total amount of L+B acid sites followed the order, BEA/TUD < BEA-hier < BEA-nano < BEA-micro (Table 6.2). The lower amount of acid sites for BEA/TUD in relation to the BEA-nano counterpart may be attributed to the fact that the composite is partly composed of zeolite, whereas BEA-nano is a bulk catalyst. For the three bulk catalysts possessing comparable Si/Al ratios (11-14), namely BEA-hier, BEA-nano and BEA-micro, the acid properties differ. Mesostructured BEA-hier possessed lower amount of acid sites (total of 331  $\mu\text{mol g}^{-1}$ ) and higher L/B ratio (2.2) than zeolites BEA-

nano and BEA-micro (L+B in the range 484-520  $\mu\text{mol g}^{-1}$ ; L/B in the range 0.6-1.6). A comparison of the materials consisting of nanocrystallites (BEA/TUD, BEA-hier, BEA-nano) *versus* microcrystals (BEA-micro), indicated that the materials possessing nanocrystallites (BEA/TUD, BEA-hier, BEA-nano) possessed mainly L acidity (L/B in the range 1.5-2.2), whereas the microcrystalline zeolite possessed mainly B acidity (L/B=0.6).

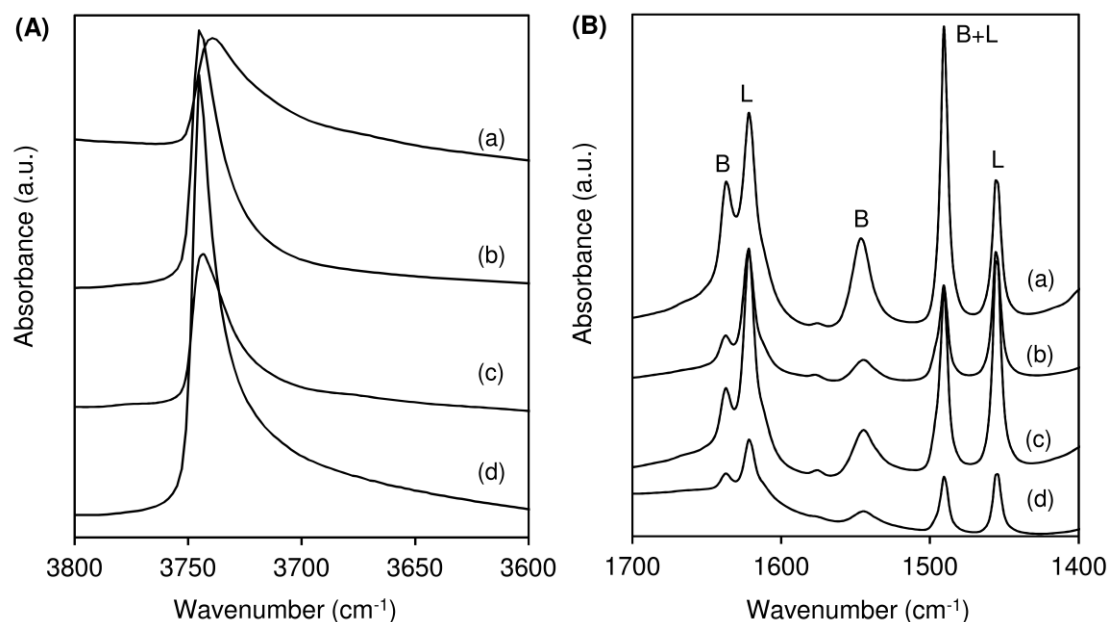


Figure 6.6. FT-IR spectra in the OH stretching region after evacuation at 450 °C (A), and FT-IR spectra of pyridine (base probe) adsorbed at 200 °C (B) for BEA-micro (a), BEA-hier (b), BEA-nano (c), and BEA/TUD (d).

Table 6.2. Acid properties of the zeolite Beta based materials.<sup>[a]</sup>

Sample	B ( $\mu\text{mol g}^{-1}$ )	L ( $\mu\text{mol g}^{-1}$ )	L+B ( $\mu\text{mol g}^{-1}$ )	L/B	$L_{450}/L_{200}$ <sup>[b]</sup>	$B_{450}/B_{200}$ <sup>[c]</sup>
BEA/TUD	78	117	195	1.5	0.55	0
BEA-nano	184	300	484	1.6	0.65	0.04
BEA-hier	105	226	331	2.2	0.57	0
BEA-micro	321	199	520	0.6	0.94	0.11
ZSM-5 <sup>[d]</sup>	338	80	418	0.2	0.71	0.43

<sup>[a]</sup> Determined by FT-IR of pyridine adsorbed at 200 °C (B=Brønsted acid sites, L=Lewis acid sites, B+L=total amount of acid sites). <sup>[b]</sup> L acid strength. <sup>[c]</sup> B acid strength.

<sup>[d]</sup> Data from Table 5.2.

Increasing the evacuation temperature from 200 °C to 450 °C led to a reduction in the amount of L and B acid sites of the Beta based materials (Table 6.2). In general, the reduction in the amount of B acid sites was always much greater ( $B_{450}/B_{200}$  in the range 0-0.11) than that of L acid sites ( $L_{450}/L_{200}$  in the range 0.55-0.94). These results suggest that the L acidity is mostly strong, and the B acidity is essentially moderate to weak. Of all Beta based materials, BEA-micro possessed the strongest acidity:  $L_{450}/L_{200}=0.94$  for BEA-micro compared to less than 0.66 for the remaining materials;  $B_{450}/B_{200}=0.11$  for BEA-micro compared to less than 0.05 for the remaining materials. The mesostructured materials BEA/TUD and BEA-hier possess comparable acid strengths, and lack strong B acidity ( $B_{450}/B_{200}=0$ ).

The benchmark catalyst ZSM-5 (Si/Al=15) obtained *via* calcination of commercial CBV3024E (Zeolyst), consists of *ca.* 0.3-0.5  $\mu\text{m}$  size crystals with a MFI topology, and uniform distributions of Al and Si (Figure 6.7 and Figure 6.20). ZSM-5 possesses  $S_{\text{BET}}=417 \text{ m}^2 \text{ g}^{-1}$  ( $S_{\text{ext}}=43 \text{ m}^2 \text{ g}^{-1}$ ),  $V_p=0.4 \text{ cm}^3 \text{ g}^{-1}$  (Table 5.1). The ratio of species  $\text{Al}_{\text{tetra}}/\text{Al}_{\text{octa}}$  was 9, based on the  $^{27}\text{Al}$  MAS NMR spectrum which exhibited two predominant peaks associated with  $\text{Al}_{\text{tetra}}$  and  $\text{Al}_{\text{octa}}$  species; Figure 6.17-B). In terms of acid properties, ZSM-5 possessed lower L/B and stronger B acidity than the Beta based materials (Table 6.2).

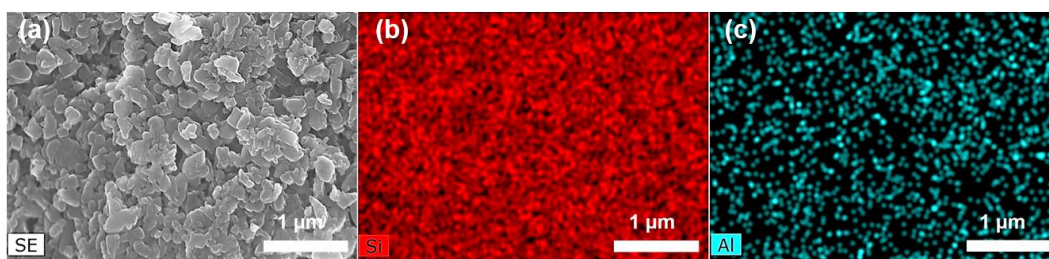


Figure 6.7. SEM image (a) and Si (b), Al (c) mappings of the commercial benchmark catalyst ZSM-5 (obtained *via* calcination of CBV3024E, Zeolyst).

### 6.3. Catalytic studies: general considerations

The different versions of zeolite Beta based materials were explored as solid acid catalysts for the oligomerization of 1-butene ( $1\text{C}_4$ ), under high pressure, continuous flow

operation, typically at 200 °C, 30 bar, and weight hourly space velocity (WHSV) of 2.2 g<sub>1C4</sub> g<sub>cat</sub><sup>-1</sup> h<sup>-1</sup>. The catalyst activation temperature (T<sub>act</sub>) was 200 °C or 450 °C during *ca.* 3 h prior to the catalytic reaction. The mesostructured materials BEA/TUD and BEA-hier, and zeolites BEA-micro and BEA-nano promoted the conversion of 1C<sub>4</sub> to higher molar mass products (Figure 6.8, Figure 6.9 and Figure 6.10; T<sub>act</sub>=200 °C). The conversions (X<sub>C4</sub>) were in the range 15-54 % (Figure 6.8 and Figure 6.9; T<sub>act</sub>=200 °C). Without catalyst, no significant reaction occurred, ascertaining the catalytic role of the materials in the oligomerization process, and negligible thermal reactions. It was formed Dcut products (i.e. with boiling point range characteristic of diesel fractions; 170-390 °C, C10-C24) and Ncut products (i.e. with boiling point range characteristic of naphtha fractions; <170 °C, C6-C10), and the mass ratios of Dcut:Ncut of the liquid products were in the range 1.5-6.6. The ratios of aromatic to aliphatic reaction products (based on GC×GC-ToFMS) were low; A<sub>arom</sub>/A<sub>aliph</sub> in the range 0.001-0.015 (Figure 6.14). The <sup>1</sup>H NMR spectra of the reaction mixtures indicated negligible contribution of aromatic rings (spectral region 6.5-9.2 ppm), which is consistent with the GC×GC-ToFMS results. Hence, the product lump distribution (PLD) curves for the different catalysts (Figure 6.10) correspond essentially to aliphatic products. The isoparaffinic ratio (*I*, determined by <sup>1</sup>H NMR spectroscopy, and reflecting the branching degree<sup>[46]</sup>) are roughly comparable for the different Beta based materials; 0.6 for zeolites BEA-nano and BEA-micro, and 0.7 for the mesostructured materials BEA-hier and BEA/TUD.

The CN values of products (Dcut plus Ncut products, without post-synthesis treatments) were determined using different correlations; specifically, those reported by O'Connor et al.<sup>[47]</sup> (CN<sub>OC</sub>) and Kapur et al.<sup>[48]</sup> (CN<sub>K</sub>). The CN<sub>OC</sub> values were comparable for all materials (40-43). It was reported in the literature CN<sub>OC</sub> values in the range 50-56 for hydrogenated diesel cuts produced *via* MODG or COD commercial processes.<sup>[49-52]</sup> The CN<sub>K</sub> values were somewhat higher for BEA-nano and BEA-micro (73-83) than BEA-hier and BEA/TUD (64-68). Literature data for commercial diesel samples indicated CN<sub>K</sub> values in the range 48-55.<sup>[48]</sup> Nevertheless, it is worth mentioning that care should be taken in comparing CN values between different works/catalytic systems, since the correlations may present deviations for samples with different characteristics (*e.g.*, fuels obtained *via* different processes or chemical routes).

Mesostructured oligomerization catalysts based on the BEA topology for 1-butene oligomerization

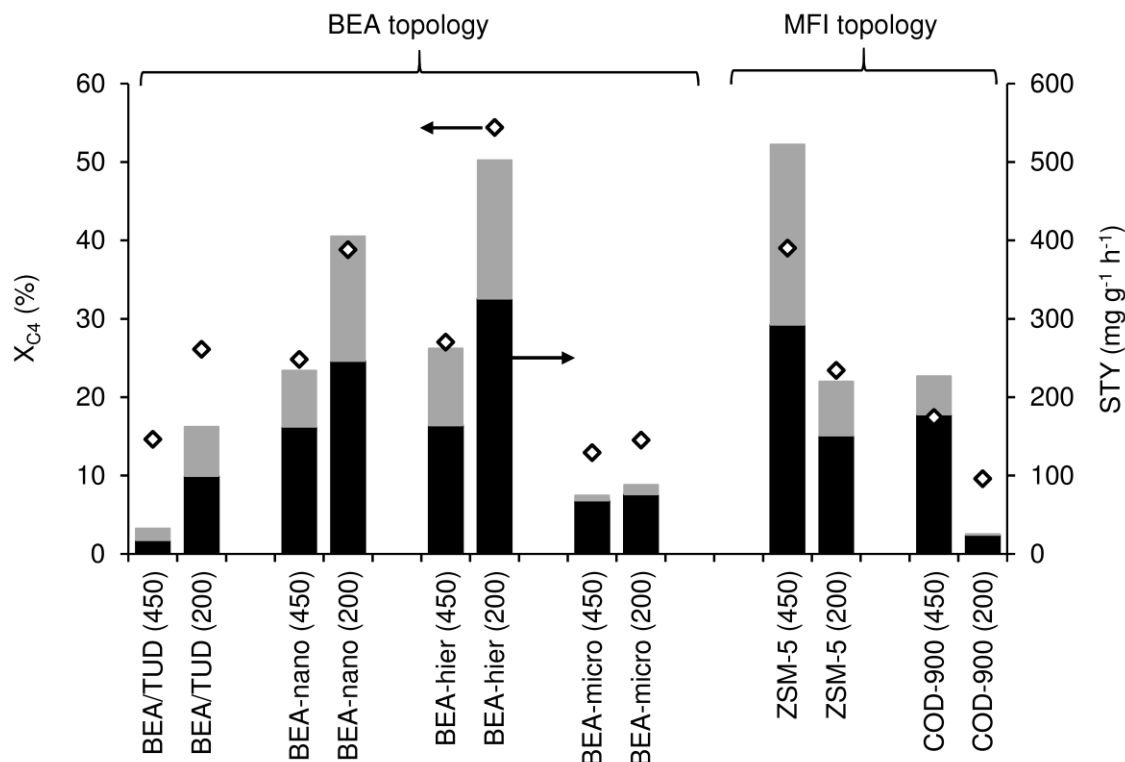


Figure 6.8. Conversion ( $\diamond$ ) and STY (bars) of Ncut (light color) and Dcut (dark color) products for the zeolite Beta based materials, and the benchmark catalysts activated at 200 °C or 450 °C prior to the catalytic reaction. Reaction conditions: 200 °C, 30 bar, WHSV=2.2 g<sub>1C4</sub> g<sup>-1</sup> h<sup>-1</sup>, TOS=8 h.

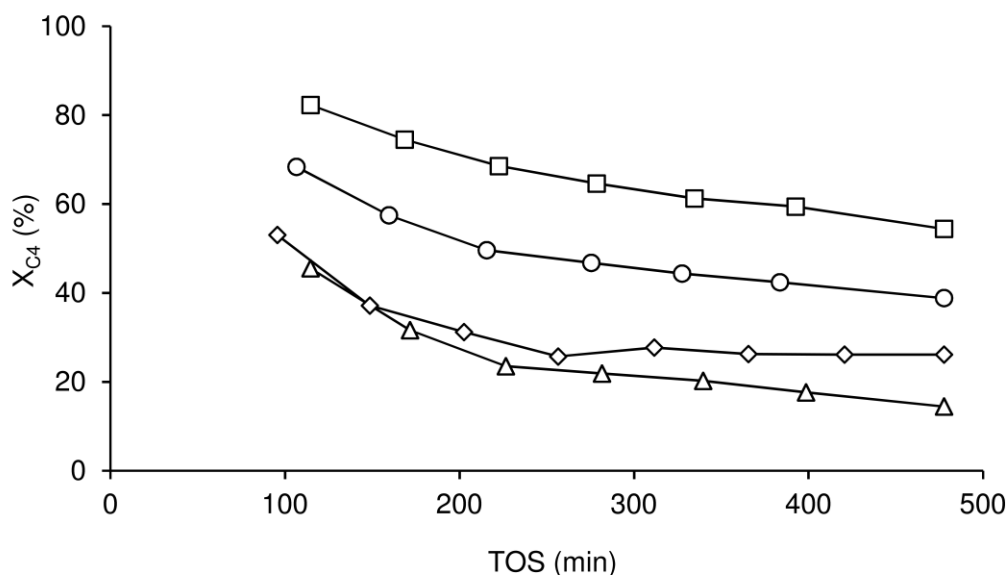


Figure 6.9. Dependence of conversion ( $X_{C4}$ ) on TOS for BEA-hier ( $\square$ ), BEA/TUD ( $\diamond$ ), BEA-nano ( $\circ$ ), and BEA-micro ( $\Delta$ ). Reaction conditions: 200 °C, 30 bar, WHSV=2.2 g<sub>1C4</sub> g<sup>-1</sup> h<sup>-1</sup>, TOS=8 h, catalyst activation temperature=200 °C.

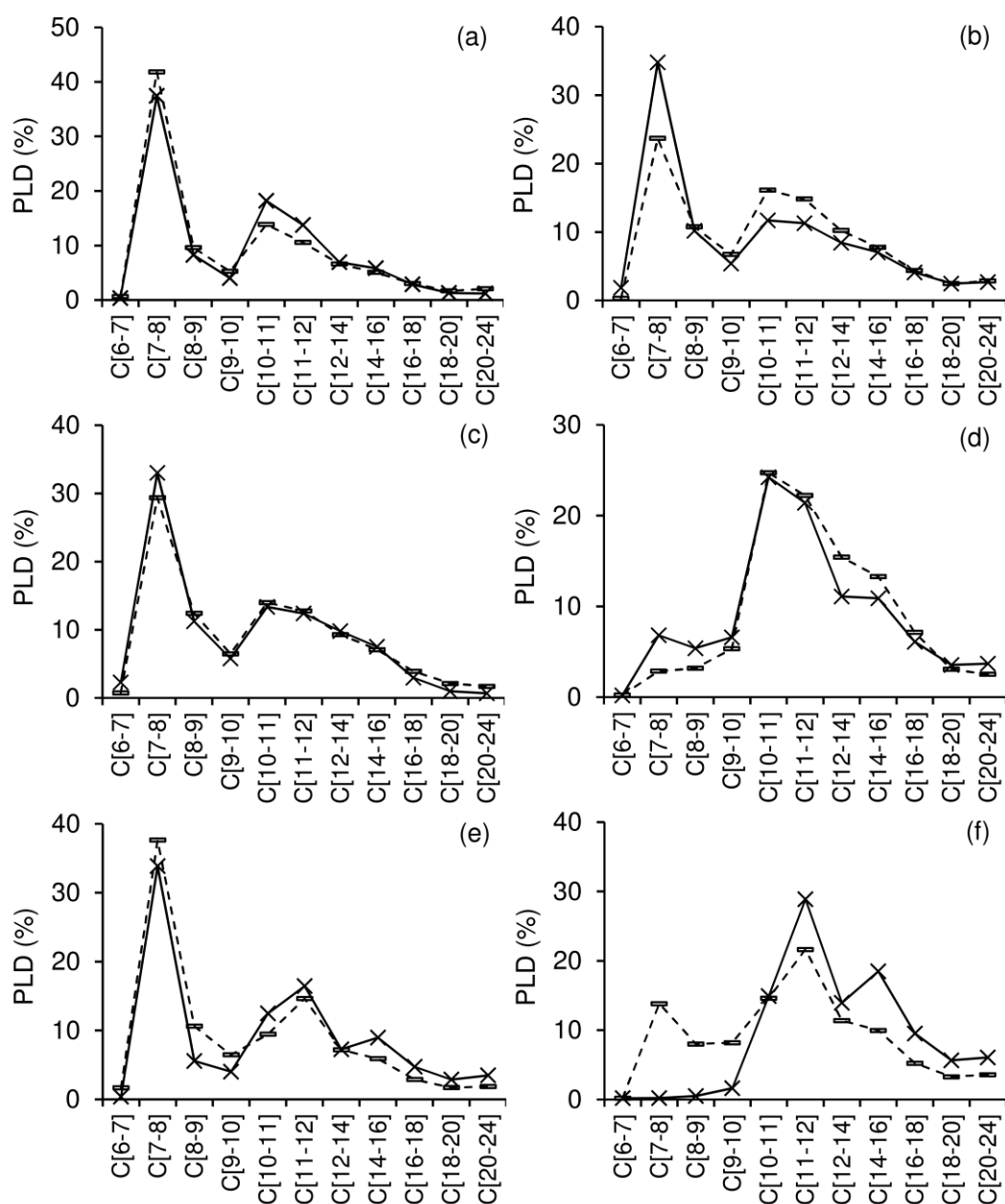


Figure 6.10. PLD profiles for the reaction of 1-butene in the presence of BEA/TUD (a), BEA-nano (b), BEA-hier (c), BEA-micro (d), ZSM-5 (e) or COD-900 (f), activated at 200 °C (solid lines) or 450 °C (dashed lines). Reaction conditions: 200 °C, 30 bar, WHSV=2.2  $\text{g}_{1\text{C}_4} \text{g}^{-1} \text{h}^{-1}$ , TOS=8 h.

#### 6.4. Influence of material properties on the catalytic performance

A comparative study for composite BEA/TUD and its zeolite counterpart BEA-nano indicated similar PLD profiles, and mass ratio  $D_{cut}:N_{cut}$  (equal to 1.6, i.e. predominance of  $D_{cut}$  over  $N_{cut}$  products) for the two materials (Figure 6.10;  $T_{act}=200\text{ }^{\circ}\text{C}$ ). No reaction of  $1C_4$  occurred over pristine silica TUD-1, ascertaining that the active phase of BEA/TUD is the zeolite component. The conversions and average space time yields of  $D_{cut}$  ( $STY_{D_{cut}}$ ) and  $N_{cut}$  ( $STY_{N_{cut}}$ ) products were lower for BEA/TUD than the counterpart BEA-nano (used in the same mass amount);  $X_{C_4}$  was 26 and 39 %, and total STY was 162 and 405  $\text{mg g}_{cat}^{-1} \text{h}^{-1}$ , respectively (Figure 6.8;  $T_{act}=200\text{ }^{\circ}\text{C}$ ). These results are likely due to the fact that the inert siliceous (matrix) accounts for a significant mass fraction of the composite catalyst (ca. 57 wt.%, discussed above). The catalytic activity expressed per amount of total acid sites (L+B) was slightly higher for BEA/TUD than BEA-nano (52 and 31  $\text{mol mol}_{L+B}^{-1} \text{h}^{-1}$ , respectively), possibly due to enhanced active site accessibility for the composite catalyst.

A comparative study for the bulk Beta type catalysts, i.e. BEA-hier, BEA-nano and BEA-micro (possess Si/Al ratio in the range 11-14), indicated that the catalytic activity expressed per mass of catalyst or per amount of total acid sites (L+B) decreased in the order, BEA-hier (21  $\text{mmol g}^{-1} \text{h}^{-1}$ ; 64  $\text{mol mol}_{L+B}^{-1} \text{h}^{-1}$ ) > BEA-nano (15  $\text{mmol g}^{-1} \text{h}^{-1}$ ; 31  $\text{mol mol}_{L+B}^{-1} \text{h}^{-1}$ ) > BEA-micro (6  $\text{mmol g}^{-1} \text{h}^{-1}$ ; 11  $\text{mol mol}_{L+B}^{-1} \text{h}^{-1}$ ) (Table 6.3, Figure 6.11). The superior results for BEA-hier may be partly due to enhanced active sites accessibility associated with the mesoporosity of this material. On the other hand, the acid properties of the materials may play important roles. Corma et al. reported that an optimal compromise between active site accessibility and acid properties of heterogeneous catalysts for diesel production, depends partly on the type of olefin to be converted, and that the introduction of mesoporosity into zeolites may be particularly important for larger olefin substrates.<sup>[53]</sup> For butene conversion, BEA-micro was the least productive, and BEA-hier the most productive catalyst;  $STY_{D_{cut}}$  and  $STY_{N_{cut}}$  of 326 and 176  $\text{mg g}_{cat}^{-1} \text{h}^{-1}$  for BEA-hier, compared to  $STY_{D_{cut}}$  and  $STY_{N_{cut}}$  of 76 and 12  $\text{mg g}_{cat}^{-1} \text{h}^{-1}$  for BEA-micro (Figure 6.8). BEA-hier seems to present the best compromise in terms of mesoporosity and acid properties of the Beta based catalysts. The  $X_{C_4}$  and STYs tended to increase with increasing molar ratio L/B, and decreased with increasing amount, density and strength of B acid sites (measured at 200  $^{\circ}\text{C}$ )

(Table 6.3, Figure 6.11). Roughly comparable relationships of acidity-catalytic performance were verified when considering the acid properties measured at 450 °C (Table 6.3, Figure 6.12). Based on these results, it seems that an enhanced relative amount of L acid sites favors the conversion of C<sub>4</sub> to higher molar mass products. Favorable effects of L *versus* B acidity was reported in the literature for the oligomerization of C<sub>4</sub> olefins over different types of catalysts.<sup>[13,54–56]</sup> Yoon et al. reported the beneficial effect of enhanced L/B ratio on the oligomerization of isobutene, for a commercially derived zeolite Beta, specifically calcined CP814E which is analogous to BEA-nano.<sup>[13]</sup> The same group also reported the beneficial role of the enhanced Lewis acidity of dealuminated zeolite Y and Y-supported AlCl<sub>3</sub> for isobutene conversion.<sup>[55,56]</sup> Although the catalyst requirements may partly depend on the type of olefin substrate, from the data reported by Li et al.<sup>[57]</sup> for the oligomerization of propene over zeolites possessing MFI topology, the conversion tended to increase with the molar ratio L/B, which somewhat parallels that verified for the Beta based catalysts.

Table 6.3. Acid properties measured at 200 °C or 450 °C on X<sub>C4</sub>, STY, and catalytic activity for the bulk Beta based catalysts (BEA-hier, BEA-nano, BEA-micro) activated at 200 °C prior to catalytic reaction. Reaction conditions: 200 °C, 30 bar, WHSV=2.2 g<sub>1C4</sub> g<sup>-1</sup> h<sup>-1</sup>, TOS=8 h.

Sample	Acid properties measured at 200 °C				Catalytic performance (T <sub>act</sub> =200 °C)				
	B/L	B (μmol g <sup>-1</sup> )	B density (meq nm <sup>-2</sup> )	B strength (B <sub>450</sub> /B <sub>200</sub> )	X <sub>C4</sub> (%)	STY (mg g <sub>cat</sub> <sup>-1</sup> h <sup>-1</sup> )		Activity	
						Ncut	Dcut	mmol g h	mmol mol <sub>L+B</sub> h
BEA-hier	0.46	105	85	0	54	176	326	21	64
BEA-nano	0.61	184	172	0	39	158	246	15	31
BEA-micro	1.61	321	332	0.43	15	12	76	6	11
Sample	Acid properties measured at 450 °C				Catalytic performance (T <sub>act</sub> =200 °C)				
	B/L	B (μmol g <sup>-1</sup> )	B density (meq nm <sup>-2</sup> )	B strength (B <sub>450</sub> /B <sub>200</sub> )	X <sub>C4</sub> (%)	STY (mg g <sub>cat</sub> <sup>-1</sup> h <sup>-1</sup> )		Activity	
						Ncut	Dcut	mmol g h	mmol mol <sub>L+B</sub> h
BEA-hier	0	0	0	-	54	176	326	21	64
BEA-nano	0.04	7	7	-	39	158	246	15	31
BEA-micro	0.18	34	35	-	15	12	76	6	11

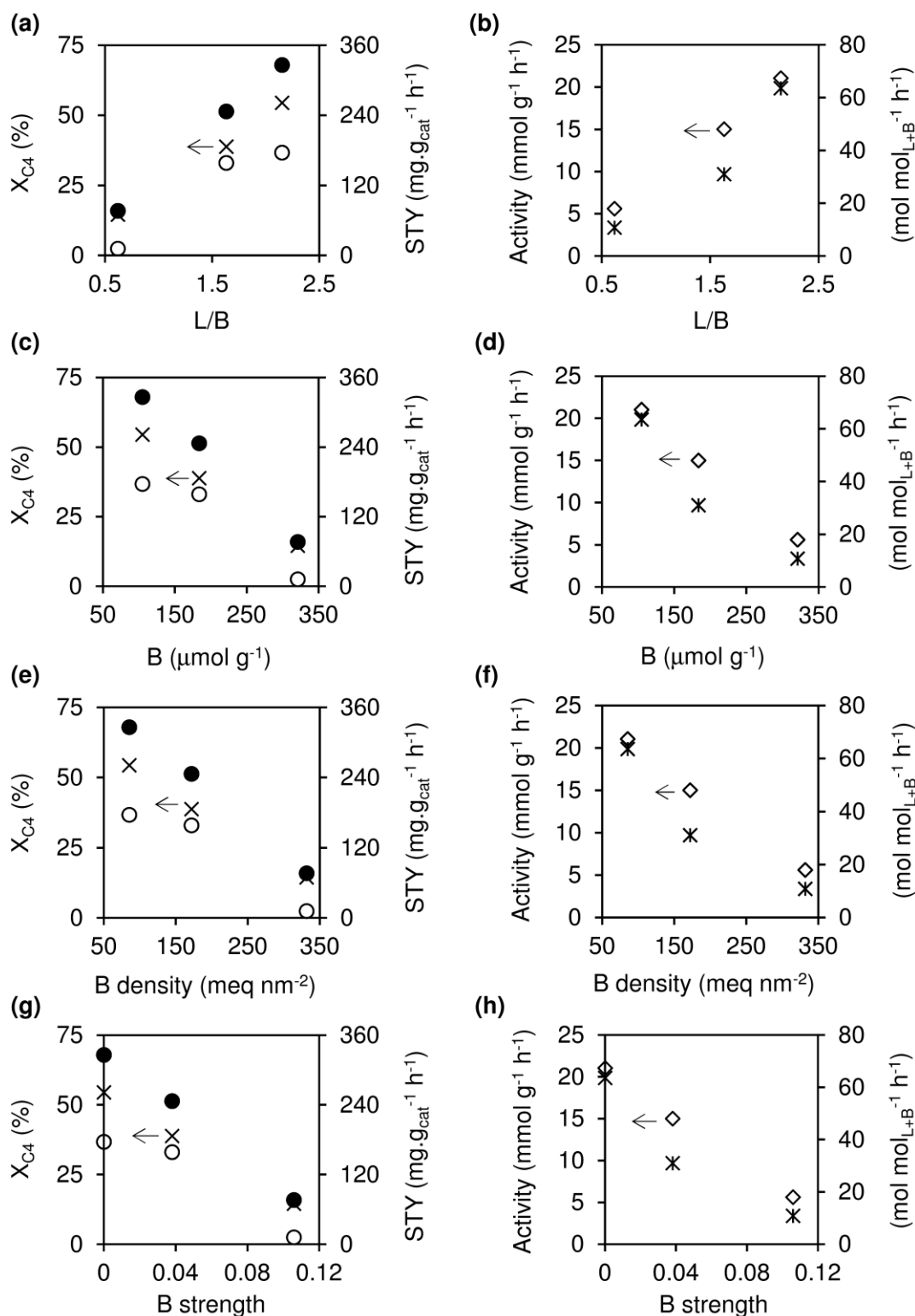


Figure 6.11. Influence of the acid properties measured at 200 °C on ((a), (c), (e), (g)) conversion (×),  $STY_{Dcut}$  (●) and  $STY_{Ncut}$  (○), and on ((b), (d), (f), (h)) catalytic activity expressed as  $mmol\ g^{-1}\ h^{-1}$  (◇) or  $mol\ mol_{L+B}^{-1}\ h^{-1}$  (\*), for the bulk Beta based catalysts (BEA-hier, BEA-nano, BEA-micro) activated at 200 °C prior to catalytic reaction. Reaction conditions: 200 °C, 30 bar,  $WHSV=2.2\ g_{IC4}\ g^{-1}\ h^{-1}$ , TOS=8 h.

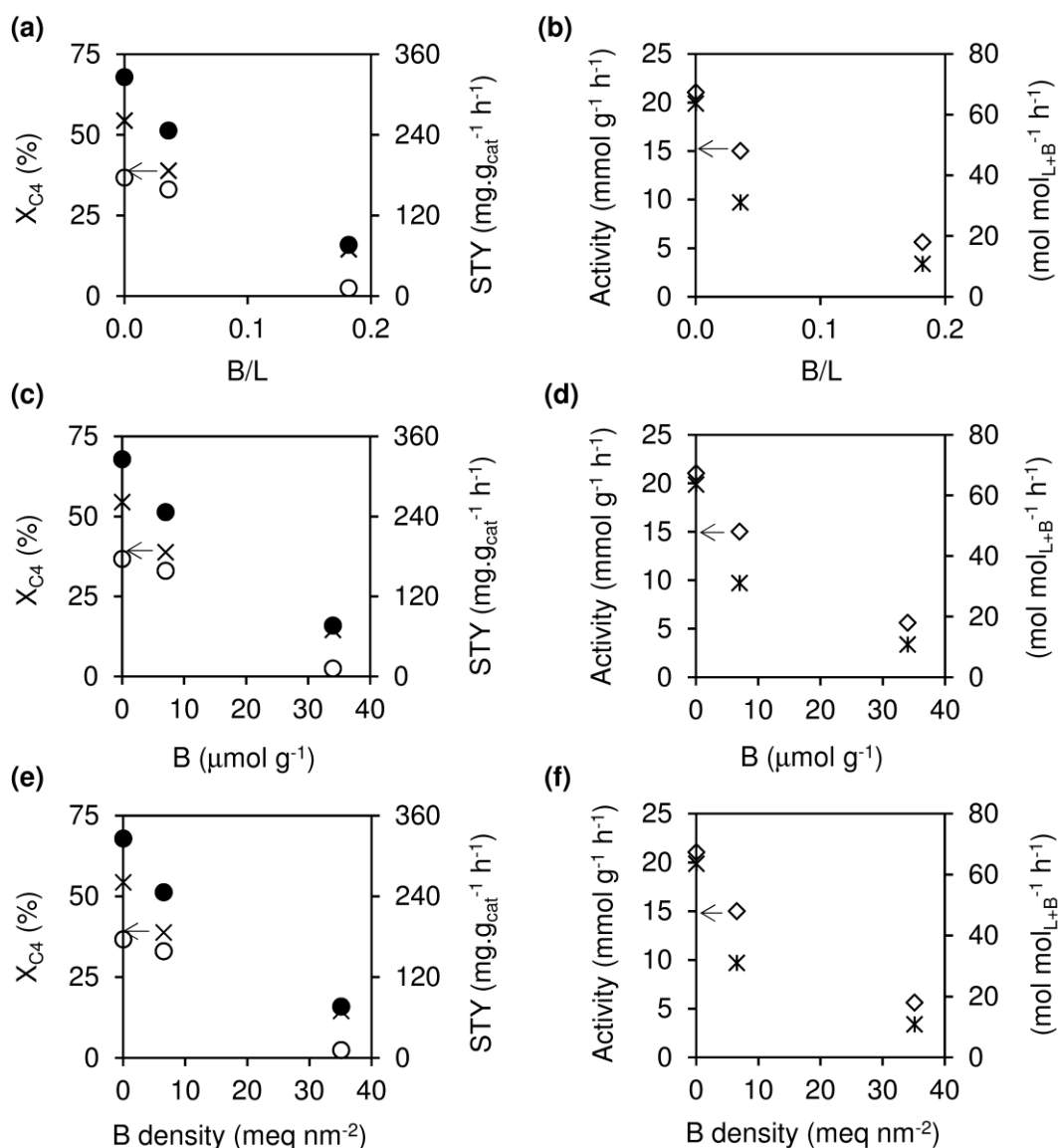


Figure 6.12. Influence of the acid properties measured at 450 °C on ((a), (c), (e)) conversion ( $\times$ ),  $STY_{Dcut}$  ( $\bullet$ ) and  $STY_{Ncut}$  ( $o$ ), and on ((b), (d), (f)) catalytic activity expressed as  $mmol\ g^{-1}\ h^{-1}$  ( $\diamond$ ) or  $mol\ mol_{L+B}^{-1}\ h^{-1}$  ( $*$ ), for the bulk Beta type catalysts (BEA-hier, BEA-nano, BEA-micro) activated at 200 °C prior to catalytic reaction. Reaction conditions: 200 °C, 30 bar,  $WHSV=2.2\ g_{C4}\ g_{cat}^{-1}\ h^{-1}$ , TOS=8 h. Note: the ratio B/L is given instead of L/B to avoid indetermination when B is zero.

## 6.5. Influence of the reaction conditions

Olefin oligomerization is an exothermic reaction, and contributes to a reduction in the number of molecules in the system.<sup>[58]</sup> Hence, the oligomerization pathways may be

avored by decreasing the reaction temperature and/or increasing the pressure.<sup>[59]</sup> The influence of temperature and pressure on the oligomerization of 1-butene, was investigated, using the catalyst BEA-hier (Figure 6.13). Increasing the reaction temperature in the range 150-250 °C (at 30 bar) led to increasing  $X_{C_4}$  (from 32 to 73 %, at 8 h on-stream) and STYs (from 142 to 849 mg  $g_{cat}^{-1} h^{-1}$ ; Figure 6.13-a), albeit the PLD profiles differed, and the mass ratio  $D_{cut}/N_{cut}$  decreased significantly from 3.2 to 1.5 (Figure 6.13-c).

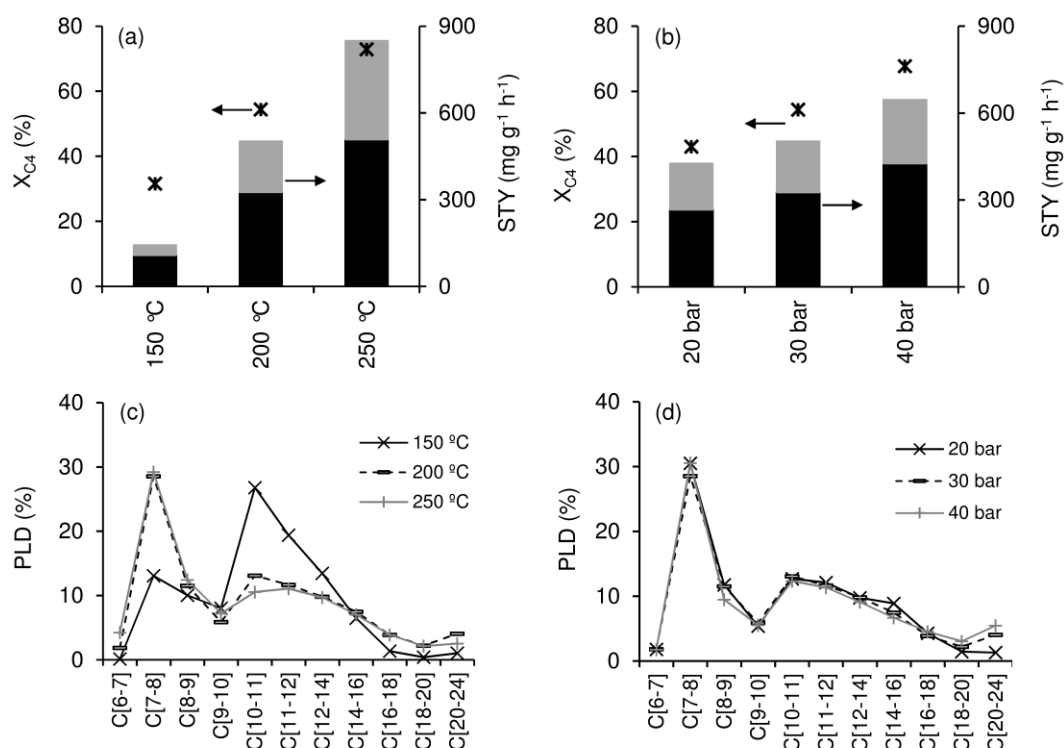


Figure 6.13. Dependence of conversion (\*) and STY (bars) of  $N_{cut}$  (light color) and  $D_{cut}$  (dark color) products ((a) and (b)), and of the PLD curves ((c) and (d)) on the reaction temperature ((a) and (c)) or pressure ((b) and (d)), in the presence of BEA-hier. Reaction conditions: catalyst activation temperature=200 °C, WHSV=2.2  $g_{1C_4}\ g^{-1}\ h^{-1}$ , TOS=8 h.

The ratio of total peak areas of aromatics to aliphatics ( $A_{arom}/A_{aliph}$ ) increased with increasing reaction temperature; from 0 at 150 °C to 0.06 at 250 °C (Figure 6.14-b). These results suggest that cracking and aromatization pathways may be favored at higher reaction temperature.<sup>[6]</sup> Increasing the reaction pressure in the range 20-40 bar (at 200 °C) improved the conversion (from 43 to 68 %, at 8 h on-stream) and STYs (from 426 to 645  $mg\ g_{cat}^{-1}\ h^{-1}$ )

(Figure 6.13-b). The PLD curves were comparable, and the mass ratio  $D_{cut}/N_{cut}$  increased slightly from 1.7 at 20 bar to 1.9 at 40 bar (Figure 6.13-d); the ratio  $A_{arom}/A_{aliph}$  varied in the range 0.01-0.04 (Figure 6.14-b). The total STY was higher at 250 °C (20 bar) and 30-40 bar (200 °C) (Figure 6.13). Operation at 30 bar, 200 °C seems a reasonable compromise in terms of conversion, mass ratio  $D_{cut}/N_{cut}$  and reduced aromatics content.

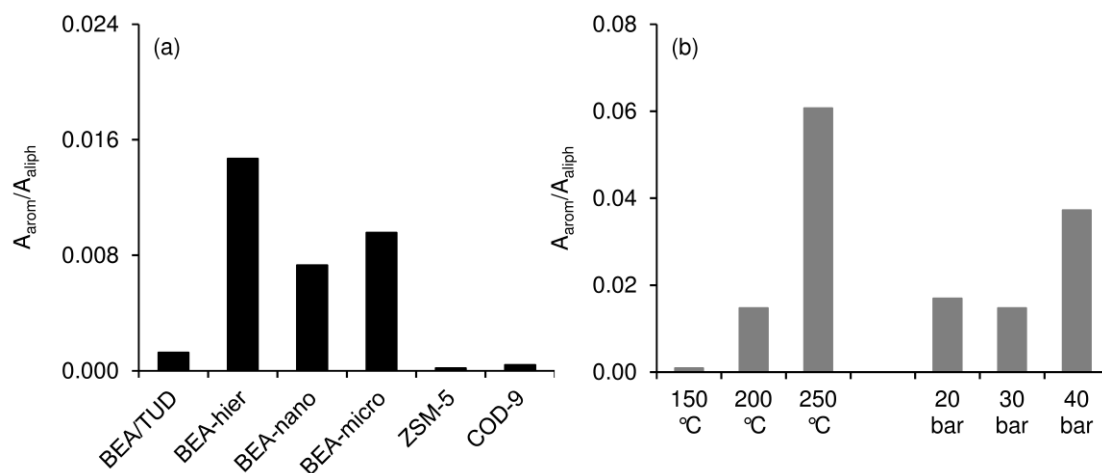


Figure 6.14. Ratio of aromatic ( $A_{arom}$ ) to aliphatic ( $A_{aliph}$ ) products ( $A_{arom}/A_{aliph}$ ; determined by GC×GC-ToFMS) of the condensed reaction products (a) for the catalysts based on the BEA or MFI topologies, or (b) for different reaction conditions using BEA-hier as catalyst. Reaction conditions: catalyst activation at 200 °C,  $WHSV=2.2 \text{ g}_{1C4} \text{ g}^{-1} \text{ h}^{-1}$ ,  $TOS=8 \text{ h}$  (for a and b); 200 °C, 30 bar for (a).

## 6.6. Catalyst stability and benchmarking

The DSC analyses of the used Beta based catalysts indicated two exothermic peaks between 280 and 550 °C, which did not appear for the original catalysts, and may be attributed to coke decomposition (Figure 6.15). The amount of coke for the mesostructured materials BEA-hier and BEA/TUD was somewhat lower (7-13 wt.% C) than for zeolites BEA-nano and BEA-micro (15-16 wt.% C). These results are somewhat in line with that reported by Corma and co-workers for the oligomerization of propene to diesel, in that the introduction of mesoporosity into zeolites may avoid severe coking (that work focused on the 10 membered-ring zeolite Theta-1).<sup>[10]</sup>

Characterization studies of the recovered Beta based catalysts indicated that the BEA topology (Figure 6.1), particle morphology (Figure S6.1), and textural properties (Table 6.4) were not drastically affected under the operation conditions used.

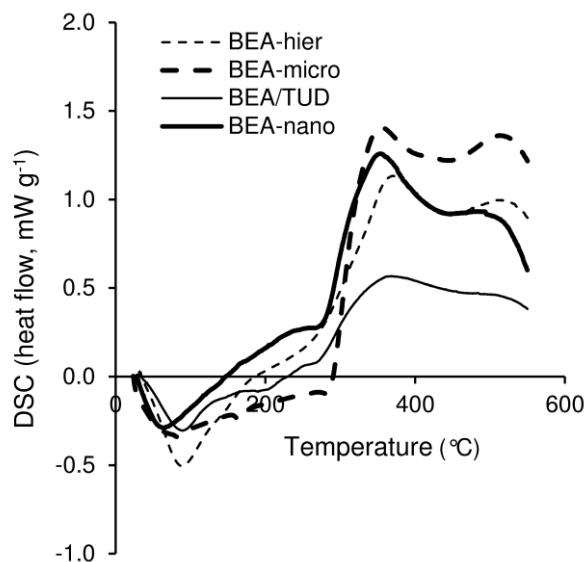


Figure 6.15. DSC curves for the used Beta based materials. Reaction conditions: catalyst activation temperature=catalytic reaction temperature=200 °C, 30 bar, WHSV=2.2 g<sub>1C4</sub> g<sub>cat</sub><sup>-1</sup> h<sup>-1</sup>, TOS=8 h.

Table 6.4. Textural properties of the catalysts before and after use (activated at 200 °C or 450 °C).<sup>[a]</sup>

Sample	S <sub>BET</sub> (m <sup>2</sup> g <sup>-1</sup> )	S <sub>ext,meso</sub> <sup>[a]</sup> (m <sup>2</sup> g <sup>-1</sup> )	V <sub>p</sub> (cm <sup>3</sup> g <sup>-1</sup> )	V <sub>micro</sub> (cm <sup>3</sup> g <sup>-1</sup> )	D <sub>p</sub> <sup>[b]</sup> (nm)
ZSM-5 <sup>[c]</sup>	417	43	0.4	0.1	-
ZSM-5 (200 °C)	393	57	0.2	0.1	-
ZSM-5 (450 °C)	373	51	0.2	0.1	-
BEA/TUD	589	355	1.4	0.1	16
BEA/TUD (200 °C)	598	494	1.5	<0.1	20
BEA/TUD (450 °C)	568	434	1.4	<0.1	20
BEA-hier	741	503	0.9	<0.1	6-9
BEA-hier (200 °C)	765	613	1.0	<0.1	6-9
BEA-hier (450 °C)	684	539	0.9	<0.1	5-9

<sup>[a]</sup> External or mesoporous specific surface area. <sup>[b]</sup> Mesopore size. <sup>[c]</sup> Data from Table 5.1.

The best-performing catalyst BEA-hier (in terms of STYs and  $X_{C_4}$ ) was reused for further 8 h on-stream. The PLD curves were similar for the two runs, albeit partial drop in conversion occurred (Figure 6.16).

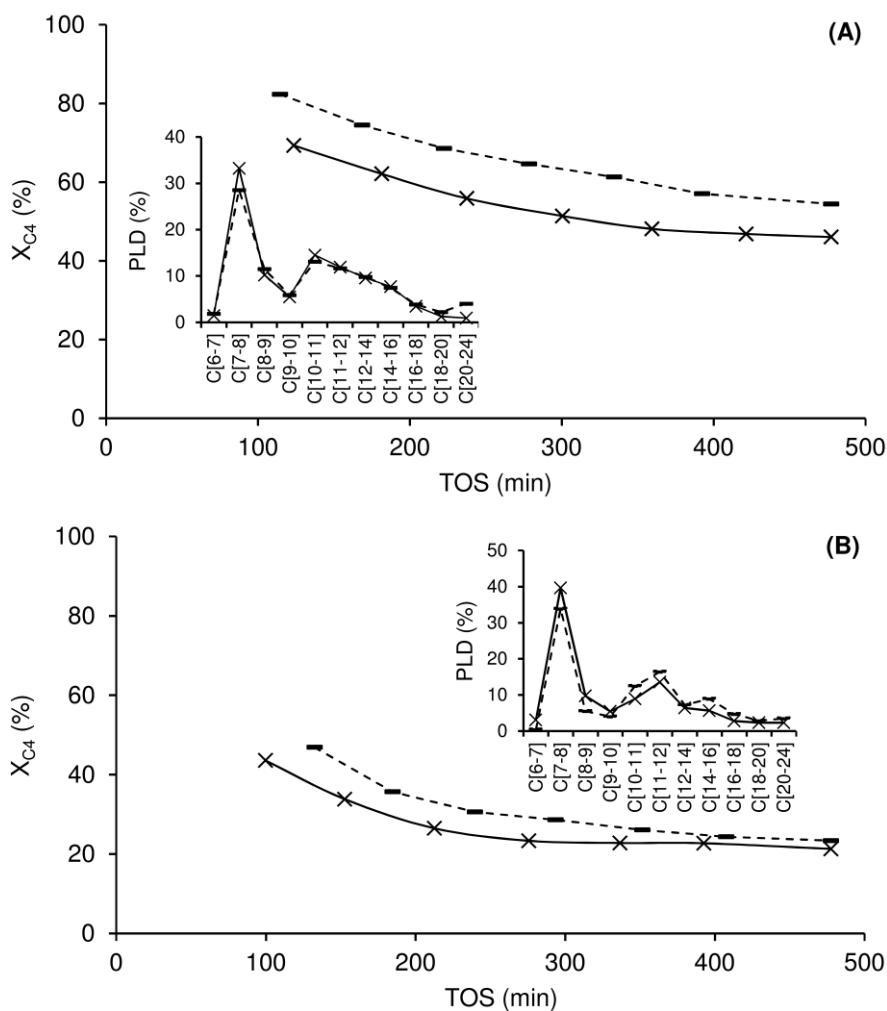


Figure 6.16. Dependence of conversion ( $X_{C_4}$ ) on TOS in the first (-), and second use after regeneration ( $\times$ ), for BEA-hier (A) and ZSM-5 (B). The inset shows the PLD curves for the two runs (with matching symbols). Reaction conditions: catalyst activation temperature=200 °C, catalytic reaction temperature=200 °C, 30 bar, WHSV=2.2  $g_{C_4} g_{cat}^{-1} h^{-1}$ , TOS=8 h for each use.

The  $^{27}Al$  MAS NMR spectra of the original and used BEA-hier catalyst were comparable (Figure 6.17). The ratio  $Al_{tetra}/Al_{octa}$  decreased from 2.2 to 1.9, which may partly explain the partial drop in catalytic activity. According to the literature, depending on the

thermal treatment and/or (de)hydration level, Al species may suffer changes in the coordination environment and adopt various configurations, which may influence the overall catalytic performance.<sup>[36,38,39,60,61]</sup> On the other hand, the precise structures and origin of Lewis acid sites of zeolites is a matter of continued debate (may be framework and/or extra-framework species, etc.), and the different types may possess different intrinsic activities.<sup>[62]</sup>

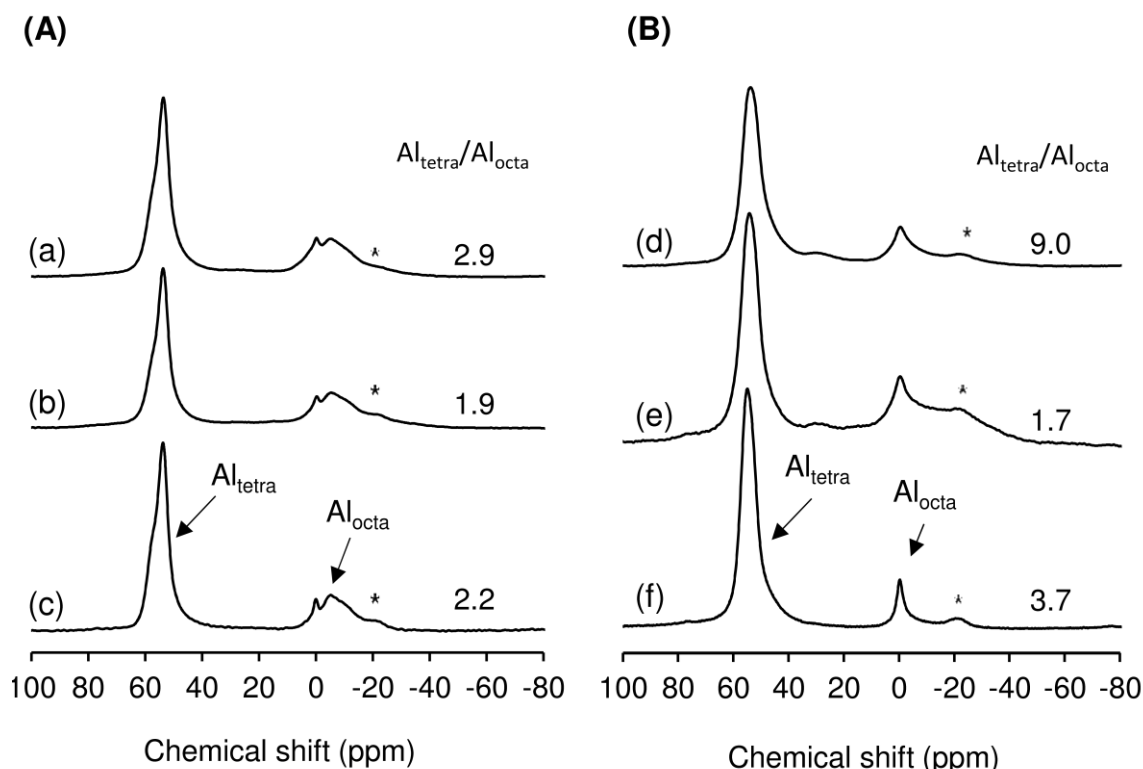


Figure 6.17.  $^{27}\text{Al}$  MAS NMR spectrum of (A) BEA-hier (used ( $T_{\text{act}}=450\text{ }^\circ\text{C}$  (a) or  $200\text{ }^\circ\text{C}$  (b)) and fresh (c)) and (B) the benchmark catalyst ZSM-5 (used ( $T_{\text{act}}=450\text{ }^\circ\text{C}$  (d) or  $200\text{ }^\circ\text{C}$  (e)) and fresh (f)). Reaction conditions: reaction temperature= $200\text{ }^\circ\text{C}$ , 30 bar, WHSV= $2.2\text{ g}_{\text{IC4}}\text{ g}_{\text{cat}}^{-1}\text{ h}^{-1}$ , TOS=8 h.

It is somewhat difficult to establish clear and fair comparisons of catalytic results between different studies reported in the literature partly due to the different operation/reaction conditions used, and sometimes the lack of sufficient data to compare the results of different works on a similar basis of calculation (Table 6.6). Hence, the catalytic performances of the Beta based materials were compared to those of commercial ZSM-5 and

COD-900 (MFI topology), which were chosen as benchmark catalysts, since they are of the type used in commercial olefin oligomerization processes.

The best-performing catalyst based on the BEA topology, namely BEA-hier stands on a higher footing than ZSM-5 and COD-900 in terms of  $X_{C_4}$ , STYs (Figure 6.8, Table 6.5). Behind BEA-hier, the catalyst BEA-nano led to superior results to the benchmark catalysts. COD-900 resembled somewhat closely the catalytic performance of BEA-micro; specifically, the former led to relatively high mass ratio of  $D_{cut}/N_{cut}$  (59), albeit low  $X_{C_4}$  (10 %) and STYs (25  $\text{mg g}_{cat}^{-1} \text{h}^{-1}$  for COD-900) (Figure 6.8 and Figure 6.10).

Table 6.5. Catalytic results for BEA-hier and the benchmark catalysts.<sup>[a]</sup>

Sample	$T_{act}=200\text{ }^{\circ}\text{C}$			$T_{act}=450\text{ }^{\circ}\text{C}$		
	$X_{C_4}$	STY ( $\text{mg g}_{cat}^{-1} \text{h}^{-1}$ )		$X_{C_4}$	STY ( $\text{mg g}_{cat}^{-1} \text{h}^{-1}$ )	
	(%)	$N_{cut}$	$D_{cut}$	(%)	$N_{cut}$	$D_{cut}$
BEA-hier	54	176	326	27	97	164
ZSM-5	23	69	151	39	230	293
COD-900	10	0.4	25	17	48	178

<sup>[a]</sup> The materials were activated at 200 °C or 450 °C prior to the catalytic reaction. Reaction conditions: 200 °C, 30 bar,  $WHSV=2.2 \text{ g}_{1C_4} \text{ g}_{cat}^{-1} \text{ h}^{-1}$ , TOS=8 h.

The BEA-hier and ZSM-5 catalysts were further compared in terms of stability (based on two runs of *ca.* 8 h on-stream; Figure 6.16). For ZSM-5, the PLD profiles and conversion at  $TOS \cong 8$  h were comparable for the two runs. These results suggest that ZSM-5 may possess steadier catalytic activity than BEA-hier (catalyst stability discussed ahead).

Table 6.6. Comparison of the catalytic results for BEA-hier and ZSM-5 (this work) to literature data, for catalysts based on the BEA or MFI zeolites, tested for the reaction of 1-butene using a fixed-bed reactor (it is included studies where feed mixtures containing 1-butene were used).<sup>[a]</sup>

Catalyst (Supplier/Preparation)	Si/Al <sup>[b]</sup>	T <sub>act</sub> <sup>[c]</sup> (°C)	P <sup>[d]</sup> (bar)	T <sup>[e]</sup> (°C)	WHSV (h <sup>-1</sup> )	Substrate <sup>[f]</sup> (%)	Diluent <sup>[g]</sup>	Conversion <sup>[h]</sup> (TOS)	Selectivity (%) <sup>[i]</sup>		Ref.
									C <sub>10</sub> -	C <sub>10</sub> +	
Beta/15-20 wt.% clay (Guild Associates)	17	500	24	225	85	90 (mol.%)	N <sub>2</sub>	X <sub>C4</sub> =9 % (6 h)	80 (mol.%)	12	[15]
Beta (Shanghai Xinnian Chem.)	16	450	10	350	2	40 (wt.%) (1C4+2C4)	butane+ propane	X <sub>(1C4+2C4)</sub> =69 % (8 h)	69 (wt.%)	31	[20]
BEA-hier	25	200	30	200	2.2	15 (mol.%) 26 (wt.%)	N <sub>2</sub>	X <sub>C4</sub> =54 % (8 h) X <sub>1C4</sub> =94 % (8 h)	48 (mol.%)	52	-
ZSM-5 (Zeolyst)	17	500	24	225	245	90 (mol.%)	N <sub>2</sub>	X <sub>C4</sub> =3 % (6 h)	86 (mol.%)	8	[15]
ZSM-5 (Zeolyst)	15	450	1	200	13.5	50 (mol.%)	N <sub>2</sub>	X <sub>1C4</sub> =10 % (21 min)	33 (wt.%) <sup>[j]</sup>	37 <sup>[j]</sup>	[12]
ZSM-5 (Shanghai Xinnian Chem.)	30 160	450	10	350	2	40 (wt.%)	butane+ propane	X <sub>(1C4+2C4)</sub> =33 % (8 h) X <sub>(1C4+2C4)</sub> =58 % (8 h)	98 (wt.%) 94.2 (wt.%)	2 5.8	[20]
ZSM-5 (Synthesized)	40	ns	50	270	12	ns	ns	X <sub>1C4</sub> =99 % (10 h)	24 (wt.%)	76	<sup>[63]</sup>
ZSM-5 (Zeolyst)	15	200	30	200	2.2	15 (mol.%) 26 (wt.%)	N <sub>2</sub>	X <sub>C4</sub> =23 % (8 h) X <sub>1C4</sub> =90 % (8 h)	44 (mol.%)	56	-

<sup>[a]</sup> ns=information not specified in the literature. Some of the values of conversion and selectivity were calculated from the data given (in the form of graphical figures or tables) in the reported study, and are approximate values. <sup>[b]</sup> Molar ratio Si/Al. <sup>[c]</sup> Catalyst activation temperature prior to the catalytic reaction. <sup>[d]</sup> Pressure of the catalytic reaction. <sup>[e]</sup> Temperature of the catalytic reaction. <sup>[f]</sup> Amount of substrate in the feed stream. The mol.% or wt.% basis is indicated in parenthesis. <sup>[g]</sup> Diluent in the feed stream. <sup>[h]</sup> Conversion of butenes (1C4=1butene; 2C4=2-butene). The values in parenthesis correspond to the TOS for which conversion was calculated. <sup>[i]</sup> Selectivity to C<sub>10</sub><sup>-</sup> or C<sub>10</sub><sup>+</sup> products. The mol.% or wt.% basis is indicated in the C<sub>10</sub><sup>-</sup> column in parenthesis. <sup>[j]</sup> The values correspond to C<sub>8</sub><sup>-</sup> and C<sub>8</sub><sup>+</sup> products.

## 6.7. Influence of catalyst activation temperature.

The influence of the catalyst activation temperature ( $T_{\text{act}}=200\text{ }^{\circ}\text{C}$ , or  $450\text{ }^{\circ}\text{C}$ ) prior to the catalytic reaction was studied for the Beta based materials and ZSM-5 (Figure 6.8 and Figure 6.10).  $T_{\text{act}}$  in the range 200-450  $^{\circ}\text{C}$  did not considerably influence the PLD profiles (Figure 6.10). The benchmark catalysts activated at 200  $^{\circ}\text{C}$  led to lower  $X_{\text{C}_4}$  and STYs than the respective materials activated at 450  $^{\circ}\text{C}$ . Conversely, the Beta based materials activated at 200  $^{\circ}\text{C}$  led to superior catalytic results than the respective materials activated at 450  $^{\circ}\text{C}$ ; this was more pronounced for the materials based on zeolite nanocrystallites, namely BEA-nano, BEA-hier and BEA/TUD. BEA-hier and ZSM-5 were further tested at an intermediate activation temperature of 325  $^{\circ}\text{C}$ , and it was verified that the catalytic results were similar to those for  $T_{\text{act}}$  of 200  $^{\circ}\text{C}$ , for the two materials (Figure S6.2). Thus, differences in catalytic results seemed more considerable for  $T_{\text{act}} > 325\text{ }^{\circ}\text{C}$ .

Characterization studies were carried out for the catalysts based on the BEA or MFI topology, in order to help understand the effect of  $T_{\text{act}}$  on the material properties. A comparative study of TGA data for all materials, suggested no clear relationship between  $T_{\text{act}}$  and the amount of coke (Figure 6.18).

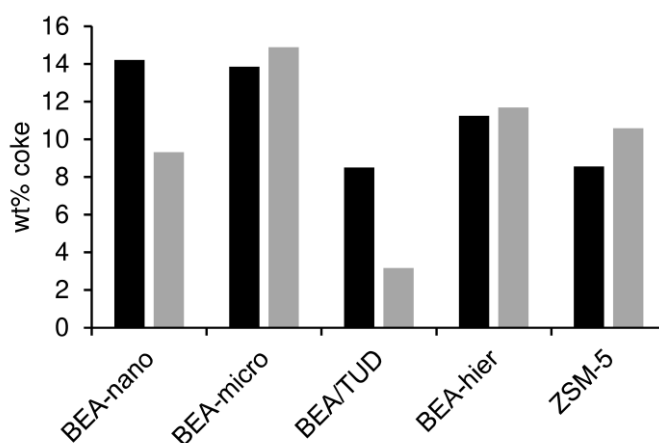


Figure 6.18. Amount of coke (based on TGA) of the Beta based materials and ZSM-5 used after activation ( $T_{\text{act}}$ ) at 200  $^{\circ}\text{C}$  (black bars) or 450  $^{\circ}\text{C}$  (grey bars). Reaction conditions: 200  $^{\circ}\text{C}$ , 30 bar,  $\text{WHSV}=2.2\text{ g}_{\text{C}_4}\text{ g}_{\text{cat}}^{-1}\text{ h}^{-1}$ , TOS=8 h.

For the composite BEA/TUD and its bulk nanocrystalline counterpart BEA-nano, the amount of coke was lower using  $T_{act}$  of 450 °C than 200 °C, with the composite leading to lower values. For BEA-hier, the amount of coke was similar using  $T_{act}$  of 200 or 450 °C, whereas catalytic activity was higher using  $T_{act}$  of 200 °C.

DSC analysis were carried out in order to gain insights into the thermal properties of the coke (Figure 6.19). Comparisons of the DSC profiles for ZSM-5 *versus* the Beta based materials, suggested that the thermal stability of coke seemed inferior for ZSM-5. For BEA-hier,  $T_{act}$  did not seem to influence significantly the type of coke. It seems that  $T_{act}$  influences different material properties.

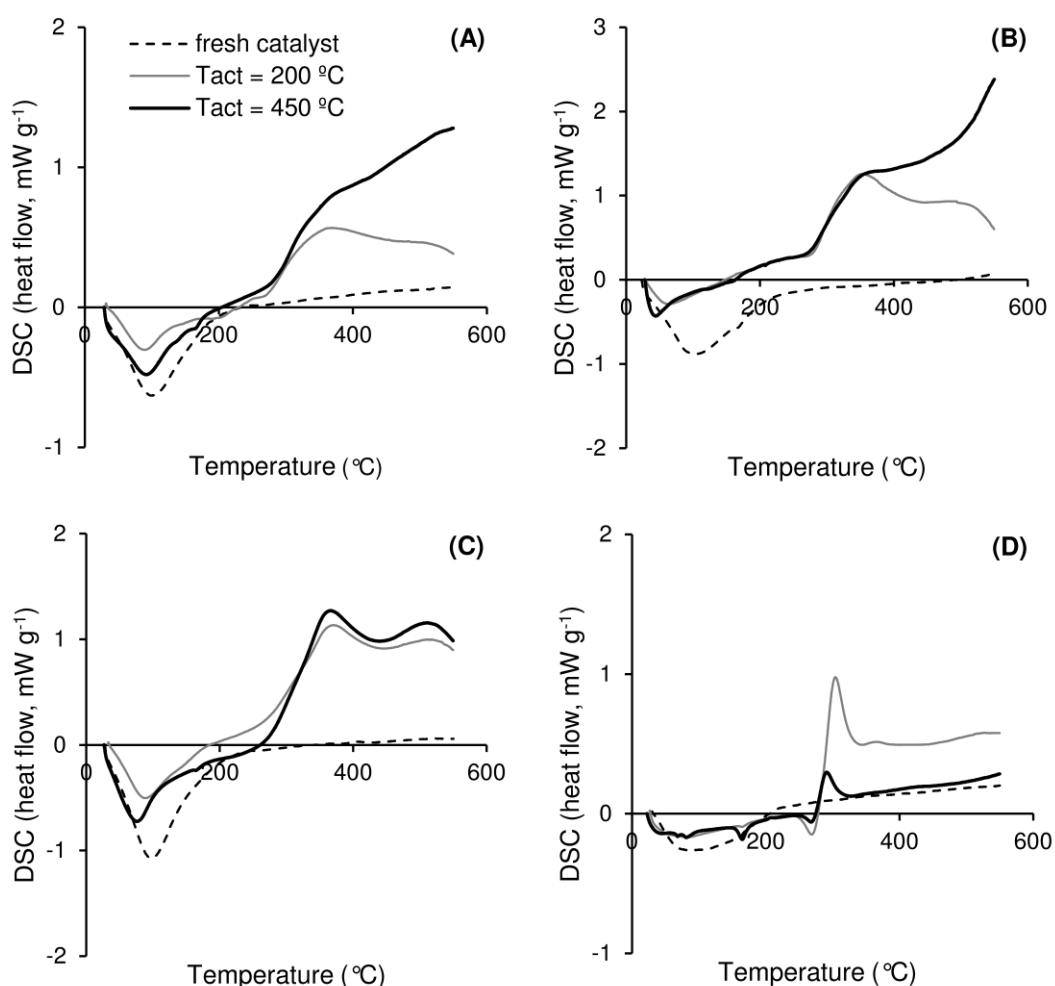


Figure 6.19. DSC curves for the BEA/TUD (A), BEA-nano (B), BEA-hier (C) and ZSM-5 (D); the results are given for the unused catalyst (dashed line), and the used catalyst activated ( $T_{act}$ ) at 200 °C (grey line) or 450 °C (black line). Reaction conditions: 200 °C, 30 bar,  $WHSV=2.2 \text{ g}_{1C4} \text{ g}_{cat}^{-1} \text{ h}^{-1}$ ,  $TOS=8 \text{ h}$ .

The PXRD patterns (Figure 6.1 and Figure 6.20), SEM images (Figure S6.1), and textural properties (Table 6.1 and Table 6.4) of the original and used catalysts ( $T_{\text{act}}=200$  °C or 450 °C) were roughly comparable. These results suggest that  $T_{\text{act}}$  up to 450 °C did not considerably affect the crystalline structure, morphology or textural properties of the materials. On the other hand, the relationships between the acid properties (measured at 200 °C or 450 °C) and  $X_{\text{C4}}$  or STYs, discussed above for the bulk Beta based catalysts activated at 200 °C (Figure 6.11 and Figure 6.12), apply similarly for the catalysts activated at 450 °C (Table S6.1, Figure S6.3 and Figure S6.4).

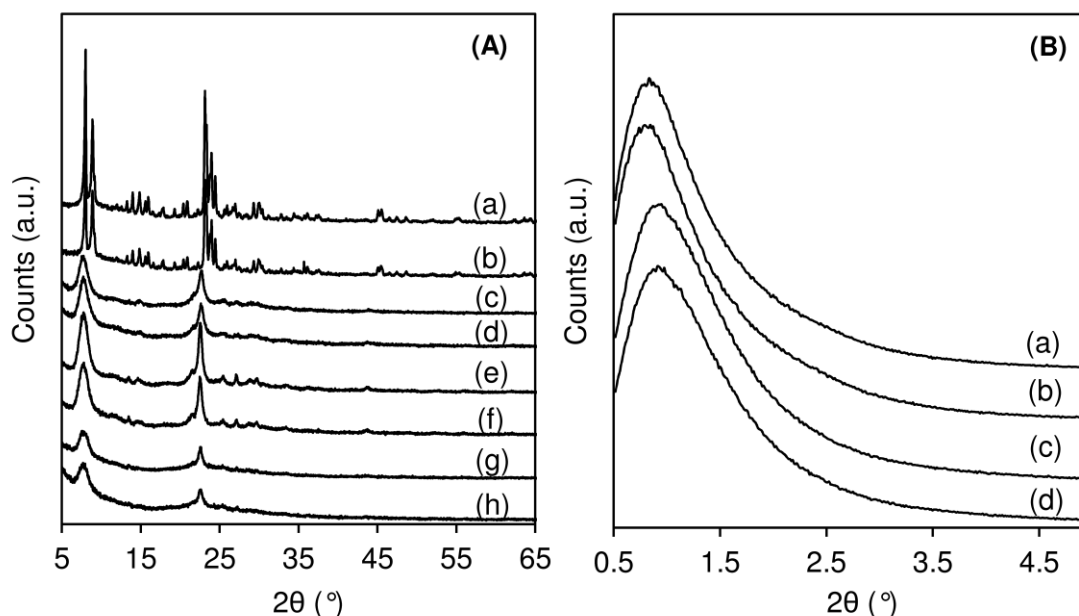


Figure 6.20. (A) PXRD patterns of ZSM-5 (fresh (a); used (b)), BEA-hier (fresh (c); used (d)), BEA-nano (fresh (e); used (f)), and BEA/TUD (fresh (g); used (h)). (B) Low angles PXRD patterns of BEA-hier (fresh (a); used (b)), BEA/TUD (fresh (c); used (d)). Reaction conditions: catalyst activation temperature=450 °C, catalytic reaction temperature=200 °C, 30 bar, WHSV=2.2 h<sup>-1</sup>.

A molecular level characterization by <sup>27</sup>Al MAS NMR spectroscopy was carried out for ZSM-5 and BEA-hier used after activation at 200 or 450 °C (Figure 6.17). For ZSM-5 it appeared a new band at *ca.* 29 ppm after use ( $T_{\text{act}}=200$  °C or 450 °C), which was not observed for the original material, and is assignable to five-coordinated aluminum species.<sup>[62,64]</sup> The ratio  $\text{Al}_{\text{tetra}}/\text{Al}_{\text{octa}}$  was higher using  $T_{\text{act}}=450$  °C than 200 °C (3.7 and 1.7, respectively), which

may partly explain the superior performance of ZSM-5 activated at the higher temperature. For BEA-hier, the values of  $Al_{tetra}/Al_{octa}$  were somewhat comparable using  $T_{act}$  of 200 °C and 450 °C (1.9-2.2), which does not (at least solely) explain the superior catalytic performance of BEA-hier activated at 200 °C compared to that for  $T_{act}=450$  °C. According to the literature, zeolite Beta based materials may possess various types of Al sites, and some may undergo alterations during catalyst activation/use: *e.g.*, formation/conversion of six-coordinated Al species partially bridged to the framework and possessing aqua, hydronium or hydroxyl ligands.<sup>[36,38,39,60,61,64–66]</sup> Water may be liberated, for example, *via* condensation of silanol groups during thermal treatment, and cause *in situ* partial hydrolysis of some surface species, altering their configurations (some of which may be reversible).<sup>[36,39]</sup> Clear assessments of the changes in the distributions of the various Al species occurring during the catalyst activation/use, and the determination of the intrinsic activities of the various effective Al sites for the target reaction system, could help gain insights into the effects of  $T_{act}$ , albeit this is not trivial.

## 6.8. Conclusions

Mesostructured versions based on the BEA topology were synthesized *via* different strategies, and explored for 1-butene oligomerization under high pressure, continuous-flow operation, typically at 200 °C, 30 bar, WHSV of 2.2  $g_{1C4} g_{cat}^{-1} h^{-1}$ . The introduction of mesoporosity into the materials led to positive effects on the catalytic reaction, in relation to commercial nanocrystalline and microcrystalline zeolite Beta (BEA-nano and BEA-micro, respectively). Specifically, a composite catalyst (BEA/TUD) consisting of nanocrystallites of zeolite Beta embedded in a mesoporous siliceous TUD-1 type matrix, possessed higher intrinsic activity than its bulk counterpart consisting of aggregated Beta nanocrystals (BEA-nano). On the other hand, a hierarchical material (BEA-hier) consisting of an arrangement of Beta nanocrystallites, possessing mesoporosity and enhanced molar ratio L/B, outperformed the commercial zeolite Beta samples, and the benchmark catalysts ZSM-5 and COD-900 (type of catalysts used in commercial oligomerization processes), in terms of conversion and STYs. BEA-hier led to 73 % conversion, space time yield (STY) of 849 mg

$\text{g}_{\text{cat}}^{-1} \text{h}^{-1}$ , mass ratio  $D_{\text{cut}}/N_{\text{cut}}$  products of 1.5, and relatively low ratio of aromatic to aliphatic products (ca. 0.06), at 8 h on-stream, 250 °C, 30 bar (WHSV of 2.2  $\text{g}_{\text{C}_4} \text{g}_{\text{cat}}^{-1} \text{h}^{-1}$ ). Decreasing reaction temperature and increasing the pressure enhanced the mass ratio  $D_{\text{cut}}/N_{\text{cut}}$  products, whereas conversion ( $X_{\text{C}_4}$ ) and space time yield (STY) tend to increase with increasing temperature and pressure. Optimization of the reaction conditions is important for improved catalytic performances. BEA-hier performed superiorly when activated (prior to catalytic reaction) at 200 °C than at 450 °C ( $T_{\text{act}}$ ), which was contrary to that verified for the benchmark catalyst ZSM-5. It was postulated that these differences may be partly related to changes in the distributions of types of Al-sites occurring during catalyst activation/use. ZSM-5 seemed to possess steadier activity upon reuse in relation to BEA-hier. In depth molecular level characterization studies (using complementary techniques; *e.g.*, some Al species may be “NMR invisible” [64]) of the changes in the types of Al sites that occur during activation/use of catalysts with different zeolite topologies, and the challenging determination of the intrinsic activities of the different types of Al species, may help to better understand the effects of  $T_{\text{act}}$ , and optimize catalytic performances for the target reaction systems.

## 6.9. References

- [1] A. Corma, S. Iborra, Oligomerization of alkenes, in: E.G., Derouane (Ed.), *Catalysts for fine chemical synthesis*, Volume 4, Microporous and mesoporous solid catalysts, John Wiley & Sons, 2006: pp. 125–140.
- [2] T. Imai, Preparation of metal oxide-supported boron fluoride catalysts, US 4407731 A, 1983.
- [3] F.T.T. Ng, G.L. Rempel, B. Nkosi, Composite catalyst for the selective oligomerization of lower alkenes and the production of high octane products, WO 2005056503 A1, 2005.
- [4] M. Sanati, C. Höرنell, S.G. Jaras, The Oligomerization of alkenes by heterogeneous catalysts, in: J.J. Spivey (Ed.), *Catalysis: Volume 14 (Specialist periodical reports)*, Royal society of chemistry, 1999: pp. 236–287.
- [5] C. Song, Properties of diesel fuels, in: *Chemistry of Diesel Fuels*, Great Britain, 2000: pp. 7–16.
- [6] A. Corma, Inorganic solid acids and their use in acid-catalyzed hydrocarbon reactions, *Chem. Re.* 95 (1995) 559–614.
- [7] A. De Klerk, Distillate production by oligomerization of Fischer - Tropsch olefins over solid phosphoric acid, *Energy & Fuels* 20 (2006) 439–445.
- [8] J.H. Coetzee, T.N. Mashapa, N.M. Prinsloo, J.D. Rademan, An improved solid phosphoric acid catalyst for alkene oligomerization in a Fischer – Tropsch refinery, *Appl. Catal. A Gen.* 308 (2006) 204–209.

- [9] J. Zhang, Y. Yan, Q. Chu, J. Feng, Solid phosphoric acid catalyst for propene oligomerization: effect of silicon phosphate composition, *Fuel Process. Technol.* 135 (2015) 2–5.
- [10] C. Martínez, E.J. Doskocil, A. Corma, Improved THETA-1 for light olefins oligomerization to diesel: influence of textural and acidic properties, *Top. Catal.* 57 (2014) 668–682.
- [11] Y.T. Kim, J.P. Chada, Z. Xu, Y.J. Pagan-Torres, D.C. Rosenfeld, W.L. Winniford, E. Schmidt, G.W. Huber, Low-temperature oligomerization of 1-butene with H-ferrierite, *J. Catal.* 323 (2015) 33–44.
- [12] A. Coelho, G. Caeiro, M.A.N.D.A. Lemos, F. Lemos, F.R. Ribeiro, 1-Butene oligomerization over ZSM-5 zeolite: Part 1 - Effect of reaction conditions, *Fuel* 111 (2013) 449–460.
- [13] J.W. Yoon, J.-S. Chang, H.-D. Lee, T.-J. Kim, S.H. Jung, Trimerization of isobutene over a zeolite beta catalyst, *J. Catal.* 245 (2007) 253–256.
- [14] N. Kumar, P. Mäki-Arvela, T. Yläsalmi, J. Villegas, T. Heikkilä, A.-R. Leino, K. Kordás, T. Salmi, D. Yu Murzin, Dimerization of 1-butene in liquid phase reaction: Influence of structure, pore size and acidity of Beta zeolite and MCM-41 mesoporous material, *Microporous Mesoporous Mater.* 147 (2012) 127–134.
- [15] M.J. Wulfers, R.F. Lobo, Assessment of mass transfer limitations in oligomerization of butene at high pressure on H-beta, *Appl. Catal. A Gen.* 505 (2015) 394–401.
- [16] E. Rossetto, B.P. Nicola, R.F. De Souza, K. Bernardo-Gusmão, S.B.C. Pergher, Heterogeneous complexes of nickel MCM-41 with beta-diimine ligands: applications in olefin oligomerization, *J. Catal.* 323 (2015) 45–54.
- [17] R. Catani, M. Mandreoli, S. Rossini, A. Vaccari, Mesoporous catalysts for the synthesis of clean diesel fuels by oligomerisation of olefins, *Catal. Today* 75 (2002) 125–131.
- [18] J.S. Lee, J.W. Yoon, S.B. Halligudi, J.S. Chang, S.H. Jung, Trimerization of isobutene over  $WO_x/ZrO_2$  catalysts, *Appl. Catal. A Gen.* 366 (2009) 299–303.
- [19] F. Tzompantzi, A. Mantilla, G. Del Angel, J.M. Padilla, J.L. Fernández, J.A.I. Díaz-Góngora, R. Gómez,  $NiO-W_2O_3/Al_2O_3$  catalysts for the production of ecological gasoline: effect of both NiO and the preparation method on the isobutene oligomerization selectivity, *Catal. Today* 143 (2009) 132–136.
- [20] X. Zhang, J. Zhong, J. Wang, J. Gao, A. Liu, Trimerization of butene over Ni-doped zeolite catalyst: effect of textural and acidic properties, *Catal. Letters* 126 (2008) 388–395.
- [21] C. Perego, R. Millini, Porous materials in catalysis: challenges for mesoporous materials, *Chem. Soc. Rev.* 42 (2013) 3956–3976.
- [22] Y. Tao, H. Kanoh, L. Abrams, K. Kaneko, Mesopore-modified zeolites: preparation, characterization, and applications, *Chem. Rev.* 106 (2006) 896–910.
- [23] D.P. Serrano, J.M. Escola, P. Pizarro, Synthesis strategies in the search for hierarchical zeolites, *Chem. Soc. Rev.* 42 (2013) 4004–4035.
- [24] J.C. Groen, J.A. Moulijn, J. Pérez-Ramírez, Desilication: on the controlled generation of mesoporosity in MFI zeolites, *J. Mater. Chem.* 16 (2006) 2121–2131.
- [25] T. Prasomsri, W. Jiao, S.Z. Weng, J. Garcia Martinez, Mesostructured zeolites: bridging the gap between zeolites and MCM-41, *Chem. Commun.* 51 (2015) 8900–8911.
- [26] P. Waller, Z. Shan, L. Marchese, G. Tartaglione, W. Zhou, J.C. Jansen, T. Maschmeyer, Zeolite nanocrystals inside mesoporous TUD-1: a high-performance catalytic composite., *Chemistry* 10 (2004) 4970–6.
- [27] R. Chal, C. Gérardin, M. Bulut, S. van Donk, Overview and industrial assessment of synthesis strategies towards zeolites with mesopores, *ChemCatChem* 3 (2011) 67–81.
- [28] K. Na, M. Choi, R. Ryoo, Recent advances in the synthesis of hierarchically nanoporous zeolites, *Microporous Mesoporous Mater.* 166 (2013) 3–19.

- [29] Y. Wei, T.E. Parmentier, K.P. de Jong, J. Zečević, Tailoring and visualizing the pore architecture of hierarchical zeolites, *Chem. Soc. Rev.* 44 (2015) 7234–7261.
- [30] K. Zhu, X. Zhou, Manipulating the architecture of zeolite catalysts for enhanced mass transfer, *Curr. Opin. Chem. Eng.* 9 (2015) 42–48.
- [31] L. Wang, Z. Zhang, C. Yin, Z. Shan, F.-S. Xiao, Hierarchical mesoporous zeolites with controllable mesoporosity templated from cationic polymers, *Microporous Mesoporous Mater.* 131 (2010) 58–67.
- [32] F.S. Xiao, L. Wang, C. Yin, K. Lin, Y. Di, J. Li, R. Xu, D.S. Su, R. Schlögl, T. Yokoi, T. Tatsumi, Catalytic properties of hierarchical mesoporous zeolites templated with a mixture of small organic ammonium salts and mesoscale cationic polymers, *Angew. Chemie - Int. Ed.* 45 (2006) 3090–3093.
- [33] Z. Shan, P.W.G. Waller, B.G. Maingay, P.J. Angevine, J.C. Jansen, C.Y. Yeh, T. Maschmeyer, F.M. Dautzenberg, L. Marchese, H.O. Pastore, Zeolite composite, method for making and catalytic application thereof, US 7,084,087 B2, 2006.
- [34] S. Lima, M.M. Antunes, A. Fernandes, M. Pillinger, M.F. Ribeiro, A.A. Valente, Catalytic cyclodehydration of xylose to furfural in the presence of zeolite H-Beta and a micro/mesoporous Beta/TUD-1 composite material, *Appl. Catal. A Gen.* 388 (2010) 141–148.
- [35] Y. Yuan, P. Tian, M. Yang, D. Fan, L. Wang, S. Xu, C. Wang, D. Wang, Y. Yang, Z. Liu, Synthesis of hierarchical beta zeolite by using a bifunctional cationic polymer and the improved catalytic performance, *RSC Adv.* 5 (2015) 9852–9860.
- [36] J.M.R. Gallo, C. Bisio, G. Gatti, L. Marchese, H.O. Pastore, Physicochemical characterization and surface acid properties of mesoporous [Al]-SBA-15 obtained by direct synthesis, *Langmuir* 26 (2010) 5791–5800.
- [37] K. Góra-Marek, M. Derewiński, P. Sarv, J. Datka, IR and NMR studies of mesoporous alumina and related aluminosilicates, *Catal. Today* 101 (2005) 131–138.
- [38] J.A. van Bokhoven, D.C. Koningsberger, P. Kunkeler, H. van Bekkum, A.P.M. Kentgens, Stepwise dealumination of zeolite Beta at specific T-sites observed with  $^{27}\text{Al}$  MAS and  $^{27}\text{Al}$  MQ MAS NMR, *J. Am. Chem. Soc.* 122 (2000) 12842–12847.
- [39] J.Z. Hu, C. Wan, A. Vjunov, M. Wang, Z. Zhao, M.Y. Hu, D.M. Camaioni, J.A. Lercher,  $^{27}\text{Al}$  MAS NMR studies of HBEA zeolite at low to high magnetic fields, *J. Phys. Chem. C* 121 (2017) 12849–12854.
- [40] W.O. Parker, A. De Angelis, C. Flego, R. Millini, C. Perego, S. Zanardi, Unexpected destructive dealumination of zeolite beta by silylation, *J. Phys. Chem. C* 114 (2010) 8459–8468.
- [41] P.J. Kunkeler, B.J. Zuurdeeg, J.C. van der Waal, J.A. van Bokhoven, D. C. Koningsberger, H. van Bekkum, Zeolite Beta: the relationship between calcination procedure, aluminum configuration, and Lewis acidity, *J. Catal.* 180 (1998) 234–244.
- [42] A. Abraham, S.-H. Lee, C.-H. Shin, S. Bong Hong, R. Prins, J.A. van Bokhoven, Influence of framework silicon to aluminum ratio on aluminum coordination and distribution in zeolite Beta investigated by  $^{27}\text{Al}$  MAS and  $^{27}\text{Al}$  MQ MAS NMR, *Phys. Chem. Chem. Phys.* 6 (2004) 3031.
- [43] A.E.W. Beers, J.A. van Bokhoven, K.M. De Lathouder, F. Kapteijn, J.A. Moulijn, Optimization of zeolite Beta by steaming and acid leaching for the acylation of anisole with octanoic acid: a structure-activity relation, *J. Catal.* 218 (2003) 239–248.
- [44] C.A. Emeis, Determination of integrated molar extinction coefficients for infrared absorption bands of pyridine adsorbed on solid acid catalysts, *J. Catal.* 141 (1993) 347–354.
- [45] S. Xing, P. Lv, J. Fu, J. Wang, P. Fan, L. Yang, Z. Yuan, Direct synthesis and characterization of pore-broadened Al-SBA-15, *Microporous Mesoporous Mater.* 239 (2017) 316–327.

- [46] J. Mühl, V. Srlica, H. Packard, Determination of fluid catalytic cracking gasoline octane number by n.m.r. spectrometry, *Fuel* 66 (1987) 1146–1149.
- [47] C.T. O'Connor, R.D. Forrester, M.S. Scurrall, Cetane number determination of synthetic diesel fuels, *Fuel* 71 (1992) 1323–1327.
- [48] G.S. Kapur, A. Ecker, R. Meusinger, Establishing quantitative structure-property relationships (QSPR) of diesel samples by proton-NMR & multiple linear regression (MLR) analysis, *Energy and Fuels* 15 (2001) 943–948.
- [49] A. De Klerk, Fischer–Tropsch refining: technology selection to match molecules, *Green Chem.* 10 (2008) 1249–1279.
- [50] C. Knottenbelt, Moss gas “gas-to-liquid” diesel fuels - An environmentally friendly option, *Catal. Today* 71 (2002) 437–445.
- [51] D. Leckel, Diesel production from Fischer-Tropsch: the past, the present, and new concepts, *Energy & Fuels* 23 (2009) 2342–2358.
- [52] H. de Lasa, G. Dogammau, A. Ravella, Fuels of the future and changing fuel needs, in: *Chemical reactor technology for environmentally safe reactors and products*, Springer-Science+Business Media, London, Ontario, 1992: pp. 1–182.
- [53] A. Corma, C. Martínez, E. Dorskocil, Designing MFI-based catalysts with improved catalyst life for C<sub>3</sub>= and C<sub>5</sub>= oligomerization to high-quality liquid fuels, *J. Catal.* 300 (2013) 183–196.
- [54] A. Mantilla, G. Ferrat, A. López-Ortega, E. Romero, F. Tzompantzi, M. Torres, E. Ortíz-Islas, R. Gómez, Catalytic behavior of sulfated TiO<sub>2</sub> in light olefins oligomerization, *J. Mol. Catal. A Chem.* 228 (2005) 333–338.
- [55] J.W. Yoon, S.H. Jung, D.H. Choo, S.J. Lee, K.-Y. Lee, J.S. Chang, Oligomerization of isobutene over dealuminated Y zeolite catalysts, *Appl. Catal. A Gen.* 337 (2008) 73–77.
- [56] J.W. Yoon, J.S. Lee, S.H. Jung, K.-Y. Lee, J.-S. Chang, Oligomerization of isobutene over aluminum chloride-loaded USY zeolite catalysts, *J. Porous Mater.* 16 (2009) 631–634.
- [57] X. Li, D. Han, H. Wang, G. Liu, B. Wang, Z. Li, J. Wu, Propene oligomerization to high-quality liquid fuels over Ni/HZSM-5, *Fuel* 144 (2015) 9–14.
- [58] S. Peratello, M. Molinari, G. Bellussi, C. Perego, Olefins oligomerization: thermodynamics and kinetics over a mesoporous silica-alumina, *Catal. Today* 52 (1999) 271–277.
- [59] C.T. O'Connor, Oligomerization, in: G. Ertl, H. Knözinger, F. Schüth, J. Weitkamp (Eds.), *Handbook of heterogeneous catalysis*, Volume 1, 2<sup>nd</sup> ed., 2008: pp. 2854–2864.
- [60] G.H. Kuehl, H.K.C. Timken, Acid sites in zeolite Beta: effects of ammonium exchange and steaming, *Microporous Mesoporous Mater.* 35 (2000) 521–532.
- [61] A.V. Toktarev, L.V. Malysheva, E.A. Paukshtis, Effect of thermal treatment conditions on the acid properties of zeolite Beta, *Kinet. Catal.* 51 (2010) 318–324.
- [62] J. Brus, L. Kobera, W. Schoefberger, M. Urbanová, P. Klein, P. Sazama, E. Tabor, S. Sklenak, A. V. Fishchuk, J. Dědeček, Structure of framework aluminum lewis sites and perturbed aluminum atoms in zeolites as determined by <sup>27</sup>Al{<sup>1</sup>H} REDOR (3Q) MAS NMR spectroscopy and DFT/molecular mechanics, *Angew. Chemie - Int. Ed.* 54 (2015) 541–545.
- [63] S. Schwarz, M. Kojima, C.T. O'Connor, Effect of silicon-to-aluminum ratio and synthesis time on high-pressure olefin oligomerization over ZSM-5, *Appl. Catal.* 56 (1989) 263–280.
- [64] L. Mafra, J.A. Vidal-Moya, T. Blasco, Structural characterization of zeolites by advanced solid state NMR spectroscopic methods, in: *Annual reports on NMR spectroscopy*, 2012: pp. 259–351.

- [65] Z. Zhao, S. Xu, M. Y. Hu, X. Bao, C.H.F. Peden, J. Hu, Investigation of aluminum site changes of dehydrated zeolite H-beta during a rehydration process by high-field solid-state NMR, *J. Phys. Chem. C*. 119 (2015) 1410–1417.
- [66] A. Guzman, I. Zuazo, A. Feller, R. Olindo, C. Sievers, J.A. Lercher, Influence of the activation temperature on the physicochemical properties and catalytic activity of La-X zeolites for isobutane/*cis*-2-butene alkylation, *Microporous Mesoporous Mater.* 97 (2006) 49–57.

# CHAPTER 7

---

## 1-Butene oligomerization over nanocrystalline MFI-based micro/mesoporous zeotypes synthesized *via* bottom-up approaches

### Abstract

The oligomerization of 1-butene was studied under high-pressure continuous-flow conditions (200-250 °C, 30-40 bar), in the presence of micro/mesoporous zeotypes based on the MFI topology, which were prepared *via* different non-destructive bottom-up strategies, such as crystallization of silanized protozeolitic units, co-

templating with a dual function template, and using a sole structure directing agent (non-surfactant and non-polymeric) to generate mesoporosity. The synthesis method influenced the material properties and consequently the catalytic performance. In targeting hydrocarbons with boiling point ranges characteristics of diesel, the zeotypes benefited from regular morphology, reduced crystallite size, mesoporosity and enhanced molar ratio of Lewis (L) to Brønsted (B) acid sites (L/B). In general, the zeotypes outperformed commercial zeolite ZSM-5. The best-performing zeotype was prepared according to the Serrano strategy based on the crystallization of silanized zeolitic seeds, and led to 97 % conversion and an average space-time yield of liquid products of 1077 mg g<sub>cat</sub><sup>-1</sup> h<sup>-1</sup>, at 250 °C, 40 bar. The zeotypes seemed more stable than the commercial zeolite, based on molecular level characterization studies of the used/regenerated catalysts, with some differences in catalytic activity.

### Oligomerisation of 1-Butene High-pressure continuous-flow

#### Acid aluminosilicate zeotypes Synthesised *via* bottom-up approaches

MFI topology  
Reduced crystallite sizes  
Regular morphology  
Mesoporosity  
Enhanced ratio Lewis/Brønsted acid sites



*Space time yield*  $\approx 1.1 \text{ g g}_{\text{cat}}^{-1} \text{ h}^{-1}$  at 250 °C, 40 bar

## CHAPTER 7

### **1-Butene oligomerization over nanocrystalline MFI-based micro/mesoporous zeotypes synthesized *via* bottom-up approaches**

7.1.	Introduction .....	213
7.2.	Synthesis of the catalytic materials .....	215
7.3.	Characterization studies of the catalytic materials .....	218
7.4.	Catalytic studies: general considerations.....	224
7.5.	Influence of material properties on the catalytic performance .....	230
7.6.	Influence of the reaction conditions .....	232
7.7.	Catalyst stability .....	233
7.8.	Conclusions .....	238
7.9.	References .....	239

## 7.1. Introduction

The importance of developing and implementing efficient and clean processes for fuel production is evident in an energy-expanding world. The great dependence of society on fossil fuels is believed to contribute to global warming, and in mitigating this problem, the solutions may involve the use of renewable sources of energy, and repurposing industrial byproducts for the production of chemicals and fuels. Light olefins are byproducts of petrochemical or Fischer-Tropsch processes,<sup>[1-4]</sup> and, on the other hand, may be obtained from renewable sources, *e.g.*, butenes from carbohydrate biomass.<sup>[5-7]</sup> The oligomerization of light olefins (C2-C5) may be a flexible technology and attractive route to produce diverse products including synthetic transportation fuels (gasoline, diesel, jet fuel) with reduced content of sulphur and aromatic compounds, drugs, detergents, lubricants and dyes.<sup>[8,9]</sup> Olefin oligomerization is favored in the presence of acid catalysts, which should be adequate for continuous-flow processes. In this sense, porous solids possessing significant specific surface area available for the catalytic reaction, are attractive. On the other hand, olefin oligomerization involves the formation of relatively bulky products, and, thus, to facilitate mass transport and maximize the portion of effectively utilized catalyst in the process, it is desirable that the solid acids possess sufficiently large pores.<sup>[10-12]</sup>

Important industrial solid acid catalysts are porous aluminosilicates. This category of materials is very versatile: amorphous or crystalline materials with different topologies, morphological, textural and acid properties may be prepared.<sup>[10-12]</sup> Most successful types of aluminosilicates applied in the industry include zeolites, which are crystalline and microporous materials. Zeolites may possess superior acid properties (*e.g.*, stronger acidity) to amorphous aluminosilicates such as ordered mesoporous materials of the type MCM-41, SBA-15 or TUD-1; the latter possess less rigid frameworks and silanol surface groups, albeit larger pores than zeolites, advantageously allowing enhanced acid sites accessibility.<sup>[2,13-16]</sup> Favorable compromise between textural and acid properties of porous solid acids is important for maximizing product yields. Another important factor for maximizing catalyst productivity is the catalyst stability. Zeolites possessing the MFI topology (medium pore, with the channel sizes of  $0.55 \times 0.51 \text{ nm}^2$  and  $0.56 \times 0.53 \text{ nm}^2$ ) are relatively robust industrial catalysts and used in commercial olefin oligomerization processes.<sup>[17-23]</sup> However, they may

present important mass transfer limitations and suffer fast catalyst deactivation in the oligomerization of olefins such as butene.<sup>[24]</sup> Hence, great attention has been drawn to the development of aluminosilicate zeotypes with reduced crystallite sizes and/or enlarged pores. The synthetic strategies for obtaining zeotypes possessing mesoporosity may be classified as top-down or bottom-up approaches.<sup>[25–28]</sup> Zeotypes prepared *via* top-down approaches were studied for olefin oligomerization, and possessed superior performances in comparison to conventional microporous zeolites; the zeotypes were based on the MFI,<sup>[29–31]</sup> MOR,<sup>[32,33]</sup> FAU<sup>[34]</sup> and TON<sup>[35]</sup> topologies.

A main difference between the top-down and bottom-up approaches is that the former may be somewhat destructive compared to the latter. Regarding the bottom-up approaches, several specific strategies (*e.g.*, with or without addition of structure-directing agents) were reported for preparing zeotypes based on different topologies and possessing mesoporosity (2–50 nm). Wang et al. and Yang et al. reported the synthesis of hydrothermally stable zeotypes based on the MFI topology, *via* (soft) co-templating protocol (denoted CoT), which involved the simultaneous use of small and large cationic ammonium-based hydrophilic templates. The mesoporosity could be fine-tuned by changing the amount of the large cationic template.<sup>[36,37]</sup> Serrano et al. reported a strategy (denoted PZSi) based on the crystallization of silanized zeolitic seeds (or protozeolitic units) possessing MFI topology, which may be followed by a treatment with a basic surfactant-containing solution (PZSiS) to rearrange the zeolitic units over the mesopore surface.<sup>[38–40]</sup> Wan et al. reported a method not requiring additional template or zeolite seeding crystals (denoted noT). The hierarchical zeotypes presented superior performances to conventional microporous ZSM-5 for different acid-catalyzed liquid or gas phase reactions, under batch or continuous-flow operation. In particular, the synthetic approach by Wan et al. led to porous solid acids that enhanced the conversion of methanol to gasoline, and was more stable towards coking.<sup>[41]</sup>

In this work, the oligomerization of 1-butene was studied under continuous-flow, at typical high-pressure conditions (200 °C, 30 bar) as in the industrial oligomerization technologies,<sup>[19,23]</sup> in the presence of zeotypes based on the MFI topology and possessing mesoporosity. The zeotypes were prepared *via* different bottom-up approaches, based on the strategies CoT, PZSi, PZSiS and noT referred above. The zeotype catalysts were benchmarked with commercial zeolite ZSM-5 possessing Si/Al ratio intermediate of the zeotypes (Si/Al=20–51). Special attention was given to aspects of catalyst stability.

## 7.2. Synthesis of the catalytic materials

The zeotype materials based on the MFI topology were synthesized *via* bottom-up approaches, and the prepared materials were denoted as hZSM-5(x)-y, where x is the Si/Al ratio giving by EDS, and y is the abbreviation of the synthesis method. The synthesis protocols were adapted from the literature: a method not requiring additional template or zeolite seeding crystals (denoted noT);<sup>[41]</sup> a method involving the crystallization of silanized zeolitic seeds (or protozeolitic units) possessing MFI topology (denoted PZSi), which may be followed by a treatment with a basic surfactant-containing solution (PZSiS) to rearrange the zeolitic units over the mesopore surface<sup>[38]</sup>; and a method based on (soft) co-templating (denoted CoT)<sup>[36]</sup>. The protocols/conditions of the synthesized zeotypes are summarized in Table 7.1.

Table 7.1. Bottom-up protocols and synthesis conditions of the zeotypes based on the MFI topology.

Synthesis step	noT	PZSi	CoT
Synthesis mixture	TEOS, TPAOH <sup>[a]</sup> , NaAlO <sub>2</sub> , H <sub>2</sub> O (50) <sup>[b]</sup>	TEOS, TPAOH, AiP, H <sub>2</sub> O (30 and 60) <sup>[b]</sup>	TEOS, TPAOH, NaAlO <sub>2</sub> , H <sub>2</sub> O (36) <sup>[b]</sup>
Aging (with stirring)	20 h, aT <sup>[c]</sup>	44 h/aT <sup>[c]</sup> ; 22 h/90 °C	3 h, 100 °C
Additional template	None	PHAPTMS, 90 °C/6 h	PDD-AM, aT <sup>[c]</sup> /15 h
Hydrothermal treatment	180 °C, 2 d <sup>[d]</sup> , static	170 °C, 7.7 d <sup>[d]</sup> , static	180 °C, 6 d <sup>[d]</sup> , static
Centrifugation, wash, dry	100 °C	110 °C	100 °C
Calcination	550 °C/5 h	550 °C/5 h	550 °C/5 h
Ion-exchange; calcination	(3×) 1.0 M NH <sub>4</sub> NO <sub>3</sub> , 50 °C/24 h; 500 °C/5 h	None	(3×) 1.0 M NH <sub>4</sub> NO <sub>3</sub> , 80 °C/2 h; 550 °C/4 h
Sample name	hZSM-5(31)-noT	hZSM-5(x)-PZSi <sup>[e]</sup>	hZSM-5(31)-CoT

<sup>[a]</sup> TPAOH as the structure-directing agent accounting for the hierarchical features. <sup>[b]</sup> Si/Al ratio of the synthesis gel. <sup>[c]</sup> aT=ambient temperature. <sup>[d]</sup> d=days. <sup>[e]</sup> x is the molar ratio Si/Al of the final material (x=20 or 51).

### Free template method (noT)

The free template method was carried out following a similar procedure to that described by Wan et al.<sup>[41]</sup> Specifically, 0.33 mmol of NaAlO<sub>2</sub>, 12.7 mmol of TPAOH solution (40 % in H<sub>2</sub>O) and 2148 mmol of milli-Q water were mixed and stirred at room temperature for 30 min. Then, 32.9 mmol of TEOS was added dropwise. The molar composition of the synthesis-gel was 1Al<sub>2</sub>O<sub>3</sub>: 101SiO<sub>2</sub>: 1.34Na<sub>2</sub>O: 39TPAOH: 7215H<sub>2</sub>O. The resulting mixture was stirred at room temperature for 22 h in order to obtain a uniform gel, followed by crystallization at 180 °C for 48 h in a PTFE-lined stainless-steel autoclave, under static, hydrothermal conditions. After cooling, the resultant product was recovered by centrifugation, washed thoroughly with milli-Q water and dried at 100 °C overnight. The solid was gently grinded using an Agate mortar and pestle and calcined at 550 °C in static air for 5 h (heating rate of 1 °C min<sup>-1</sup>). The protonic form was obtained by ion-exchange with 1.0 M NH<sub>4</sub>NO<sub>3</sub> aqueous solution (1 g of calcined sample per 10 mL of solution), at 50 °C, under stirring. The solution was renewed two times, every 24 h. Finally, the solid was centrifuged, washed with milli-Q water, dried at 100 °C overnight, and calcined at 500 °C in static air for 5 h (heating rate of 1 °C min<sup>-1</sup>), giving a material denoted hZSM-5(31)-noT (noT stands for no additional template).

### Crystallization of silanized protozeolitic units (PZSi)

The method of silanization of protozeolitic units was employed following a similar procedure to that described by Serrano et al.<sup>[38]</sup> Specifically, the precursor ZSM-5 solution was prepared by mixing 8.11 mmol of TPAOH, 928 mmol of milli-Q water, 42.3 mmol of TEOS and 0.71 mmol of AiP for hZSM-5(51)-PZSi or 1.41 mmol of AiP for hZSM-5(20)-PZSi. The molar composition of the synthesis-gel was 1Al<sub>2</sub>O<sub>3</sub>: 120SiO<sub>2</sub>: 23TPAOH: 3000H<sub>2</sub>O for hZSM-5(51)-PZSi and 1Al<sub>2</sub>O<sub>3</sub>: 60SiO<sub>2</sub>: 11.5TPAOH: 1500H<sub>2</sub>O for hZSM-5(20)-PZSi. For the two materials, the mixture was aged at room temperature for 44 h and precrystallized under reflux and stirring (100 rpm) at 90 °C for 22 h. The resulting protozeolitic units were functionalized using 8 mol.% of PHAPTMS (with respect to the silica content in the initial gel), and the silanization reaction was performed at 90 °C for 6 h, under reflux, followed by crystallization at 170 °C during 184 h (for hZSM-5(51)-PZSi) or 186 h (for hZSM-5(20)-PZSi), in a PTFE-lined stainless-steel autoclave, under static,

hydrothermal conditions. After cooling, the resultant product was recovered by centrifugation, washed thoroughly with milli-Q water and dried at 110 °C overnight. The solid was gently grinded using an Agate mortar and pestle and calcined at 550 °C in static air for 5 h (heating rate of 1 °C min<sup>-1</sup>), giving the material hZSM-5(x)-PZSi (PZSi stands for ProtoZeolic units subjected to Silanization), where x stands for the Si/Al ratio of the synthesis gel.

The resulting hZSM-5(51)-PZSi material was submitted to a mesopore narrowing treatment. Specifically, 1.0 g of material was dispersed in 62.8 g of a 0.37 M NH<sub>4</sub>OH aqueous solution containing 0.7 g of CTAB. The resulting mixture was stirred at room temperature for 30 min, and then subjected to a hydrothermal treatment under static conditions, for 20 h at 150 °C in a PTFE-lined stainless-steel autoclave. The resultant product was recovered by centrifugation, washed thoroughly with milli-Q water and dried at 110 °C overnight. The solid was gently grinded using an Agate mortar and pestle and calcined at 550 °C in static air for 5 h (heating rate of 1 °C min<sup>-1</sup>), giving a material denoted hZSM-5(47)-PZSiS (PZSiS stands for ProtoZeolic units subjected to Silanization, followed by Surfactant treatment). This protocol does not require ion-exchange since no alkaline source is used.

### **Soft co-templating method (CoT)**

The co-templating method was carried out following a similar procedure to that described by Wang et al.<sup>[36]</sup> Specifically, 0.43 mmol of NaAlO<sub>2</sub>, 9.8 mmol of TPAOH and 31.0 mmol of TEOS were mixed with 1268 mmol of milli-Q water under stirring and aged at 100 °C for 3 h. Then, 3.0 mmol of PDD-AM were added into the reaction mixture. The molar composition of the synthesis-gel was 1Al<sub>2</sub>O<sub>3</sub>: 72SiO<sub>2</sub>: 1.3 Na<sub>2</sub>O: 23TPAOH: 4000H<sub>2</sub>O. The mixture was stirred for 15-16 h at room temperature, and then was transferred into a PTFE-lined stainless-steel autoclave for crystallization at 180 °C for 144 h. The solid product was separated by centrifugation, washed thoroughly with milli-Q water and dried at 100 °C overnight. The solid was gently grinded using an Agate mortar and pestle and calcined at 550 °C in static air for 5 h (heating rate of 1 °C min<sup>-1</sup>). The protonic form was obtained by ion-exchange with 1.0 M NH<sub>4</sub>NO<sub>3</sub> aqueous solution (1 g of calcined sample per 10 mL of solution), at 80 °C, under stirring. The solution was renewed three times, every 2

h. Finally, the solid was centrifuged, washed with milli-Q water, dried at 100 °C overnight, and calcined at 550 °C in static air for 4 h (heating rate of 1 °C min<sup>-1</sup>), giving a material denoted hZSM-5(31)-CoT (CoT stands for co-template).

### 7.3. Characterization studies of the catalytic materials

The MFI features of the materials prepared were ascertained by PXRD diffraction, which showed the characteristic reflections in the range 7-57° 2 $\theta$ , with the most intense peaks at 7-8° and 23-24° 2 $\theta$  (Figure 7.1-A).<sup>[42,43]</sup> Low angle PXRD showed a broad peak in the range 0.5-1.5° 2 $\theta$ , likely associated with the mesoporous features of the zeotypes prepared (Figure 7.1-B).

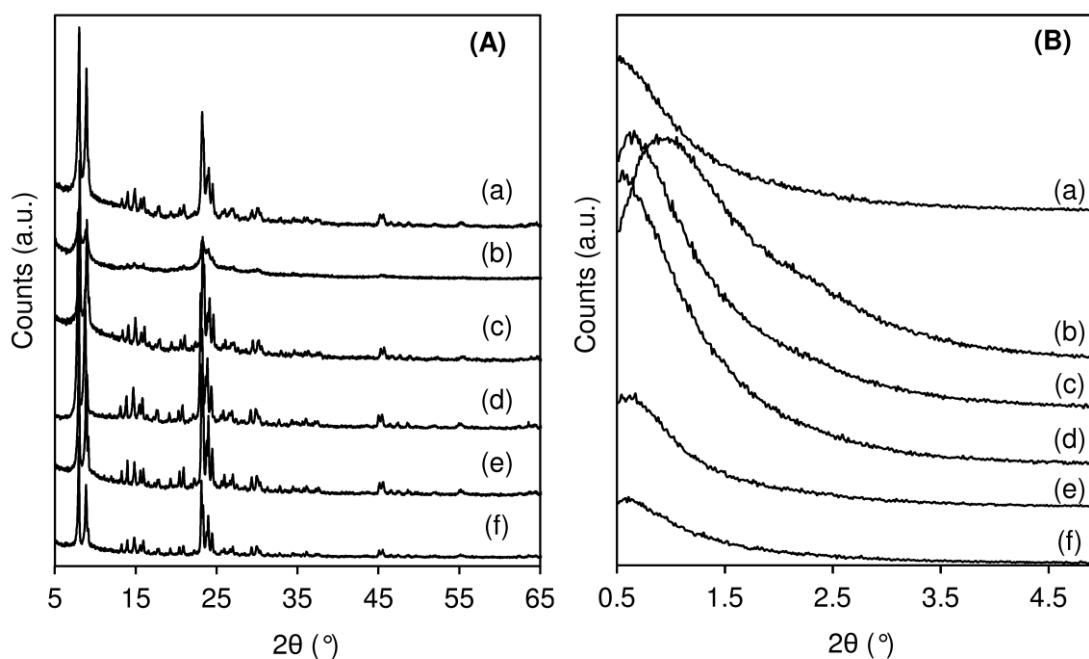


Figure 7.1. (A) Wide angles and (B) Low angles PXRD patterns for hZSM-5(31)-noT (a), hZSM-5(20)-PZSi (b), hZSM-5(51)-PZSi (c), hZSM-5(47)-PZSiS (d), hZSM-5(31)-CoT (e), and ZSM-5(29) (f).

1-Butene oligomerization over nanocrystalline MFI-based micro/mesoporous zeotypes synthesized *via* bottom-up approaches

Figure 7.2 shows the SEM and STEM images of the zeotypes. The noT and the PZSi(S) protocols led to materials consisting of pseudo-spherical aggregates ( $\approx 200$ -400 nm in size, Figure 7.2-a,d,g,j) of nanocrystalites ( $\approx 10$ -60 nm, Figure 7.2-c,f,i,l), somewhat in agreement with literature data for similarly prepared materials.<sup>[38,41]</sup> The PZSiS protocol involving a final surfactant treatment seemed to lead to some coalescence (Figure 7.2-k), forming larger nanocrystalites of  $\approx 30$ -60 nm compared to  $\approx 10$ -20 nm for PZSi. The CoT protocol led to irregular aggregates (ca. 1-1.5  $\mu\text{m}$ ) of nanocrystalites ( $\approx 30$ -40 nm), Figure 7.2-m,n,o. Commercial ZSM-5 zeolite (ZSM-5(29)) consists of small microcrystals (100-300 nm, Figure 7.2-p,q,r). EDS (Table 7.2) and Si and Al mappings (Figure 7.3) suggested that the materials possessed uniform dispersions of metal/metalloid surface species, and the molar ratios Si/Al were in the range 20-51 (Table 7.2).

Table 7.2. Elemental analyses and textural properties of the MFI-based materials.<sup>[a]</sup>

Sample	Si/Al <sup>[a]</sup>	Textural properties						$D_p$ <sup>[d]</sup> (nm)
		$S_{\text{BET}}$ ( $\text{m}^2\text{g}^{-1}$ )	$S_{\text{meso}}$ <sup>[b]</sup> ( $\text{m}^2\text{g}^{-1}$ )	% $S_{\text{meso}}$	$V_p$ ( $\text{cm}^3\text{g}^{-1}$ )	$V_{\text{micro}}$ <sup>[c]</sup> ( $\text{cm}^3\text{g}^{-1}$ )	% $V_{\text{micro}}$	
hZSM-5(31)-noT	31	308	168	54	0.46	0.04	8	2-10
hZSM-5(20)-PZSi	20	721	308	43	0.74	0.09	12	2-5
hZSM-5(51)-PZSi	51	558	289	52	0.77	0.07	10	2-7
hZSM-5(47)-PZSiS	47	464	275	59	0.76	0.05	7	2-5
hZSM-5(31)-CoT	31	853	140	16	0.48	0.25	52	2-5
ZSM-5(29)	29	334	97	29	0.47	0.17	36	-

<sup>[a]</sup> Molar ratio determined by EDS. <sup>[b]</sup> External/mesoporous specific surface area. <sup>[c]</sup> Micropore volume (calculated for  $p/p_0 \approx 0.99$ ). <sup>[d]</sup> Mesopore size range. For all materials, the micropore size distribution (based on DFT) indicated a median pore size in the range 0.55-0.57 nm.

The materials possessed BET specific surface area ( $S_{\text{BET}}$ ) in the range 308-853  $\text{m}^2\text{g}^{-1}$  (Table 7.2), and both micro- and mesoporosity (micropore sizes of 0.55-0.57 nm, and mesopore sizes of 2-10 nm, Figure 7.2). For the prepared zeotypes excluding hZSM-5(31)-CoT, the portion of specific mesopore surface area ( $S_{\text{meso}}$ ) was in the range 43-59 %, and that of micropore volume was 7-12 %. The material hZSM-5(31)-CoT possessed highest  $S_{\text{BET}}$  (853  $\text{m}^2\text{g}^{-1}$ ), albeit the portion of microporous volume was considerable (52 %). The commercial zeolite ZSM-5(29) possessed the lowest  $S_{\text{meso}}$ .

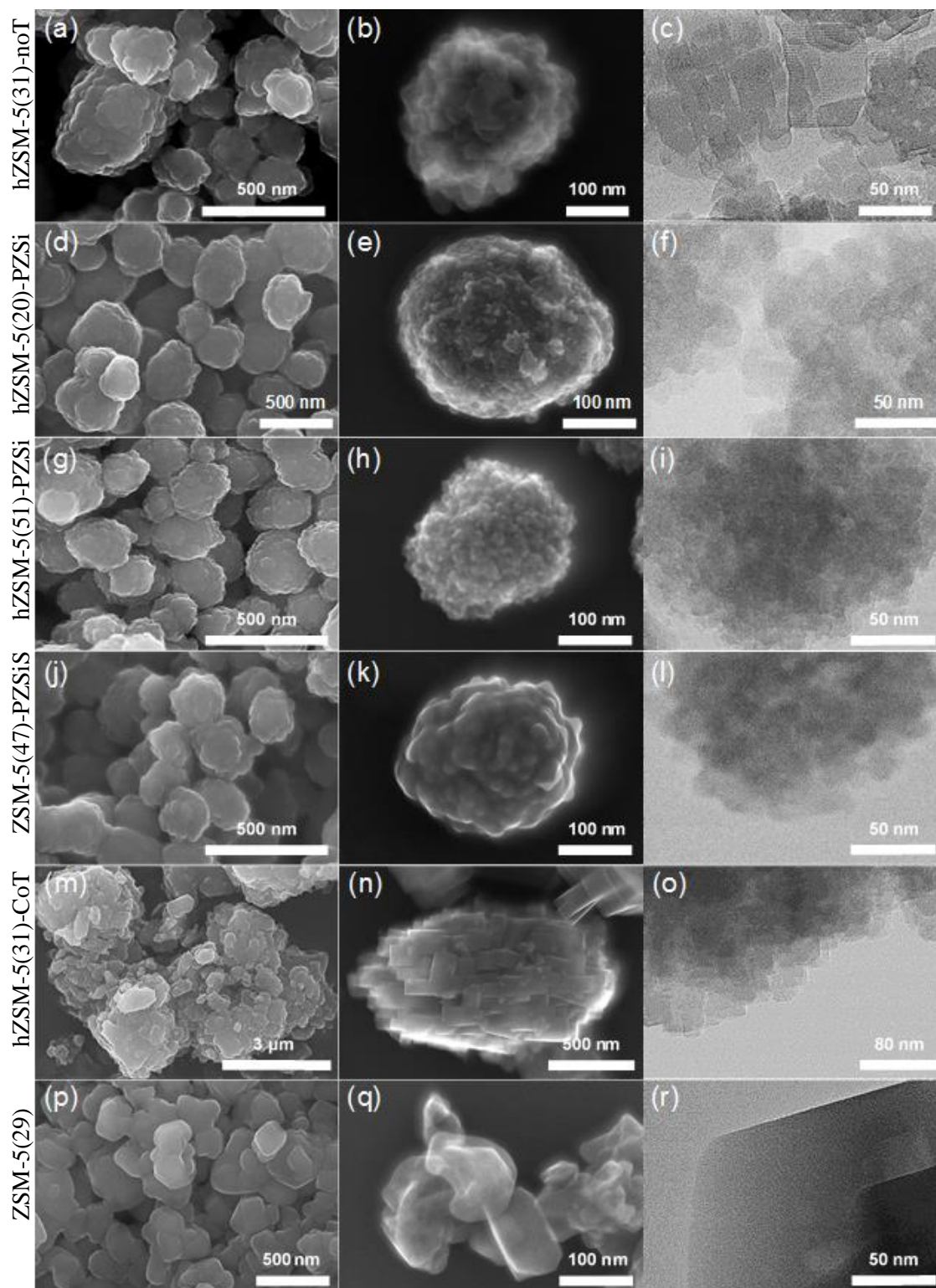


Figure 7.2. SEM (left column, a,d,g,j,m,p) and STEM (middle and right columns) images of hZSM-5(31)-noT (a, b, c), hZSM-5(20)-PZSi (d, e, f), hZSM-5(51)-PZSi (g, h, i), hZSM-5(47)-PZSiS (j, k, l), hZSM-5(31)-CoT (m, n, o), and ZSM-5(29) (p, q, r).

1-Butene oligomerization over nanocrystalline MFI-based micro/mesoporous zeotypes synthesized *via* bottom-up approaches

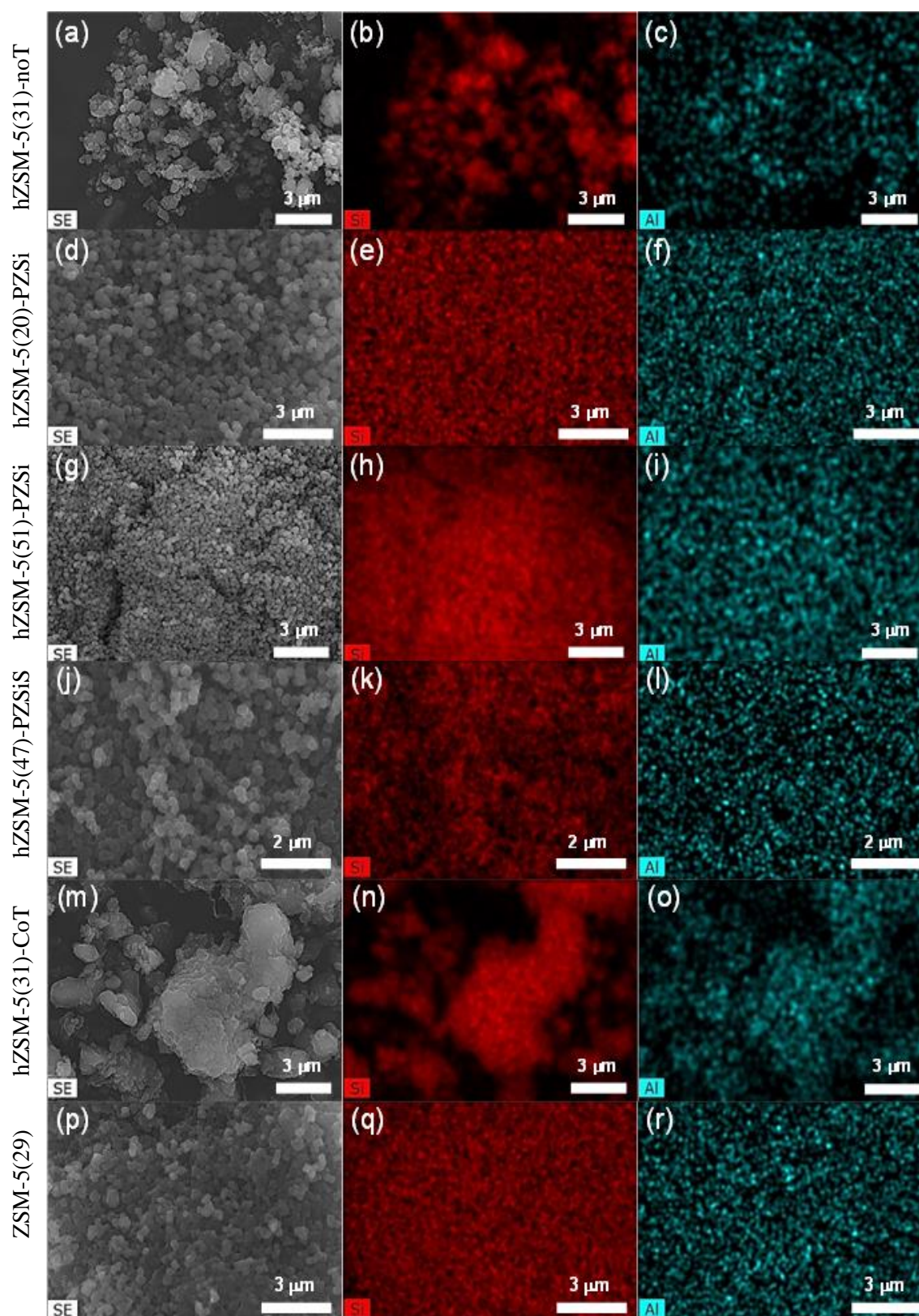


Figure 7.3. Chemical (Al, Si) mappings of ZSM-5(31)-noT (a, b, c), hZSM-5(20)-PZSi (d, e, f), hZSM-5(51)-PZSi (g, h, i), hZSM-5(47)-PZSiS (j, k, l), hZSM-5(31)-CoT (m, n, o), and ZSM-5(29) (p, q, r).

The materials were characterized at the molecular level by  $^{27}\text{Al}$  MAS NMR spectroscopy to identify the types of Al species, and FT-IR spectroscopy using pyridine as base probe to investigate the surface acidity.  $^{27}\text{Al}$  MAS NMR spectroscopy indicated that all materials exhibited a main resonance centered at *ca.* 55 ppm assignable to four-coordinated (framework) aluminum species ( $\text{Al}_{\text{tetra}}$ ), and a small resonance at *ca.* 0 ppm assignable to six-coordinated Al species ( $\text{Al}_{\text{octa}}$ ) which may be bonded or not to the framework (Figure 7.4, Table 7.3).<sup>[46]</sup> The ratio  $\text{Al}_{\text{tetra}}/\text{Al}_{\text{octa}}$  (determined *via* deconvolution of the spectra and integration of the peaks) were in the range 3-13 for the zeotypes and 16 for zeolite ZSM-5(29). The lower  $\text{Al}_{\text{tetra}}/\text{Al}_{\text{octa}}$  together with the above FT-IR spectroscopic results for the zeotypes, suggest that these may possess more defect sites than the zeolite, which may be partly associated with the reduced crystallite sizes of the zeotypes.

FT-IR spectroscopy of the dehydrated materials (self-supported samples) showed a band centered at *ca.* 3743  $\text{cm}^{-1}$ , and a shoulder at *ca.* 3730  $\text{cm}^{-1}$ , which seemed more pronounced for the zeotypes than zeolite ZSM-5(29) (Figure 7.5-A). The band at *ca.* 3743  $\text{cm}^{-1}$  is assignable to the OH stretching vibration of isolated silanol groups, and that at *ca.* 3730  $\text{cm}^{-1}$  may be due to weakly perturbed silanol groups (*e.g.*, defect sites).<sup>[44,45]</sup>

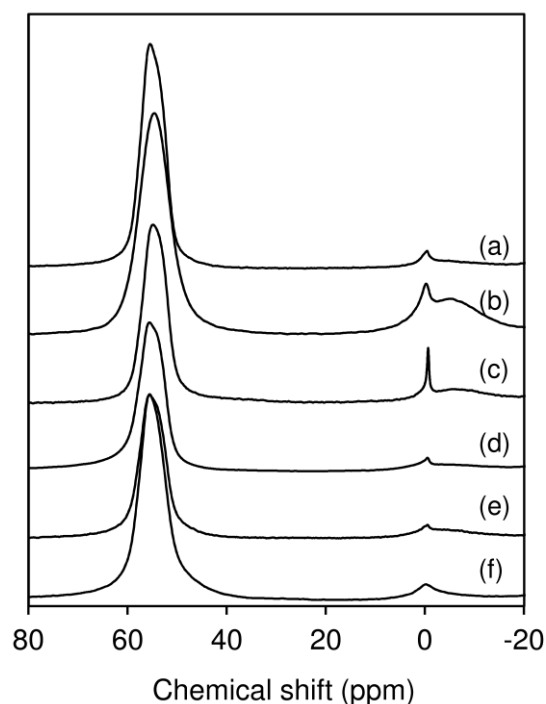


Figure 7.4.  $^{27}\text{Al}$  MAS NMR spectra for hZSM-5(31)-noT (a), hZSM-5(20)-PZSi (b), hZSM-5(51)-PZSi (c), hZSM-5(47)-PZSiS (d), hZSM-5(31)-CoT (e), and ZSM-5(29) (f).

## 1-Butene oligomerization over nanocrystalline MFI-based micro/mesoporous zeotypes synthesized *via* bottom-up approaches

The acid properties measured by FT-IR spectroscopy of adsorbed pyridine (base probe) are indicated in Table 7.3. All materials exhibited bands at  $\approx 1540$  and  $1455\text{ cm}^{-1}$  assigned to Brønsted and Lewis acid sites (Figure 7.5-B).<sup>[47]</sup> In general, the zeotypes and zeolite ZSM5(29) possessed essentially strong Lewis acid sites ( $L_{450}/L_{200}$  in the range  $\sim 0.5$ -1) and weak/moderate Brønsted acidity ( $B_{450}/B_{200} < 0.3$ ) (Table 7.3). Zeolite ZSM-5(29) possessed the higher amount of total acid sites (L+B) than the zeotypes. Of the zeotypes, hZSM-5(31)-noT and hZSM-5(20)-PZSi possessed highest (and similar) L+B ( $251$ - $252\text{ }\mu\text{mol g}^{-1}$ ). The noT and CoT protocols gave materials possessing comparable or stronger acidity to zeolite ZSM-5(29), whereas the PZSi protocol gave materials possessing weaker acidity. Changing the Si/Al ratio of the materials prepared *via* the PZSi protocol influenced L+B and the molar ratio L/B, without affecting significantly the acid strength; L+B and L/B increased with decreasing Si/Al ratio (Table 7.3). The zeotype hZSM-5(20)-PZSi possessed the highest molar ratio L/B of 1.3, compared to  $< 0.6$  for the remaining materials.

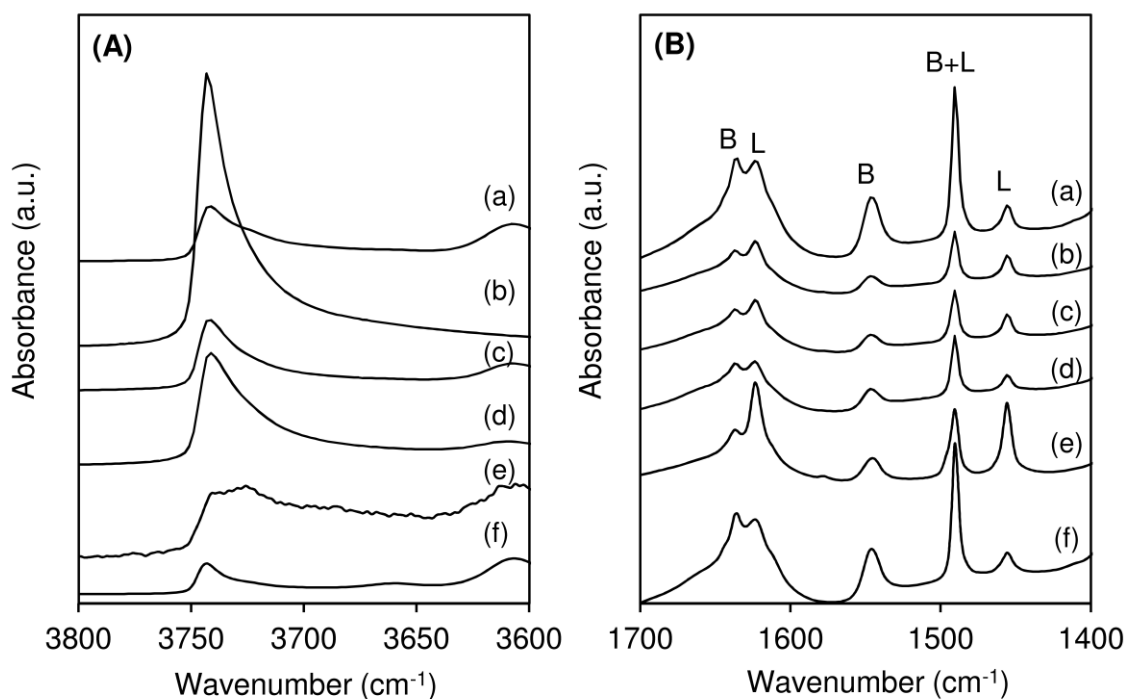


Figure 7.5. FT-IR spectra in the OH stretching region after evacuation at  $450\text{ }^{\circ}\text{C}$  (A), and FT-IR spectra of pyridine (base probe) adsorbed at  $200\text{ }^{\circ}\text{C}$  (B) for hZSM-5(31)-noT (a), hZSM-5(20)-PZSi (b), hZSM-5(51)-PZSi (c), hZSM-5(47)-PZSiS (d), hZSM-5(31)-CoT (e), and ZSM-5(29) (f).

Table 7.3. Al-species and acid properties of the MFI-based materials.

Sample	Al species <sup>[a]</sup>			Acid properties <sup>[b]</sup>		
	% Al <sub>tetra</sub>	% Al <sub>octa</sub>	L+B ( $\mu\text{mol g}^{-1}$ )	L/B	L <sub>450</sub> /L <sub>200</sub>	B <sub>450</sub> /B <sub>200</sub>
hZSM-5(31)-noT	91	9	252	0.19	1.01	0.25
hZSM-5(20)-PZSi	75	25	251	1.34	0.47	0.06
hZSM-5(51)-PZSi	81	19	132	0.59	0.61	0.04
hZSM-5(47)-PZSiS	93	7	147	0.33	0.59	0.04
hZSM-5(31)-CoT	88	12	152	0.26	1.02	0.14
ZSM-5(29)	94	6	365	0.22	0.85	0.21

<sup>[a]</sup> Determined by <sup>27</sup>Al MAS NMR spectroscopy. <sup>[b]</sup> Determined by FT-IR of pyridine adsorbed at 200 °C; B=Brønsted acid sites, L=Lewis acid sites, B+L=total amount of acid sites.

#### 7.4. Catalytic studies: general considerations

The MFI-based materials prepared *via* the bottom-up synthetic approaches were tested for the oligomerization of 1-butene (1C<sub>4</sub>), under high-pressure (30 bar) continuous-flow conditions, at 200 °C, and weight hourly space velocity (WHSV) of 2.2 g<sub>1C<sub>4</sub></sub> g<sub>cat</sub><sup>-1</sup> h<sup>-1</sup>. Previous studies using Beta type catalysts (Chapter 6) showed that these conditions were a good compromise for targeting diesel cut products with low aromatics content; and for WHSV of 2.2 g<sub>1C<sub>4</sub></sub> g<sub>cat</sub><sup>-1</sup> h<sup>-1</sup> it was verified that mass transfer limitations are avoided (section 3.6). All materials prepared were effective in converting 1-butene (1C<sub>4</sub>) to higher molar mass products. The gaseous effluent stream contained essentially unreacted 1C<sub>4</sub> and its isomers *cis*-2-butene and *trans*-2-butene. The conversion of total butenes (X<sub>C<sub>4</sub></sub>) was in the range 27-77 % (Figure 7.6 and Figure 7.8). The liquid product lump distribution (PLD) curves correspond to products possessing number of carbon atoms in the range C<sub>6</sub>-C<sub>24</sub>, i.e. products with boiling point ranges corresponding to the 170 °C cut (C<sub>6</sub>-C<sub>10</sub>) characteristic of naphtha type products (Ncut), and the 170-390 °C cut (C<sub>10</sub>-C<sub>24</sub>) characteristic of diesel type products (Dcut) (Figure 7.7). A comparative study for all materials, indicated that the zeotypes possessed different catalytic activity and led to different average space-time yields of liquid products (STY). Higher catalytic activity seemed accompanied by a greater production of higher molar mass products (Figure 7.9). In general, the zeotypes performed superiorly to commercial zeolite ZSM-5(29) (X<sub>C<sub>4</sub></sub>=27 %, STY=58 mg g<sub>cat</sub><sup>-1</sup> h<sup>-1</sup>, Figure 7.6).

1-Butene oligomerization over nanocrystalline MFI-based micro/mesoporous zeotypes synthesized *via* bottom-up approaches

The best-performing zeotype was hZSM-5(20)-PZSi, which led to  $X_{C_4}=77\%$  and  $STY=791$   $\text{mg g}_{\text{cat}}^{-1} \text{h}^{-1}$ , with the predominance of Dcut products (mass ratio of Dcut:Ncut=2.1 and  $STY_{\text{Dcut}}=534$   $\text{mg g}_{\text{cat}}^{-1} \text{h}^{-1}$ , TOS=7 h).

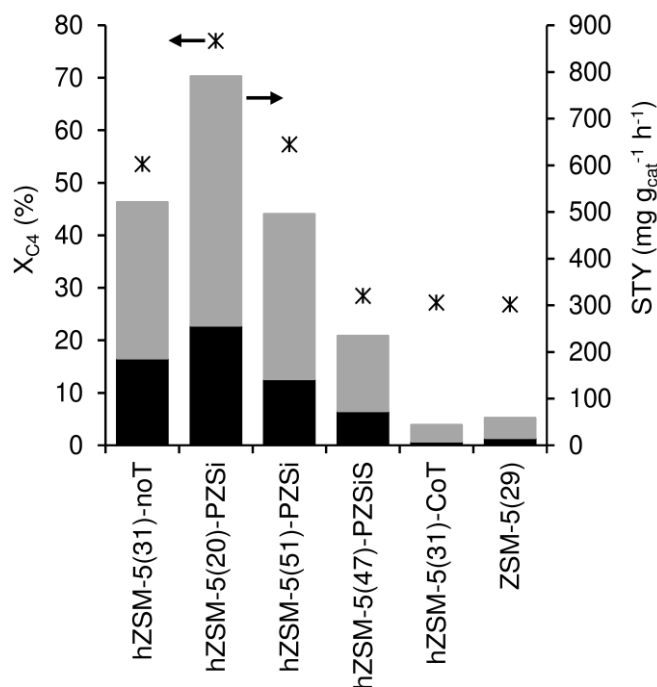


Figure 7.6. Conversion (\*) and STY (bars) of Ncut (dark colour) and Dcut (light colour) products for the MFI-based materials prepared and the benchmark catalyst ZSM-5(29). Reaction conditions: 200 °C, 30 bar,  $WHSV=2.2$   $\text{g}_{1C_4} \text{g}_{\text{cat}}^{-1} \text{h}^{-1}$ , TOS=7 h,  $T_{\text{act}}=450$  °C.

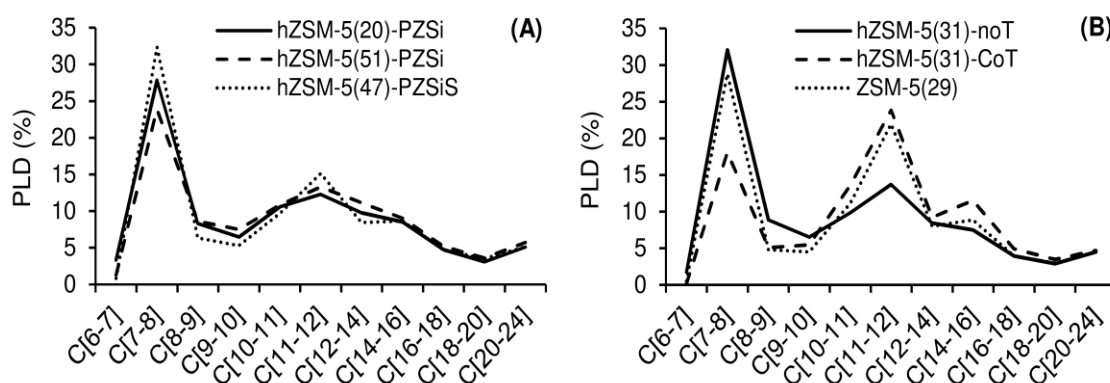


Figure 7.7. PLD profiles for the liquid products of the reaction of 1-butene in the presence of the MFI-based materials: (A) hZSM-5(20)-PZSi (solid line), hZSM-5(51)-PZSi (dashed line), hZSM-5(47)-PZSiS (dotted line), and (B) hZSM-5(31)-noT (solid line), hZSM-5(31)-CoT (dashed line), and ZSM-5(29) (dotted line). Reaction conditions: 200 °C, 30 bar,  $WHSV=2.2$   $\text{g}_{1C_4} \text{g}_{\text{cat}}^{-1} \text{h}^{-1}$ , TOS=7 h,  $T_{\text{act}}=450$  °C.

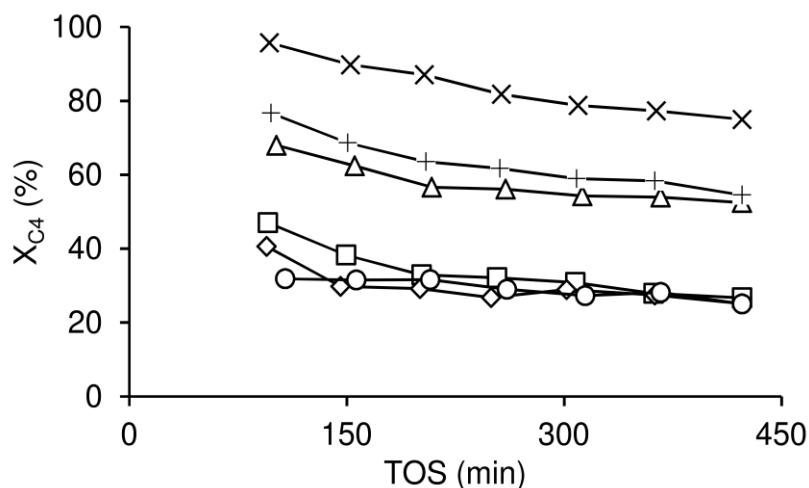


Figure 7.8. Dependence of conversion on TOS for hZSM-5(31)-noT ( $\Delta$ ), hZSM-5(20)-PZSi ( $\times$ ), hZSM-5(51)-PZSi (+), hZSM-5(47)-PZSi ( $\square$ ), hZSM-5(31)-CoT ( $\diamond$ ), and ZSM-5(29) (o). Reaction conditions: 200 °C, 30 bar, WHSV=2.2 g<sub>1C4</sub> g<sub>cat</sub><sup>-1</sup> h<sup>-1</sup>, TOS=7 h, T<sub>act</sub>=450 °C.

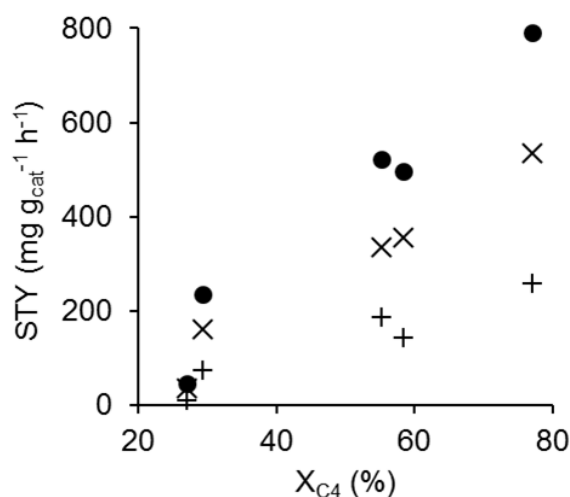


Figure 7.9. STY as a function of X<sub>C4</sub> for the MFI-based materials prepared (STY total (●), STY<sub>Dcut</sub> (x), and STY<sub>Ncut</sub> (+)). Reaction conditions: 200 °C, 30 bar, WHSV=2.2 g<sub>1C4</sub> g<sub>cat</sub><sup>-1</sup> h<sup>-1</sup>, TOS=7 h, T<sub>act</sub>=450 °C.

The overall reaction mechanism of these systems may be very complex, involving for example, primary/secondary cracking and alkylation reactions, besides isomerization (*e.g.*, double bond or methyl shifts) and oligomerization.<sup>[48]</sup> The relative amount of aromatic products (H<sub>ar</sub>) and the isoparaffinic ratio (*I*), which reflects the degree of branching of the liquid products, were determined by <sup>1</sup>H NMR spectroscopic analysis of the liquid reaction

products. For all materials,  $H_{ar} < 0.2$  %, indicating very low aromatics content. The low aromatics content and the absence of heteroatoms are advantages of light olefin oligomerization routes for synthesizing clean fuels. The  $I$  values were in the range 0.47-0.59, based on the O'Connor or Kapur methods.<sup>[49,50]</sup> These results are advantageously lower than that reported in Chapter 6 for a mesostructured zeotype based on the BEA topology ( $I \approx 0.62$ ), tested under similar 1C4 reaction conditions. An estimation of the cetane number (CN, based on the O'Connor method<sup>[49]</sup>) indicated values in the range 43-50 (noteworthy, without post-treatments such as hydrogenation that increase the CN<sup>[51]</sup>). Literature data for CN of diesel cuts produced in commercial processes, and commercial diesel samples were in the range 48-56.<sup>[20,50,52-54]</sup>

The results for the best-performing catalyst hZSM-5(20)-PZSi ( $X_{C4} = 77$  %,  $STY = 791$   $\text{mg g}_{cat}^{-1} \text{h}^{-1}$ , mass ratio  $D_{cut}/N_{cut} = 2.1$ ) compare favorably to literature data for several types of aluminosilicates, tested under similar 1C4 reaction conditions (200 °C, 30 bar): mesoporous aluminosilicates possessing amorphous pore walls (Chapter 5); versions of (large-pore) zeolite Beta such as microcrystalline or nanocrystalline zeolite Beta (Chapter 6); and a composite of BEA nanocrystals embedded in a mesoporous siliceous matrix (Chapter 6) (Table 7.4). Interesting results were reported for a hierarchical zeotype based on the BEA topology ( $T_{act} = 200$  °C) which led to  $X_{C4}$  (54 %), and  $STY$  of  $502 \text{ mg g}_{cat}^{-1} \text{h}^{-1}$ , and commercial zeolite ZSM-5 with  $Si/Al = 15$  ( $T_{act} = 450$  °C) which led to  $X_{C4} = 39$  % and  $STY = 523 \text{ mg g}_{cat}^{-1} \text{h}^{-1}$  (Chapter 6). Several studies reported 1C4 conversion over commercial ZSM-5, under different reaction conditions; one of the best results in terms of selectivity to diesel products was reported by Schwarz et al., specifically, 76 wt.% diesel selectivity at 99 % 1C4 conversion (conversion of total butenes not specified), at 270 °C, 50 bar (Table 7.4).<sup>[55]</sup> Under roughly comparable temperature and pressure conditions to those used by Schwarz et al., Li et al. reported the conversion of butene (isomer not specified), over a ZSM-5 type material synthesized hydrothermally using hemicellulose, the initiator ammonium persulphate and tetramethylethylenediamine, which led to 88 % diesel selectivity at 91 % conversion, 40 bar, 270 °C ( $WHSV = 4.8 \text{ g}_{1C4} \text{ g}_{cat}^{-1} \text{h}^{-1}$ ) (Table 7.4); this material possessed 17 %  $S_{meso}$  and 33 %  $V_{micro}$  compared to 13 %  $S_{meso}$  and 38 %  $V_{micro}$  for ZSM-5 prepared in a conventional fashion, which together with the higher amount of total acid sites of the former, led to improved catalytic performance in relation to the conventional zeolite.<sup>[56]</sup>

Table 7.4. Comparison of the catalytic results for hZSM-5(20)-PZSi (this work) to literature data, for catalysts based on the MFI topology, tested for the reaction of butene (the isomer is not always specified) using a fixed-bed reactor (includes studies where the feed was multicomponent and contained 1-butene).<sup>[a]</sup>

Catalyst (Supplier/Preparation)	Si/Al <sup>[b]</sup>	T <sub>act</sub> <sup>[c]</sup> (°C)	P <sup>[d]</sup> (bar)	T <sup>[e]</sup> (°C)	WHSV (h <sup>-1</sup> )	Substrate <sup>[f]</sup> (%)	Diluent <sup>[g]</sup>	Conversion of C4 substrates <sup>[h]</sup> (TOS)	Selectivity (%) <sup>[i]</sup>		Ref.
									C10 <sup>-</sup>	C10 <sup>+</sup>	
hZSM-5(20)-PZSi	20	450	30	200	2.2	15 (mol.) 26 (wt.)	N <sub>2</sub>	X <sub>C4</sub> =75 % (7 h) X <sub>1C4</sub> =96 % (7 h)	46 (mol.)	54	Chapter 7
ZSM-5 (Synthesized)	25	500	40	270	4.8	ns	N <sub>2</sub>	X <sub>C4</sub> =91 % (24 h)	12 (ns %)	88	[56]
ZSM-5 (Zeolyst)	40	500	24	225	245	90 (mol.)	N <sub>2</sub>	X <sub>C4</sub> =3 % (6 h)	86 (mol.)	8	[24]
ZSM-5 (Zeolyst)	15	450	1	200	13.5	50 (mol.)	N <sub>2</sub>	X <sub>1C4</sub> =10 % (21 min)	33 (wt.) <sup>[j]</sup>	37 <sup>[j]</sup>	[57]
ZSM-5 (Shanghai Xinnian Chem.)	30 160	450	10	350	2	40 (wt.)	butane+ propane	X <sub>(1C4+2C4)</sub> =33 % (8 h) X <sub>(1C4+2C4)</sub> =58 % (8 h)	98 (wt.) 4.2 (wt.)	25.8	[58]
ZSM-5 (synthesized)	40	ns	50	270	12	99.5 (wt.)	-	X <sub>1C4</sub> =99 % (10h)	24 (wt.) <sup>[k]</sup>	76 <sup>[k]</sup>	[55]
ZSM-5 (Zeolyst)	15	200	30	200	2.2	15 (mol.) 26 (wt.)	N <sub>2</sub>	X <sub>C4</sub> =23 % (8 h) X <sub>1C4</sub> =90 % (8 h)	44 (mol.)	56	Chapter 5
ZSM-5 (Zeolyst)	40	ns	15	300	ns	77 (n.s %)	butanes	X <sub>C4</sub> =98 % (ns)	85 (wt.) <sup>[l]</sup>		[59]
ZSM-5 (Zeolyst- modified)	40	ns	15	300	ns	77 (n.s %)	butanes	X <sub>C4</sub> =96 % (8 h)	89 (wt.) <sup>[l]</sup>		[59]
ZSM-5 (Synthesized)	29	550	15	300	3.3	77 (n.s %)	butanes	X <sub>C4</sub> =75 % (4.2 h)	78 (mol.)	22	[60]
ZSM-5 (Zeolyst)	30	ns	1	300	ns	30 (mol.)	N <sub>2</sub>	X <sub>1C4</sub> =68 (25 min)	ns	ns	[61]
Ferrierite (Zeolyst)	10	500	6.9	200	0.03	2 (mol.)	He	X <sub>C4</sub> =19; X <sub>1C4</sub> =91 (10h)	60 (mol.)	8.5	[62]
	10	500	6.9	250	0.03	2 (mol.)	He	X <sub>C4</sub> =77; X <sub>1C4</sub> =96 (10h)	50 (mol.)	4	[62]
Beta/15-20 wt.% clay (Guild Associates)	17	500	24	225	85	90 (mol.)	N <sub>2</sub>	X <sub>C4</sub> =9 % (6 h)	80 (mol.)	12	[24]

Table 7.4. (continued)

Catalyst (Supplier/Preparation)	Si/Al <sup>[b]</sup>	T <sub>act</sub> <sup>[c]</sup> (°C)	P <sup>[d]</sup> (bar)	T <sup>[e]</sup> (°C)	WHSV (h <sup>-1</sup> )	Substrate <sup>[f]</sup> (%)	Diluent <sup>[g]</sup>	Conversion of C <sub>4</sub> substrates <sup>[h]</sup> (TOS)	Selectivity (%) <sup>[i]</sup>		Ref.
									C10 <sup>-</sup>	C10 <sup>+</sup>	
Beta (Shanghai Xinnian Chem.)	16	450	10	350	2	40 (wt.%) (1C4+2C4)	butane+ propane	X <sub>(1C4+2C4)</sub> =69 % (8 h)	69 (wt.%)	31	[58]
Hierarchical Beta	25	200	30	200	2.2	15 (mol.%) 26 (wt.%)	N <sub>2</sub>	X <sub>C4</sub> =54 % (8 h) X <sub>1C4</sub> =94 % (8 h)	48 (mol.%)	52	Chapter 6
Mesoporous Al-TUD-1	18	450	30	200	2.2	15 (mol.%) 26 (wt.%)	N <sub>2</sub>	X <sub>C4</sub> =33 % (8 h) X <sub>1C4</sub> =89 % (8 h)	54 (mol.%)	46	Chapter 5

<sup>[a]</sup> ns=information not specified in the literature. Some of the values of conversion and selectivity were calculated from the data given (in the form of graphical figures or tables) in the reported study, and are approximate values. <sup>[b]</sup> Molar ratio Si/Al. <sup>[c]</sup> T<sub>act</sub> prior to the catalytic reaction. <sup>[d]</sup> Pressure of the catalytic reaction. <sup>[e]</sup> Temperature of the catalytic reaction. <sup>[f]</sup> Amount of substrate in the feed stream. The mol.% or wt.% basis is indicated in parenthesis. <sup>[g]</sup> Diluent in the feed stream. <sup>[h]</sup> Conversion of butenes (1C4=1butene; 2C4=2-butene). The values in parenthesis correspond to the TOS for which conversion was calculated. <sup>[i]</sup> Selectivity to C10<sup>-</sup> or C10<sup>+</sup> products. The mol.% or wt.% basis is indicated in the C10<sup>-</sup> column in parenthesis. <sup>[j]</sup> The values correspond to C8<sup>-</sup> and C8<sup>+</sup> products. <sup>[k]</sup> Selectivity to C12<sup>-</sup> or C12<sup>+</sup> products. <sup>[l]</sup> The values correspond to C5<sup>+</sup> products.

## 7.5. Influence of material properties on the catalytic performance

Conversion followed the order ( $X_{C4}$ ): hZSM-5(31)-CoT (27 %)  $\approx$  hZSM-5(47)-PZSiS (28 %) < hZSM-5(31)-noT (54 %)  $\approx$  hZSM-5(51)-PZSi (57 %) < hZSM-5(20)-PZSi (77 %). On the other hand, the total STY followed the order ( $\text{mg g}_{\text{cat}}^{-1} \text{h}^{-1}$ ): hZSM-5(31)-CoT (43) < hZSM-5(47)-PZSiS (235) < hZSM-5(51)-PZSi (496) < hZSM-5(31)-noT (521) < hZSM-5(20)-PZSi (791). Direct relationships between the catalytic activity and the textural or acid properties could not be clearly established considering all materials at once. The catalytic performance may result from complex interplay of several properties including morphology, texture and acidity, which, in turn, depend on the synthesis protocol. It is important to reduce the number of variables in comparative studies to gain insights into structure-activity relationships. The materials prepared *via* the protocols CoT and noT possess the same molar ratio Si/Al (31) and roughly comparable  $S_{\text{meso}}$  (140 and 168  $\text{m}^2 \text{g}^{-1}$ , respectively), Table 7.2. Yet, their catalytic performances were very different, with hZSM-5(31)-noT performing far superiorly to hZSM-5(31)-CoT;  $X_{C4}$  of 54 and 27 %, and STY of 522 and 43  $\text{mg g}_{\text{cat}}^{-1} \text{h}^{-1}$ , respectively. Zeotype hZSM-5(31)-noT possessed more regular morphology (Figure 7.2), lower  $V_{\text{micro}}$  and higher amount of acid sites (Table 7.3) than hZSM-5(31)-CoT, which may result in a higher amount of effective (accessible) active sites in the former case, favoring the oligomerization reaction.

Zeolite ZSM-5(29) possessed highest amount of acid sites, albeit its catalytic activity was similar to the least active material prepared namely hZSM-5(31)-CoT. The larger crystallite sizes (micron range) and relatively low  $S_{\text{meso}}$  of ZSM-5(29) may account for longer diffusional pathways and important steric hindrance effects. Hence, nanocrystallinity, mesoporosity and regular morphology seem important features to meet superior catalytic performances.

The materials based on the PZSi synthetic approach were consisted of pseudo-spherical aggregates of nanocrystalites of 10-60 nm in size, and possessed comparable  $V_p$ ,  $V_{\text{micro}}$  and  $S_{\text{meso}}$  (275-308  $\text{m}^2 \text{g}^{-1}$ ) and acid strengths. However, their catalytic performances were different, which seemed to be related to the relative amount of Lewis acid sites. Specifically,  $X_{C4}$  and STY increased with L/B, being highest for hZSM-5(20)-PZSi (Figure

7.10). Thus, the Lewis acidity seems favorable for the catalytic reaction. These results are in agreement with literature data for the oligomerization of C4 olefins; *e.g.*, 1C4 conversion over zeotypes possessing BEA topology (Chapter 6), and isobutene conversion over commercial zeolite Beta,<sup>[63]</sup> dealuminated zeolite Y or zeolite Y-supported AlCl<sub>3</sub><sup>[34,64]</sup>. Since the material properties requirements may be different for olefins of different carbon chain lengths,<sup>[29]</sup> comparisons have been restricted to C4 olefins. The post-synthesis surfactant treatment of hZSM-5(51)-PZSi gave hZSM-5(47)-PZSiS, which did not lead to improved X<sub>C4</sub> or STY (Figure 7.6); these results may be partly due to the lower L/B of hZSM-5(47)-PZSiS (Table 7.3).

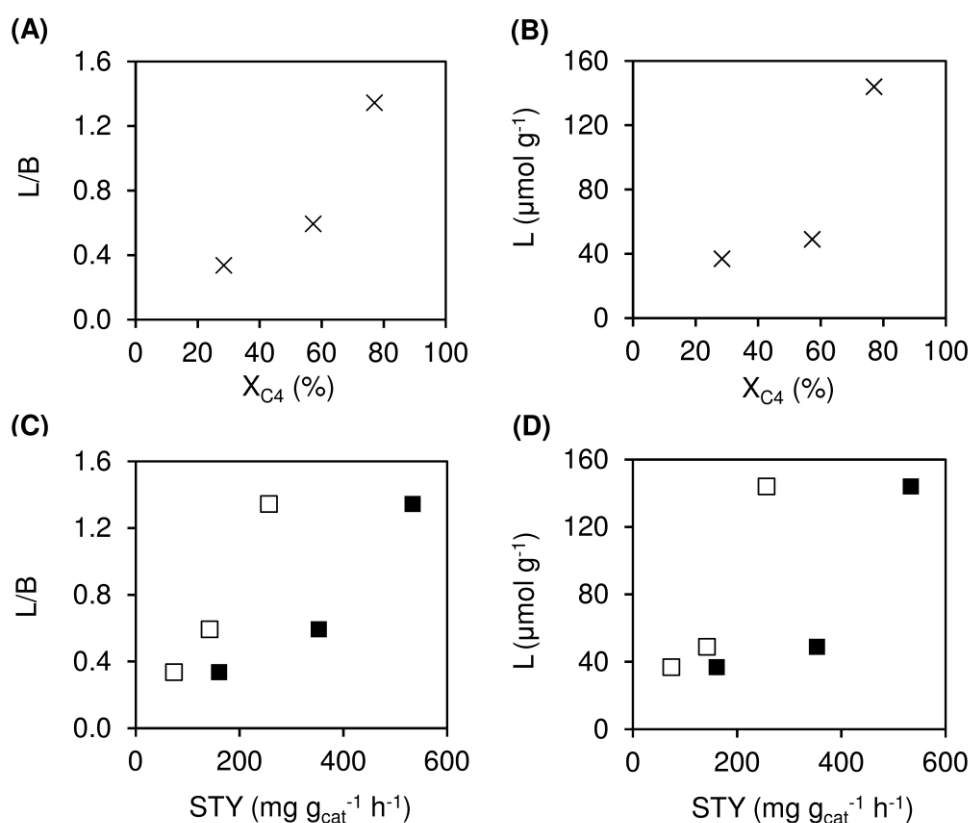


Figure 7.10. Influence of the acid properties measured at 200 °C on X<sub>C4</sub> (x), (a, b), STYDcut (■) and STYNeut (□) (c, d), for the catalysts prepared according to the PZSi(S) protocols, namely hZSM-5(20)-PZSi, hZSM-5(51)-PZSi, and hZSM-5(47)-PZSiS. Reaction conditions: 200 °C, 30 bar, WHSV=2.2 g<sub>1C4</sub> g<sub>cat</sub><sup>-1</sup> h<sup>-1</sup>, TOS=7 h, T<sub>act</sub>=450 °C.

Overall, the noT and PZSi synthetic strategies seem promising for preparing zeotype catalysts for olefin oligomerization. One of the parameters that may be varied in all synthesis protocols is the Si/Al ratio, which may influence the acid properties of the final materials. The material prepared *via* the noT protocol (Si/Al=31) possessed intermediate Si/Al ratio of the two PZSi based materials (20-51). Nevertheless, hZSM-5(31)-noT resembled somewhat closely the catalytic performance of hZSM-5(51)-PZSi and was outperformed by hZSM-5(20)-PZSi. The PZSi protocol seems to advantageously give materials with enhanced L/B ratio and  $S_{\text{ext,meso}}$  for butene oligomerization.

## 7.6. Influence of the reaction conditions

The most active catalyst hZSM-5(20)-PZSi was further tested under different reaction conditions (Table 7.5). The catalyst activation temperature ( $T_{\text{act}}$ ) of 200 °C or 450 °C prior to the oligomerization reaction led to comparable catalytic results (similar  $X_{C_4}$  and STY at 200 °C, 30 bar).

Table 7.5. Influence of the catalyst activation temperature ( $T_{\text{act}}$ ) and reaction conditions (T, P) on the catalytic reaction.

Conditions			$X_{C_4}$ (%)	STY (mg g <sup>-1</sup> h <sup>-1</sup> )			Dcut/Ncut
$T_{\text{act}}$ (°C)	T (°C)	P (bar)		Ncut	Dcut	Total	
200	200	30	77	272	543	815	2.0
450	200	30	77	257	534	791	2.1
450	250	30	87	414	611	1025	1.5
450	250	40	97	408	669	1077	1.6

Different results were reported in the literature for micro-mesoporous zeotypes based on the BEA topology, for which higher  $T_{\text{act}}$  led to poorer catalytic results;  $T_{\text{act}}$  may affect the coordination environment (and configuration) of the Al species of the BEA framework (Chapter 5). Conversion and STY increased with increasing reaction temperature from 200

to 250 °C, whereas the mass ratio  $D_{cut}/N_{cut}$  decreased from 2.1 to 1.5. Hence, while the total productivity may be favored by increasing the temperature, albeit the relative amount of  $D_{cut}$  products decreases, which is consistent with the fact that the oligomerization reaction is exothermic. Increasing the reaction pressure from 30 to 40 bar led to enhanced  $X_{C4}$  (87 and 97 %, respectively) and  $STY_{D_{cut}}$  (611 and 669  $mg\ g_{cat}^{-1}\ h^{-1}$ , respectively) at 250 °C. These results are consistent with the fact that oligomerization leads to reduction in the total number of molecules in the reaction system, and thus may be favored with increased pressure.

## 7.7. Catalyst stability

The catalyst stabilities of hZSM-5(20)-PZSi and hZSM-5(51)-PZSi were investigated, and compared to zeolite ZSM-5(29), at 200 °C, 30 bar and WHSV of 2.2  $g_{1C4}\ g_{cat}^{-1}\ h^{-1}$ . The originally pristine white solid catalysts turned brown in color after the catalytic reaction. The carbon content of the washed/dried catalysts was *ca.* 13 wt.% C (based on elemental analysis). DSC analysis of the used catalysts under air atmosphere indicated an endothermic process occurring at temperature lower than 200 °C, which was likely the desorption of physisorbed water and other volatiles (exemplified for hZSM-5(20)-PZSi in Figure 7.11). Additionally, an exothermic process with an onset at *ca.* 280 °C occurred for the used catalysts, but not for the unused ones. The exothermic process was likely the combustion of coke deposits. The catalysts were regenerated by the thermal treatment at 550 °C and turned off-white in color, suggesting that most of the coke was removed, as could be verified by DSC (Figure 7.11).

The regenerated catalysts were characterized in what regards the morphology (SEM, TEM), composition (EDS), crystal structure (PXRD), textural properties ( $N_2$  adsorption), surface Al species ( $^{27}Al$  MAS NMR) and acid properties (FT-IR spectroscopy of adsorbed pyridine). For the three catalysts, the MFI crystalline structure was essentially preserved during the catalytic process (Figure 7.12-A), and the morphology (Figure S7.2) and textural properties remained similar (Table 7.6).

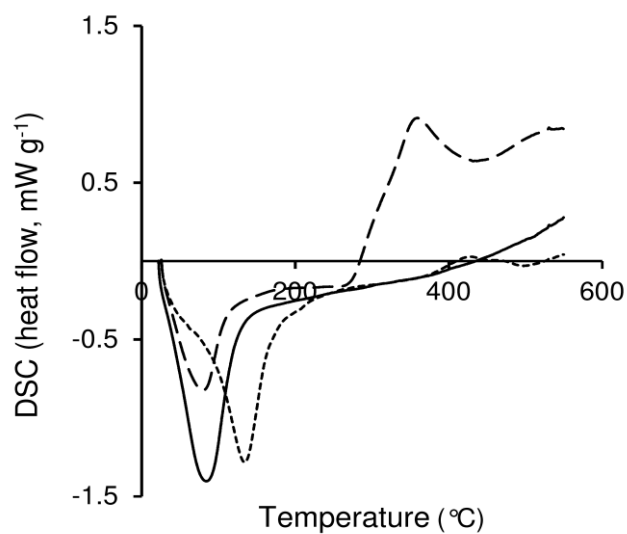


Figure 7.11. DSC curves for hZSM-5(20)-PZSi (solid line), and the respective used solid after washing and drying (dashed line) or after calcination at 550 °C to remove the organic matter from the solid catalyst (dotted line). Reaction conditions: 200 °C, 30 bar, WHSV=2.2 g<sub>1C4</sub> g<sub>cat</sub><sup>-1</sup> h<sup>-1</sup>, TOS=7 h, T<sub>act</sub>=450 °C.

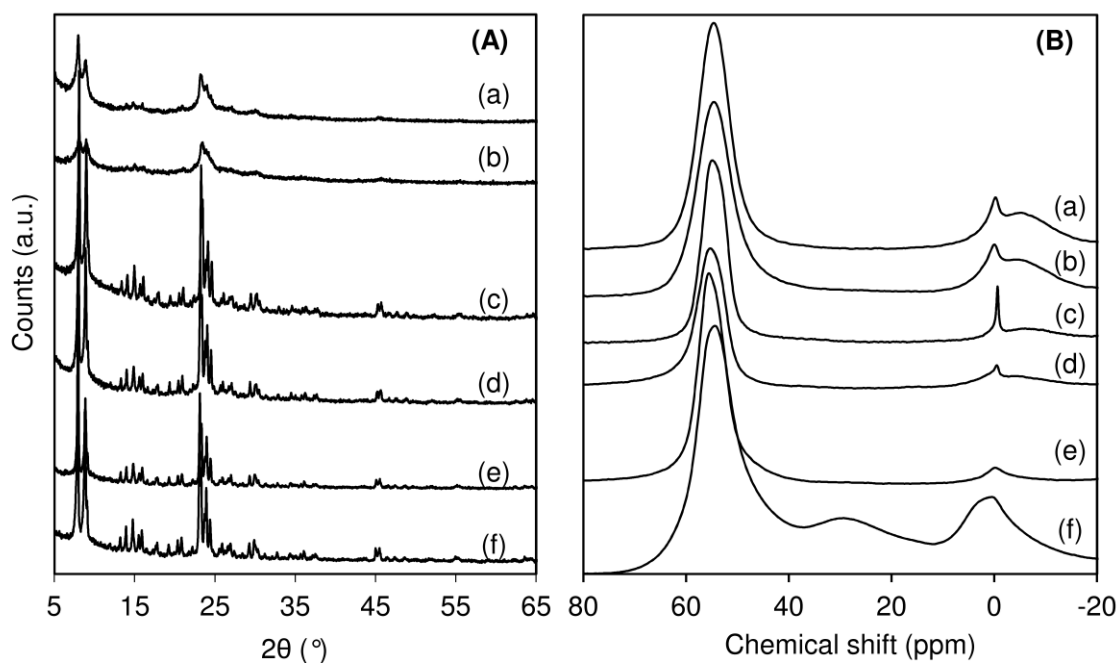


Figure 7.12. PXRD patterns (A) and <sup>27</sup>Al MAS NMR spectra (B) for hZSM-5(20)-PZSi (fresh (a); used (b)), hZSM-5(51)-PZSi (fresh (c); used (d)), and ZSM-5(29) (fresh (e); used (f)).

Table 7.6. Elemental analyses and textural properties of the original and used MFI-based materials.<sup>[a]</sup>

Sample	Si/Al <sup>[a]</sup>	Textural properties				
		S <sub>BET</sub> (m <sup>2</sup> g <sup>-1</sup> )	S <sub>meso</sub> <sup>[b]</sup>	V <sub>p</sub> (cm <sup>3</sup> g <sup>-1</sup> )	V <sub>micro</sub> <sup>[c]</sup>	D <sub>p</sub> <sup>[d]</sup> (nm)
hZSM-5(20)-PZSi	20	721	308	0.74	0.09	2-5
	(21)	(713)	(350)	(0.86)	(0.07)	(2-5)
hZSM-5(51)-PZSi	51	558	289	0.77	0.07	2-7
	(49)	(528)	(278)	(0.73)	(0.06)	(2-5)
ZSM-5(29)	29	334	97	0.47	0.17	-
	(17)	(386)	(85)	(0.68)	(0.15)	-

<sup>[a]</sup> Molar ratio determined by EDS (values in parenthesis are for the used catalysts). <sup>[b]</sup> External/mesoporous specific surface area. <sup>[c]</sup> Micropore volume (calculated for  $p/p_0 \approx 0.99$ ). <sup>[d]</sup> Mesopore size range. For all materials, the micropore size distribution (based on DFT) indicated a median pore size in the range 0.55-0.57 nm (values in parenthesis are for the used catalysts).

For the zeotypes, the Si/Al ratio remained roughly constant, and molecular level characterization studies indicated the predominance of Al<sub>tetra</sub> species and comparable L/B ratio (Table 7.7). The most pronounced difference was slight decrease of L+B for the used catalyst hZSM-5(20)-PZSi. The commercial zeolite ZSM-5(29) suffered drop in the Si/Al ratio, %Al<sub>tetra</sub> and L+B, which was accompanied by the appearance of five-coordinated Al species (band at *ca.* 25 ppm due to Al<sub>penta</sub>) (Figure 7.12-B) and slight increase in L/B. Based on the results regarding the material properties, the zeotypes seemed more stable than the zeolite.

The catalysts were used for two consecutive 7 h on-stream cycles, with an intermediate step of catalyst regeneration, consisting of washing the catalyst several times, with dichloromethane, drying at 60 °C overnight, and calcination at 600 °C for 6 h (heating rate of 1 °C min<sup>-1</sup>). From the first to the second cycle it was verified partial catalyst deactivation, which was more pronounced for the zeotypes (X<sub>C4</sub> at TOS=7 h decreased by a factor of *ca.* 1.44) than ZSM-5(29) (X<sub>C4</sub> decreased by a factor of *ca.* 1.4) (Figure 7.13). The drop in activity for ZSM-5(29) somewhat correlates with the changes in surface Al<sub>tetra</sub> species and acid properties of the use catalyst (discussed above). For the zeotypes, the partial catalyst deactivation does not correlate with the characterization results, which indicated that

the physicochemical properties of the materials were fairly well preserved, especially in the case of hZSM-5(51)-PZSi.

Table 7.7. Al-species and acid properties of the original and used MFI-based materials.

	Al species <sup>[a]</sup>		Acid properties <sup>[b]</sup>			
	% Al <sub>tetra</sub>	% Al <sub>octa</sub>	L+B ( $\mu\text{mol g}^{-1}$ )	L/B	L <sub>450</sub> /L <sub>200</sub>	B <sub>450</sub> /B <sub>200</sub>
hZSM-5(20)-PZSi	75 (75)	25 (25)	251 (188)	1.34 (1.65)	0.47 (0.39)	0.06 (0)
hZSM-5(51)-PZSi	81 (97)	19 (3)	132 (138)	0.59 (0.61)	0.61 (0.62)	0.04 (0.06)
ZSM-5(29)	94 (57) <sup>[c]</sup>	6 (22)	365 (202)	0.22 (0.64)	0.85 (0.48)	0.21 (0.16)

<sup>[a]</sup> Determined by <sup>27</sup>Al MAS NMR spectroscopy (values in parenthesis are for the used catalysts). <sup>[b]</sup> Determined by FT-IR of pyridine adsorbed at 200 °C; B=Brønsted acid sites, L=Lewis acid sites, B+L=total amount of acid sites (values in parenthesis are for the used catalysts). <sup>[c]</sup> Five-coordinated Al species were formed (band at *ca.* 25 ppm in the <sup>27</sup>Al MAS NMR spectrum).

The MFI based materials possess crystallographically different Al species, for which the intrinsic activity and stability may be different. Molecular-level changes may occur during the catalytic process, which are difficult to track by the characterization studies of the solids recovered after the catalytic reaction. Although the original and used zeotypes exhibited similar <sup>27</sup>Al MAS NMR spectra, it is important to consider that there may exist “NMR-invisible” Al species.<sup>[65–67]</sup> Woolery et al. reported for MFI zeolites that treatment at high temperature may lead to the hydrolysis of Al-O bonds (*e.g.*, less stable Al species subjected to local stress in a confined environment) and the formation of “NMR-invisible” Al species of Lewis type.<sup>[46]</sup> The extent of the hydrolysis of the framework species may increase with temperature.<sup>[65]</sup> Accordingly, the reaction conditions and the temperature distribution along the catalytic bed may affect the catalyst stability. The Al<sub>tetra</sub> species may undergo hydrolysis to give framework-bonded Al<sub>octa</sub> species; the latter may react reversibly to give Al<sub>tetra</sub> species by the interaction with base molecules such as pyridine, which was used as probe for measuring the acid properties.<sup>[65]</sup> Hence, although the molecular-level characterization studies based on the spectroscopic techniques <sup>27</sup>Al MAS NMR and FT-IR

1-Butene oligomerization over nanocrystalline MFI-based micro/mesoporous zeotypes synthesized *via* bottom-up approaches

of adsorbed pyridine gave similar results for the original and used hZSM-5(51)-PZSi catalysts, for example, this does not rule out the possibility of occurring in situ changes of surface species; it is not trivial to track these possible modifications, and assess the intrinsic activities and relative amounts of the in situ modified surface species in order to study their influence on the catalytic reaction.

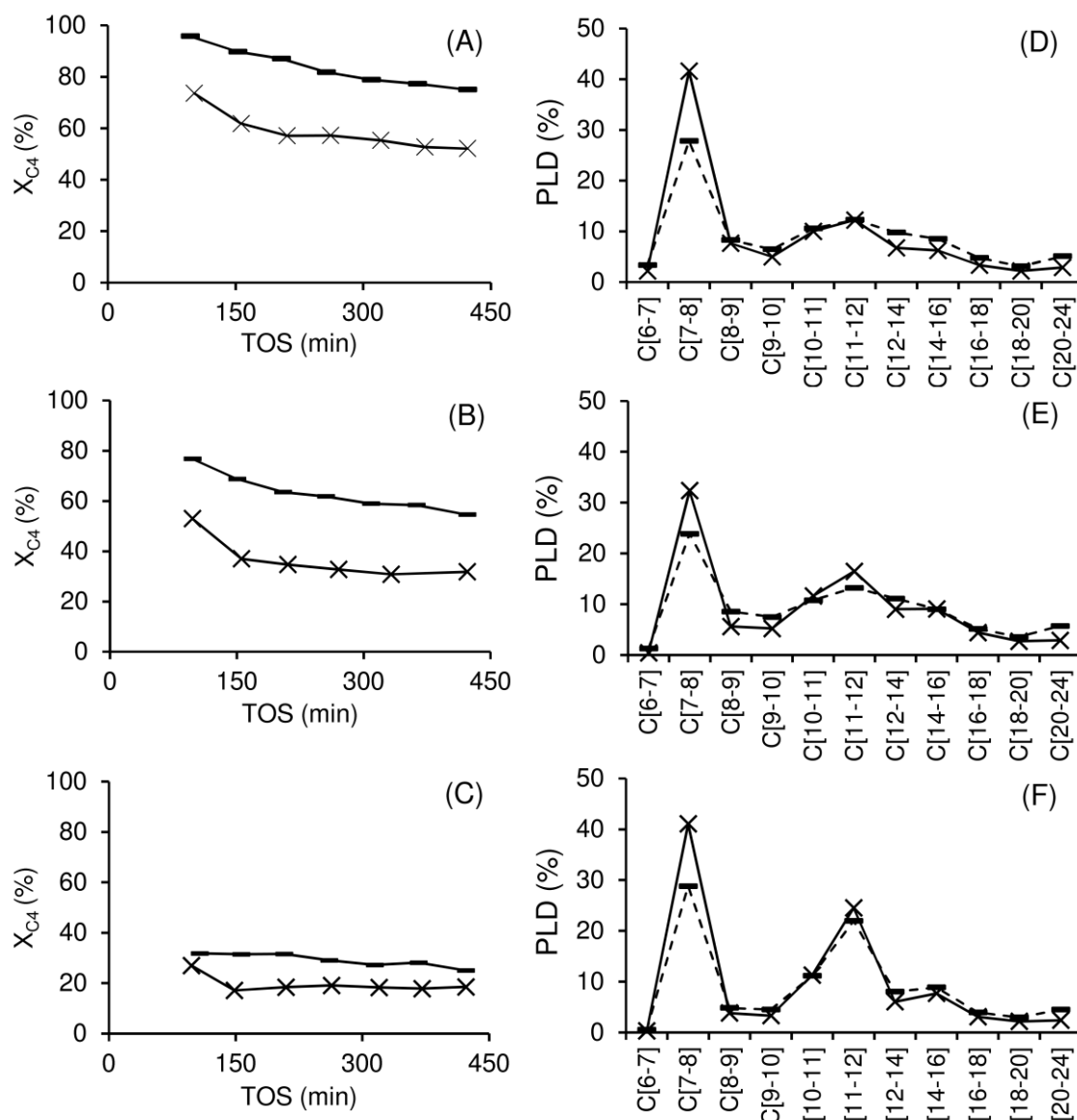


Figure 7.13. Dependence of conversion ( $X_{C_4}$ ) on TOS for hZSM-5(20)-PZSi (A), hZSM-5(51)-PZSi (C) and ZSM-5(29) (E) in the first (-) and second cycle using the regenerated catalyst (x). PLD curves for the two cycles (with matching symbols) for hZSM-5(20)-PZSi (B), hZSM-5(51)-PZSi (D), and ZSM-5(29) (F).

## 7.8. Conclusions

Non-destructive bottom-up synthetic approaches led to MFI-based zeotype catalysts with favorable morphological, textural and acid properties for olefin oligomerization to higher molar mass products, under high-pressure continuous-flow conditions. In general, the zeotypes consisting of morphologically regular aggregates of nanocrystallites and possessing mesoporosity outperformed microcrystalline zeolite ZSM-5 in 1-butene oligomerization, at 200 °C, 30 bar (even though the zeolite possessed the highest amount of total acid sites). The best performing zeotype was hZSM-5(20)-PZSi (Si/Al=20), prepared *via* the Serrano et al. strategy (PZSi) based on the crystallization of silanized protozeolitic units; 77 % conversion of butenes, average space time yield of liquid products of 791 mg  $g_{\text{cat}}^{-1} \text{ h}^{-1}$  (7 h on-stream) and mass ratio  $D_{\text{cut}}/N_{\text{cut}}=2$ . These results compared favorably to literature data for several aluminosilicates tested under similar 1-butene oligomerization reaction conditions. The materials prepared *via* the PZSi approach seemed to benefit from enhanced mesoporosity and L/B ratio for butene oligomerization.

Characterization studies indicated that the morphology, structure, composition, textural and acid properties of the zeotypes were essentially preserved during the catalytic reaction and the catalyst regeneration processes. Molecular-level characterization of the zeotypes and the zeolite, suggested superior stability of the former in what concerns the Al-species and acid properties. However, partial drop in catalytic activity was verified for the regenerated catalysts, possibly due to changes in surface chemical properties occurring *in situ*, under the operating conditions. It is not trivial to track these changes by characterization studies of the catalysts recovered after the reaction. While envisaging zeotypes as promising catalysts for olefin oligomerization, important future challenges include *in situ* high temperature characterization studies to track possible changes in surface chemical species occurring under the operating conditions, and gain more insights into effective structure-activity relationships, which may aid in the improvement of material properties to meet superior performances.

## 7.9. References

- [1] E. Kriván, I. Valkai, J. Hancsók, Investigation of production of motor fuel components on heterogeneous catalyst with oligomerization, *Top Catal.* 56 (2013) 831–838.
- [2] G. Bellussi, F. Mizia, V. Calemma, P. Pollesel, R. Millini, Oligomerization of olefins from Light Cracking Naphtha over zeolite-based catalyst for the production of high quality diesel fuel, *Microporous Mesoporous Mater.* 164 (2012) 127–134.
- [3] M.A. Maseloane, Dimerization of naphtha-range Fischer-Tropsch olefins into diesel-range products over zeolite H-ZSM-5 and amorphous silica-alumina, University of Cape Town, 2011.
- [4] A. De Klerk, Distillate production by oligomerization of Fischer-Tropsch olefins over solid phosphoric acid, *Energy & Fuels* 20 (2006) 439–445.
- [5] J.Q. Bond, D.M. Alonso, D. Wang, R.M. West, J.A. Dumesic, Integrated catalytic conversion of  $\gamma$ -valerolactone to liquid alkenes for transportation fuels, *Science* 327 (2010) 1110–1114.
- [6] J.Q. Bond, A.A. Upadhye, H. Olcay, G.A. Tompsett, J. Jae, R. Xing, D.M. Alonso, D. Wang, T. Zhang, R. Kumar, A. Foster, S.M. Sen, C.T. Maravelias, R. Malina, S.R.H. Barrett, R. Lobo, C.E. Wyman, J. a. Dumesic, G.W. Huber, Production of renewable jet fuel range alkanes and commodity chemicals from integrated catalytic processing of biomass, *Energy Environ. Sci.* 7 (2014) 1500–1523.
- [7] D.M. Alonso, J.Q. Bond, J.C. Serrano-Ruiz, J.A. Dumesic, Production of liquid hydrocarbon transportation fuels by oligomerization of biomass-derived C<sub>9</sub> alkenes, *Green Chem.* 12 (2010) 992–999.
- [8] C.P. Nicholas, Applications of light olefin oligomerization to the production of fuels and chemicals, *Appl. Catal. A Gen.* 543 (2017) 82–97.
- [9] A. Corma, S. Iborra, Oligomerization of Alkenes, in: *E.G., Derouane (Ed.), Catalysts for fine chemical synthesis, Volume 4, Microporous mesoporous solid catalysts*, John Wiley & Sons, 2006: pp. 125–140.
- [10] J. Weitkamp, Zeolites and catalysis, *Solid State Ionics* 131 (2000) 175–188.
- [11] P.M.M. Blauwhoff, J.W. Gosselink, E.P. Kieffer, S.T. Sie, W.H.J. Stork, Zeolites as catalysts in industrial processes, in: J. Weitkamp, L. Puppe (Eds.), *Catalysis and zeolites: fundamentals and applications*, Springer Berlin Heidelberg, Berlin, Heidelberg, 1999: pp. 437–538.
- [12] J. Cejka, H. van Bekkum, *Zeolites and ordered mesoporous materials: progress and prospects*, Volume 157, 1<sup>st</sup> ed., Elsevier Science, 2005.
- [13] A. Corma, From microporous to mesoporous molecular sieve materials and their use in catalysis, *Chem. Rev.* 97 (1997) 2373–2420.
- [14] B. Chiche, E. Sauvage, F. Di Renzo, I.I. Ivanova, F. Fajula, Butene oligomerization over mesoporous MTS-type aluminosilicates, *J. Mol. Catal. A Chem.* 134 (1998) 145–157.
- [15] J.P.G. Pater, P.A. Jacobs, J.A. Martens, Oligomerization of hex-1-ene over acidic aluminosilicate zeolites, MCM-41, and silica-alumina co-gel catalysts: a comparative study, *J. Catal.* 184 (1999) 262–267.
- [16] Y. Tao, H. Kanoh, L. Abrams, K. Kaneko, Mesopore-modified zeolites: preparation, characterization, and applications, *Chem. Rev.* 106 (2006) 896–910.
- [17] J.T.F. Degnan, Applications of zeolites in petroleum refining, *Top. Catal.* 13 (2000) 349–356.

- [18] N. V. Choudary, B.L. Newalkar, Use of zeolites in petroleum refining and petrochemical processes: recent advances, *J. Porous Mater.* 18 (2011) 685–692.
- [19] S.A. Tabak, A.A. Avidan, F.J. Krambeck, Production of synthetic gasoline and diesel fuel from non-petroleum resources, *Am. Chem. Soc., Div. Fuel Chem.* 31 (1986) 293–299.
- [20] C. Knottenbelt, Mossgas “gas-to-liquid” diesel fuels - An environmentally friendly option, *Catal. Today* 71 (2002) 437–445.
- [21] R.O. Minnie, Catalytic conversion of olefins to diesel and gasoline fuel, WO 2006091986 A1, 2006.
- [22] A. de Klerk, E. Furimsky, Catalysis in the upgrading of Fischer–Tropsch syncrude, in: *Catalysis in the refining of Fischer–Tropsch syncrude*, 2010: pp. 40–164.
- [23] A. V. Lavrenov, T.R. Karpova, E.A. Buluchevskii, E.N. Bogdanets, Heterogeneous oligomerization of light alkenes: 80 years in oil refining, *Catal. Ind.* 8 (2016) 316–327.
- [24] M.J. Wulfers, R.F. Lobo, Assessment of mass transfer limitations in oligomerization of butene at high pressure on H-beta, *Appl. Catal. A Gen.* 505 (2015) 394–401.
- [25] D.P. Serrano, J.M. Escola, P. Pizarro, Synthesis strategies in the search for hierarchical zeolites, *Chem. Soc. Rev.* 42 (2013) 4004–35.
- [26] R. Chal, C. Gérardin, M. Bulut, S. van Donk, Overview and industrial assessment of synthesis strategies towards zeolites with mesopores, *ChemCatChem* 3 (2011) 67–81.
- [27] K. Zhu, X. Zhou, Manipulating the architecture of zeolite catalysts for enhanced mass transfer, *Curr. Opin. Chem. Eng.* 9 (2015) 42–48.
- [28] J. Pérez-Ramírez, C.H. Christensen, K. Egeblad, C.H. Christensen, J.C. Groen, Hierarchical zeolites: enhanced utilisation of microporous crystals in catalysis by advances in materials design, *Chem. Soc. Rev.* 37 (2008) 2530.
- [29] A. Corma, C. Martínez, E. Dskocil, Designing MFI-based catalysts with improved catalyst life for C<sub>3</sub>= and C<sub>5</sub>= oligomerization to high-quality liquid fuels, *J. Catal.* 300 (2013) 183–196.
- [30] X. Wang, X. Hu, C. Song, K.W. Lux, M. Namazian, T. Imam, Oligomerization of biomass-derived light olefins to liquid fuel: effect of alkali treatment on the HZSM-5 catalyst, *Ind. Eng. Chem. Res.* 56 (2017) 12046–12055.
- [31] N.A.S. Amin, D.D. Anggoro, Dealuminated ZSM-5 zeolite catalyst for ethylene oligomerization to liquid fuels, *J. Nat. Gas Chem.* 11 (2002) 79–86.
- [32] C. Bertrand-Drira, X.-W. Cheng, T. Cacciaguerra, P. Trens, G. Melinte, O. Ersen, D. Minoux, A. Finiels, F. Fajula, C. Gerardin, Mesoporous mordenites obtained by desilication: mechanistic considerations and evaluation in catalytic oligomerization of pentene, *Microporous Mesoporous Mater.* 213 (2015) 142–149.
- [33] M.J. van Niekerk, C.T. O’Connor, J.C.Q. Fletcher, Methanol conversion and propene oligomerization productivity of dealuminated large-pore mordenites, *Ind. Eng. Chem. Res.* 35 (1996) 697–702.
- [34] J.W. Yoon, S.H. Jung, D.H. Choo, S.J. Lee, K.-Y. Lee, J.S. Chang, Oligomerization of isobutene over dealuminated Y zeolite catalysts, *Appl. Catal. A Gen.* 337 (2008) 73–77.
- [35] C. Martínez, E.J. Dskocil, A. Corma, Improved THETA-1 for light olefins oligomerization to diesel: influence of textural and acidic properties, *Top. Catal.* 57 (2014) 668–682.
- [36] L. Wang, Z. Zhang, C. Yin, Z. Shan, F.-S. Xiao, Hierarchical mesoporous zeolites with controllable mesoporosity templated from cationic polymers, *Microporous Mesoporous Mater.* 131 (2010) 58–67.
- [37] Q. Yang, H. Zhang, M. Kong, X. Bao, J. Fei, X. Zheng, Hierarchical mesoporous ZSM- 5 for the dehydration of methanol to dimethyl ether, *Chinese J. Catal.* 34 (2013) 1576–1582.

1-Butene oligomerization over nanocrystalline MFI-based micro/mesoporous zeotypes synthesized *via* bottom-up approaches

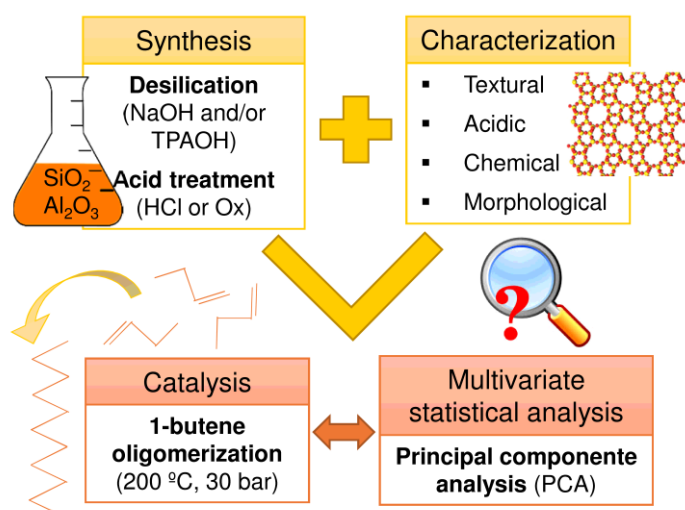
- [38] D.P. Serrano, J.M. Escola, R. Sanz, R.A. Garcia, A. Peral, I. Moreno, M. Linares, Hierarchical ZSM-5 zeolite with uniform mesopores and improved catalytic properties, *New J. Chem.* 40 (2016) 4206–4216.
- [39] D.P. Serrano, J. Aguado, G. Morales, J.M. Rodríguez, A. Peral, M. Thommes, J.P. Epping, B.F. Chmelka, Molecular and meso- and macroscopic properties of hierarchical nanocrystalline ZSM-5 zeolite prepared by seed silanization, *Chem. Mater.* 21 (2009) 641–654.
- [40] D.P. Serrano, J. Aguado, J.M. Escola, J.M. Rodríguez, A. Peral, Hierarchical zeolites with enhanced textural and catalytic properties synthesized from organofunctionalized seeds, *Chem. Mater.* 18 (2006) 2462–2464.
- [41] Z. Wan, W. Wu, W. Chen, H. Yang, D. Zhang, Direct synthesis of hierarchical ZSM-5 zeolite and its performance in catalyzing methanol to gasoline conversion, *Ind. Eng. Chem. Res.* 53 (2014) 19471–19478.
- [42] A.S. Al-Dughaiter, H. de Lasa, HZSM-5 Zeolites with different SiO<sub>2</sub>/Al<sub>2</sub>O<sub>3</sub> ratios. Characterization and NH<sub>3</sub> desorption kinetics, *Ind. Eng. Chem. Res.* 53 (2014) 15303–15316.
- [43] M.M.J. Treacy, J.B. Higgins, Collection of simulated XRD powder patterns for zeolites, ELSEVIER, 2001.
- [44] K. Góra-Marek, M. Derewiński, P. Sarv, J. Datka, IR and NMR studies of mesoporous alumina and related aluminosilicates, *Catal. Today* 101 (2005) 131–138.
- [45] J.M.R. Gallo, C. Bisio, G. Gatti, L. Marchese, H.O. Pastore, Physicochemical characterization and surface acid properties of mesoporous [Al]-SBA-15 obtained by direct synthesis, *Langmuir* 26 (2010) 5791–5800.
- [46] G.L. Woolery, G.H. Kuehl, H.C. Timken, A.W. Chester, J.C. Vartuli, On the nature of framework Brønsted and Lewis acid sites in ZSM-5, *Zeolites* 2449 (1997) 288–296.
- [47] J.M. Campelo, F. Lafont, J.M. Marinas, Pt/SAPO-5 and Pt/SAPO-11 as catalysts for the hydroisomerization and hydrocracking of n-octane, *J. Chem. Soc., Faraday Trans.* 91 (1995) 1551–1555.
- [48] M. Henry, M. Bulut, W. Vermandel, B. Sels, P. Jacobs, D. Minoux, N. Nesterenko, S. van Donk, J.P. Dath, Low temperature conversion of linear C<sub>4</sub> olefins with acid ZSM-5 zeolites of homogeneous composition, *Appl. Catal. A, Gen.* 413–414 (2012) 62–77.
- [49] C.T. O'Connor, R.D. Forrester, M.S. Scurrall, Cetane number determination of synthetic diesel fuels, *Fuel* 71 (1992) 1323–1327.
- [50] G.S. Kapur, A. Ecker, R. Meusinger, Establishing quantitative structure-property relationships (QSPR) of diesel samples by proton-NMR & multiple linear regression (MLR) analysis, *Energy and Fuels* 15 (2001) 943–948.
- [51] A. de Klerk, Can Fischer-Tropsch syncrude be refined to on-specification diesel fuel?, *Energy & Fuels* 23 (2009) 4593–4604.
- [52] H. de Lasa, G. Dogammau, A. Ravella, Fuels of the future and changing fuel needs, in: *Chemical reactor technology for environmentally safe reactors and products*, Springer-Science+Business Media, London, Ontario, 1992: pp. 1–182.
- [53] D. Leckel, Diesel production from Fischer-Tropsch: the past, the present, and new concepts, *Energy & Fuels* 23 (2009) 2342–2358.
- [54] A. De Klerk, Fischer–Tropsch refining: technology selection to match molecules, *Green Chem.* 10 (2008) 1249–1279.
- [55] S. Schwarz, M. Kojima, C.T. O'Connor, Effect of silicon-to-aluminum ratio and synthesis time on high-pressure olefin oligomerization over ZSM-5, *Appl. Catal.* 56 (1989) 263–280.

- [56] C. Li, J. Du, H. Wang, X. Li, S.S. Zhu, G. Liu, J. Wu, A hemicellulose modified HZSM-5 and their application in the light olefins oligomerization to high-quality liquid fuels reaction, *Catal. Commun.* 102 (2017) 89–92.
- [57] A. Coelho, G. Caeiro, M.A.N.D.A. Lemos, F. Lemos, F.R. Ribeiro, 1-Butene oligomerization over ZSM-5 zeolite: Part 1 - Effect of reaction conditions, *Fuel* 111 (2013) 449–460.
- [58] X. Zhang, J. Zhong, J. Wang, J. Gao, A. Liu, Trimerization of butene over Ni-doped zeolite catalyst: effect of textural and acidic properties, *Catal. Letters* 126 (2008) 388–395.
- [59] A.G. Popov, D.A. Fedosov, I.I. Ivanova, O.S. Vedernikov, A.V. Kleimenov, D.O. Kondrashev, V.D. Miroshkina, P.A. Abrashenkov, S.E. Kuznetsov, A ZSM-5 zeolite-based catalyst for oligomerization of the butane–butylene fraction, *Pet. Chem.* 56 (2016) 237–243.
- [60] A.G. Popov, V.S. Pavlov, I.I. Ivanova, Effect of crystal size on butenes oligomerization over MFI catalysts, *J. Catal.* 335 (2016) 155–164.
- [61] P. Borges, R.R. Pinto, M.A.N.D.A. Lemos, F. Lemos, J.C. Védrine, E.G., Derouane, F.R. Ribeiro, Light olefin transformation over ZSM-5 zeolites. A kinetic model for olefin consumption, *Appl. Catal. A Gen.* 324 (2007) 20–29.
- [62] Y.T. Kim, J.P. Chada, Z. Xu, Y.J. Pagan-Torres, D.C. Rosenfeld, W.L. Winniford, E. Schmidt, G.W. Huber, Low-temperature oligomerization of 1-butene with H-ferrierite, *J. Catal.* 323 (2015) 33–44.
- [63] J.W. Yoon, J.-S. Chang, H.-D. Lee, T.-J. Kim, S.H. Jung, Trimerization of isobutene over a zeolite beta catalyst, *J. Catal.* 245 (2007) 253–256.
- [64] J.W. Yoon, J.S. Lee, S.H. Jung, K.-Y. Lee, J.-S. Chang, Oligomerization of isobutene over aluminum chloride-loaded USY zeolite catalysts, *J. Porous Mater.* 16 (2009) 631–634.
- [65] L. Mafra, J.A. Vidal-Moya, T. Blasco, Structural characterization of zeolites by advanced solid state NMR spectroscopic methods, in: annual reports on NMR spectroscopy, 2012: pp. 259–351.
- [66] P. V. Wiper, J. Amelse, L. Mafra, Multinuclear solid-state NMR characterization of the Brønsted/Lewis acid properties in the BP HAMS-1B (H-[B]-ZSM-5) borosilicate molecular sieve using adsorbed TMPO and TBPO probe molecules, *J. Catal.* 316 (2014) 240–250.
- [67] S. Hayashi, K. Jimura, N. Kojima, Acid property of MFI-type zeolites probed by trimethylphosphine oxide studied by solid-state NMR, *Microporous Mesoporous Mater.* 186 (2014) 101–105.

# CHAPTER 8

---

## Modified versions of zeolite ZSM-5 synthesized *via* top-down approaches for oligomerization of 1-butene



### Abstract

The oligomerization of light olefins, obtainable from fossil/renewable sources and refinery streams, is an attractive route to produce clean synthetic fuels and added-value chemicals. ZSM-5 is a type of catalyst used in commercial olefin oligomerization processes. Using appropriate modification procedures, it was possible to prepare catalysts

with improved performances. Various modified versions of commercially available ZSM-5 were prepared and investigated for 1-butene oligomerization under high-pressure, continuous-flow operation (30 bar, 200 °C). Simple, up-scalable top-down strategies involving base-acid treatments of ZSM-5 led to catalysts possessing enlarged pores and the required acidity for converting 1-butene to higher molar mass products. In targeting diesel type products, the modified catalysts led to up to 86 % butenes conversion, space time yield of 852 mg g<sub>cat</sub><sup>-1</sup> h<sup>-1</sup> and mass ratio diesel:naphtha cuts of 2.2. Characterization studies and multivariate/principal component analysis helped categorize the differently prepared catalysts, and gain insights into complex interplay of material properties influencing the catalytic reaction.

## CHAPTER 8

### **Modified versions of zeolite ZSM-5 synthesized *via* top-down approaches for oligomerization of 1-butene**

8.1.	Introduction .....	245
8.2.	Synthesis of the catalytic materials .....	246
8.3.	Characterization studies of the catalytic materials .....	250
8.4.	Methods of statistical analysis of data .....	260
8.5.	Principal component analysis (PCA) of the material properties .....	262
8.6.	Catalytic studies: general considerations .....	264
8.7.	Influence of material properties on the catalytic performance .....	267
8.8.	Conclusions .....	273
8.9.	References .....	273

## 8.1. Introduction

The oligomerization of light olefins, such as ethene, propene and butenes, represents an attractive route to produce ecofriendly synthetic fuels with low content of aromatics and sulphur, and added value chemicals such as dyes, plasticizers and detergents.<sup>[1,2]</sup> R&D efforts in the fields of materials and chemical engineering continue aiming at the development of efficient eco-friendly production processes of distillates. Zeolites appear as interesting catalysts, since they are relatively robust, versatile (tunable properties), some are readily available and reached industrial application (*e.g.*, MFI, FAU, BEA topologies). The ordered microporous systems of zeolites confer them shape-selectivity properties, albeit internal mass transfer limitations may be important, along with pore blockage and fast catalyst deactivation, especially when the desired reaction products are relatively bulky molecules, such as oligomers.<sup>[3,4]</sup>

Thus, great focus has been put on developing improved versions of zeolites with enhanced active sites accessibility, allowing facilitated mass transfer in/out of the pores, while benefiting from zeotype features (structural order at the atomic level, tunable surface properties and shape-selectivity).<sup>[5-9]</sup> This may be accomplished with the introduction of mesoporosity in zeolites *via* bottom-up or top-down synthetic approaches.<sup>[10-16]</sup> In the former case, mesoporosity is formed by hard templating (*e.g.*, carbonaceous or polymeric compounds),<sup>[17-19]</sup> soft templating (*e.g.*, surfactants, organosilanes),<sup>[20-22]</sup> or indirect templating methods (*e.g.*, steam-assisted and solid-phase crystallization).<sup>[23-25]</sup> In top-down approaches, mesoporosity is introduced by strategically removing framework atoms from pre-made zeolites; *e.g.*, desilication *via* alkaline treatment,<sup>[26-29]</sup> and dealumination *via* acid treatment or steaming at high temperature.<sup>[26,29-32]</sup> The top-down strategies are advantageously cheaper, relatively easy to reproduce and scale-up for larger production.<sup>[10,15,33]</sup> Zeotypes based on the MFI,<sup>[26,30,34]</sup> MOR,<sup>[11,35]</sup> FAU<sup>[36]</sup> and TON<sup>[37]</sup> topologies were prepared *via* top-down strategies. MFI versions were reported as effective catalysts, for example, for selective catalytic cracking of 1-butene,<sup>[38-40]</sup> and 2-methyl-2-butene<sup>[41]</sup> to light olefins; and for propene and pentene oligomerization to higher molecular weight products.<sup>[26]</sup>

Depending on the type of olefin, the relationships of material properties-catalytic activity may differ.<sup>[26]</sup> On the other hand, depending on the starting zeolite, the modification treatments may influence differently the material properties. For example, the effectiveness of desilication *via* alkaline treatment depends on factors such as topology, molar ratio Si/Al and crystal size of the starting zeolite. Thus desilication may be accomplished using strong inorganic bases (SIB protocol) such as NaOH leading to relatively fast hydrolysis and dissolution of the silicon species,<sup>[29]</sup> or, alternatively, quaternary ammonium hydroxides (QAH protocol) where the ammonium cations may act as a protective barrier at the surface of the zeolite crystals allowing moderate alkaline hydrolysis<sup>[28,42]</sup>. Desilication may be followed by moderate acid treatments to remove extra-framework aluminum species and/or inorganic debris.<sup>[29,43]</sup>

Considering the versatility and simplicity of top-down strategies, we sought to prepare and explore improved versions of ZSM-5 (the zeolite type used for commercial oligomerization processes)<sup>[44–46]</sup> for the oligomerization of 1-butene, under continuous-flow, high-pressure conditions (200 °C, 30 bar). Materials with distinct properties were prepared *via* SIB or QAH procedures or a combination of both (mixB), starting from commercial zeolite ZSM-5 possessing relatively low molar Si/Al ratio. The studies reported herein comprise establishing appropriate top-down modification protocols of ZSM-5 to meet superior catalytic performances for 1-butene conversion to diesel type products, understanding the influence of material properties on the catalytic reaction, and obtaining high space time yields of diesel cuts for catalysts prepared under optimized conditions.

## 8.2. Synthesis of the catalytic materials

The catalysts were prepared *via* top-down strategies starting from HZSM-5 (protonic form) which was obtained by calcining commercial (microcrystalline) zeolite NH<sub>4</sub>ZSM-5 (Si/Al=15, CBV3024E), at 550 °C for 5 h (heating rate of 1 °C min<sup>-1</sup>). HZSM-5 was subjected to desilication using NaOH (SIB procedure), TPAOH (QAH procedure) or a combination of both bases (mixB procedure), and acid treatment using HCl (Cl) or oxalic acid (Ox), adapting

different procedures (Figure 8.1).<sup>[26–29]</sup> Table 8.1 summarizes the conditions of the different protocols and the respective catalysts' names.

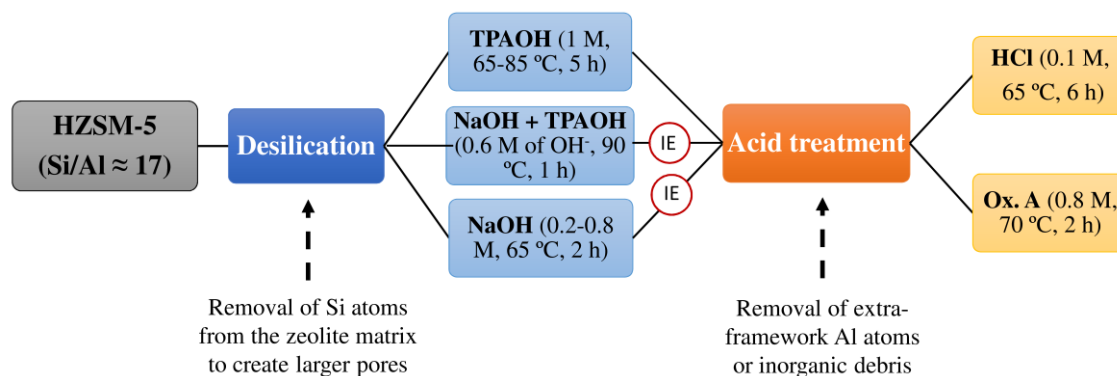


Figure 8.1. Top-down synthetic approaches employed for the synthesis of the MFI based micro/mesoporous zeotypes.

### Desilication

HZSM-5 was treated with NaOH which is a strong inorganic base (SIB procedure), according to the procedure described in the literature.<sup>[29]</sup> Specifically, an aqueous solution of NaOH (0.2, 0.4, 0.6 or 0.8 M) was added to HZSM-5 (30 cm<sup>3</sup> of solution per gram of solid) under stirring at 65 °C, and kept at this temperature for 2 h. Subsequently, the mixture was cooled using an ice bath; after *ca.* 10-15 min, the solid was separated by centrifugation and washed thoroughly with distilled water at 80 °C, until pH=7. Finally, the solid was dried overnight at 110 °C, giving pre-MZS-x, where x stands for the NaOH molar concentration used.

Alternatively, HZSM-5 was treated with TPAOH which is a quaternary ammonium hydroxide (QAH procedure), in a similar fashion to the SIB procedure, but using 1.0 M aq. TPAOH instead of NaOH, according to the procedure described in the literature.<sup>[28]</sup> The TPAOH solution was added to HZSM-5 (30 cm<sup>3</sup> of solution per gram of solid) under stirring at 65 or 85 °C, for 5 h. Subsequently, the mixture was cooled using an ice bath for *ca.* 10-15 min, the solid was separated by centrifugation and washed thoroughly with distilled water until pH=7. The resultant solid was dried overnight at 80 °C, giving pre-MZS-TPA-y, where

TPA stand for TPAOH and  $y$  stands for the temperature ( $^{\circ}\text{C}$ ) of the alkaline treatment ( $y=65, 85$ ).

HZSM-5 was treated in a similar fashion to the SIB or QAH procedures, albeit using an aqueous solution of NaOH plus TPAOH (mixB procedure) in a total concentration of NaOH plus TPAOH of 0.6 M (molar ratio of  $\text{TPA}^+/\text{Na}^+$  of 0.4), according to the procedure described in the literature.<sup>[27]</sup> This solution was added to HZSM-5 (25  $\text{cm}^3$  of solution per gram of solid), and the resultant mixture was stirred for 1 h at 90  $^{\circ}\text{C}$ . Subsequently, the mixture was cooled using an ice bath for *ca.* 10-15 min, the solid was separated by centrifugation and washed thoroughly with distilled water until  $\text{pH}=7$ , and then dried overnight at 60  $^{\circ}\text{C}$ , giving pre-MZS-TPA/Na.

### **Ion-exchange**

All desilicated materials prepared *via* the SIB or mixB procedures were converted to the acid form *via* ion-exchange using 100  $\text{cm}^3$  of 0.1 M aq.  $\text{NH}_4\text{NO}_3$  solution per gram of solid, and stirring for 24 h at 25  $^{\circ}\text{C}$ . The liquid phase was renewed twice (every 24 h) with new  $\text{NH}_4\text{NO}_3$  solution. Subsequently, the solids were separated by centrifugation, washed with distilled water and dried overnight at 60  $^{\circ}\text{C}$ . A portion of the ion-exchanged solid was calcined, and the remaining portion (not calcined) was subjected to acid treatment as described ahead. The ion-exchange step was not required for the QAH procedure.

The ion-exchanged materials pre-MZS- $x$  and pre-MZS-TPA- $y$  were calcined at 500  $^{\circ}\text{C}$  for 5 h (heating rate of 1  $^{\circ}\text{C min}^{-1}$ ), giving MZS- $x$  and MZS-TPA- $y$ , respectively, where  $x$  stands for the NaOH concentration and  $y$  stands for the temperature of the desilication treatment. The material pre-MZS-TPA/Na was calcined at 600  $^{\circ}\text{C}$  for 4 h (heating rate of 5  $^{\circ}\text{C min}^{-1}$ ) giving MZS-TPA/Na.

### **Acid treatment**

The desilicated materials MZS- $x$ , MZS-TPA- $y$  and MZS-TPA/Na were treated with hydrochloric acid (for the removal of inorganic debris from the pores<sup>[29,47-49]</sup>), or oxalic acid (for the removal of extra-framework aluminum species, likely located closer to the external

Modified versions of zeolite ZSM-5 synthesized *via* top-down approaches for oligomerization of 1-butene

surface<sup>[12,26]</sup>). Specifically, a 0.8 M aq. oxalic acid solution was added to the solid (100 cm<sup>3</sup> of solution per gram of solid) at 70 °C, for 2 h, or, alternatively, 0.1 M aq. of HCl solution was added to the solid (100 cm<sup>3</sup> of solution per gram of solid), and the resultant mixtures were stirred for 6 h at 65 °C. Subsequently, the solids were filtered, washed with milli-Q water until pH=7 and dried overnight at 60 °C. Finally, the materials were calcined at 500 °C for 5 h (heating rate of 1 °C min<sup>-1</sup>), giving MZS-x-Ox, MZS-x-Cl, MZS-TPA-y-Cl and MZS-TPA/Na-Cl, where Ox and Cl stands for acid treatment using oxalic acid or hydrochloric acid, respectively.

Table 8.1. Top-down protocols and synthesis conditions of the MFI based catalysts.

		Top-down strategies		Catalyst
Desilication Procedure		Ion-exchange <sup>[a]</sup>	Acid treatment	
SIB	NaOH 0.2-0.8 M 65 °C, 2 h	yes	no	MZS-0.2
				MZS-0.4
				MZS-0.6
				MZS-0.8
		yes	Oxalic acid 0.8 M 70 °C, 2 h	MZS-0.2-Ox
				MZS-0.4-Ox
		MZS-0.6-Ox		
		yes	HCl 0.1 M 65 °C, 6 h	MZS-0.2-Cl
				MZS-0.4-Cl
				MZS-0.6-Cl
				MZS-0.8-Cl
QAH <sup>[b]</sup>	TPAOH 1.0 M 65 °C or 85 °C, 5 h	no	no	MZS-TPA-65
				MZS-TPA-85
		no	HCl 0.1 M 65 °C, 6 h	MZS-TPA-65-Cl
				MZS-TPA-85-Cl
MixB	TPAOH 0.18 M + NaOH 0.42 M TPA <sup>+</sup> /Na <sup>+</sup> =0.4 90 °C, 1 h	yes	no	MZS-TPA/Na
		yes	HCl 0.1 M 65 °C, 6 h	MZS-TPA/Na-Cl

<sup>[a]</sup> Ion-exchange using an aqueous solution of NH<sub>4</sub>NO<sub>3</sub>, followed by washing, drying (and calcination for the materials that were not subjected to further acid treatment). <sup>[b]</sup> These materials were not fully characterized partly due to their poor catalytic performances.

### 8.3. Characterization studies of the catalytic materials

The protonic form HZSM-5 ( $\text{Si/Al} \approx 17$ ,  $S_{\text{BET}} = 431 \text{ m}^2\text{g}^{-1}$ ,  $S_{\text{meso}} = 54 \text{ m}^2\text{g}^{-1}$ ) of commercial microcrystalline  $\text{NH}_4\text{ZSM-5}$  was subjected to different base-acid treatments (Figure 8.1), leading to modified materials (Table 8.1) with Si/Al ratio in the range 3-122 (Table 8.2). The alkaline treatments were carried out using NaOH (SIB procedure giving MZS-x, where x stands for the molar concentration of NaOH ( $x = 0.2, 0.4, 0.6$  or  $0.8$ ), tetrapropylammonium hydroxide (QAH procedure giving MZS-TPA-y, where y is the temperature of the alkaline treatment = 65 or 85 °C) or mixed tetrapropylammonium hydroxide plus NaOH (mixB procedure giving MZS-TPA/Na). In general, it was verified that the Si/Al ratio decreased from *ca.* 17 for the parent zeolite HZSM-5 to values in the range 3-16 after the alkaline treatment. The drop in Si/Al ratio was far more pronounced for the SIB and mixB procedures in relation to the QAH one. The latter procedure did not influence significantly the Si/Al ratio ( $\text{Si/Al} = 16$  for MZS-TPA-65 and MZS-TPA-85, compared to 17 for HZSM-5) suggesting that desilication was negligible. For the SIB procedure (MZS-x), the Si/Al ratio decreased with increasing NaOH concentration (x) due to enhanced removal of silicon species from HZSM-5 (Figure 8.2).

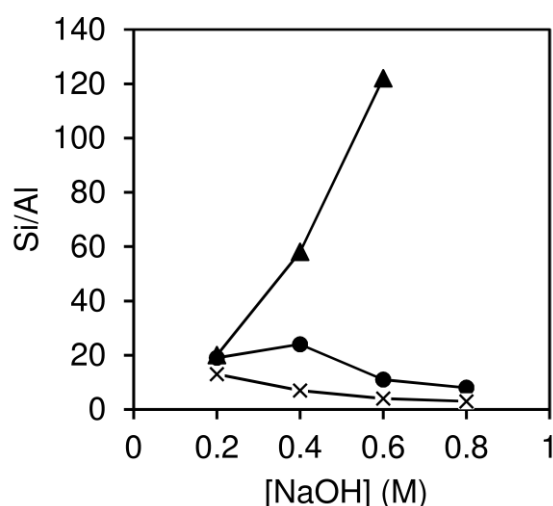


Figure 8.2. Si/Al molar ratio as function of the NaOH concentration for the materials prepared by the SIB procedure without acid treatment (×), with acid treatment using HCl (●) or oxalic acid (▲).

Table 8.2. Composition and textural properties of HZSM-5 and its modified versions.

Catalyst	Si/Al	S <sub>BET</sub> [m <sup>2</sup> g <sup>-1</sup> ]	S <sub>meso</sub> [m <sup>2</sup> g <sup>-1</sup> ]	V <sub>p</sub> [cm <sup>3</sup> g <sup>-1</sup> ]	V <sub>meso</sub> [cm <sup>3</sup> g <sup>-1</sup> ]	IHF <sup>[a]</sup>
MZS-0.2	13	439	176	0.64	0.52	0.41
MZS-0.2-Cl	19	453	149	0.64	0.51	0.39
MZS-0.2-Ox	20	483	189	0.67	0.54	0.49
MZS-0.4	7	414	271	1.08	1.03	0.23
MZS-0.4-Cl	24	564	291	1.23	1.11	0.65
MZS-0.4-Ox	58	564	267	1.21	1.08	0.65
MZS-0.6	4	232	175	0.99	0.96	0.09
MZS-0.6-Cl	11	494	255	1.23	1.12	0.54
MZS-0.6-Ox	122	596	269	1.39	1.24	0.76
MZS-0.8	3	136	114	0.94	0.93	0.03
MZS-0.8-Cl	8	374	272	1.08	1.03	0.25
MZS-TPA-65	16	410	59	0.55	0.41	0.16
MZS-TPA-65-Cl	19	424	65	0.56	0.41	0.19
MZS-TPA-85	16	414	66	0.49	0.34	0.20
MZS-TPA-85-Cl	17	413	67	0.48	0.33	0.20
MZS-TPA/Na	5	275	178	0.81	0.77	0.15
MZS-TPA/Na-Cl	21	604	285	1.24	1.10	0.80
HZSM-5	17 <sup>[b]</sup>	431	54	0.36	0.18	0.18
MZS-0.4-Cl-r <sup>[c]</sup>	-	498	312	1.15	1.06	0.49

<sup>[a]</sup> Indexed hierarchy factor (IHF) =  $V_{\text{micro}}/V_{\text{micro,HZSM-5}} \times S_{\text{meso}}/S_{\text{meso,MZS-0.4-Cl}}$ , where  $V_{\text{micro,HZSM-5}} = 0.18 \text{ cm}^3 \text{ g}^{-1}$  and  $S_{\text{meso,MZS-0.4-Cl}} = 291 \text{ m}^2 \text{ g}^{-1}$ .<sup>[47]</sup> <sup>[b]</sup> Si/Al=15 in the technical bulletin for the parent commercial NH<sub>4</sub>ZSM-5. <sup>[c]</sup> Results for the used catalyst, after thermal treatment.

Desilication was followed by acid treatment using oxalic acid (Ox) or HCl (Cl), which led to increased Si/Al ratio (Table 8.2), especially for materials obtained *via* the SIB and mixB procedures. These results may be attributed to the removal of inorganic debris and/or extra-framework aluminum species, likely formed in greater amounts during the SIB and mixB treatments than the QAH one. The materials MZS-x-Ox possessed higher Si/Al ratio than the HCl treated counterparts MZS-x-Cl, suggesting that the Ox treatment enhanced dealumination.

The desilication procedure/conditions may influence the crystallinity. Figure 8.3 shows the powder XRD patterns for HZSM-5 and its modified versions. The materials prepared *via* the SIB procedure with x=0.2 (namely, MZS-0.2, MZS-0.2-Cl, MZS-0.2-Ox)

or the QAH procedure (MZS-TPA- $y$ , MZS-TPA- $y$ -Cl) exhibited reflections associated with the MFI topology, the most intense appearing in the ranges  $7-8^\circ 2\theta$  and  $23-24^\circ 2\theta$ .<sup>[50,51]</sup> These materials seemed relatively crystalline, by comparison to the XRD pattern of HZSM-5. The SIB ( $x \geq 4$ ) and mixB procedures had more pronounced effects on structural order; peak intensities decreased in the order, SIB/ $x=0.2 > \text{SIB}/x=0.4 > (\text{SIB}/x=0.6; \text{mixB})$ , and SIB/ $x=0.8$  led to lack of crystallinity.

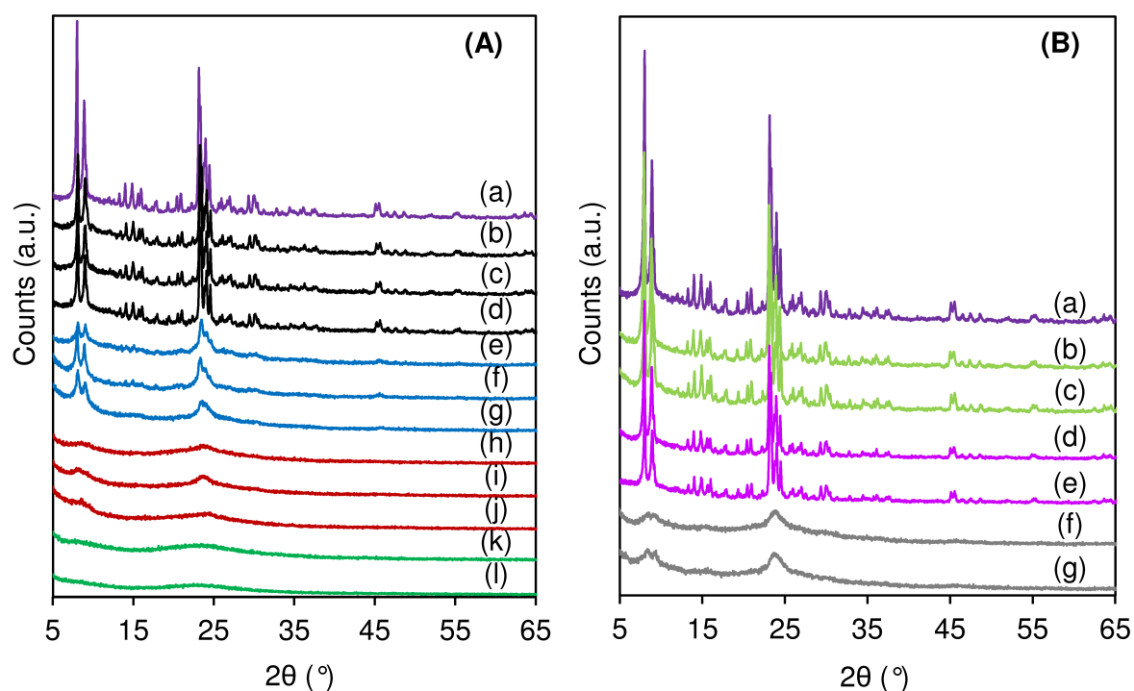


Figure 8.3. Powder XRD patterns for (A) the materials prepared *via* the SIB procedure: HZSM-5 (a), MZS-0.2 (b), MZS-0.2-Cl (c), MZS-0.2-Ox (d), MZS-0.4 (e), MZS-0.4-Cl (f), MZS-0.4-Ox (g), MZS-0.6 (h), MZS-0.6-Cl (i), MZS-0.6-Ox (j), MZS-0.8 (k), and MZS-0.8-Cl (l); and for (B) materials prepared *via* QAH and mixB procedures: HZSM-5 (a), MZS-TPA-65 (b), MZS-TPA-65-Cl (c), MZS-TPA-85 (d), MZS-TPA-85-Cl (e), MZS-TPA/Na (f), and MZS-TPA/Na-Cl (g).

Morphologically, HZSM-5 and its modified versions consisted of aggregates of irregular sizes (up to  $\approx 700$  nm) and formed by pseudo-spherical particles (Figure 8.4); exceptionally, MZS-0.8 consisted of relatively small aggregates, which may be related to the lack of crystallinity. For all materials, some particles of *ca.* 100 nm could be distinguished. However, with the modification treatments, partial particle coalescence seemed to occur,

making it difficult to identify the particle size ranges. The literature for desilicated zeolites referred to coalescence associated with the formation of mesopores, likely involving reactions between vicinal defect sites.<sup>[52,53]</sup> It was also referred the occurrence of external surface roughening, especially for materials prepared from zeolites possessing relatively low ratio Si/Al (less than *ca.* 25).<sup>[54,55]</sup> On the other hand, it was reported that less stable silicon species may be formed during modification treatments, and migrate and condense with silanol groups in different locations, as a type of healing process (during dealumination).<sup>[52]</sup> One may hypothesize that the apparent particle coalescence for the MZS materials may be due to interactions between external surface defects of crystallites in close proximity, and/or these interactions may occur *via* the intermediacy of extra-framework species (formed during desilication).

The nitrogen adsorption-desorption isotherms showed increasing adsorption capacity at high relative pressure ( $p/p_0 > 0.9$ ), attributable to multilayer adsorption on the external surface (Figure 8.5). This feature was less pronounced for HZSM-5 and its modified versions resulting from the SIB/ $x=0.2$  and QAH procedures. The SIB/ $(x \geq 0.4)$  and mixB treated materials exhibited a hysteresis loop (Figure 8.5), enhanced portion of mesoporosity ( $\% S_{\text{meso}}$ ,  $\% V_{\text{meso}}$ ) and reduced portion of microporosity ( $\% V_{\text{micro}}$ ), Figure 8.6. A comparative study for the MZS- $x$  materials, indicated that  $S_{\text{meso}}$  and  $V_{\text{meso}}$  were highest for  $x=0.4$  ( $271 \text{ m}^2 \text{ g}^{-1}$  and  $1.03 \text{ cm}^3 \text{ g}^{-1}$ ), suggesting that the SIB/ $(x=0.4)$  protocol was favorable for introducing mesoporosity in HZSM-5 (Table 8.2).

The increased  $S_{\text{meso}}$  ( $54 \text{ m}^2 \text{ g}^{-1}$  for HZSM-5 *versus*  $114\text{-}271 \text{ m}^2 \text{ g}^{-1}$  for alkaline-treated materials) and  $V_{\text{meso}}$  ( $0.18 \text{ cm}^3 \text{ g}^{-1}$  for HZSM-5 *versus*  $0.51\text{-}1.03 \text{ cm}^3 \text{ g}^{-1}$ ) were accompanied by decreased Si/Al ratio (Table 8.2) and structural order (Figure 8.3). The limited mesopore formation *via* the QAH procedure may be partly due to the relatively low Si/Al ratio of the parent zeolite HZSM-5,<sup>[28]</sup> since high framework aluminum content suppresses intracrystalline silicon extraction.<sup>[12]</sup> The SIB ( $x \geq 0.4$ ) and mixB treated materials possessed relatively narrow mesopore size distribution curves in the range 2-6 nm (Figure S8.1). HZSM-5 and its versions modified *via* the SIB procedure with  $x=0.2$  or 0.8, or the QAH procedure, exhibited poorly defined mesopore size distribution curves, which was attributed, on the one hand, to the poor effectiveness of the SIB/ $(x=0.2)$  and QAH procedures for introducing mesoporosity (Table 8.2), and, on the other hand, to the severity of the SIB/ $(x=0.8)$  procedure in causing structural collapse (Figure 8.3).

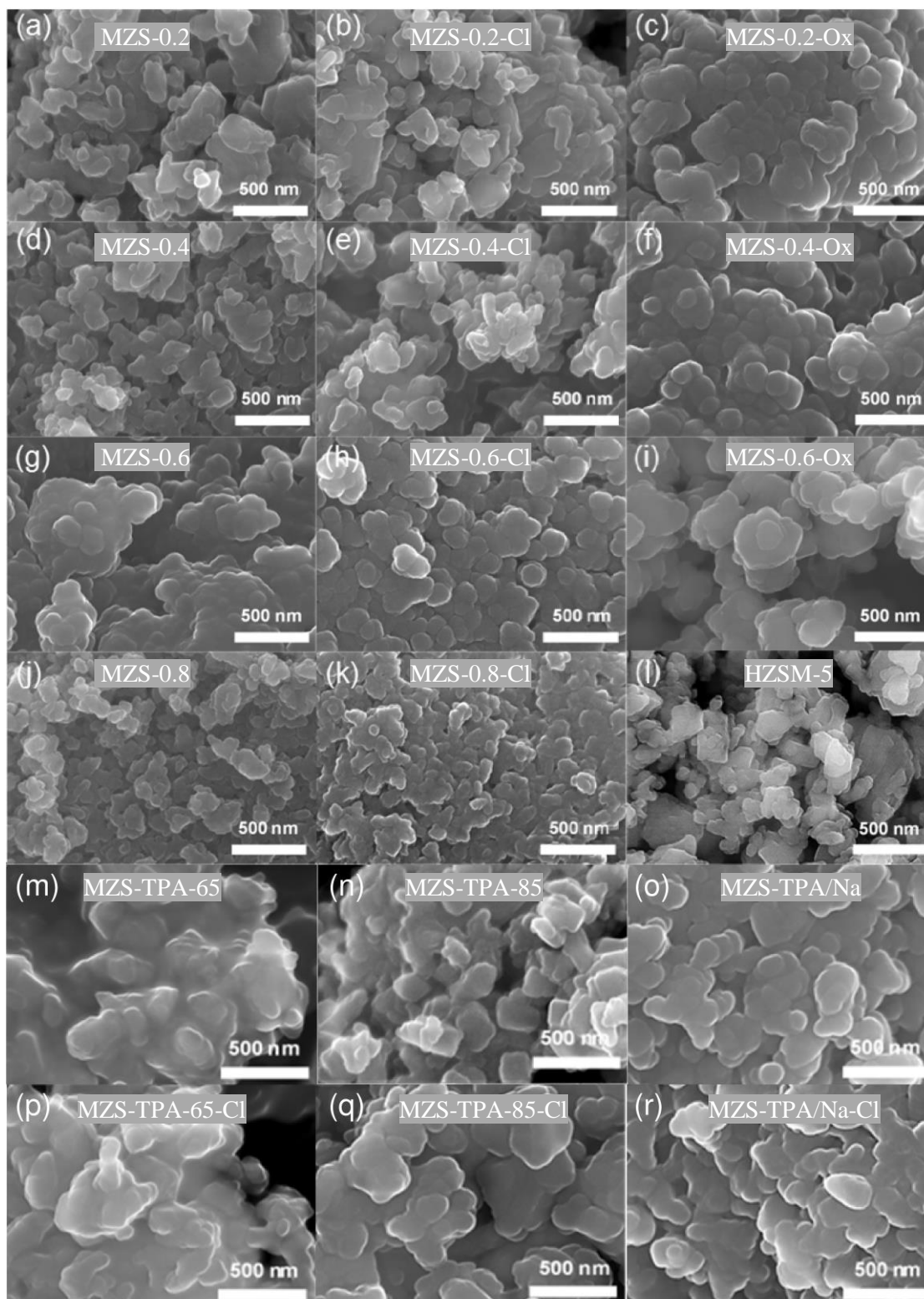


Figure 8.4. SEM images of the materials prepared *via* the SIB procedure: MZS-0.2 (a), MZS-0.2-Cl (b), MZS-0.2-Ox (c), MZS-0.4 (d), MZS-0.4-Cl (e), MZS-0.4-Ox (f), MZS-0.6 (g), MZS-0.6-Cl (h), MZS-0.6-Ox (i), MZS-0.8 (j), MZS-0.8-Cl (k), and HZSM-5 (l); and the materials prepared *via* the QAH and mixB procedures: MZS-TPA-65 (m), MZS-TPA-85 (n), MZS-TPA/Na (o), MZS-TPA-65-Cl (p), MZS-TPA-85-Cl (q), and MZS-TPA/Na-Cl (r).

Modified versions of zeolite ZSM-5 synthesized *via* top-down approaches for oligomerization of 1-butene

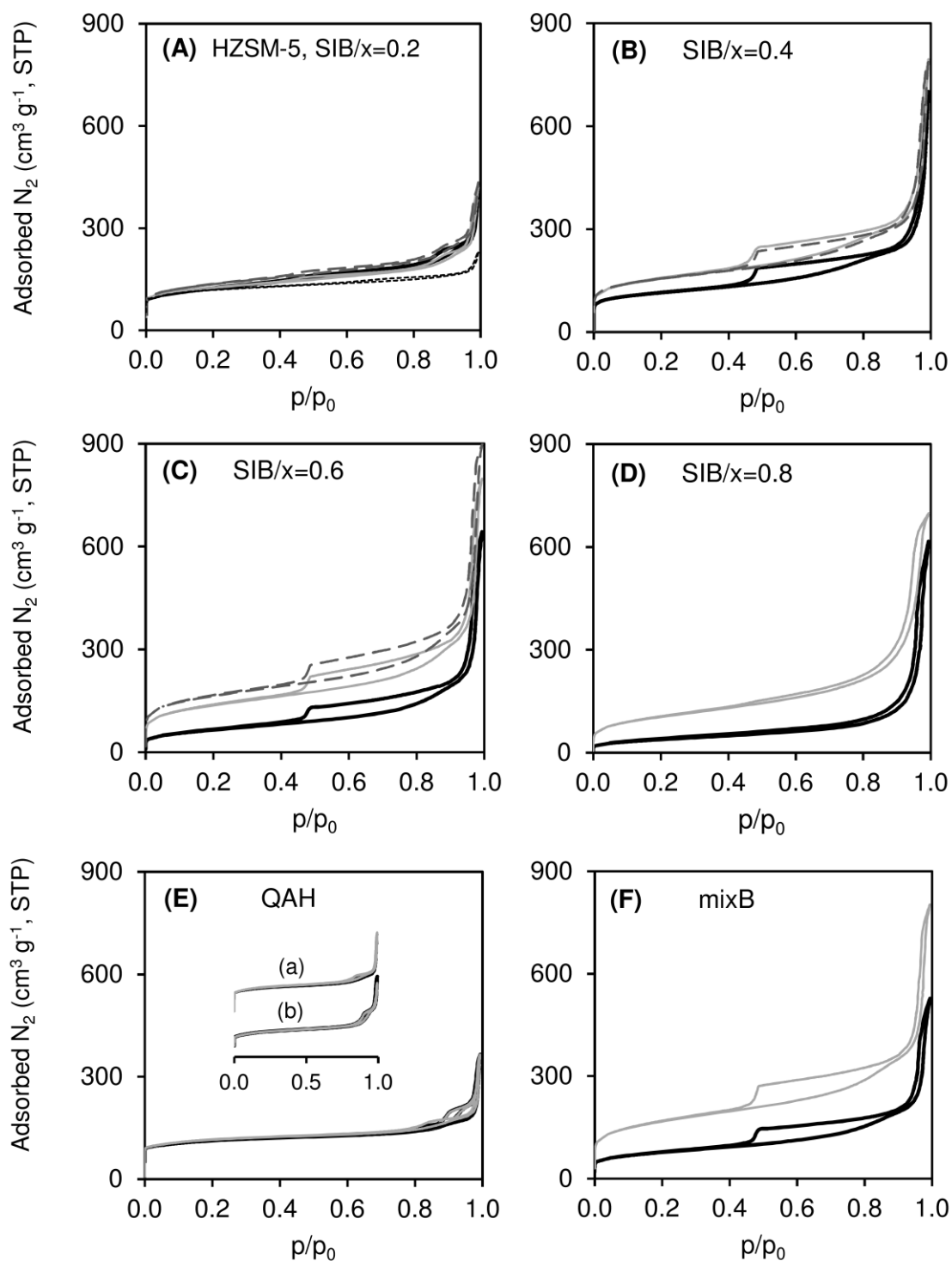


Figure 8.5. Nitrogen adsorption-desorption isotherms (at  $-196\text{ }^{\circ}\text{C}$ ) for materials prepared by SIB procedure using NaOH concentration of 0.2 M (A), 0.4 M (B), 0.6 M (C) or 0.8 M (D); and materials prepared by QAH (E) and mixB (F) procedures. Materials without acid (Ox, Cl) treatment - thick black lines; materials treated with oxalic acid - wide dashed lines in (A), (B), (C); materials treated with HCl - grey lines; HZSM-5 - dotted black line in (A). The inset in (E) shows, separately, the pairs (a) MZS-TPA-65 and MZS-TPA-65-Cl, and (b) MZS-TPA-85 and MZS-TPA-85-Cl for better visualization.

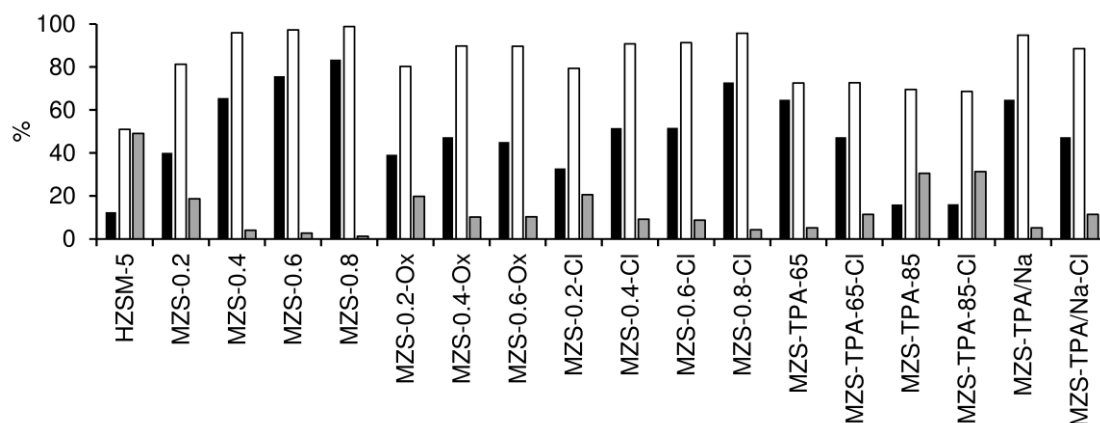


Figure 8.6. Proportion of mesoporous specific surface area (black), mesoporous volume (white) and microporous volume (grey) of each material ( $\%S_{\text{meso}}=S_{\text{meso}}/S_{\text{BET}}\times 100$ ;  $\%V_i=V_i/V_p\times 100$  where  $i$  is micro or meso and  $V_p$  is the total pore volume).

The acid treatment is important to remove inorganic debris and/or extra-framework Al species (Table 8.2).<sup>[26,43,47]</sup> For the desilicated materials MZS- $x$  and MZS-TPA/Na, the acid treatment step led to enhanced  $S_{\text{BET}}$ ,  $V_p$  and  $V_{\text{micro}}$  (Table 8.2), without affecting significantly the mesopore size distribution (Figure S8.1). In general, the impact of the acid treatment was pronounced on  $S_{\text{meso}}$  (up to 139 % increase in relation to the corresponding desilicated materials) and  $V_{\text{meso}}$  (up to 42 % increase). The  $S_{\text{meso}}$  was highest for MZS-0.4-Cl ( $291 \text{ m}^2 \text{ g}^{-1}$ ) and MZS-TPA/Na-Cl ( $285 \text{ m}^2 \text{ g}^{-1}$ ) (Table 8.2). For the QAH treated materials, the impact of the acid treatment on the textural properties was not significant, which is consistent with the above discussion regarding the ineffectiveness of this procedure for desilication of the parent zeolite HZSM-5.

The indexed hierarchy factor (IHF) reflects the efficiency of the desilication process in introducing mesoporosity without drastically affecting microporosity (Table 8.2).<sup>[47]</sup> The acid-treated materials possessed higher IHF (0.20-0.80) than the parent zeolite HZSM-5 (0.18), with the highest IHF values being verified for MZS-0.4-Cl, MZS-0.4-ox, MZS-0.6-ox and MZS-TPA/Na-Cl. Hence, top-down strategies contemplating Ox or Cl treatment after desilication, *via* mixB or SIB/( $x=0.4, 0.6$ ) procedures, may give good compromises of enhanced  $S_{\text{meso}}$  with partial preservation of  $V_{\text{micro}}$ . Advantageously, the mineral acid (HCl) may be used in much lower concentration and lower temperature than the organic acid.

Figure 8.7 shows the  $^{27}\text{Al}$  MAS NMR spectra of HZSM-5 and the modified materials. All materials exhibited a peak centered at *ca.* 55 ppm assigned to four-coordinated aluminum species ( $\text{Al}_{\text{tetra}}$ ). In general, desilication led to enhanced relative amount of five- ( $\text{Al}_{\text{penta}}$ ) and six-coordinated ( $\text{Al}_{\text{octa}}$ ) aluminum species (peaks centred at *ca.* 28 ppm and 0 ppm, respectively), which seemed to be more pronounced for stronger alkaline conditions ( $\text{SIB}/(x \geq 0.6)$ , mixB), Figure 8.7, Table 8.3. The acid treatment (Ox, Cl) led to considerable reduction in the relative amounts of  $\text{Al}_{\text{penta}}$  and  $\text{Al}_{\text{octa}}$  species, and enhanced  $\text{Al}_{\text{tetra}}$  (Table 8.3). These results together with the increase of the Si/Al ratio upon acid treatment, indicated that this step led to the removal extra-framework Al species and/or inorganic debris containing aluminum. FT-IR spectroscopy of the dehydrated materials showed a band at  $\approx 3745 \text{ cm}^{-1}$  assignable to silanol groups on the external surface (Figure 8.8-B).<sup>[56,57]</sup> The relative intensity of this band was more pronounced for the modified materials than HZSM-5, likely due to the desilication process leading to the formation of defect sites. HZSM-5 and related materials modified *via* the SIB procedure with  $x=0.2$  or  $0.4$  exhibited a band at  $\approx 3610 \text{ cm}^{-1}$  assignable to structural acidic O-H groups.<sup>[56,58]</sup>

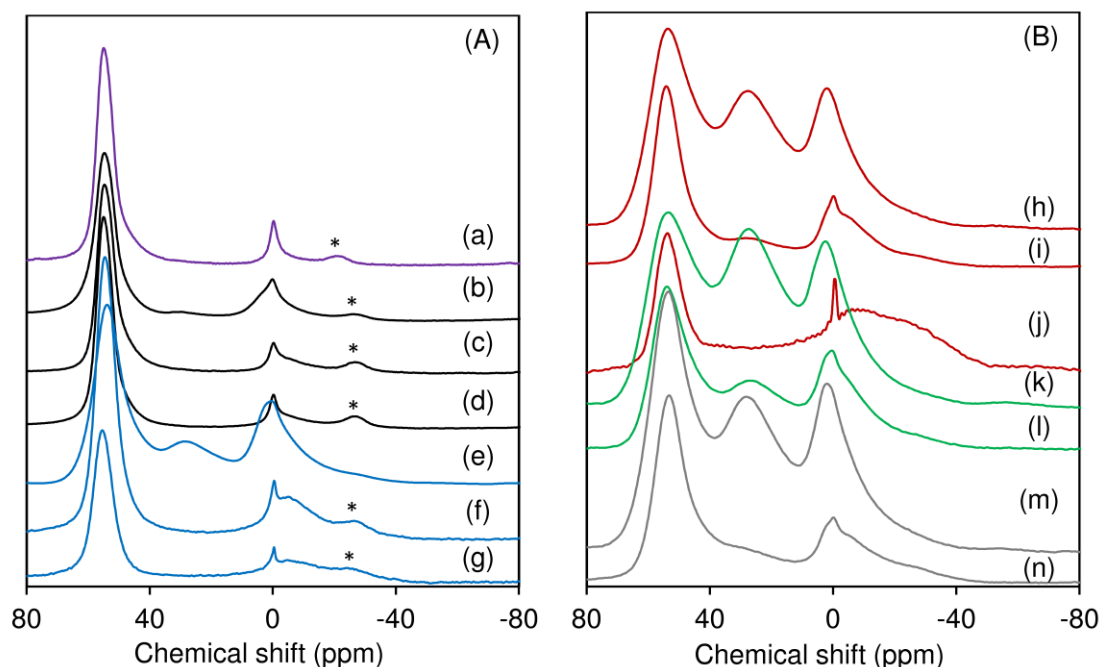


Figure 8.7.  $^{27}\text{Al}$  MAS NMR spectra for (A) HZSM-5 (a), MZS-0.2 (b), MZS-0.2-Cl (c), MZS-0.2-Ox (d), MZS-0.4 (e), MZS-0.4-Cl (f), MZS-0.4-Ox (g), and (B) MZS-0.6 (h), MZS-0.6-Cl (i), MZS-0.6-Ox (j), MZS-0.8 (k), MZS-0.8-Cl (l), MZS-TPA/Na (m), and MZS-TPA/Na-Cl (n). The asterisk denotes side bands.

FT-IR spectroscopy of adsorbed pyridine as base probe indicated that all materials exhibited bands centered at *ca.* 1540 and 1455  $\text{cm}^{-1}$  associated with pyridinium ions (related to Brønsted (B) acid sites) and coordinated pyridine (Lewis (L) acid sites), respectively (Figure 8.8-A). Upon desilication, the amount and density of L+B (and B) acid sites decreased and the molar ratio L/B increased (Table 8.3, Figure S8.2) which is somewhat consistent with the  $^{27}\text{Al}$  MAS NMR spectroscopic data in that  $\text{Al}_{\text{tetra}}$  decreased and  $\text{Al}_{\text{penta}}$  increased (Figure 8.7). For the SIB treated materials, the acid treatment (Ox, Cl) led to decreased L/B ratio, which was more pronounced using oxalic acid (Table 8.3). Of the modified materials, MZS-0.2-Cl possessed the highest amount of total acid sites, albeit reduced mesoporosity and undefined mesopore size distribution. On the other hand, MZS-0.6-Ox possessed the lowest amount of total acid sites, albeit enhanced mesoporosity and relatively narrow mesopore size distribution (Table 8.3).

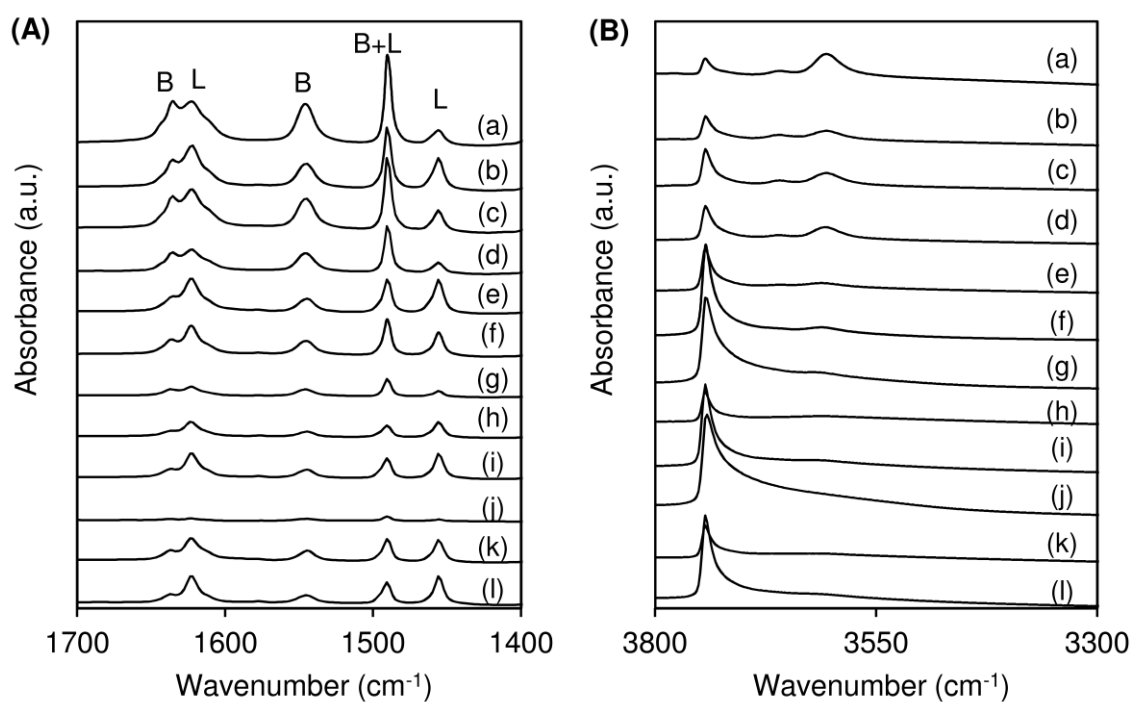


Figure 8.8. FT-IR spectra of pyridine (base probe) adsorbed at 200 °C (A), and FT-IR spectra in the OH stretching region after evacuation at 450 °C (B) for HZSM-5 (a), MZS-0.2 (b), MZS-0.2-Cl (c), MZS-0.2-Ox (d), MZS-0.4 (e), MZS-0.4-Cl (f), MZS-0.4-Ox (g), MZS-0.6 (h), MZS-0.6-Cl (i), MZS-0.6-Ox (j), MZS-TPA/Na (k), and MZS-TPA/Na-Cl (l).

Modified versions of zeolite ZSM-5 synthesized *via* top-down approaches for oligomerization of 1-butene

For each MZS-x material, the Ox and Cl treatments led to similar acid strengths: the B acid strength was, in general, mostly moderate; and the L acid strength was mostly strong for MZS-x-Ox and MZS-x-Cl with x=0.2, 0.4 ( $L_{450}/L_{200} \geq 0.63$ ), and mostly moderate for the remaining acid-treated materials ( $L_{450}/L_{200} \leq 0.45$ ) (Table 8.3). The materials MSZ-0.6 and MSZ-TPA/Na, prepared using similar total alkaline concentration (i.e.  $[\text{OH}^-]=0.6$  M), possessed roughly comparable Si/Al ratio, morphological, textural and acid properties, suggesting that the SIB and mixB procedures using comparable conditions may impact similarly on the material properties. In summary, Figure 8.9 shows positive and negative variations of material properties (Si/Al ratio, acidity, texture) due to the alkaline (SIB, mixB) and acid treatments.

Table 8.3. Types of aluminum species and acid properties of selected catalysts.

Catalyst	Al species <sup>[a]</sup>		Acid properties <sup>[b]</sup>			
	% Al <sub>tetra+penta</sub> (Al <sub>penta</sub> /Al <sub>tetra</sub> )	% Al <sub>octa</sub>	L+B [ $\mu\text{mol g}^{-1}$ ]	L/B	L <sub>450</sub> /L <sub>200</sub>	B <sub>450</sub> /B <sub>200</sub>
MZS-0.2	89 (0.02)	11	346	0.64	0.56	0.26
MZS-0.2-Cl	83 (0.00)	17	342	0.31	0.79	0.33
MZS-0.2-Ox	87 (0.00)	13	288	0.26	0.86	0.25
MZS-0.4	88 (0.37)	12	347	1.29	0.08	0.75
MZS-0.4-Cl	71 (0.00)	29	250	0.80	0.63	0.13
MZS-0.4-Ox	80 (0.00)	20	108	0.39	0.77	0.07
MZS-0.6	59 (0.80)	41	126	1.63	0.29	0.00
MZS-0.6-Cl	74 (0.23)	26	253	1.50	0.35	0.05
MZS-0.6-Ox	74 (0.33)	26	33	0.35	0.34	0.00
MZS-TPA/Na	56 (0.73)	44	181	1.11	0.34	0.04
MZS-TPA/Na-Cl	74 (0.32)	26	213	1.72	0.45	0.00
HZSM-5	75 (0.00)	25	415	0.18	0.87	0.42

<sup>[a]</sup> Determined by <sup>27</sup>Al MAS NMR spectroscopy. <sup>[b]</sup> Determined by FT-IR spectroscopy of adsorbed pyridine at 200 °C; B=Brønsted acid sites, L=Lewis acid sites, B+L=total amount of acid sites.

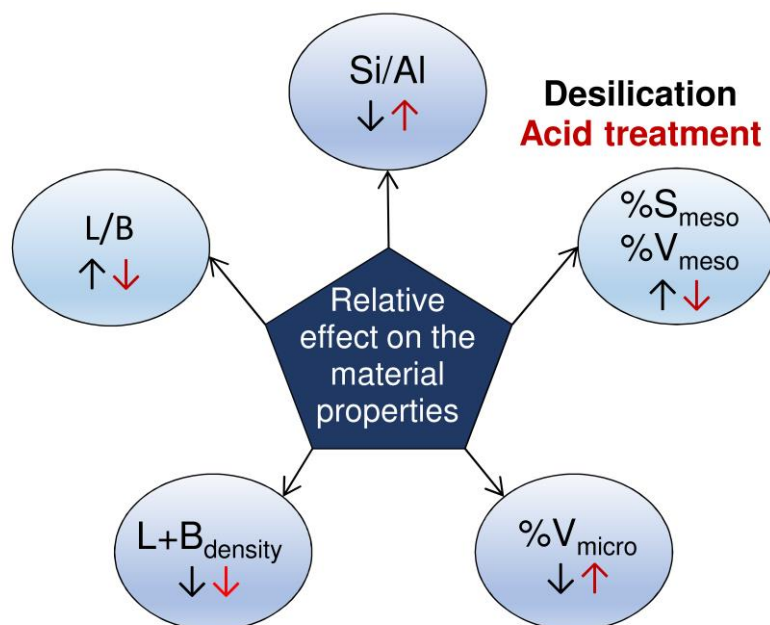


Figure 8.9. Changes in textural and acid properties of the materials prepared by the SIB and mixB procedures: black arrows – after desilication; red arrows – after the acid treatment; (↑) represents an increase and (↓) a decrease.

#### 8.4. Methods of statistical analysis of data

In analyzing a large set of material properties that may be somehow related, one may advantageously employ a multivariate statistical tool, such as principal component analysis (PCA), since it allows to reduce a large set of variables to a smaller set of principal components that still contains most of the information of the large set, decreasing the complexity of the analyses.<sup>[59]</sup> The PCA methodology was reported by Castaño and coworkers<sup>[60]</sup> for fluid catalytic cracking over faujasite Y zeolites, and by Vayenas and coworkers<sup>[61]</sup> for hydrotreatment of lube oil over metal oxides, allowing valuable insights into key parameters affecting the catalytic reactions.

PCA was carried out using XLSTAT statistical analysis software, to help categorize the prepared materials according to their properties based on the complementary characterization studies, and, on the other hand, identify best-performing catalysts based on the catalytic results. For each PCA study, it was necessary to generate a data matrix with the

observations (rows) and variables (columns). For the PCA of the materials properties, the data matrix contemplated the following properties: amount and strength of B and L acid sites,  $S_{\text{BET}}$ ,  $S_{\text{meso}}$ ,  $V_{\text{meso}}$ , and  $V_{\text{micro}}$  (Table 8.4). A more detailed matrix included additionally the IHF, ratio  $\text{Al}_{\text{penta}}/\text{Al}_{\text{tetra}}$  and  $\% \text{Al}_{\text{tetra+penta}}$  (Table S8.1). The observations were the materials prepared *via* the SIB and mixB procedures, with or without (Ox, Cl) acid treatment, and HZSM-5. On the other hand, PCA of the catalytic results was carried out for selected materials, and the data matrix contemplated:  $X_{\text{C}_4}$ , mass ratio  $D_{\text{Cut}}/N_{\text{Cut}}$ , STY and  $\text{STY}_{D_{\text{Cut}}}$  (Table S8.2).

It was chosen the PCA type for computation (either correlation matrix (Pearson or Spearman) or covariance matrix), the significance level, and the desired outputs (*e.g.*, descriptive statistics, eigenvalues, factor scores, squared cosines, correlation circle, biplot with variables and observations). Then, it was necessary to select the x and y axis with the factors with higher total variance to represent the data. In this work, the data were analyzed using the Pearson correlation, with statistically significant level of 95 % ( $p < 0.05$ ), and the factors F1 and F2 were selected for the x axis (principal component 1 (PC1)) and y axis (principal component 2 (PC2)), respectively. When analyzing the PCA results, it was important to: (i) analyze the eigenvalues to evaluate the quality of the projections (if the total variance is too low, it is preferred to reselect the variables and/or observations); (ii) analyze the correlation circle chart to check if some variable is located close to the center (in that case any interpretation on that variable may be hazardous); (iii) analyze the squared cosines table, which gives an idea of the quality of the representation of a given variable on the PCA axis (if the square cosines are close to zero, the more careful has to be the interpretation of the results in terms of trends on the corresponding axis); (iv) analyze the PCA biplot in order to establish relationships between variables and identify trends between variables and observations. The analyses of the points (i) to (iii) of the different PCAs allowed to verify that it was appropriate to analyze the resultant PCA biplots with F1 and F2 as principal components (high total variance). Figure S8.3 is a schematic representation of the procedure used for carrying out the PCA, using, as example, the data matrix of Table 8.4.

Special caution is required when analyzing the variables  $B_{\text{strength}}$  and L in the biplots of Figure 8.10 and Figure S8.4, since they present relatively low squared cosines for F1 and F2.

Table 8.4. Data matrix used in the construction of the PCA biplot (Figure 8.10).

Material	B $\mu\text{mol g}^{-1}$	L $\mu\text{mol g}^{-1}$	L <sub>Strength</sub>	B <sub>Strength</sub>	S <sub>BET</sub> $\text{m}^2 \text{g}^{-1}$	S <sub>meso</sub> $\text{m}^2 \text{g}^{-1}$	V <sub>micro</sub> $\text{cm}^3 \text{g}^{-1}$	V <sub>meso</sub> $\text{cm}^3 \text{g}^{-1}$
M-0.2	211	134	0.6	0.26	439	176	0.12	0.52
M-0.2-Ox	228	60	0.9	0.25	483	189	0.13	0.54
M-0.2-Cl	261	81	0.8	0.33	453	149	0.13	0.51
M-0.4	152	195	0.1	0.75	414	271	0.04	1.03
M-0.4-Ox	77	30	0.8	0.07	564	267	0.12	1.08
M-0.4-Cl	138	111	0.6	0.13	564	291	0.11	1.11
M-0.6	48	78	0.3	0.00	232	175	0.03	0.96
M-0.6-Ox	24	9	0.3	0.00	596	269	0.14	1.24
M-0.6-Cl	101	152	0.4	0.05	494	255	0.11	1.12
TPA/Na	86	95	0.3	0.04	275	178	0.04	0.77
TPA/Na-Cl	78	135	0.4	0.00	604	285	0.14	1.10
ZSM-5	353	62	0.9	0.42	431	54	0.17	0.18

## 8.5. Principal component analysis (PCA) of the material properties

Figure 8.10 shows the PCA biplot with eight variables (i.e., materials properties) and twelve samples prepared *via* the SIB or mixB procedures, with or without acid treatment (the data were taken from Table 8.4). The first two components accounted for *ca.* 75 % of the variance of the data (PC1: 45 % and PC2: 29 %). Hence, the prepared materials could be differentiated along the x- and y-axis. Specifically, three sets of materials could be identified in the PCA biplot of Figure 8.10. Group 1 (blue) regards materials prepared using relatively low concentration of NaOH, with or without acid treatment (namely, MZS-0.2, MZS-0.2-Cl, MZS-0.2-Ox). Group 2 (green) comprises materials prepared using higher alkaline (OH<sup>-</sup>) concentration, without acid treatment (MZS-0.4, MZS-0.6, MZS-TPA/Na). Group 3 (purple) regards materials prepared using higher alkaline concentration, with acid treatment (MZS-0.4-Cl, MZS-0.4-Ox, MZS-0.6-Cl, MZS-0.6-Ox, MZS-TPA/Na-Cl). Group 1 is located closer to the parent zeolite HZSM-5, on the left side of the biplot which is characterized by higher microporosity (V<sub>micro</sub>) and acid strengths. Groups 2 and 3 are located on the right side of the biplot which is characterized by higher mesoporosity (S<sub>meso</sub>, V<sub>meso</sub>). In particular, Group 3 (upper-right region of the biplot) possessed higher S<sub>BET</sub>, V<sub>micro</sub> and L

acid strength than Group 2 (bottom-right region of the biplot). Hence, the acid treatment step led to a gain in terms of specific surface area and microporosity, in combination with mesoporosity.

A PCA biplot (Figure S8.4) was determined using a larger set of material properties, i.e. including %Al<sub>tetra+penta</sub>, ratio Al<sub>penta</sub>/Al<sub>tetra</sub> and IHF (Table S8.1). Although there was a somewhat greater dispersion of the results and a decrease of the total variance of the data by the principal components, the same three groups of materials could be distinguished. Regarding the types of Al species, Group 1 was characterized by higher %Al<sub>tetra+penta</sub> and lower ratio Al<sub>penta</sub>/Al<sub>tetra</sub>, which is consistent with the less effective desilication for this group of materials. Group 2 was characterized by higher ratio Al<sub>penta</sub>/Al<sub>tetra</sub>, which may related to significant amounts of extra-framework species and/or inorganic debris present in these (non-acid- treated) materials, making them less attractive for catalytic application. Overall, Group 3 was characterized by higher IHF, i.e. greater desilication efficiency.

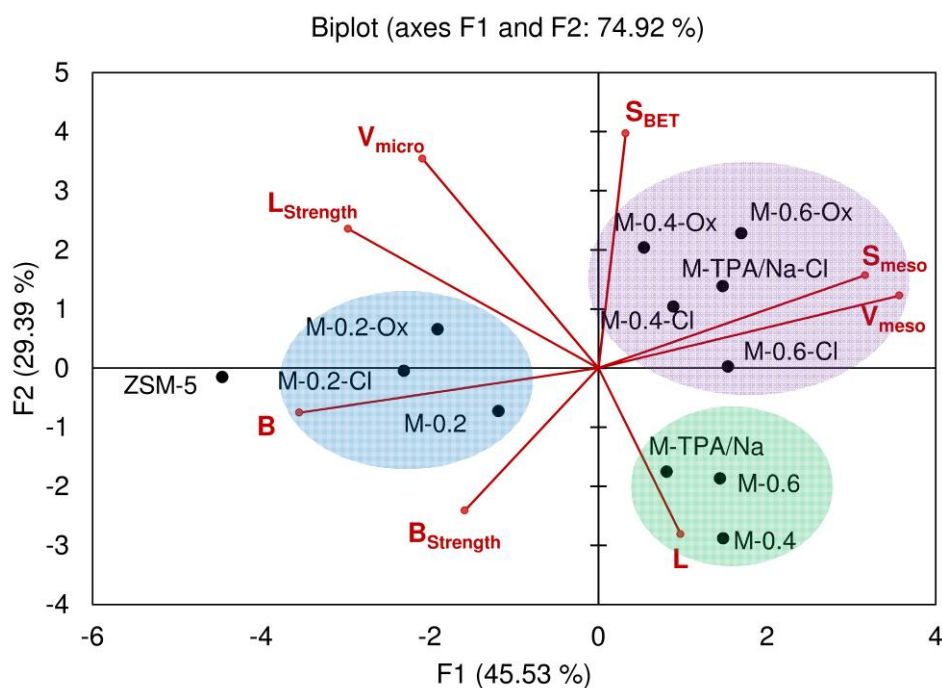


Figure 8.10. Two-dimensional principal component analysis biplot; the variables are represented in red color and the observations in black color; the colored circles signalize three different groups of materials (Group 1 (blue), Group 2 (green), Group 3 (purple)). PCA biplot (PC1: 45.53 % and PC2: 29.39 %) categorizing the materials according to their properties.

## 8.6. Catalytic studies: general considerations

The MFI-based materials prepared *via* the top-down approaches were tested for the oligomerization of 1-butene (1C<sub>4</sub>), under high-pressure (30 bar) continuous-flow conditions, at 200 °C, using a weight hourly space velocity (WHSV) of 2.2 g<sub>1C<sub>4</sub></sub> g<sub>cat</sub><sup>-1</sup> h<sup>-1</sup>. The design and operation conditions of the catalytic reactor were optimized for plug flow pattern with negligible diffusional limitations (Chapter 4). All materials prepared promoted olefin conversion to higher molar mass products (Figure 8.11 and Figure 8.12). The catalyst activation temperature (T<sub>act</sub>) of 200 °C or 450 °C prior to the oligomerization reaction led to similar X<sub>C<sub>4</sub></sub> and STY. The conversion of butenes (X<sub>C<sub>4</sub></sub>) were in the range 10-86 % and the total space time yields (STY) were in the range 19-852 mg g<sub>cat</sub><sup>-1</sup> h<sup>-1</sup>. In general, higher catalytic activity was accompanied by greater production of higher molar mass products (Figure 8.13). Figure 8.14 shows the PLD curves; the mass ratio of Dcut:Ncut was in the range 1.0-3.7, indicating the favorable formation of the 170-390 °C cut characteristic of diesel products (Dcut) over the <170 °C cut characteristic of naphtha products (Ncut).

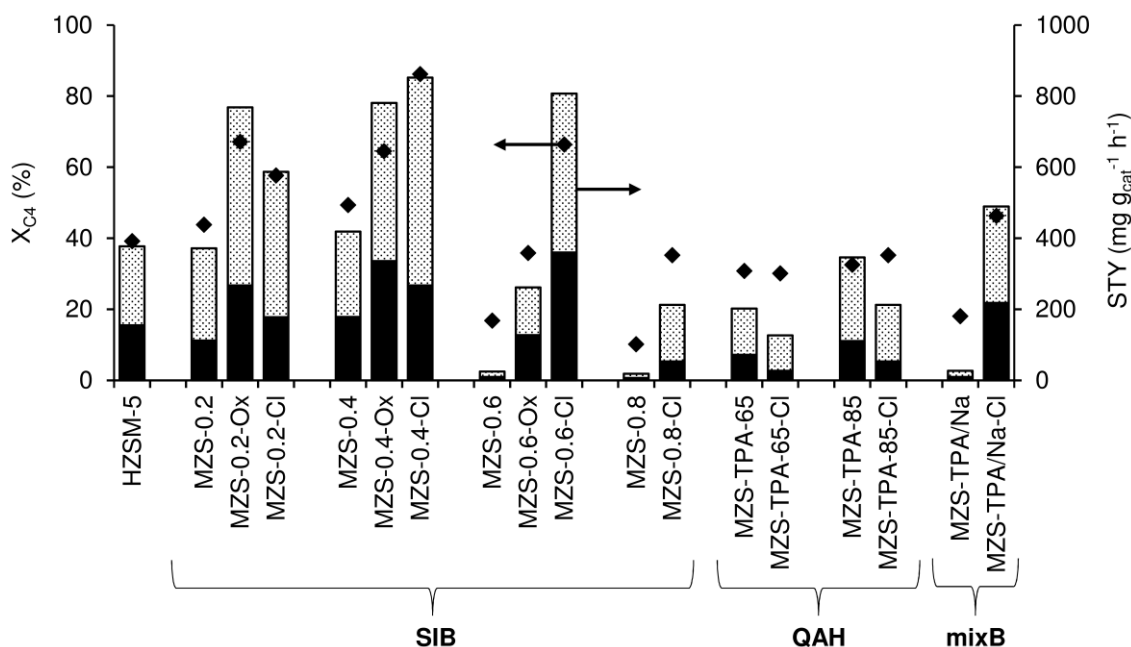


Figure 8.11. Conversion (●) and STY (bars) of Ncut (black bars) and Dcut (grey bars) products for the MFI-based materials prepared and the benchmark catalyst HZSM-5. Reaction conditions: 200 °C, 30 bar, WHSV=2.2 g<sub>1C<sub>4</sub></sub> g<sub>cat</sub><sup>-1</sup> h<sup>-1</sup>, TOS=7 h, T<sub>act</sub>=450 °C.

Modified versions of zeolite ZSM-5 synthesized *via* top-down approaches for oligomerization of 1-butene

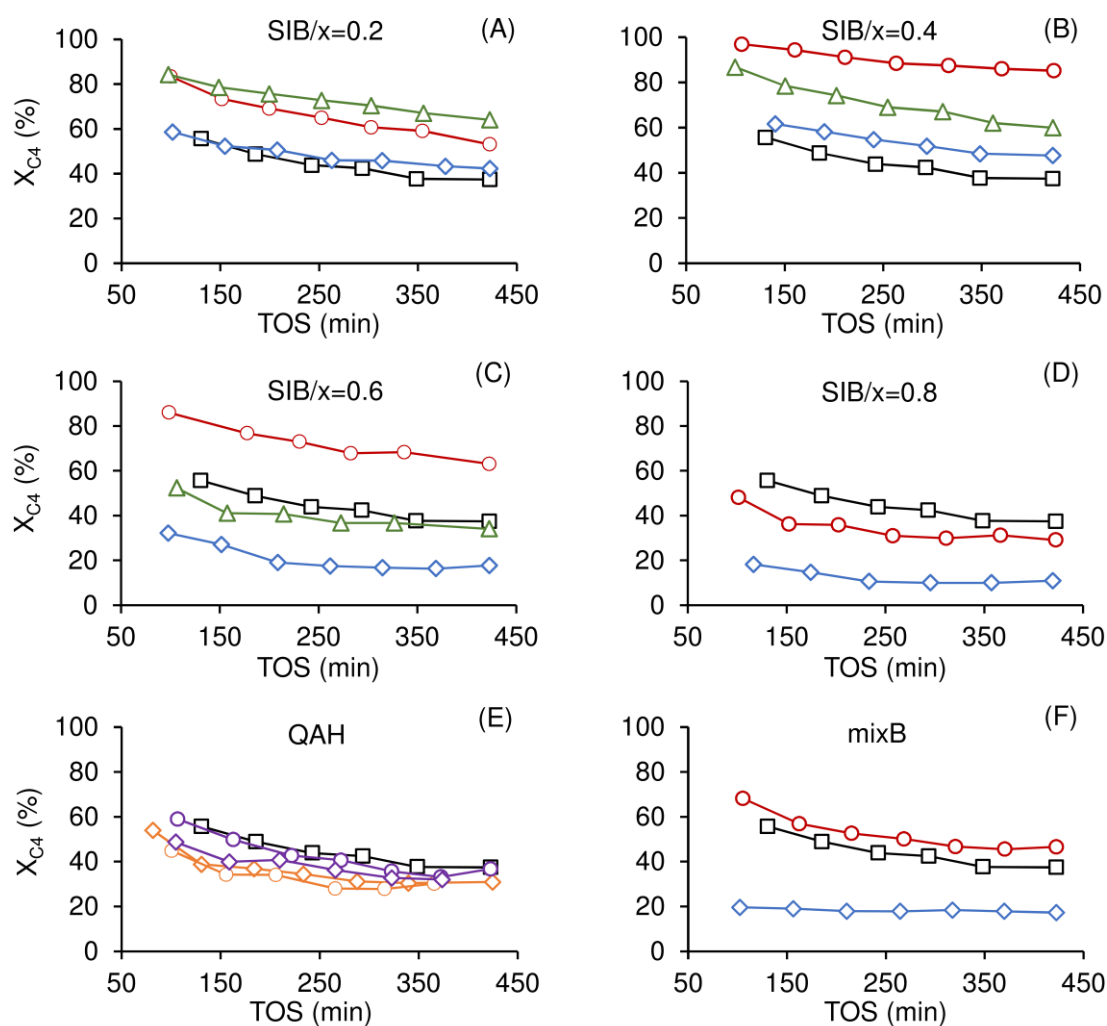


Figure 8.12. Dependence of conversion of butenes on TOS for materials prepared by the SIB procedure using NaOH concentration of 0.2 M (A), 0.4 M (B), 0.6 M (C) or 0.8 M (D); and materials prepared by the QAH (E; orange (65 °C), purple (85 °C)) and mixB (F) procedures: ( $\diamond$ ) - materials without acid treatment; ( $\Delta$ ) - materials treated with oxalic acid; ( $\circ$ ) - materials treated with HCl; ( $\square$ ) - commercial HZSM-5. Reaction conditions: 200 °C, 30 bar, WHSV=2.2 g<sub>1C4</sub> g<sub>cat</sub><sup>-1</sup> h<sup>-1</sup>, TOS=7 h, T<sub>act</sub>=450 °C.

HZSM-5 led to intermediate catalytic results of the modified materials;  $X_{C_4}$ =39 %,  $STY$ =377 mg g<sub>cat</sub><sup>-1</sup> h<sup>-1</sup>, mass ratio Dcut:Ncut=1.4 (Figure 8.11). A comparative study for the desilicated materials (without acid treatment) and HZSM-5 indicated that the SIB/( $x \leq 0.4$ ) led to slightly improved catalytic activity ( $X_{C_4}$ =44-49 %,  $STY$ =372-419 mg g<sub>cat</sub><sup>-1</sup> h<sup>-1</sup>, whereas for  $x > 0.4$  the catalytic performance dropped significantly ( $X_{C_4}$ =10-17 %;  $STY$ =19-25 mg g<sub>cat</sub><sup>-1</sup> h<sup>-1</sup>), Figure 8.11. Catalyst MZS-0.8-Cl performed very poorly, since, although it possessed higher  $S_{meso}$  and  $V_{meso}$  than HZSM-5 (Table 8.2), it lacked crystallinity (Figure

8.3). The QAH and mixB procedures (without acid treatment) led to lower  $X_{C4}$  and STY than HZSM-5. For the QAH procedure, the acid treatment did not bring advantages to the catalytic performance ( $X_{C4}$  was roughly comparable with or without acid treatment). However, for the SIB and mixB procedures, the acid (Ox, Cl) treatment led to considerable improvements in catalytic performances compared to the same procedures without acid treatment (Figure 8.11).

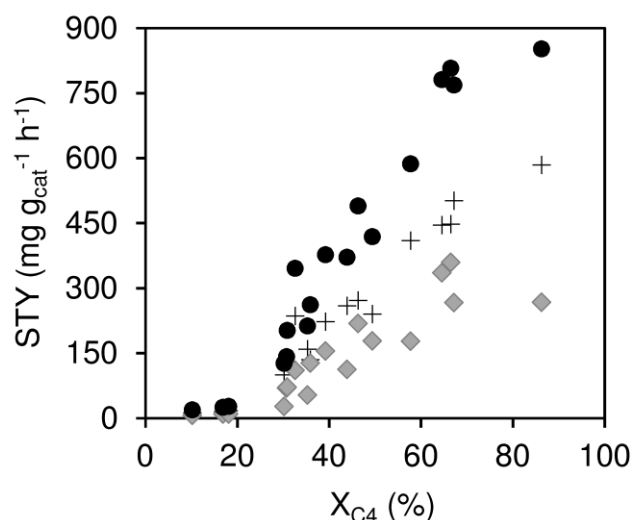


Figure 8.13. STY as a function of  $X_{C4}$ , under approximately steady state conditions, for the different catalysts prepared (STY total (●), STY<sub>Dcut</sub> (+), and STY<sub>Ncut</sub> (◆)). Reaction conditions: 200 °C, 30 bar, WHSV=2.2 g<sub>1C4</sub> g<sub>cat</sub><sup>-1</sup> h<sup>-1</sup>, TOS=7 h, T<sub>act</sub>=450 °C.

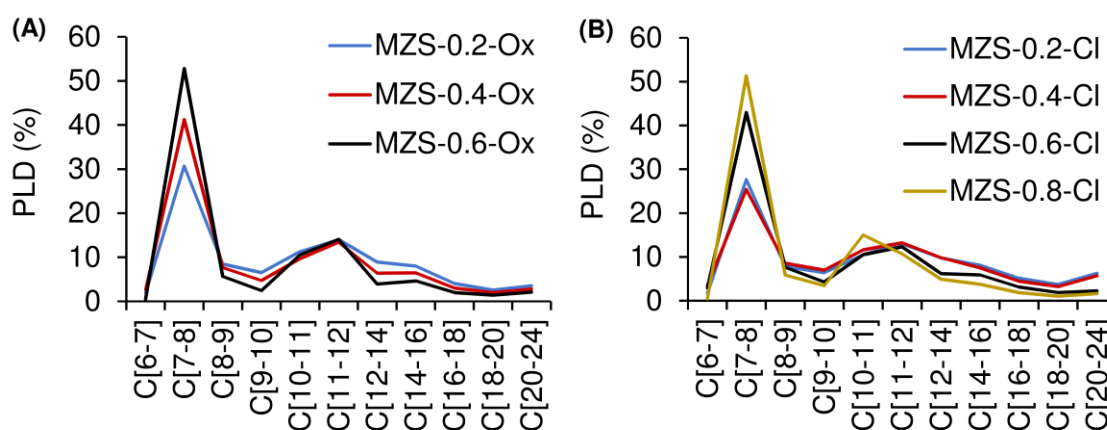


Figure 8.14. Product lump distributions (PLD) curves for the liquid products of the reaction of 1-butene, in the presence of the catalysts prepared *via* the SIB procedure with acid treatment using (A) oxalic acid or (B) HCl. The NaOH concentration was 0.2 M (blue), 0.4 M (red), 0.6 M (black) or 0.8 M (yellow). Reaction conditions: 200 °C, 30 bar, WHSV=2.2 g<sub>1C4</sub> g<sub>cat</sub><sup>-1</sup> h<sup>-1</sup>, TOS=7 h, T<sub>act</sub>=450 °C.

Olefin oligomerization systems involve complex reaction mechanisms where, besides oligomerization, various side reactions may occur such as cracking (primary, secondary), alkylation and isomerizations (double bond, methyl shifts).<sup>[62–65]</sup> The liquid products were analyzed by <sup>1</sup>H NMR spectroscopy to determine the relative amount of aromatic products ( $H_{ar}$ ), isoparaffinic ratio ( $I$ ), and the cetane number (CN, based on the O'Connor method) of the mixtures (Table S8.3).<sup>[66]</sup> The isoparaffinic ratios  $I$  (reflects the branching degree) were in the range 0.52–0.60 for the prepared catalysts. These results are advantageously lower than that reported in Chapter 6 for a mesostructured zeotype based on the BEA topology ( $I \approx 0.62$ ). The  $H_{ar}$  was less than 0.35 %, indicating that the prepared catalysts led to very low aromatics content which is an important advantage of olefin oligomerization routes to clean synthetic fuels. The estimated CN values were in the range 41–46, which serves for rough comparisons, since the products were not subjected to post-treatments (*e.g.*, hydrogenation increases CN<sup>[67,68]</sup>). CN values in the range 48–56 were reported in the literature for diesel cuts produced in commercial processes or commercial diesel samples.<sup>[69–72]</sup>

## 8.7. Influence of material properties on the catalytic performance

A comparative study for the three groups of materials identified using the multivariate, principal component analysis (PCA) tool, indicated that Group 2 catalysts (Figure 8.10) were poorly performing (Figure 8.11); these catalysts were prepared *via* the SIB or mixB procedures using intermediate alkaline ( $OH^-$ ) concentration of 0.4–0.6 M, without acid treatment, and presented miscellaneous properties which may be partly due to the presence of inorganic debris and/or extra-framework Al species (not removed after desilication). The PCA biplot contemplating the IHF (Figure S8.4) indicated that Group 2 materials possessing lower IHF than the respective acid treated materials (Group 3), performed inferiorly.

A comparative study of Groups 1 and 3 (Figure 8.10 and Figure 8.11) pointed to the importance of balancing the textural and acid properties. Group 1 possessed higher amount and strength of B acid sites, and lower mesoporosity (and IHF) than Group 3 materials

(Figure 8.10, Figure S8.4); and Group 3 possessed enhanced  $S_{\text{BET}}$ ,  $S_{\text{meso}}$ ,  $V_{\text{meso}}$  and IHF. Although MZS-0.2-Cl (Group 1) possessed higher amount and strength of B acid sites ( $261 \mu\text{mol g}^{-1}$  and 0.33, respectively, Table 8.3) than the Group 3 materials MZS-0.6-Cl and MZS-0.4-Ox ( $77\text{-}101 \mu\text{mol g}^{-1}$  and 0.05-0.07, respectively, Table 8.3), the latter catalysts performed superiorly in 1C4 conversion (Figure 8.11) likely benefiting from enhanced mesoporosity (Table 8.2). On the other hand, MZS-0.2-Ox (Group 1), and MZS-0.4-Ox and MZS-0.6-Cl (Group 3) led to comparably good catalytic results ( $X_{\text{C}_4}=65\text{-}67\%$ ,  $\text{STY}=769\text{-}808 \text{ mg g}_{\text{cat}}^{-1} \text{ h}^{-1}$ ,  $D_{\text{cut}}/N_{\text{cut}}=1.2\text{-}1.9$ , Figure 8.11). While MZS-0.2-Ox seemed to benefit in terms of B acidity, Group 3 materials benefitted in terms of mesoporosity.

A PCA study was also carried out for data matrix with the catalytic performance parameters ( $D_{\text{Cut}}/N_{\text{Cut}}$ ,  $\text{STY}$ ,  $\text{STY}_{D_{\text{Cut}}}$ ,  $X_{\text{C}_4}$ ) of selected samples (Table S8.2). Figure 8.15 shows the PCA biplot determined with 4 variables (catalytic results) and 9 samples of Groups 1 and 3 (Group 2 was excluded, since these materials possessed considerable amounts of inorganic debris, which does not seem interesting for catalytic application). The first two components accounted for *ca.* 99 % of the variance of the data (PC1: 77 % and PC2: 22 %), which provides a reliable interpretation of the results. The upper side of the PCA biplot represents higher ratio  $D_{\text{Cut}}/N_{\text{Cut}}$  which applies for Group 1, i.e. materials characterized by higher acidity and lower mesoporosity, and, on the other hand, MZS-0.4-Cl which is characterized by medium acidity and higher mesoporosity and IHF. The right side of the biplot represents higher conversion of butenes, total  $\text{STY}$  and  $\text{STY}_{D_{\text{Cut}}}$ , which applies for some materials of Groups 1 and 3. In particular, MZS-0.4-Cl is located on the upper, far-right side of the biplot (Figure 8.15), suggesting that it is the most promising for the production of diesel type products at high conversion of butenes;  $X_{\text{C}_4}=86\%$ ,  $\text{STY}=852 \text{ mg g}_{\text{cat}}^{-1} \text{ h}^{-1}$ ,  $D_{\text{cut}}/N_{\text{cut}}=2.2$  (Figure 8.11). MZS-0.4-Cl possessed intermediate amount of B acid sites (the highest of Group 3;  $138 \mu\text{mol g}^{-1}$ , Table 8.4), besides mesoporosity. Brønsted acidity may favor olefin oligomerization,<sup>[26,73-76]</sup> although the acid sites accessibility seems particularly important for 1-butene conversion. The PCA biplots suggested that mesoporosity and B acidity are inversely related (since these variables are located on opposite quadrants), which calls for a balance. Figure 8.16 shows  $X_{\text{C}_4}$  and  $\text{STY}$  ( $D_{\text{cut}}$ ,  $N_{\text{cut}}$ ) *versus* amount of B acid sites (and L+B, although the main effect was that of B) for the acid-treated materials. These results further support that superior catalytic performances may be met when mesoporosity and intermediate amounts of B (and total) acid sites prevail.

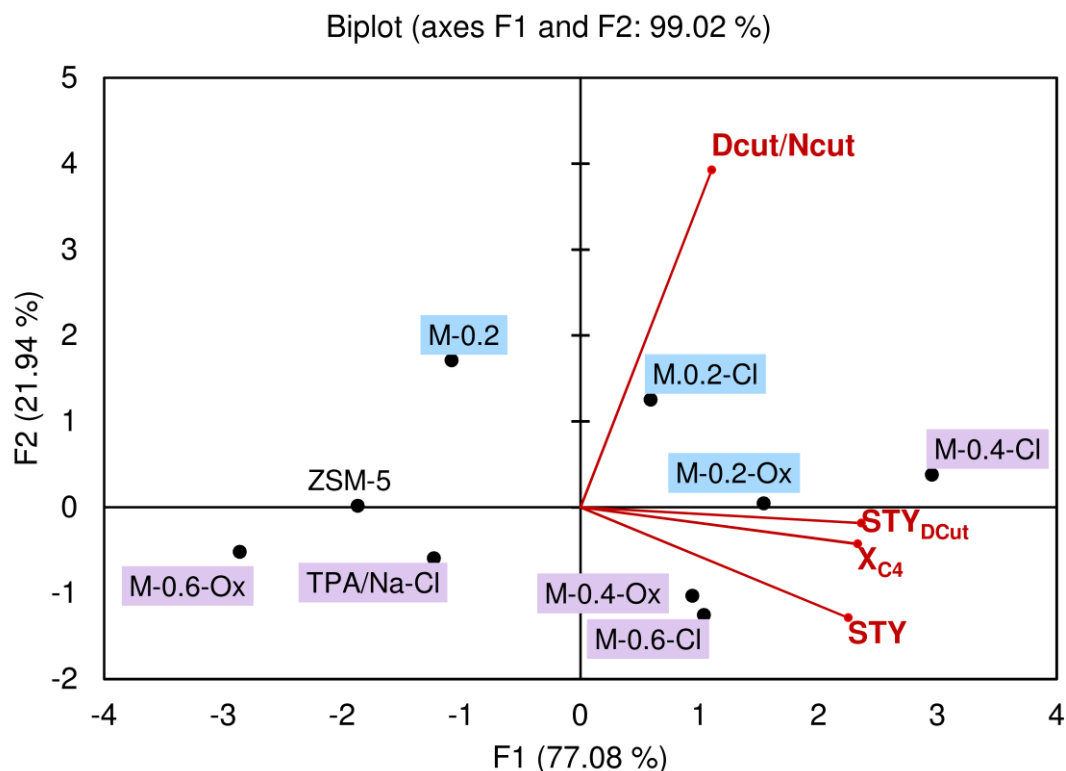


Figure 8.15. Two-dimensional principal component analysis biplot; the variables are represented in red color and the observations in black color; the colored highlights signalize three different groups of materials (Group 1 (blue), Group 2 (green), Group 3 (purple)). PCA biplot (PC1: 77.08 % and PC2: 21.94 %) categorizing the materials according to their catalytic performance.

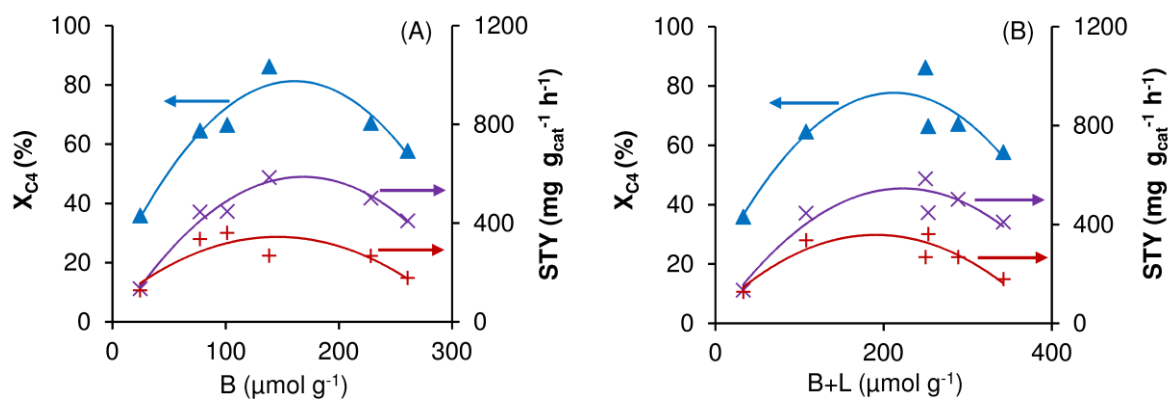


Figure 8.16. Influence of amount of Brønsted acid sites (A) and total amount of acid sites (B) on X<sub>C4</sub> (▲), STY<sub>DCut</sub> (×) and STY<sub>Ncut</sub> (+), for the catalysts MZS-x-Ox and MZS-x-Cl. Reaction conditions: 200 °C, 30 bar, WHSV=2.2 g<sub>1C4</sub> g<sub>cat</sub><sup>-1</sup> h<sup>-1</sup>, TOS=7 h, T<sub>act</sub>=450 °C.

Various effects of acid properties on 1-butene conversion were reported in the literature. Henry et al. reported higher selectivity towards dimers (and, to a smaller extent, trimers) at 220°C for a ZSM-5 sample with Si/Al=20 and possessing higher amount of B acid sites, in relation to another ZSM-5 sample with Si/Al=169.<sup>[77]</sup> Popov et al. reported that 1C<sub>4</sub> oligomerization over zeolite ZSM-5 was favored by B acid sites located in the subsurface of polycrystals, and that B acid sites located on the external surface favored not only oligomerization, but also side reactions such as hydride transfer and cracking.<sup>[74]</sup> In a different study for ZSM-5, the results indicated that conversion and selectivity to diesel increased with increasing amount of B acid sites, at 270 °C/40 bar.<sup>[91]</sup> A comparative study of zeolite Beta and mesoporous aluminosilicate MCM-41 by Kumar et al. indicated favorable effects of mild B acidity of MCM-41 on oligomerization, compared to zeolite Beta possessing more (and stronger) B acid sites.<sup>[78]</sup>

The stabilities of the catalysts MZS-0.2-Cl, MZS-0.2-ox, MZS-0.4-ox, MZS-0.4-Cl and MZS-0.6-Cl were compared based on the drop of X<sub>C<sub>4</sub></sub> with time on-stream (Figure 8.12). The drop of X<sub>C<sub>4</sub></sub> was less pronounced for MZS-0.4-Cl (10 % decrease) than the remaining materials (18-28 % decrease), suggesting that MZS-0.4-Cl was more stable. The used catalysts were brownish in colour, attributable to coke, as confirmed by elemental (EA) and thermal (TGA, DSC) analyses. The amount of coke was in the range 11-14 wt.% (based on the mass loss in the temperature range 200-800 °C, TGA), and EA indicated carbon contents in the range 8-12 wt.%. Figure 8.17 exemplifies the DSC analysis for MZS-0.4-Cl; an endothermic curve below *ca.* 220 °C was due to desorption of physisorbed water/volatiles, and, on the other hand, an exothermic process associated with coke decomposition occurred above *ca.* 270 °C for the used catalyst (and not for original catalyst).

The used catalyst MZS-0.4-Cl was thermally treated at 600 °C (heating rate of 1 °C min<sup>-1</sup>). Thermal analyses and EA gave similar results for the original *versus* treated catalysts (2.8 and 2.9 wt.% mass loss, respectively; 0.58 and 0.78 wt.% C, respectively; Figure 8.18), suggesting that the treatment was effective in removing coke. The resultant regenerated catalyst MZS-0.4-Cl-r was used for a second catalytic run of *ca.* 7 h on-stream (Figure 8.18). The product lump distribution (PLD) curves were similar (inset of Figure 8.18), and conversion decreased slightly by a factor of 1.13 (based on conversion at *ca.* 7 h on-stream). The regenerated catalyst exhibited comparable powder XRD pattern to the original catalyst

(Figure 8.19-A), and the two solids possessed comparable textural properties (Figure 8.19-B, Table 8.2).

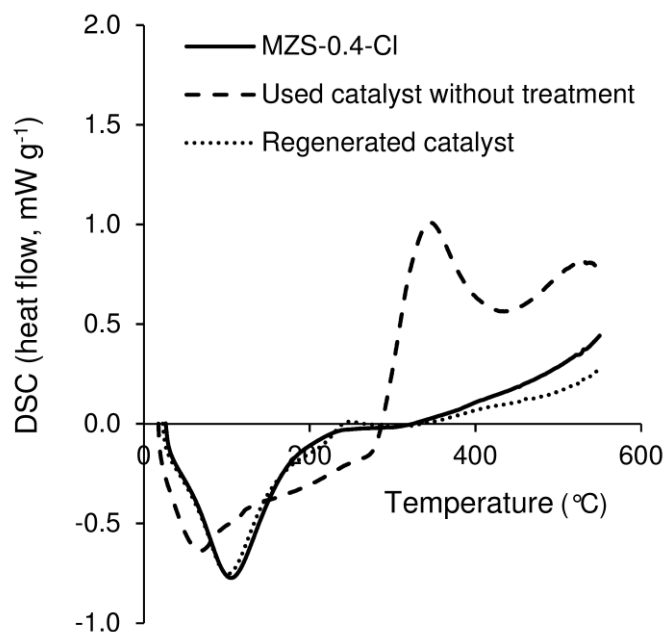


Figure 8.17. DSC analysis of the original, used and thermally regenerated catalyst MZS-0.4-Cl. Reaction conditions: 200 °C, 30 bar, WHSV=2.2 g<sub>1C4</sub> g<sub>cat</sub><sup>-1</sup> h<sup>-1</sup>, TOS=7 h, T<sub>act</sub>=450 °C.

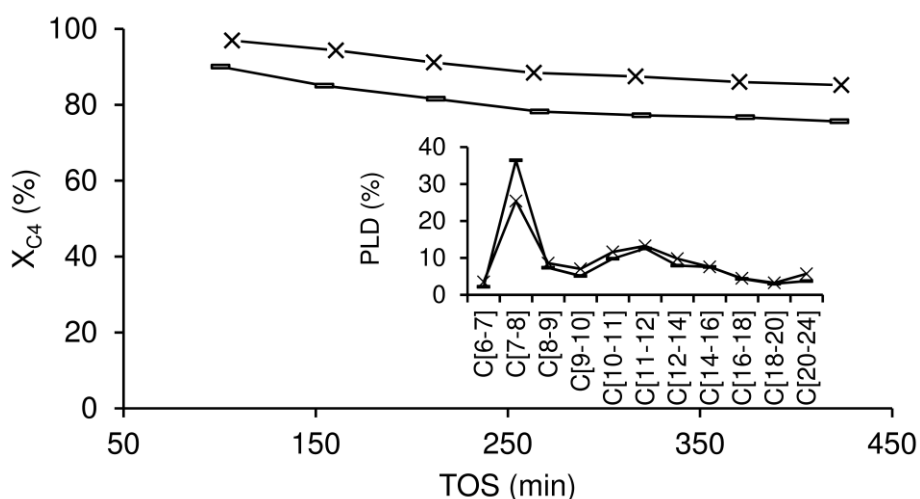


Figure 8.18. Catalytic stability of MZS-0.4-Cl for consecutive 7 h on-stream runs (original catalyst (x); regenerated catalyst MZS-0.4-Cl-r (-)); the inset is the product lump distributions (PLD) curves for the liquid products of the reaction of 1-butene in the presence of the original (x) or the regenerated (-) catalysts. Reaction conditions: 200 °C, 30 bar, WHSV=2.2 g<sub>1C4</sub> g<sub>cat</sub><sup>-1</sup> h<sup>-1</sup>, TOS=7 h, T<sub>act</sub>=450 °C.

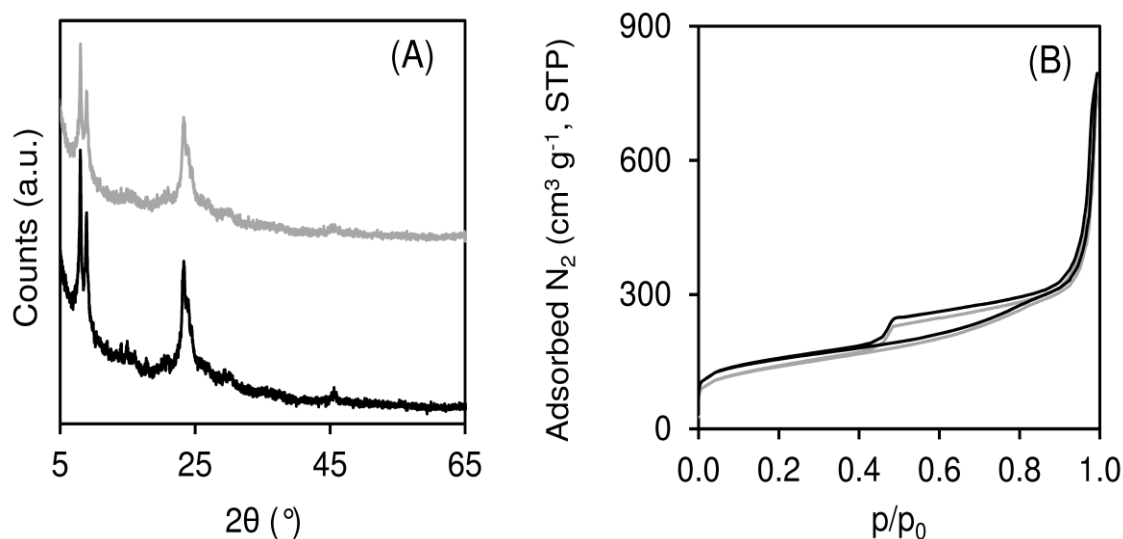


Figure 8.19. (A) Powder XRD patterns for the original (black line) and recovered (grey line) solids. (B) N<sub>2</sub> adsorption-desorption isotherms (at -196 °C) for the original (black line) and recovered (grey line) solids. Reaction conditions: 200 °C, 30 bar, WHSV=2.2 g<sub>1C4</sub> g<sub>cat</sub><sup>-1</sup> h<sup>-1</sup>, TOS=7 h, T<sub>act</sub>=450 °C.

Fair comparisons of the catalytic results to literature data are not straightforward partly due to the considerable number of parameters involved in these reaction processes, which are different between studies or not always specified. Conversion and selectivity depend on several factors such as process conditions and types of catalysts.<sup>[79]</sup> Table 7.4 contemplates the catalytic results (conversions; selectivity towards C10<sup>-</sup> and C10<sup>+</sup> products) of literature data for zeolites and modified zeolites tested for butenes oligomerization using fixed-bed reactors. Based on rough comparisons, MZS-0.4-Cl seemed to perform quite well (86 % butenes conversion and 56 mol.% selectivity to C10<sup>+</sup> products). At higher reaction pressure (40-50 bar) and temperature (270 °C), it was reported relatively high C10<sup>+</sup> selectivity at high conversions for two hydrothermally synthesized ZSM-5 samples:<sup>[80,81]</sup> however, for one of the studies, the type of butene isomer used as substrate and the feed composition were not specified (the catalyst possessed  $S_{\text{meso}}=68 \text{ m}^2 \text{ g}^{-1}$ , comparable to  $S_{\text{meso}}=54 \text{ m}^2 \text{ g}^{-1}$  for HZSM-5 in this work),<sup>[80]</sup> and for the other study no textural properties of the catalyst were indicated.<sup>[81]</sup>

## 8.8. Conclusions

ZSM-5 - type of catalyst used in commercial oligomerization processes - may be modified *via* top-down synthetic approaches to meet superior catalytic performances for converting 1-butene (derivable from (non)renewable sources) to higher molar mass products characteristic of diesel and naphtha cuts, under high-pressure continuous-flow conditions (200 °C, 30 bar). Solid catalysts prepared using appropriate base and acid treatments, outperformed the (calcined) commercial acid catalyst HZSM-5, even though the latter possessed higher amount of total acid sites. Among the superior catalysts, MZS-0.4-Cl (Si/Al=24) prepared *via* desilication using 0.4 M NaOH and acid treatment using HCl, led to 86 % conversion of butenes, space time yield of liquid products (STY) of 852 mg g<sub>cat</sub><sup>-1</sup> h<sup>-1</sup> (7 h on-stream) and mass ratio D<sub>cut</sub>/N<sub>cut</sub> of 2.2, whereas HZSM-5 led to conversion=39 %, STY=377 mg g<sub>cat</sub><sup>-1</sup> h<sup>-1</sup>, D<sub>cut</sub>/N<sub>cut</sub>=1.4. Catalytic studies combined with characterization and multivariate/principal component analysis studies, suggested that superior catalytic performances for 1-butene oligomerization may be met in an intermediate range of acid sites concentrations and prevailing mesoporosity. Protocols involving alkaline treatment using NaOH or mixed NaOH/TPAOH, and acid treatment using HCl or oxalic acid seem effective for modifying commercial microcrystalline HZSM-5 zeolites possessing relatively low Si/Al ratios, to produce adequate catalysts for reactions involving relatively bulky molecules.

## 8.9. References

- [1] C.P. Nicholas, Applications of light olefin oligomerization to the production of fuels and chemicals, *Appl. Catal. A Gen.* 543 (2017) 82–97.
- [2] A. Corma, S. Iborra, Oligomerization of alkenes, in: *E.G., Derouane (Ed.), Catalysts for fine chemical synthesis, Volume 4, Microporous and mesoporous solid catalysts*, John Wiley & Sons, 2006: pp. 125–140.
- [3] M.J. Wulfers, R.F. Lobo, Assessment of mass transfer limitations in oligomerization of butene at high pressure on H-beta, *Appl. Catal. A Gen.* 505 (2015) 394–401.
- [4] J. Weitkamp, S. Ernst, L. Puppe, Shape-selective catalysis in zeolites, in: *Catalysis and zeolites: fundamentals and applications*, 1999: pp. 327–376.
- [5] J. Pérez-Ramírez, C.H. Christensen, K. Egeblad, C.H. Christensen, J.C. Groen, Hierarchical zeolites: enhanced utilisation of microporous crystals in catalysis by advances in materials design, *Chem. Soc. Rev.* 37 (2008) 2530.

- [6] K. Zhu, X. Zhou, Manipulating the architecture of zeolite catalysts for enhanced mass transfer, *Curr. Opin. Chem. Eng.* 9 (2015) 42–48.
- [7] E. Koohsaryan, M. Anbia, Nanosized and hierarchical zeolites: A short review, *Cuihua Xuebao/Chinese J. Catal.* 37 (2016) 447–467.
- [8] C.H. Christensen, K. Johannsen, E. Törnqvist, I. Schmidt, H. Topsøe, C.H. Christensen, Mesoporous zeolite single crystal catalysts: diffusion and catalysis in hierarchical zeolites, *Catal. Today* 128 (2007) 117–122.
- [9] Y. Ji, H. Yang, W. Yan, Catalytic cracking of *n*-hexane to light alkene over ZSM-5 zeolite: Influence of hierarchical porosity and acid property, *Mol. Catal.* 448 (2018) 91–99.
- [10] R. Chal, C. Gérardin, M. Bulut, S. van Donk, Overview and industrial assessment of synthesis strategies towards zeolites with mesopores, *ChemCatChem* 3 (2011) 67–81.
- [11] C. Bertrand-Drira, X. wei Cheng, T. Cacciaguerra, P. Trens, G. Melinte, O. Ersen, D. Minoux, A. Finiels, F. Fajula, C. Gerardin, Mesoporous mordenites obtained by desilication: Mechanistic considerations and evaluation in catalytic oligomerization of pentene, *Microporous Mesoporous Mater.* 213 (2015) 142–149.
- [12] J.C. Groen, J.A. Moulijn, J. Pérez-Ramírez, Desilication: on the controlled generation of mesoporosity in MFI zeolites, *J. Mater. Chem.* 16 (2006) 2121–2131.
- [13] D.P. Serrano, J.M. Escola, P. Pizarro, Synthesis strategies in the search for hierarchical zeolites, *Chem. Soc. Rev.* 42 (2013) 4004–4035.
- [14] Y. Tao, H. Kanoh, L. Abrams, K. Kaneko, Mesopore-modified zeolites: preparation, characterization, and applications, *Chem. Rev.* 106 (2006) 896–910.
- [15] K. Na, M. Choi, R. Ryoo, Recent advances in the synthesis of hierarchically nanoporous zeolites, *Microporous Mesoporous Mater.* 166 (2013) 3–19.
- [16] X. Vu, U. Armbruster, A. Martin, Micro/mesoporous zeolitic composites: recent developments in synthesis and catalytic applications, *Catalysts* 6 (2016) 183–206.
- [17] Z. Liu, D. Wu, S. Ren, X. Chen, M. Qiu, G. Liu, G. Zeng, Y. Sun, Facile one-pot solvent-free synthesis of hierarchical ZSM-5 for methanol to gasoline conversion, *RSC Adv.* 6 (2016) 15816–15820.
- [18] K. Zhu, K. Egeblad, C.H. Christensen, Mesoporous carbon prepared from carbohydrate as hard template for hierarchical zeolites, *Eur. J. Inorg. Chem.* (2007) 3955–3960.
- [19] R.J. White, A. Fischer, C. Goebel, A. Thomas, A sustainable template for mesoporous zeolite synthesis, *J. Am. Chem. Soc.* 136 (2014) 2715–2718.
- [20] L. Wang, Z. Zhang, C. Yin, Z. Shan, F.-S. Xiao, Hierarchical mesoporous zeolites with controllable mesoporosity templated from cationic polymers, *Microporous Mesoporous Mater.* 131 (2010) 58–67.
- [21] D.P. Serrano, J.M. Escola, R. Sanz, R.A. Garcia, A. Peral, I. Moreno, M. Linares, Hierarchical ZSM-5 zeolite with uniform mesopores and improved catalytic properties, *New J. Chem.* 40 (2016) 4206–4216.
- [22] L. Meng, B. Mezari, M.G. Goesten, E.J.M. Hensen, One-step synthesis of hierarchical ZSM-5 using cetyltrimethylammonium as mesoporegen and structure-directing agent, *Chem. Mater.* 29 (2017) 4091–4096.
- [23] Y. Wang, J. Song, N.C. Baxter, G.T. Kuo, S. Wang, Synthesis of hierarchical ZSM-5 zeolites by solid-state crystallization and their catalytic properties, *J. Catal.* 349 (2017) 53–65.
- [24] K. Möller, B. Yilmaz, R.M. Jacubinas, U. Müller, T. Bein, One-step synthesis of hierarchical zeolite beta *via* network formation of uniform nanocrystals, *J. Am. Chem. Soc.* 133 (2011) 5284–5295.

- [25] O. Mazaheri, R.J. Kalbasi, Preparation and characterization of Ni/mZSM-5 zeolite with a hierarchical pore structure by using KIT-6 as silica template: an efficient bi-functional catalyst for the reduction of nitro aromatic compounds, *RSC Adv.* 5 (2015) 34398–34414.
- [26] A. Corma, C. Martínez, E. Dorskocil, Designing MFI-based catalysts with improved catalyst life for C<sub>3</sub>= and C<sub>5</sub>= oligomerization to high-quality liquid fuels, *J. Catal.* 300 (2013) 183–196.
- [27] Q. Shen, L. Zhang, M. Wu, C. He, W. Wei, N. Sun, Y. Sun, Post-synthesis of mesoporous ZSM-5 zeolites with TPAOH-assisted desilication and determination of activity performance in N<sub>2</sub>O decomposition, *J. Porous Mater.* 24 (2017) 759–767.
- [28] S. Abelló, A. Bonilla, J. Pérez-Ramírez, Mesoporous ZSM-5 zeolite catalysts prepared by desilication with organic hydroxides and comparison with NaOH leaching, *Appl. Catal. A Gen.* 364 (2009) 191–198.
- [29] M.M. Antunes, S. Lima, A. Fernandes, A.L. Magalhães, P. Neves, C.M. Silva, M.F. Ribeiro, D. Chadwick, K. Hellgardt, M. Pillinger, A.A. Valente, MFI acid catalysts with different crystal sizes and porosity for the conversion of furanic compounds in alcohol media, *ChemCatChem* 9 (2017) 2747–2759.
- [30] N.A.S. Amin, D.D. Anggoro, Dealuminated ZSM-5 zeolite catalyst for ethylene oligomerization to liquid fuels, *J. Nat. Gas Chem.* 11 (2002) 79–86.
- [31] E.H. Yuan, Z. Tang, Z. Mo, G. Lu, A new method to construct hierarchical ZSM-5 zeolites with excellent catalytic activity, *J. Porous Mater.* 21 (2014) 957–965.
- [32] P.J. Kooyman, P. van Der Waal, H. van Bekkum, Acid dealumination of ZSM-5, *Zeolites* 18 (1997) 50–53.
- [33] P. Losch, T.C. Hoff, J.F. Kolb, C. Bernardon, J.-P. Tessonnier, B. Louis, Mesoporous ZSM-5 zeolites in acid catalysis: Top-Down vs. Bottom-Up approach, *Catalysts* 7 (2017) 225.
- [34] X. Wang, X. Hu, C. Song, K.W. Lux, M. Namazian, T. Imam, Oligomerization of biomass-derived light olefins to liquid fuel: effect of alkali treatment on the HZSM-5 catalyst, *Ind. Eng. Chem. Res.* 56 (2017) 12046–12055.
- [35] M.J. van Niekerk, C.T. O'Connor, J.C.Q. Fletcher, Methanol conversion and propene oligomerization productivity of dealuminated large-pore mordenites, *Ind. Eng. Chem. Res.* 35 (1996) 697–702.
- [36] J.W. Yoon, S.H. Jung, D.H. Choo, S.J. Lee, K.-Y. Lee, J.S. Chang, Oligomerization of isobutene over dealuminated Y zeolite catalysts, *Appl. Catal. A Gen.* 337 (2008) 73–77.
- [37] C. Martínez, E.J. Dorskocil, A. Corma, Improved THETA-1 for light olefins oligomerization to diesel: influence of textural and acidic properties, *Top. Catal.* 57 (2014) 668–682.
- [38] E. Epelde, J.I. Santos, P. Florian, A.T. Aguayo, A.G. Gayubo, J. Bilbao, P. Castaño, Controlling coke deactivation and cracking selectivity of MFI zeolite by H<sub>3</sub>PO<sub>4</sub> or KOH modification, *Appl. Catal. A Gen.* 505 (2015) 105–115.
- [39] A. Abdalla, P. Arudra, S.S. Al-Khattaf, Catalytic cracking of 1-butene to propylene using modified H-ZSM-5 catalyst: a comparative study of surface modification and core-shell synthesis, *Appl. Catal. A Gen.* 533 (2017) 109–120.
- [40] M. Ibáñez, E. Epelde, A.T. Aguayo, A.G. Gayubo, J. Bilbao, P. Castaño, Selective dealumination of HZSM-5 zeolite boosts propylene by modifying 1-butene cracking pathway, *Appl. Catal. A Gen.* 543 (2017) 1–9.
- [41] S. Mitchell, M. Boltz, J. Liu, J. Pérez-Ramírez, Engineering of ZSM-5 zeolite crystals for enhanced lifetime in the production of light olefins *via* 2-methyl-2-butene cracking, *Catal. Sci. Technol.* 7 (2017) 64–74.

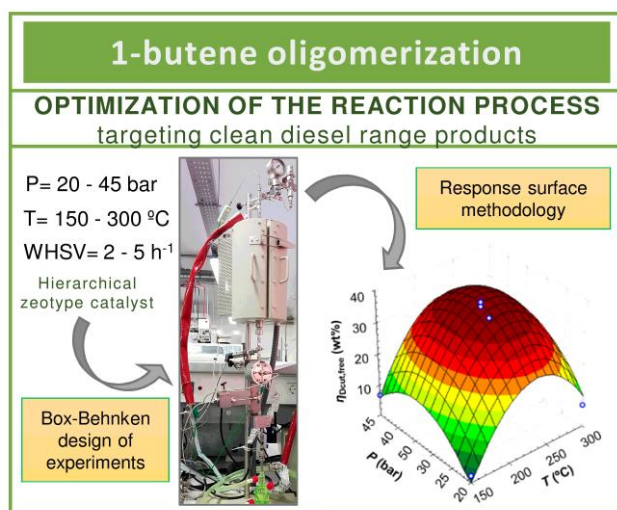
- [42] Y. He, M. Liu, C. Dai, S. Xu, Y. Wei, Z. Liu, X. Guo, Modification of nanocrystalline HZSM-5 zeolite with tetrapropylammonium hydroxide and its catalytic performance in methanol to gasoline reaction, *Cuihua Xuebao/Chinese J. Catal.* 34 (2013) 1148–1158.
- [43] R. Caicedo-Realpe, J. Pérez-Ramírez, Mesoporous ZSM-5 zeolites prepared by a two-step route comprising sodium aluminate and acid treatments, *Microporous Mesoporous Mater.* 128 (2010) 91–100.
- [44] C. Knottenbelt, Mossgas “gas-to-liquid” diesel fuels - An environmentally friendly option, *Catal. Today* 71 (2002) 437–445.
- [45] A. de Klerk, E. Furimsky, Catalysis in the upgrading of Fischer–Tropsch syncrude, in: *Catalysis in the refining of Fischer–Tropsch syncrude*, 2010: pp. 40–164.
- [46] A. V. Lavrenov, T.R. Karpova, E.A. Buluchevskii, E.N. Bogdanets, Heterogeneous oligomerization of light alkenes: 80 years in oil refining, *Catal. Ind.* 8 (2016) 316–327.
- [47] D. Verboekend, S. Mitchell, M. Milina, J.C. Groen, J. Pérez-Ramírez, Full compositional flexibility in the preparation of mesoporous MFI zeolites by desilication, *J. Phys. Chem. C.* 115 (2011) 14193–14203.
- [48] M.-C. Silaghi, C. Chizallet, P. Raybaud, Challenges on molecular aspects of dealumination and desilication of zeolites, *Microporous Mesoporous Mater.* 191 (2014) 82–96.
- [49] R. Caicedo-Realpe, J. Pérez-Ramírez, Mesoporous ZSM-5 zeolites prepared by a two-step route comprising sodium aluminate and acid treatments, *Microporous Mesoporous Mater.* 128 (2010) 91–100.
- [50] A.S. Al-Dughaiter, H. de Lasa, HZSM-5 zeolites with different SiO<sub>2</sub>/Al<sub>2</sub>O<sub>3</sub> ratios. characterization and NH<sub>3</sub> desorption kinetics, *Ind. Eng. Chem. Res.* 53 (2014) 15303–15316.
- [51] M.M.J. Treacy, J.B. Higgins, *Collection of simulated XRD powder patterns for zeolites*, ELSEVIER, 2001.
- [52] Y. Wei, T.E. Parmentier, K.P. de Jong, J. Zečević, Tailoring and visualizing the pore architecture of hierarchical zeolites, *Chem. Soc. Rev.* 44 (2015) 7234–7261.
- [53] Z. Qin, B. Shen, Z. Yu, F. Deng, L. Zhao, S. Zhou, D. Yuan, X. Gao, B. Wang, H. Zhao, H. Liu, A defect-based strategy for the preparation of mesoporous zeolite y for high-performance catalytic cracking, *J. Catal.* 298 (2013) 102–111.
- [54] T.C. Hoff, D.W. Gardner, R. Thilakarathne, J. Proano-Aviles, R.C. Brown, J.P. Tessonnier, Elucidating the effect of desilication on aluminum-rich ZSM-5 zeolite and its consequences on biomass catalytic fast pyrolysis, *Appl. Catal. A Gen.* 529 (2017) 68–78.
- [55] D. Verboekend, J. Pérez-Ramírez, Desilication mechanism revisited: highly mesoporous all-silica zeolites enabled through pore-directing agents, *Chem. - A Eur. J.* 17 (2011) 1137–1147.
- [56] K. Góra-Marek, M. Derewiński, P. Sarv, J. Datka, IR and NMR studies of mesoporous alumina and related aluminosilicates, *Catal. Today* 101 (2005) 131–138.
- [57] J.M.R. Gallo, C. Bisio, G. Gatti, L. Marchese, H.O. Pastore, Physicochemical characterization and surface acid properties of mesoporous [Al]-SBA-15 obtained by direct synthesis, *Langmuir* 26 (2010) 5791–5800.
- [58] B.H. Chiche, F. Fajula, E. Garrone, Formation of conjugated iminium ions from pyridine on dealuminated mazzite, *J. Catal.* 146 (1994) 460–467.
- [59] I.T. Jolliffe, *Principal component analysis*, 2<sup>nd</sup> ed., Springer, 2002.
- [60] J.I. Alvira, I. Hita, E. Rodríguez, J.M. Arandes, P. Castaño, A data-driven reaction network for the fluid catalytic cracking of waste feeds, *Processes* 6 (2018) 243–257.
- [61] A.N. Pasadakis, C. Yiokari, N. Varotsis, C. Vayenas, Characterization of hydrotreating catalysts using the principal component analysis, *Appl. Catal. A Gen.* 207 (2001) 333–341.

- [62] L. Ying, J. Zhu, Y. Cheng, L. Wang, X. Li, Kinetic modeling of C2-C7 olefins interconversion over ZSM-5 catalyst, *J. Ind. Eng. Chem.* 33 (2016) 80–90.
- [63] A. de Klerk, Fischer-Tropsch refining, University of Pretoria, 2011.
- [64] Y.T. Kim, J.P. Chada, Z. Xu, Y.J. Pagan-Torres, D.C. Rosenfeld, W.L. Winniford, E. Schmidt, G.W. Huber, Low-temperature oligomerization of 1-butene with H-ferrierite, *J. Catal.* 323 (2015) 33–44.
- [65] M. Sanati, C. Hörnell, S.G. Jaras, The oligomerization of alkenes by heterogeneous catalysts, in: J.J. Spivey (Ed.), *Catalysis, Volume 14 (Specialist periodical reports)*, Royal society of chemistry, 1999: pp. 236–287.
- [66] C.T. O'Connor, R.D. Forrester, M.S. Scurrall, Cetane number determination of synthetic diesel fuels, *Fuel* 71 (1992) 1323–1327.
- [67] J.A. Tilton, W.M. Smith, W.G. Hockberger, Production of high cetane number diesel fuels by hydrogenation, *Ind. Eng. Chem.* 40 (1948) 1269–1273.
- [68] R.J. Ellis, R.J. Bennett, R. Berndt, J. Brandt, J. Cattananch, G. Crociani, B. Patrick, Opportunities and costs to upgrade the quality of automotive diesel fuel, CONCAWE Reports. (1988). [https://www.concawe.eu/wp-content/uploads/2017/01/rpt\\_88-52ocr-2004-01313-01-e.pdf](https://www.concawe.eu/wp-content/uploads/2017/01/rpt_88-52ocr-2004-01313-01-e.pdf) (accessed October 26, 2018).
- [69] G.S. Kapur, A. Ecker, R. Meusinger, Establishing quantitative structure-property relationships (QSPR) of diesel samples by proton-NMR & multiple linear regression (MLR) analysis, *Energy and Fuels* 15 (2001) 943–948.
- [70] A. De Klerk, Fischer-Tropsch refining: technology selection to match molecules, *Green Chem.* 10 (2008) 1249–1279.
- [71] D. Leckel, Diesel production from Fischer-Tropsch: the past, the present, and new concepts, *Energy & Fuels* 23 (2009) 2342–2358.
- [72] Chevron, Diesel Fuels Technical Review, (2007). <https://www.chevron.com/--/media/chevron/operations/documents/diesel-fuel-tech-review.pdf>.
- [73] A.N. Mlinar, P.M. Zimmerman, F.E. Celik, M. Head-Gordon, A.T. Bell, Effects of Brønsted-acid site proximity on the oligomerization of propene in H-MFI, *J. Catal.* 288 (2012) 65–73.
- [74] A.G. Popov, V.S. Pavlov, I.I. Ivanova, Effect of crystal size on butenes oligomerization over MFI catalysts, *J. Catal.* 335 (2016) 155–164.
- [75] M.R. Díaz-Rey, C. Paris, R. Martínez-Franco, M. Moliner, C. Martínez, A. Corma, Efficient oligomerization of pentene into liquid fuels on nanocrystalline Beta zeolites, *ACS Catal.* 7 (2017) 6170–6178.
- [76] M. Bjørgen, K.P. Lillerud, U. Olsbye, S. Bordiga, A. Zecchina, 1-butene oligomerization in brønsted acidic zeolites: mechanistic insights from low-temperature in situ FTIR spectroscopy, *J. Phys. Chem. B.* 108 (2004) 7862–7870.
- [77] M. Henry, M. Bulut, W. Vermandel, B. Sels, P. Jacobs, D. Minoux, N. Nesterenko, S. van Donk, J.P. Dath, Low temperature conversion of linear C4 olefins with acid ZSM-5 zeolites of homogeneous composition, *Appl. Catal. A, Gen.* 413–414 (2012) 62–77.
- [78] N. Kumar, P. Mäki-Arvela, T. Yläsalmi, J. Villegas, T. Heikkilä, A.R. Leino, K. Kordás, T. Salmi, D. Yu Murzin, Dimerization of 1-butene in liquid phase reaction: Influence of structure, pore size and acidity of Beta zeolite and MCM-41 mesoporous material, *Microporous Mesoporous Mater.* 147 (2012) 127–134.
- [79] O. Muraza, Maximizing diesel production through oligomerization: a landmark opportunity for zeolite research, *Ind. Eng. Chem. Res.* 54 (2015) 781–789.

- [80] C. Li, J. Du, H. Wang, X. Li, S.S. Zhu, G. Liu, J. Wu, A hemicellulose modified HZSM-5 and their application in the light olefins oligomerization to high-quality liquid fuels reaction, *Catal. Commun.* 102 (2017) 89–92.
- [81] S. Schwarz, M. Kojima, C.T. O'Connor, Effect of silicon-to-aluminum ratio and synthesis time on high-pressure olefin oligomerization over ZSM-5, *Appl. Catal.* 56 (1989) 263–280.

# CHAPTER 9

## Optimization of heterogeneous catalytic oligomerization of 1-butene by design of experiments and response surface methodology



### Abstract

Oligomerization of light olefins aims at the production of clean, sulphur-free fuels or fuel additives with reduced aromatics content, and useful chemicals. Commercial heterogeneous catalytic oligomerization technologies were developed to meet market demands in flexible fashions, whereby the operating conditions were adjustable in favor of the desired product specifications and yields. These strategies are examples of the importance of optimizing

oligomerization reaction processes, which are complex systems and difficult to predict *via* rigorous kinetic modelling. Multivariate statistics techniques, namely, the design of experiments (DoE) and response surface methodology (RSM) allow the expeditious determination of the optimal operating conditions, yet are presently unexploited for light olefins oligomerization processes. This work deals with the optimization of olefin oligomerization by DoE/RSM, with the analytical input of Comprehensive Two-Dimensional Gas Chromatography with Time-of-Flight Mass Spectrometry (GC×GC-ToFMS) used for characterizing the complex product mixtures. The optimization studies were carried out for the conversion of 1-butene – derivable from fossil or renewable sources of organic carbon - over a hierarchical zeotype catalyst, under continuous-flow operation, targeting clean diesel range products. DoE/RSM and GC×GC-ToFMS allowed optimizing the product yields in a refined fashion to contemplate quality features such as reduced aromatics content.

## CHAPTER 9

### **Optimization of heterogeneous catalytic oligomerization of 1-butene by design of experiments and response surface methodology**

9.1.	Introduction .....	281
9.2.	Synthesis of the catalytic materials .....	283
9.3.	Design of experiments and response surface methodology.....	284
9.3.	Characterization studies of the catalytic materials .....	287
9.4.	Catalytic studies: general considerations.....	289
9.5.	Optimization studies of 1-butene oligomerization .....	294
9.6.	Conclusions .....	299
9.7.	References .....	300

## 9.1. Introduction

Light olefins (ethene, propene, butenes) have long been key industrial building blocks partly due to their availability and relative cheapness. The oligomerization of light olefins - which may derive from fossil fuels or renewable sources such as cellulosic biomass<sup>[1,2]</sup> – may lead to clean synthetic fuels and useful chemicals.<sup>[3–6]</sup> Over the years, commercialized olefin oligomerization technologies have been strategically developed for the transportation fuels sector. Nearly a century ago, Universal Oil Products (UOP) developed the CatPoly technology (1930s)<sup>[7,8]</sup> which converted propene/butene mixtures derived from Fischer-Tropsch processes to gasoline and diesel range products, using solid phosphoric acid as catalyst (Table 2.5). Following, Mobil Olefins to Gasoline and Distillates (MOGD)<sup>[9,10]</sup> and Conversion of Olefins to Distillates (COD)<sup>[11,12]</sup> emerged as flexible technologies allowing a broad range of operating conditions in “Gasoline Mode” or “Distillate Mode”, using zeolite ZSM-5 type catalyst (Table 9.1).<sup>[10,12,13]</sup> More recently, Axens developed the Polyfuel technology for maximal production of distillates, by converting light olefins derived from gasoline to distillates, using amorphous silica-alumina (ASA; IP 811) as catalyst (Table 2.5).<sup>[14]</sup>

Table 9.1. Gasoline and distillate mode operating conditions used in light olefins oligomerization technologies.

<b>Technology</b>	<b>Operation mode</b>	<b>P (bar)</b>	<b>T (°C)</b>	<b>WHSV (h<sup>-1</sup>)</b>	<b>Ref.</b>
Catpoly	Gasoline	30-40	180-200	0.5-1	[13]
MOGD	Gasoline	4-30	230-375	0.5-2	[12]
	Distillate	42-70	190-315	0.5-1.5	
COD	Gasoline	58	223-350	0.5	[10]
	Distillate	58	233-350	0.5	

Research efforts continue to be made in the fields of material science and catalysis to develop efficient heterogeneous catalytic oligomerization processes.<sup>[15–22]</sup> The efficiency passes through the maximization of catalyst productivity and optimization of the operating conditions. In particular, the operating conditions influence the thermodynamics and kinetics

of the global process. However, the development of rigorous kinetic models of complex reaction systems such as olefins oligomerization, is not trivial. Oligomerization involves consecutive reactions of light olefins to oligomers, and the latter may undergo multiple reactions such as skeletal and double bond isomerization, disproportionation, hydrogen transfer reactions, cyclization and cracking.<sup>[23]</sup> The operating conditions will influence the relative rates of the various pathways, and lead to product mixtures with different properties such as branching degree, molecular weight and boiling point.<sup>[24,25]</sup> For example, oligomerization reactions are highly exothermic and involve reduction of the total number of moles of the system. Hence, low temperature ( $< 200\text{ }^{\circ}\text{C}$ ) and high pressure may be thermodynamically favorable. However, at relatively low temperature, the chain growth may slow down, and at relatively high temperature (especially  $> 300\text{ }^{\circ}\text{C}$ ) undesired reactions such as cracking, hydrogen transfer and disproportionation may be favored.<sup>[26,27]</sup>

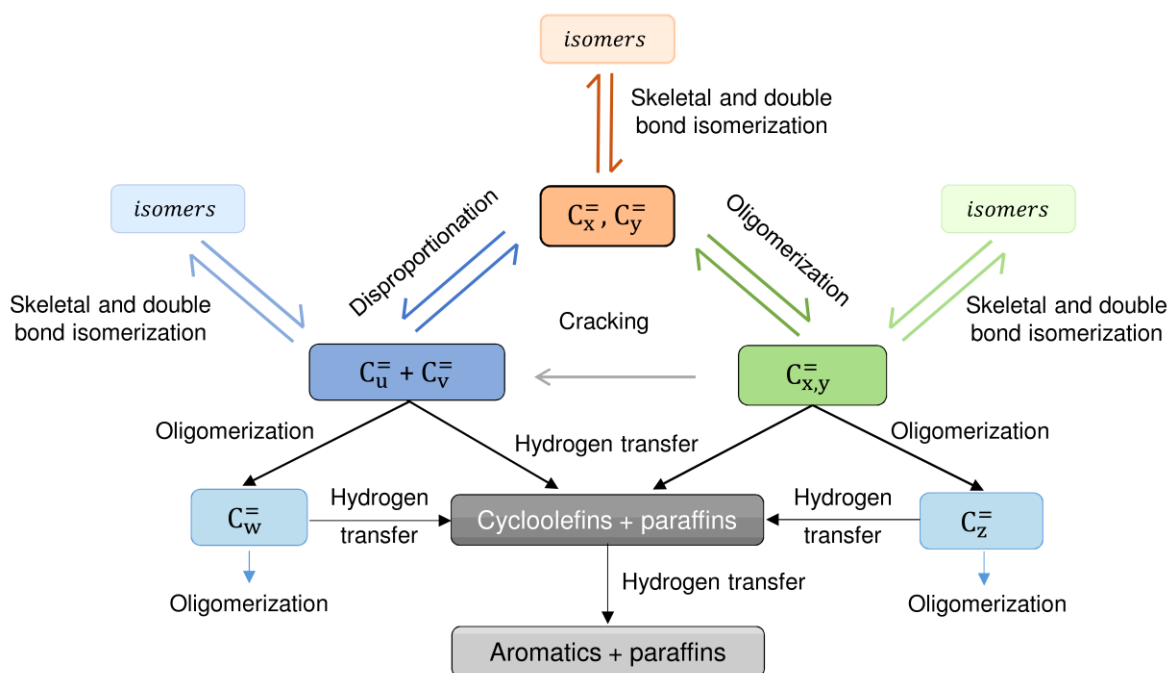


Figure 9.1. Light olefin oligomerization reaction and possible pathways involved in the complex reaction system ( $x, y, u, v, w$  and  $z$  are the carbon number).

The expeditious optimization of complex reaction systems may be accomplished using multivariate statistical tools, specifically, design of experiments (DoE) and response surface methodology (RSM). Applying DoE/RSM to a set of catalytic assays allows the

identification of main factors influencing catalytic reaction process indicators.<sup>[28]</sup> RSM may represent non-linear relationships between independent variables and responses of system, being useful in several research subjects such as supercritical fluid extraction,<sup>[29–31]</sup> Fischer-Tropsch synthesis,<sup>[32]</sup> adsorption<sup>[33]</sup> and chromatography.<sup>[34]</sup> Despite its great potential, there is only one study of the optimization of olefin oligomerization using DoE/RSM tools, to the best of our knowledge. Specifically, Echaroj et al.<sup>[35]</sup> employed DoE/RSM to optimize the production of fuels and lubricant oils *via* the oligomerization of a heavy olefin (1-decene) over sulfated alumina catalysts, at atmospheric pressure.

In this work, DoE/RSM tools are employed, for the first time, for the optimization of light olefin oligomerization, specifically of 1-butene, under high-pressure continuous-flow conditions, using a hierarchical zeotype catalyst (namely, hierZ-MFI, prepared *via* a top-down approach from commercial zeolite ZSM-5). DoE/RSM tools shed light on the interplay of temperature, pressure and weight hourly space velocity influencing 1-butene conversion and product yields, and helped determine, expeditiously, the optimal operating conditions for maximizing yields of clean diesel range products (free of aromatics).

## 9.2. Synthesis of the catalytic materials

The catalyst was prepared *via* the top-down approach, starting from commercial (microcrystalline) zeolite NH<sub>4</sub>ZSM-5, in a similar fashion to that described in Chapter 8. Specifically, NH<sub>4</sub>ZSM-5 was calcined at 550 °C for 5 h (heating rate of 1 °C min<sup>-1</sup>) giving H-ZSM-5. H-ZSM-5 was treated with an aqueous solution of 0.4 M NaOH (30 cm<sup>3</sup> of solution per gram of solid) under stirring at 65 °C and kept at this temperature for 2 h. Subsequently, the solution was cooled using an ice bath, for *ca.* 10-15 min. The solid was separated by centrifugation and thoroughly washed with distilled water at 80 °C until pH=7, and dried overnight at 110 °C. The obtained material, in its alkaline (sodium) form, was converted to the acid form *via* ion-exchange, using 100 cm<sup>3</sup> of 0.1 M aq. NH<sub>4</sub>NO<sub>3</sub> solution per gram of solid and stirring for 24 h, at 25 °C; the liquid phase was renewed twice (every 24 h). The solid was separated by centrifugation, washed with distillate water and dried overnight at 60 °C. The ion-exchanged material was treated with hydrochloric acid to remove

inorganic debris obstructing the pores and/or extra-framework aluminum species.<sup>[36–38]</sup> Specifically, 0.1 M aq. HCl was added to the solid (100 cm<sup>3</sup> of solution per gram of solid) and stirred for 6 h at 65 °C; the solid was filtered, washed with milli-Q water until pH=7 and dried overnight at 60 °C. Finally, the material was calcined at 500 °C for 5 h (heating rate of 1 °C min<sup>-1</sup>), giving the hierarchical zeotype hierZ-MFI.

### 9.3. Design of experiments and response surface methodology

DoE and RSM consists of mathematical and statistical methods which systematize and treat experimental data, in order to screen and optimize a studied response (dependent variable) as a function of direct and crossed factors (independent variables). DoE/RSM minimizes the number of experimental runs necessary for optimizing the process when rigorous kinetic modelling is difficult. In the RSM it is necessary to select the independent variables (factors) of the system, the experimental range of values of the factors (minimum and maximum limits), the degrees of variation of the factors (levels), and the experimental design method (e.g. Box-Benken, full factorial, Doehlert matrix, Taguchi, etc.).<sup>[28,39]</sup>

For 1-butene oligomerization over hierZ-MFI, three factors were considered, namely total pressure (P), reaction temperature (T), and weight hourly space velocity (W), in the following ranges of operating conditions (factors): 20-45 bar, 150-300 °C, 2-5 g<sub>1C4</sub> g<sub>cat</sub><sup>-1</sup> h<sup>-1</sup>, respectively (Table 9.2). The choice of these ranges was based on the known operating conditions of commercial oligomerization technologies (Table 9.1),<sup>[10,12,13]</sup> and the ranges of operating conditions allowable in our catalytic reactor setup. Three levels were considered for each factor (independent variable), which were codified according to Eq. (1).

$$X_k = \frac{x_k - x_0}{\Delta x_k} \quad (1)$$

where  $X_k$  and  $x_k$  are respectively the codified and real values of the independent variable,  $x_0$  is the value of the central point of the independent variable, and  $\Delta x_k$  is the step change (based on the levels).

Table 9.2. Levels and codification of the factors (independent variables) used in the optimization of the catalytic oligomerization process.

Factor	Variable		Level correspondence		
	Real	Coded	-1	0	1
Pressure (bar)	P	X <sub>P</sub>	20	32.5	45
Temperature (°C)	T	X <sub>T</sub>	150	225	300
Weight hourly space velocity (h <sup>-1</sup> )	W	X <sub>W</sub>	2.0	3.5	5.0

The experimental design for RSM was Box-Behnken (BB) which is a flexible design and very efficient in terms of the number of required runs. The BB design consisted of a three-level incomplete factorial design comprising fifteen catalytic assays performed in a random fashion (three of the assays were replicates of the central point  $x_0$ ).<sup>[39]</sup> The following responses (dependent variables) were investigated (Table 9.3):  $X_{C4}$  is the conversion of butenes,  $\eta_{Dcut}$  is the yield of products corresponding to the 170-390 °C cut characteristic of diesel type products (Dcut),  $\eta_{Ncut}$  is the yield of products corresponding to the <170 °C cut characteristic of naphtha type products (Ncut),  $\eta_{Arom}$  is the yield of aromatics,  $\eta_{Dcut,free}$  is the yield of Dcut free of aromatics and  $\eta_{Ncut,free}$  is the yield of Ncut free of aromatics.

The fittings of empirical models to the data led to response surfaces of the studied factors.<sup>[39]</sup> Each response is described by a second order polynomial function of codified factors (Eq. (2)).

$$Y = \beta_0 + \beta_1 X_P + \beta_2 X_T + \beta_3 X_W + \beta_{11} X_P^2 + \beta_{22} X_T^2 + \beta_{33} X_W^2 + \beta_{12} X_P X_T + \beta_{13} X_P X_W + \beta_{23} X_T X_W \quad (2)$$

where  $Y$  is a response,  $X_P$ ,  $X_T$  and  $X_W$  are the codified factors,  $\beta_0$  is a constant that includes the residual value,  $\beta_i$  are the model coefficients for the linear effects,  $\beta_{ii}$  are the coefficients associated with quadratic effects, and  $\beta_{ij}$  are the coefficients associated with interaction effects. The model coefficients were determined by regression analysis of the experimental results, using STATISTICA software (version 5.1, StatSoft Inc., Tulsa, USA) for statistical treatment of the data. The analysis of variance (ANOVA) was carried out to evaluate the statistical significance of the factors and interactions using Fisher's test, and its associated probability level (p-value) for a confidence interval of 90 %. T-tests were employed to study the significance ( $\beta \neq 0$ ) of the coefficients determined for each model. The coefficient of

determination ( $R^2$ ) and its adjusted values ( $R_{\text{adj}}^2$ ) were used to evaluate the goodness of fit of the regression models.

The fitted polynomial equations gave rise to the response surface plots showing the relationship between factors and responses, and allowing to determine optimal conditions. The goodness of fit of the statistical model to the experimental data was evaluated by the average absolute relative deviation, AARD (Eq. (3)).

$$AARD(\%) = \frac{100}{N} \times \sum_{i=1}^N \left| \frac{y_i^{\text{calc}} - y_i^{\text{exp}}}{y_i^{\text{exp}}} \right| \quad (3)$$

where  $N$  is the number of data points, and  $y_i^{\text{calc}}$  and  $y_i^{\text{exp}}$  are the calculated and experimental values of the response, respectively.

Table 9.3. Performance parameters (responses) for the evaluation of 1-butene oligomerization.

Performance parameters	Formula	Eq.
Conversion of butenes (mol.%)	$X_{C4} = \frac{F_{1C4in} - F_{C4out}}{F_{1C4in}} \times 100$	(4)
Yield of diesel cut, Dcut (wt.%)	$\eta_{\text{Dcut}} = \eta \times x_{\text{Dcut}}^{[a]}$	(5)
Yield of naphtha cut, Ncut (wt.%)	$\eta_{\text{Ncut}} = \eta \times (1 - x_{\text{Dcut}})$	(6)
Yield of aromatics (wt.%)	$\eta_{\text{Arom}} = \eta \times x_{\text{Arom}}^{[b]}$	(7)
Yield of Dcut, free of aromatics (wt.%)	$\eta_{\text{Dcut,free}} = \eta_{\text{Dcut}} \times (1 - x_{\text{Arom}})$	(8)
Yield of Ncut, free of aromatics (wt.%)	$\eta_{\text{Ncut,free}} = \eta_{\text{Ncut}} \times (1 - x_{\text{Arom}})$	(9)

[a]  $\eta = X_{C4} \times S$ ;  $S = \frac{m_{\text{Dcut}} + m_{\text{Ncut}}}{m_{1C4,in} - m_{C4,out}}$ ;  $x_{\text{Dcut}} = \frac{\frac{n_{\text{Dcut}}}{M_{\text{Dcut}}}}{\frac{n_{\text{Dcut}}}{M_{\text{Dcut}}} + \frac{n_{\text{Ncut}}}{M_{\text{Ncut}}}}$ ; [b]  $x_{\text{Arom}}$  was determined based on GC×GC-ToFMS.

### 9.3. Characterization studies of the catalytic materials

The prepared material hierZ-MFI possessed a Si/Al molar ratio of *ca.* 25, which was higher than that of the parent zeolite H-ZSM-5 (Si/Al=15), attributed to the post-synthesis treatments. Figure 9.2 shows similar morphology of H-ZSM-5 and hierZ-MFI, and the two materials exhibited the reflections associated with the MFI topology (most intense peaks at 8-9° 2 $\theta$  and 23-24° 2 $\theta$ ). The modified material hierZ-MFI was less crystalline than the parent zeolite, which is in agreement with that reported in the literature for synthesis strategies involving post-synthesis introduction of mesoporosity in zeolites.<sup>[40,41]</sup> The elemental mappings of hierZ-MFI showed uniform distributions of Si and Al (Figure 9.2).

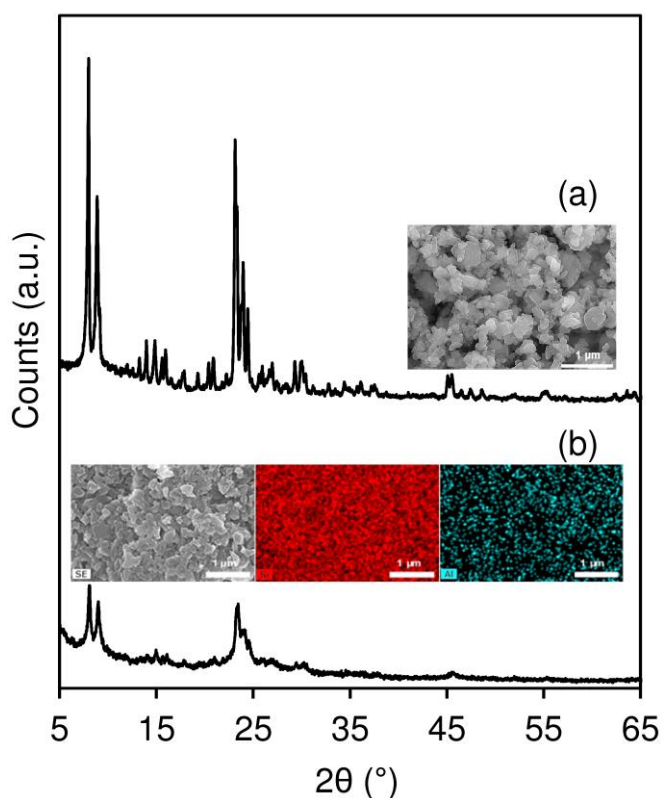


Figure 9.2. PXRD patterns for H-ZSM-5 (a) and hierZ-MFI (b), and respective SEM images (and Si (red), Al (blue) mapping for hierZ-MFI).

Zeolite H-ZSM-5 exhibited a Type I adsorption isotherm with a slight increase in uptake at high relative pressure due to multilayer adsorption on the external surface of some

relatively small crystals (Figure 9.2). The modified material hierZ-MFI exhibited a hysteresis loop with a step at  $p/p_0 \approx 0.40$  of the desorption branch, associated with mesoporosity. The BET specific surface area ( $S_{\text{BET}}$ ) was higher for hierZ-MFI;  $S_{\text{BET}} = 688 \text{ m}^2 \text{ g}^{-1}$  compared to  $431 \text{ m}^2 \text{ g}^{-1}$  for H-ZSM-5, partly due to the enhanced mesoporosity of hierZ-MFI ( $S_{\text{meso}}$  and  $V_{\text{meso}}$  of  $299 \text{ m}^2 \text{ g}^{-1}$  and  $1.164 \text{ cm}^3 \text{ g}^{-1}$ , respectively). The increased mesoporosity was accompanied by reduced microporosity of hierZ-MFI ( $V_{\text{micro}} = 0.118 \text{ cm}^3 \text{ g}^{-1}$ , compared to  $0.175 \text{ cm}^3 \text{ g}^{-1}$  for H-ZSM-5). The pore size distribution of hierZ-MFI was centred at 1.4 and 3.8 nm (Figure 9.3-A).  $^{27}\text{Al}$  MAS NMR spectroscopic studies indicated that H-ZSM-5 and hierZ-MFI exhibited peaks at *ca.* 55 ppm and 0 ppm assigned to four- ( $\text{Al}_{\text{tetra}}$ ) and six-coordinated ( $\text{Al}_{\text{octa}}$ ) aluminum species, respectively (Figure 9.3-B). Based on the peaks areas, the ratio  $\text{Al}_{\text{tetra}}/\text{Al}_{\text{octa}}$  was 8.3 and 3.5 for H-ZSM-5 and hierZ-MFI, respectively. The decrease of  $\text{Al}_{\text{tetra}}/\text{Al}_{\text{octa}}$  may be partly associated with the decreased crystallinity resulting from the introduction of mesoporosity.

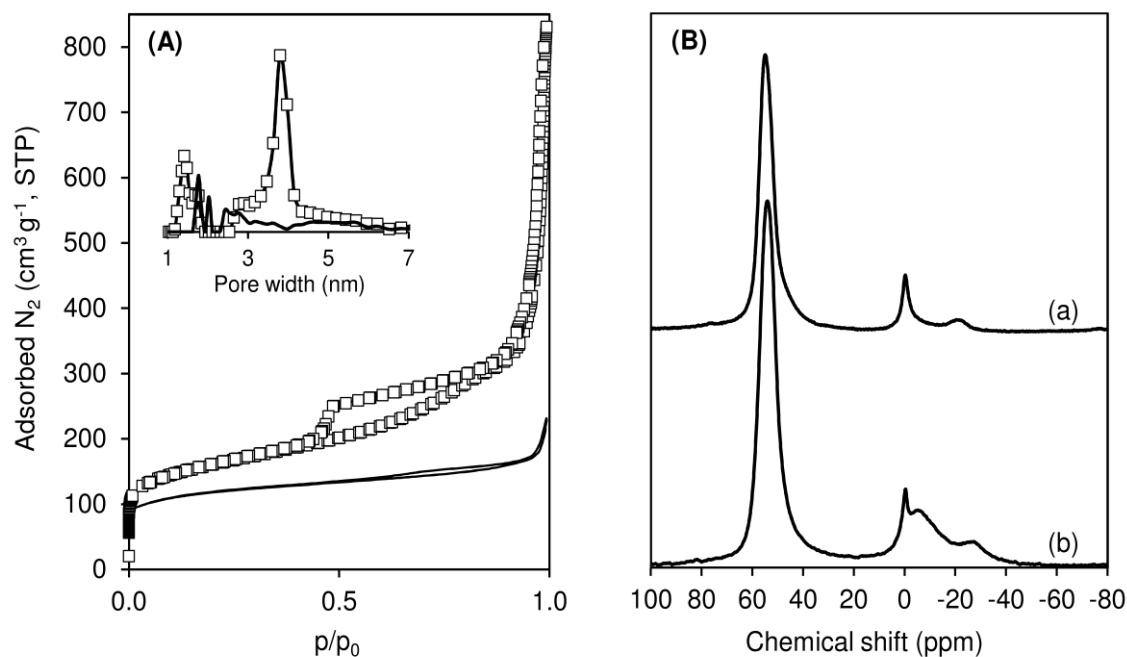


Figure 9.3. (A) Nitrogen adsorption-desorption isotherms at -196 K for H-ZSM-5 (-) and hierZ-MFI ( $\square$ ). The inset shows the respective pore size distribution curves (with matching lines). (B)  $^{27}\text{Al}$  MAS NMR spectra for HZSM-5 (a) and hierZ-MFI (b).

#### 9.4. Catalytic studies: general considerations

The reaction of 1-butene was carried out under high-pressure, continuous-flow conditions to target diesel type products, using hierZ-MFI as heterogeneous acid catalyst. Table 9.2 lists the ranges of reaction conditions used: 150-300 °C reaction temperature (T), 20-45 bar reaction pressure (P), and weight hourly space velocity (W) of 2-5  $\text{g}_{1\text{C}_4} \text{g}_{\text{cat}}^{-1} \text{h}^{-1}$ . Compounds with boiling point ranges characteristic of naphtha and diesel cuts (Ncut and Dcut, respectively) were formed. The product mixtures obtained under the different reaction conditions were analyzed by GC×GC-ToFMS and  $^1\text{H}$  nuclear magnetic resonance (NMR) spectroscopy. GC×GC-ToFMS revealed the complexity of the multicomponent mixtures, as exemplified in Figure 9.4 for sample 1 obtained under the conditions 225 °C, 32.5 bar, 3.5  $\text{g}_{1\text{C}_4} \text{g}_{\text{cat}}^{-1} \text{h}^{-1}$ , and sample 2 obtained at 300 °C, 45 bar, 3.5  $\text{g}_{1\text{C}_4} \text{g}_{\text{cat}}^{-1} \text{h}^{-1}$ . Mainly aliphatic products were formed. Table 9.4 lists the identified aliphatic products for the two samples. The products included branched linear and cyclic, saturated and unsaturated aliphatic compounds such as methylundecenes, dodecene, trimethyloctenes, hexadecane and dimethylcyclohexenes.<sup>[42–71]</sup> The aromatics contents were in the range 0-22 % (Table S9.1), and consisted essentially of substituted phenyl, indane and tetrahydronaphthalene type compounds and, to much smaller extent, naphthalene type diaromatics (Table S9.2). According to the literature, oligomerization processes may involve the various types of chemical reactions besides oligomerization (which may involve carbenium ions as chain carriers, giving products possessing multiples of 4 carbon atoms) such as co-oligomerization (involving olefins with an odd number of carbon atoms, isomerization (double bond or alkyl group shifts), dehydrogenation, hydrogen transfer, cracking (e.g. carbenium ion/bimolecular catalytic cracking involving  $\beta$ -scission; protolytic cracking), cyclization and dehydrocyclization (aromatization), Figure 9.1.<sup>[9,72–76]</sup>

The cetane number (CN), isoparaffinic index (I), and aromatics content were determined by  $^1\text{H}$  NMR spectroscopy (Table S9.1), based on the O'Connor method.<sup>[77]</sup> The total aromatics content was in the range 0-5 %. The I, which reflects the branching degree, was in the range 0.48-0.70, somewhat consistent with the GC×GC-ToFMS studies indicating the formation of several branched products (Table 9.4). The CN's were in range 37-49, which is reasonable considering that the product mixtures were not further treated; e.g.

consecutive hydrogenation leads to enhanced CN.<sup>[78]</sup> Literature data of CN for diesel cuts produced in commercial processes or commercial diesel samples were in the range 48-56.<sup>[11,79-82]</sup> Noteworthy, the aromatics contents determined by <sup>1</sup>H NMR spectroscopy and GC×GC-ToFMS presented a roughly linear dependency (Figure S9.1), with GC×GC-ToFMS giving higher values than <sup>1</sup>H NMR spectroscopy likely due to higher sensitivity of the former technique.

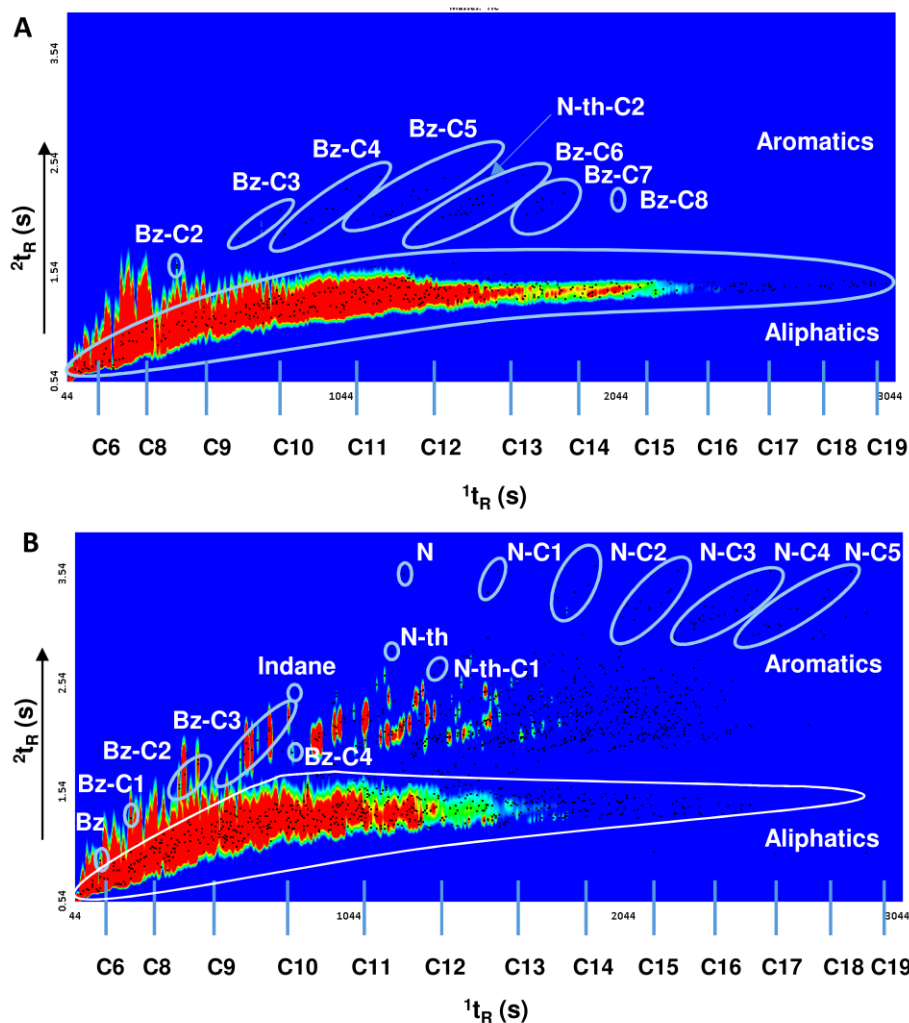


Figure 9.4. GC×GC-ToFMS total ion chromatogram contour plot of the reaction product mixture for (A) sample 1 (225 °C, 32.5 bar, 3.5 g  $g_{cat}^{-1} h^{-1}$ ) and (B) sample 2 (300 °C, 45 bar, 3.5 g  $g_{cat}^{-1} h^{-1}$ ):  $^1t_R$  (horizontal axis) and  $^2t_R$  (vertical axis) stand for retention time (s) for the primary and secondary GC columns, respectively; as a guide, the compounds of the standard mixture (linear hydrocarbons,  $C_i$  where  $i$  is the number of carbon atoms) eluted from the first column are signaled in the  $^1t_R$  axis. The symbols denote types of chemical compounds, namely: Bz- $C_i$ =alkyl benzenes (monocyclic), N- $C_i$ =alkyl naphthalenes, and N-th- $C_i$ =alkyl tetrahydronaphthalenes, where  $C_i$  is the total number of carbon atoms in substituent groups per molecule.

Optimization of heterogeneous catalytic oligomerization of 1-butene by design of experiments and response surface methodology

Table 9.4. Aliphatic products formed in the catalytic reactions of 1-butene, at 225 °C, 32.5 bar, 3.5 g<sub>1C4</sub> g<sub>cat</sub><sup>-1</sup> h<sup>-1</sup> (sample 1), or 300 °C, 45 bar, 3.5 g<sub>1C4</sub> g<sub>cat</sub><sup>-1</sup> h<sup>-1</sup> (sample 2).<sup>[a]</sup>

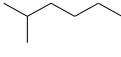
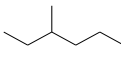
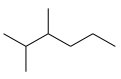
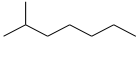
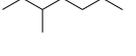
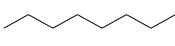
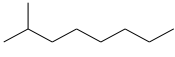
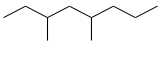
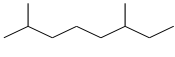
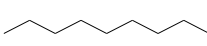
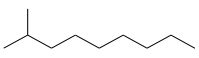
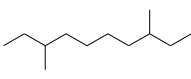
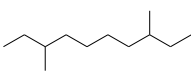
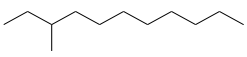
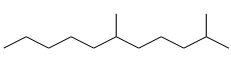
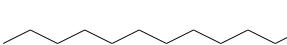
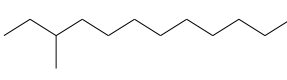
Chemical structure	Name	Sim. <sup>[b]</sup>	RI <sup>[c]</sup>		Ref.
			Exp.	Rpt.	
<i>Linear aliphatics</i>					
	2-methylbutane	926	570	578	[42]
	2-methylpentane	917	588	577	[43]
	3-methylpentane*	945	595	590	[42]
	2,4-dimethylpentane*	908	619	623	[54]
	2-methylhexane	885	643	657	[54]
	3-methylhexane	822	674	674	[43]
	2,3-dimethylhexane	851	740	754	[54]
	2-methylheptane	928	746	761	[54]
	3-methylheptane	936	758	769	[54]
	octane	912	800	800	[65]
	2-methyloctane*	869	862	856	[54]
	3,5-dimethyloctane*	938	926	927	[43]
	2,6-dimethyloctane,	916	934	937	[43]
	nonane	932	900	900	[66]
	2-methylnonane*	920	965	964	[67]
	3,8-dimethyldecane*	712	1126	1140	[68]
	2,9-dimethyldecane	943	1130	1130	[69]
	3-methylundecane*	898	1173	1173	[43]
	2,6-dimethylundecane*	927	1218	1216	[70]
	Dodecane*	925	1203	1200	[71]
	3-methyldodecane*	926	1273	1271	[70]

Table 9.4. (Continued)

Chemical structure	Name	Sim. <sup>[b]</sup>	RI <sup>[c]</sup>		Ref.
			Exp.	Rpt.	
	hexadecane	941	1613	1600	[44]
	2-ethyl-3-methyl-1-butene*	845	661	663	[45]
	3-methyl-2-pentene	942	607	610	[46]
	3,4-dimethyl-2-pentene*	909	631	670	[47]
	3-ethyl-4-methyl-2-pentene*	897	722	736	[48]
	3-methyl-2-hexene*	931	673	702	[49]
	3-ethyl-2-hexene*	887	789	790	[50]
	3-ethyl-2,5-dimethyl-1,3-hexadiene	843	947	-	
	4,6-dimethyl-1-heptene*	857	884	-	
	2,6-dimethyl-1-heptene*	898	862	853	[51]
	3-heptene*	935	667	698	[46]
	2-methyl-3-heptene*	880	752	752	[49]
	4-ethyl-3-heptene*	857	878	884	[52]
	2,3-dimethyl-3-heptene*	880	830	837	[53]
	2,6-dimethyl-3-heptene*	873	839	815	[55]
	4-ethyl-3-octene	861	936	-	
	3,3-dimethyl-1-octene*	903	995	-	
	2,6-dimethyl-2-octene*	899	959	966	[56]

Table 9.4. (Continued)

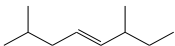
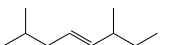
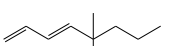
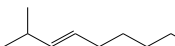
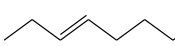
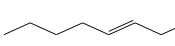
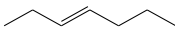
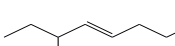
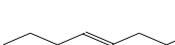
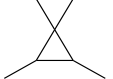
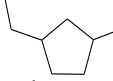
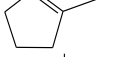
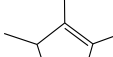
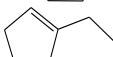
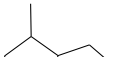
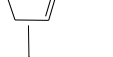
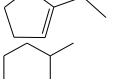
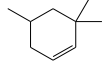
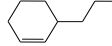
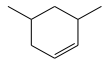
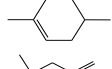
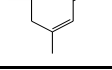
Chemical structure	Name	Sim. <sup>[b]</sup>	RI <sup>[c]</sup>		Ref.
			Exp.	Rpt.	
<i>Linear aliphatics</i>					
	2,6-dimethyl-4-octene	840	954	-	
	2,3,6-trimethyl-1-4-octene*	815	988	-	
	5,5-dimethyl-1,3-octadiene	812	993	-	
	2-methyl-3-nonene*	910	995	-	
	3-decene*	896	954	993	[57]
	4-decene*	851	954	992	[58]
	5-decene*	898	973	984	[59]
	4-undecene*	906	1051	1081	[60]
	9-methyl-3-undecene*	902	1108	-	
	3-methyl-4-undecene*	843	1086	-	
	4-dodecene*	903	1148	1180	[61]
<i>Cyclic aliphatics</i>					
	1,1-diethyl cyclopropane*	854	643	673	[62]
	1,1,2,3-tetramethyl cyclopropane*	835	655	-	
	1-ethyl-3-methylcyclopentane	915	777	787	[45]
	1-methylcyclopentene	956	631	636	[42]
	1,2,3-trimethylcyclopentene	943	698	715	[63]
	1-ethylcyclopentene	817	728	753	[42]
	2-ethyl-3-methylcyclopentene	926	830	-	
	2-ethyl-3-methylcyclopentene	926	830	-	
	methylcyclohexane	827	692	715	[42]

Table 9.4. (Continued)

Chemical structure	Name	Sim. <sup>[b]</sup>	RI <sup>[c]</sup>		Ref.
			Exp.	Rpt.	
<i>Cyclic aliphatics</i>					
	3,3,5-trimethyl cyclohexene*	875	918	-	
	3-propylcyclohexene	849	949	-	
	3,5-dimethylcyclohexene	878	813	-	
	1,4-dimethyl-1-cyclohexene*	954	817	818	[64]
	1,5,5-trimethyl-3-methylenecyclohexene	849	1046	-	

<sup>[a]</sup> \* Signalizes products of sample 2 which were also present in sample 1. <sup>[b]</sup> Similarity (Sim.) of the mass spectra. <sup>[c]</sup> Retention Index (RI) determined experimentally (Exp.) and RI values reported in the literature (Rpt).

## 9.5. Optimization studies of 1-butene oligomerization

The catalytic system of 1-butene oligomerization was optimized *via* DoE/RSM, with the practical goal of maximizing production of clean fuels with low aromatics contents. Table 9.3 lists the performance parameters for the catalytic reaction system, which were determined experimentally under different operating conditions. The performance parameters were the conversion of butenes ( $X_{C4}$ ), yields of total Ncut ( $\eta_{Ncut}$ ) and Dcut products ( $\eta_{Dcut}$ ), yield of Ncut free of aromatics ( $\eta_{Ncut,free}$ ), yield of Dcut free of aromatics ( $\eta_{Dcut,free}$ ), and yield of total aromatics ( $\eta_{Arom}$ ). Regarding the operating conditions, it was investigated the influence of the reaction pressure (P), reaction temperature (T) and weight hourly space velocity (W). Table 9.5 indicates the experimental design matrix based on a three-level Box-Behnken design with three factors (operating conditions) in terms of uncoded units, and the responses (catalytic results). The conversion of butenes ( $X_{C4}$ ) ranged from 27 % (32.5 bar, 150 °C, 5 g<sub>1C4</sub> g<sub>cat</sub><sup>-1</sup> h<sup>-1</sup>) to 97 % (45 bar, 225 °C, 2 g<sub>1C4</sub> g<sub>cat</sub><sup>-1</sup> h<sup>-1</sup>). The yield of Dcut products ( $\eta_{Dcut}$ ) ranged from 2 % (20 bar, 150 °C, 3.5 g<sub>1C4</sub> g<sub>cat</sub><sup>-1</sup> h<sup>-1</sup>) to 39 % (32.5 bar, 225 °C, 3.5 g<sub>1C4</sub> g<sub>cat</sub><sup>-1</sup> h<sup>-1</sup>), and that of Ncut ( $\eta_{Ncut}$ ) ranged from 11 % (20 bar, 150 °C, 3.5 g<sub>1C4</sub> g<sub>cat</sub><sup>-1</sup> h<sup>-1</sup>) to 75 % (20 bar, 300 °C, 3.5 g<sub>1C4</sub> g<sub>cat</sub><sup>-1</sup> h<sup>-1</sup>), Table 9.5. The yield of

Optimization of heterogeneous catalytic oligomerization of 1-butene by design of experiments and response surface methodology

aromatics ( $\eta_{\text{Arom}}$ ) ranged from 0 % for all assays carried out at  $T=150$  °C, to *ca.* 18.2 % for the reaction conditions 20 bar, 300 °C and  $3.5 \text{ g}_{\text{1C4}} \text{ g}_{\text{cat}}^{-1} \text{ h}^{-1}$ , Table 9.5.

Table 9.5. Experimental design matrix using a three-level Box-Behnken design with three factors (in terms of uncoded units) and the experimental responses.

Run	Factors			Responses					
	<i>P</i> (bar)	<i>T</i> (°C)	<i>W</i> (h <sup>-1</sup> )	<i>X</i> <sub>C4</sub> (mol.%)	$\eta_{\text{Dcut}}$ (wt.%)	$\eta_{\text{Ncut}}$ (wt.%)	$\eta_{\text{Arom}}$ (wt.%)	$\eta_{\text{Dcut,free}}$ (wt.%)	$\eta_{\text{Ncut,free}}$ (wt.%)
1	20	150	3.5	35	2	11	0.0	2	11
2	20	300	3.5	95	14	75	18.2	7	63
3	45	150	3.5	32	7	15	0.0	7	15
4	45	300	3.5	94	25	64	16.9	16	56
5	20	225	2.0	70	21	30	0.5	21	30
6	20	225	5.0	41	11	23	0.1	11	22
7	45	225	2.0	97	27	48	1.7	27	47
8	45	225	5.0	66	21	35	0.2	21	34
9	32.5	150	2.0	37	8	14	0.0	8	14
10	32.5	150	5.0	27	3	12	0.0	3	12
11	32.5	300	2.0	96	28	62	15.5	20	55
12	32.5	300	5.0	94	24	65	5.7	21	62
13	32.5	225	3.5	82	37	35	0.4	36	35
14	32.5	225	3.5	83	39	35	0.5	38	35
15	32.5	225	3.5	87	38	37	0.5	38	37

Regression analysis was carried out for the data set in their coded form, considering the influence of individual factors (linear and quadratic effects) on the responses, and interactions between factors. The reduced models for the responses of the DoE were based on selected factors/interactions (Table 9.6); the reduced models with the codified variables are given in Table S9.3. The selection of the factors/interactions was based on the corresponding effect bars given by the Pareto charts (Table 9.5 (a-c) and Table 9.6 (a-c)). The factors/interactions for which the effect bars passed the statistical significance boundary line ( $p\text{-value}=0.1$ ) were very significant which, together with some additional factors/interactions that were close to the statistical significance boundary line, were contemplated in the models, resulting in reasonable fittings to the experimental data ( $R^2 > 0.91$  and  $R_{\text{adj}}^2 > 0.88$ , Table 9.6 and Table S9.3).

The response surface plots are given in Figure 9.5(d-i) and Figure 9.6(d-g), showing the influence of the different factors on the catalytic reaction of 1-butene. The BB design data were reasonably well fitted by second order polynomial quadratic equations; the average absolute relative deviations (AARDs) between the experimental and calculated results (by the RSM reduced models) were in the range of 10-28 % (Table 9.7). For further validation of the regression models, a catalytic test was carried out using different operating conditions (45 bar, 255 °C, 2.0 g<sub>1C4</sub> g<sub>cat</sub><sup>-1</sup> h<sup>-1</sup>) from those of the design matrix; the models provided reliable estimates of the catalytic data, giving comparable results to the experimental results of this test (Table 9.7).

Table 9.6. Reduced models for the responses of the DoE.

Reduced model	$R^2$	$R_{adj}^2$
$X_{C4}(\%) = -212.361 + 3.678 P + 1.4138 T + 19.17 W - 0.0491 P^2 - 0.0022186 T^2 - 3.6009 W^2$	0.932	0.881
$\eta_{Dcut}(\text{wt.}\%) = -238.902 + 4.7818 P + 1.3407 T + 19.3113 W - 0.06876 P^2 - 0.0027184 T^2 - 3.0729 W^2$	0.982	0.969
$\eta_{Ncut}(\text{wt.}\%) = -31.327 + 1.1152 P + 0.08705 T - 1.6617 W + 0.0008852 T^2 - 0.003955 P \times T$	0.955	0.929
$\eta_{Arom}(\text{wt.}\%) = 24.1831 - 0.34945 T + 3.9041 W + 0.00115355 T^2 - 0.021677 T \times W$	0.911	0.876
$\eta_{Dcut,free}(\text{wt.}\%) = -244.94 + 4.9728 P + 1.4792 T + 14.38 W - 0.07214 P^2 - 0.003245 T^2 - 2.7804 W^2 + 0.0154 T \times W$	0.973	0.945
$\eta_{Ncut,free}(\text{wt.}\%) = -42.26 + 0.2529 P + 0.30767 T$	0.932	0.921

Table 9.7. Experimental and calculated responses (by the RSM reduced models) for the catalytic assay performed at 45 bar, 255 °C, 2.0 g<sub>1C4</sub> g<sub>cat</sub><sup>-1</sup> h<sup>-1</sup>, and the AARDs for this catalytic assay and for the RSM reduced models.

Responses, AARDs	$X_{C4}$ (%)	$\eta_{Dcut}$ (wt.%)	$\eta_{Ncut}$ (wt.%)	$\eta_{Dcut,free}$ (wt.%)	$\eta_{Ncut,free}$ (wt.%)
Experimental	96	36	52	28	47
Calculated	94	28	50	24	48
AARD (catalytic test) (%)	2	21	4	12	0.4
AARD (RSM models) (%)	10	17	13	22	10

The dependencies of butenes conversion ( $X_{C4}$ ) on the operating conditions (P, T, W) are given by the response surface plots of Figure 9.5 (d,g). The  $X_{C4}$  increased with increasing T and P, and decreasing W (i.e. increasing residence time), in agreement with literature data for light olefins oligomerization over zeolites or zeotypes of different topologies (e.g. H-ferrierite<sup>[73]</sup>, ZSM-5<sup>[83]</sup>). Figure 9.5(e,h) shows the  $\eta_{Dcut}$  response surface plots, indicating that  $\eta_{Dcut}$  increased with increasing P and, to a smaller extent, with increasing T, reaching an optimal of 35-40 wt.%, in the ranges 220-270 °C, 30-40 bar, 2.5-3.5 g<sub>1C4</sub> g<sub>cat</sub><sup>-1</sup> h<sup>-1</sup>; increasing further the T, led to decreasing  $\eta_{Dcut}$ .

A comparative study of the  $\eta_{Dcut}$  (Figure 9.5(e,h)) and  $\eta_{Ncut}$  (Figure 9.5 (f,i)) response surface plots indicated that in the higher T range (above *ca.* 235-240 °C),  $\eta_{Dcut}$  decreased with the concomitant increase of  $\eta_{Ncut}$ . Hence, too high T led to reduction in the molar mass of the products, likely due to cracking reactions.<sup>[84]</sup> Cracking reactions may be accompanied by dehydrocyclization reactions leading to mono- and polyaromatic products,<sup>[23,85]</sup> which may impact negatively on the fuel quality and eco-friendliness. Thus, it is important to check the influence of the operating conditions on the production of aromatics. In this sense, a refined analysis was carried out considering the fraction of aromatics in the Dcut and Ncut products. The product mixtures obtained for the higher T range seemed to possess considerable amounts of aromatics, as exemplified in Figure 9.4 comparing sample 1 (products of the reaction at 225 °C) and sample 2 (products of the reaction at 300 °C). GC×GC-ToFMS analyses (discussed above) indicated that the greatest portion of aromatics belonged to the Dcut (Table S9.4).

Figure 9.6 (d-g) shows the response surface (RSM) plots for  $\eta_{Arom}$ ,  $\eta_{Dcut,free}$  and  $\eta_{Ncut,free}$ . Considerable formation of aromatics began at temperatures above 225 °C (Figure 9.6(d)). In the high T range (above *ca.* 225 °C), the aromatics formation increases with decreasing W, reaching 18 wt.%, at 300 °C, 2 g<sub>1C4</sub> g<sub>cat</sub><sup>-1</sup> h<sup>-1</sup> (pressure range 20-45 bar). This trend matches literature data for 1-butene conversion over H-ferrierite (based on the yields of aromatics, calculated from the reported results of conversion and selectivity to aromatics).<sup>[73]</sup> E. Epelde et al.<sup>[84]</sup> reported that 1-butene conversion may involve series of oligomerization-cracking reactions and subsequent aromatization. Thus, the consecutive reactions leading to aromatics may be favored by longer residence times (especially in the high T range).

The  $\eta_{Dcut,free}$  increased with increasing P and T, and decreasing W, reaching maximum of 34-38 wt.% in the range 220-250 °C, 30-40 bar and 2.5-3.5  $g_{1C4} g_{cat}^{-1} h^{-1}$  (Figure 9.6(e,g)). The  $\eta_{Ncut,free}$  surface plot showed increasing yields with increasing P and especially T, leading to 61 wt.% yield, at 300 °C, 45 bar (Figure 9.6(f)). In the higher T range,  $\eta_{Ncut,free}$  was greater than  $\eta_{Dcut,free}$ . However, these harsh reaction conditions lead to considerable production of aromatics (up to 18 wt.% at 300 °C).

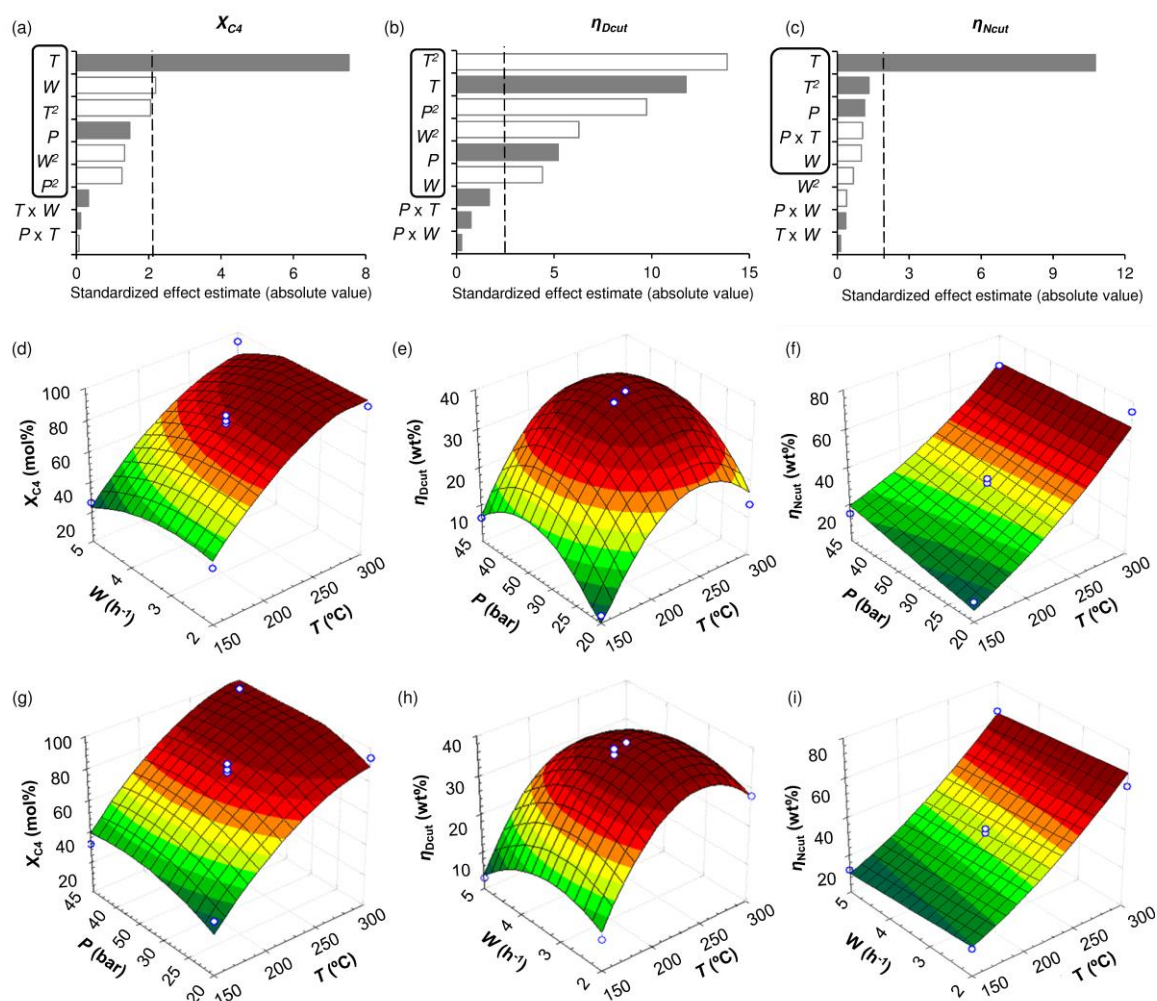


Figure 9.5. Pareto charts of (a)  $X_{C4}$ , (b)  $\eta_{Dcut}$  and (c)  $\eta_{Ncut}$  considering the Box-Behnken design of Table 9.5 with confidence interval of 90 % and p-value=0.10; black and white bars refer to positive and negative impacts, respectively. Response surface plots of (d,g)  $X_{C4}$ , (e,h)  $\eta_{Dcut}$ , (f,i)  $\eta_{Ncut}$  as function of temperature, pressure or WHSV (imposing the other variable at their zero level, i.e. (d,h,i) have P=32.5 bar, and (e,f,g) have W=3.5  $g_{1C4} g_{cat}^{-1} h^{-1}$ ). Dots represent the experimental results.

## Optimization of heterogeneous catalytic oligomerization of 1-butene by design of experiments and response surface methodology

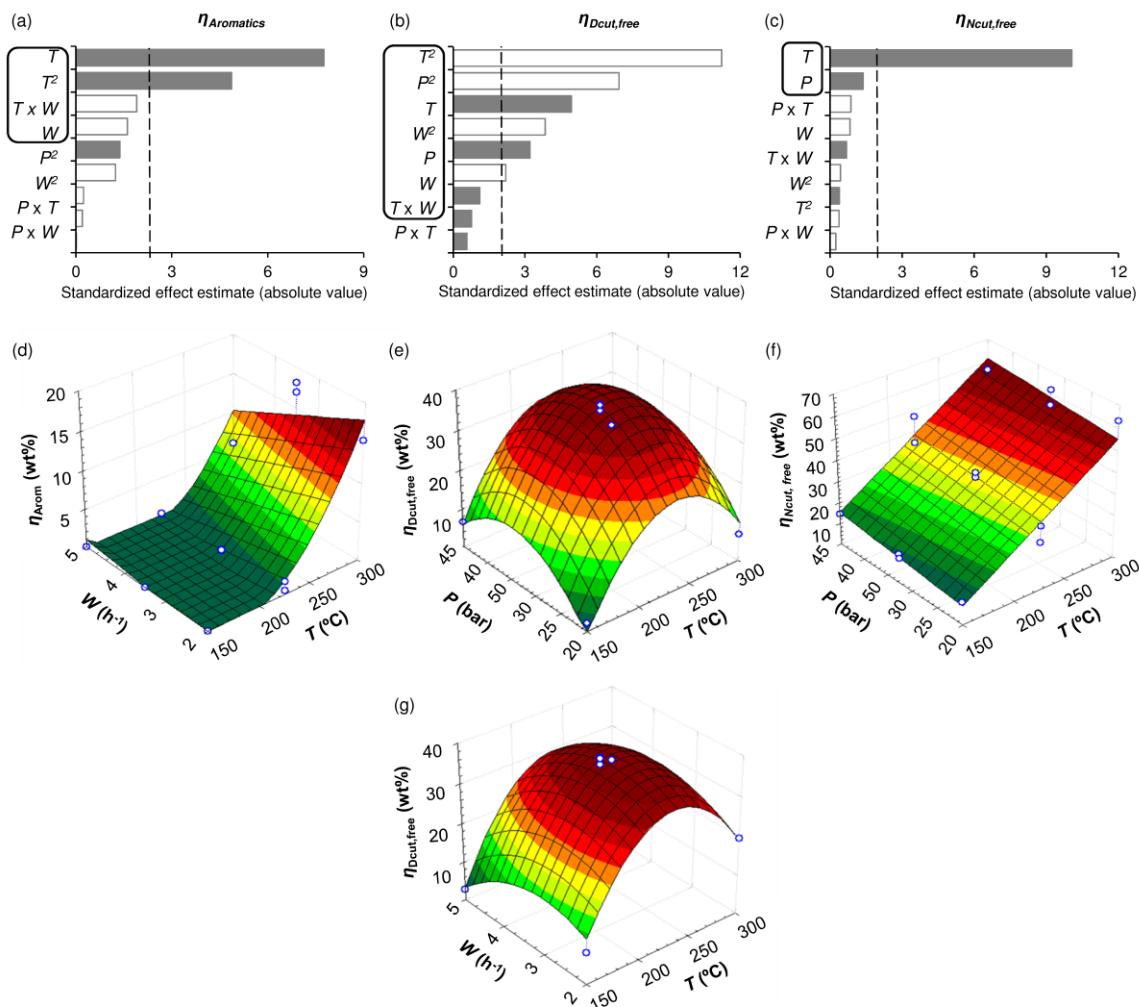


Figure 9.6. Pareto charts of (a)  $\eta_{Arom}$ , (b)  $\eta_{Dcut,free}$  and (c)  $\eta_{Ncut,free}$  considering the Box-Behnken design of Table 9.5 with confidence interval of 90 % and p-value=0.10; black and white bars refer to positive and negative impacts, respectively. Response surface plots of (d)  $\eta_{Arom}$ , (e,g)  $\eta_{Dcut,free}$ , (f)  $\eta_{Ncut,free}$  as function of temperature, pressure or WHSV (imposing the other variable at their zero level, i.e. (e) have  $W=3.5 \text{ g}_{1C4} \text{ g}_{cat}^{-1} \text{ h}^{-1}$  and (g) have  $P=32.5 \text{ bar}$ ). Dots represent the experimental results.

## 9.6. Conclusions

The acid-catalyzed oligomerization of light olefins is a complex reaction system where the yields and characteristics of the products depend on interplay of several operating conditions, which requires careful optimization. However, these reaction systems present high complexity. The present study highlights that a Box-Behnken design with response

surface methodology (DoE/RSM) is an effective expeditious tool for optimizing these complex reaction systems. DoE/RSM was coupled with GC×GC-ToFMS (which allowed product quality assessment) for optimizing the continuous flow reaction of 1-butene over a micro/mesoporous zeotype (hierZ-MFI, Si/Al~25) to maximize the production of diesel range products, free of aromatics ( $\eta_{\text{Dcut,free}}$ ). The optimal conditions (temperature, pressure and weight hourly space velocity) given by the regression models were in the ranges: 220–250 °C, 30–40 bar and 2.5–3.5 g<sub>1C4</sub> g<sub>cat</sub><sup>-1</sup> h<sup>-1</sup>, which led to  $\eta_{\text{Dcut,free}}$  of 34–38 %, and  $\eta_{\text{Arom}}$  of 0–5 %. The results indicated that intermediate conditions of reaction pressure, temperature and residence time allowed maximizing the production of clean diesel range products, while avoiding aromatics and cracking products. Overall, DoE/RSM, which is presently unexploited for light olefins oligomerization processes, may be a powerful evaluation tool in the development of flexible technologies to meet market demands for high quality fuels. Coupling DoE/RSM with diverse analytical techniques used for product quality assessments, allows the expeditious optimization of simultaneously product yields and quality, which is hardly achievable *via* phenomenological modeling (involving complex, time-consuming numerical optimization).

## 9.7. References

- [1] D.M. Alonso, J.Q. Bond, J.C. Serrano-Ruiz, J.A. Dumesic, Production of liquid hydrocarbon transportation fuels by oligomerization of biomass-derived C<sub>9</sub> alkenes, *Green Chem.* 12 (2010) 992–999.
- [2] J.Q. Bond, D.M. Alonso, D. Wang, R.M. West, J.A. Dumesic, Integrated catalytic conversion of  $\gamma$ -valerolactone to liquid alkenes for transportation fuels, *Science* 327 (2010) 1110–1114.
- [3] C.P. Nicholas, Applications of light olefin oligomerization to the production of fuels and chemicals, *Appl. Catal. A Gen.* 543 (2017) 82–97.
- [4] A. V. Lavrenov, T.R. Karpova, E.A. Buluchevskii, E.N. Bogdanets, Heterogeneous oligomerization of light alkenes: 80 years in oil refining, *Catal. Ind.* 8 (2016) 316–327.
- [5] O. Muraza, Maximizing diesel production through oligomerization: a landmark opportunity for zeolite research, *Ind. Eng. Chem. Res.* 54 (2015) 781–789.
- [6] A. Corma, S. Iborra, Oligomerization of alkenes, in: E.G. Derouane (Ed.), *Catalysts for fine chemical synthesis, Volume 4, Microporous and mesoporous solid catalysts*, John Wiley & Sons, 2006: pp. 125–140.
- [7] A. De Klerk, Distillate production by oligomerization of Fischer - Tropsch olefins over solid phosphoric acid, *Energy & Fuels* 20 (2006) 439–445.
- [8] V. Ipatieff, B.B. Corson, G. Egloff, Polymerization, a new source of gasoline, *Ind. Eng. Chem.* 27 (1935) 1077–1081.

Optimization of heterogeneous catalytic oligomerization of 1-butene by design of experiments and response surface methodology

- [9] S.A. Tabak, F.J. Krambeck, W.E. Garwood, Conversion of propylene and butylene over ZSM-5 catalyst, *AIChE J.* 32 (1986) 1526–1531.
- [10] M.N. Harandi, H. Owen, Integrated staged conversion of methanol to gasoline and distillate, US 4899002 A, 1988.
- [11] C. Knottenbelt, Moss gas “gas-to-liquid” diesel fuels - An environmentally friendly option, *Catal. Today* 71 (2002) 437–445.
- [12] R.O. Minnie, Catalytic conversion of olefins to diesel and gasoline fuel, WO 2006091986 A1, 2006.
- [13] P. Leprince, Oligomerization, in: J.-P. Wauquier (Ed.), *Petroleum refining, Volume 3, Conversion processes*, Editions TECHNIP, 2001: pp. 321–332.
- [14] Axens, PolyFuel, <http://www.axens.net/product/technology-licensing/20071/polyfuel.html> (accessed March 24, 2016).
- [15] J.C. Groen, J.A. Moulijn, J. Pérez-Ramírez, Desilication: on the controlled generation of mesoporosity in MFI zeolites, *J. Mater. Chem.* 16 (2006) 2121–2131.
- [16] D.P. Serrano, J.M. Escola, P. Pizarro, Synthesis strategies in the search for hierarchical zeolites, *Chem. Soc. Rev.* 42 (2013) 4004–4035.
- [17] Y. Tao, H. Kanoh, L. Abrams, K. Kaneko, Mesopore-modified zeolites: preparation, characterization, and applications, *Chem. Rev.* 106 (2006) 896–910.
- [18] K. Na, M. Choi, R. Ryoo, Recent advances in the synthesis of hierarchically nanoporous zeolites, *Microporous Mesoporous Mater.* 166 (2013) 3–19.
- [19] X. Vu, U. Armbruster, A. Martin, Micro/mesoporous zeolitic composites: recent developments in synthesis and catalytic applications, *Catalysts* 6 (2016) 183–206.
- [20] R. Chal, C. Gérardin, M. Bulut, S. van Donk, Overview and industrial assessment of synthesis strategies towards zeolites with mesopores, *ChemCatChem* 3 (2011) 67–81.
- [21] M.S. Holm, E. Taarning, K. Egeblad, C.H. Christensen, Catalysis with hierarchical zeolites, *Catal. Today* 168 (2011) 3–16.
- [22] Y. Wei, T.E. Parmentier, K.P. de Jong, J. Zečević, Tailoring and visualizing the pore architecture of hierarchical zeolites, *Chem. Soc. Rev.* 44 (2015) 7234–7261.
- [23] M. Sanati, C. Hörnell, S.G. Jaras, The oligomerization of alkenes by heterogeneous catalysts, in: J.J. Spivey (Ed.), *Catalysis: Volume 14 (Specialist periodical reports)*, Royal society of chemistry, 1999: pp. 236–287.
- [24] Chevron, Diesel Fuels Technical Review, (2007). <https://www.chevron.com/-/media/chevron/operations/documents/diesel-fuel-tech-review.pdf>.
- [25] J. Speight, *The chemistry and technology of petroleum*, 4<sup>th</sup> ed., CRC press, 2014.
- [26] L. Ying, J. Zhu, Y. Cheng, L. Wang, X. Li, Kinetic modeling of C2-C7olefins interconversion over ZSM-5 catalyst, *J. Ind. Eng. Chem.* 33 (2016) 80–90.
- [27] C.T. O’Connor, Oligomerization, in: G. Ertl, H. Knözinger, F. Schüth, J. Weitkamp (Eds.), *Handbook of heterogeneous catalysis, volume 1*, 2<sup>nd</sup> ed., 2008: pp. 2854–2864.
- [28] M.A. Bezerra, R.E. Santelli, E.P. Oliveira, L.S. Villar, L.A. Escalera, Response surface methodology (RSM) as a tool for optimization in analytical chemistry, *Talanta* 76 (2008) 965–977.
- [29] A.F. Silva, M.M.R. De Melo, C.M. Silva, Supercritical solvent selection (CO<sub>2</sub> versus ethane) and optimization of operating conditions of the extraction of lycopene from tomato residues: Innovative analysis of extraction curves by a response surface methodology and cost of manufacturing hybrid app, *J. Supercrit. Fluids* 95 (2014) 618–627.

- [30] R.M.A. Domingues, M.M.R. de Melo, E.L.G. Oliveira, C.P. Neto, A.J.D. Silvestre, C.M. Silva, Optimization of the supercritical fluid extraction of triterpenic acids from *Eucalyptus globulus* bark using experimental design, *J. Supercrit. Fluids* 74 (2013) 105–114.
- [31] V.H. Rodrigues, M.M.R. de Melo, I. Portugal, C.M. Silva, Supercritical fluid extraction of *Eucalyptus globulus* leaves. Experimental and modelling studies of the influence of operating conditions and biomass pretreatment upon yields and kinetics, *Sep. Purif. Technol.* 191 (2018) 173–181.
- [32] Y. Sun, J. Wei, J.P. Zhang, G. Yang, Optimization using response surface methodology and kinetic study of Fischer-Tropsch synthesis using SiO<sub>2</sub> supported bimetallic Co-Ni catalyst, *J. Nat. Gas Sci. Eng.* 28 (2016) 173–183.
- [33] J.M. Pinheiro, S. Salústio, A.A. Valente, C.M. Silva, Adsorption heat pump optimization by experimental design and response surface methodology, *Appl. Therm. Eng.* 138 (2018) 849–860.
- [34] J.P.S. Aniceto, S.P. Cardoso, C.M. Silva, General optimization strategy of simulated moving bed units through design of experiments and response surface methodologies, *Comput. Chem. Eng.* 90 (2016) 161–170.
- [35] S. Echaroj, M. Santikunaporn, S. Chavadej, Oligomerization of 1-decene over sulfated alumina catalysts for the production of synthetic fuels and lubricants: modelling and verification, *React. Kinet. Mech. Catal.* 121 (2017) 629–644.
- [36] D. Verboekend, A.M. Chabaneix, K. Thomas, J.-P. Gilson, J. Pérez-Ramírez, Mesoporous ZSM-22 zeolite obtained by desilication: peculiarities associated with crystal morphology and aluminum distribution, *CrystEngComm.* 13 (2011) 3408–3416.
- [37] M.-C. Silaghi, C. Chizallet, P. Raybaud, Challenges on molecular aspects of dealumination and desilication of zeolites, *Microporous Mesoporous Mater.* 191 (2014) 82–96.
- [38] R. Caicedo-Realpe, J. Pérez-Ramírez, Mesoporous ZSM-5 zeolites prepared by a two-step route comprising sodium aluminate and acid treatments, *Microporous Mesoporous Mater.* 128 (2010) 91–100.
- [39] D.C. Montgomery, Design and analysis of experiments, 9<sup>th</sup> ed., Wiley, 2017.
- [40] A.S. Al-Dughaiter, H. de Lasa, HZSM-5 zeolites with different SiO<sub>2</sub>/Al<sub>2</sub>O<sub>3</sub> ratios. Characterization and NH<sub>3</sub> desorption kinetics, *Ind. Eng. Chem. Res.* 53 (2014) 15303–15316.
- [41] M.M.J. Treacy, J.B. Higgins, Collection of simulated XRD powder patterns for zeolites, ELSEVIER, 2001.
- [42] LECO Corporation, Determination of hydrocarbon components in petroleum naphthas, 2010. [http://www.leco.co.za/wp-content/uploads/2011/06/PEG\\_PETROLEUM\\_NAPHTHAS\\_ASTM\\_D5134\\_203-821-190.pdf](http://www.leco.co.za/wp-content/uploads/2011/06/PEG_PETROLEUM_NAPHTHAS_ASTM_D5134_203-821-190.pdf).
- [43] X. Zhang, L. Ding, Z. Sun, L. Song, T. Sun, Study on quantitative structure–retention relationships for hydrocarbons in FCC gasoline, *Chromatographia* 70 (2009) 511–518.
- [44] Hexadecane-Kovats Retention Index, <https://pubchem.ncbi.nlm.nih.gov/compound/hexadecane#section=Kovats-Retention-Index> (accessed December 26, 2018).
- [45] H.-S. Laboratory, Procedure for the detailed hydrocarbon analysis of gasolines by single column high efficiency (capillary) column gas chromatography, 1997. <http://www.arb.ca.gov/cc/semiconductors/semiconductors.htm>.
- [46] P. Ciccioli, A. Cecinato, E. Brancaleoni, M. Frattoni, A. Liberti, Use of carbon adsorption traps combined with high resolution gas chromatography – mass spectrometry for the analysis of polar and non-polar C<sub>4</sub>-C<sub>14</sub> hydrocarbons involved in photochemical smog formation, *J. High Resolut. Chromatogr.* 15 (1992) 75–84.

Optimization of heterogeneous catalytic oligomerization of 1-butene by design of experiments and response surface methodology

- [47] Trans-3,4-Dimethyl-2-Pentene-Kovats Retention Index, <https://pubchem.ncbi.nlm.nih.gov/compound/638068#section=Experimental-Properties> (accessed December 26, 2018).
- [48] 3-Ethyl-4-Methyl-2-Pentene-Kovats Retention Index, <https://pubchem.ncbi.nlm.nih.gov/compound/5352666#section=Kovats-Retention-Index> (accessed December 26, 2018).
- [49] Supelco, Petrocol DH Columns Catalog No. 24160-U, (2012). <https://www.sigmaaldrich.com/content/dam/sigma-aldrich/docs/Supelco/Datasheet/1/w97949.pdf> (accessed December 26, 2018).
- [50] 3-Ethyl-2-Hexene-Kovats Retention Index, <https://pubchem.ncbi.nlm.nih.gov/compound/5352663#section=Kovats-Retention-Index> (accessed December 26, 2018).
- [51] 2,6-Dimethyl-1-Heptene-Kovats Retention Index, [https://pubchem.ncbi.nlm.nih.gov/compound/2\\_6-Dimethyl-1-heptene#section=Kovats-Retention-Index](https://pubchem.ncbi.nlm.nih.gov/compound/2_6-Dimethyl-1-heptene#section=Kovats-Retention-Index) (accessed December 26, 2018).
- [52] 4-Ethyl-3-heptene-Kovats Retention Index, <https://pubchem.ncbi.nlm.nih.gov/compound/5364679#section=Kovats-Retention-Index> (accessed December 26, 2018).
- [53] 2,3-Dimethyl-3-heptene-Retention index (Kovats), <http://www.chemspider.com/Chemical-Structure.4516879.html> (accessed December 26, 2018).
- [54] P.A. Martos, A. Saraullo, J. Pawliszyn, Estimation of air/coating distribution coefficients for solid phase microextraction using retention indexes from linear temperature-programmed capillary gas chromatography. Application to the sampling and analysis of total petroleum hydrocarbons in air, *Anal. Chem.* 69 (1997) 402–408.
- [55] 2,6-Dimethyl-3-heptene, <https://webbook.nist.gov/cgi/cbook.cgi?ID=C2738183&Units=SI&Mask=2000#Gas-Chrom> (accessed December 15, 2018).
- [56] A.A. Swigar, R.M. Silverstein, Monoterpenes: infrared, mass, <sup>1</sup>H NMR, and <sup>13</sup>C NMR spectra, and Kováts indices, Aldrich Chemical Company, Milwaukee, WI, USA, 1981.
- [57] C.M. White, J. Hackett, R.R. Anderson, S. Kail, P.S. Spock, Linear temperature programmed retention indices of gasoline range hydrocarbons and chlorinated hydrocarbons on cross-linked polydimethylsiloxane, *J. High Resolut. Chromatogr.* 15 (1992) 105–120.
- [58] R.J. Laub, J.H. Purnell, Specific retention volumes, retention indices, and family-plot regressions of aliphatic, alicyclic, and aromatic hydrocarbon solutes with OV-101 poly (dimethylsiloxane) stationary phase, *J. High Resolut. Chromatogr. & Chromatogr. Commun.* 11 (1988) 649–660.
- [59] Cis-5-Decene-Kovats Retention, Index [https://pubchem.ncbi.nlm.nih.gov/compound/\\_Z\\_-5-Decene#section=Kovats-Retention-Index](https://pubchem.ncbi.nlm.nih.gov/compound/_Z_-5-Decene#section=Kovats-Retention-Index) (accessed Dec 26, 2018).
- [60] 4-Undecene, (4E)-Kovats Retention Index, [https://pubchem.ncbi.nlm.nih.gov/compound/4-Undecene\\_\\_E\\_-#section=Kovats-Retention-Index](https://pubchem.ncbi.nlm.nih.gov/compound/4-Undecene__E_-#section=Kovats-Retention-Index) (accessed December 26, 2018).
- [61] Trans-4-Dodecene-Kovats Retention Index, <https://pubchem.ncbi.nlm.nih.gov/compound/5364443#section=Kovats-Retention-Index> (accessed December 26, 2018).
- [62] 1,1-Diethylcyclopropane-Kovats Retention Index, [https://pubchem.ncbi.nlm.nih.gov/compound/1\\_1-Diethylcyclopropane#section=Kovats-Retention-Index](https://pubchem.ncbi.nlm.nih.gov/compound/1_1-Diethylcyclopropane#section=Kovats-Retention-Index) (accessed December 26, 2018).

- [63] 1,2,3-Trimethylcyclopentene-Kovats Retention Index, [https://pubchem.ncbi.nlm.nih.gov/compound/1\\_2\\_3-Trimethylcyclopentene#section=Kovats-Retention-Index](https://pubchem.ncbi.nlm.nih.gov/compound/1_2_3-Trimethylcyclopentene#section=Kovats-Retention-Index) (accessed December 26, 2018).
- [64] 1,4-Dimethylcyclohexene-Kovats Retention Index, [https://pubchem.ncbi.nlm.nih.gov/compound/1\\_4-Dimethylcyclohexene#section=Kovats-Retention-Index](https://pubchem.ncbi.nlm.nih.gov/compound/1_4-Dimethylcyclohexene#section=Kovats-Retention-Index) (accessed December 26, 2018).
- [65] Octane-Kovats Retention Index, <https://pubchem.ncbi.nlm.nih.gov/compound/octane#section=Kovats-Retention-Index> (accessed December 26, 2018).
- [66] Nonane-Kovats Retention Index, <https://pubchem.ncbi.nlm.nih.gov/compound/nonane#section=Kovats-Retention-Index> (accessed January 6, 2019).
- [67] C. Vendeuvre, F. Bertocini, D. Thiébaud, M. Martin, M.-C. Hennion, Evaluation of a retention model in comprehensive two-dimensional gas chromatography, *J. Sep. Sci.* 28 (2005) 1129–1136.
- [68] 3,8-Dimethyldecane-Kovats Retention Index, [https://pubchem.ncbi.nlm.nih.gov/compound/3\\_8-Dimethyldecane#section=Kovats-Retention-Index](https://pubchem.ncbi.nlm.nih.gov/compound/3_8-Dimethyldecane#section=Kovats-Retention-Index) (accessed December 26, 2018).
- [69] F. Khorasheh, M.R. Gray, M.L. Selucky, Correlation for Kovats retention index of C9-C26 monoalkyl and polymethyl alkanes and alkenes, *J. Chromatogr.* 481 (1989) 1–16.
- [70] P.C.J. Hayes, E.W. Pitzer, Kovats indices as a tool in characterizing hydrocarbon fuels in temperature programmed glass capillary gas chromatography. Part 1. Qualitative identification, 1981, [https://archive.org/details/DTIC\\_ADA111389/page/n1](https://archive.org/details/DTIC_ADA111389/page/n1) (accessed Dec 26, 2018).
- [71] Dodecane-Kovats Retention Index, <https://pubchem.ncbi.nlm.nih.gov/compound/8182#section=Kovats-Retention-Index> (accessed December 26, 2018).
- [72] N. Kumar, P. Mäki-Arvela, T. Yläsalmi, J. Villegas, T. Heikkilä, A.-R. Leino, K. Kordás, T. Salmi, D. Yu Murzin, Dimerization of 1-butene in liquid phase reaction: Influence of structure, pore size and acidity of Beta zeolite and MCM-41 mesoporous material, *Microporous Mesoporous Mater.* 147 (2012) 127–134.
- [73] Y.T. Kim, J.P. Chada, Z. Xu, Y.J. Pagan-Torres, D.C. Rosenfeld, W.L. Winniford, E. Schmidt, G.W. Huber, Low-temperature oligomerization of 1-butene with H-ferrierite, *J. Catal.* 323 (2015) 33–44.
- [74] G. Bellussi, F. Mizia, V. Calemma, P. Pollesel, R. Millini, Oligomerization of olefins from Light Cracking Naphtha over zeolite-based catalyst for the production of high quality diesel fuel, *Microporous Mesoporous Mater.* 164 (2012) 127–134.
- [75] A. Abdalla, P. Arudra, S.S. Al-Khattaf, Catalytic cracking of 1-butene to propylene using modified H-ZSM-5 catalyst: A comparative study of surface modification and core-shell synthesis, *Appl. Catal. A Gen.* 533 (2017) 109–120.
- [76] S. Kotrel, H. Knözinger, B.C. Gates, The Haag–Dessau mechanism of protolytic cracking of alkanes, *Microporous Mesoporous Mater.* 35–36 (2000) 11–20.
- [77] C.T. O'Connor, R.D. Forrester, M.S. Scurrall, Cetane number determination of synthetic diesel fuels, *Fuel* 71 (1992) 1323–1327.
- [78] A. de Klerk, Can Fischer-Tropsch syncrude be refined to on-specification diesel fuel?, *Energy & Fuels* 23 (2009) 4593–4604.

Optimization of heterogeneous catalytic oligomerization of 1-butene by design of experiments and response surface methodology

- [79] H. de Lasa, G. Dogammau, A. Ravella, Fuels of the future and changing fuel needs, in: Chemical reactor technology for environmentally safe reactors and products, Springer-Science+Business Media, London, Ontario, 1992: pp. 1–182.
- [80] D. Leckel, Diesel production from Fischer-Tropsch: the past, the present, and new concepts, *Energy & Fuels* 23 (2009) 2342–2358.
- [81] A. De Klerk, Fischer–Tropsch refining: technology selection to match molecules, *Green Chem.* 10 (2008) 1249–1279.
- [82] G.S. Kapur, A. Ecker, R. Meusinger, Establishing quantitative structure-property relationships (QSPR) of diesel samples by proton-NMR & multiple linear regression (MLR) analysis, *Energy and Fuels* 15 (2001) 943–948.
- [83] A. Coelho, G. Caeiro, M.A.N.D.A. Lemos, F. Lemos, F.R. Ribeiro, 1-Butene oligomerization over ZSM-5 zeolite: Part 1 - Effect of reaction conditions, *Fuel* 111 (2013) 449–460.
- [84] E. Epelde, J.I. Santos, P. Florian, A.T. Aguayo, A.G. Gayubo, J. Bilbao, P. Castaño, Controlling coke deactivation and cracking selectivity of MFI zeolite by H<sub>3</sub>PO<sub>4</sub> or KOH modification, *Appl. Catal. A Gen.* 505 (2015) 105–115.
- [85] J.R. Shahrouzi, D. Guillaume, P. Rouchon, P. Da Costa, Stochastic simulation and single events kinetic modeling: application to olefin oligomerization, *Ind. Eng. Chem. Res.* 47 (2008) 4308–4316.



# CHAPTER 10

---

## Conclusions and future work



### Chapter 10

#### Conclusions and future work

10.1.	General conclusions .....	308
10.2.	Future work.....	315
10.3.	References.....	317

## 10.1. General conclusions

In face of the fast world population growth and increasing globalization and development especially in non-Organization for Economic Co-operation and Development (non-OECD) countries, continued efforts need to be made in the different energetic sectors (industrial, transportation, buildings) in order to satisfy the high worldwide energy demand while, at the same time, reducing the environmental impact and enhancing energetic security. Particularly in the transportation sector important advances have been made regarding the efficiency of internal combustion engine (ICE) vehicles, and the share of electric and bio-based fuels vehicles is increasing. The shared mobility is also a good solution that has been increasing in recent years. In spite of the great advances, the current and future scenarios indicate that fossil fuels, mainly gasoline and diesel (>60 %), will predominate in the fuels demand worldwide. Particularly in the European Union, the diesel demand will continue to increase, whereas the gasoline demand is decreasing. Thus, it is essential to develop and invest in efficient technologies for producing clean synthetic fuels, with low content of sulphur-containing and aromatic compounds. The oligomerization of light olefins appears as a promising route to produce clean synthetic fuels and valorize low cost olefinic streams derived from the petrochemical and Fischer-Tropsch (FT) industries, or from renewable sources such as cellulosic biomass. Currently, the olefin oligomerization technologies COD (MFI type catalyst) and CatPoly (SPA catalyst) are in operation at FT refineries in the Republic of South Africa.

Despite the important improvements accomplished in oligomerization technologies, there are continued research efforts in the fields of material science and catalysis to develop catalytic materials with superior performances in terms of activity, stability and selectivity to diesel type products. Zeolites appeared as promising catalysts due to their high internal surface area, high thermal stability, versatility, acidic features, and ordered microporous systems conferring them interesting shape-selectivity properties. However, internal mass transfer limitations may be important, leading to pore blockage and fast catalyst deactivation, especially when the desired reaction products are relatively bulky molecules. Recent materials research is focused on developing zeotypes to overcome mass transfer limitations and steric hindrance effects associated with microporous zeolites. In this thesis, special

attention was given to porous aluminosilicates (Figure 10.1), which are a huge and versatile category of solid materials, some of which reached industrial applications as catalysts.

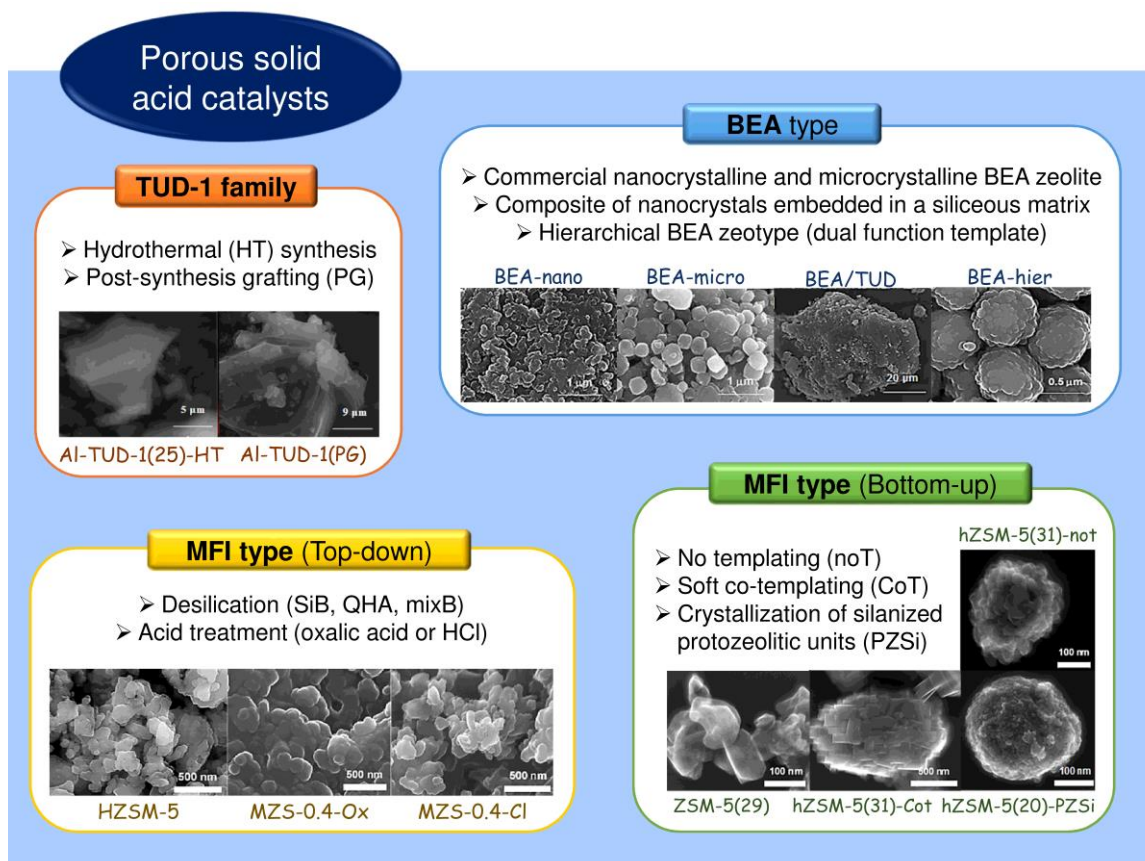


Figure 10.1. Summary of the porous solid acid catalysts explored in this work.

The prepared catalytic materials were explored for the oligomerization of 1-butene, under high pressure and continuous fixed bed operation, targeting diesel range products. The catalytic performances of the materials were evaluated in terms of activity, product selectivity and stability, based on experimental studies and multivariate statistical tools for establishing activity relationships; and were benchmarked with commercially available zeolites and a catalyst based on the MFI topology (COD-9) that was developed for the COD commercial oligomerization technology. The characteristics of the catalytic reaction products were studied by comprehensive two-dimensional gas chromatography coupled to time-of-flight mass spectrometry (GC×GC-ToFMS) and Nuclear Magnetic Resonance (NMR) spectroscopy.

Mesoporous TUD-1 type aluminosilicates prepared *via* hydrothermal synthesis (HT) or post-synthesis grafting (PG) approaches without surfactants (an eco-friendly feature), possessed large mesopore sizes (10-14 nm) and essentially Lewis acidity of moderate strength (Chapter 5). These materials performed superiorly to an ordered mesoporous aluminosilicate synthesized using surfactant mixtures. In particular, Al-TUD-1(25)-HT possessed good stability for 32 h on-stream, albeit it did not outperform the commercial zeolite ZSM-5, which may be partly attributed to the overall mild acidity of the mesoporous silicate. Hence, further work was focused on transforming zeolites into hierarchical zeolitic materials (zeotypes) possessing micro- and mesoporosity.

A hierarchical zeotype based on the BEA topology (BEA-hier, Si/Al=11) was synthesized *via* soft template methodology using a relatively low-cost dual function cationic polymer that acted simultaneously as micro- and mesopore former (Chapter 6). BEA-hier consisted of an arrangement of nanocrystallites, possessing mesoporosity ( $S_{\text{meso}}=503 \text{ m}^2 \text{ g}^{-1}$ ) and enhanced molar ratio of Lewis (L) to Brønsted (B) acid sites ( $L/B=2.2$ ,  $B+L=331 \mu\text{mol g}^{-1}$ ). This catalyst outperformed commercial nanocrystalline and microcrystalline Beta zeolites, as well as ZSM-5 and COD-900, in terms of conversion of butenes and space time yields of liquid products (STY). The synthesis method involving a dual function polymeric template is non-destructive and may be adapted for synthesizing hierarchical zeotypes of different topologies such as MFI that corresponds to that of catalysts used in the olefin oligomerization industrial process (South African). MFI zeotypes may also be prepared without using additional templates.

MFI-based zeotypes were prepared *via* different non-destructive bottom-up approaches, which included the use of an appropriate dual function template (CoT), or not using additional template (noT) (Chapter 7). In general, the materials consisted of somewhat regular shaped aggregates of nanocrystallites, possessing mesoporosity, and were effective for olefin oligomerization. Characterization studies indicated that the morphology, structure, composition, textural and acid properties of the zeotypes were essentially preserved during the catalytic reaction and the catalyst regeneration processes. The materials prepared *via* the noT and CoT procedures possessed stronger acidity and inferior mesoporous specific surface area than the materials prepared *via* a methodology that involved crystallization of silanized protozeolitic units (PZSi). The latter synthesis methodology led to the best-performing

catalyst, namely hZSM-5(20)-PZSi (Si/Al=20,  $S_{\text{meso}}=308 \text{ m}^2 \text{ g}^{-1}$ , L/B=1.34, B+L=251  $\mu\text{mol g}^{-1}$ ). However, the PZSi procedure used relatively expensive organosilanes and scaling up of the hydrothermal synthesis may not be trivial. Post-synthesis modifications of commercially and readily available materials may be easier to scale up and implement industrially.

Commercial zeolite ZSM-5 possessing relatively low Si/Al molar ratio (15) was modified *via* top-down approaches leading to superior catalysts (Chapter 8). Catalytic and characterization studies combined with principal component analysis (PCA) suggested that an intermediate range of acid sites concentrations and enhanced mesoporosity favored the oligomerization reaction. One of the best-performing was MZS-0.4-Cl (Si/Al=24,  $S_{\text{meso}}=291 \text{ m}^2 \text{ g}^{-1}$ , L/B=0.80, B+L=250  $\mu\text{mol g}^{-1}$ ) prepared *via* desilication using 0.4 M NaOH and acid treatment using HCl. This catalyst led to the highest conversion of butenes (86 %) and STY of liquid products (852  $\text{g g}_{\text{cat}}^{-1} \text{ h}^{-1}$ ).

The influence of the catalyst activation temperature (prior to the catalytic reaction) was investigated for the different zeotypes. The BEA based catalysts performed superiorly when activated at 200 or 320 °C than at 450 °C, which was opposite to that verified for commercial ZSM-5. These differences may be partly attributed to changes in the distributions of the types of Al-sites occurring during catalyst activation/use. The activation temperature (200 °C or 450 °C) did not influence significantly the performances of the MFI based zeotypes prepared *via* bottom-up or top-down approaches.

For the best-performing catalysts of each family of materials studied in Chapters 5, 6 and 7, namely Al-TUD-1(25)-HT, BEA-hier and hZSM-5(20)-PZSi (Figure 10.1), it was studied the influence of the reaction pressure and temperature, in order to meet superior performances. The catalytic activity was enhanced by increasing the reaction temperature and pressure. Decreasing reaction temperature and increasing the pressure enhanced the mass ratio of diesel to naphtha range products ( $D_{\text{cut}}/N_{\text{cut}}$ ). Based on GC×GC-ToFMS analysis, the types of products formed were mainly aliphatic hydrocarbons, and relatively low amounts of aromatics at 200 °C and 30 bar.

PCA analysis of all materials studied in this thesis was carried out for overall comparisons of the catalytic performances (Figure 10.2) and relationships with the material properties (Figure 10.3), based on the data matrix of Table S10.1. For the two PCA biplots, the total variance was greater than 80 % and the squared cosines of the variables and

observations were sufficiently high to allow meaningful analyses of the biplots with F1 and F2 as principal components. Based on Figure 10.2, the materials may be classified in two main groups, according to their performances in relation to commercial zeolites: (i) the poorer performing (pink circle) and (ii) the superior performing (blue circle) catalysts. The poorer performing catalysts (pink circle) led to lower or similar conversion of butenes ( $X_{C4}$ ), STY and space time yield of diesel type products ( $STY_{Dcut}$ ) to the commercial zeolites (yellow highlighted names). This group comprises the mesoporous TUD-1 type aluminosilicates (Chapter 5), the composite material BEA/TUD (Chapter 6), the micro/mesoporous MFI zeotype prepared *via* the co-templating method (hZSM-5(31)-CoT, Chapter 7) and the materials prepared by top-down approach (MZS-0.6-Ox, Chapter 8). The best-performing group (blue circle) led to higher  $X_{C4}$ , STY and  $STY_{Dcut}$  than the commercial zeolites, and comprises BEA-hier (Chapter 6) and MFI-based zeotypes prepared *via* bottom-up (Chapter 7) or top-down (Chapter 8) approaches. One of the best catalysts was prepared *via* the top-down approach, namely MZS-0.4-Cl (green highlighted name), Chapter 8. For the poorer performing group,  $X_{C4}$  was in the range 15-36 %, STY in the range 26-288 g  $g_{cat}^{-1} h^{-1}$ ,  $STY_{Dcut}$  in the range 26-166 g  $g_{cat}^{-1} h^{-1}$  and Dcut selectivity (for the liquid products) in the range 21-87 wt.%, whereas the superior performing one led to 46-86 %  $X_{C4}$ , 490-852 g  $g_{cat}^{-1} h^{-1}$  STY, 271-584 g  $g_{cat}^{-1} h^{-1}$   $STY_{Dcut}$  and 55-71 wt.% Dcut selectivity.

Figure 10.3 shows the PCA biplot considering the materials properties (texture and acidity); the materials were highlighted according to the classification of Figure 10.2. Apparently, there is no clear direct relation between the catalytic performance parameters and the material properties, suggesting complex interplay of the material properties. The TUD-1 type aluminosilicates, belonging to the poorer performing group, are characterized by higher mesoporosity (left side of the biplot) and lower acid strength (located opposite to the right side of the biplot). The materials MZS-0.2-Ox and MZS-0.2-Cl prepared *via* top-down approach using relatively low NaOH concentration (Chapter 8) and hZZSM-5(31)-not prepared *via* bottom-up approach without template (Chapter 7) possessed similar textural and acid properties (high acid strength and inferior mesoporosity) and belonged to the superior performing group (compared to commercial zeolites). The remaining materials were located in the central region of the biplot, being characterized by intermediate textural and acid properties, and most of these materials belonged to the superior performing group, which included the best-performing catalyst MZS-0.4-Cl.

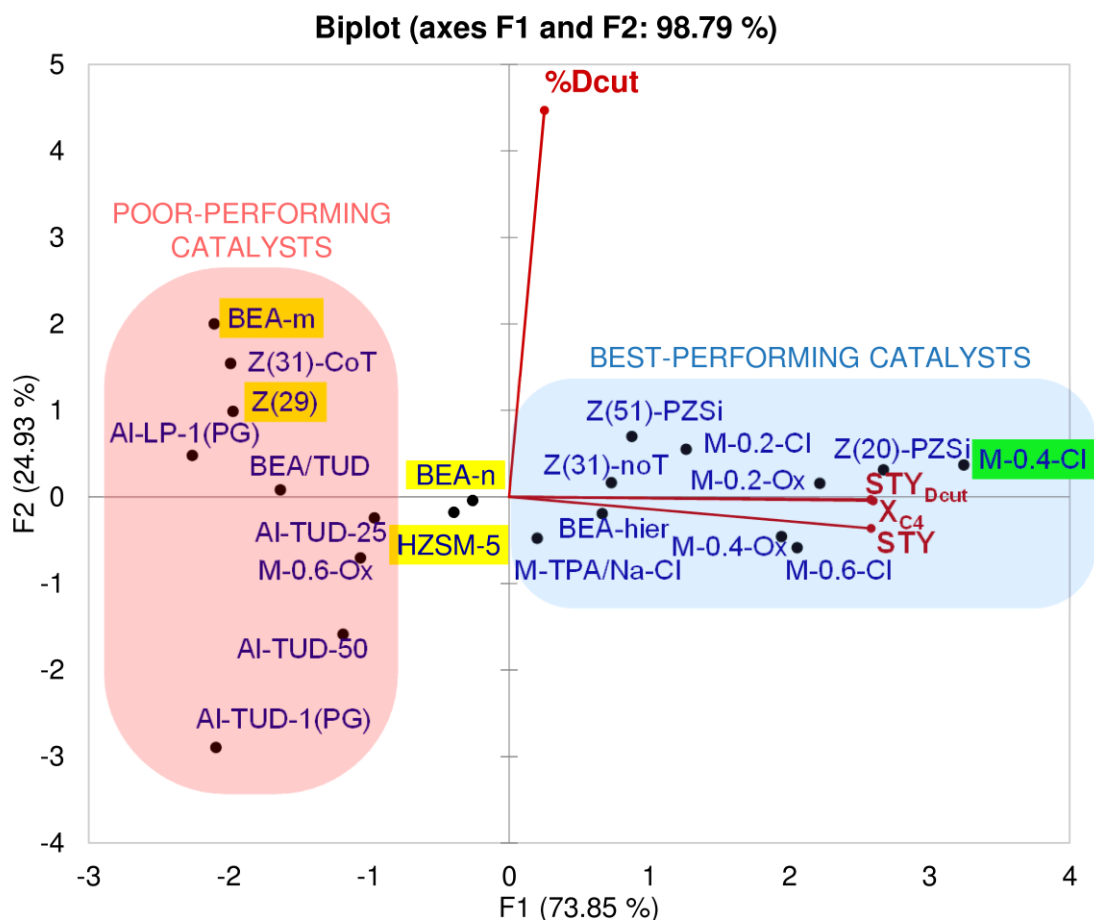


Figure 10.2. PCA biplot (PC1: 73.85 % and PC2: 24.93 %) categorizing the materials according to their catalytic performances. The variables are represented in red text and the observations in blue text. The blue and pink colored regions signalize, respectively, the superior and poorer performing materials, in comparison to the commercial zeolites (yellow). In green is highlighted the best performing catalyst of all the studied materials. The samples names are abbreviated for better visualization: M represents MZS, Z<sub>x</sub> represents hZSM-5 (where x is the value of the molar ratio Si/Al), n represents nano and m represents micro, Al-TUD-25=Al-TUD-1(25)-HT, Al-TUD-50=Al-TUD-1(50)-HT.

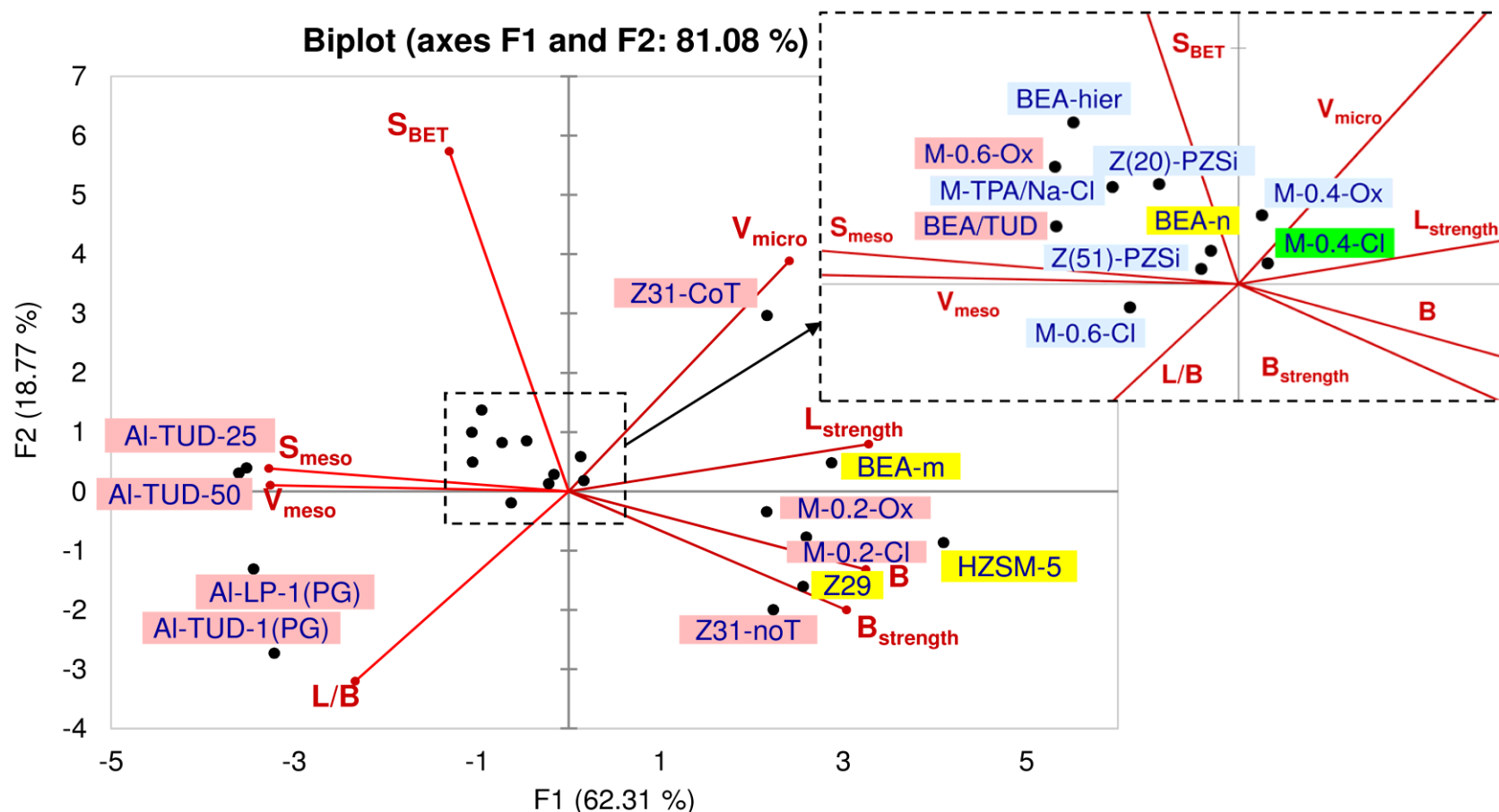


Figure 10.3. PCA biplot (PC1: 61.58 % and PC2: 18.75 %) categorizing the materials according to their properties. The variables are represented in red text and the observations in blue text. The blue and pink highlights (of sample names) signalize, respectively, the superior and poorer performing materials in comparison to the commercial zeolites (yellow), according to Figure 10.2. In green is highlighted the best performing catalyst of all the studied materials. The samples names are abbreviated for better visualization: M represents MZS,  $Z_x$  represents hZSM-5 (where  $x$  is the value of the molar ratio Si/Al), n represents nano and m represents micro, AI-TUD-25=AI-TUD-1(25)-HT, AI-TUD-50=AI-TUD-1(50)-HT.

An optimization study of olefin oligomerization was carried out for the best performing catalyst, MZS-0.4-Cl, in order to maximize the yields as well as the quality (reduced aromatics content) of diesel range products. The optimization was based on a Box-Behnken design of experiments (DoE) and response surface methodology (RSM), which are statistical tools that systematize and treat experimental data, in order to screen and optimize a studied response as a function of direct and crossed factors, minimizing the number of experimental assays necessary for optimizing the process; this is particularly valuable when rigorous kinetic modelling is difficult. DoE/RSM may be a powerful evaluation tool in the development of flexible technologies to meet market demands for high quality fuels. This thesis includes the first DoE/RSM study reported (to the best of my knowledge) for light olefin oligomerization. The factors evaluated were the reaction temperature, pressure and WHSV, and the responses were conversion, yields of Dcut and Ncut products, yields of aromatics and yields of Dcut and Ncut range products free of aromatic compounds. The reaction products obtained under the different reaction conditions were analyzed by GC×GC-ToFMS. It was verified that the optimal operating windows to obtain high yields of diesel type products with low aromatics were: 220-250 °C, 30-40 bar and 2.5-3.5 g<sub>1C4</sub> g<sub>cat</sub><sup>-1</sup> h<sup>-1</sup>, which led to 34-38 % yield of Dcut products free of aromatics, and less than 5 % yield of aromatic compounds (mainly monocyclic). In the higher temperature range (>250 °C), the amounts of naphtha type products increased, albeit the fraction of aromatics was considerable.

## 10.2. Future work

This thesis focused on the oligomerization of 1-butene over different types of heterogeneous acid catalysts. Next, the best performing catalysts identified in this thesis may be studied for the oligomerization of mixtures of olefins, mimicking the olefinic streams of the industrial processes. For example, the C<sub>4</sub> stream of a Fluid Catalytic Cracking (FCC) unit may be 20-40 % isobutane, 10-25 % isobutene, 10-25 % 1-butene, 10-20 % 2-butenes, 10-20 % n-butane, 0-0.5 % 1,3-butadiene.<sup>[1]</sup>

Innovative, promising catalysts are being discovered for the petrochemical industry as a result of the continued advances in materials science and engineering. New catalysts should be considered for olefin oligomerization. Motivated by the demonstrated advantages of introducing mesoporosity in MFI zeolites *via* bottom-up or top-down approaches, it is encouraged to explore different zeolite topologies (*e.g.*, FER, BEA, TON, FAU) prepared using similar synthesis strategies and compare the performances with the MFI based zeotypes, especially in terms of catalyst stability over long time on-stream.

According to the literature, materials synthesized hydrothermally from clays may possess relatively high mechanical and hydrothermal stabilities and pore sizes, which may enhance the accessibility to the acid sites.<sup>[2,3]</sup> The synthesis of zeolites possessing different topologies (FAU, BEA, MFI) from readily available natural clays (*e.g.*, kaolin, rectorite), with controllable Si/Al ratio, are viewed as promising routes to produce catalysts for industrial applications, with low production cost and environmental impact. These types of materials may deserve some attention. Attempts were made along this thesis to prepare MFI zeolites from clays, specifically using a kaolin type found in Portugal and Spain (Figure S10.2). The crystalline phase of the material was very sensitive to the synthesis conditions (Figure S10.3). ZSM-5 was obtained using a molar Si/Al ratio of the synthesis gel of 25, but required the addition of considerable amounts of colloidal silica to the synthesis mixture. This catalyst performed poorly, leading to 16 % conversion of butenes. The synthesis conditions needed to be optimized, for which DoE/RSM may be a helpful tool.

The acid properties influenced considerably the catalytic performances of the materials. The introduction of transition metals (*e.g.*, Ni and Zr) in zeolites is thoroughly reported in the literature for ethene oligomerization and, to a smaller extent, for the oligomerization of other olefins. These modifications led to enhanced catalytic stability and favored the oligomerization reaction. It may be interesting to study the effects of introducing different metals in the best-performing zeotypes.

The DoE/RSM statistical optimization tool helped determine, in expeditious fashions, the optimal operating regions and understand the influence of the reaction conditions. This tool may be useful for tuning the material properties for promising synthesis methodologies. The synthesis parameters (*e.g.*, Si/Al ratio, amount of structure directing

agent, synthesis time and temperature) may be optimized within ranges that lead to the desired crystalline phases of the materials.

Another challenge is to develop rigorous phenomenological models contemplating kinetics, equilibrium and conservation laws, for the simulation and optimization studies of oligomerization continuous flow processes.

### 10.3. References

- [1] T. Streich, H. Kömpel, J. Geng, M. Renger, Secure the best benefits from C4 hydrocarbon processing-Part 1: Separation sequences, *Hydrocarb. Process.* June (2016) 73–78.
- [2] B. Shen, P. Wang, Z. Yi, W. Zhang, X. Tong, Y. Liu, Q. Guo, J. Gao, C. Xu, Synthesis of zeolite beta from kaolin and its catalytic performance for FCC naphtha aromatization, *Energy and Fuels* 23 (2009) 60–64.
- [3] B. Wei, H. Liu, T. Li, L. Cao, Y. Fan, Natural rectorite mineral: a promising substitute of kaolin for *in-situ* synthesis of fluid catalytic cracking catalysts, *AIChE J.* 56 (2010) 2913–2922.



## Appendix A

Supplementary Material - Chapter 3.....	320
Supplementary Material - Chapter 4.....	329
Supplementary Material - Chapter 6.....	332
Supplementary Material - Chapter 7.....	336
Supplementary Material - Chapter 8.....	338
Supplementary Material - Chapter 9.....	343
Supplementary Material - Chapter 10.....	348
References of Appendix A.....	350

## Supplementary Material - Chapter 3

### Description of Setup 1

A schematic representation of Setup 1 is presented in Figure 3.4 (Chapter 3) and in Figure S3.1 and Figure S3.2. The feed section (A) comprised the following equipment: (A1) bottle of nitrogen gas (AirLiquid, 99.999 %); (A2) bottle of 1-butene (Praxair, 99.6 %); (A3) mass flow controller (MFC, Bronkhorst, EL-FLOW F-201CV, 3-500 mL min<sup>-1</sup>, pressure up to 64 bar, -10 to 70 °C); (A4) syringe pump (CHEMYX, Nexus 6000, with capacity of 20 mL, minimal volumetric flow of 0.1 nL min<sup>-1</sup>, accuracy < ±0.04 % error, pressure up to 78 bar, 10 to 50 °C); (A5) ice bath; (A6-A8) needle valves (Hy-lok, NV1-H-2TPK-S316, pressure up to 340 bar, temperature up to 315 °C); (A9-A11) check valves (Hy-lok, 700 series model CV1-H-2T-S316, pressure up to 206 bar, temperature up to 191 °C); (A12) relief valve (Parker, 4M4F-RH4A-VT-SS, -26 °C to 204 °C); (A13) manometer (Wika); (A14) pressure transducer (Sensor Techniques, KTE630GL0, output of 0-10V); and (A15) pressure indicator (Paralab).

The reaction section (B) comprised the following equipment: (B1) tubular reactor (Paralab, custom made, stainless-steel 316, length of 400 mm, internal diameter (I.D.) of 16 mm and external diameter (O.D.) of 22 mm, temperature up to 800 °C); (B2) thermocouple (Omega, type K, CAIN-IM15U-450, temperature up to 650 °C); (B3) temperature PID controller (Shinko, model ACS); (B4) tubular oven equipped with thermocouple (Termolab); (B5) oven temperature PID controller and indicator (Eurotherm, model 2116); (B6) pressure transducer (Omega, PX319-1KGI, pressure up to 69 bar, accuracy of ±0.25 %, output of 4-20 mA); (B7) manometer (Wika); (B8) filter (Paralab); (B9) back-pressure regulator (BPR, Equilibar, Primary Research series, model LF1, diaphragm of polyamide, pressure up to 55 bar, temperature up to 150 °C); (B10) BPR manual regulator (TESCOM, 44-1700 Series, maximum inlet pressure of 55.2 bar, -26 to 60 °C); and (B11-B14) needle valves (Hy-lok, NV1-H-2TPK-S316, pressure up to 340 bar, temperature up to 315 °C).

The products section (C) comprised the following equipment: (C1-C4) needle valves (Hy-lok, NV1-H-2TPK-S316, pressure up to 340 bar, temperature up to 315 °C); (C5) jacketed trap (Paralab, stainless steel 316, capacity of 20 mL); (C6) bath (Thermo/HAAKE, model DC10-K10 with immersion circulator, operates at 20 to 100 °C (with tap water) or –

30 to 100 °C (with an appropriate liquid refrigerant)); (C7) loops system, composed by a 6 port 2-position manual valve (VICI, 4C6WE, pressure up to 27 bar, temperature up to 225 °C), and a 12 multi-position trapping path ST selector (VICI, EMT4CST12MWT), equipped with 0.5 mL loops (Paralab, pressure up to 13 bar, temperature up to 300 °C); and (C8) gas chromatograph (GC, DANI, Master Fast) equipped with FID detector, split/splitless injector, and capillary column ValcoBond VB-1 (VICI, 60 m length, 0.25 mm ID, 1.50 µm column film thickness, with dimethylpolysiloxane phase, maximum temperature of 340/360 °C).

All three sections of laboratory Setup 1 are composed by stainless steel 316 tubes with O.D. of 1/8 and 1/16 inches, some of them heated by heating hoses (represented by red lines), and by two closed heated boxes (represented by red squares), to avoid condensation of reactants or reaction products. These heated sections possess temperature controls and indicators (A16, B15 and C9 for the hoses, and B16 and C10 for the boxes). The set-point of the several pieces of equipment is set *via* a specific lab view software, created by Paralab, for this specific oligomerization setup.

### Operation of Setup 1

Setup 1 was based on a robust and versatile design to perform oligomerization reactions at atmospheric or high pressure, up to 45-50 bar, and a wide range of temperatures, up to 600 °C. Before each experiment, the required amount of catalyst, in powdered form, was loaded into the reactor, and packed between two quartz wool discs (Elemental Microanalysis, 16 mm of diameter and 5 mm thick) supported in six stainless steel cylinders (16 mm of diameter and 20-30 mm length), in order to form a fixed bed in the middle zone of the vertical tubular reactor, where the temperature was uniform. These cylinders had helical cracks in their lateral surface and a small opening in the middle to facilitate the flow of reactant and products. The catalyst was activated *in situ* at 500 °C for 3 h, under nitrogen flow (20 mL/min). Afterwards, the reactor temperature and the feed line was set to the desired reaction temperature. The temperature of the reactor effluent line and the main heated box (comprising the BPR) was 200 and 150 °C, respectively. The temperature of the jacketed trap was 0-5 °C, using a bath with external circulation, and a mixture (1:1 (v/v)) of ethylene glycol and distilled water as refrigerant. The syringe pump was filled with 1-butene by opening valve A6 and keeping the remaining valves closed. The ice bath was filled

with a mixture of ice and salt in a mass proportion of 10:1 (temperature of *ca.* -10 °C), in order to fill the syringe pump with 1-butene in the liquid state (a low filling rate of 0.05-0.1 mL/min was recommendable).

To operate at high pressure, it was necessary to pressurize the installation with nitrogen (50-80 mL/min), by rotating the BPR regulator and opening the valves A6, B13, C2 and C3, while keeping the remaining valves closed. On the other hand, to operate at atmospheric pressure, it was necessary to reduce the pressure of the feed line of 1-butene to atmospheric pressure, by rotating the BPR regulator and opening the valves A6, B11, B12, B14, C1 and C3, while keeping the remaining valves closed. Figure S3.1 and Figure S3.2 show a schematic representation of the fluid circuit in Setup 1 for atmospheric pressure and high-pressure operation, respectively.

After the installation being properly prepared, at the desired pressure and temperature, the flow rates of nitrogen and 1-butene were set. The catalytic reaction started when the pressure of the syringe pump line equaled the pressure of the installation, and then valve A8 was opened. Regardless the desired pressure of the reaction, during the catalytic reaction valve C4 was opened, valve C3 is closed, and the 6 port 2-position manual valve was placed in the “Load” position, in order to sample the effluent gas phase (non-condensed compounds) into the loops of the trapping selector, in regular intervals of *ca.* 1 h, with a loading time of 1-2 min per loop (pre-programed in the lab view software). After loading every loop, the 6 port 2-position manual valve was placed in the “Inject” position in order to inject the gas sample from the loops into the GC column for subsequent analysis. In turn, the liquid reaction products were condensed in the cold trap and, at the end of the reaction, were collected and manually injected into the same GC. After the reaction, 20 mL/min of nitrogen was passed through the installation during 30-60 min to carry some of the products retained inside the installation to the trap.

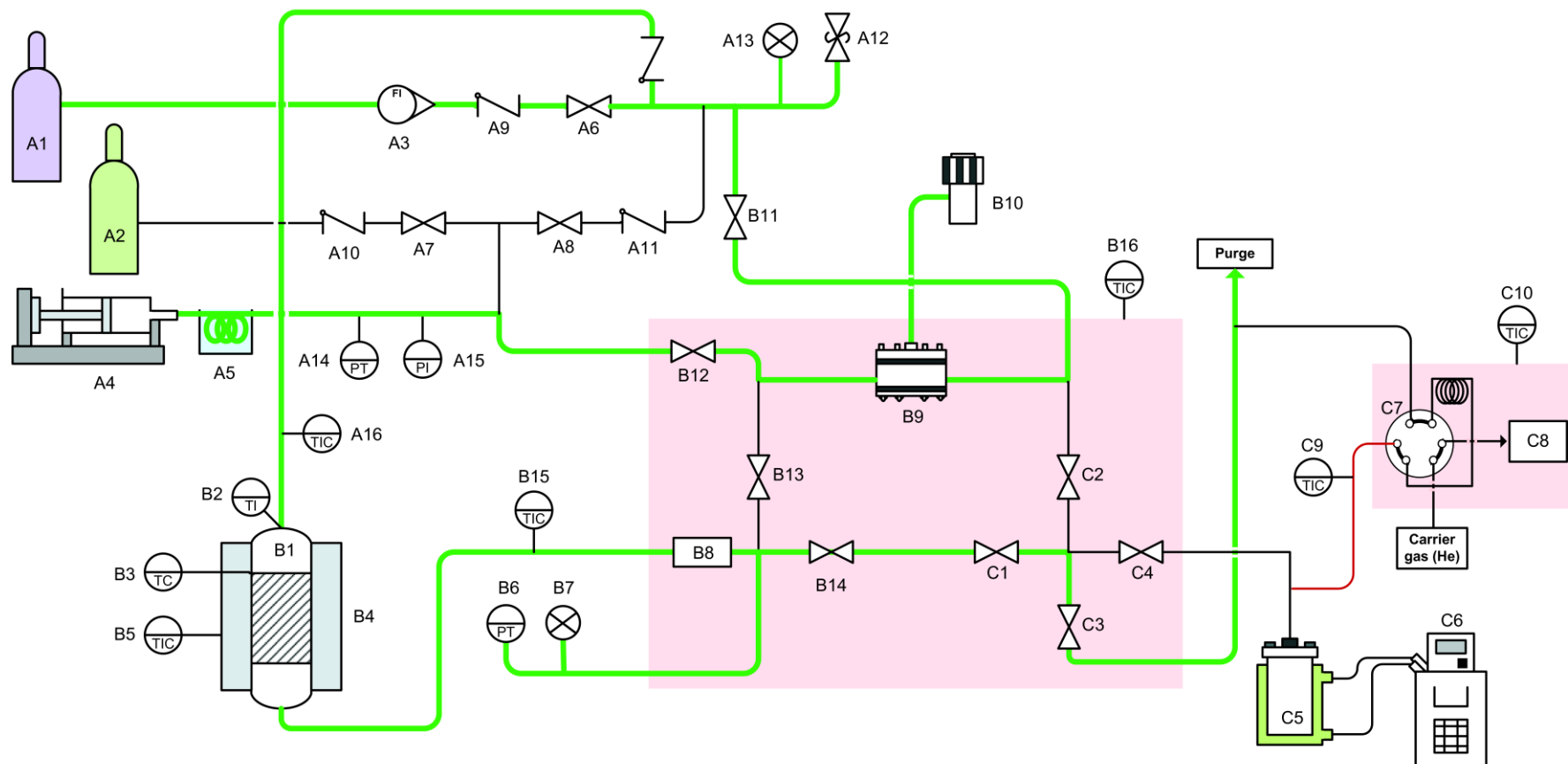


Figure S3.1. Fluid circuit (represented by the green lines) in Setup 1 for atmospheric-pressure operation.

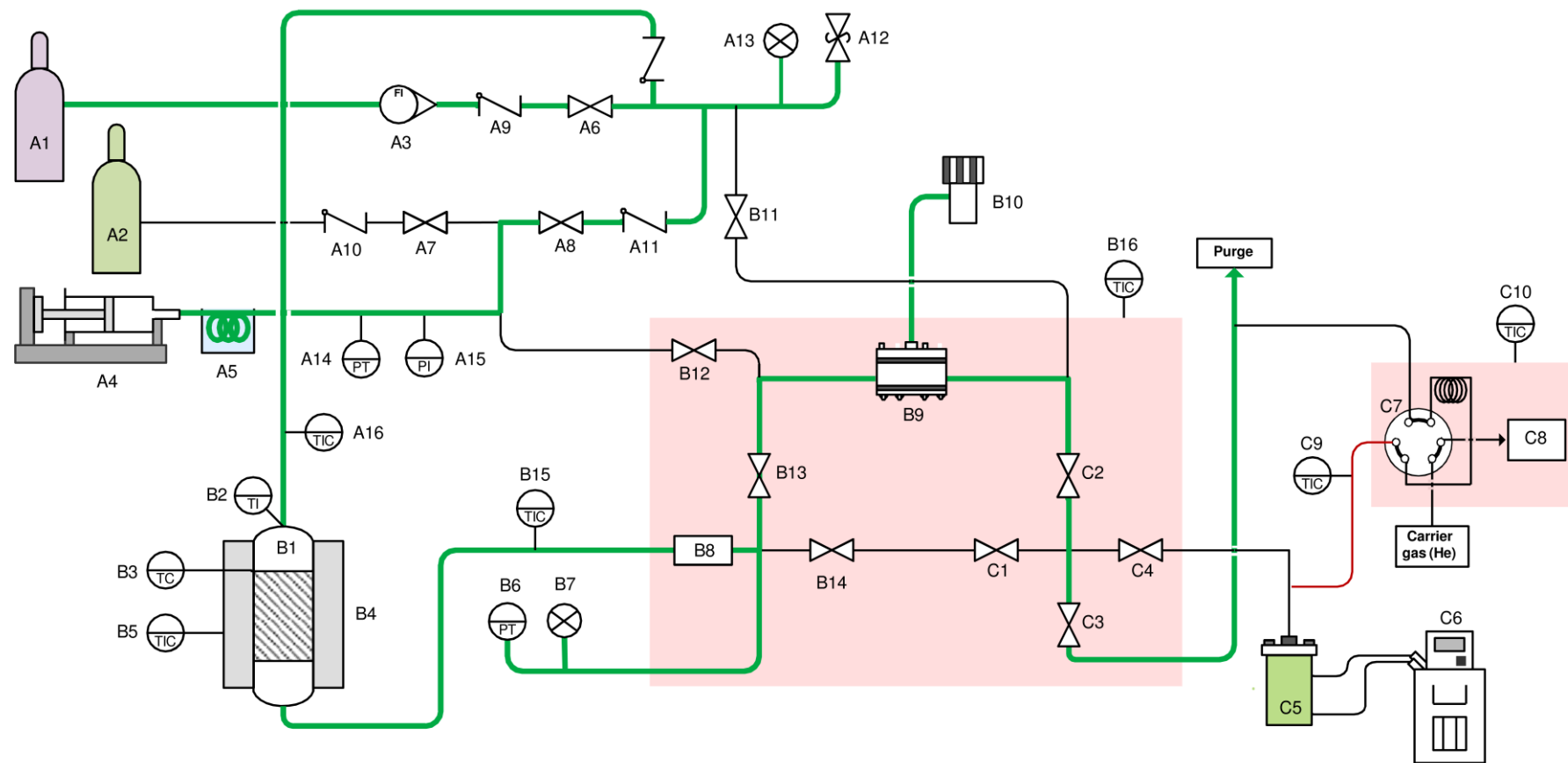


Figure S3.2. Fluid circuit (represented by the green lines) in Setup 1 for the high-pressure operation.

### Determination of nitrogen and 1-butene volumetric flow rates

For each catalytic assay it was necessary to determine the required volumetric flow rate of nitrogen and 1-butene, based on (i) the parameters of the reaction such as temperature, pressure, mass of catalyst, weight hourly space velocity (WHSV), and initial molar composition of 1-butene; and (ii) the ambient temperature and pressure. The flow rate values determined served as set-point for the equipment controlling the flow rate of these compounds, namely the mass flow controller (MFC) for nitrogen and the syringe pump for 1-butene. The volumetric flow rate of 1-butene ( $Q_v(1C4)$ ) was calculated based on the mass flow rate of 1-butene (which is the product of WHSV and mass of catalyst ( $m_{cat}$ )), and the density of 1-butene under the olefin feed conditions (ambient temperature and the desired reaction pressure), according to Eq. (S3.1).

$$Q_v(1C4) = \frac{WHSV \times m_{cat}}{\rho(1C4)_{feed}} \quad (S3.1)$$

The volumetric flow rate of nitrogen ( $Q_v(N_2)$ ) was calculated based on (i) the mass flow rate ( $Q_m(C_4)$ ) and molar composition ( $mol\%(C_4)$ ) of 1-butene, and (ii) the nitrogen density ( $\rho(N_2)_{cal}$ ) at the conditions of the calibration of the MFC (0 °C, atmospheric pressure), according to Eq. (S3.2). The volumetric flow rate of nitrogen ( $Q_v(N_2)_{MFC}$ ) to be the set-point of the MFC was then obtained from the MFC calibration curve (Figure S3.3), according to Eq. (S3.3), that relates the measured (real) nitrogen volumetric flow rate ( $Q_v(N_2)$ , measured using a bubble meter at ambient temperature and pressure) to the nitrogen volumetric flow rate of the MFC set-point. This calibration is especially required when working in the lower flow rate region of the MFC, due to the low accuracy of the equipment for small flow rates.

$$mol\%(C_4) = \frac{\frac{Q_m(C_4)}{M(C_4)}}{\frac{Q_m(C_4)}{M(C_4)} + \frac{Q_v(N_2) \cdot \rho(N_2)_{cal}}{M(N_2)}} \quad (S3.2)$$

$$Q_v(N_2)_{MFC} = 1.0268 \times Q_v(N_2) - 2,7563 \quad (S3.3)$$

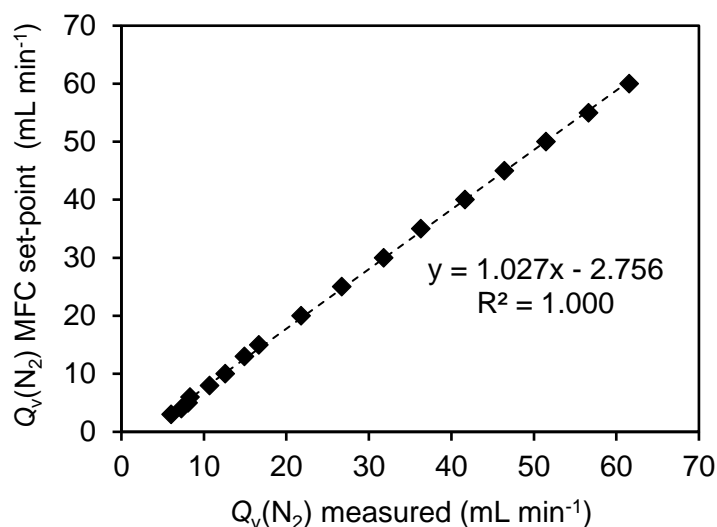


Figure S3.3. Mass flow controller (MFC) calibration curve.

The density of 1-butene and nitrogen were obtained using the Peng-Robinson equation of state (PREOS),<sup>[1]</sup> Eq. (S3.4) to Eq. (S3.8), which is a function of temperature, pressure, the critical properties and acentric factor of the fluid (Table S3.1).

$$\rho = \frac{M}{V_m} \quad (\text{S3.4})$$

$$P = \frac{RT}{V_m - b} - \frac{a \cdot \alpha}{V_m^2 - 2bV_m - b^2} \quad (\text{S3.5})$$

$$a = \frac{0.45724 R^2 T_c^2}{P_c} \quad (\text{S3.6})$$

$$b = \frac{0.0778 RT_c}{P_c} \quad (\text{S3.7})$$

$$\alpha = [1 + (0.37464 + 1.54226\omega - 0.26992\omega^2)(1 - T_r^{0.5})]^2 \quad (\text{S3.8})$$

where  $V_m$  is molar volume,  $P$  is pressure,  $T_c$  is critical temperature,  $T_r$  is the reduced temperature,  $P_c$  is critical pressure, and  $\omega$  is the acentric factor. Table A1 lists the critical values and the acentric factor for the fluids.

Table S3.1. Critical properties and acentric factor of 1-butene and nitrogen.

	$P_c$ (MPa)	$T_c$ (K)	$\omega$
1-Butene	4.02	419.5	0.184495
Nitrogen	3.4	126.2	0.0377215

Table S3.2. Yields of different products considered in the material balances, for the different materials (Chapter 5-8) tested in the 1-butene oligomerization at 200 °C, 30 bar and WHSV of 2.2 g<sub>1C4</sub> g<sub>cat</sub><sup>-1</sup> h<sup>-1</sup>.<sup>[a]</sup>

	Materials	Yield (wt%)					Total	
		1C4 unc. <sup>[b]</sup>	C4 isomers	C5 <sup>+</sup> gas	C6 <sup>+</sup> liquid	Washing <sup>[c]</sup>		coke <sup>[d]</sup>
Chapter 5	Al-TUD-1(25)-HT	10	51	16	13	0.3	0.05	91
	Al-TUD-1(50)-HT	9	48	15	13	4	0.06	88
	Al-TUD-1(PG)	11	64	12	4	0.5	0.04	91
	Al-LP(PG)	11	63	12	1	0.2	0.05	87
Chapter 6	BEA-nano	8	42	16	19	5	0.21	90
	BEA-micro	10	65	12	4	1	0.21	92
	BEA-hier	5	29	16	23	11	0.16	84
	BEA/TUD	9	59	13	7	2	0.13	91
	COD-9	10	68	9	1	2	0.14	91
Chapter 7	hZSM-5(31)-noT	7	35	14	26	5	0.13	88
	hZSM-5(20)-PZSi	3	13	16	36	13	0.27	79
	hZSM-5(51)-PZSi	6	31	13	23	10	0.25	83
	hZSM-5(47)-PZSiS	10	56	13	11	1	0.25	91
	hZSM-5(31)-CoT	11	59	7	2	0.1	0.17	80
	ZSM-5(29)	10	61	8	2	0.4	0.20	81
Chapter 8	MZS-0.2	8	43	13	17	2	n.m.	84
	MZS-0.2-Ox	5	22	15	35	9	n.m.	86
	MZS.0.2-Cl	5	28	14	27	10	n.m.	85
	MZS-0.4	7	39	13	19	3	n.m.	81
	MZS-0.4-Ox	5	24	16	36	6	n.m.	87
	MZS-0.4-Cl	2	8	16	39	15	0.14	81
	MZS-0.6	11	68	10	2	1	n.m.	92
	MZS-0.6-Ox	9	51	13	12	0	n.m.	85
	MZS-0.6-Cl	5	23	17	37	5	n.m.	87
	MZS-0.8	10	76	6	1	0	n.m.	93
	MZS-0.8-Cl	9	56	12	7	1	n.m.	85
	MZS-TPA-65	9	54	12	9	1	n.m.	86
	MZS-TPA-65-Cl	9	58	9	6	1	n.m.	83
	MZS-TPA-85	9	53	12	16	3	n.m.	93
	MZS-TPA-85-Cl	9	49	16	10	3	n.m.	86
	MZS-TPA/Na	11	71	7	2	0	n.m.	91
	MZS-TPA/Na-Cl	7	40	15	23	3	n.m.	88
	HZSM-5	8	47	12	17	1	n.m.	86

<sup>[a]</sup> n. m. stands for not measured. <sup>[b]</sup> Unconverted 1-butene. <sup>[c]</sup> Products recovered from the washing of the used catalyst. <sup>[d]</sup> Determined based on % of C (EA) per mass of hydrated solid (Eq. S3.9-3.10).

Table S3.3. Yields of different products considered in the material balances, for the hierZ-MFI (Chapter 9) tested in the 1-butene oligomerization at different reaction conditions.<sup>[a]</sup>

	Reaction conditions			Yield (wt%)						Total
	P (bar)	T (°C)	WHSV (h <sup>-1</sup> )	1C4 unc. <sup>[b]</sup>	C4 isomers	C5 <sup>+</sup> gas	C6 <sup>+</sup> liquid	Washing <sup>[c]</sup>	coke	
Chapter 9 (hierZ-MFI)	20	150	3.5	6	58	10	3	4	n.m.	82
	20	300	3.5	4	1	55	34	1	n.m.	94
	45	150	3.5	8	59	11	12	7	n.m.	96
	45	300	3.5	4	1	38	51	1	n.m.	95
	20	225	2	4	22	17	37	13	n.m.	94
	20	225	5	8	49	11	25	3	n.m.	96
	45	225	2	2	1	33	43	10	n.m.	88
	45	225	5	5	25	16	43	6	n.m.	95
	32.5	150	2	7	54	10	14	11	n.m.	96
	32.5	150	5	7	65	11	5	3	n.m.	91
	32.5	300	2	3	1	39	51	2	n.m.	95
	32.5	300	5	4	2	29	60	1	n.m.	95
	32.5	225	3.5	4	12	18	56	5	n.m.	95
	32.5	225	3.5	4	10	18	58	5	n.m.	95
	32.5	225	3.5	3	7	23	55	6	n.m.	94
	45	255	2	3	1	38	51	2	n.m.	94

<sup>[a]</sup> n. m. stands for not measured. <sup>[b]</sup> Unconverted 1-butene. <sup>[c]</sup> Products recovered from the washing of the used catalyst.

## Supplementary Material - Chapter 4

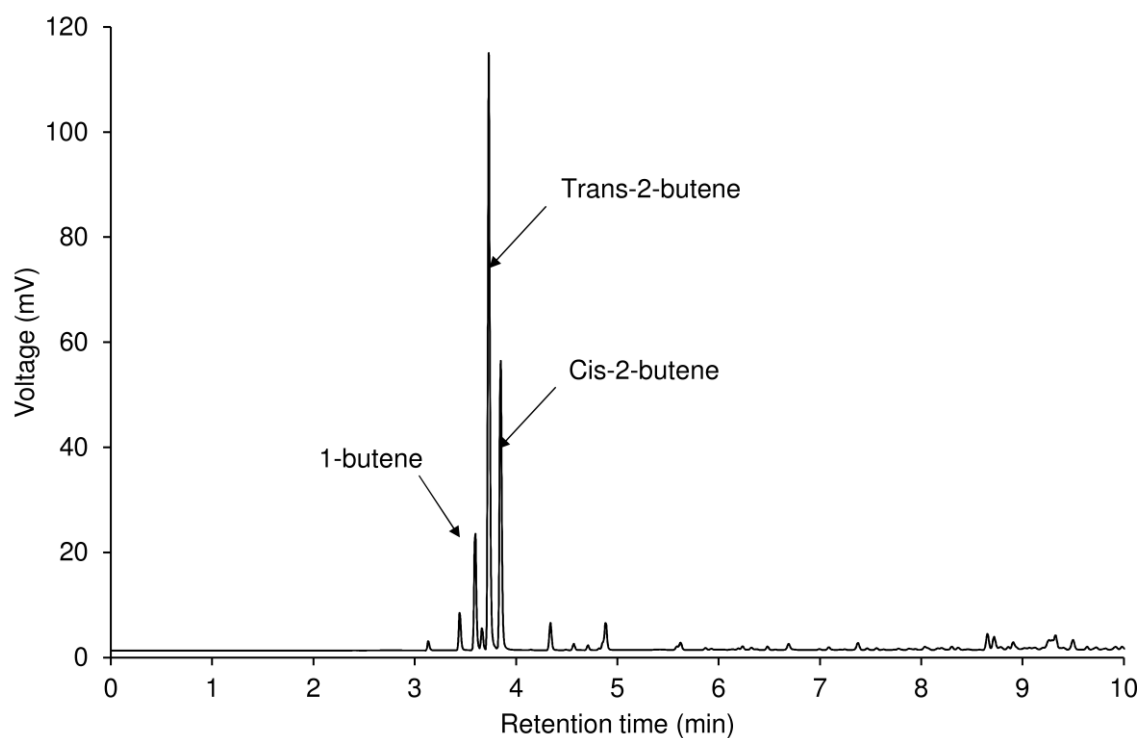


Figure S4.1. Chromatogram of the gas phase reaction products of the 1-butene oligomerization over BEA-hier (Chapter 6) at 200 °C, 30 bar and  $2.2 \text{ g}_{\text{C}_4} \text{ g}_{\text{cat}}^{-1} \text{ h}^{-1}$ , obtained using Master Fast GC-FID with the analysis method described in Chapter 3.

Table S4.1. Butene isomers distributions for the different materials tested in the 1-butene oligomerization at 200 °C, 30 bar and WHSV of 2.2 g<sub>1C4</sub> g<sub>cat</sub><sup>-1</sup> h<sup>-1</sup>.

	Materials	Distributions (%)			C4 isomers/1C4	<i>trans/cis</i>
		1C4	<i>trans</i> -C4	<i>cis</i> -C4		
Chapter 5	Al-TUD-1(25)-HT	17	51	32	4.9	1.59
	Al-TUD-1(50)-HT	16	52	32	5.1	1.61
	Al-TUD-1(PG)	15	52	33	5.7	1.60
	Al-LP(PG)	15	52	33	5.7	1.60
Chapter 6	BEA-nano	15	53	32	5.8	1.68
	BEA-micro	12	55	33	7.4	1.69
	BEA-hier	15	54	31	5.7	1.70
	BEA/TUD	14	53	32	5.9	1.67
	COD-9	13	55	32	6.9	1.72
Chapter 7	hZSM-5(31)-noT	17	51	32	5.0	1.60
	hZSM-5(20)-PZSi	22	49	29	3.6	1.66
	hZSM-5(51)-PZSi	17	52	31	5.0	1.65
	hZSM-5(47)-PZSiS	15	53	32	5.7	1.64
	hZSM-5(31)-CoT	16	52	32	5.4	1.61
	ZSM-5(29)	14	53	32	6.1	1.64
Chapter 8	MZS-0.2	16	52	32	5.3	1.60
	MZS-0.2-Ox	18	51	31	4.6	1.64
	MZS.0.2-Cl	17	52	32	5.0	1.63
	MZS-0.4	16	52	32	5.3	1.65
	MZS-0.4-Ox	18	51	31	4.6	1.65
	MZS-0.4-Cl	27	46	28	2.8	1.67
	MZS-0.6	14	53	32	6.0	1.65
	MZS-0.6-Ox	14	54	32	6.0	1.68
	MZS-0.6-Cl	18	51	31	4.5	1.67
	MZS-0.8	14	53	32	6.0	1.65
	MZS-0.8-Cl	14	54	32	6.1	1.69
	MZS-TPA-65	15	53	32	5.7	1.64
	MZS-TPA-65-Cl	14	54	32	6.2	1.66
	MZS-TPA-85	15	53	32	5.8	1.64
	MZS-TPA-85-Cl	15	52	33	5.5	1.59
	MZS-TPA/Na	14	53	32	6.1	1.66
	MZS-TPA/Na-Cl	15	53	32	5.5	1.66
	HZSM-5	15	52	32	5.5	1.62

Table S4.2. Butene isomers distributions for the different materials tested in different operating conditions.

		P (bar)	T (°C)	WHSV (h <sup>-1</sup> )	1C4	<i>trans</i> - C4	<i>cis</i> - C4	C4 isomers/ 1C4	<i>trans/cis</i>
Thermodynamics			150		10	55	34	8.6	1.6
		30	200	--	13	52	35	6.4	1.5
			250		16	49	35	5.1	1.4
		20	150		10	55	34	8.6	1.6
	40			10	55	35	8.9	1.6	
Chapter 5	Al-TUD- 1(25)-HT		150		11	57	32	8.1	1.8
		30	200	2.2	17	51	32	4.9	1.6
			250		23	47	30	3.4	1.5
		20	200	2.2	15	52	32	5.5	1.6
	40			15	53	32	5.6	1.7	
	30	200	1.3	17	52	31	4.9	1.6	
			3.1	15	53	32	5.7	1.7	
Chapter 6	BEA-hier		150		9	60	30	9.6	2.0
		30	200	2.2	14	55	31	6.1	1.8
			250		25	45	30	3.0	1.5
		20	200	2.2	14	55	31	6.3	1.8
	40			17	53	30	5.0	1.8	
Chapter 7	hZSM- 5(20)-PZSi	30	200		21	49	30	3.7	1.7
			250	2.2	29	45	26	2.4	1.7
		40	250		65	21	13	0.5	1.6
Chapter 9	hierZ-MFI	20		3.5	10	59	31	9.1	1.9
		45	150	3.5	11	58	31	8.2	1.8
		32.5		2	11	58	31	8.0	1.8
		32.5		5	10	59	31	9.2	1.9
		20		3.5	81	12	7	0.2	1.6
		20	300	3.5	77	14	9	0.3	1.5
		45		2	80	13	7	0.2	1.7
		45		5	68	19	13	0.5	1.4
		20		2	17	52	31	5.0	1.7
		20	225	5	14	54	32	6.0	1.7
		45		2	65	22	14	0.5	1.6
		45		5	17	52	31	4.8	1.6
		32.5		3.5	35	40	25	1.9	1.6
		32.5		3.5	26	45	29	2.8	1.6
32.5	3.5	29		44	28	2.5	1.6		

## Supplementary Material - Chapter 6

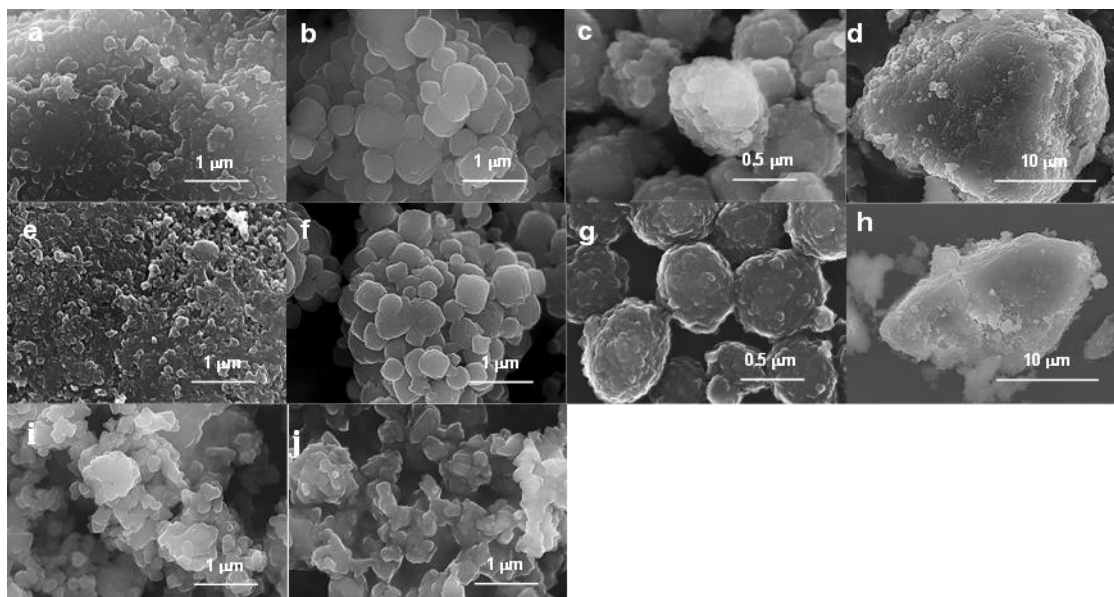


Figure S6.1. SEM images for the spent catalysts BEA-nano (a, e), BEA-micro (b, f), BEA-hier (c, g), BEA/TUD (d, h), and ZSM-5 (i, j). Reaction conditions: catalyst activation temperature=200 °C (a, b, c, d, i) or 450 °C (e, f, g, h, j), catalytic reaction temperature=200 °C, 30 bar, WHSV=2.2 g<sub>1C4</sub> g<sub>cat</sub><sup>-1</sup> h<sup>-1</sup>, TOS=8 h.

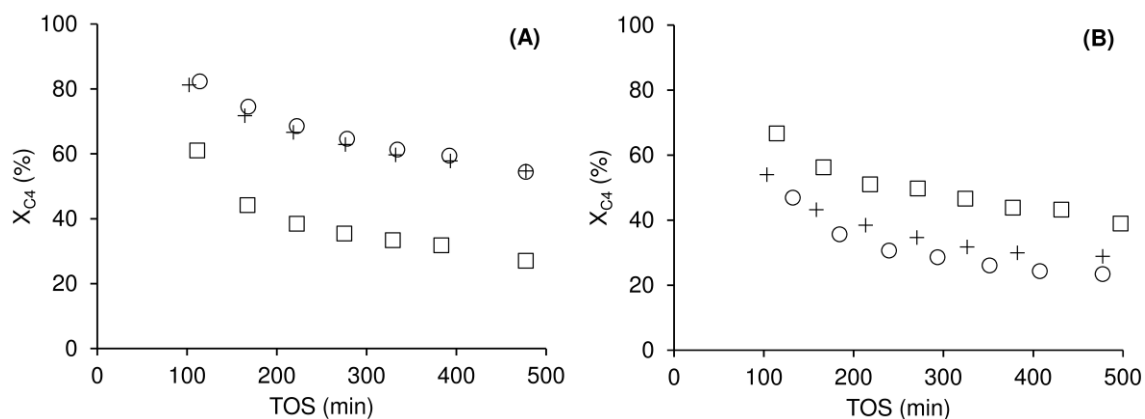


Figure S6.2. Dependence of conversion ( $X_{C_4}$ ) on TOS for (A) BEA-hier and (B) ZSM-5, at different catalyst activation temperatures: 200 °C (o), 325 °C (+) and 450 °C (□). Reaction conditions: 200 °C, 30 bar, WHSV=2.2 g<sub>1C4</sub> g<sub>cat</sub><sup>-1</sup> h<sup>-1</sup>, TOS=8 h.

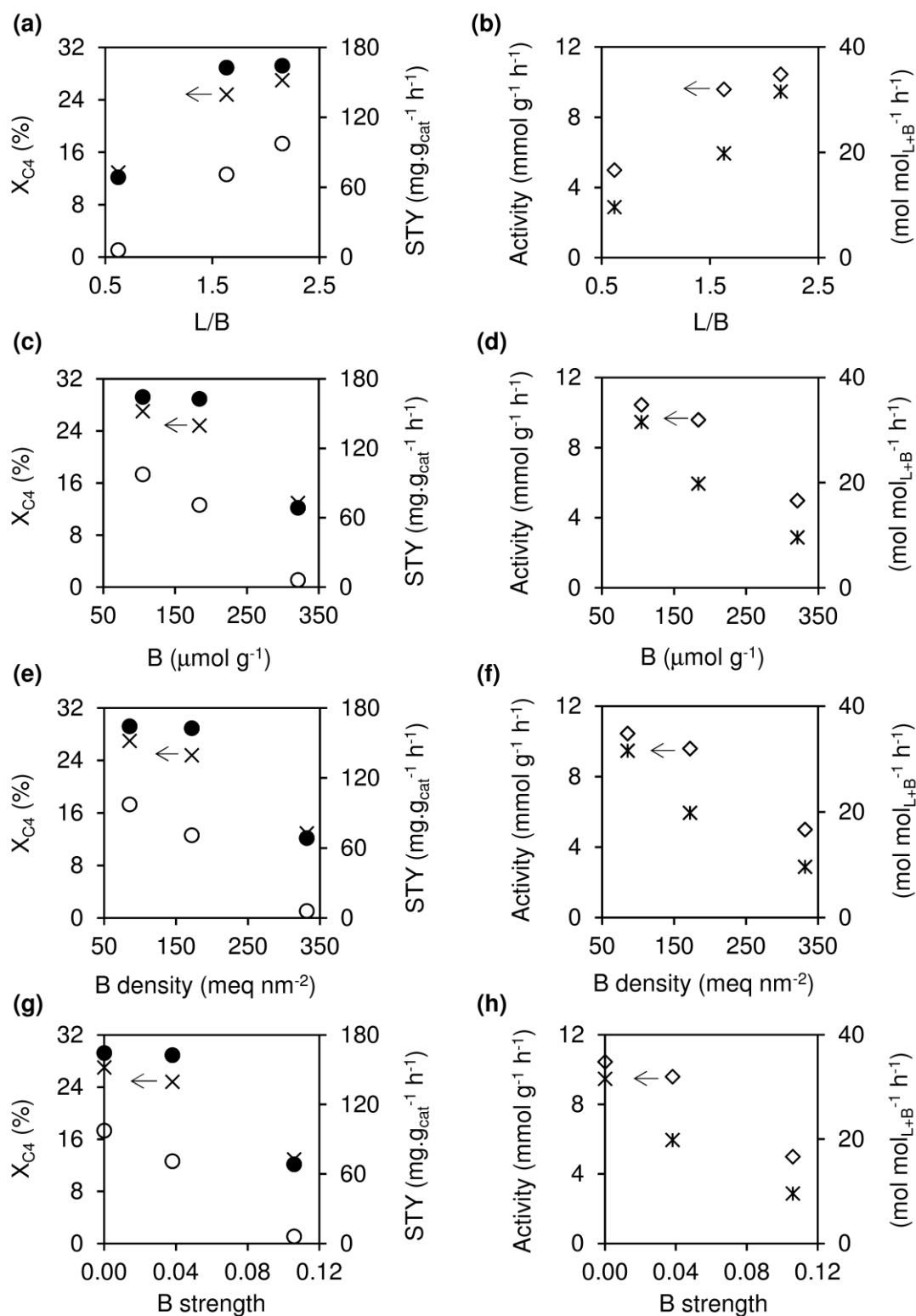


Figure S6.3. Influence of the acid properties measured at 200 °C on ((a), (c), (e), (g)) conversion (x),  $\text{STY}_{\text{Dcut}}$  (•) and  $\text{STY}_{\text{Ncut}}$  (o), and on ((b), (d), (f), (h)) catalytic activity expressed as  $\text{mmol.g}^{-1} \text{h}^{-1}$  (◊) or  $\text{mol.mol}_{L+B}^{-1} \text{h}^{-1}$  (\*), for the bulk Beta based catalysts (BEA-hier, BEA-nano, BEA-micro) activated at 450 °C prior to catalytic reaction. Reaction conditions: 200 °C, 30 bar,  $\text{WHSV}=2.2 \text{ g}_{\text{IC4}} \text{ g}_{\text{cat}}^{-1} \text{h}^{-1}$ , TOS=8 h.

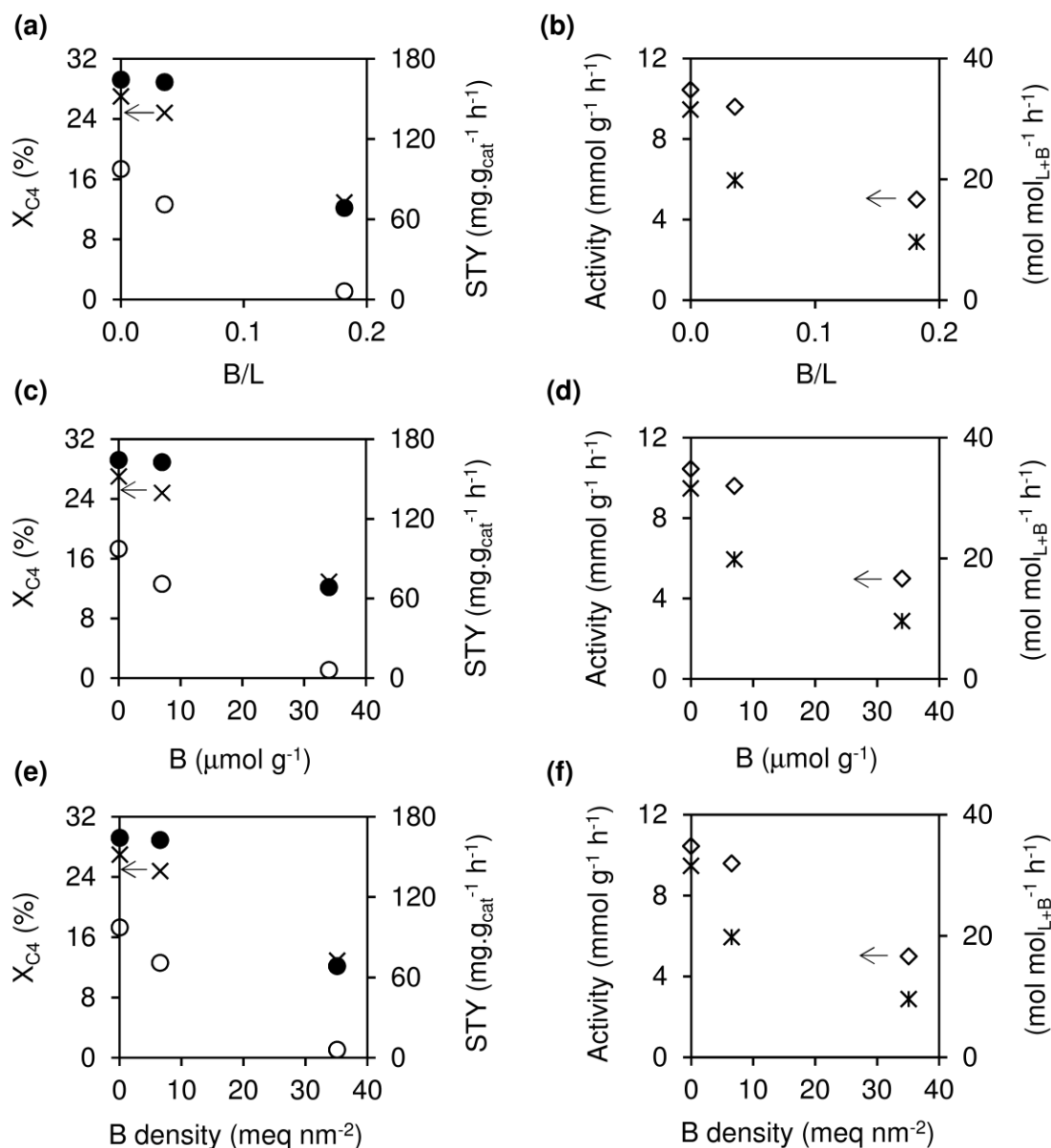


Figure S6.4. Influence of the acid properties measured at 450 °C on ((a), (c), (e)) conversion ( $\times$ ), STY<sub>Decut</sub> ( $\bullet$ ) and STY<sub>Ncut</sub> ( $\circ$ ), and on ((b), (d), (f)) catalytic activity expressed as  $\text{mmol} \text{g}^{-1} \text{h}^{-1}$  ( $\diamond$ ) or  $\text{mol} \text{mol}_{L+B}^{-1} \text{h}^{-1}$  ( $*$ ), for the bulk Beta type catalysts (BEA-hier, BEA-nano, BEA-micro) activated at 450 °C prior to catalytic reaction. Reaction conditions: 200 °C, 30 bar, WHSV=2.2  $\text{g}_{\text{IC4}} \text{g}_{\text{cat}}^{-1} \text{h}^{-1}$ , TOS=8 h. Note: the ratio B/L is given instead of L/B to avoid indetermination when B is zero.

Table S6.1. Acid properties measured at 200 °C or 450 °C on X<sub>C4</sub>, STY, and catalytic activity for the bulk Beta based catalysts (BEA-hier, BEA-nano, BEA-micro) activated at 200 °C prior to catalytic reaction. Reaction conditions: 200 °C, 30 bar, WHSV=2.2 g<sub>1C4</sub> g<sub>cat</sub><sup>-1</sup> h<sup>-1</sup>, TOS=8 h.

Sample	Acid properties measured at 200 °C				Catalytic performance (T <sub>act</sub> =450 °C)				
	B/L	B (μmol g <sup>-1</sup> )	B density (meq nm <sup>-2</sup> )	B strength (B <sub>450</sub> /B <sub>200</sub> )	X <sub>C4</sub> (%)	STY (mg g <sub>cat</sub> <sup>-1</sup> h <sup>-1</sup> )		Activity	
						Ncut	Dcut	mmol g h	mmol mol <sub>L+B</sub> h
BEA-hier	0.46	105	85	0	27	97	164	10	32
BEA-nano	0.61	184	172	0	25	71	163	10	20
BEA-micro	1.61	321	332	0.43	13	6	68	5	10
Sample	Acid properties measured at 450 °C				Catalytic performance (T <sub>act</sub> =450 °C)				
	B/L	B (μmol g <sup>-1</sup> )	B density (meq nm <sup>-2</sup> )	B strength (B <sub>450</sub> /B <sub>200</sub> )	X <sub>C4</sub> (%)	STY (mg g <sub>cat</sub> <sup>-1</sup> h <sup>-1</sup> )		Activity	
						Ncut	Dcut	mmol g h	mmol mol <sub>L+B</sub> h
BEA-hier	0	0	0	-	27	97	164	10	32
BEA-nano	0.04	7	7	-	25	71	163	10	20
BEA-micro	0.18	34	35	-	13	6	68	5	10

**Supplementary Material - Chapter 7**

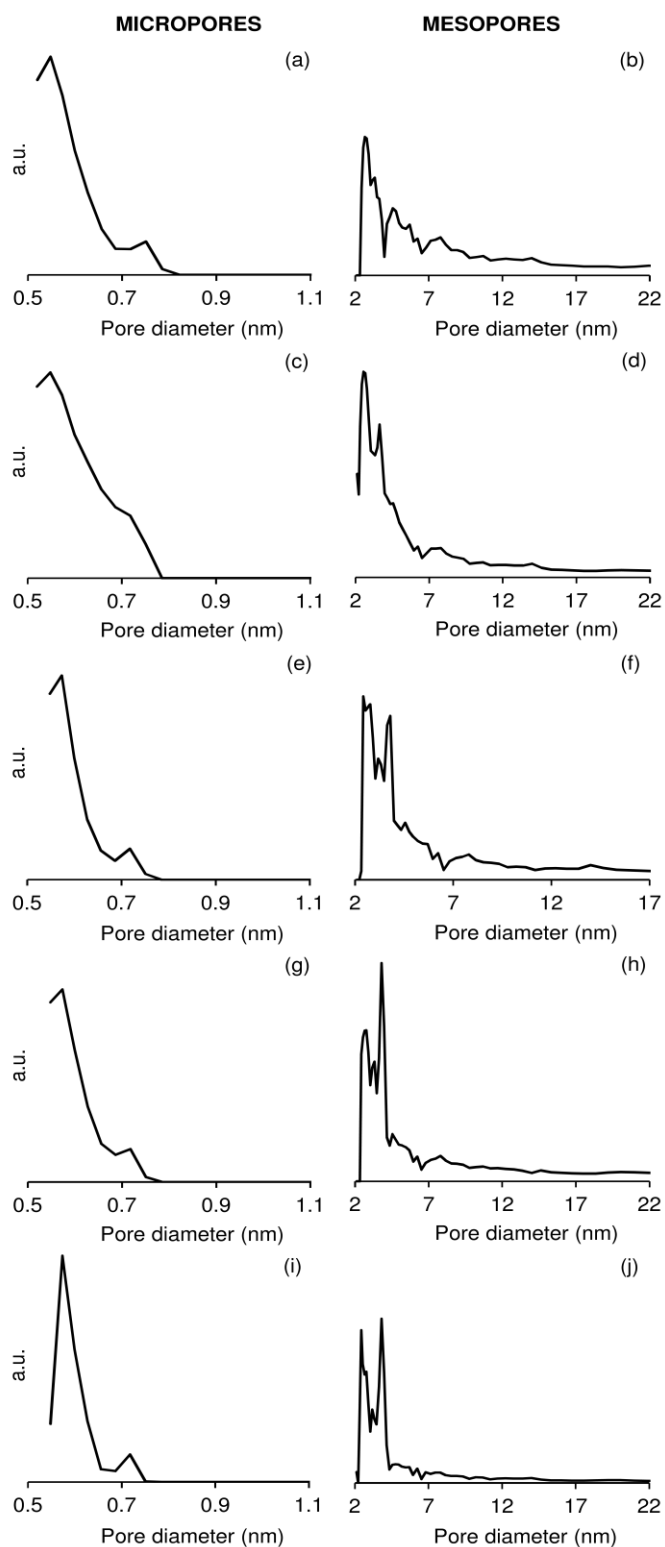


Figure S7.1. Pore size distribution curves (DFT method) for hZSM-5(31)-noT (a, b), hZSM-5(20)-PZSi (c, d), hZSM-5(51)-PZSi (e, f), hZSM-5(47)-PZSiS (g, h), and hZSM-5(31)-CoT (i, j).

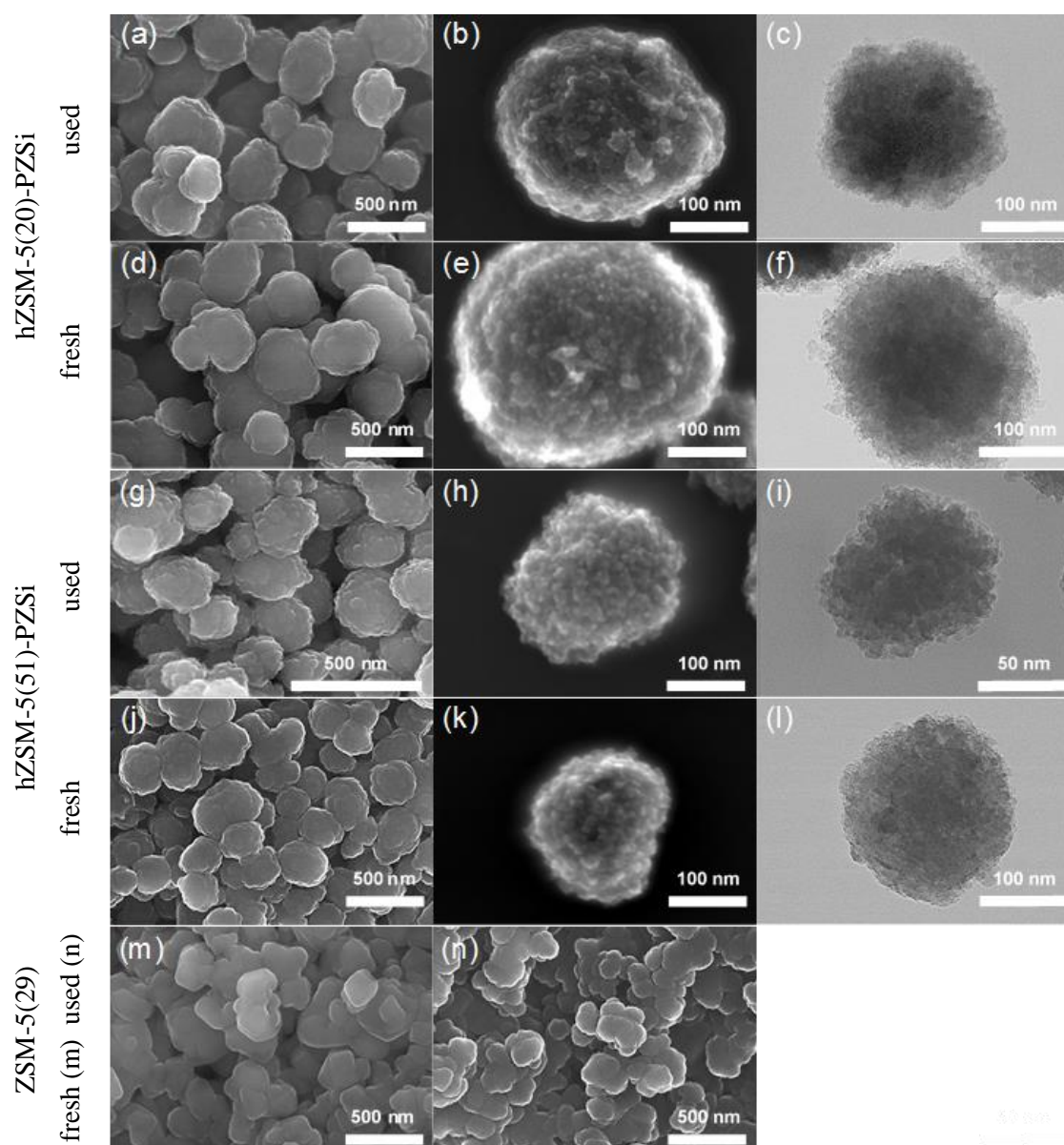


Figure S7.2. SEM and TEM images for the unused (a, b, c, g, h, i, m) and used (d, e, f, j, k, l, n) catalysts hZSM-5(20)-PZSi (a to f), hZSM-5(51)-PZSi (g to l), and ZSM-5(29) (m, n). Reaction conditions: 200 °C, 30 bar, WHSV=2.2 g<sub>1C4</sub> g<sub>cat</sub><sup>-1</sup> h<sup>-1</sup>, TOS=7 h, catalyst activation temperature=450 °C.

## Supplementary Material - Chapter 8

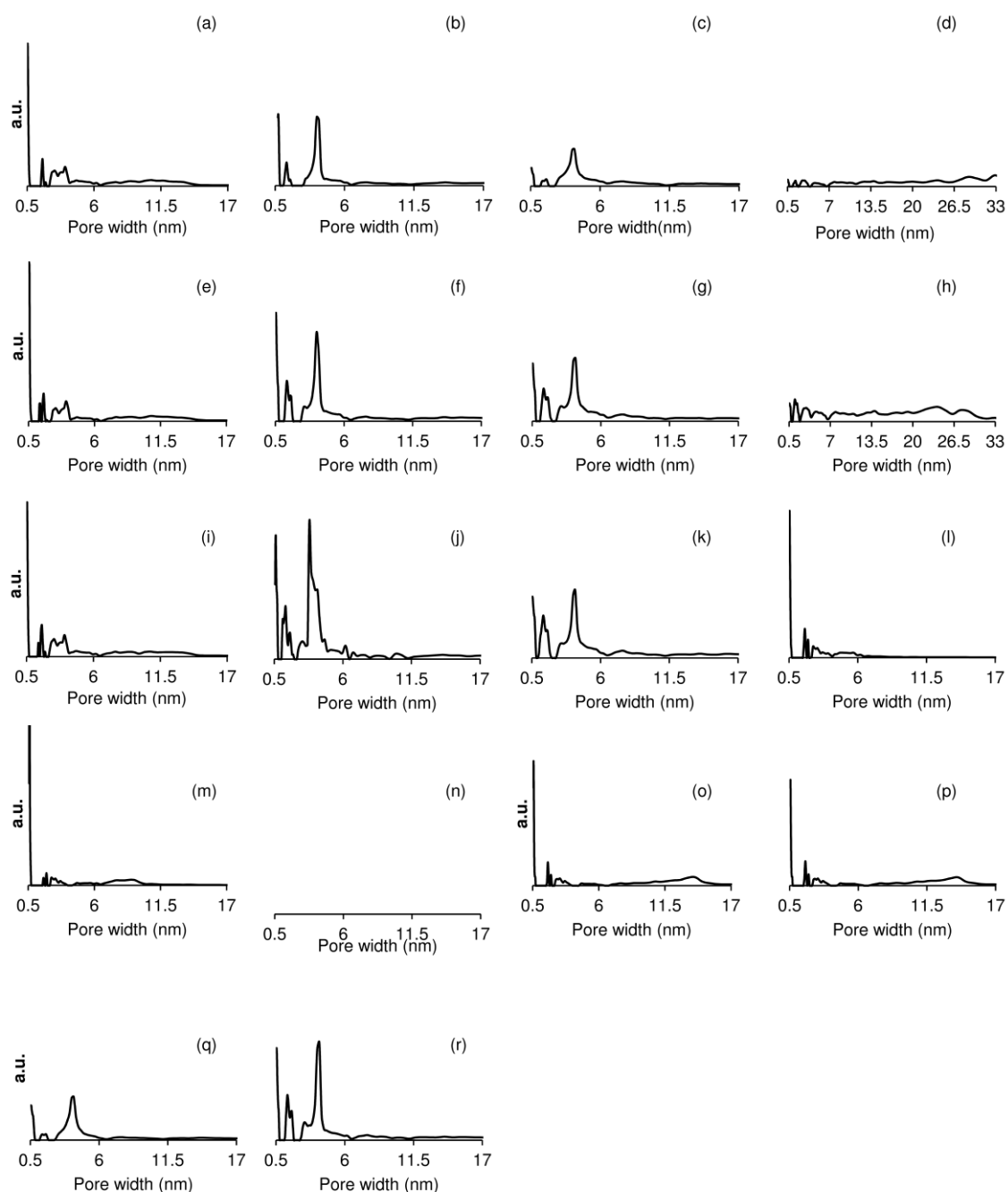


Figure S8.1. Pore size distribution curves (DFT method) for MZS-0.2 (a), MZS-0.4 (b), MZS-0.6 (c), MZS-0.8 (d), MZS-0.2-Cl (e), MZS-0.4-Cl (f), MZS-0.6-Cl (g), MZS-0.8-Cl (h), MZS-0.2-Ox (i), MZS-0.4-Ox (j), MZS-0.6-Ox (k), HZSM-5 (l), MZS-TPA-65 (m), MZS-TPA-65-Cl (n), MZS-TPA-85 (o), MZS-TPA-85-Cl (p), MZS-TPA/Na (q) and MZS-TPA/Na-Cl (r).

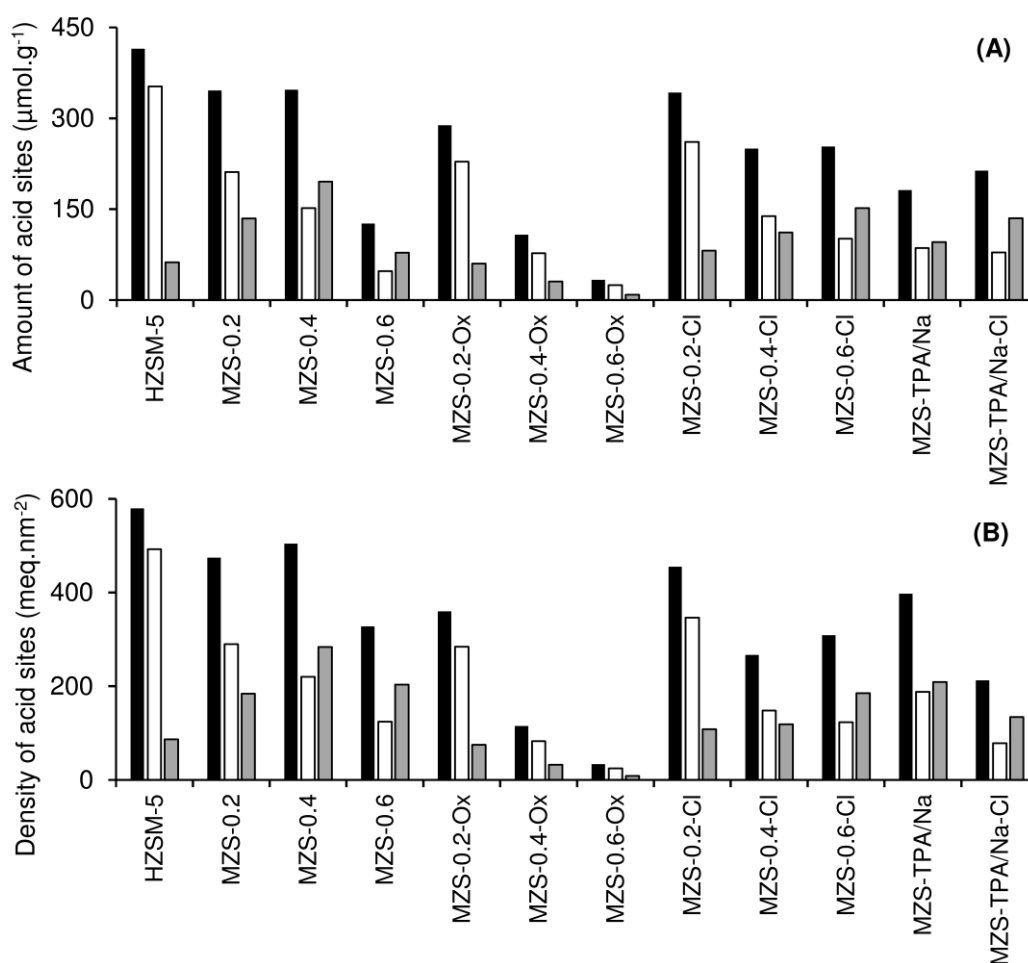


Figure S8.2. (A) Amount and (B) density of total (Brønsted plus Lewis) acid sites (black), and amounts of Brønsted (white) or Lewis (grey) acid sites for each catalyst.

Table S8.1. Data matrix used in the construction of the PCA biplot of Figure S8.4.

Material	IHF	Al <sub>penta</sub> /Al <sub>tetra</sub>	%Al <sub>tetra+penta</sub>
<b>M-0.2</b>	0.41	0.02	89
<b>M-0.2-Ox</b>	0.49	0	87
<b>M-0.2-Cl</b>	0.39	0	83
<b>M-0.4</b>	0.23	0.37	88
<b>M-0.4-Ox</b>	0.65	0	80
<b>M-0.4-Cl</b>	0.65	0	71
<b>M-0.6</b>	0.09	0.8	59
<b>M-0.6-Ox</b>	0.76	0.33	74
<b>M-0.6-Cl</b>	0.54	0.23	74
<b>TPA/Na</b>	0.15	0.73	56
<b>TPA/Na-Cl</b>	0.80	0.32	74
<b>ZSM-5</b>	0.18	0	75

Table S8.2. Data matrix used in the construction of the PCA biplot of Figure 8.15.

<b>Material</b>	<b>X<sub>C4</sub></b> %	<b>STY</b> mg g <sub>cat</sub> <sup>-1</sup> h <sup>-1</sup>	<b>STY<sub>Deut</sub></b> mg g <sub>cat</sub> <sup>-1</sup> h <sup>-1</sup>	<b>Deut/Ncut</b>
<b>M-0.2</b>	44	372	259	2.3
<b>M-0.2-Ox</b>	67	769	502	1.9
<b>M-0.2-Cl</b>	58	587	409	2.3
<b>M-0.4-Ox</b>	65	781	445	1.3
<b>M-0.4-Cl</b>	86	852	584	2.2
<b>M-0.6-Ox</b>	36	262	134	1.1
<b>M-0.6-Cl</b>	66	808	448	1.2
<b>TPA/Na-Cl</b>	46	490	271	1.2
<b>ZSM-5</b>	39	377	222	1.4

Table S8.3. Cetane number, paraffin index and content of aromatic compounds for the best catalysts.

Catalyst	CN	I	%H <sub>ar</sub>
HZSM-5	46	0.53	0.00
MZS-0.2	46	0.52	0.00
MZS-0.2-Ox	45	0.54	0.02
MZS-0.2-Cl	45	0.53	0.04
MZS-0.4	42	0.59	0.34
MZS-0.4-Ox	44	0.55	0.06
MZS-0.4-Cl	44	0.56	0.17
MZS-0.6-Ox	46	0.52	0.06
MZS-0.6-Cl	43	0.57	0.05
MZS-0.8-Cl	41	0.60	0.12
MZS-TPA/Na-Cl	43	0.57	0.07

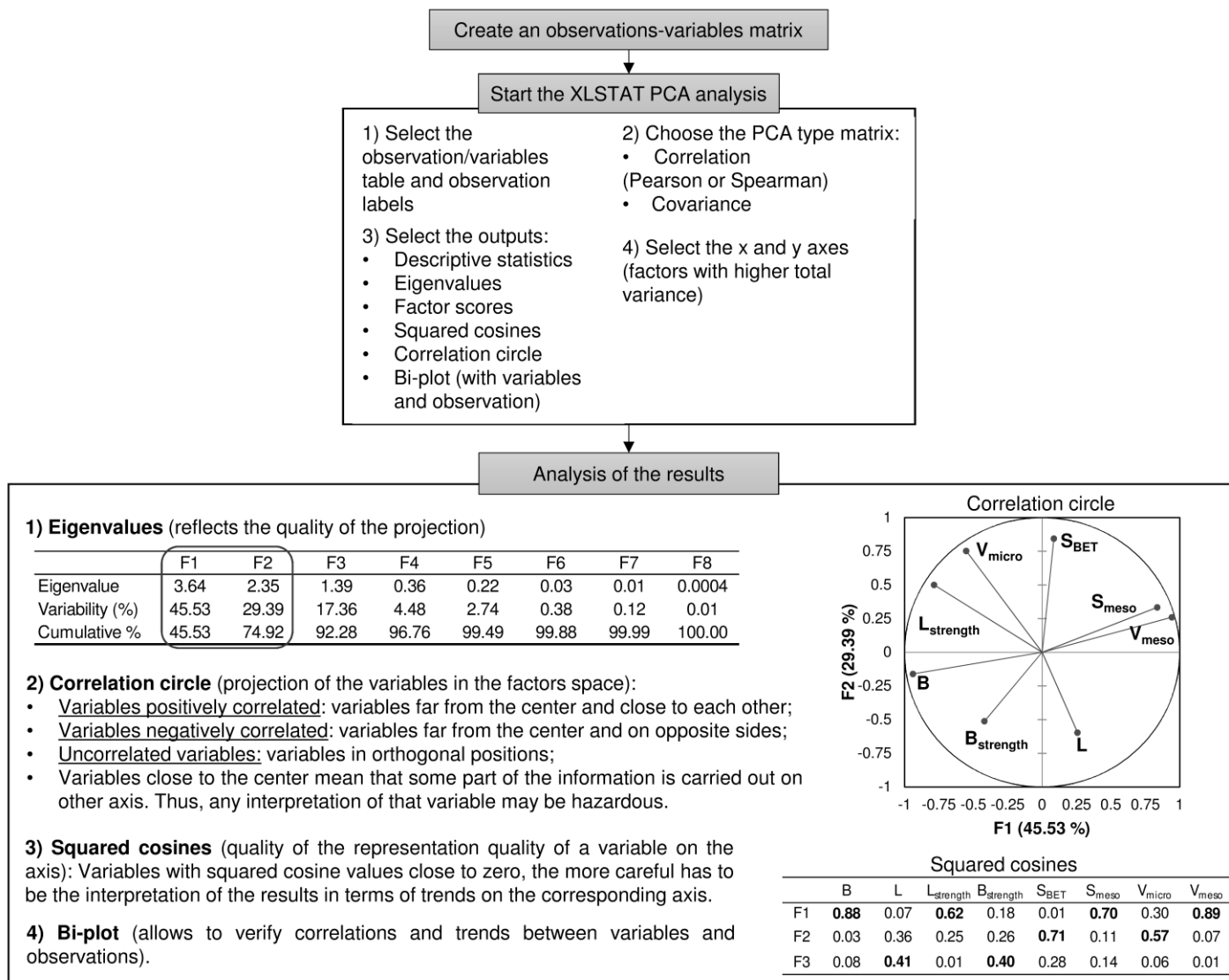


Figure S8.3. Scheme of the PCA analysis of the data matrix of Table 8.4.

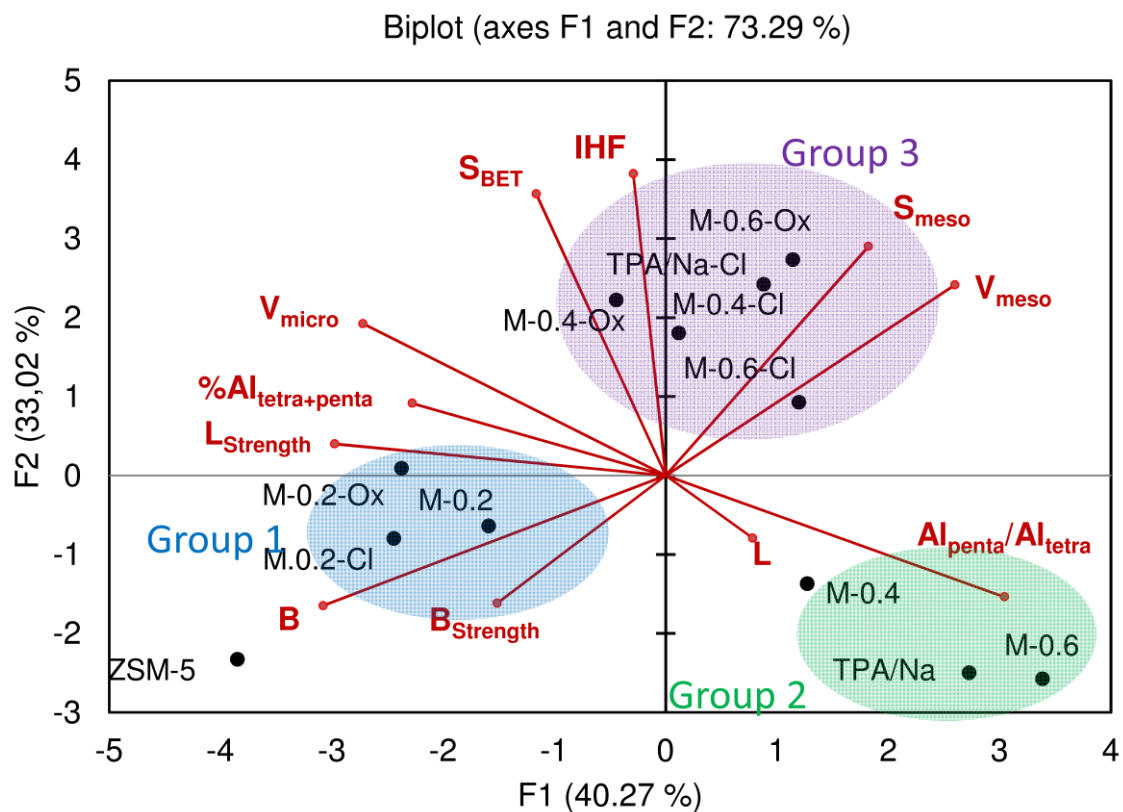


Figure S8.4. Two-dimensional principal component analysis biplot (PC1: 40.27 % and PC2: 33.02 %) categorizing the materials according to their properties. The set of material properties was enlarged (in relation to Figure 8.10 (Chapter 8)), and includes  $\%Al_{tetra+penta}$ , ratio  $Al_{penta}/Al_{tetra}$  and  $IHF$  (Table S8.1). The variables are represented in red color and the observations are signaled in black color. The colored highlights of the sample names indicate the groups of materials according to the PCA biplot presented in Figure 8.10: Group 1 (blue), Group 2 (green), Group 3 (purple).

## Supplementary Material - Chapter 9

Table S9.1. Aromatic and diaromatic contents determined by GC×GC-ToFMS, and aromatic content, isoparafinic index and cetane number determined by <sup>1</sup>H NMR, for the different assays.

Run	Operating conditions			GC×GC-ToFMS		<sup>1</sup> H NMR		
	<i>T</i> (°C)	<i>P</i> (bar)	<i>W</i> (h <sup>-1</sup> )	%Ar	%DiAr	%Ar	<i>I</i>	<i>CN</i>
1	20	150	3.5	0.06	0.00	0.00	0.61	41
2	20	300	3.5	21.61	1.41	4.71	0.52	46
3	45	150	3.5	0.00	0.00	0.02	0.70	37
4	45	300	3.5	17.58	3.48	3.62	0.48	49
5	20	225	2.0	0.97	1.10	0.41	0.60	41
6	20	225	5.0	0.03	0.00	0.07	0.55	44
7	45	225	2.0	1.73	0.00	0.58	0.55	44
8	45	225	5.0	0.13	0.00	0.07	0.59	42
9	32.5	150	2.0	0.00	0.00	0.05	0.56	44
10	32.5	150	5.0	0.00	0.00	0.00	0.62	40
11	32.5	300	2.0	12.00	2.25	3.28	0.59	42
12	32.5	300	5.0	3.16	0.40	1.28	0.50	47
13	32.5	225	3.5	0.41	0.00	0.17	0.53	46
14	32.5	225	3.5	0.67	0.00	0.26	0.50	47
15	32.5	225	3.5	0.64	0.00	0.25	0.54	45

Table S9.2. Aromatic products formed in the catalytic reactions of 1-butene, at 225 °C, 32.5 bar, and 3.5 g g<sub>cat</sub><sup>-1</sup> h<sup>-1</sup> (sample 1), or 300 °C, 45 bar, and 3.5 g g<sub>cat</sub><sup>-1</sup> h<sup>-1</sup> (sample 2).<sup>[a]</sup>

Chemical structure <sup>[b]</sup>	Name	Sim. <sup>[c]</sup>	RI <sup>[d]</sup>		Ref.
			Exp.	Rpt.	
	benzene	733	631	641	[2]
C1-subst 	toluene	980	728	748	[3]
C2-subst 	ethylbenzene	926	843	842	[2]
	o-xylene	966	875	872	[3]
	m-xylene*	979	852	850	[2]

Table S9.2. (continued)

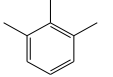
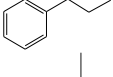
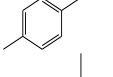
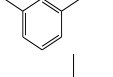
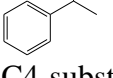
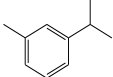
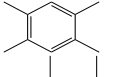
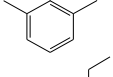
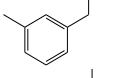
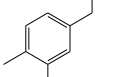
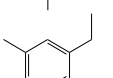
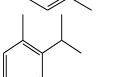
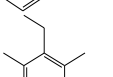
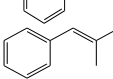
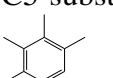
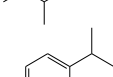
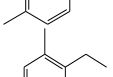
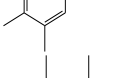
Chemical structure <sup>[b]</sup>	Name	Sim. <sup>[c]</sup>	RI <sup>[d]</sup>		Ref.
			Exp.	Rpt.	
<b>C3-subst</b>					
	1,2,3-trimethylbenzene	976	1000	1007	[4]
	propylbenzene	968	937	935	[2]
	1-ethyl-4-methylbenzene*	975	944	945	[2]
	1-ethyl-3-methylbenzene	957	942	943	[2]
	(1-methylethyl)benzene	947	908	907	[2]
<b>C4-subst</b>					
	1-methyl-3-(1-methylethyl)benzene	978	1006	1005	[2]
	1,2,4,5-tetramethylbenzene*	969	1103	1098	[2]
	1-ethyl-2,3-dimethylbenzene	962	1041	1086	[2]
	1-methyl-3-propylbenzene*	897	1033	1035	[2]
	4-ethyl-1,2-dimethylbenzene	970	1068	1067	[2]
	2-ethyl-1,4-dimethylbenzene*	968	1064	1060	[2]
	o-cymene*	905	1006	1020	[2]
	2-ethyl-1,3-dimethylbenzene*	961	1073	1074	[5]
	(2-methyl-1-propenyl)benzene	875	1058	1067	[6]
<b>C5-subst</b>					
	pentamethylbenzene*	960	1260	1261	[7]
	1-methyl-4-(1-methylpropyl)benzene*	882	1121	1100	[8]
	1-ethyl-2,4,5-trimethylbenzene	908	1118	1173	[9]
	2,4-dimethyl-1-(1-methylethyl)benzene	942	1101	1123	[10]

Table S9.2. (continued)

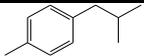
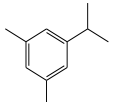
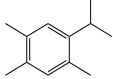
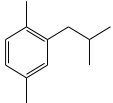
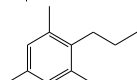
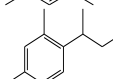
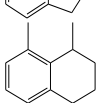
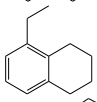
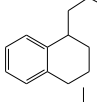
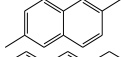
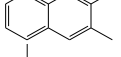
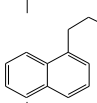
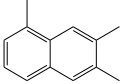
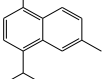
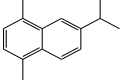
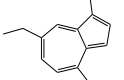
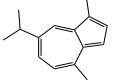
Chemical structure <sup>[b]</sup>	Name	Sim. <sup>[c]</sup>	RI <sup>[d]</sup>		Ref.
			Exp.	Rpt.	
	1-methyl-4-(2-methylpropyl)benzene	918	1086	1089	[11]
	1,3-dimethyl-5-(1-methylethyl)benzene	933	1116	1113	[12]
<b>C6-subst</b>					
	1,2,4-trimethyl-5-(1-methylethyl)benzene*	869	1247	1234	[13]
	1,4-dimethyl-2-(2-methylpropyl)benzene*	945	1242	1242	[14]
	1,3,5-trimethyl-2-propylbenzene*	954	1298	-	
	2,4-dimethyl-1-(1-methylpropyl)benzene*	883	1211	1198	[15]
<b>Bicyclics</b>					
	indane	951	1011	1013	[3]
	1-methylindan	945	1063	1078	[16]
	1,2,3,4-tetrahydro-1,8-dimethylnaphthalene*	945	1219	-	
	5-ethyl-1,2,3,4-tetrahydronaphthalene	948	1332	1354	[6]
	1,2,3,4-tetrahydro-1-propylnaphthalene	883	1379	1389	[16]
	1,2-dihydro-2,5,8-trimethylnaphthalene	852	1455	-	
	naphthalene	947	1154	1156	[16]
	2,6-dimethylnaphthalene	973	1374	1377	[16]
	2-ethylnaphthalene	922	1416	1414	[17]
	2,3-dimethylnaphthalene	960	1385	1395	[18]
	1,4-dimethylnaphthalene	962	1404	1409	[16]
	1-propylnaphthalene	916	1456	1463	[19]
	1,4,6-trimethylnaphthalene	940	1527	1509	[20]

Table S9.2. (continued)

Chemical structure <sup>[b]</sup>	Name	Sim. <sup>[c]</sup>	RI <sup>[d]</sup>		Ref.
			Exp.	Rpt.	
	1,6,7-trimethylnaphthalene	927	1496	1533	[7]
	1,4,5,8-tetramethylnaphthalene	941	1653	-	
	1,6-dimethyl-4-(1-methylethyl)naphthalene	838	1685	1682	[21]
	6-isopropyl-1,4-dimethylnaphthalene	864	1841	-	
	7-ethyl-1,4-dimethylazulene	899	1673	1674	[22]
	1,4-dimethyl-7-(1-methylethyl)azulene	893	1791	1734	[23]
	9-ethyl-1,2,3,4,5,6-hexahydroanthracene	751	1830/	-	

<sup>[a]</sup> \* Signalizes products of sample 1 which were also present in sample 2. <sup>[b]</sup> C<sub>n</sub>-subst with n=1-6, denotes the total number of carbon atoms in the substituent groups. <sup>[c]</sup> Similarity of the mass spectra (Sim.). <sup>[d]</sup> Retention Index (RI) determined experimentally (Exp.) and RI values reported in the literature (Rpt).

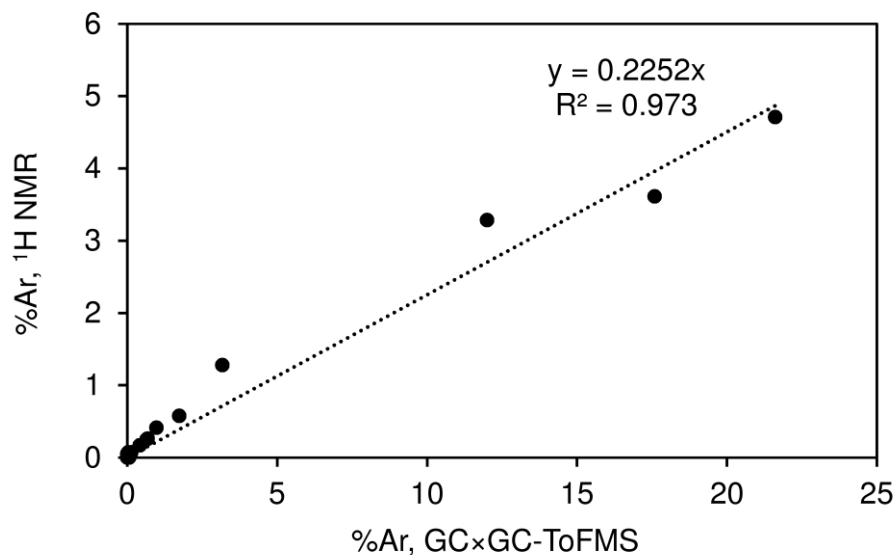


Figure S9.1. Aromatics contents (%Ar) determined by <sup>1</sup>H NMR spectroscopy *versus* that determined by GCxGC-ToFMS.

Table S9.3. Reduced experimental models, with codified variables, for the responses of the DoE.

Reduced model	$R^2$	$R^2_{adj}$
$X_{C4}(\%) = 84.084 + 6.08 X_P + 31.16 X_T - 9.06 X_W - 7.67 X_P^2 - 12.48 X_T^2 - 8.10 X_W^2$	0.932	0.881
$\eta_{Dcut}(\%wt) = 37.87 + 3.91 X_P + 8.81 X_T - 3.30 X_W - 10.74 X_P^2 - 15.29 X_T^2 - 6.91 X_W^2$	0.982	0.969
$\eta_{Ncut}(\%wt) = 34.58 + 2.817 X_P + 26.764 X_T - 2.492 X_W + 4.979 X_T^2 - 3.708 X_P \times X_T$	0.955	0.929
$\eta_{Arom}(\%wt) = 0.549 + 7.03 X_T - 1.46 X_W + 6.489 X_T^2 - 2.44 X_T \times X_W$	0.911	0.876
$\eta_{Dcut,free}(\%wt) = 37.42 + 3.545 X_P + 5.463 X_T - 2.427 X_W - 11.27 X_P^2 - 18.25 X_T^2 - 6.26 X_W^2 + 1.732 X_T \times X_W$	0.973	0.945
$\eta_{Ncut,free}(\%wt) = 35.18 + 3.16 X_P + 23.07 X_T$	0.932	0.921

Table S9.4. Aromatics distribution in the Dcut and Ncut products.

Run	Operating conditions			Aromatics distribution (%)	
	$T$ (°C)	$P$ (bar)	$W$ (h <sup>-1</sup> )	Dcut	Ncut
1	20	150	3.5	64	35
2	20	300	3.5	87	13
3	45	150	3.5	99	1
4	45	300	3.5	100	0
5	20	225	2.0	95	5
6	20	225	5.0	0	0
7	45	225	2.0	84	16
8	45	225	5.0	94	6
9	32.5	150	2.0	0	0
10	32.5	150	5.0	58	42
11	32.5	300	2.0	84	16
12	32.5	300	5.0	95	5
13	32.5	225	3.5	86	14
14	32.5	225	3.5	63	37
15	32.5	225	3.5	100	0

## Supplementary Material - Chapter 10

Table S10.1. Data matrix used in the construction of the PCA biplots of Figure 10.2 and Figure 10.3.

	Material	Materials acid properties				Materials textural properties				Catalytic performance parameters			
		B ( $\mu\text{mol g}^{-1}$ )	L/B	L <sub>strength</sub>	B <sub>strength</sub>	S <sub>BET</sub> ( $\text{m}^2 \text{g}^{-1}$ )	S <sub>meso</sub> ( $\text{m}^2 \text{g}^{-1}$ )	V <sub>micro</sub> ( $\text{m}^2 \text{g}^{-1}$ )	V <sub>meso</sub> ( $\text{m}^2 \text{g}^{-1}$ )	X <sub>C4</sub> (%)	STY ( $\text{g g}_{\text{cat}}^{-1} \text{h}^{-1}$ )	STY <sub>Dcut</sub> ( $\text{g g}_{\text{cat}}^{-1} \text{h}^{-1}$ )	%Dcut
Chapter 5	Al-TUD-25	44	3.0	0.33	0.00	741	741	0.00	1.70	33	288	166	58
	Al-TUD-50	28	3.6	0.33	0.00	687	687	0.03	2.07	35	274	108	40
	Al-TUD-1(PG)	8	14.9	0.18	0.00	397	397	0.02	1.18	21	100	96	21
	Al-LP-1(PG)	17	10.1	0.22	0.00	559	559	0.01	1.39	22	26	26	66
Chapter 6	BEA-n	184	1.6	0.65	0.04	645	260	0.07	1.03	39	405	246	61
	BEA-m	321	0.6	0.94	0.11	583	20	0.16	0.19	15	88	76	87
	BEA-hier	105	2.2	0.57	0.00	741	503	0.12	0.78	54	502	326	59
	BEA/TUD	78	1.5	0.56	0.00	589	355	0.10	1.30	26	162	100	61
Chapter 7	Z31-noT	212	0.2	1.01	0.25	308	168	0.04	0.42	54	521	335	64
	Z20-PZSi	107	1.3	0.47	0.06	721	308	0.09	0.65	77	791	534	68
	Z51-PZSi	83	0.6	0.61	0.04	558	289	0.07	0.69	57	496	353	71
	Z31-CoT	120	0.3	1.02	0.14	853	140	0.25	0.23	27	43	35	80
	Z29	299	0.2	0.85	0.21	334	97	0.08	0.38	27	58	43	73
Chapter 8	M-0.2-Ox	228	0.3	0.86	0.25	483	189	0.13	0.54	67	769	502	65
	M-0.2-Cl	261	0.3	0.79	0.33	453	149	0.13	0.51	58	587	409	70
	M-0.4-Ox	77	0.4	0.77	0.07	564	267	0.12	1.08	65	781	446	57
	M-0.4-Cl	138	0.8	0.63	0.13	564	291	0.11	1.11	86	852	584	69
	M-0.6-Ox	24	0.3	0.34	0.00	596	269	0.14	1.24	36	262	134	51
	M-0.6-Cl	101	1.5	0.35	0.05	494	255	0.11	1.12	66	808	448	55
	M-TPA/Na-Cl	78	1.7	0.45	0.00	604	285	0.14	1.10	46	490	271	55
	HZSM-5	353	0.2	0.87	0.42	431	54	0.17	0.18	39	377	222	59

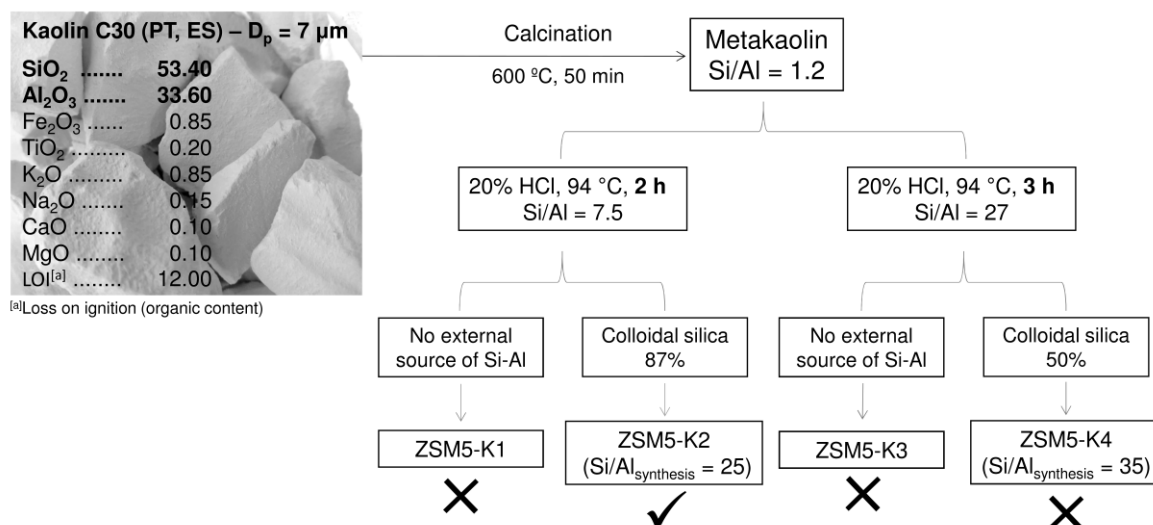


Figure S10.1. Preparation of ZSM-5 from kaolin C30 (Sibelco) according to the procedure described in refs. [24,25], using different acid treatments of metakaolin, with or without addition of external source of Si and Al ('X' stands for materials without ZSM-5 crystalline phase and 'V' stands for material with ZSM-5 crystalline phase).

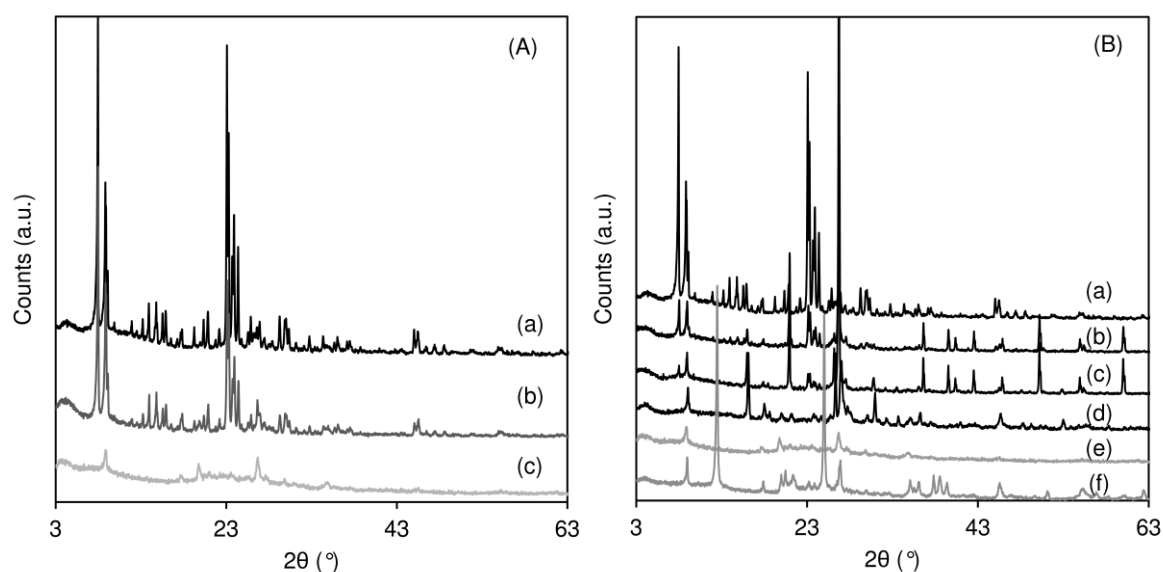


Figure S10.2. (A) PXRD patterns of ZSM-5 zeolite (CBV3024E, Zeolyst) (a), ZSM5-K2 (b) and metakaolin (c). (B) PXRD patterns of ZSM-5 zeolite (CBV3024E, Zeolyst) (a), ZSM5-K4 (b), ZSM5-K3 (c), ZSM5-K1 (d), metakaolin (e), and kaolin C30 (f).

**References of Appendix A**

- [1] J.S. Lopez-Echeverry, S. Reif-Acherman, E. Araujo-Lopez, Peng-Robinson equation of state: 40 years through cubics, *Fluid Phase Equilib.* 447 (2017) 39–71.
- [2] P.A. Martos, A. Saraullo, J. Pawliszyn, Estimation of air/coating distribution coefficients for solid phase microextraction using retention indexes from linear temperature-programmed capillary gas chromatography. Application to the sampling and analysis of total petroleum hydrocarbons in air, *Anal. Chem.* 69 (1997) 402–408.
- [3] P.C.J. Hayes, E.W. Pitzer, Kovats indices as a tool in characterizing hydrocarbon fuels in temperature programmed glass capillary gas chromatography. Part 1. Qualitative identification, 1981.  
[https://archive.org/details/DTIC\\_ADA111389/page/n1](https://archive.org/details/DTIC_ADA111389/page/n1) (accessed Dec 26, 2018).
- [4] 1,2,3-Trimethylbenzene-Kovats Retention Index  
[https://pubchem.ncbi.nlm.nih.gov/compound/1\\_2\\_3-trimethylbenzene#section=Kovats-Retention-Index](https://pubchem.ncbi.nlm.nih.gov/compound/1_2_3-trimethylbenzene#section=Kovats-Retention-Index) (accessed Dec 26, 2018).
- [5] A. Orav, T. Kailas, M. Müürisepp, J. Kann, Composition of the oil from waste tires. 2. Fraction boiling at 160-180 °C, *Proc. Est. Acad. Sci. Chem.* 48 (1999) 136–140.
- [6] C.M. White, J. Hackett, R.R. Anderson, S. Kail, P.S. Spock, Linear temperature programmed retention indices of gasoline range hydrocarbons and chlorinated hydrocarbons on cross-linked polydimethylsiloxane, *J. High Resolut. Chromatogr.* 15 (1992) 105–120.
- [7] A. Waggott, I.W. Davies, Identification of organic pollutants using linear temperature programmed retention indices (LTPRIs) - Part II, 1984.  
<http://dwi.defra.gov.uk/research/completed-research/reports/dwi0383.pdf>
- [8] E. Matisová, E. Juranyiová, P. Kurán, E. Brandsteterová, A. Kocan, S. Holotík, Analysis of multi-component mixtures by high-resolution capillary gas chromatography and combined gas chromatography-mass spectrometry. II. Trace aromatics in an n-alkane matrix, *J. Chromatogr.* 552 (1991) 301–312.
- [9] E. Matisová, M. Rukřiglová, J. Krupčík, E. Kovacicová, S. Holotík, Identification of alkylbenzenes up to C<sub>12</sub> by capillary gas chromatography and combined gas chromatography-mass spectrometry, *J. Q/ Chromatogr.* 455 (1988) 301–309.
- [10] 2,4-Dimethyl-1-Propan-2-Ylbenzene-Kovats Retention Index  
<https://pubchem.ncbi.nlm.nih.gov/compound/20832#section=Kovats-Retention-Index> (accessed Dec 26, 2018).
- [11] 1-Methyl-4-(2-Methylpropyl)Benzene-Kovats Retention Index  
<https://pubchem.ncbi.nlm.nih.gov/compound/21240#section=Kovats-Retention-Index> (accessed Dec 26, 2018).
- [12] 5-Isopropyl-M-Xylene-Kovats Retention Index  
<https://pubchem.ncbi.nlm.nih.gov/compound/5-Isopropyl-m-xylene#section=Kovats-Retention-Index> (accessed Dec 26, 2018).
- [13] 1,2,4-trimethyl-5-(1-methylethyl)benzene  
<https://webbook.nist.gov/cgi/cbook.cgi?ID=C10222954&Units=SI&Mask=2000#Gas-Chrom> (accessed Dec 15, 2018).
- [14] 1-Isobutyl-2,5-Dimethylbenzene-Kovats Retention Index  
<https://pubchem.ncbi.nlm.nih.gov/compound/41508#section=Kovats-Retention-Index>

- Index (accessed Dec 26, 2018).
- [15] 2,4-dimethyl-1-(1-methylpropyl)benzene  
<https://webbook.nist.gov/cgi/cbook.cgi?ID=C1483609&Units=SI&Mask=2000#Gas-Chrom> (accessed Dec 15, 2018).
- [16] P.C. Jr. Haynes, E.W. Pitzer, Disengaging solutes in shale- and petroleum-derived jet fuels by altering GC programmed temperature rates, *J. Hi. Res. Chromatogr. Chromatogr. Comm.* 8 (1985) 230-242.
- [17] 2-Ethyl-naphthalene -Kovats Retention Index  
<https://pubchem.ncbi.nlm.nih.gov/compound/2-ethylnaphthalene#section=Kovats-Retention-Index> (accessed Dec 15, 2018).
- [18] P. Bredael, Retention Indices of Hydrocarbons on SE-30, *J. Hi. Res. Chromatogr. Chromatogr. Comm.* 5 (1982) 325-328.
- [19] 1-Propyl-naphthalene-Kovats Retention Index  
<https://pubchem.ncbi.nlm.nih.gov/compound/33800#section=Kovats-Retention-Index> (accessed Dec 26, 2018).
- [20] 1,4,6-Trimethyl-naphthalene-Kovats Retention Index  
[https://pubchem.ncbi.nlm.nih.gov/compound/1\\_4\\_6-trimethylnaphthalene#section=Kovats-Retention-Index](https://pubchem.ncbi.nlm.nih.gov/compound/1_4_6-trimethylnaphthalene#section=Kovats-Retention-Index) (accessed Dec 26, 2018).
- [21] J.R. Kuate, J.M. Bessièrè, G. Vilarem, P.H.A. Zollo, Chemical composition and antidermatophytic properties of the essential oils from leaves, flowers and fruits of *Cupressus lusitanica* Mill from Cameroon, *Flavour Fragr. J.* 21 (2006) 693-697.
- [22] C. Bicchi, A. Binello, A.D. Amato, P. Rubiolo, Reliability of Van den Dool retention indices in the analysis of essential oils, *J. Chromatogr. Sci.* 37 (1999) 288-294.
- [23] Guaiazulene-Kovats Retention Index  
<https://pubchem.ncbi.nlm.nih.gov/compound/3515#section=Kovats-Retention>
- [24] A.S. Kovo, O. Hernandez, S.M. Holmes, Synthesis and characterization of zeolite Y and ZSM-5 from Nigerian Ahoko Kaolin using a novel, lower temperature, metakaolinization technique, *J. Mater. Chem.* 19 (2009) 6207-6212.
- [25] A. Duan, G. Wan, Y. Zhang, Z. Zhao, G. Jiang, J. Liu, Optimal synthesis of micro/mesoporous beta zeolite from kaolin clay and catalytic performance for hydrodesulfurization of diesel, *Catal. Today* 175 (2011) 485-493.